

UNITED STATES DEPARTMENT OF THE INTERIOR  
GEOLOGICAL SURVEY

---

PROCEEDING OF  
WORKSHOP XLVI

**The 7th U.S. - Japan Seminar on Earthquake Prediction**

Sponsored by the

INTERNATIONAL PROGRAM OF THE NATIONAL SCIENCE FOUNDATION

JAPAN SOCIETY FOR THE PROMOTION OF SCIENCE

U. S. GEOLOGICAL SURVEY

12 - 15 September 1988

---



**Open-File Report 90-98**

This report was prepared under contract to the U. S. Geological Survey and has not been reviewed for conformity with U.S.G.S. editorial standards or with the North American Stratigraphic Code. Opinions and conclusions expressed herein do not necessarily represent those of the USGS. Any use of trade, product, or firm names is for descriptive purposes only and does not imply endorsement by the U.S. Government

MENLO PARK, CALIFORNIA

1990

UNITED STATES DEPARTMENT OF THE INTERIOR

GEOLOGICAL SURVEY

---

PROCEEDINGS OF

WORKSHOP XLVI

**The 7th U.S. - Japan Seminar on Earthquake Prediction**

Volume 1

Sponsored by the

INTERNATIONAL PROGRAM OF THE NATIONAL SCIENCE FOUNDATION  
JAPAN SOCIETY FOR THE PROMOTION OF SCIENCE  
U. S. GEOLOGICAL SURVEY

12 - 15 September 1988

Convenors

Hiroo Kanamori  
Seismological Laboratory  
California Institute of Technology  
Pasadena, California, 91125, U.S.A.

Takeshi Mikumo  
Disaster Prevention Research Institute  
Kyoto University, Uji  
Kyoto 611, Japan

Organizing Committee

Hiroo Kanamori  
Carl Kisslinger  
John Filson

California Institute of Technology  
CIRES, University of Colorado  
U. S. Geological Survey

Administrator

Wanda H. Seiders  
U. S. Geological Survey

**Open-File Report 90-98**

Compiled by  
Muriel Jacobson

This report was prepared under contract to the U. S. Geological Survey and has not been reviewed for conformity with USGS editorial standards or the North American Stratigraphic Code. Opinions and conclusions expressed herein do not necessarily represent those of the USGS. Any use of trade, product, or firm names is for descriptive purposes only and does not imply endorsement by the U.S. Government.

1990

## TABLE OF CONTENTS

|   | Page |
|---|------|
| Summary and Acknowledgments:<br>Carl Kisslinger, Takeshi Mikumo and Hiroo Kanamori. . . . .   | i    |
| List of Participants. . . . .   | xii  |
| <br>SESSION I   |      |
| Regional variation in the seismicity before large shallow earthquakes<br>Kiyoo Mogi . . . . .   | 1    |
| Relation of aftershock distribution in time and space to the pre-mainshock<br>seismicity pattern<br>Carl Kisslinger and E. R. Engdahl . . . . .                         | 11   |
| Seismotectonic zonation based on the characteristics of active faults in Japan<br>Yoshihiro Kinugasa . . . . .  | 15   |
| Time dependent peninsula tectonics and earthquake prediction in Japan<br>Minoru Tanaka and Tetsuro Imakiire. . . . .  | 18   |
| Loci and maximum size of thrust earthquakes and the mechanics of the<br>shallow region of subduction zones<br>Daniel E. Byrne, Dan M. Davis, and Lynn R. Sykes. . . . . | 34   |
| Seismic activity in the Tokai area, Central Japan<br>H. Aoki, F. Yamazaki, and T. Ooida . . . . .   | 59   |
| <br>SESSION II  |      |
| Recent progress of electromagnetic studies for the earthquake prediction in Japan<br>Takeshi Yukutake. . . . .  | 63   |
| Parkfield, California earthquake prediction experiment - A status report<br>William H. Bakun. . . . .   | 68   |
| Classification of earthquake precursors and regularity of precursor appearance<br>Kazuo Hamada. . . . .   | 72   |
| Conclusions from social science research on earthquake prediction research<br>in the United States for the period of 1974 through 1988<br>Dennis S. Miletì . . . . .    | 80   |
| Temporal variations of seismic activity and some precursors before recent<br>intraplate earthquakes in southwest Japan<br>Takeshi Mikumo. . . . .                       | 85   |
| Prediction of large aftershocks on the basis of quiescence<br>R. E. Habermann and Frederic H. Creamer. . . . .  | 93   |

|  |     |
|--|-----|
| Coseismic changes in groundwater radon<br>H. Wakita, G. Igarashi, Y. Nakamura, Y. Sano and K. Notsu . . . . .  | 99  |
| A more precise chronology of earthquakes produced by the San Andreas fault<br>in southern California<br>Kerry Sieh, Minze Stuiver and David Brillinger . . . . . | 104 |
| New directions in the U. S. earthquake prediction program<br>Robert W. Wesson . . . . .  | 105 |
| The outline of the sixth earthquake prediction plan of Japan<br>Kazuhiko Otake . . . . .   | 109 |

### SESSION III

|  |     |
|--|-----|
| Rapid determination of source parameters<br>Adam M. Dziewonski . . . . .   | 114 |
| Earthquake phenomena observation system (EPOS) --- new JMA system for<br>earthquake prediction and tsunami warning services ---<br>Kenshiro Tsumura . . . . .  | 115 |
| On mitigating rapid onset natural disasters: project THRUST (Tsunami<br>Hazards Reduction Utilizing Systems Technology)<br>E. N. Bernard, R. R. Behn, G. T. Hebenstreit, F. I. Gonzales, P. Krumpel,<br>J. F. Lander, E. Lorca, P. M. McManamon, and H. B. Milburn . . . . . | 125 |
| Deep ocean tsunami and seismic wave observations: three recent gulf<br>of Alaska events<br>F. I. Gonzales and E. N. Bernard. . . . .   | 131 |
| Pasadena very broad-band system and its use for real-time seismology<br>Hiroo Kanamori . . . . .   | 135 |
| A real-time processing system of Tohoku University seismic network and recent<br>microearthquake activity<br>Akira Hasegawa, Norihito Umino and Akio Takagi . . . . .  | 143 |
| Seismic monitoring in southern California; plans for the future and<br>present realities<br>Thomas H. Heaton. . . . .  | 147 |
| The application of foreshocks to real-time earthquake hazard assessment in<br>southern California<br>Lucile M. Jones and Paul A. Reasenber . . . . .   | 151 |
| Real-time earthquake warning<br>M. Nafi Toksöz, Anton M. Dainty, John T. Bullitt and Robert Cicerone. . . . .  | 163 |
| A model for real time prediction of large earthquakes<br>Karen C. McNally. . . . .   | 174 |

## SESSION IV

|   |     |
|---|-----|
| Earthquake fault slip estimation from geologic, geodetic and seismological observations: implications for earthquake mechanics and prediction research<br>Wayne Thatcher and Manuel G. Bonilla. . . . . | 200 |
| Data Collection Network System of University Group and some recent results of crustal movements<br>Hiroshi Ishii. . . . .   | 214 |
| Spatial and temporal correlation between coda $Q^{-1}$ and seismicity<br>Keiiti Aki. . . . .  | 219 |
| Comparative strain measurement of the NRLM tunnel by an interferometer and a distance meter<br>Tadanao Oh'ishi and Katuo Seta . . . . .   | 221 |
| Repeating earthquakes: Characteristics and implications<br>William L. Ellsworth and Lynn D. Dietz . . . . .   | 226 |
| Gravity studies of active faults in Japan<br>Yukio Hagiwara. . . . .  | 246 |
| Foreshocks, aftershocks and earthquake recurrence<br>James H. Dieterich . . . . .   | 251 |
| Implications of fault creep studies for the mechanics of faulting<br>Robert L. Wesson . . . . .   | 258 |
| Observation status of the Japanese geodetic satellite "Ajisai" and precise baseline determination by using the Transportable Laser Ranging Station (HTLRS)<br>Yoshio Kubo and Minoru Sasaki . . . . .   | 262 |
| Conferences to Date. . . . .  | 273 |

## Summary

### Seventh U.S.-Japan Earthquake Prediction Research Seminar: Use of Real-Time Earthquake Information for Hazard Warning.

by

Carl Kisslinger, Takeshi Mikumo, and Hiroo Kanamori

For the seventh time since 1964, a seminar on earthquake prediction has been convened under the U.S.-Japan Cooperation in Science Program. The purpose of the seminar was to provide an opportunity for researchers from the two countries to share recent progress and future plans in the continuing effort to develop the scientific basis for predicting earthquakes and practical means for implementing prediction technology as it emerges. Thirty-six contributors, 15 from Japan and 21 from the U.S., met in Morro Bay, California, September 12-14. The following day they traveled to nearby sections of the San Andreas fault, including the site of the Parkfield prediction experiment. The convenors of the seminar were Hiroo Kanamori, Seismological Laboratory, Caltech, for the U.S., and Takeshi Mikumo, Disaster Prevention Research Institute, Kyoto University, for Japan. Funding for the participants came from the U.S. National Science Foundation and the Japan Society for the Promotion of Science, supplemented by other agencies in both countries.

The special theme for this seminar was the use of real-time information in the formulation of warnings of impending earthquakes and associated hazards. The papers and lively discussion ranged over the whole subject of earthquake prediction, from the fundamental physics of earthquake processes to the interface between science and society in the implementation of prediction technology. Tom Heaton, USGS, who chaired the concluding discussion session, summarized the principal topics as:

- \* seismicity sequences: foreshocks, aftershocks, and their relation to background seismicity.
- \* characteristic earthquakes.
- \* slip in subduction-zone earthquakes: where does it occur and how does it relate to the accretionary prism, sediment thickness, and other geological variables?
- \* non-seismological precursory anomalies: strain, geoelectrical, and geochemical.
- \* the present capability to process and use real time data for predictions and warnings, including tsunami warnings.
- \* the fundamental physics of instabilities and creep (which couples back into all of the above topics).

Other topics that were addressed included new results from geological studies of active faults, advances in seismic instrumentation and technology for remotely accessing centralized digital data bases, and the correlation of Bouguer gravity anomalies with seismogenic zones and subsurface faults in Japan.

The earthquake prediction problem is treated on three time scales: long-term (decades), intermediate-term (a few years), and short-term (a few weeks to a few hours). The work reported during

the seminar supports the general outlook that the most promising approaches to prediction, each applicable to one or more of these time scales, are (1) geological studies of fault systems and paleoseismological studies, (2) analysis of the time-dependent distribution of seismicity in space and time, (3) observations of crustal deformation, which may be manifested by a variety of phenomena (uplift, tilt, strain, gravity changes, etc.). Specific precursory anomalies that might arise from changes in rock properties or ambient conditions as a major event approaches are still being sought and tested.

#### Real-time Data Processing and Short-term Warnings

The capability to treat data in real-time and use the results for warnings, the special topic of this seminar, pertains primarily to short-term predictions, or even warnings that an earthquake has already occurred and that its effects (strong shaking, tsunami) will arrive soon at places away from the source. Modern data acquisition and computational systems have made real-time processing of earthquake-related data a reality in both countries, though not yet in general use in either.

Locations, magnitudes, focal mechanisms and other source parameters can be known within some tens of minutes after an event from the analysis of data telemetered to a suitably equipped center from either teleseismic stations or regional networks. Broadband data from even a single station can yield important (though not unique) results quickly.

The Japan Meteorological Agency (JMA) has installed a system called Earthquake Phenomena Observation System (EPOS) that can process 512 channels of seismic data and 512 channels of other data (e.g., strain, tilt, sea-level) on an on-line real-time basis. EPOS is used for tsunami warning and earthquake prediction services. Recent tsunami advisories, a primary JMA responsibility, were issued within about 7 minutes of the earthquake occurrence. JMA is also responsible for the short-term prediction of the expected Tokai earthquake. For this task, the Agency monitors the data continuously and if anomalous changes are seen, the Earthquake Assessment Committee will be assembled promptly. Almost any data in EPOS, including real-time data, can be displayed on a large screen in the specially equipped room in which the Committee meets. Thus, the Committee can quickly and efficiently assess the situation on the basis of the most recent observations.

Current seismic activity in the Tokai region has also been monitored continuously by university seismograph networks. The characteristic features of this seismicity, together with examples of focal mechanisms, were discussed in detail.

The National Oceanic and Atmospheric Administration and the U.S. Army Corps of Engineers are cooperating in a recently established program to monitor portions of the Aleutian Trench with high potential for tsunamigenic earthquakes with bottom pressure recorders. The devices are capable of detecting the tsunami in deep water and the data can be rapidly transmitted to the Pacific Tsunami Warning Center, which has responsibility for warnings for the Pacific basin.

The current capabilities and the potential applications for

the real-time processing of data from the dense regional university networks in several parts of Japan and in the southern California region of the U.S. were described to the meeting. The typical Japanese university analysis system, which is linked to the telemetered station network, automatically detects events, reads the arrival times of P and S waves, and locates the events. For example, the Tohoku University system locates about 9000 earthquakes per year. Reliability checks carried out by comparison to manual processing and comparison of the resulting seismicity distributions with those mapped from earlier work have shown the systems to be functioning very well.

The Southern California system is based on 250 telemetered stations, operated jointly by the USGS and Caltech. Currently about 15,000 events are located each year, with analysis completed within several days of real time. Systems under development should allow near real-time locations in the future.

From the prediction viewpoint, the payoff from near real-time processing comes from the ability to recognize anomalies that might denote the imminence of a strong event and to formulate a warning. The science has not yet had a full test of its capability to do this, but mechanisms to try are in place in both countries.

The prediction experiment at Parkfield, California is the centerpiece of the current U.S. program. The project is designed to determine if short-term precursors to an earthquake in the magnitude 6 range can be detected and interpreted rapidly, to enable the U.S.G.S. to make a closely timed prediction. The data from many sensors in the Parkfield area are telemetered to Menlo Park, where they are processed in almost real time. The experiment is an attempt at practical implementation of the results of much research during the past decade, and, if the results are positive, it is a step toward the development of an operational earthquake forecasting system. The observation and data handling system described to the seminar will certainly provide excellent data for research on earthquake processes, even if short-term prediction turns out not to work for the next Parkfield earthquake. The criteria established for making decisions on various levels of alert called for by the observations will also be tested as the experiment progresses. Finally, the effectiveness of the system established to communicate the prediction to the government of California and of their response will also be tested.

Many earthquakes are preceded by foreshocks, but the identification of an event as a foreshock prior to the occurrence of the mainshock has proven to be a difficult and elusive task. An alternative approach that is being tried is to estimate the probability that, given the occurrence of a small-to-moderate earthquake, a larger event will occur near the same place shortly afterwards. This approach is a key element in the Parkfield plan, based on what occurred during the previous two Parkfield earthquakes. Determinations of the spatial and temporal behavior of foreshock sequences and the regional history of foreshock occurrence are being combined in an effort to do real-time estimation of the increase of hazard implied by the occurrence of a moderate event in parts of California. A study of past foreshock sequences

has revealed that, after the largest foreshock has occurred, these sequences decay in a manner very similar to aftershock sequences.

The California Earthquake Prediction Evaluation Council has developed a procedure for real-time, short-term predictions of large ( $M \geq 7.0$ ) earthquakes in eight identified seismic gaps in the state. The basis of the procedure is the assumption that every  $M \geq 6$  earthquake within 50 km of four gaps in southern California and every  $M \geq 5$  earthquake within 20 km of four gaps in northern California are foreshocks to a  $M \geq 7$  mainshock, to occur within 5 days. The predictions are issued as earthquake "advisories". The false alarm rate, judged from historical data, should be acceptable from the viewpoint of public reaction. Problems to be solved include the decision as to which gap will rupture when a postulated foreshock occurs, and what to do about differences in magnitudes for the same earthquake determined by different organizations.

A search for systematics among a large number of reported precursors to Japanese earthquakes, based on many different types of geophysical, geochemical and geodetic observations, yielded a suggested relation, for short-term precursors (less than 40 days), for the probability of occurrence of a strong earthquake, given the observation of one of these precursors. Discussion brought out the principal problem with evaluating the significance of reported anomalies as true precursors. Many published reports, especially early ones, do not provide a basis for critically evaluating the validity of the report or any information on false alarms or failures to predict when the particular phenomenon is used.

The limit of a short-term real-time warning system is one that responds within tens of seconds of the occurrence of an earthquake, to provide a reliable estimate of the location, origin time, and size, and then calculate the area at risk, while the rupture is occurring. Signals from a network of instruments deployed along a fault (which, of course, must be pre-selected as having a high potential for a damaging earthquake), are monitored to detect promptly that something has occurred. The signals are used to track the rupture, locate the source, and estimate the seismic moment release in real time as the event progresses. Information that a potentially destructive event has occurred can be transmitted quickly to critical facilities, so that systems to limit or prevent damage can be actuated before the ground motion reaches the sites. A prototype system has been designed and tested on data from two recent California earthquakes and simulated data for the great 1857 event by a group at MIT.

### Prediction Research

The empiricism that characterized early prediction research is no longer acceptable in either country. Much of the research discussed at the seminar is directed toward gaining a fundamental understanding of seismogenesis that is adequate for interpreting observations of anomalies preceding earthquakes and the co-seismic and post-seismic phenomena associated with strong earthquakes, as well as for designing future observation programs. Results of studies of subduction zones ( a subject that has not

figured prominently in the U.S. program), the San Andreas and associated faults in California, and intraplate events in the Japanese islands were presented and debated.

Geological investigations of active faults are one source of essential information. A seismotectonic zonation for upper plate events within the Japanese Islands, based on a geological investigation of the regional characteristics of active faults was offered. Improvements in dating techniques have led to a more precise chronology of earthquake ruptures on the southern San Andreas fault. A shorter average interval for the most recent 10 events (131 years) has been found, but also a much greater variability of the inter-event times. The finding that these events tended to cluster in time, with long intervals between, reinforces doubts about the validity of using long-term average rates for estimating the current seismic hazard for this fault. On the other hand, the more precise dates increase the ability to correlate events between sites in efforts to evaluate the size of paleoseismic events.

Detailed gravity surveys in Japan revealed evidence of strike-slip movements on a latent active fault, as well as correlations between short wavelength negative Bouguer anomalies and microearthquake activity in some regions.

Hot discussion was provoked by a paper on the role of the accretionary prism and sedimentation rates on the distribution of seismic slip in subduction zones. In many subduction settings, an aseismic strip is observed to lie between the intra-plate activity near the trench and the abundant seismicity in the main thrust zone. The debate focussed on whether this aseismic section can be explained as due to the presence of weak materials in the accretionary prism above the downgoing slab in all known cases.

The distribution of co-seismic fault slip can be estimated independently from: (1) direct geological observations, (2) modelling of geodetic observations, and (3) modelling of waveforms recorded by seismographs. A U.S.G.S. study has looked at what each of these approaches reveals about the true fault slip. They have examined how the distributions, which often look quite different, can be reconciled, and how the combination can be used to document the complexities of fault rupture.

The details of the spatial and temporal distributions of earthquake sequences provide constraints on theoretical models of earthquake processes. Pre-mainshock distributions have been demonstrated to be a promising basis for intermediate-term predictions. Patterns observed prior to mainshocks and during the aftershock sequences were described for all of the tectonic settings mentioned earlier, with examples drawn from California, the Aleutian Islands, and Japan.

Results from Japan are mainly based on regional JMA observations and partly on local observations by university networks. Data from a number of large earthquakes around Japan support the concept that pre-event seismicity may vary according to three different patterns (quiescence, gradual increase, or concentrated swarm), depending on the region. In addition, there is evidence that variations in the long-term rate of seismicity observed concurrently in different regions might be attributed to slight

changes in tectonic stress.

During discussions of case histories from northern and central California and from the central Aleutians, the participants seemed to accept the evidence that clusters of aftershocks tend to occur in the same places as clusters of events during the pre-mainshock period, and that this behavior is closely tied to the concept of a "characteristic earthquake". Rates of decay of aftershocks with time are being studied for possible ways in which to predict strong aftershocks in real time, as well as for the information these rates may contain about fault zone properties.

The rate of decay of the seismic signal recorded at local or regional distances is measured by an attenuation parameter called "coda Q". Temporal variations in coda-Q have been tested in various settings as a precursor. Recent work shows that the distribution of attenuation measured this way correlates well with seismicity, being low (high Q) in tectonically stable regions and high in young active areas. The temporal correlation is more complex, with cases of both higher and lower attenuation prior to a mainshock having been detected. The clustering of fractures before a mainshock may explain coda-Q changes, as well as seismicity precursors of various kinds.

The capability to determine rapidly the source parameters of large numbers of moderate to strong earthquakes, globally distributed, from broad-band digital seismograms has been put into routine use in the past few years. The large data base, containing consistently determined focal mechanisms, is valuable not only for general geodynamics research, but also for studies directed towards intermediate-term prediction.

Crustal deformation observations have been a key element in the Japanese prediction program from its beginning. Elevation changes observed on the Boso and Miura Peninsulas since 1923 have been interpreted in terms of subduction processes. This effort at "peninsula tectonics" suggests a periodic modulation of the secular variation, with a period of 19-20 years, and short-period variations related to time-dependent subduction processes. About 100 crustal deformation observatories use a variety of strainmeters and tiltmeters to monitor zones of seismotectonic importance. The data are telemetered to the Earthquake Prediction Data Center at the Earthquake Research Institute, University of Tokyo. Data showing the subsidence of Omaezaki in the Tokai district since 1976 and uplift of the northeast sector of the Izu Peninsula since mid-1980 were displayed as products of levelling data analysis.

Work on non-seismological precursors to earthquakes, reported by Japanese participants, places more emphasis on fundamental studies than on correlations of anomalies with subsequent earthquakes. The investigation of resistivity, electrical potential, and geomagnetic anomalies in the neighborhood of faults are being carried out in an effort to clarify the role of ground water in earthquake processes and in accounting for geoelectromagnetic changes that have been observed prior to some earthquakes.

Geochemical precursors, especially changes in radon concentration in groundwater, have been controversial and poorly understood (and often suspect) phenomena for a long time. No U.S.

research on this topic was reported. One of the problems has been that observations at two sites at about the same distance from an epicenter might show an anomaly at one and not the other. Evidence of co-seismic and pre-seismic changes in radon concentration in a well or in soils on active faults in northeastern and southwestern Japan was presented. The observation of co-seismic changes in the well is not only interesting in itself, but the absence of any significant radon changes at another well about 50 km away on the same fault shows that, indeed, some wells are more sensitive than others to whatever produces the radon fluctuations. Such observations seem useful for identifying the best wells to use for future tests of the radon precursor hypothesis.

### **Fault Physics and Instrumentation Development**

Although many of the observational studies reviewed in the seminar have produced results that are important for understanding earthquake processes, few new theoretical results and no new laboratory findings were included. Two U.S.G.S. papers considered fundamental aspects of faulting. One of these examined the role of fault creep, with emphasis on how creep acts to redistribute and concentrate stress around the strong points on the fault that ultimately fail to produce earthquakes. From the prediction viewpoint, an important conclusion is that intervals of time during which aseismic fault slip occurs should be regarded as periods of enhanced probability for an earthquake. The other study is part of a continuing effort to develop a comprehensive theory of earthquake nucleation, one that will account for the time dependence of foreshock and aftershock occurrence, as well as inter-event times of mainshocks. An important suggestion from the work is that the duration of aftershock sequences are directly related to the recurrence time of mainshocks, a result that is supported by the data shown.

Development of new instruments is important for future progress in the two national prediction programs. The National Research Laboratory for Metrology, Tsukuba, has developed a facility for comparative performance tests of devices for geodetic measurements. Results from two years of operation of a laser extensometer and a laser distance measurement instrument in a specially prepared tunnel showed the close correspondence of the two, to within a few microstrains, but with an unexplained phase shift of about 48 days between the two sets of measurements. The multi-channel portable field unit that has been developed for the PASSCAL program of the Incorporated Research Institutions for Seismology was described and displayed.

Research on the social, economic, and political consequences of earthquake predictions has been underway in the U.S. from the earliest days of the prediction research program. A review of findings during the past 15 years revealed that long-term and short-term predictions, while eliciting different public responses, are not likely to have serious impacts on the target communities. Intermediate-term predictions (a few years) may have negative economic impacts, as well as positive effects.

## Future Plans

Plans for future prediction research efforts were discussed for the U.S. by R.L. Wesson, U.S.G.S., and for Japan by K. Otake, Geographical Survey Institute. The Sixth Earthquake Prediction Plan of Japan was presented to the Government very recently. The plan calls for a comprehensive program, in which observations and analysis will continue for specified Areas of Intensified Observation, with expanded efforts in both long-term and short-term prediction. The effort is to be supported by a variety of fundamental research studies, instrumentation development projects, and work on the prediction system.

The U.S. Five Year Plan, 1989-1993, for the National Earthquake Hazards Reduction Program was in the late stages of preparation at the time of the seminar. Therefore, a less specific program plan was outlined. Instead "likely candidates for increased emphasis" during future years were put forward. These include: geologic and seismologic studies for long-term prediction, geodetic measurements, borehole observations, rheology of faults zones, combined use of short-period and broad-band networks, and computer modelling of earthquake processes.

The participants came away from the seminar with a general feeling that, while there is very much work still to be done, especially on short-term predictions, much progress has been achieved in both national programs. Above all, there is no doubt as to the value to both countries of these more-or-less regularly scheduled opportunities for representatives of the active research communities to come together in a relaxed atmosphere, conducive to thorough airing of progress and problems.

Those contributing to the seminar were: K. Aki (University of Southern California), H. Aoki (Nagoya University), W.H. Bakun (USGS), E.N. Bernard (NOAA/PMEL), A. Dainty (MIT), J.H. Dieterich (USGS), A.M. Dziewonski (Harvard University), W.L. Ellsworth (USGS), J. Fowler (IRIS), F. Gonzalez (NOAA/PMEL), R.E. Habermann (NOAA/NGDC), Y. Hagiwara (University of Tokyo), K. Hamada (National Research Center for Disaster Prevention), A. Hasegawa (Tohoku University), T.H. Heaton (USGS), H. Ishii (University of Tokyo), D. Johnson (NSF), L.M. Jones (USGS), H. Kanamori (Caltech), Y. Kinugasa (Geological Survey of Japan), C. Kisslinger (University of Colorado), K.C. McNally (University of California, Santa Cruz), T. Mikumo (Kyoto University), D. Miletic (Colorado State University), K. Mogi (University of Tokyo), T. Oh'ishi (National Research Laboratory of Metrology), K. Otake (Geographical Survey Institute), Y. Okada (National Research Center for Disaster Prevention), K.E. Sieh (Caltech), L.R. Sykes (Columbia University), M. Tanaka (Geographical Survey Institute), W.R. Thatcher (USGS), K. Tsumura (JMA), H. Wakita (University of Tokyo), R. Wesson (USGS), T. Yukutake (University of Tokyo).

## Acknowledgments

This seminar was partially supported by the International Program of the National Science Foundation, Grant No. INT-8715928 (expenses for travel and subsistence of U. S. non-government participants), Japan Society for the Promotion of Science and Kagami Memorial Foundation of Tokyo-Kaijo Co. (expenses for the Japanese participants), and the U. S. Geological Survey.

The convenors and participants are grateful to Wanda Seiders (U. S. Geological Survey) and Dee Page (California Institute of Technology) for their assistance in the logistics for the seminar.

## Opening Remarks by Mr. Kazuhiko Otake

It is my great pleasure to have an opportunity to greet you at the 6th Joint Meeting of the U.J.N.R. Panel on Earthquake Prediction Technology here in Menlo Park.

On behalf of the Japanese members and their guests, I would like to convey my gratitude to Dr. Wesson, the chairman of the United States U.J.N.R. Panel, and the Panel members for inviting us to the meeting.

The panel was established in 1979 under the agreement between the two countries, with the aim to work jointly towards the improvement of earthquake prediction technology, and the current meeting marks the sixth, based on mutual understanding and efforts. At the last joint meeting, many subjects were discussed, including the Parkfield earthquake prediction experiment. Since then, various exchanges in research projects and a very active extensive exchange of information have been in progress, including the laser ranging and VLBI experiment between the two countries.

In Japan, after the last joint meeting, the 1986 eruption of Izu-Oshima Volcano at its summit crater occurred on November 15. By the fissure eruption on both the caldera floor and the flank of the main cone, all the habitants were evacuated from the island. This evacuation lasted about one month. The Japanese Government made an emergency plan to establish a monitoring and observation system on the volcanic activity, for judging the safety of the return of the people to the island. Fortunately, there was no human damages.

Concerning the earthquakes, middle class deep earthquakes occurred off the east coast of Chiba prefecture (M6.7, d=58 km) on December 17, 1987 and in eastern Tokyo (M6.0, d=100 km) on March 18, 1988. The east coast of Chiba prefecture suffered from liquefaction failure and other damages by the earthquake. From this experience, it was considered essential to also prepare a detailed land use plan from the viewpoint of disaster prevention.

Needless to say, earthquake prediction is extremely important for reducing the loss of life and property in Japan due to earthquake hazard.

Under these circumstance, the Sixth 5-year Earthquake Prediction Project of Japan was authorized by the Geodesy Council in July 1988, which will be in effect April of 1989. In this project, the following points are emphasized,

- (1) Since high accuracy in prediction of the time of the occurrence is rather more important than that of location and size for long and short range prediction, the main theme on prediction of earthquakes is shifted from "development and research" to "observation and research".
- (2) Concerning observation and research, with respect to earthquake prediction of the inland type originating directly beneath the Metropolitan and Urban areas, telemetering system improving the routine monitoring system and research on the mechanism of premonitory phenomena are strongly promoted for short range prediction. However, there are many problems which must be solved, especially in the Metropolitan area.
- (3) For this purpose, intensive observation and research in the specified test fields with high priority is carried out. As an example, the area near the northern Sagami trough has been selected not only from the viewpoint of being a very important subject area but also because of the fact that it was specified as a test field with high priority.

- (4) Application of space techniques to prediction research including GPS, VLBI, laser ranging and use of telecommunication satellites for transmission of monitoring data.

This Joint Meeting is the first meeting which is held under the joint auspices of the 7th U.S.-Japan Seminar on Earthquake Prediction. I believe that the papers presented will significantly contribute to earthquake prediction technology in the world.

Lastly, I would like to express our hearty gratitude to Dr. Wesson and the U.S. panel members, including the seminar convener in making all necessary preparations for the meetings.

I would like to introduce the members of the Japanese Panel and guests. The members attending are Dr. Kazuo Hamada of the National Research Center for Disaster Prevention, Dr. Minoru Tanaka of the Geographical Survey Institute, Dr. Tadanao Oh'ishi of the National Research Laboratory of Metrology, Dr. Yoshihiro Kinugasa of the Geological Survey of Japan, and I am from the Geographical Survey Institute.

Japanese Panel members have traditionally been affiliated with government agencies. However, in view of the fact that important observations and research are also in progress in the academic field, I welcome with great pleasure Prof. Takeshi Mikumo of Kyoto University, who was the convener of the Japanese members for the 7th U.S.-Japan Earthquake Prediction Seminar, and Prof. Harumi Aoki of Nagoya University, who was in charge of summarizing the Sixth Earthquake Prediction Plan of Japan. Our other guest is Dr. Yoshimitsu Okada of the National Research Center for Disaster Prevention.

## LIST OF PARTICIPANTS

AKI, Keiiti  
Department of Geological Science  
University of Southern California  
Los Angeles, California 90089-074

AOKI, Harumi  
Department of Science  
Nagoya University, Furo-cho,  
Chikusa-ku, Nagoya 464, Japan

BAKUN, William H.  
U. S. Geological Survey  
345 Middlefield Road, MS977  
Menlo Park, California 94025

BERNARD, Eddie N.  
NOAA/Pacific Marine Environmental Lab.  
7600 Sand Point Way, N.E.  
Seattle, Washington 98115

DAINTY, Anton M.  
Department of Earth, Atmospheric and  
Planetary Science  
Massachusetts Institute of Technology  
Cambridge, Massachusetts 02139

DIETERICH, James H.  
U. S. Geological Survey  
345 Middlefield Road, MS977  
Menlo Park, California 94025

DZIEWONSKI, Adam M.  
Department of Earth and Planetary Sciences  
Harvard University  
Cambridge, Massachusetts 02138

ELLSWORTH, William L.  
U. S. Geological Survey  
345 Middlefield Road, MS977  
Menlo Park, California 94025

HABERMANN, Ray E.  
National Geophysical Data Center  
NOAA, NESDIS E/GC4  
325 Broadway  
Boulder, Colorado 80303

HAGIWARA, Yukio  
Earthquake Research Institute  
University of Tokyo, Yayoi 1-1-1  
Bunkyo-ku, Tokyo, 113, Japan

HAMADA, Kazuo  
National Center For Disaster Prevention

HASEGAWA, Akira  
Department of Science  
Tohoku University, Aoba, Aramaki  
Sendai 980, Japan

HEATON, Thomas H.  
U. S. Geological Survey  
525 Wilson Avenue  
Pasadena, California 91106

ISHII, Hiroshi  
Earthquake Research Institute  
University of Tokyo, Yayoi 1-1-1  
Bunkyo-ku, Tokyo 113, Japan

JOHNSON, Douglas  
Division of Earth Sciences  
National Science Foundation  
Washington, D. C. 20550

JONES, Lucile M.  
U. S. Geological Survey  
525 Wilson Avenue  
Pasadena, California 91106

KANAMORI, Hiroo  
Seismological Laboratory  
California Institute of Technology  
Pasadena, California 91125

KINUGASA, Yoshihiro  
Geological Survey of Japan  
Yatabe-cho, Tsukuba  
Ibaraki Pref. 305, Japan

KISSLINGER, Carl  
CIRES  
University of Colorado  
Boulder, Colorado 80309

McNALLY, Karen C.  
Earthscience Board  
University of California, Santa Cruz  
Santa Cruz, California 95064

MIKUMO, Takeshi  
Disaster Prevention Research Institute  
Kyoto University, Uji  
Kyoto 611, Japan

MILETI, Dennis  
Hazard Assessment Laboratory  
Department of Earth Resources  
Colorado State University  
Fort Collins, Colorado 80523

MOGI, Kiyoo  
Earthquake Research Institute  
University of Tokyo  
Yayoi 1-1-1  
Bunkyo-ku, Tokyo 113, Japan

OHISHI, Tadanao  
National Laboratory of Meteorology

OKADA, Y.  
National Center for Disaster Prevention

OTAKE, T.  
Geographical Survey Institute

SIEH, Kerry E.  
Division of Geological and Planetary Sciences  
California Institute of Technology  
Pasadena, California 91125

SYKES, Lynn R.  
Lamont-Doherty Geological Observatory  
Columbia University  
Palisades, New York 10964

TANAKA, Minoru  
Geographical Survey Institute

THATCHER, Wayne R.  
U. S. Geological Survey  
345 Middlefield Road, MS977  
Menlo Park, California 94025

TSUMURA, Kenshiro  
Japan Meteorological Agency  
Otemachi 1-3-4, Chiyoda-ku  
Tokyo 100, Japan

WAKITA, Hiroshi  
Department of Science  
University of Tokyo  
Hongo 7-3-1, Bunkyo-ku  
Tokyo 113, Japan

WESSON, Robert L.  
U. S. Geological Survey  
12201 Sunrise Valley Drive  
Reston, Virginia 22092

YUKUTAKE, Takeshi  
Earthquake Research Institute  
University of Tokyo  
Yayoi 1-1-1  
Bunkyo-ku, Tokyo, Japan

# Regional Variation in the Seismicity Before Large Shallow Earthquakes

Kiyoo Mogi

Earthquake Research Institute, University of Tokyo, Tokyo, Japan

The seismicity before and after large shallow earthquakes around the Japanese islands is examined systematically based on the revised JMA earthquake catalog (1982) and the Seismological Bulletin of JMA until the present time. In this paper, the seismicity pattern leading up to the principal shock was compared with the aftershock region, which is considered to be the focal region of the main shock.

The method used in this paper is as follows: Epicentral distribution of earthquakes for each year was obtained for a rather long time span, and the changes were observed. Next, similarly patterned periods were combined in several pages of maps and finally refined to a few maps showing the changes in seismicity pattern as simply as possible. In the subduction zones, earthquakes of focal depth less than 80 km were plotted, while earthquakes shallower than 40 km were plotted in other regions.

As the rupture zones of major earthquake, the most widely used method is to plot the region of aftershocks immediately following the main shock, usually for one day after. However, since the earthquakes under study in this paper are relatively large (M 4-5), the number of aftershocks is low in some cases, making it difficult to express the rupture region of the main shock. Considering this difficulty, the aftershock region was obtained from the distribution of aftershocks plotted for a two-day period following the main shock in this paper. This is, for all practical purposes, the same as plotting aftershocks within one day after the main shock. A comparison was made of the aftershock region immediately following the main shock and the seismicity pattern preceding the large earthquake.

The results show a variety of differences in the change of seismicity patterns over time. These different cases can be classified into three types (A, B, C) (Figure 1). In Type A, seismic activity becomes very low prior to a large earthquake in its focal region (creating a seismic gap of the second kind). In Type B, a seismic quiescence in the focal region is not observed before a large earthquake, and seismic activity rather increases gradually in the focal region and its vicinity. In Type C, seismic activity increases steadily without a predominant principal earthquake ever occurring, i.e. a swarm pattern.

Locations of these three types of earthquakes are shown in Figure 1. The results of this study show the close relationship between differences in seismicity pattern prior to large earthquake and the submarine topography. Type A earthquakes occur where the submarine topography is quite simple, Type B earthquakes where it is complex, such as in a subduction zone disturbed by oceanic ridges or active tectonic lines, and Type C earthquakes where seamounts subduct beneath the continental plate at the deep sea trench, creating very complex submarine topography. Where

the submarine topography in the focal region is simple and flat, earthquake fault surface might be relatively homogeneous; where the submarine topography is more complex, the fault itself is also more complex. Thus, it is deduced that the differences in seismicity patterns among these three types is due to the irregularity of their faults.

As an example of Type A, the case of the 1973 Nemuro-hanto-oki earthquake is shown in Figures 2, 3, and 4. This earthquake occurred off the southern coast of the Nemuro Peninsula, Hokkaido, on June 17, 1973. This earthquake was of the low angle thrust type (Shimazaki, 1974), and its magnitude was M 7.4, Mw 7.8. Figures 2a, b, and c show the epicentral distributions of earthquakes of M 5.0 or larger before the large earthquake in the region, while Figure 3 shows the location of the main shock and the distribution of aftershocks in the two-day period immediately following. For the seven-year period of 1952-1958 shown in Figure 2a, seismicity within the aftershock region was high. For the next 7-year period shown in Figure 2b (1959-1965), seismic activity was low in the southern half of the aftershock region, but remained active in the northern half. However, from 1966 until the main shock occurred on June 17, 1973 (a period of 7.5 years) seismic activity within the aftershock region became very low and the surrounding region was active (Figure 2c). In this case, the area of the seismic gap is practically the same as that of the aftershock region.

Utsu (1972) pointed out that seismic activity prior to the Nemuro-hanto-oki earthquake was low for the period from 1961-1970. The seismic gap he described is larger than the one indicated here, with a slightly more southerly position and so somewhat different from the aftershock region of this earthquake. This difference is due to the difference in period observed (his being 1961) and illustrates the importance which must be given to the selection of observation periods.

In Figure 2c, the quiescent region, just west of the aftershock region of the 1973 earthquake, can be recognized. This corresponds to the rupture zone of the 1952 Tokachi-oki earthquake of M 8.2.

In summary, a clear precursory seismic quiescence appeared before this earthquake from 1966 and the quiescent region corresponds closely to the aftershock region. This is a clear case of Type A. The submarine topography in the focal region of this earthquake shown in Figure 4 is very simple.

As an example of Type C, the case of the Ibaraki-ken-oki earthquakes is shown in Figures 5 and 6. Figures 5a and b show the epicentral distribution of the earthquakes (1960-1961) off the east coast of Ibaraki prefecture, Honshu. In the Ibaraki-ken-oki region, activity including earthquakes of M 6~7 has occurred repeatedly, showing the swarm type pattern wherein seismicity builds gradually until a peak is reached, then decreases gradually. A tendency for activity to concentrate along a belt running NW-SE can be seen. Figure 6 shows the submarine topography in this region, in which the axis of the Japan Trench is indicated by a solid line. In this figure, we find several seamounts east of the trench and a very complicated configuration of the sea bottom to the west. One seamount in particular, the Kashima First Seamount indicated by a thick arrow, breaks down at the trench axis. It is deduced that this seamount is subducting beneath the Eurasia Plate as the Pacific Plate moves (A. Mogi

and Nishizawa, 1980). The complexity of the sea bottom configuration of the landward side is most probably caused by seamounts similarly subducting beneath the land. The region where seismic activity is high runs northwest from the area where it is thought that seamounts are being pushed under the upper plate. This is the same direction as the movement of the Pacific Plate itself.

The results are summarized in Figure 1 and Table 1. In Figure 1, Type A earthquakes are indicated by solid circles, Type B semi-solid and Type C by open circles. Simplified structural characteristics are also shown. Figure 1 clearly shows that almost every earthquake of M 7.5 or larger around the Japanese islands has been of Type A. The appearance of a seismic gap of the second kind is therefore a fairly common phenomenon, and can be helpful for the long-term prediction of earthquakes.

Finally, a hypothesis is presented explaining the mechanism of these different seismicity patterns prior to a large earthquake.

In the case of Type A, the fault surface is generally even, with small undulations. In the initial stage, small-scale asperities, which correspond to small contact portions on the fault surfaces, distribute at random, and as stress increases, small to medium-size ruptures occur at stress concentrated portions. By this process, the fault plane becomes more uniform and stronger, and so seismic quiescence appears in this part. When the stress reaches the ultimate strength of the main asperity, a large earthquake occurs by a rupture of the asperity. The mechanism of seismic quiescence presented here is nearly similar to those by Mogi (1977) and Kanamori (1981).

In the case of Type B, the fault surface is not even, but fairly complex. As stress increases, contact areas between fault surfaces increases also, but the fault plane does not become uniform. Stress concentrates at many points on the fault plane, and small and medium-size ruptures continue to occur. Then asperities combine, rupturing at the same time causing a large earthquake. Examples of this type of irregular fault surface are found at structurally complex areas, such as the subduction zone disturbed by oceanic ridges or active tectonic lines.

In the case of Type C, the fault surface is extremely complex, and ruptures of small and medium-size asperities continue to occur at points where stress is concentrated. In this case, the predominant large rupture can not occur. This type of extremely complex fault surface may be caused by strong structural disturbances, such as subduction of an oceanic plate with seamounts.

A final explanation in Table 1 is required regarding the normal fault type of earthquake, which is shown to exhibit a seismicity pattern resembling Type B. The above-mentioned cases were discussed in terms of compressive stress fields; however, in this case, a tensile stress field applies. As stress increases in a tensile stress field, structural uniformity does not occur, and small to medium-size ruptures occur before the main rupture. This would, therefore, show the same pattern of seismicity as Type B.

## References

- Japan Meteorological Agency, Catalogue of relocated major earthquakes in and near Japan (1926-1960), pp. 109, 1982.
- Kanamori, H., The nature of seismicity patterns before large earthquakes, In: D. W. Simpson and P. G. Richards (Editors), Earthquake Prediction, Maurice Ewing Ser., 4, Am. Geophys. Union, Washington, D.C., pp. 1-19, 1981.
- Mogi, A. and Nishizawa, K., Breakdown of a seamount on the slope of the Japan Trench, Proc. Japan Acad., 56 (Ser. B): 257-259, 1980.
- Mogi, K., Seismic activity and earthquake prediction, Proc. Earthquake Predict. Symp. 1976, 203-214, 1977 (in Japanese).
- Shimazaki, K., Nemuro-Oki earthquake of June 17, 1973: A lithospheric rebound at the upper half of the interface. Phys. Earth Planet. Inter., 39: 314-327, 1974.
- Utsu, T., Large earthquakes near Hokkaido and the expectancy of the occurrence of a large earthquake off Nemuro, Rep. Coord. Comm. Earthquake Predict., 7: 7-13, 1972 (in Japanese).

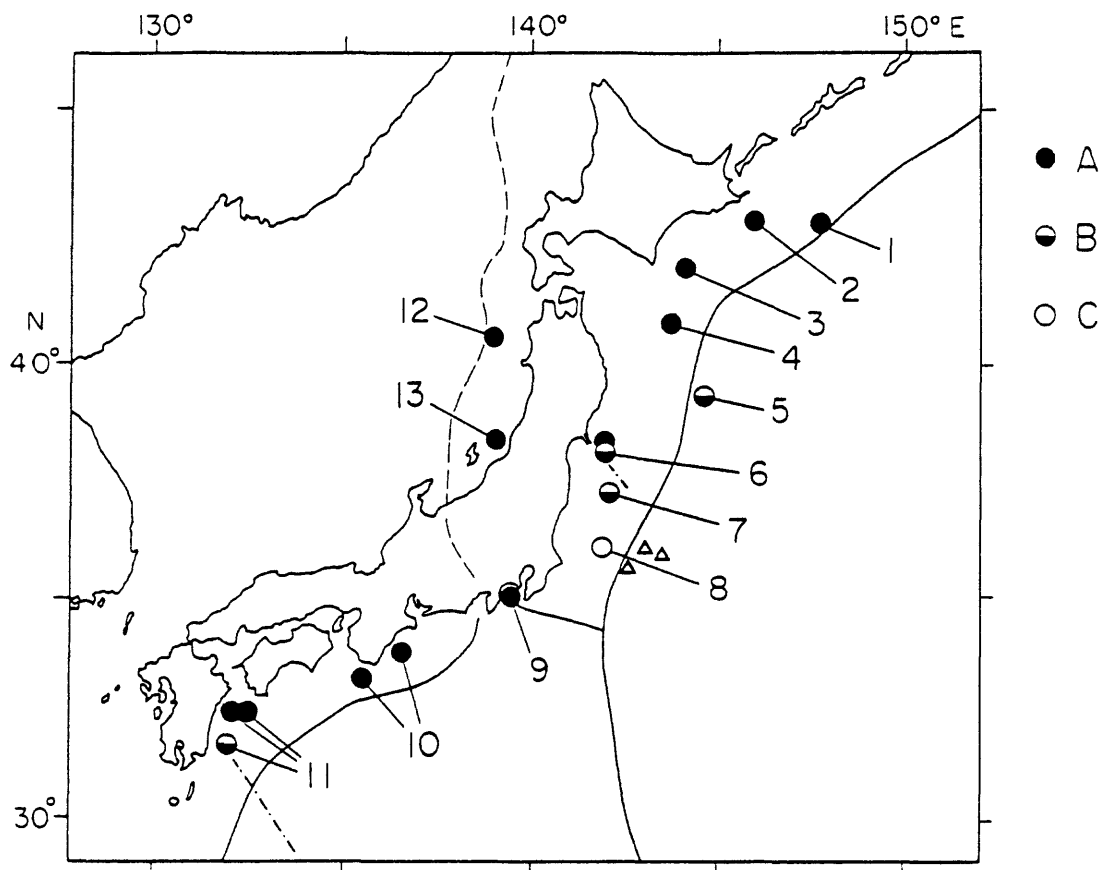
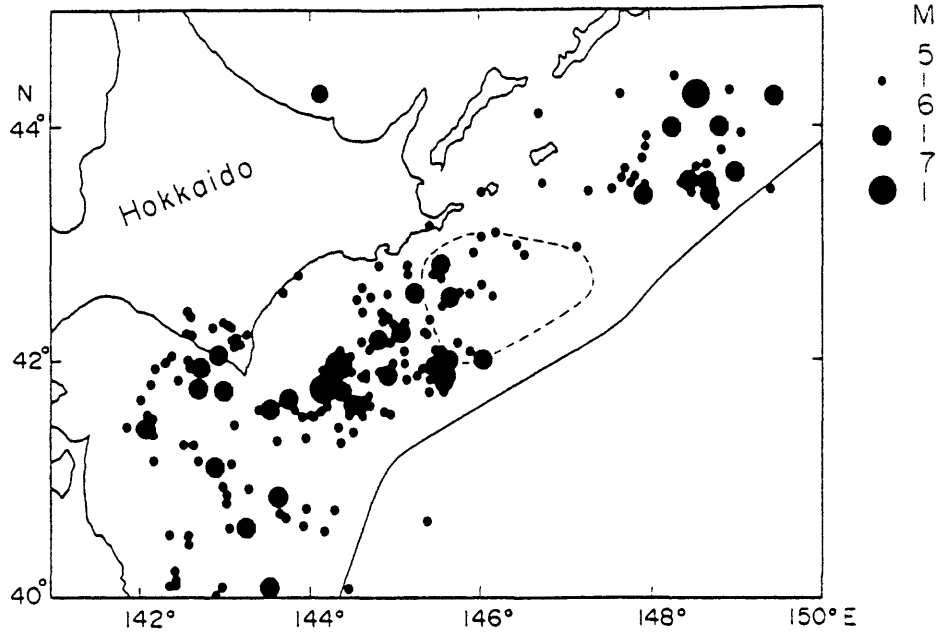


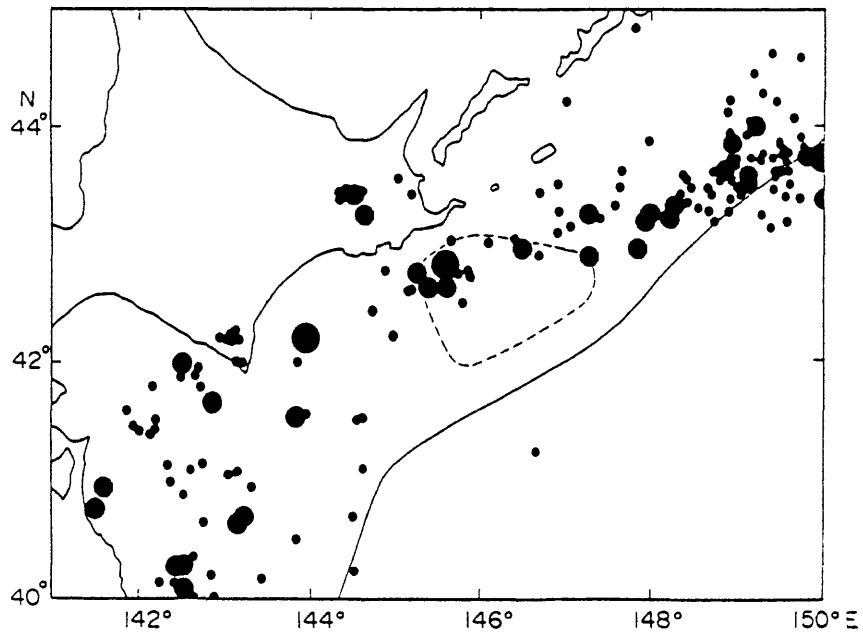
Figure 1 Epicentral distribution of earthquakes of Type A, Type B and Type C. Triangle: seamount; chain line: oceanic ridge or active tectonic line; solid curve: deep sea trench or trough; broken line: plate boundary proposed by Nakamura (1983).

1952 - 1958



(a)

1959 - 1965



(b)

Figure 2 Epicentral distributions of shallow earthquakes (focal depth <80km) before the 1973 Nemuro-hanto-oki earthquake. The broken curve shows the aftershock region of the 1973 earthquake and the solid line shows the axis of the Kurile Trench. (a) 1952-1958; (b) 1959-1965; (c) 1966-June 16, 1973.

1966-1973. 6. 16

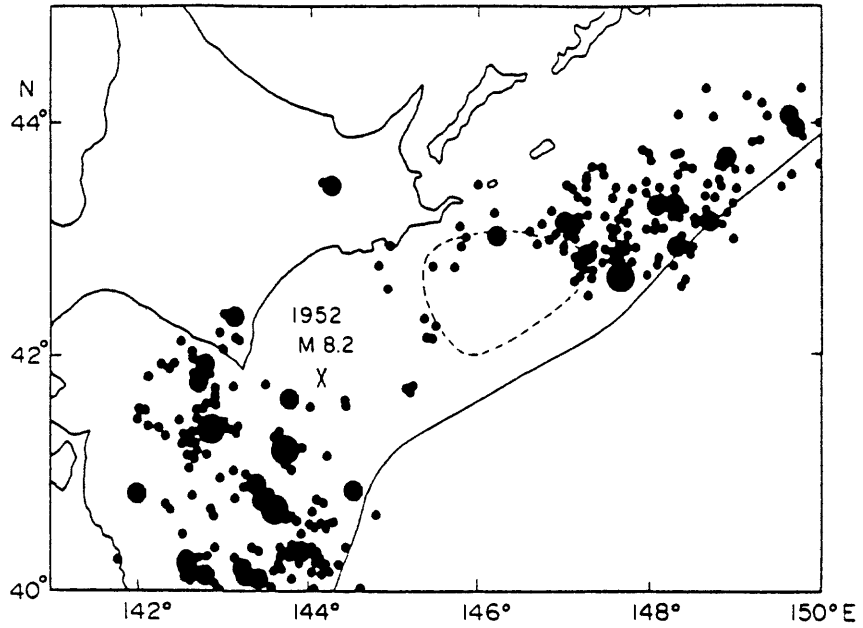


Figure 2(c)

1973.6.17(12<sup>h</sup>55<sup>m</sup>) - 1973.6.19(12<sup>h</sup>54<sup>m</sup>)

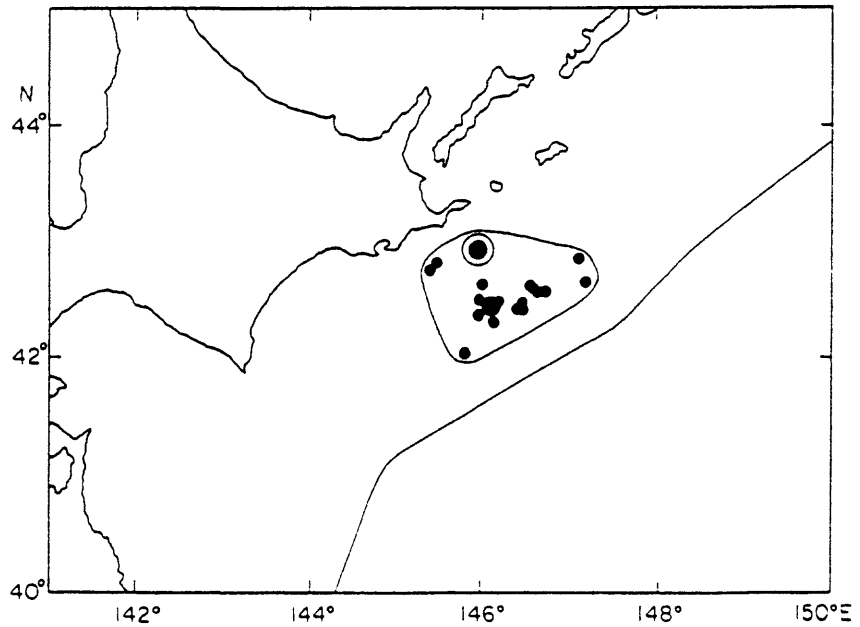


Figure 3 The main shock (double circle) and aftershocks within a two-day period of the Nemuro-hanto-oki earthquake of June 17, 1973.

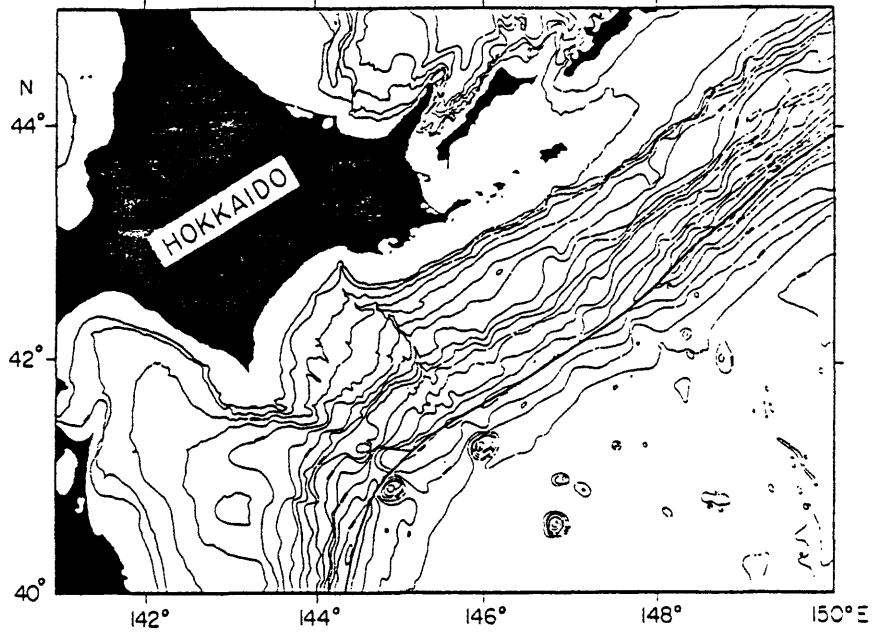


Figure 4 Submarine topography in and around the focal region of the 1973 Nemuro-hanto-oki earthquake. Solid line: the axis of the Kurile Trench.

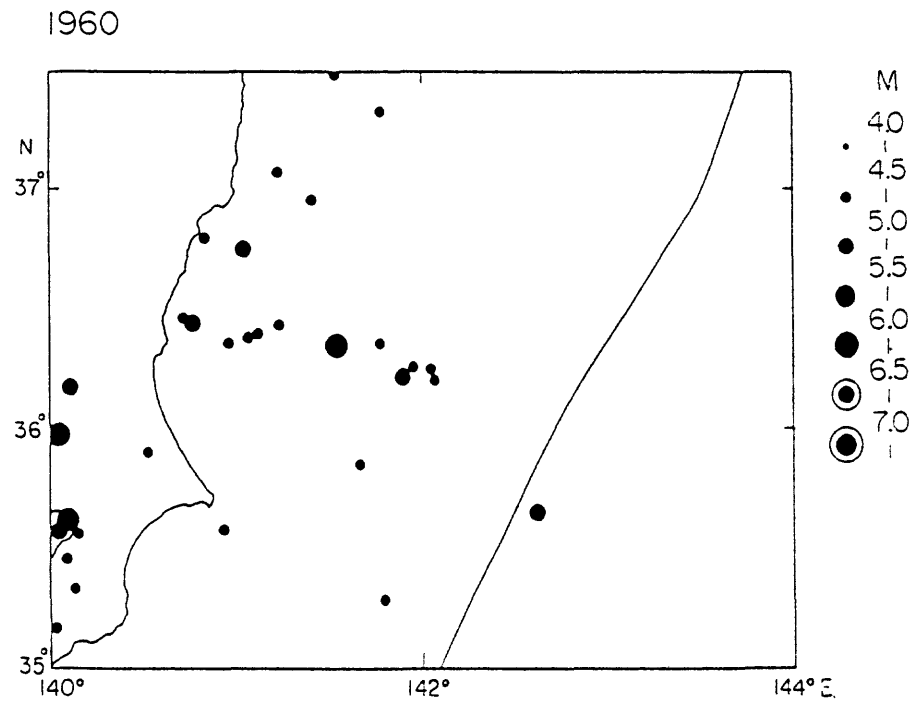


Figure 5(a) Epicentral distributions of shallow earthquakes which occurred off the east coast of the Ibaraki prefecture, Honshu, during the period from 1960 to 1961. The solid line shows the axis of the Japan Trench. (a) 1960; (b) 1961.

1961

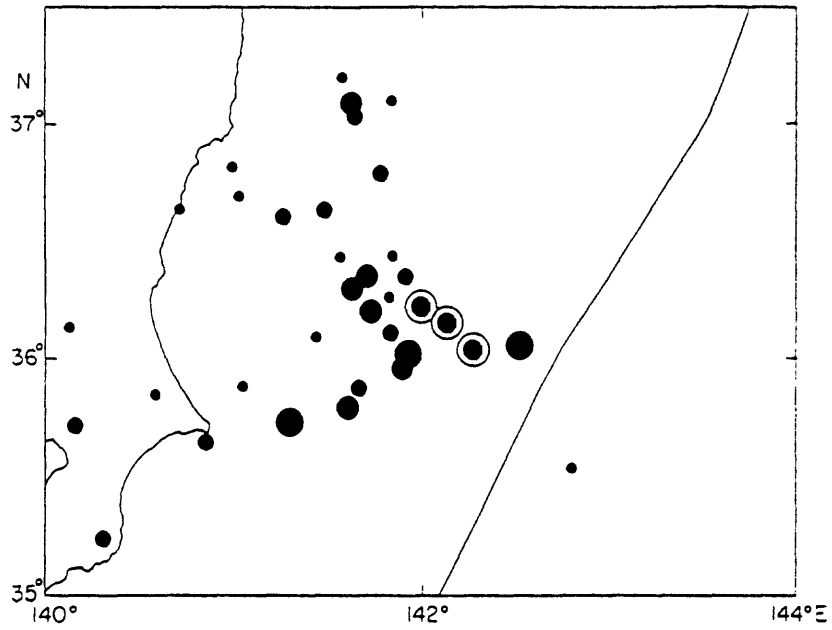


Figure 5(b)

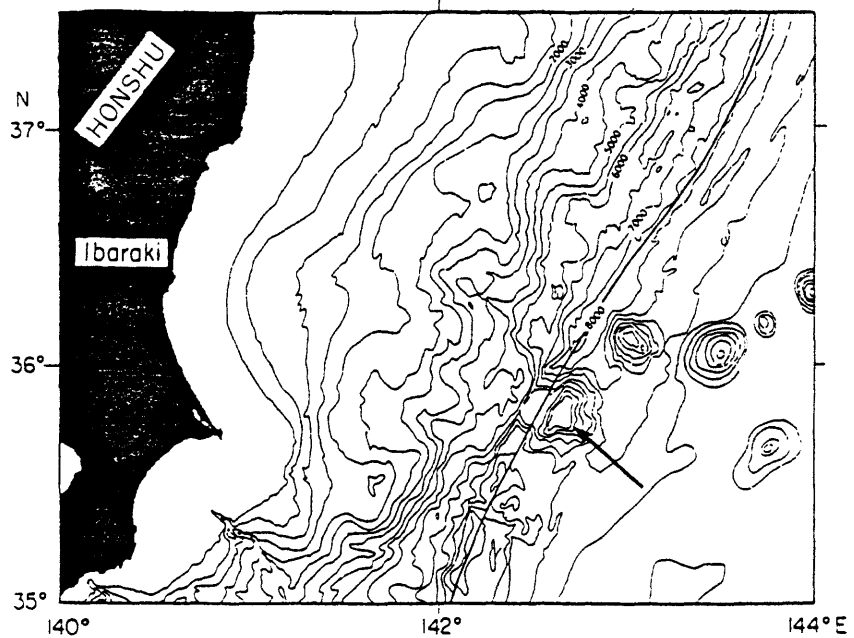


Figure 6 Submarine topography in the region off the east coast of Ibaraki prefecture. A solid line shows the axis of the Japan Trench and a thick arrow indicates the Kashima First Seamount.

Table 1

|                 |    | Seismicity<br>before the large<br>earthquake | Maximum<br>magnitude of<br>the earthquake | Tectonic<br>structure            |
|-----------------|----|--|---|----------------------------------|
| Thrust<br>fault | A  | Seismic<br>quiescence                        | ~ 8                                       | Homogeneous                      |
|                 | B  | Increasing<br>activity                       | ~ 7.5                                     | Complex                          |
|                 | C  | Swarm type                                   | ~ 6 - 7                                   | Extremely<br>complex             |
| Normal<br>fault | B' | Increasing<br>activity                       | ~ 8                                       | ( Extension<br>stress<br>field ) |

## Relation of Aftershock Distribution in Time and Space to the Pre-Mainshock Seismicity Pattern

C. Kisslinger (CIRES, University of Colorado, Boulder, CO 80309) and E. R. Engdahl (U.S. Geological Survey, Denver, CO 80225)

The distribution in time and space of seismicity prior to a major earthquake, the details of the rupture processes during the mainshock, and the characteristics of the aftershock sequence are all manifestations of the physics of seismogenesis. The increasing availability of high-quality data makes it possible to determine the details of all three of these phases of the earthquake cycle with resolution and reliability that are adequate to provide meaningful constraints on models. Here we investigate the relations among the phenomena observed during the three phases. The quantitative understanding that will follow from the analysis of a number of cases, in various tectonic settings, and the synthesis of the findings will provide an improved basis for approaches to the prediction of future events.

In this study, the spatial distribution of the aftershocks of the Andreanof Islands earthquake of May 7, 1986 ( $M_w$  8.0) has been compared with the distribution of seismicity during the 22 years prior to the event. The aftershock distribution has also been compared to the distribution of seismic quiescence at the microearthquake level during 40 months before the mainshock, for that part of the rupture zone for which data are available from the Central Aleutians Seismic Network, and with the distribution of moment release during the mainshock, as derived by others.

The objectives of the study of the rate of decay of aftershock activity are: (1) to determine if the rates are significantly different for different faults, (2) to interpret significant differences in decay rates in terms of the mechanical properties of the fault, and (3) to search for changes in aftershock occurrence rate that might be precursory to strong aftershocks. The temporal behavior of the Andreanof aftershock sequence has been modelled by fitting the Modified Omori relation to the teleseismically derived data for the first 350 days. The rate of decay of activity is expressed as the p-value in  $n(t)=K(t+c)^{-p}$ , where  $n(t)$  is the number of events per unit time at time  $t$ . The p-values have been derived for the entire aftershock zone, as well as for subdivisions defined on the basis of the seismicity distribution: the upper and lower parts of the main thrust plane, and the upper plate.

The primary data base for this work was the catalog of central Aleutian earthquakes, January, 1964 - April, 1987, as re-located by Engdahl. A lower magnitude cutoff of  $m_b$  4.7 was applied to this catalog, but in a modified form. A combination of the reported USGS  $m_b$  (minimum 4.3) and the number of stations reporting the event (minimum 15) was used to either eliminate or include some events for which the reported magnitude was almost certainly erroneous. The Central Aleutians catalog, based on the CIRES network, was used to provide detailed data down to the  $M_D$  2.3 level for the part of the rupture zone west of the May 7, 1986 epicenter, for August, 1974 - May 6, 1986 and for the earliest part of the aftershock sequence.

The principal conclusions of the analysis of the spatial distribution are:

(1) the overall distribution of aftershocks agrees closely with the seismicity distribution during the preceding 22 years for the same section of the Aleutians seismic zone. Events are distributed all along the upper thrust plane, but the lower thrust plane was active only in the segment west of the mainshock epicenter.

(2) the aftershocks are concentrated in definite clusters, separated by regions of no activity. With one exception, these clusters are in the same place as the clusters of events prior to the mainshock. One group of aftershocks did fill in a hole in the pre-event distribution, in the upper thrust plane, close to the epicenter to the southwest.

(3) for that part of the rupture zone monitored by the local network, the early aftershocks in the local catalog and the teleseismic aftershocks show a distinct concentration in the place in which the sharpest and most persistent quiescence had occurred prior to the mainshock, and where major moment release occurred during the event.

The results of the analysis of the temporal behavior and b-value determinations are summarized in Table 1.

(1) for all aftershocks,  $m_b \geq 4.7$ , the rate of decay, as given by the p-value in the Modified Omori relation, is 0.87, with a b-value of 1.27. For the upper thrust plane, within which 68.5% of the aftershocks occurred,  $p=0.94$ ,  $b=1.30$ . For the lower thrust plane, with 23.5% of the aftershocks,  $p=0.72$ ,  $b=1.7$  (this high b-value is suspect because of the narrow range of magnitudes in the data set). For the small group of upper plate events, most of which occurred in a short time interval,  $p=1.26$ ,  $b=0.95$ .

(2) the upper plate activity is interpreted as triggered activity and not part of the primary aftershock sequence. If these events are removed, the p-value hardly changes, but the fit to the Modified Omori relation is improved, as indicated by the smaller value of the mean difference.

(3) The low p-value and high b-value in the lower thrust plane indicate that this part of the fault zone has significantly different properties than the upper thrust plane. Both values point to a heterogeneous fault surface, containing a large number of small asperities scattered over it. The absence of activity on the eastern part of the lower plane is still to be explained.

(4) the b-value for the whole aftershock zone during the 22 years before the mainshock was 1.15. For the thrust zone only, b was 1.20. No significant difference in pre-event and aftershock b-values is seen.

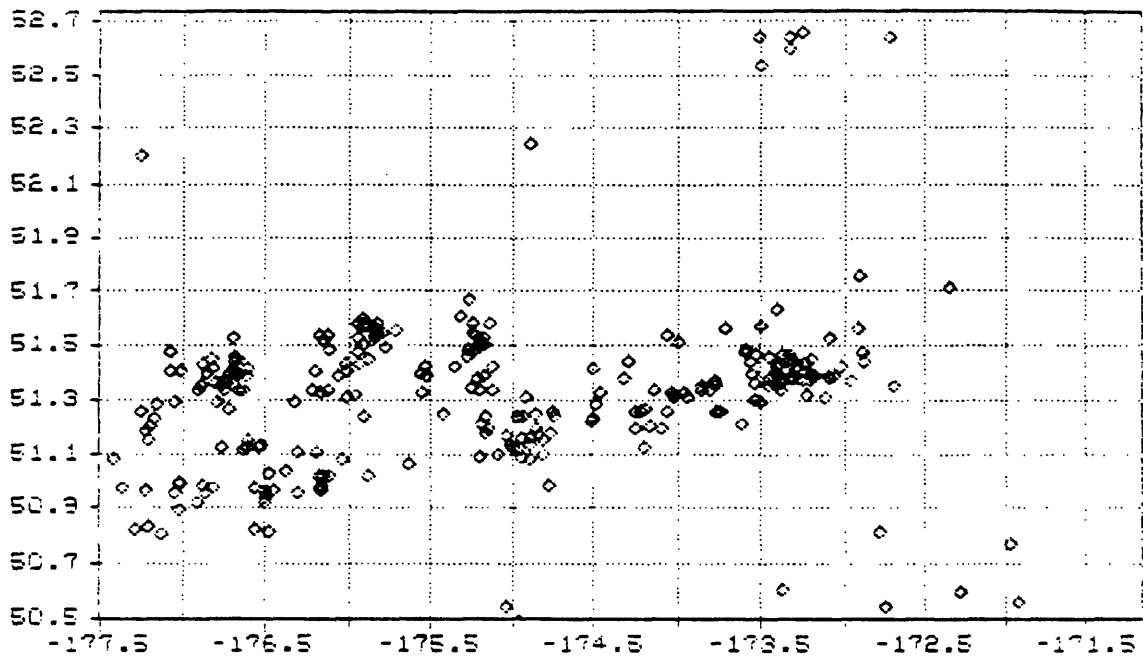
The concentration of aftershocks, as well as of major moment release in the mainshock, within the zone of pronounced quiescence, lends support to the interpretation of the quiescence as an intermediate-term precursor to this major earthquake.

Table 1

Summary of Modified Omori Fits to Subsets of the Aftershocks

| Subset             | No. events  | p     | b    | Mean dif (number-FLT) |
|--------------------|-------------|-------|------|-----------------------|
| All aftershocks    | 238         | 0.868 | 1.27 | 0.236±4.410           |
| All $m_b \geq 5$   | 95          | 0.918 |      | 0.365±2.669           |
| Upper thrust       | 163 (68.5%) | 0.935 | 1.30 | 0.396±2.871           |
| Lower thrust       | 56 (23.5%)  | 0.719 | 1.73 | 0.378±1.473           |
| Upper plate        | 19 (8%)     | 1.262 | 0.95 | 0.600±1.885           |
| All-upper plate    | 219 (92%)   | 0.876 |      | 0.118±3.600           |
| East of epicenter  | 89 (37.4%)  | 0.982 |      | 0.453±3.960           |
| Upper thrust, east | 71          | 0.994 |      | 0.486±3.240           |
| West of epicenter  | 149 (62.6%) | 0.835 |      | 0.411±2.466           |
| Upper thrust, west | 92          | 0.942 |      | 0.461±1.568           |

640101-860506,  $h \leq 50$  km



860507-870430

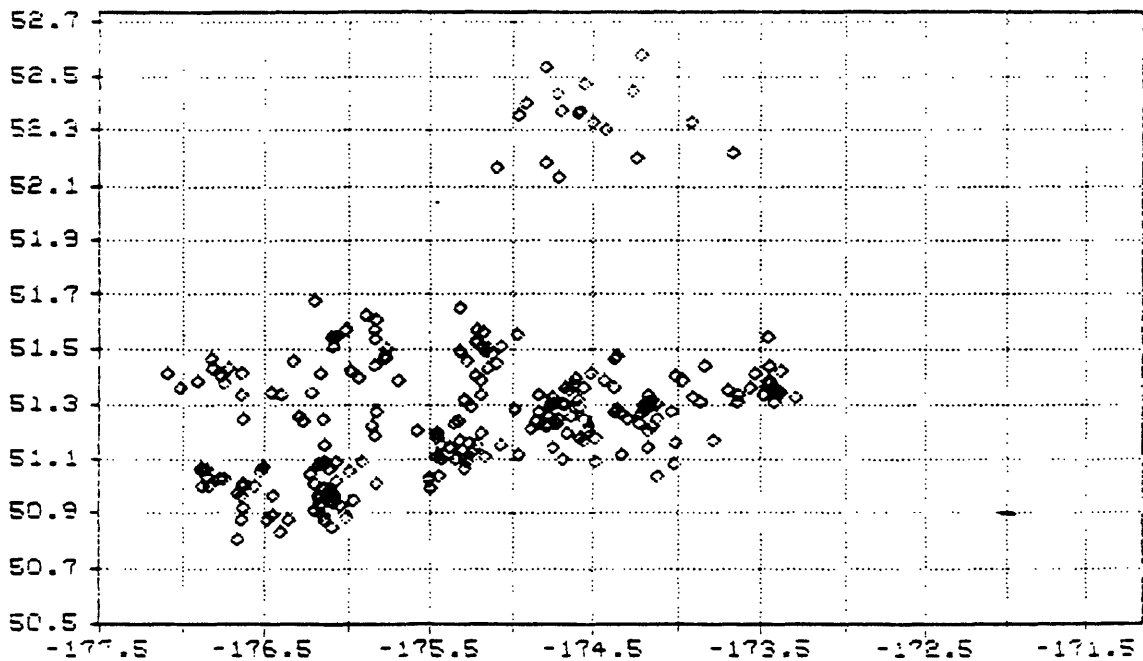


Figure 1. Top: Pre-event Seismicity, 1964 - April 1986  
Bottom: Aftershocks,  $m_b \geq 4.7$

Aftershocks vs. time,  $\geq 4.7$  &  $\geq 5.0$

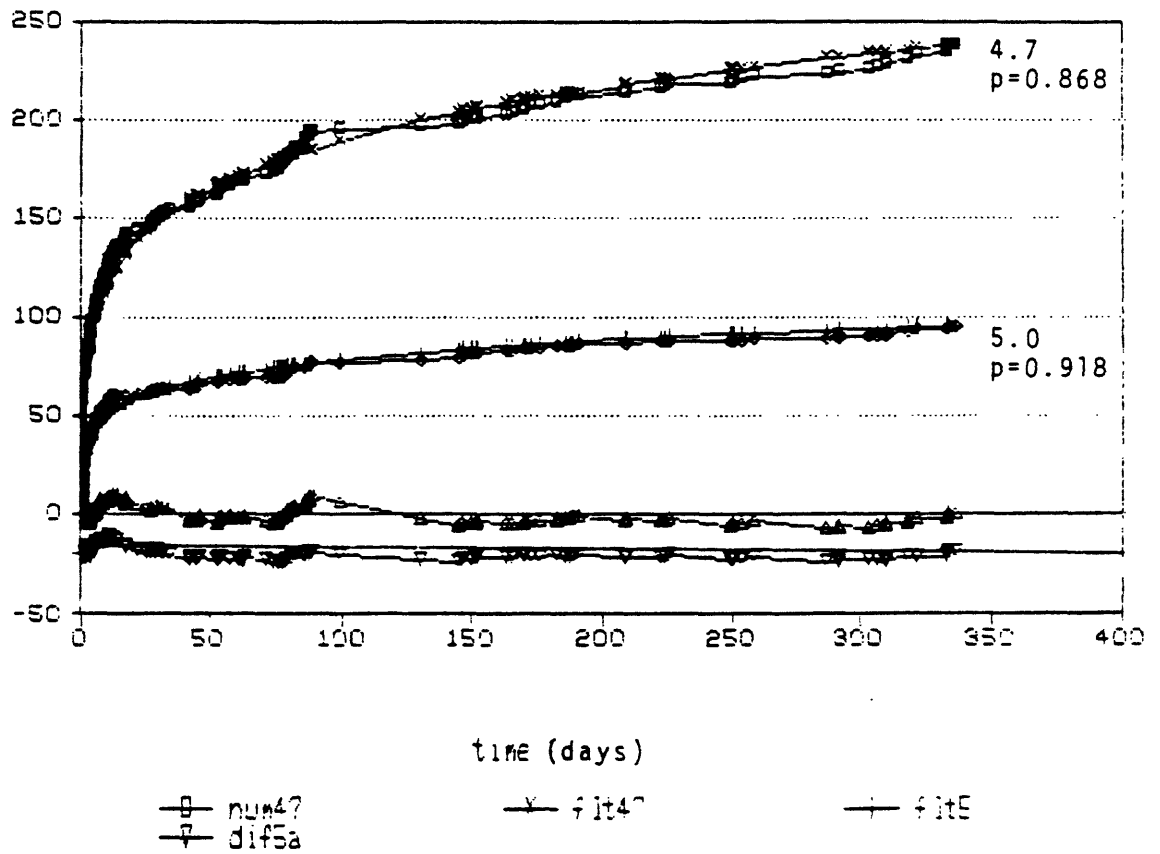


Figure 2. Modified Omori fit to the aftershocks for two magnitude cutoff values.

## Seismotectonic Zonation based on the Characteristics of Active Faults in Japan

Yoshihiro KINUGASA  
Geological Survey of Japan  
1-1-3 Higashi, Tsukuba, Ibaraki, 305 Japan

One of the major themes of the Sixth Earthquake Prediction Plan of Japan is the earthquake prediction research of intra-plate earthquakes. Seismotectonic study provides basic data for this research as well as being one of the major products of the research itself. This paper deals with seismotectonic zonation based on the regional characteristics of active faults.

The definition of an active fault in this study follows that of Bonilla [Bonilla, 1970]. The distribution of active faults was re-examined by the staff of the Geological Survey of Japan [GSJ, 1982-1987] during the period of the Fifth Earthquake Prediction Plan and summarized in the Quaternary Maps of Japan [JAQR, 1987].

Active faults in Japan are scattered over the country as shown in Fig.1-a. However, careful examination of the active faults reveals certain regional characteristics. For instance, dip-slip faults are predominant in northern Japan and strike-slip faults in western Japan. Also, the distribution density of active faults shows a remarkable contrast between the coastal area of the Japan Sea and that of the Pacific Ocean.

In this study, fault length is also used as one of the factors of regional characteristics because fault length is the function of earthquake magnitude as shown in the empirical relations between the length of earthquake surface breaks and the magnitude of historical earthquakes.

Grouping and segmentation are important factors in the evaluation of fault length. In this study, faults along the same geological structure are considered as a group, and the length of this group which includes individual fault segments is evaluated.

Evaluation of the length of very long faults such as the Median Tectonic line requires the concept of segmentation. Although a significant amount of work has been undertaken on this concept much still remains to be investigated. Also, because such long faults usually take the role of seismotectonic boundaries, they are shown as seismotectonic boundaries in this study.

Based on these regional characteristics of active faults, seismotectonic provinces and boundaries are defined as shown in Fig.1-b. Within each province active faults have similar characteristics such as slip sense and length. The characteristic length of faults in a region implies the characteristic magnitude of earthquakes in that region.

Boundaries can be classified into two kinds, active boundaries which accompany active faults and inactive boundaries without active faults. An active boundary is considered to be a seismotectonic province without width because it has earthquake potential in the same manner as a seismic province.

Some distinctive features of the regional characteristics of active faults can be summarized as follows:

1: High distribution density in central Japan (Kinki and Kyubu regions) and these regions are broken into small pieces of seismotectonic provinces.

2: Distribution density contrast between the coastal area of the Japan Sea and that of the Pacific Ocean, which can be seen in the northern part of the main island (Tohoku region) and central Japan.

3: Coincidence of major active faults with the above mentioned boundary of the distribution density. The boundary can be described as an "Active Fault Front" in a similar sense to the Volcanic Front and the Aseismic Front.

4: Discontinuity of the Active Fault Front behind the junction of trenches is notable, such as Kuril-Japan trench junction and Japan-Bonin junction, while no remarkable discontinuity can be seen behind the Nankai-Ryukyu junction.

5: Zonation map of Hokkaido (Northern Island) shows peculiar features in comparison with other areas, and it is thought that these features might have been caused by interaction of the Pacific, Eurasian and North-American Plates.

6: Coincidence of the seismotectonic boundaries with older geologic structures such as the boundary of the Neogene volcanic and non-volcanic regions. Not only the active parts of the Median Tectonic Line but also the inactive parts of it takes the role of the boundary and of the Active Fault Front.

#### References

Bonilla, M. G., Surface faulting and related effects, in Wiegel, R. L. ed. Earthquake Engineering, Prentice-Hall Inc., 47-74, 1970.

Geological Survey of Japan, 1:500,000 Neotectonic Map Series (14 sheets), 1982-1987.

Japan Association of Quaternary Research (ed.), Quaternary Maps of Japan, Univ. of Tokyo Press, 1987.

Fig-a. ACTIVE FAULTS IN JAPANESE ISLANDS  
based on GSJ'S 1:500,000 NEOTECTONIC MAPS

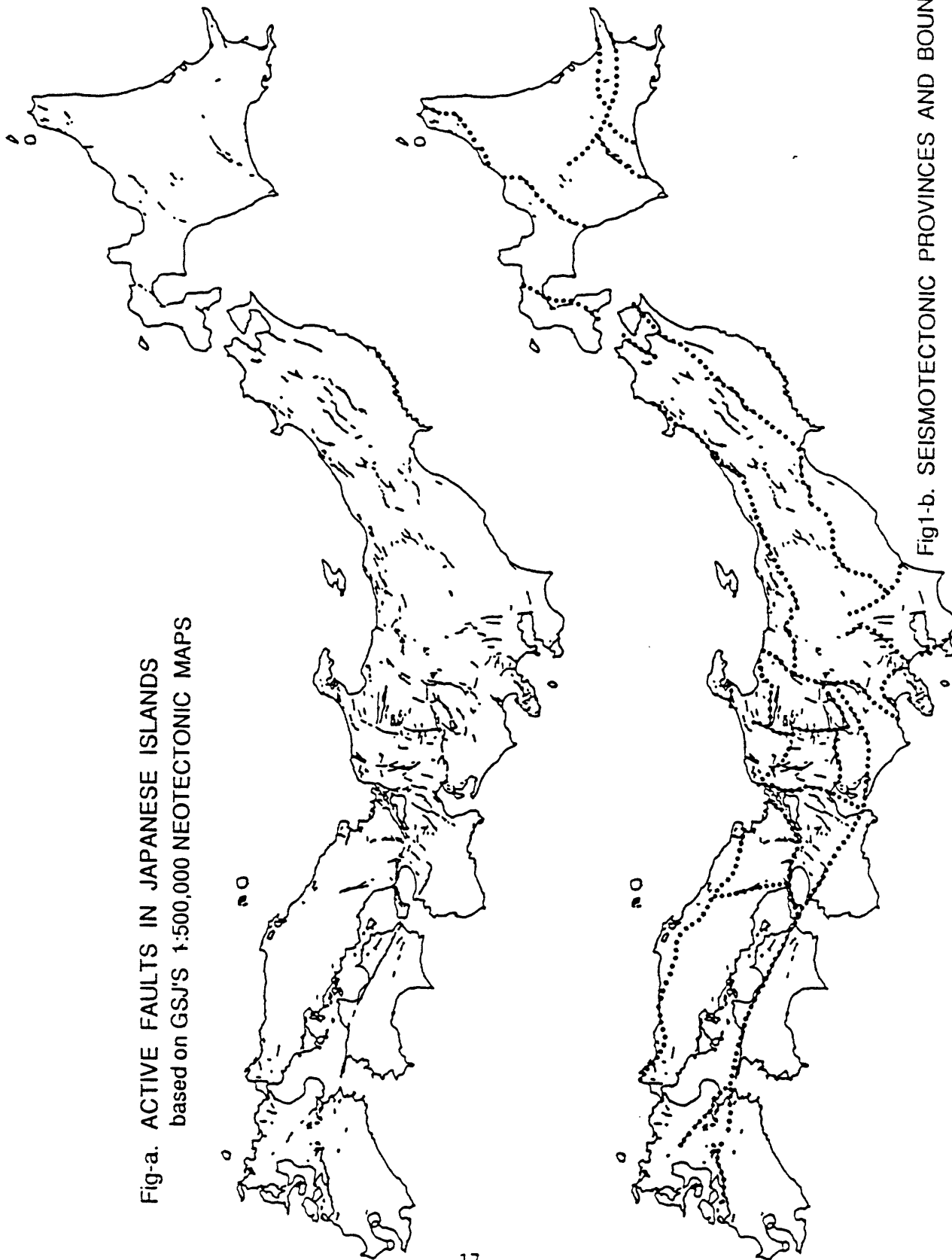


Fig1-b. SEISMOTECTONIC PROVINCES AND BOUNDARIES

TIME DEPENDENT PENINSULA TECTONICS AND  
EARTHQUAKE PREDICTION IN JAPAN

by

Minoru Tanaka

and

Tetsuro Imakiire

Geographical Survey Institute  
Tsukuba, Ibaraki, 305 Japan

Submitted to the 7th U.S.-Japan Seminar  
on Earthquake Prediction( Sept.12-15,  
1988, Morro Bay, California)

September, 1988

MINORU TANAKA and TETSURO IMAKIIRE (Geographical Survey Institute, Tsukuba, Ibaraki, 305, Japan)

## ABSTRACT

For earthquake prediction through the detection of an anomalous crustal deformation, it is considered to be a very useful method to closely examine the present state of crustal deformation on peninsulas jutting out into the trench or the trough, where they are regarded as very large monitoring sensors in detecting the anomalous deformation. In the southern Kanto and Tokai region, peninsulas are confronted with the Philippine sea plate, and located under the influence of the Pacific plate, and moreover, their tectonic behaviors show the various fluctuations due to these subducting plates. We call them "Time Dependent Peninsula Tectonics" and have been investigating them mainly by geodetic means from about 1980 to detect a uniform deformation in the various fluctuations through the subduction process. As an example of the investigation, Miura and Boso peninsulas are selected, because many geodetic data on them have been accumulated since the 1923 Great Kanto Earthquake(M7.9).

The outline of this investigation on the time dependent peninsula tectonics is as follows;

- (1) secular variation related to some periodic change, i.e., about 19-20 years variation hypothesis,
- (2) short-period variation related to time dependent subduction process, i.e., fault creep dislocation model or time dependent plate bending model,
- (3) annual variation related to seasonal change in groundwater or tide.

These results are reported as preliminary ones.

## 1. Introduction

Detection of long term anomalous variation of crustal deformation from precise repetitional geodetic surveys is very important for earthquake prediction in Japan, especially in the southern Kanto-Tokai area. Therefore, investigation on peninsula tectonics was carried out in the Miura and Boso peninsulas, where they are regarded as large monitoring sensors to grasp short range prediction.

In the Miura peninsula, the southern tip of coastside near the Sagami trough continues subsiding uniformly relative to the north inland side, and large sporadic changes in this uniform subsiding trend have been observed by the repetitional leveling surveys. These sporadic vertical changes have been pointed out recently by Fujita(1978) to correlate with large earthquakes(M>7.5) which occurred along the Japan trench or Sagami trough. In interpreting this phenomenon, the fault creep dislocation model was proposed by Fujita and Kaidzu(1985) on the assumption that the main fault plane (right lateral fault) at the time of the 1923 Great Kanto Earthquake as calculated by Kanamori and Ando(1973) is divided into three segments and some parts of the segment continues to creep slowly in the direction of the landward side along the fault.

On the other hand, based on the mechanism of earthquake generation in the Kanto-Tokai area, the unified plate model for interpreting the tectonics was proposed by Kasahara

and Hamada(1981) and Kasahara(1985). Tanaka et.al.(1986) attempted to interpret the recent crustal deformation in the Miura and Boso peninsulas by the time dependent plate bending model, in association with the above model.

In this investigation on the time dependent peninsula tectonics, the following three points are reported,

- (1) secular change in height of datum related to some periodic change; 19-20 years variation hypothesis,
- (2) short period crustal deformation in the Miura and Boso peninsulas related to time dependent subduction process,
- (3) annual variation related to seasonal changes in height and tide.

Investigations have been carried out since 1980 and are still continuing. We report the results obtained so far on earthquake prediction.

## 2. Secular change in height of the tip of the Miura peninsula

Fig.1 shows the location map of the leveling route in the southern Kanto district used for this investigation. Secular change in height of leveling datum showed the abrupt subsidence of 86mm in average at the time of the 1923 Great Kanto Earthquake (M 7.9) i.e., 85.4mm from the net adjustment by fixing many stable bench marks on the surrounding route in the northern Kanto district, and 87.3mm from the direct leveling from datum to Aburatsubo Tidal Station correcting the tidal difference at the time of the earthquake. Fig.2 shows the secular change in tidal level at Aburatsubo Tidal Station after the 1923 earthquake. In this figure, about 19-20 years variation due to secular change in ocean tide is seen. Fig.3 shows the secular change in height of datum obtained from direct repetitional precise leveling between datum and the fixed point at Aburatsubo Tidal Station, and corrected by only a linear gradient of Fig.2 without considering the individual changes in large tidal variations. The obtained secular trend has three maximum peaks, i.e., about 1934, about 1953 and about 1970. On the other hand, tidal level has also maximum peaks in about 1927, about 1944, about 1963, and about 1985 as shown in Fig.2. Height change of datum relative to the fix point at Aburatsubo T.S. is expected to have some periodic changes such as about 19-20 years variation. Fig.2 is considered to show the tidal variation having about 7-8 years deviation to Fig.3, though it may be a half cycle deviation in itself. Fig.4 shows the secular changes in height of BMF25, BM35-1 and BM5367-2 relative to datum for reference. From these results, the macroscopic tidal loading effect in the southern Kanto area is suggested to play an important role in the time dependent peninsula tectonics. According to this hypothesis, the next large sporadic change in height after the 1968-70 event may be seen in about 1992-3. At any rate, secular change in geoidal undulation can also be pointed out from the above results. It was found that the interaction between oceanographic effects (Nishi and Tanaka,1974) and time dependent peninsula tectonics through subduction process is very important for long range prediction.

## 3. Short period crustal deformation in the Miura and Boso peninsulas

In order to detect the different short period crustal deformation between the tips of the Miura and Boso peninsulas, we investigated the leveling results obtained in the southern Kanto area. Fig.5 shows the secular variation of the tip of Miura(BM5367-2) relative to BMF25(upper) and BM35-1(bottom). The bottom figure is given by Fujita and Kaidzu(1985) and fault creep dislocation model was proposed to interpret the large

sporadic change in about 1968 in this figure. This evidence that their presented fault segment is creeping along the main fault is not clear at the present time, though recently, it has been pointed out that the contour line of the upper surface of the Philippine sea plate appears to be discontinued beneath the Tokyo Bay (Ishida, 1986).

Fig.6 shows two results of vertical changes obtained from net adjustment in the southern Kanto area during the periods from 1972-1977 and 1978-1981 and from 1978-81 to 1984-85 relative to both datum and Uchiura Tidal Station. In these figures, the phenomena which appear commonly as a tectonic variation can be pointed out in the following areas,

1. upheaval near Katsuura Tidal Station,
2. upheaval near Ito, the eastern part of Izu peninsula.
3. upheavals near the eastern part of Tokyo near datum and near the south of Chiba city (recovery of ground subsidence ? ),
4. subsidence of tips of peninsulas,
5. subsiding inclination toward Suruga trough at the western coast side of Izu peninsula.

These short period variations on peninsula tectonics suggest the time dependent bending effect produced by the Philippine sea plate under the influence of the Pacific plate, when referred to the unified plate model.

In order to show this more clearly, secular variations for the period from 1968 to 1988 in the tips of the Miura and Boso peninsulas were investigated.

Fig.7 shows the secular change in elevation of BM5367-2 near Aburatsubo T.S. relative to BM36-1 (Fujisawa) and BMF25 (Yokohama) (upper figure), and the secular change in elevation of BM3880 (Tateyama) in the tip of Boso peninsula relative to BM3864 (Futtsu) in the middle part of the Boso peninsula (bottom figure).

In the upper figure, the difference given by black circle (●) and white circle (○) is considered to show that BMF25 side has a tendency of upheaving relatively to BM36-1 side after 1975, because the difference is larger than the propagation error between these BM points by precise leveling. The double circle (◎) shows the results by leveling carried out in summer (May-June). The difference between surveys in summer (○) and winter (●) shows seasonal change in height, which is very likely to have tendencies of being small, when Miura's tip shows the upheaval for the period from 1983 to 1985 and moreover, of being large when Miura's tip shows the gradual subsidence during the period from 1986 to 1988. This is seen in the tip of Boso as shown by the difference between white (○) and black (●) circles. These seasonal variations are discussed in the following chapter.

Concerning short period variation related to time dependent subduction process, the tip of Miura shows the upheaval from 1968 to 1972 and the gradual subsidence from 1972 to 1988, while the tip of Boso shows gradual subsidence from 1972 to 1973 and step-like upheaval from 1973 to 1988. The surrounding earthquakes are represented by arrows in the bottom figure. The Off East of Hachijojima earthquakes (1972 M7.0 and M7.2) have been regarded as a start point to the recent active crustal deformation near the southern Kanto area (Mogi, 1979) and moreover, regarded as being earthquake occurrences through their relative motion in plate boundary between the Philippine sea and the Pacific plates (Kasahara, 1985).

Concerning the time dependent tectonic fluctuation on these peninsulas, two interpretations are possible, i.e., fault creep dislocation model and time dependent plate bending model. Because of insufficient detailed survey data in the Boso peninsula to obtain any decisive results, no conclusion has been reached now. However, recent deep earthquake occurrences near the plate boundary are suggested to be produced as a phenomenon in releasing the increasing bending effect of Philippine sea plate from the Pacific plate.

Under these circumstances that the tip of Boso near Tateyama continues upheaving anomalously under the long-term slow subsidence, the phenomenon which seems to be

related to the forerunner of the earthquake of just under Tateyama(M5.3, d=70km, Aug.12, 1988) was detected from the extensometer data at the Tateyama Crustal Observatory in the tip of Boso (Fig.8), though this small earthquake is considered to be due to the internal deformation of Philippine sea plate (Kasahara,1988, private communication).

#### 4. Seasonal change in height of the tips of peninsulas in the southern Kanto-Tokai area

In order to detect an anomalous crustal deformation from geodetic means and predict the forthcoming Tokai earthquake, repetitional precise leveling survey has been carried out since 1962 between Kakegawa(BM140-1) and Omaezaki(BM2595), and specifically done four times a year since 1981. Moreover, this detailed precise leveling with a short period and a short distance has been carried out by Shizuoka prefecture since 1982. The recent results are shown in Fig.9.

From these results, clear seasonal changes in height having the pattern of subsidence in winter and upheaval in summer were detected. Concerning the origin, ground water model could not output the amplitude of this seasonal change. The tidal loading model using the Voigt model to explain the phase difference of about 2-3 month's delay of elevation change from tidal change could not similarly output the amplitude (Tanaka, 1981). Tajima et.al.(1984) presented elastic buoyancy deformation model to explain both the phase and amplitude. Their analyzed elevation data is in disagreement with recent tidal phase as far as phase difference is concerned. Inouchi and Hosono (1987) found strong correlation of the phase between changes in elevation and in day time tidal level. They pointed out that it is due to the difference between the day time(10AM-4PM) survey value and all day mean values of tidal level. However, a little difference is still observed from their phase comparison between changes in height of BM2595 and day time mean sea level at Omaezaki Tidal Station, and another important problem on output of amplitude has been left unsolved. In order to detect each proper vertical variation of a peninsula from the detailed precise leveling in various peninsulas other than Omaezaki peninsula, the detailed precise leveling has been carried out in the Miura and Boso peninsulas as an example to compare with the phase of vertical variation in Omaezaki. The results are shown in Fig.10 and Fig.11.

From these investigations, the phases on seasonal vertical variations in Miura and Boso peninsulas were curiously found to have the tendency of being delayed about 7 days and 20 days in comparison with the phase in Omaezaki, respectively. The phase in Miura varies with the direction of leveling route, which moves from south to north, and is considered to agree with that in tidal change within an accuracy of about one month or so. Therefore making choices of appropriate direction of leveling route, showing maximum inclination to tidal force, is very important for this investigation.

In the tip of the Miura peninsula, amplitude of seasonal change in elevation became small when showing upheaval during the period from 1983 to 1985. That is, as shown in Fig.7, it is found that the amplitude of seasonal change in elevation becomes small when ground level ascends (increasing bending mode), and vice versa (releasing bending mode) and only then, these investigations are pointed out to be very useful in short range prediction as seen also in the example of August in 1986(Fig.9).

#### 5. Conclusion

The outline of the investigation on time dependent peninsula tectonics is as follows.

- (1) Secular crustal deformation related to about 19-20 years variation was detected from both secular changes in tidal level at Aburatsubo and in height of datum. These facts are considered to show the long term time dependent geoidal undulation. Then.

it is very important for long range prediction to make clear the interaction between ocean tide and time dependent peninsular tectonics through subduction process, especially in the Kanto-Tokai area.

(2) It is possible to interpret the recent crustal deformation on peninsular tectonics in the southern Kanto area by the time dependent plate bending model, when considering recent deep earthquake occurrences through their relative motion in the plate boundary between the Philippine Sea plate and the Pacific plate.

(3) Detection of secular changes in amplitude from seasonal changes in height given by detailed precise leveling is very important for short range earthquake prediction in this area. It was found that this method is also very useful in detecting seasonal geoidal undulation. In this type of investigation, the choice of the leveling route is a problem in itself.

Such an investigation on time dependent peninsula tectonics through geodetic means including detection of seasonal variation will be a great help in solving the problem of short-range earthquake prediction for practical use in the Kanto-Tokai area, though there are many points which must be solved.

We are pleased to acknowledge the considerable assistance of Mr. T.Gomi.

## 6. References

Fujita N., Tilt of Miura peninsula, Rep. Coord. Comm. Earthq. Predict., 19, 51-53, 1978 (in Japanese)

Fujita N. and M. Kaidzu, Vertical movement in the south Kanto - existence of creep plane -, J. Geod. Soc. Japan, 31, 333-339, 1985 (in Japanese)

Inouchi, N and T.Hosono, On the yearly change of ground movement detected by precise leveling surveys connecting Kakegawa to Omaezaki, Shizuoka prefecture, Japan, J. Geod. Soc. Japan, 347-359, 33, 1987 (in Japanese)

Ishida M., The configuration of the Philippine sea and the Pacific plates as estimated from the high-resolution microearthquake hypocenters in the Kanto-Tokai district, Japan, Rep. NRCDP, 1-19, 36, 1986 (in Japanese)

Kanamori H. and M.Ando, Fault parameters of the Great Kanto Earthquake of 1923, in Publication for 50th Anniversary of Great Kanto Earthquake, 1923, 89-101, Earthquake Res. Inst., Univ. of Tokyo, 1973 (in Japanese)

Kasahara K., Patterns of crustal activity associated with the convergence of three plates in the Kanto-Tokai area, central Japan, Rep. NRCDP, 33-137, 35, 1985 (in Japanese)

Kasahara K. and K.Hamada, A plate model consistent with the tectonics of the Kanto-Tokai area, Japan, in Proceeding of the 2nd Joint Meeting of the U.J.N.R. Panel on Earthquake Prediction Technology, 85-97, U.S. Geological Survey, Open File Rep. 82-180, 1981

Mogi K., Izu - Recent crustal activity, The CCEP in Its First Decade, 121-140, 1979 (in Japanese)

- Nishi S. and M.Tanaka, Long period oceanographic effect estimated from secular variation of mean sea level, J. Geod. Soc. Japan, 225-226, 20, 1974
- Tanaka M., Correlation between change in elevation of the Omaezaki peninsula and sea level change, Report at the sectional meeting of Area of intensified observation in CCEP, Aug. 17, 1981 (unpublished)
- Tanaka M., A.Yoshimura and K.Sugita, Recent secular vertical variation in datum, Miura and Boso peninsulas - possibility of about 19 years variation - , G.S.I. Journal, 74-79, 63, 1986 (in Japanese)
- Tajima M., N.Matsumoto and M.Kaidzu, Relation between seasonal variation of the Omaezaki peninsula and sea level change, J. Geod. Soc. Japan, 107-113, 30, 1984

## Figure Captions

Fig.1, Location map of the leveling route used for this investigation in the southern Kanto district.

Fig.2, Secular change in height of Aburastubo Tidal Station(Fixed mark) relative to Aburastubo annual mean sea level.

Fig.3, Secular change in height of Leveling Datum during the period of 64 years relative to the mean sea level at the Aburastubo tidal fixed mark.

Fig.4, Secular changes in height of Miura Peninsula(First order leveling point) relative to Leveling Datum.

Fig.5, Secular changes in height of the tip of Miura(BM5367.2) relative to BMF25 and BM35.1.

Fig.6, Vertical changes obtained by the net adjustment in the southern Kanto district relative to Uchiura tidal station( ) and Datum).

Fig.7, Secular changes in height of the tips of Miura and Boso peninsulas.

Fig.8, Secular changes of extensometers at Tateyama Crustal Observatory, Monthly mean values (upper) and Daily mean values(bottom).

Fig.9, Secular changes in height of Omaezaki(BM2595) relative to Kakegawa(BM 140-1) by G.S.I. (upper) and Seasonal changes in height between short route(2 km) by the detailed short period repetitional leveling carried out by the Shizuoka prefecture relative to EMSF2129(bottom).

Fig.10, Changes in height of BM5364(Hayama) and BM5364-1(Yokosuka) relative to BM5363-1 in the tip of Miura peninsula.

Fig.11, Changes in height of BM3877(south) relative to BM3876(north) in the tip of Boso peninsula.

Fig.1, Location map of the leveling route in the south Kanto district used for this investigation

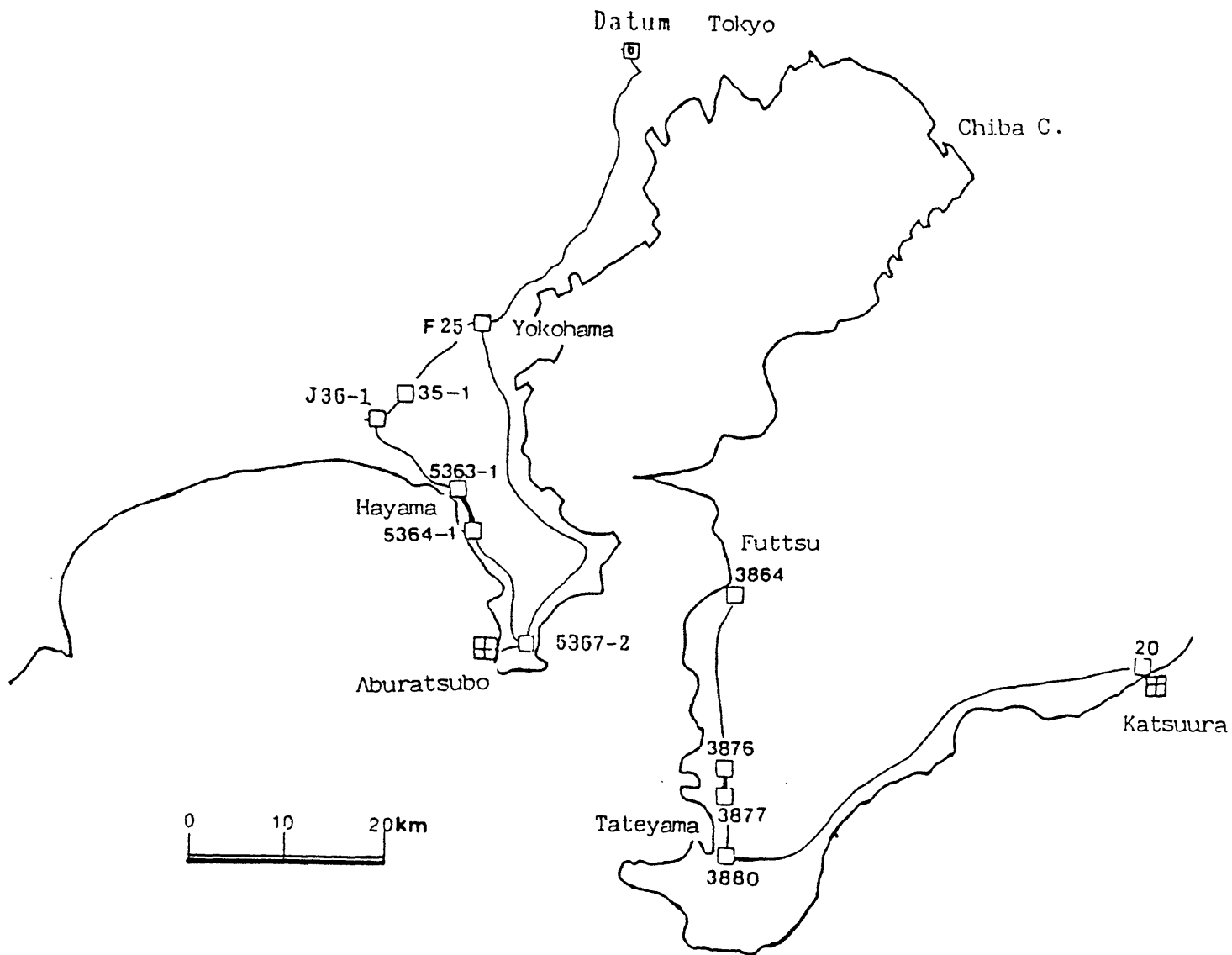


Fig.2, Secular change in height of Aburatsubo tidal station (Fixed mark) relative to Aburatsubo annual mean sea level

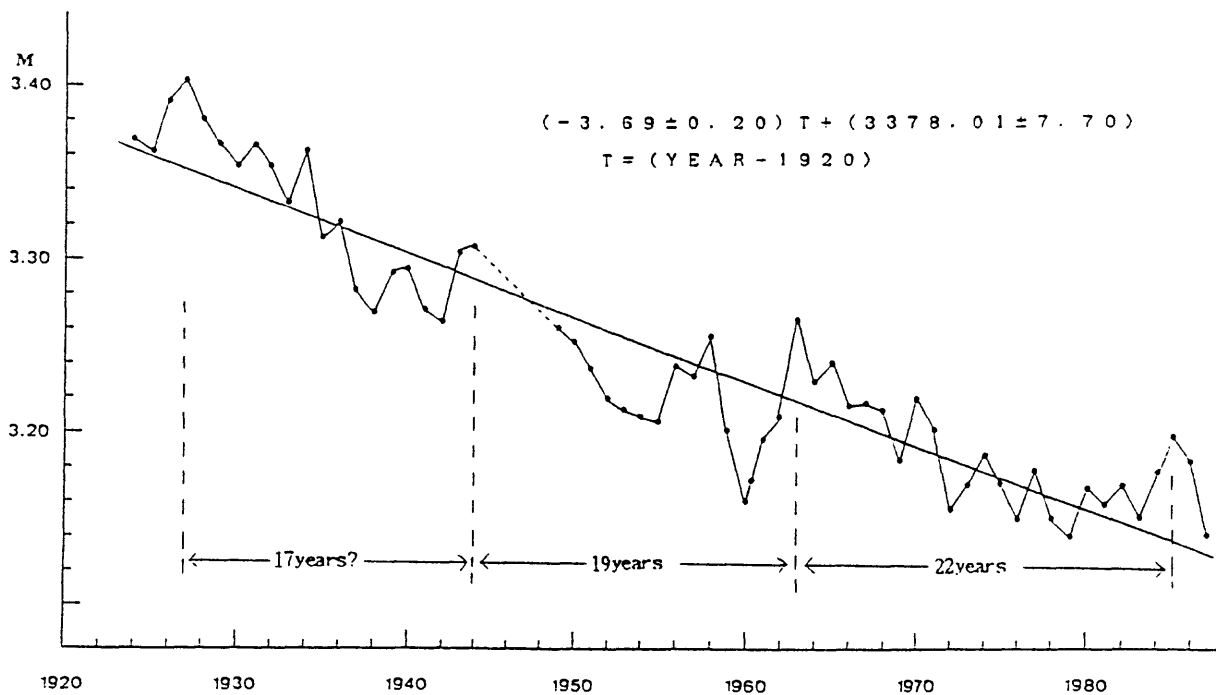


Fig.3, Secular change in height of Leveling Datum during the period of 64 years relative to the mean sea level at the Aburatsubo tidal fixed mark

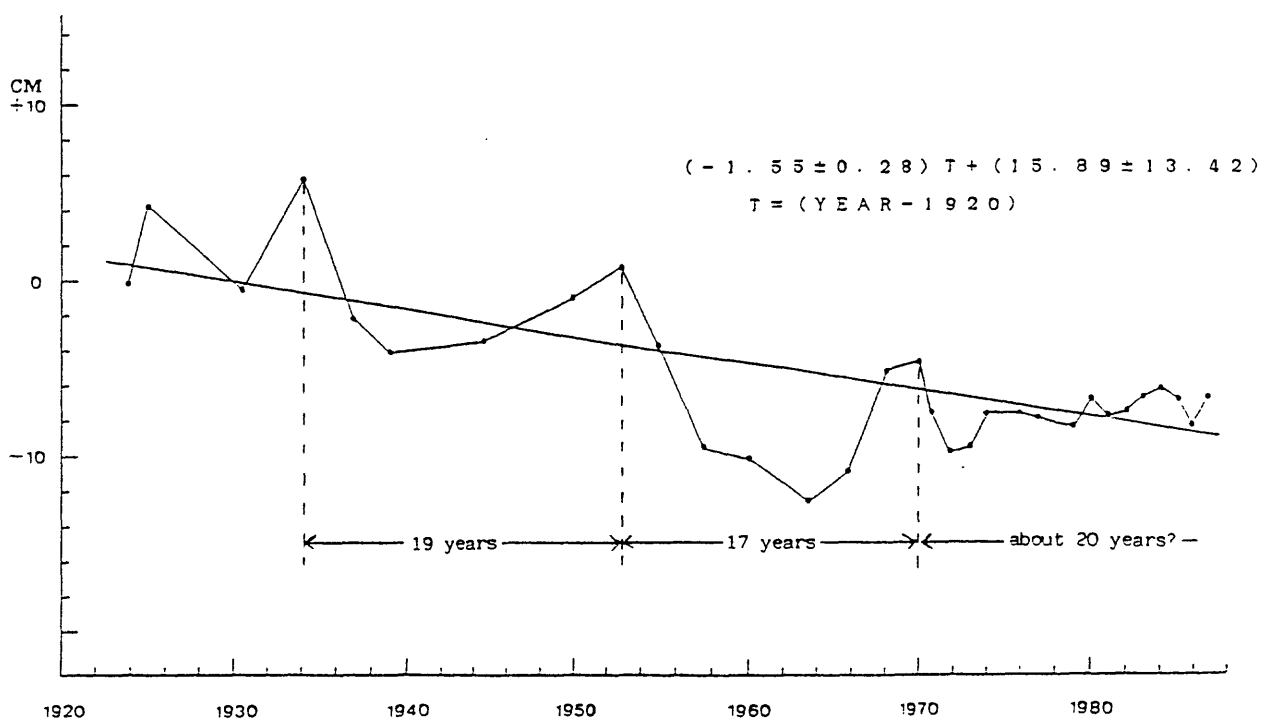


Fig.4, Secular change in height of Miura Peninsula (First order leveling point) relative to the Leveling Datum

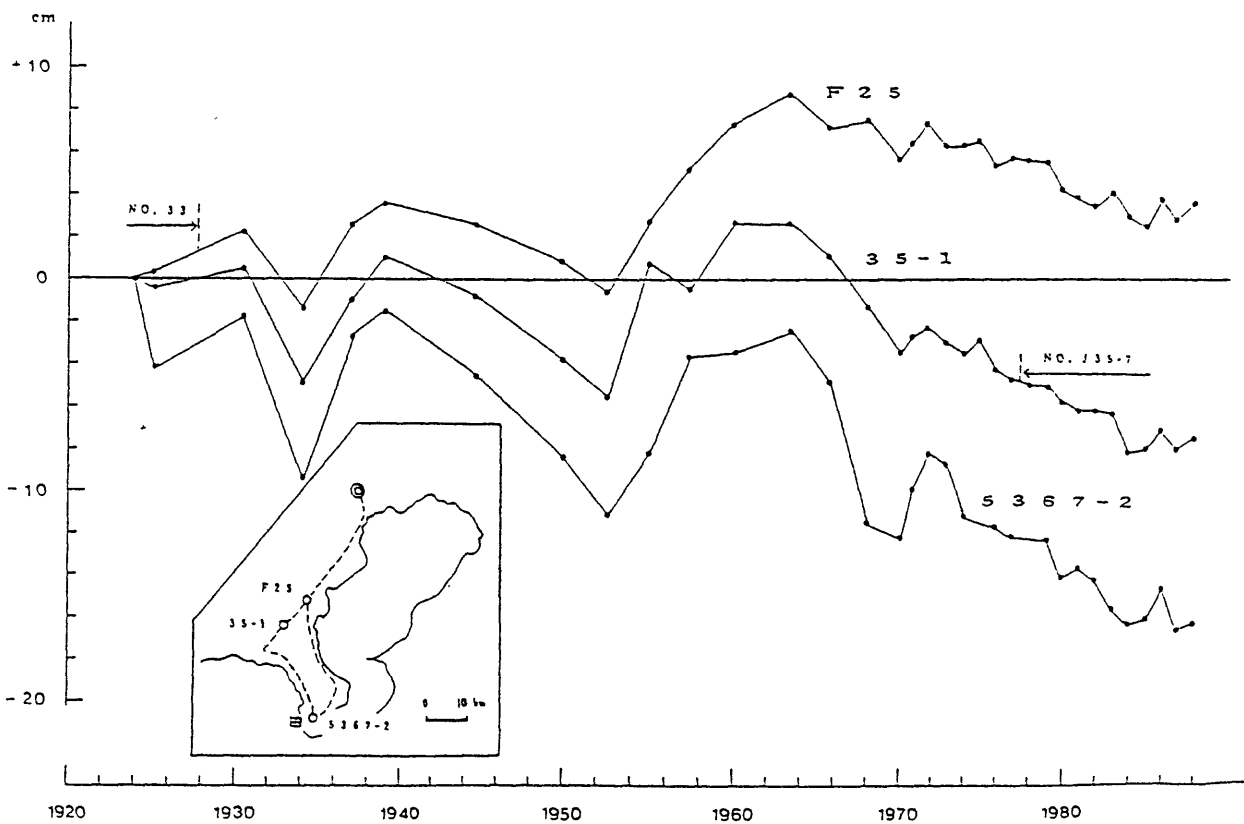


Fig.5, Secular change in height of the tip of Miura (BM5367.2) relative to BMF25 and BM35.1.

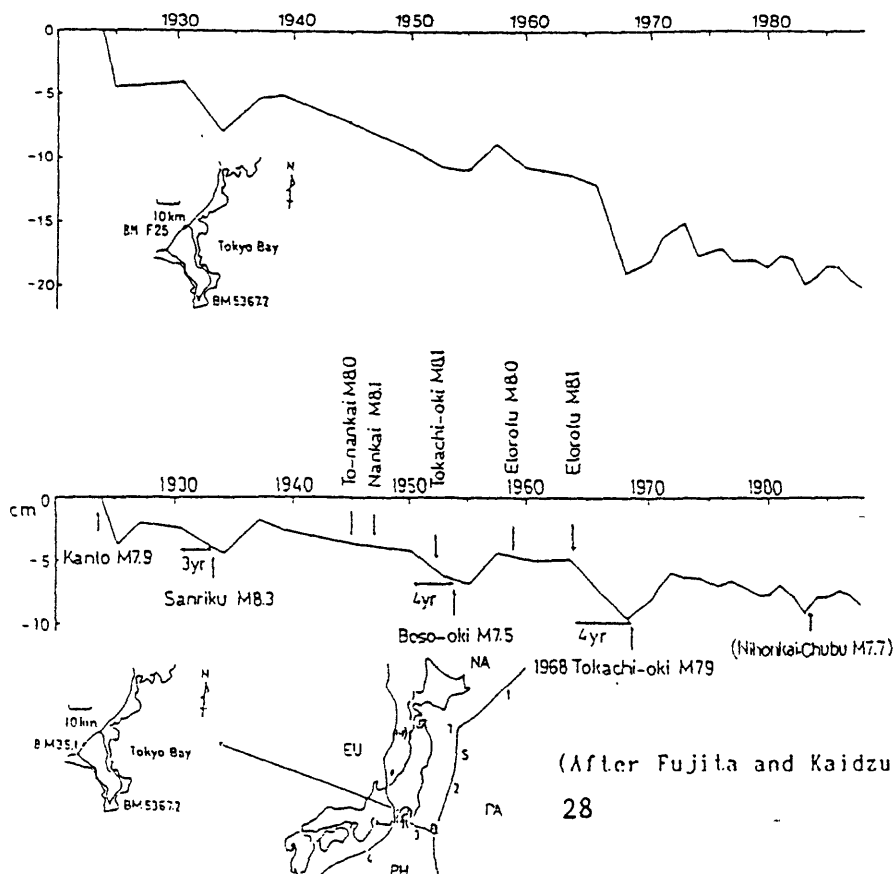
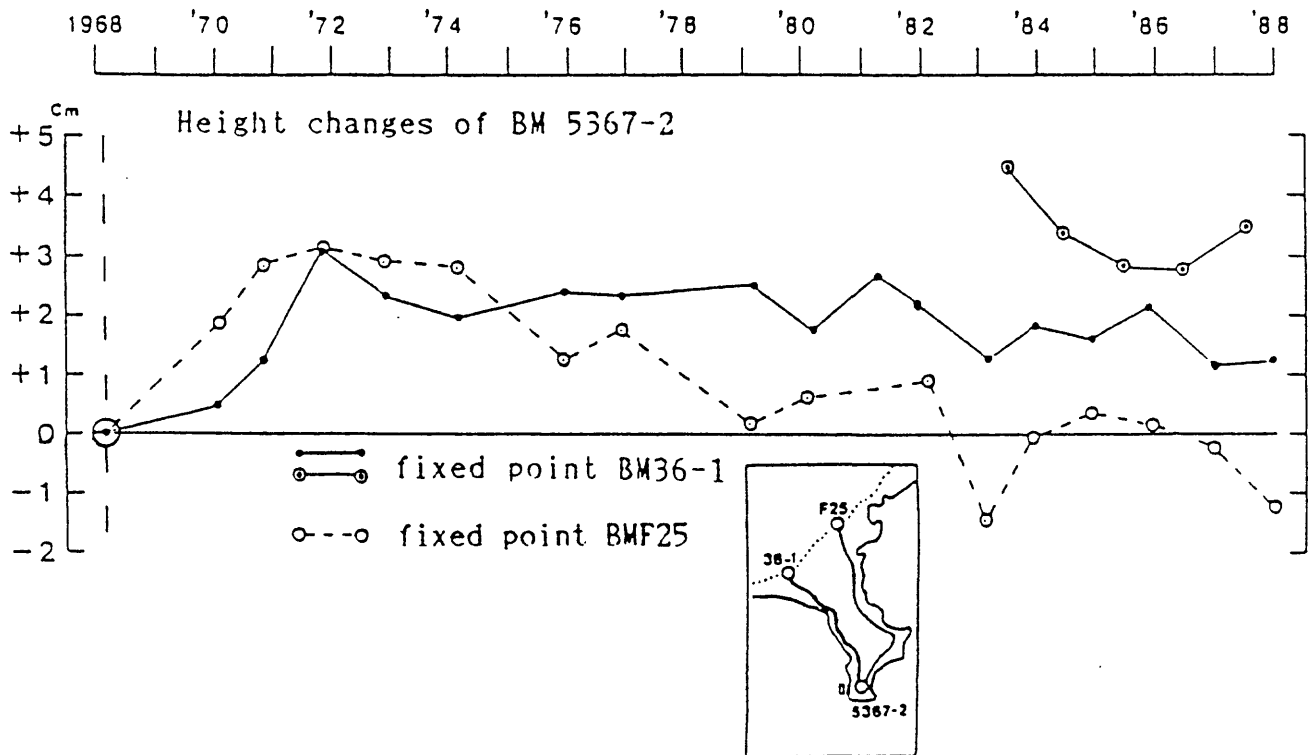




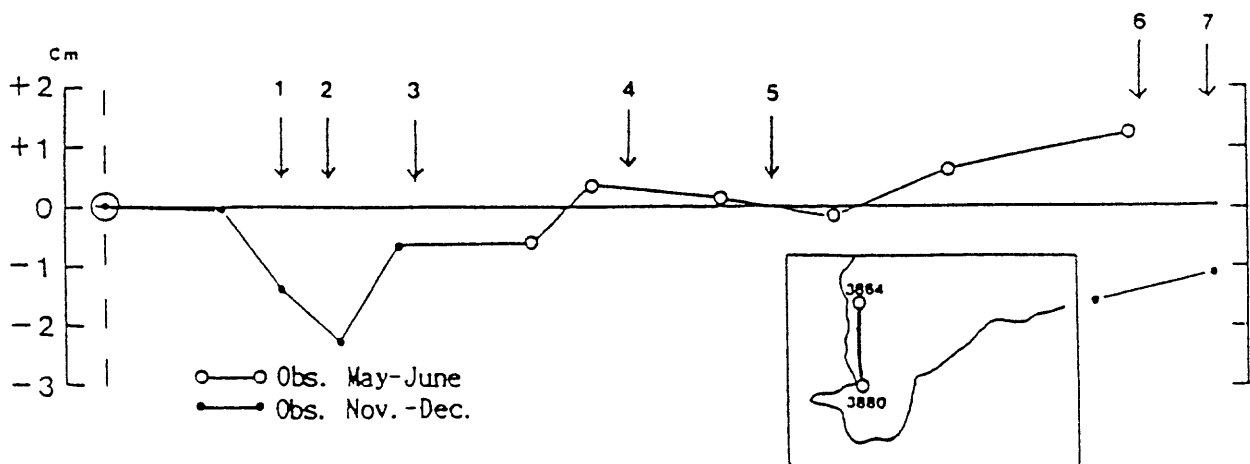
Fig.7,

Secular changes in height of the tips of Miura and Boso peninsulas



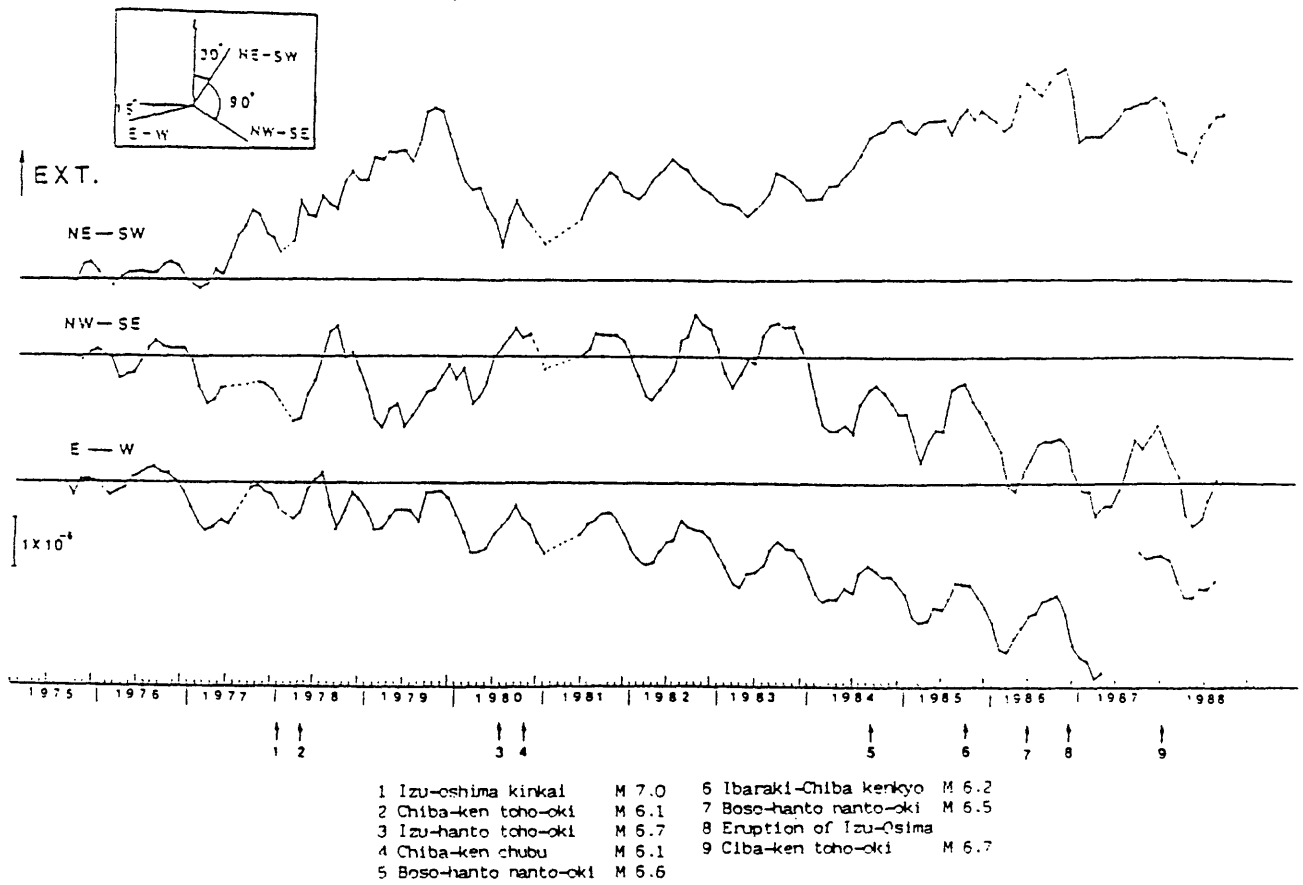
Height change of BM3880

fixed point BM3864



- |                          |       |
|--------------------------|-------|
| 1 Hachijo-jima kinkai    | M 7.0 |
| 2 Hachijo-jima toho-oki  | M 7.2 |
| 3 Izu-hanto oki          | M 6.9 |
| 4 Izu-Oshima kinkai      | M 7.0 |
| 5 Izu-hanto toho-oki     | M 6.7 |
| 6 eruption of Izu-Oshima |       |
| 7 Chiba-ken toho-oki     | M 6.7 |

Fig.8, Secular change of extensometer at Tateyama Crustal Observatory  
(monthly Mean value)



Change of extensometer at Tateyama Crustal Observatory (Daily mean value)

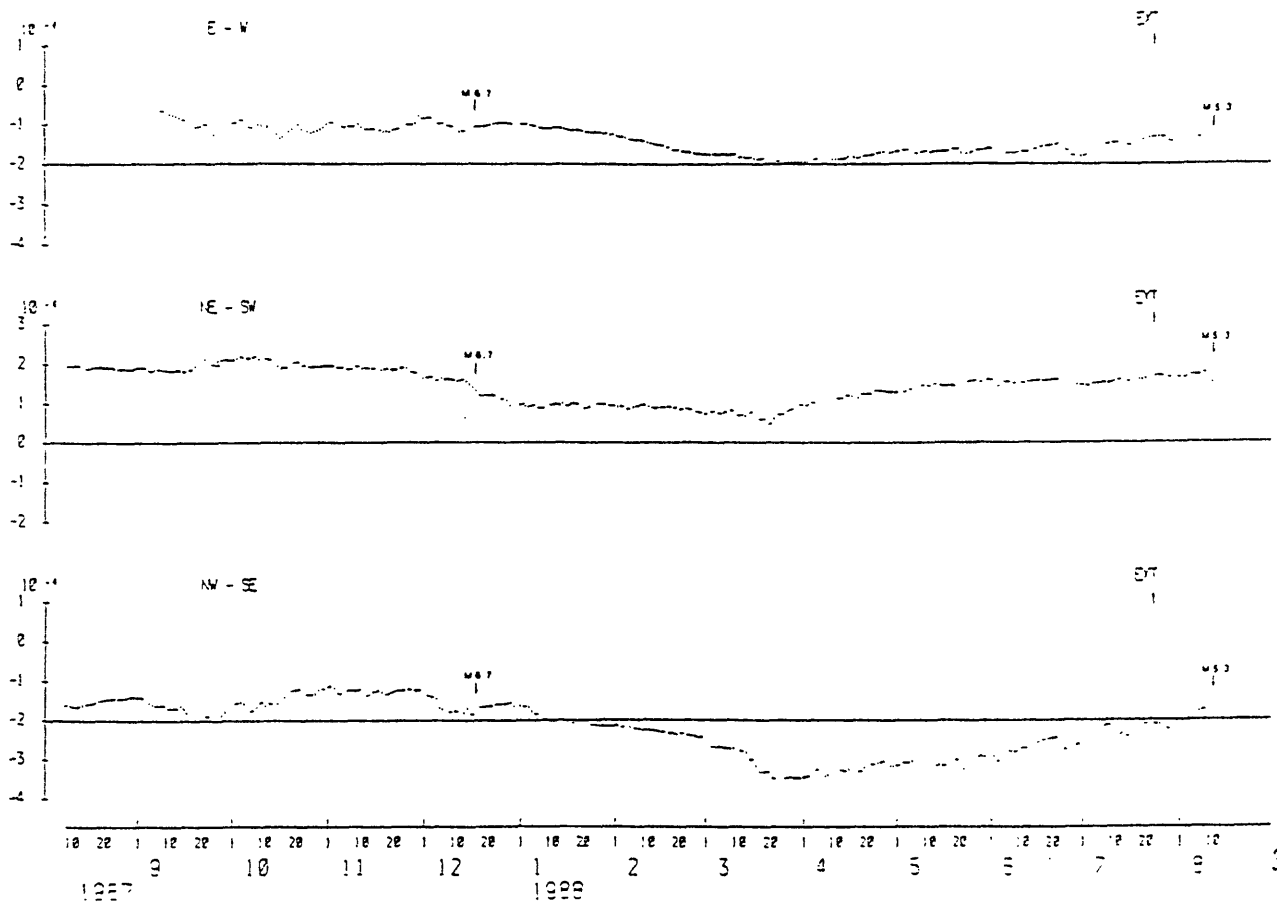
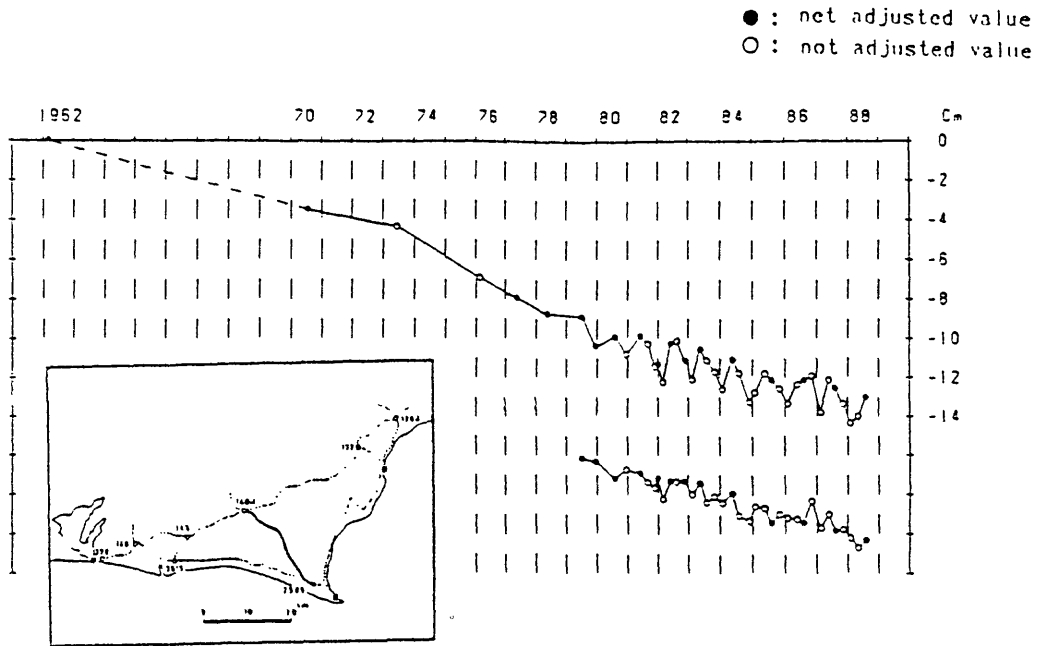


Fig.9, Secular change in height of Omaezaki(BM2595) relative to Kakegawa(BM140-1)



Seasonal changes in height between short route(2km) by short period  
repetitional leveling surveys carried out by Shizuoka prefecture

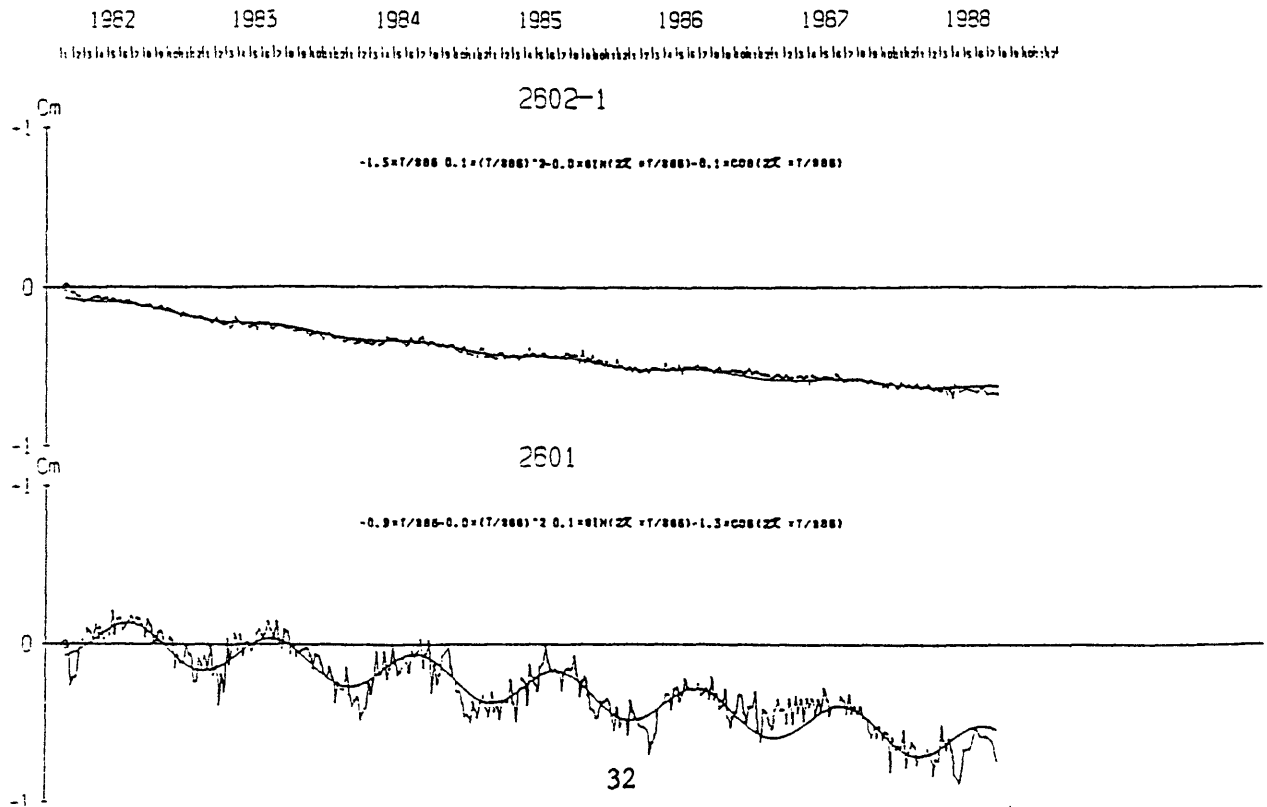


Fig.10, Changes in height of BM5364(Hayama) and BM5364-1(Yokosuka) relative to BM5363-1 in the tip of Miura Peninsula

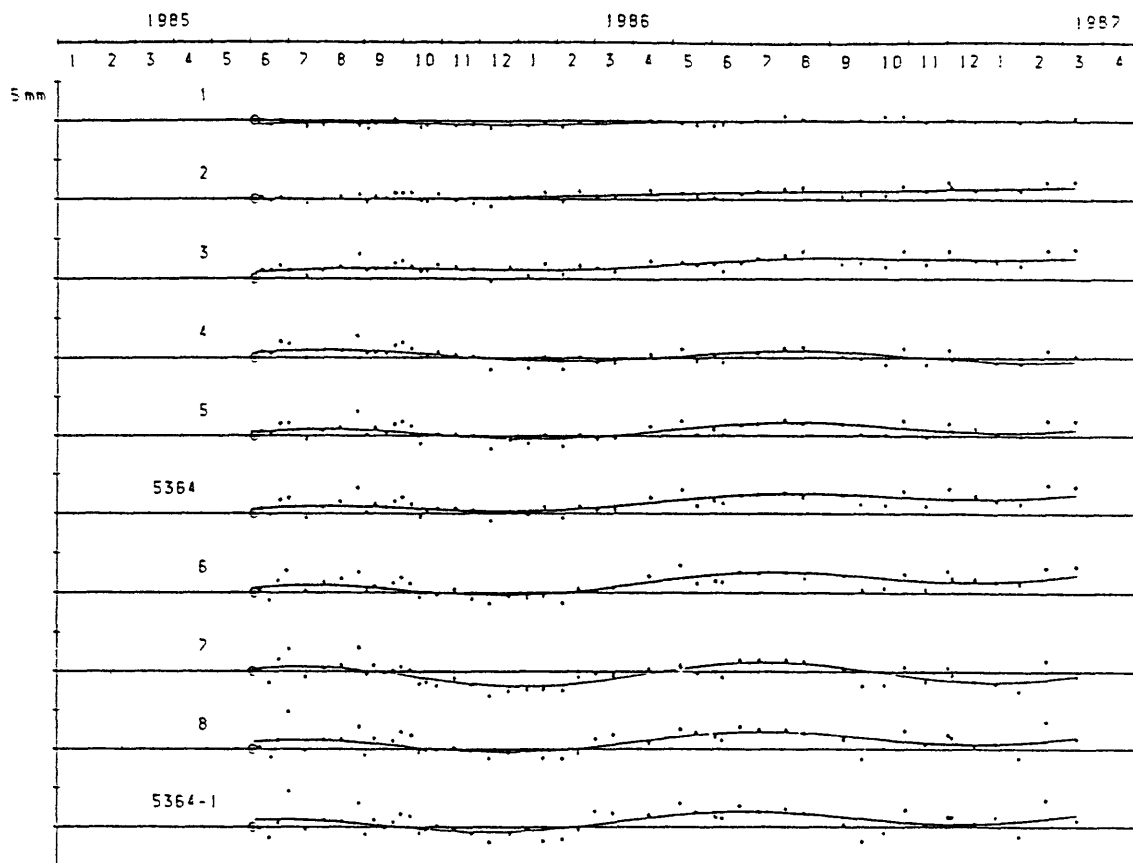
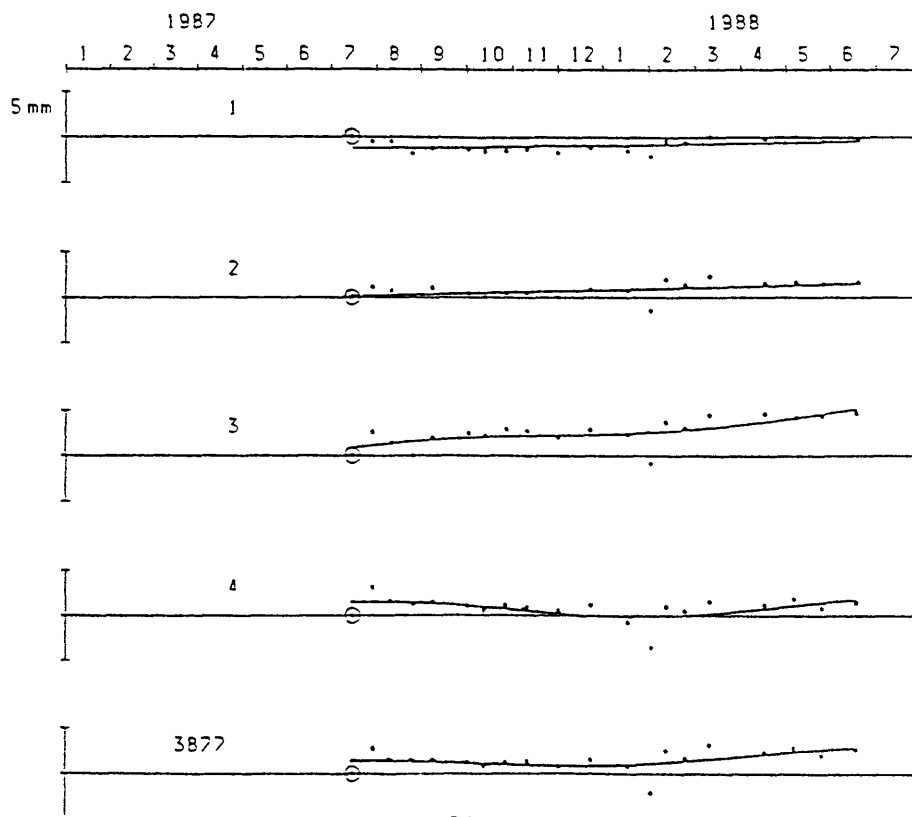


Fig.11, Changes in height of BM3877(south) relative to BM3876(north) in the tip of Boso Peninsula



LOCI AND MAXIMUM SIZE OF THRUST  
EARTHQUAKES AND THE MECHANICS OF THE  
SHALLOW REGION OF SUBDUCTION ZONES

Daniel E. Byrne,<sup>1,2</sup> Dan M. Davis,<sup>3</sup>  
and Lynn R. Sykes<sup>1,2</sup>

*Abstract.* Earthquakes do not extend updip along the plate interface at most subduction zones all of the way to the plate boundary at the trench axis or deformation front. Rather, the shallowest part of that interface moves mainly through stable, aseismic slip. That part of the plate boundary, referred to here as the aseismic zone, occurs along the base of an accreted wedge of young sediments. The probable primary cause for the existence of this aseismic zone is the stable slip properties of the unconsolidated and semiconsolidated sediments in that zone. Subducted sediment is progressively dewatered and underplated to the base of the overriding plate. Through this process, more consolidated rocks eventually come into contact at depth across both sides of the plate boundary. From the point where sufficiently hard rock is found across the plate interface, that interface will change its slip behavior to unstable stick-slip sliding, which is characteristic of consolidated material under most conditions. This type of motion is accommodated seismically as episodic slip in large earthquakes. The location of this transition to seismic behavior, referred to as the seismic front, marks the deep end of the aseismic zone and the top of the seismogenic zone, i.e.,

that part of the plate interface that moves primarily in thrust earthquakes. Several convergent plate margins are discussed to illustrate the seismic front and the aseismic zone. We find that the seismic front defined by smaller earthquakes that occur during the interval between large events is nearly the same as that for large events as inferred from the locations of their aftershocks. The location of the seismic front is important for making estimates of the maximum possible size of thrust earthquakes along the plate boundary because it delimits the trenchward limit of the potential rupture area of these events. The size of large thrust earthquakes is proportional to rupture area and to at least the cube of the downdip width,  $W$ , of that area. Thus by defining the location of the seismic front for convergent margins it is possible to make better estimates of  $W$  and hence to deduce the maximum size of future interplate earthquakes. The average repeat time of such events is also related to  $W$  and so better estimates of average repeat time are possible from improved knowledge of  $W$ . The hypothesis that the location of the seismic front is related to the maximum depth of subduction of unconsolidated sediment has implications for forearc mechanics. We use a mechanical analysis, laboratory modeling, and multichannel seismic information to develop a simple model explaining the growth of forearcs. The outer-arc high or trench-slope break that occurs arcward of most accretionary wedges represents an abrupt change in the critical taper of the accretionary wedge. We argue that that change is caused by a large arcward increase in the strength of the material within the overriding plate. That stronger material is called the backstop. Our laboratory modeling experiments indicate that a backstop with a trenchward-dipping upper surface results in the development of an overlying structure that includes all of the primary morphologic features observed in modern forearcs. In our modeling an accretionary wedge

---

<sup>1</sup>Lamont-Doherty Geological Observatory, Palisades, New York.

<sup>2</sup>Also at Department of Geological Sciences of Columbia University, New York.

<sup>3</sup>Department of Earth and Space Sciences, State University of New York at Stony Brook.

develops trenchward of the backstop, an outer-arc high develops above the trenchward toe of the backstop, and farther arcward a passive forearc basin forms above the stronger material of the backstop. This model is consistent with the observation that earthquakes do not extend updip along the plate interface all the way to the trench axis. We hypothesize that plate motion is accommodated seismically along the base of the consolidated backstop and mostly or entirely aseismically trenchward of the toe of the backstop along the base of the accretionary wedge. At several margins the seismic front is approximately coincident with the outer-arc high, supporting this interpretation.

INTRODUCTION

The plate boundaries at subduction zones are the loci of the largest known earthquakes and of many smaller magnitude events as well, but the shallowest parts of the same plate boundaries are often areas of persistent aseismicity. The observation that interplate seismicity does not extend updip

all the way to the outcrop of the plate boundary near the trench axis or deformation front has been made by workers at a number of subduction zones [e.g., Engdahl, 1977; Frolich et al., 1982; Chinn and Isacks, 1983; Hirata et al., 1983]. The presence of this shallow aseismic region indicates that the seismogenic zone (i.e., that part of the plate boundary that moves predominantly in large or great thrust earthquakes) is limited in its updip extent by a transition in the mode of interplate slip. In this paper we call the location of the trenchward limit of seismicity within the overriding plate and along the plate interface the seismic front after the usage of House and Jacob [1983], and we refer to the region between the trench axis and the seismic front as the aseismic zone (Figure 1). We conclude that the seismic front marks a transition from stable to stick-slip frictional sliding along the plate boundary similar to that described for strike-slip faults by Marone and Scholz [1988]. The aseismic zone is probably caused by the presence of unconsolidated, overpressured sediment along the shallow part of the plate boundary. Along the seismogenic zone, more consolidated

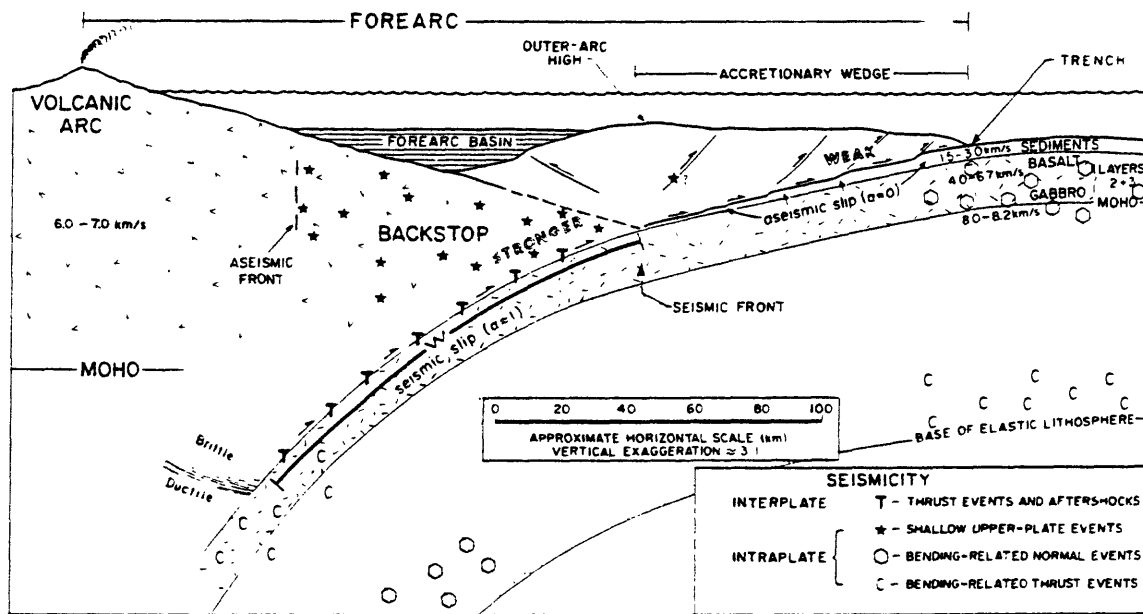


Fig. 1. Schematic cross section of the shallow (approximately the upper 50 km) part of a subduction zone illustrating our forearc model. Major features are named, a schematic distribution of earthquakes is shown, and some representative P wave velocities are given. The ratio of seismic slip to total slip as defined by Sykes and Quittmeyer [1981] is  $\alpha$ . The backstop consists of stronger material, and has an upper surface that dips trenchward beneath the weaker sediments of the forearc basin and accretionary wedge. The backstop affects the mechanics of the overlying sediments and is responsible for the development of the outer-arc high and the relatively undisturbed sediments of the forearc basin. Interplate thrust earthquakes, T, do not occur along the entire plate interface but stop at a point that we define as the seismic front. Earthquakes within the upper plate also occur mainly arcward (i.e., to the left) of this point. The seismic front is coincident with the outer-arc high at many margins, suggesting that the presence of the stronger material of the backstop affects the style of deformation along the plate boundary in addition to influencing morphology. Interplate earthquakes do not occur below the brittle-ductile transition where higher temperatures favor stable sliding. The location of this transition and of the seismic front determine the width of the seismogenic zone, W, the downdip extent of rupture in large thrust earthquakes.

rock is in contact along both sides of the boundary resulting in stick-slip frictional behavior.

The rupture area of an earthquake is proportional to its seismic moment. This fact has been used in previous studies in assessment of the seismic potential of subduction zones (i.e., the maximum size of interplate thrust events) by estimating the potential rupture area of future large earthquakes [e.g., Sykes and Quittmeyer, 1981; Chinn and Isacks, 1983; Peterson and Seno, 1984]. These studies, however, did not take the shallow aseismic zone into account in their estimates of the downdip width of the seismogenic zone. The aseismic zone can be very large in some margins and much if not all of it does not contribute appreciably to seismic moment release. Thus, we suggest that in future estimates of the potential rupture area of large interplate thrust earthquakes, workers must recognize and remove the aseismic zone from consideration of potential rupture area.

Unconsolidated sediment along the plate boundary results in aseismic slip as discussed below [Marone and Scholz, 1988]; therefore we infer that the seismic front marks not only a transition in frictional slip stability, but the deep limit of unconsolidated material along the plate boundary as well. The presence or absence of earthquakes as a function of depth along the plate boundary can therefore shed light on the distribution of failure modes within the rocks in the shallow part of subduction zones. To develop this idea we extend the mechanical analysis of Davis et al. [1983] for accretionary wedges to include the entire forearc. Our analysis indicates that the large decrease in the slope of the ocean floor represented by outer-arc highs or trench-slope breaks arcward of accretionary wedges may be explained by the presence of stronger material below these features. This stronger material at depth within the forearc is referred to as the backstop. We compliment our mechanical analysis with laboratory modeling. Using a very simple model, we are able to reproduce all of the primary structures that are commonly observed in forearcs. The seismic front is interpreted to be the shallow limit of the contact between the consolidated material of the backstop and consolidated material of the lower plate.

This paper brings together seismological and morphological information bearing upon the modes of interplate slip at convergent plate boundaries and on the mechanics and structure of forearcs. We employ earthquake locations, a simple mechanical analysis, laboratory experiments, and some multichannel seismic profiles to develop and discuss a simple model for forearc morphology and mechanics. With the resultant model we offer an explanation for the modes of interplate slip, for the formation of outer-arc highs and trench-slope breaks, and we suggest a relationship between these near-surface structures, the deeper structure of forearcs, and the distribution of shallow seismicity.

#### SHALLOW DISTRIBUTION OF EARTHQUAKES IN SUBDUCTION ZONES

Earthquakes occur in three different settings within the shallow (upper 50 km) part of subduction zones: within the

overriding plate, along the plate interface, and within the plate being subducted (Figure 1). These three zones vary between and along convergent margins in their extent and in the relative intensity of their seismic activity. Thrust-faulting earthquakes occur along the plate boundary, defining the seismogenic zone. The world's largest known earthquakes are of this type. Earthquakes within the overriding plate have various focal mechanisms that are indicative of the state of stress within the upper plate, and only occur arcward of the seismic front. Trenchward of the seismic front, within the accretionary wedge, sediments deform totally or nearly totally by aseismic processes [Chen et al., 1982]. Most margins also have earthquakes that occur within the lower plate with normal faulting focal mechanisms that are thought to be caused by bending [e.g., Stauder, 1968; Ward, 1983].

In most subduction zones, however, earthquakes do not occur within the upper plate or along the plate interface near the trench axis or deformation front and for some distance arcward of that point. This area lacks both smaller magnitude events that occur during the interseismic period between large or great thrust events as well as aftershocks of large or great earthquakes [Chen, 1981]. The shallowest part of the upper plate is commonly built primarily from unconsolidated sediments that have been accreted onto the overlying plate and underplated beneath it forming an accretionary wedge. The absence or near absence of events within the accretionary wedge and along its underlying plate boundary indicates that motion in this region occurs mainly or totally in an aseismic manner. Large thrust earthquakes that nucleate at depth may propagate updip into this zone, but the slip properties of unconsolidated sediment, which we describe in a later section, lead us to conclude that earthquakes will not nucleate along the part of the plate boundary that is rich in unconsolidated or semiconsolidated sediments. Because of the very low rigidity of these sediments any motion of this shallowest part of the plate boundary during large earthquakes would not contribute significantly to the total seismic moment release. Thus the seismogenic zone is limited in depth extent, with a shallow cutoff that occurs at the seismic front. The distance between the seismic front and the trench axis can be quite large for some margins, reaching distances of over 200 km in extreme cases. The term seismic front should not be confused with the aseismic front [e.g., Yoshii, 1979], which is the limit of upper plate seismicity toward the arc (Figure 1). The seismic region of most forearcs is bounded by this aseismic front at its arcward end and by the seismic front, to which we refer in this paper, at its trenchward end.

It is useful to describe the distribution of earthquakes in tectonic settings where event locations are very accurate such as the San Andreas strike-slip fault system for comparison with the distribution observed at subduction zones where most locations are not as accurate. Earthquake locations are very accurate along much of the San Andreas system because of the high density of nearby seismometers. An example of the depth distribution of earthquake hypocenters there is provided by the work of Doser and Kanamori [1986], who relocated over 1000 earthquakes recorded in the Imperial Valley of

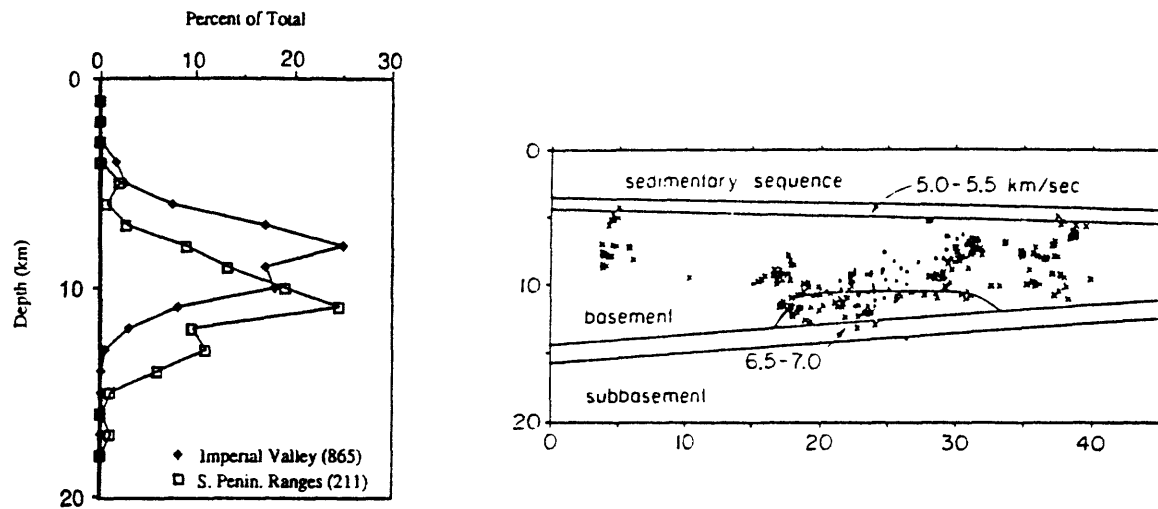


Fig. 2. Cross sections of relocated earthquakes (right diagram) and percentage of events as a function of depth for the San Andreas strike-slip fault system in the Imperial Valley of southern California. Structural interpretation is based on a large refraction study of Fuis et al. [1982]. Note that the aseismic zone extends from the surface to a depth of about 4–5 km, i.e., down to the velocity transition that marks the deep limit of the shallow sedimentary sequence. Figure from Doser and Kanamori [1986].

southern California. The resulting focal depths have a precision of  $\pm 2$  km. The frequency–depth distribution of these events (Figure 2) indicates an aseismic zone within the uppermost 4–5 km. The seismogenic zone (defined here by small-to-moderate-sized events) extends between depths of approximately 5 and 15 km. A large earthquake occurred in 1979 along the Imperial Valley fault. Studies of this event indicate that maximum coseismic displacement occurred at depths greater than 5 km [Hartzell and Helmberger, 1982] and that the maximum stress release was concentrated between 9 and 11 km [Quin and Boatwright, 1987]. Such studies indicate that the shallow aseismic region persists even in large earthquakes. The aseismic zone in this example occurs within and is probably caused by the presence of unconsolidated sediment that is approximately 4 to 5 km thick in the Imperial Valley as determined by a large refraction experiment [Fuis et al., 1982]. At the deeper limit of the seismogenic zone higher temperatures cause aseismic slip, resulting in a second transition in frictional slip stability [Scholz, 1988].

In subduction zones the plate boundary dips at a very shallow angle; consequently, the plate boundary is much wider in downdip extent than it is for nearly vertical strike-slip faults. The subduction and accretion of young sediments along the shallow part of that boundary cause the aseismic zone to be disproportionately wider in subduction zones than that observed along strike-slip faults. The deeper frictional transition at the base of the seismogenic zone also occurs very deep in subduction zones because the subduction of the cold slab lowers the geothermal gradient [e.g., Watanabe et al., 1977]. We show below that the seismic front and aseismic zone are observed in subduction zones where well-located

hypocenters are available. Accurate hypocentral locations in subduction zones generally require a local network on the arc combined with event relocations and, ideally, an ocean bottom seismometer study. In the following sections the distribution of shallow seismicity is described for some of those arcs for which the most accurate hypocentral locations are available.

#### *Adak Region, Central Aleutian Arc*

The University of Colorado has maintained a seismic network in the Adak Island area of the central Aleutian arc near  $177^{\circ}\text{W}$  for nearly a decade [Scherbaum and Kisslinger, 1984]. In addition to a local network on the volcanic arc, several ocean bottom seismometer (OBS) studies have been conducted over the forearc and trench axis seaward of Adak [Chen et al., 1982; Frolich et al., 1982]. A cross section of hypocenters of moderate-sized earthquakes from Engdahl and Gubbins [1987] shows the general distribution of seismicity (Figure 3). Both the local network and teleseismic data were used to relocate these events. They occurred in the period between the large shocks of 1957 and 1986, and are therefore called interseismic events. The location of this cross section is shown in Figure 4. Multichannel seismic (MCS) studies across the forearc in that region show an accretionary wedge approximately 60 km wide abutting the Hawley Ridge outer-arc high at its arcward (northward) end; arc basement does not appear to extend trenchward beyond Hawley ridge [Scholl and Ryan, 1986].

Earthquakes are observed near the trench within the Pacific plate as it bends downward just prior to being underthrust beneath the North American plate. Within and along the base

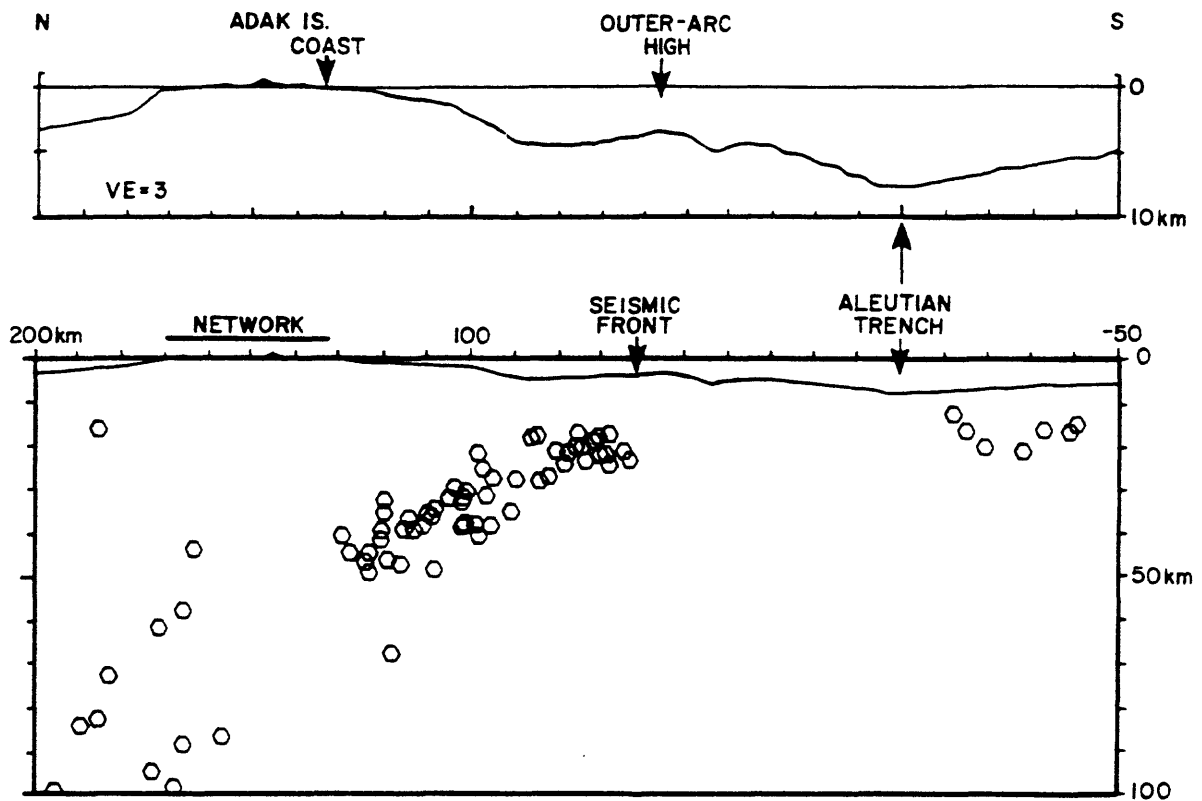


Fig. 3. Bathymetric profile and cross section of earthquake hypocenters in the central Aleutians along line A-B of Figure 4. Upper figure shows bathymetry vertically exaggerated by a factor of 3; there is no vertical exaggeration in the lower figure. Hypocenters were relocated by Engdahl and Gubbins [1987] using local network and teleseismic arrival times for the time period of approximately 1975–1985. Most of the events are of magnitude 4.8 and greater. The hypocenters define a sharp seismic front. Note the absence of seismicity in the region between the trench axis and the seismic front. The seismic front defined by these larger earthquakes is slightly arcward of that in Figure 4. In this and following figures the 0-km horizontal reference is placed at the trench axis. Solid line marked network shows aperture of seismic net on Adak.

of the upper plate, an aseismic zone extends north approximately 60 km from the trench axis. At that point there is a sharp onset of seismicity that we define to be the seismic front. Engdahl [1977] notes that although the Adak network has the sensitivity to detect small earthquakes between the trench and the seismic front, very few events have been reported from that area, an observation supported by the OBS surveys described below. This indicates that the aseismic zone is not an artifact of detection capability. The available focal mechanisms of earthquakes within the upper plate indicate predominantly normal faulting with a minor strike-slip component, suggesting east-west extension parallel to the arc [LaForge and Engdahl, 1979]. Thrust-faulting focal mechanisms are found for events beneath the upper plate earthquakes, and these are interpreted to define the plate boundary [LaForge and Engdahl, 1979; Ekström and Engdahl, 1987]. Thus the seismic front delimits both interplate and upper plate earthquakes

Two OBS studies in the Adak Island area, one over the forearc and one near the trench axis [Frolich et al., 1982], confirm the observations from the Adak network (Figure 5). These investigations located a number of small, shallow earthquakes in the subducting plate seaward of and beneath the trench axis. Composite focal mechanisms of these events show normal faulting that is indicative of north-south extension related to the bending of the Pacific plate [Chen et al., 1982; Frolich et al., 1982]. While the OBS arrays were sensitive enough to detect very small events within the forearc, no earthquakes were observed in the zone that is aseismic in Figures 3 and 5.

In addition to the earthquakes described above, the Adak region experienced a great shock in 1957 (8.6  $M_w$ ) and a large event in 1986 (8.0  $M_w$ ). Using data from the Adak network, C. Kisslinger and others (unpublished data, 1987) located the first three days of aftershocks of the 1986 earthquake (Figure 4). The trenchward limit of these aftershocks is quite sharp

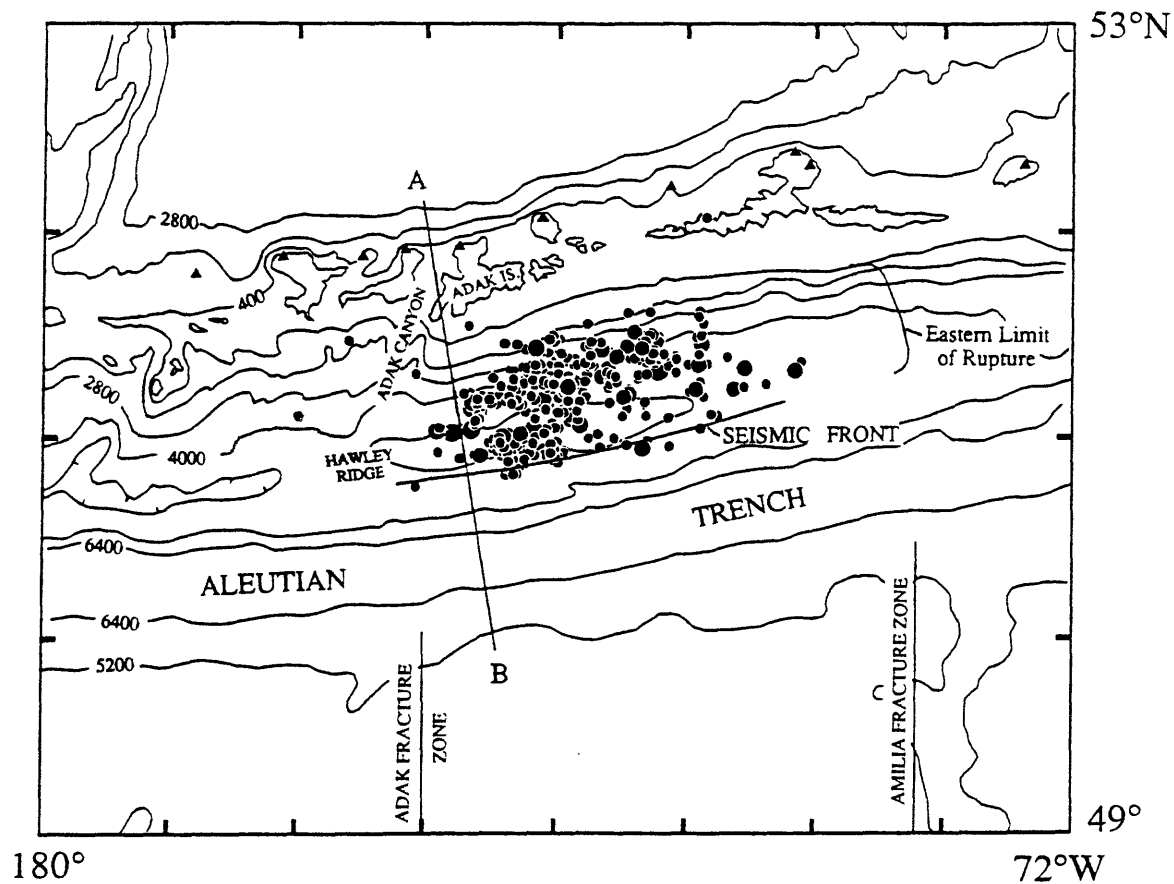


Fig. 4. Map of Central Aleutians showing the locations of the first 3 days of aftershocks of the 1986 Andreanof Islands earthquake ( $8.0 M_w$ ). Locations are from Adak network (C. Kisslinger, unpublished data, 1987). Events outside the network to the east are not located by the net; hence the easternmost limit of rupture as defined by the Preliminary Determination of Epicenters of the U.S. Geological Survey is indicated. These events clearly define a seismic front that is coincident with the trenchward edge of Hawley Ridge, the outer-arc high. Line A-B is the location of the cross sections in Figures 3 and 5. Triangles indicate active volcanoes. Contour interval is 1200 m.

and defines a seismic front that is approximately coincident with that defined by the interseismic events in Figure 3. The 1986 aftershock and the OBS data sets both show a seismic front that is slightly trenchward ( $<10$  km) of that indicated by the events in Figure 3. The interseismic-period events (Figure 3) are generally larger than most of the 1986 aftershocks and OBS events. The small difference in the estimates of the location of the seismic front may be related to this magnitude difference. The locations of the aftershocks of the 1957 event are not well determined [Boyd, 1986], but they do indicate an aseismic region between the seismic front and the trench axis. The correlation between the seismic front of these data sets indicates that hypocenters of smaller, interseismic events can be used to delimit the trenchward limit of seismic rupture in large earthquakes.

The hypocentral locations provided by the different data sets in the Adak region are among the best available for a

subduction zone. These data show a clear aseismic zone approximately 60 km in width ending in a sharp seismic front arcward (northward) of which is the seismogenic zone.

#### *Japan Trench, Tohoku District, Honshu*

The Tohoku District in northeastern Honshu is the site of a seismic network situated over a seismically very active subduction zone. The wide forearc there is interrupted by a midslope terrace [von Huene et al., 1982] that occurs approximately 35-km arcward (westward) of the trench axis (Figure 6). The midslope terrace is coincident with a transition from continental to intermediate crustal velocity structure [Murauchi and Ludwig, 1980] and may mark the trenchward limit of older material that was accreted during a subduction episode that ceased in the Paleocene [von Huene et al., 1982].

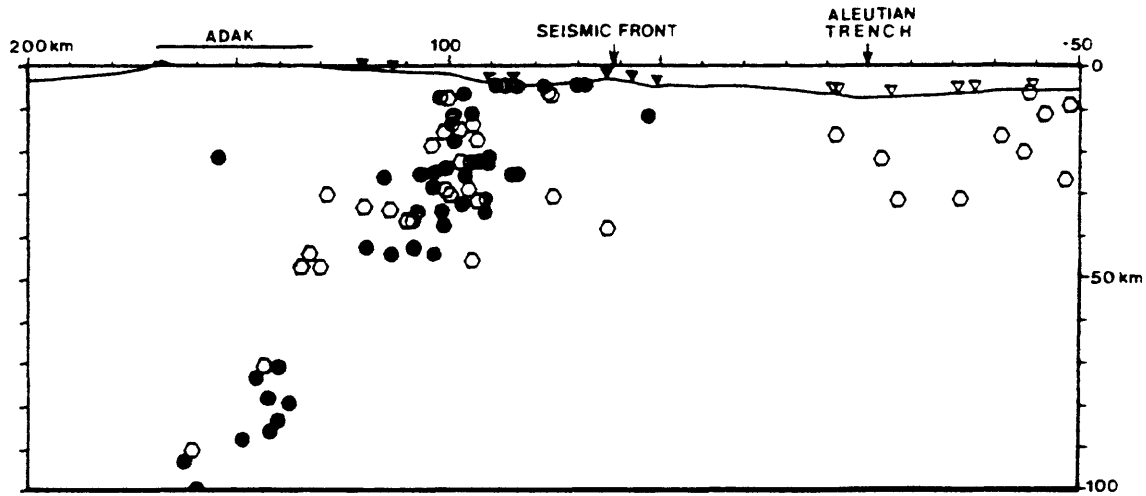


Fig. 5. Cross section along line A-B of Figure 4 of earthquake hypocenters located by two ocean bottom seismometer (OBS) arrays [Frolich et al., 1982]. Triangles on ocean floor indicate OBS locations projected into section. Solid triangles and circles are OBS and earthquake locations from a 1978 survey, and open symbols are from a 1979 survey. In both studies, OBS observations were supplemented with data from the Adak network. Seismic front is same as that identified in Figure 3 and is not as sharply defined with this data set. Note, nevertheless, that a region of little or no detectable seismicity between the trench and the seismic front is still clearly observed. OBS surveys were able to detect earthquakes down to very small magnitudes; thus even small events occurring in this quiet region would have been observed. This indicates that the trenchward toe of the forearc is relatively aseismic for earthquakes of all magnitudes.

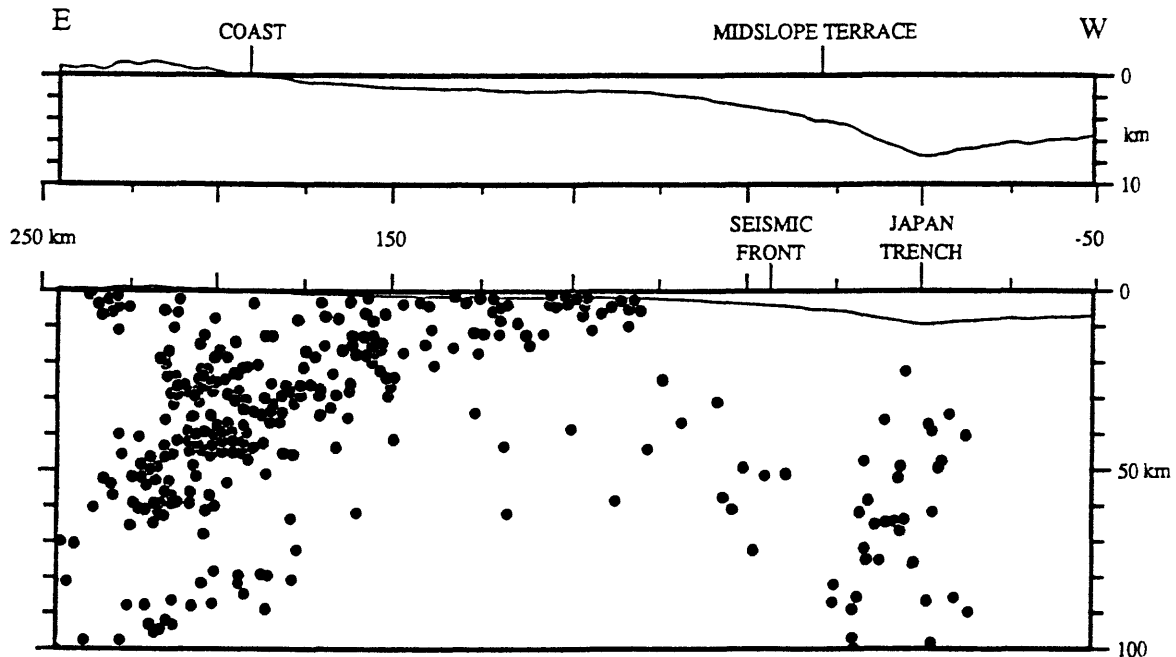


Fig. 6. Bathymetric profile and earthquake hypocenters along a cross section perpendicular to the Japan Trench at 40°N latitude. Earthquake hypocenters located by the Tohoku seismic network [Hasegawa et al., 1976; Abe, 1978]. Upper figure shows bathymetry vertically exaggerated by a factor of 3; there is no vertical exaggeration in the lower figure. The locations are not very accurate near the trench axis but clearly indicate a region with little or no seismicity arcward of the trench axis. The position of seismic front is taken from the data shown in Figure 7. Bathymetry is from MCS line 78-4 [Nasu et al., 1979].

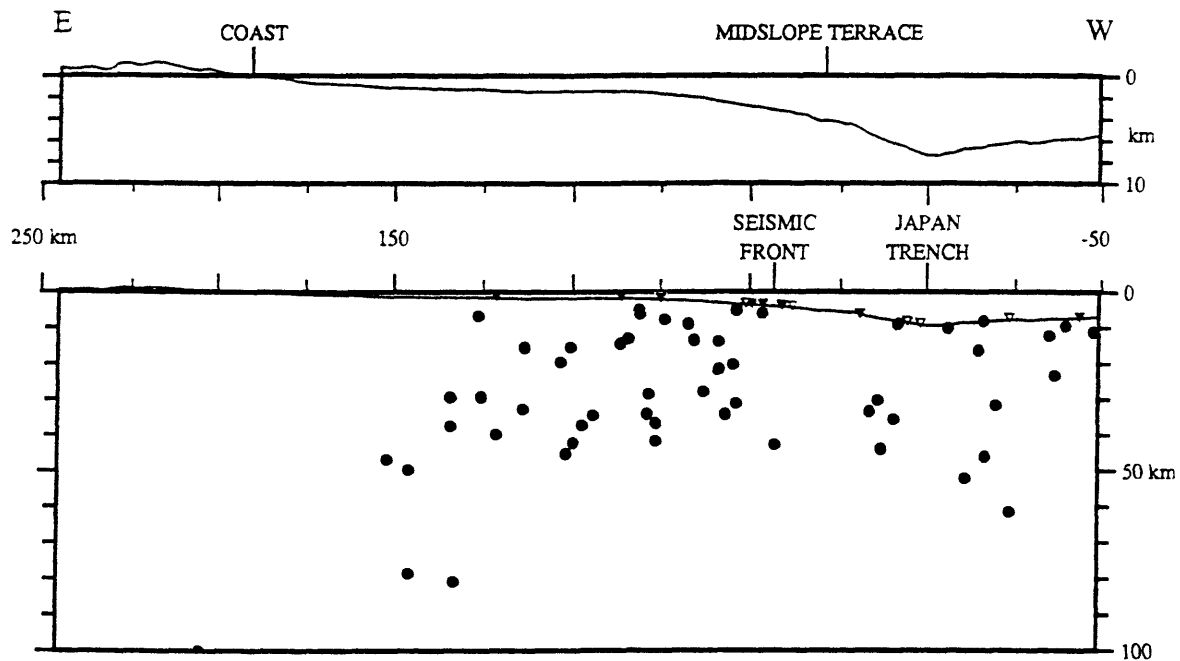


Fig. 7. Bathymetric profile and hypocentral cross section as in Figure 6. Hypocenters are from OBS surveys [Hirata et al., 1983, 1985]. Triangles on the ocean floor indicate the locations of OBS sites projected into section. Note the region of low seismicity between the seismic front and the trench axis. The seismic front occurs near the midslope terrace that appears to mark the trenchward extent of continental crust as discussed in text. The hypocenters are more accurate than those of Figure 6, and the location of the seismic front for this region of the Japan trench is based on these events.

The locations from the Tohoku network (Figure 6) have not been relocated as have events from the Adak region (Figure 3). Thus network locations for events near the trench are probably not as accurate. This is evidenced by the large range in earthquake depths beneath the trench, which is probably an artifact of poor depth control [Hirata et al., 1983]. A similar distribution of seismicity, although inferior to the local network locations, is seen from data compiled by the International Seismological Center [e.g., Yoshii, 1979].

More accurate near-trench locations are provided by the OBS surveys of Hirata et al. [1983, 1985] that were conducted near the axis of the Japan Trench in 1980 and 1981. Locations of events from these studies are shown in cross section in Figure 7. The OBS studies found a large number of small earthquakes near the trench axis within the lower plate as well as a nearly aseismic zone just arcward of the trench with little or no interplate or upper plate seismicity. All the locatable events beneath the aseismic zone are deep enough to clearly be within the lower plate. We define the seismic front to occur 45 km from the trench axis based on the onset of seismicity. Arcward of that position, earthquakes occur within the upper plate and probably along the plate boundary (Figure 7). The aseismic zone as determined by the OBS data is not as wide as one would estimate from the local network data of Figure 6. Given the better resolution of near-

trench events detected by the OBS arrays, we use those locations to define the seismic front. The location of the seismic front is nearly coincident with the midslope terrace, which suggests that a transition in plate boundary slip mode occurs in the vicinity of a transition to stronger forearc material. This combined data set thus indicates a clear, aseismic zone and a seismic front for the subduction zone of northeastern Japan.

#### *Examples From Other Subduction Zones*

A seismic network has been operated in the Shumagin Islands of the Aleutian arc near 160°W on the Alaskan Peninsula since 1973 [Davies and House, 1979]. No OBS experiments have been conducted there to supplement the data from the network. Nonetheless, a nearly aseismic zone approximately 60 km in width is observed arcward of the trench (Figures 8 and 9). Seismic activity increases greatly just trenchward of the shelf edge. We take the location of this increase to be the seismic front. Because the network is able to detect events above magnitude 2.5 throughout this area, and because normal faulting events are observed within the Pacific plate near the trench axis (Figure 9), we conclude that the aseismic zone is real and not an artifact of detection capability.

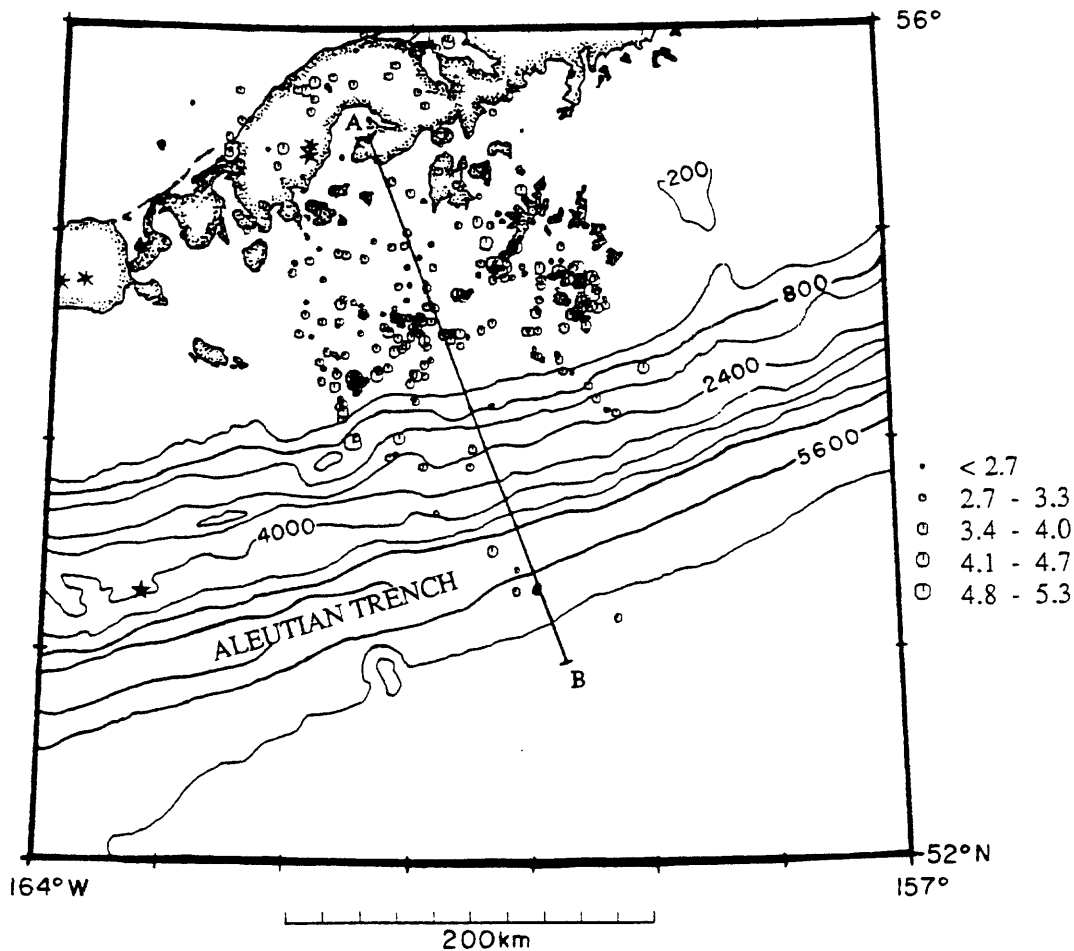


Fig. 8. Map of earthquakes located using data from the seismic network in the Shumagin Islands of the eastern Aleutian arc. Data shown represent all events of magnitude 2.5 and greater observed between 1979 and 1985 within a 150-km-wide region from the central part of network, which includes best hypocentral locations. Note that level of seismicity greatly decreases seaward of 200-m contour. Line A-B is the trace of the cross section shown in Figure 9. Except for 200 m, the contour interval is 800 m. Asterisks indicate active volcanoes. Star is the epicenter of the unusual 1946 earthquake.

The Shumagin shelf is composed of a thick Cretaceous sequence of accreted sediments that is intruded by quartz-dioritic batholiths of Tertiary age [Burk, 1965]. MCS lines farther east suggest that the bulk of the forearc between the shelf edge and the trench axis is made up of accreted and underplated sediment [von Huene, 1986]. Reyners and Coles [1982] determined that earthquakes within the upper plate involve predominantly strike-slip faulting with the P axis (a rough estimate of the direction of maximum compressive stress) being nearly horizontal and oriented in the direction of relative plate convergence. Reyners and Coles found focal mechanisms of the thrust type for a number of earthquakes within the arcward dipping zone of events between depths of 15 and 45 km arcward of the seismic front. These earthquakes are taken to define the plate boundary. Seismicity deeper than these interplate events occurs within the downgoing Pacific

plate. An earthquake occurred trenchward of the seismic front (Figure 8) in 1946 (7.4  $M_s$ ) that was unusual in many respects. It generated a tsunami comparable to that expected for a magnitude 9.2 earthquake [Davies et al., 1981], and may be related to the subduction of a seamount [Sykes, 1971]. The seismicity of the Shumagin region otherwise exhibits a well developed aseismic zone and a clear seismic front.

As in the central Aleutians, an example of an aseismic zone delimited by the aftershocks of a large earthquake is seen in the Oaxaca region of southern Mexico. Four large ( $M > 7$ ) earthquakes have occurred along this section of the southern margin of Mexico since 1960. A study of the seismicity in the region of the largest of these events, the 1978 Oaxaca earthquake, began just 20 days prior to the occurrence of the main shock [Singh et al., 1980; Stewart et al., 1981]. The earthquakes of the 1978 sequence were well located using data

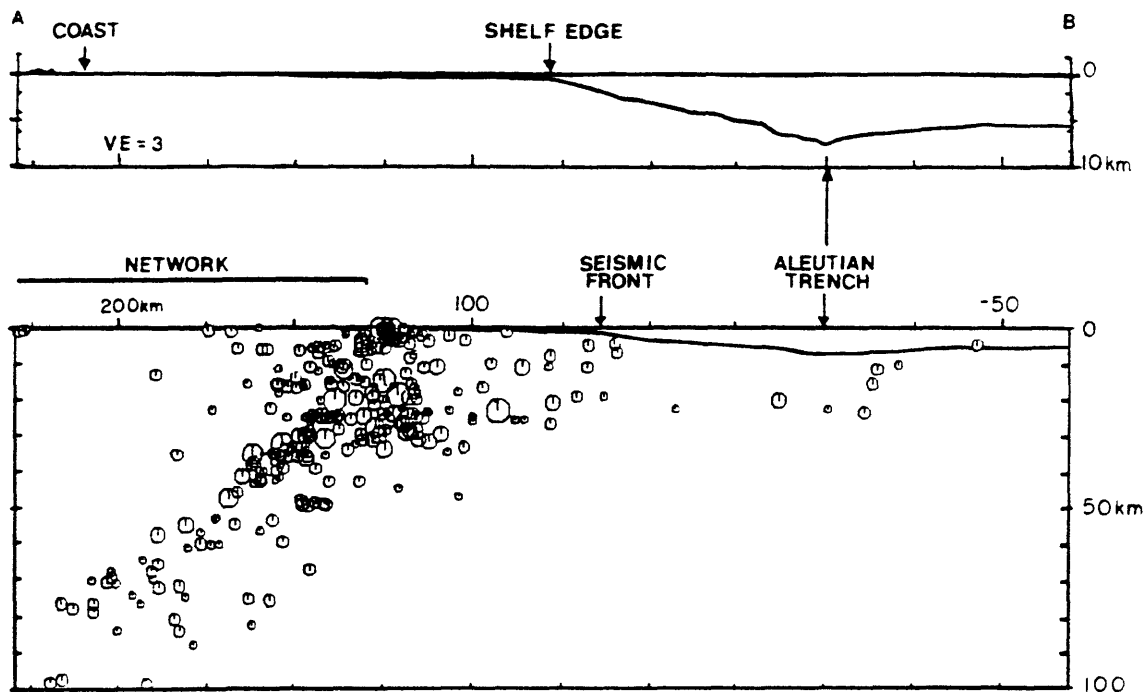


Fig. 9. Cross section of bathymetry and earthquake hypocenters along line A-B of Figure 8. As in Figure 3, the upper figure shows bathymetry vertically exaggerated by a factor of three, and the lower figure has no vertical exaggeration. Note the region of low seismicity between the trench and the seismic front and the much higher activity arcward of the seismic front. The shelf edge and seismic front are nearly coincident.

from local stations of this study, and they indicate an aseismic zone along the shallowest part of the plate boundary (Figure 10). The relocated aftershocks extend closer to the trench axis than in any of the other margins described thus far. Nonetheless, an aseismic zone approximately 25 km wide is observed, arcward of which the shallowest aftershocks occur. Only a small and relatively young accretionary wedge has developed along this margin [Moore et al., 1982b], and schists have been cored 35 km from the trench axis in Deep Sea Drilling Project site 489 [Watkins et al., 1982]. The narrowness of the sedimentary portion of the forearc has been attributed to continental truncation with renewed accretion commencing in the Late Miocene [Karig et al., 1978]. The Oaxaca region is therefore another example in which seismicity extends trenchward only as far as consolidated forearc material.

An example of a very wide aseismic zone comes from the southern Lesser Antillean subduction zone. Because of the massive amount of sediment supplied by the Orinoco River in South America the southern part of this margin has developed a forearc that extends trenchward (eastward) over 350 km from the volcanic arc. The sediments are sufficiently thick that no bathymetric expression of a trench occurs; rather, an accretionary wedge extends arcward from a deformation front (i.e., the outcrop of the plate boundary) for approximately 200 km to the Barbados Ridge Complex, a broad outer-arc high

[Westbrook et al., 1984]. Epicentral locations for events recorded by local networks between 1977 and 1981 [McCann and Ryan, 1984] illustrate the wide aseismic zone that also extends arcward over 200 km from the deformation front (Figure 11). Most events are of magnitude 3 and greater. The accuracy of these locations is poor in comparison to those for the margins discussed previously. However, the forearc in the southern Lesser Antilles is sufficiently wide that the features of interest are, nonetheless, easily discerned. A marked increase in seismicity, the location of which we define as the seismic front, extends along the entire arc. The same seismicity pattern is seen in locations of teleseismic data (not shown in Figure 11) [e.g., Stein et al., 1982]. It is not clear how many of these earthquakes are interplate thrust events and how many are intraplate because hypocentral depths are generally not very accurate. But because few events occur within the lower plate as it bends beneath the accretionary wedge arcward of the outer-arc high, there is no reason to expect a sudden increase in such events at the seismic front. Therefore we infer that most of the events associated with the seismic front occur within the upper plate or along the plate interface.

All of the above subduction zones exhibit an aseismic zone along the shallowest part of the plate boundary. That zone gives way to the seismogenic zone at the seismic front. Available evidence indicates that the seismic front is a fixed

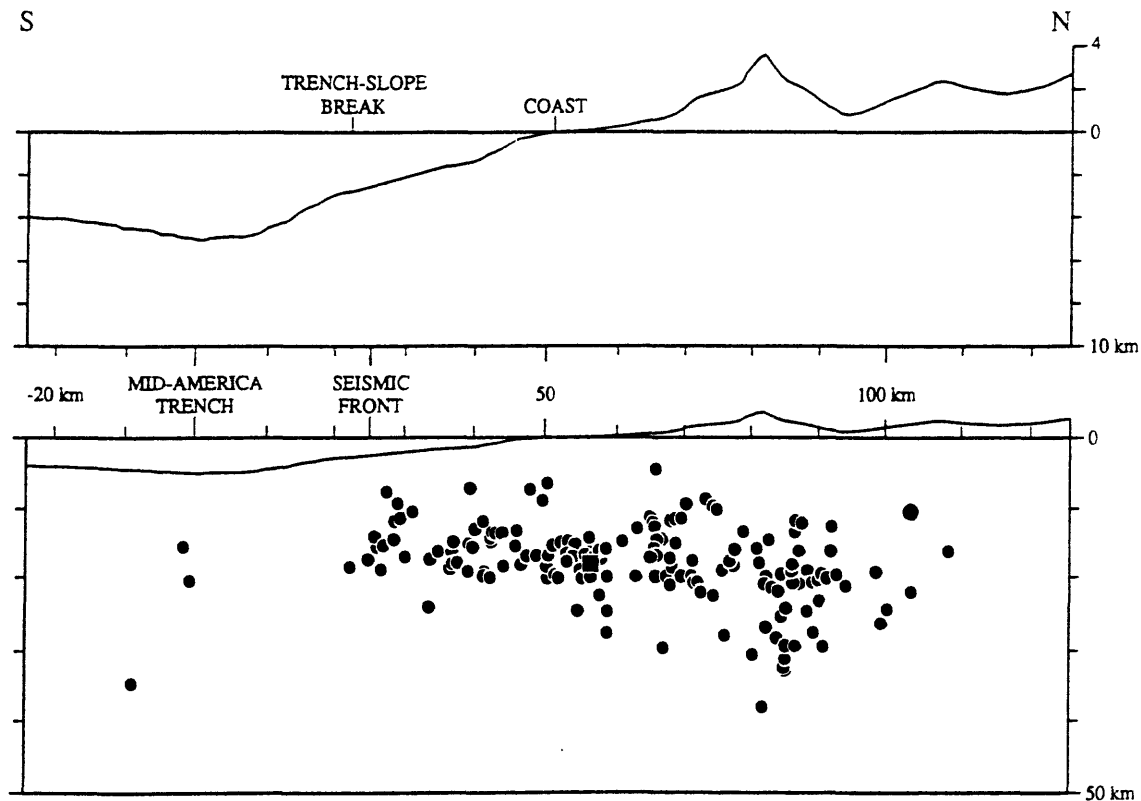


Fig. 10. North-south cross section of bathymetry and earthquake hypocenters along the Middle America Trench at 96.8°W in southern Mexico. Hypocenters are aftershocks of the 1978 Oaxaca event located by Stewart et al. [1981]. Square denotes location of main shock. Bathymetry is taken from MCS line YQ712 of Oregon State University, and is shown with a vertical exaggeration of 3 in the upper figure. Note that the seismic front occurs near the trench-slope break approximately 25 km from the trench axis.

boundary for both interseismic events and for large and great earthquakes at any given place. We suggest further that neither the aseismic zone nor the seismic front are unusual features and that they would be observed at most convergent margins given sufficiently accurate earthquake detection and location.

*Shallow Seismicity and the Seismic Potential of Subduction Zones*

A great deal of variability exists among and along subduction zones in the maximum size of plate boundary earthquakes. A part of this variability has been ascribed to differences in some key parameters, the most important being the age of the plate being subducted and the convergence velocity [Kanamori, 1971; Uyeda and Kanamori, 1979; Ruff and Kanamori, 1980, 1983]. A regression relation for the maximum size thrust event based on these two parameters alone, however, indicates considerable scatter of the data points. We think that other factors may play more dominant roles for some margins, and hence must be considered in studies of seismic potential. In particular, we conclude that

the nature of the zone of plate contact is a major factor in controlling the maximum size and the average repeat time of thrust events. An example of such dependence is the observed variation in the maximum size of thrust earthquakes along the Japan trench where neither plate age nor convergence velocity change significantly along the arc. In the northern part of that subduction zone, earthquakes greater than magnitude 8 occur, but farther south only events up to magnitude 7.8 are observed (and most are smaller than 7.5) [Kawakatsu and Seno, 1983]. Mogi [1987] attributes this change in seismic potential to a variation along strike in seafloor topography, with smooth seafloor being subducted in the north and rough seafloor characterized by many seamounts being subducted in the south.

Because rupture area ultimately determines the size of an earthquake, a more direct way of estimating the size of future or potential large earthquakes may be to estimate the maximum rupture area. This area is the product of the downdip width,  $W$ , of the seismogenic zone (Figure 1) and the length along strike,  $L$ .  $W$  is a very important parameter in estimating the size of large earthquakes because seismic moment,  $M_0$ , is very sensitive to it, as shown below. The

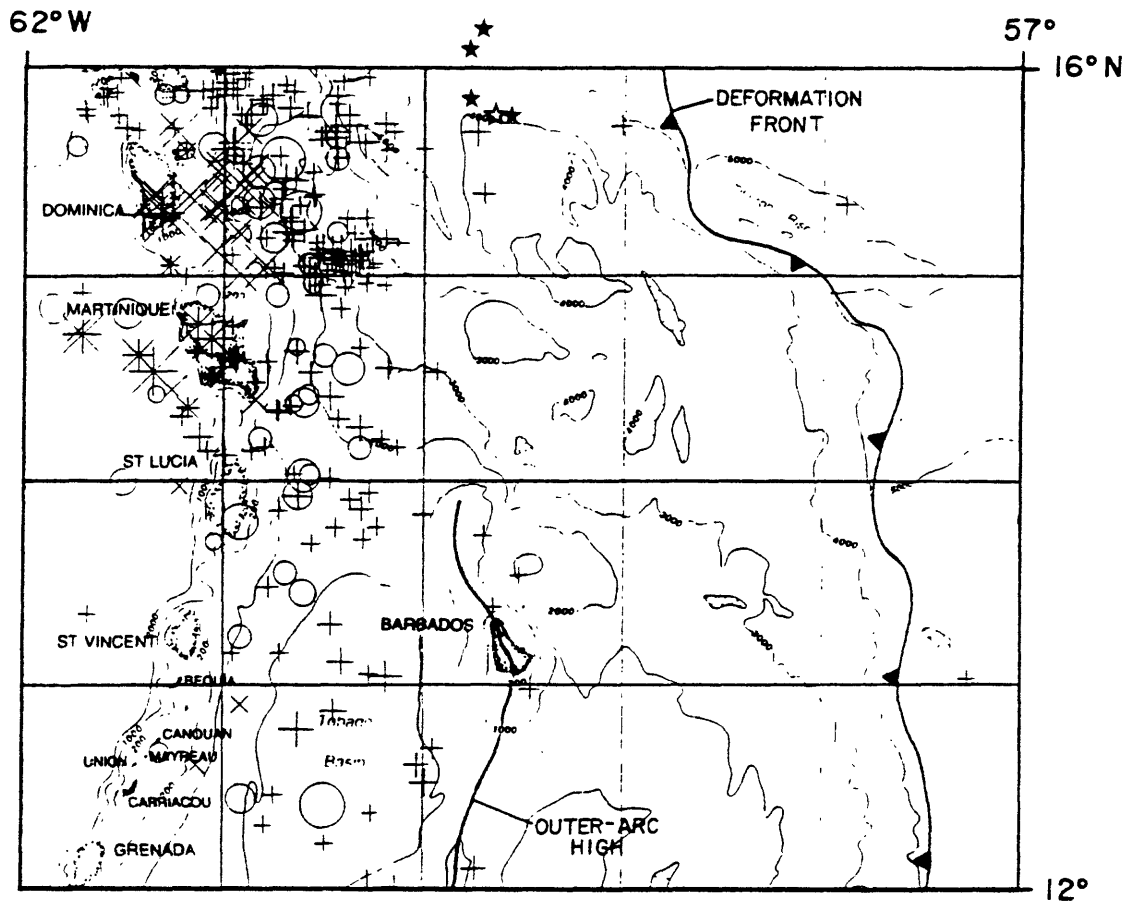


Fig. 11. Map of earthquake epicenters in the Lesser Antilles. Earthquake locations are from local networks for events occurring between 1977 and 1981 as compiled by McCann and Ryan [1984]. Symbols indicate earthquake depth: plus sign, 0-50; circle, 51-100; cross, 101-150; asterisk, 151-200; and Y, greater than 200 km. Relative size of symbol reflects number of stations reporting. Most events are of magnitude 3 and greater. Note the decrease in seismicity trenchward (eastward) of the outer-arc high. The seismic front, i.e., eastern limit of high seismic activity near 60°, is coincident with the outer-arc high in the southern Lesser Antilles. North of 14° the bathymetry indicates more complexity, probably caused by the subduction of aseismic ridges such as the Tiburon Rise. The stars near 59.7°W are the epicenters of the 1969 sequence of events within the downgoing plate; the open star is the main shock. Contours are in meters.

location of the shallow limit of seismic slip has not been considered previously, yet its location is crucial in making accurate determinations of  $W$ . Many studies have assumed that the locked portion of the plate interface extends all the way to its outcrop at the trench axis [e.g., Robinson, 1978, 1986; Sykes and Quitmeyer, 1981; Reyners and Coles, 1982; Peterson and Seno, 1984], thereby seriously overestimating  $W$ . By taking the seismic front to define the trenchward limit of the seismogenic zone, a better estimate of  $W$  and therefore of  $M_0$  can be made.

The shallow, sediment-rich portion of the plate boundary does not contribute significantly to the seismic moment release in large earthquakes even if such ruptures propagate updip into that part of the interface. The seismic moment of

an earthquake is proportional to the rigidity of the material through which the event ruptures. The rigidity of the sediments along the shallow part of the plate boundary is much lower than that of deeper, more consolidated rock. Thus, this low-rigidity part of the plate boundary should be removed from  $W$  in making estimates of the maximum possible seismic moment release in large earthquakes.

The downdip width of the seismogenic zone is delimited by the seismic front at its shallow end and by the temperature-controlled transition to stable sliding at depth. A complete determination of  $W$  therefore also requires an estimate of the location of that deep limit. Laboratory experiments indicate that a transition from velocity weakening to velocity strengthening occurs at high temperature [Slesky, 1978]. The

and Rice [1986] show that the deep limit to seismic rupture along strike-slip faults in continental rocks occurs at approximately the 300°C isotherm. The same is expected in subduction zones except that the thermal gradients are lower, and so the depth of the 300°C isotherm is approximately three times greater. Because the dip of the plate interface generally increases with depth, a small error in the depth estimate of the shallow limit will be more significant in a determination of  $W$  than an equivalent error for the deeper limit.

Given improved estimates of  $W$ , better determinations of seismic moments of future large thrust earthquakes are in turn possible because moment is related to  $W$  through

$$M_0 = \mu ULW \quad (1)$$

where  $\mu$  is rigidity,  $U$  is the average slip over the rupture zone, and  $L$  times  $W$  is the rupture area (length along strike times downdip width).

Chinnery [1969] and others find that average slip,  $U$ , is proportional to the product of static stress drop, downdip width, and a geometrical constant that is a function of the aspect ratio  $L/W$ . Sykes and Quittmeyer [1981] used available repeat time information and this relation to study large plate boundary earthquakes. They found that static stress drop,  $\Delta\sigma$ , increases with increasing  $W$  for thrust events. Even though they probably overestimated  $W$  for several events, it is safe to conclude that  $U$  is proportional to  $W^n$ , where  $n \geq 1$ . Other workers have argued that the gross static stress drop is approximately constant for large earthquakes [e.g., Kanamori and Anderson, 1975; Kanamori, 1977], in which case  $n$  would be equal to 1. The rupture length is controlled by structural features transverse to the trench, by major changes in the subduction zone strike [Davies et al., 1981], and by the locations of the rupture zones of previous earthquakes. In addition,  $L$  usually increases with  $W$  [Sykes and Quittmeyer, 1981]. Thrust earthquakes at subduction zones generally have rupture areas with lengths roughly two or three times their widths [e.g., Abe, 1975]. This is true even for most of the greatest earthquakes, with notable exceptions being the 1960 Chile and the 1957 and 1965 Aleutian events for which  $L$  was considerably greater. Thus  $L$  increases roughly linearly with  $W$  and on rare occasions somewhat faster than linearly. Hence, to first order, we can write  $L = kW$  where  $k$ , the aspect ratio, is generally equal to 2 to 3. Substitution of these functions of  $W$  into (1) yields

$$M_0 \propto W^{(2+n)} \quad (2)$$

where  $n \geq 1$ .

Equation (2) indicates that  $M_0$  is proportional to at least  $W$  cubed for most large earthquakes and is therefore very sensitive to  $W$ . Several other authors have found that  $M_0$  is proportional to rupture area to the three-halves power [e.g., Aki, 1972; Abe, 1975; Kanamori and Anderson, 1975; Kanamori, 1977] which is the same as  $W^3$  for rupture zones with a nearly constant aspect ratio and  $n=1$  (i.e.,  $\Delta\sigma$  constant). Thus the ability to define the width of the seismogenic zone,  $W$ , can be very important in determining the maximum seismic moment for a given segment of a convergent plate boundary. It should be realized that  $W$  has previously been

seriously overestimated for many large thrust events. This in turn has resulted in incorrect estimates of the average slip and the static stress drop since they have usually been calculated from estimates of  $M_0$ ,  $L$ , and  $W$ . Unlike  $W$ ,  $L$  is usually relatively well determined either from aftershock locations or from direct measurements of very long-period seismic waves.

$W$  is also proportional to the average repeat time of large earthquakes along given segments of convergent margins [Sykes and Quittmeyer, 1981; Astiz and Kanamori, 1984]. Average repeat time,  $T_r$ , is equal to the average seismic slip,  $U$ , divided by the convergence velocity,  $V_c$ , divided by the ratio of seismic slip to total slip,  $\alpha$ . Again, writing  $U$  in terms of  $W^n$  and assuming that  $\alpha$  is nearly constant, we can write average repeat time as

$$T_r \equiv b W^n / V \quad (3),$$

where  $b$  is constant. If one assumes that stress drop is approximately constant ( $n=1$ ), then repeat time is proportional to  $W$ . Astiz and Kanamori [1984] derive an equivalent relation between  $T_r$  and  $M_0$ .

Thus, by defining the location of the seismic front for a convergent margin, we are able to estimate better the width of the seismogenic zone and hence to calculate both the maximum size of possible interplate events and their average repeat times.

#### *Causes of the Aseismic Zone Within and Along the Base of Accretionary Wedges*

Accretionary wedges make up the shallowest, near-trench part of forearc regions (Figure 1). They are commonly composed of sediments that are accreted to the toe of the overriding plate, underplated along its base, and/or deposited along its upper surface. Significantly, it is this shallow region of the overriding plate and of the plate boundary that behaves aseismically. We thus conclude that it is the unconsolidated and overpressured nature of the newly accreted sediments that is responsible for the existence of the aseismic zone within and along the base of accretionary wedges.

The sediments that make up accretionary wedges are derived from the plate that is being subducted, from the adjacent volcanic arc or continent, or from both. In this paper we have referred to these as young sediments in order to distinguish them from older (e.g., Cretaceous), lithified sediments that make up part of the backstop at a number of convergent margins. The abundance of such sediment determines the rate at which an accretionary wedge develops. The sediments available for accretion commonly include pelagic and hemipelagic marine sediments with varying amounts of terrigenous sediments. They generally have very high initial porosity and very low permeability. The process of accretion subjects these sediments to increasing pressure resulting in dewatering and consolidation. When accretion occurs rapidly, however, which is the case for most active convergent plate boundaries, low-permeability sediments are not able to drain fast enough to follow a normal compaction process, and high pore fluid pressures develop. Pore fluid pressures in excess of

hydrostatic lead to an effective normal stress within the sedimentary matrix that is less than lithostatic. As pore pressure approaches the lithostatic value, effective normal stress approaches zero. Low effective normal stress results in low shear strength, which in turn means that such a material is not able to store up the high level of shear stress released as sudden slip during large earthquakes. Experimental work further suggests that low normal stress favors stable, aseismic slip rather than simply decreasing the size of potential stick-slip events [Dieterich, 1978]. Many and perhaps most modern accretionary wedges are likely sites of very high pore fluid pressures. Evidence from deep sea drilling is suggestive of pore fluid pressures near lithostatic within the toe of the Lesser Antilles accretionary wedge [e.g., Moore, Biju-Duval et al., 1982a]. Highly elevated pore fluid pressures are probably present within accretionary wedges at a number of other subduction zones as well [von Huene and Lee, 1983]. Hence, the shallowest portions of many subduction zones are particularly well suited for the presence of elevated pore fluid pressures and should thus be expected to deform aseismically as is observed.

Recent laboratory experiments provide another explanation for the aseismic zone by suggesting that unconsolidated materials experience inherently stable, aseismic slip behavior [e.g., Logan et al., 1981; Zhang et al., 1987; Marone et al., 1988]. Zhang et al. [1987] find that there is a transition, which is dependent upon porosity and effective confining pressure, from 'ductile' to 'brittle' behavior in highly porous sandstone. At higher porosity, earthquake instability can be ruled out because there is no shear localization or stress drop. At lower porosity, strain softening makes a runaway earthquake instability possible. Marone et al. [1988] investigated the frictional properties of unconsolidated quartz gouge under saturated drained conditions and constant normal stress during triaxial shear. Other studies of gouge have often used very thin layers and may therefore have observed the slip between gouge and hard rock rather than slip within the gouge itself [e.g., Byerlee and Summers, 1976; Dieterich, 1981]. Marone et al. found stable sliding at approximately constant shear stress after a peak stress was reached. They also found that slip occurs with a higher coefficient of friction for higher slip rates, thus exhibiting velocity strengthening. Slip is therefore stable in unconsolidated quartz gouge in that it requires more energy to slip at higher velocities. Consolidated or solid samples of quartz and granite, on the other hand, exhibit unstable, stick-slip behavior [Dieterich, 1979; Ruina, 1983; Tullis and Weeks, 1986]. The difference observed in the slip stability between consolidated and unconsolidated samples suggests that consolidation is primarily responsible for the change in frictional slip.

At some convergent plate margins the presence of marine clays may also affect the nature of slip. Summers and Byerlee [1977] showed that expanding clays such as montmorillonite and smectite exhibit stable sliding and low friction because the layers of molecular water within their structure cause them to act as solid lubricants. Higher pressures and temperatures

dehydrate the clays and cause them to lose their lubricating property [Logan et al., 1981]. Thus such clays provide another reason to expect stable slip at shallow depth at margins in which the sediment column on the subducting plate includes a high percentage of expanding clay.

The primary factor that determines the nature of slip within the sediments seems to be the state of their compaction. Several secondary parameters interact to influence that state at a given subduction zone. The type of material making up the sedimentary column is one such parameter because the material properties of initial porosity and permeability determine the rate at which the sediment can be drained and compacted. Another obvious parameter that determines sediment consolidation is the thickness of the sediments available for subduction. A thick sequence of clastic material with high permeability, for example, may be dewatered and consolidated under relatively low pressures, while an equally thick sequence of highly impermeable clay will drain only very slowly. In this instance the clay sequence would cause an aseismic zone that is much wider than the clastic sediment. Therefore through the combined effects of pore fluid pressure, velocity strengthening behavior, and low friction clays, the sediments along the shallow part of the plate boundary cause stable, aseismic slip; earthquakes (which are essentially unstable slip events) of any size should not be expected to nucleate there. This would explain the absence of seismicity along the sediment-lined portion of the plate boundary at subduction zones.

The shallowest portion of the plate boundary at subduction zones is often called a decollement. The decollement preferentially occurs along the weakest available interface, which is likely to be that with the highest pore-fluid pressure [von Huene and Lee, 1983]. As sediment near the decollement is dewatered and compacted, it becomes stronger than adjacent, less deformed sediment. When this happens the decollement will abandon that interface and slip will begin to occur within deeper, weaker material [Moore and Byrne, 1987]. Thus the plate boundary steps farther downsection with distance from the trench axis, resulting in accretion to the base of the upper plate (i.e., underplating) [e.g., Aoki et al., 1983; Westbrook and Smith, 1983; Fisher and Byrne, 1987]. At margins where an extremely large volume of sediment is being subducted (>3 km at the deformation front) the decollement may never step downsection through the entire sediment column. Thus at such zones, semiconsolidated sediment may line the plate boundary to great depths. At most margins, however, a more moderate amount of sediment is present. Therefore, the bulk of the sediment that is subducted past the deformation front will eventually be underplated, compacted and lithified. Once the bulk of the unconsolidated sediment is compacted and/or removed from the active slip boundary we should expect the plate boundary to begin exhibiting unstable, stick-slip behavior [Marone and Scholz, 1988]. Because a seismic front marks the trenchward extent of stick-slip frictional behavior, we hypothesize that it also marks the trenchward limit of contact of consolidated

rock across the plate boundary; the aseismic zone then approximately delimits that part of the plate boundary that is lined with unconsolidated sediment.

## SHALLOW SEISMICITY AND THE MECHANICS OF FOREARC REGIONS

### *Forearc Mechanics*

The mechanics of accretionary wedges have been well studied using various assumptions about rheology [e.g., Chapple, 1978; Davis et al., 1983; Emerman and Turcotte, 1983]. Such studies, however, have not considered the entire forearc. The distribution of seismicity along the plate boundary and within the overriding forearc can be used to map out frictional instability and, indirectly, to infer the gross state of consolidation of material there. In this paper we use the critical taper model proposed by Davis et al. [1983]. After a brief description of the main elements of that model, we apply it to the entire forearc and discuss the resulting implications for forearc structure and seismicity.

Accretionary wedges are considered to be analogous to snow or soil being pushed by a bulldozer. These deforming masses acquire a wedge shape as a consequence of forces exerted upon them, primarily shear along their bases [Davis et al., 1983]. Pushing a sufficiently weak layer of material forward will result in the layer deforming internally, rather than sliding *en masse*. The layer becomes shorter and thicker near the end that is being pushed while the distant end of the layer remains motionless. This process eventually leads to the formation of a wedge. The wedge continues to grow by internal deformation without sliding along its base until a critical taper is reached, at which time it will be the thinnest body that is sufficiently strong to slide along its base without further internal deformation. At subduction zones this steady state situation is generally not achieved. Erosion and/or continued accretion in addition to time-dependent sedimentary behavior require some deformation to continue within the wedge.

The development of a wedge shape is a simple consequence of the forces acting on the wedge and can be explained by considering two adjacent vertical columns in an accretionary wedge. Any given vertical column must have an integrated strength sufficient to overcome the basal frictional resistance of the entire extent of the wedge trenchward of itself if it is to push that part of the wedge forward. The required strength is related to the distance of the column from the toe of the wedge and to the frictional resistance along the decollement. A second column immediately behind the first must be strong enough to support the load borne by the first and, in addition, to overcome the additional frictional resistance along the base of the first column. All else being equal, the integrated strength of a column increases with its height, and so, if the wedge is at its minimum possible (critical) taper, the second column must be taller than the first. If it is not, internal deformation will take place within the wedge until the second

column has reached a sufficient height for slip to occur along the base of the wedge trenchward of it. This mechanical requirement for increasingly taller columns leads to the formation of a body that is wedge shaped in cross section. An accretionary wedge with a planar decollement will have an upper surface (the seafloor) with a constant dip if it is made of a noncohesive material, a concave upward profile if it has a constant, nonzero cohesion, and a convex upward profile for the case in which cohesion increases with distance from the trench [Dahlen et al., 1984; Dahlen, 1984; Zhao et al., 1986]. The latter type of profile is observed for many accretionary wedges.

At the arcward end of accretionary wedges, outer-arc highs or trench-slope breaks occur [Karig, 1974]. Trench-slope breaks and outer-arc highs form an abrupt change in the critical taper of the accretionary wedge; hence they indicate large changes in the factors controlling wedge taper. One possible explanation for that change is a steepening of the dip of the decollement. This would allow a wedge to continue to thicken arcward and maintain a critical taper even though the slope of the water-sediment interface decreases. Neither the distribution of seismicity nor mechanical considerations of a bending plate, however, indicate any sudden steepening of the subducting slab beneath the outer-arc high. Another possible explanation is that the change in slope is an expression of the base of the accretionary wedge, the decollement, reaching the brittle-ductile transition. This would lower the friction along the decollement, producing a flattening of the surface of the accretionary wedge [Davis et al., 1983]. While this may be an explanation for a few of the largest accretionary wedges, it alone cannot be a general explanation for the development of trench-slope breaks because both large and small wedges show similar morphology, albeit on different scales. Other explanations for the change in slope that we consider unlikely include a sudden change to a lower coefficient of friction or to higher pore fluid pressures along the decollement beneath the topographic high because basal friction generally increases and pore fluid pressure generally decreases with distance from the deformation front.

An alternative cause for the development of an outer-arc high, and the one that we favor, is a relatively large horizontal gradient in shear strength within the overriding plate. The near-trench convexity of the cross sectional shape of many accretionary wedges has been attributed to a similar, but less marked, horizontal gradient in strength [e.g., Zhao et al., 1986]. The mechanical requirement that each successive column must be stronger than the one trenchward of it can be accomplished either by increasing height or, obviously, by increasing shear strength. We suggest that the change in slope of the forearc is a reflection of a change to more consolidated rock within the upper plate. Depending on the strength contrast, stronger material could support the same differential stress as several times its own height of weak, incompletely lithified, and possibly overpressured sediments. Thus a column of sediment underlain by stronger material gains a large boost in integrated strength and therefore no longer needs additional height to provide increased strength.

### *The Backstop*

We follow previous workers [e.g., Silver et al., 1985; Brandon, 1986] in using the term backstop to describe the stronger basement material presumed to exist below the arcward end of forearcs (Figures 1 and 2). This term is sometimes applied to the interface between strong and weak material, but in this paper we use it to describe the strong material itself. The backstop acts mechanically as a load-bearing member, supporting an increasing amount of the compressive stress as it thickens arcward. Weak sediments are thus allowed to ride passively on top of the stronger material of the backstop, shielded or isolated from shear stresses along the base of the backstop. Forearc basins occur arcward of accretionary wedges and outer-arc highs and are commonly much less intensely deformed than the sediments of the accretionary wedge. Some landward tilting of originally horizontal layers accompanies the uplift of the back of the accretionary wedge [e.g., Karig, 1977; Karig et al., 1980; Lewis and Hayes, 1985]. The fact that weak sedimentary basins can remain essentially undeformed in the midst of strongly compressional convergent margins indicates that they are largely decoupled or isolated from the lateral stress transmitted from the plate boundary. While forearc basins have been observed and commented upon for many years, few previous attempts have been made to explain mechanistically their presence and general lack of deformation. We interpret the relative lack of deformation within forearc basins to indicate that a backstop beneath them supports and carries the compressional stress. We hypothesize that a backstop of strong material whose upper surface dips trenchward explains the development of common morphologic features of forearcs as well as the distribution of shallow seismicity.

The property that distinguishes the backstop is its higher state of consolidation compared to that of the sediments above and arcward of it. Its actual lithology is not very important from a strength point of view, and it may be composed of a number of lithologies, from those associated with volcanic arc rocks to various sorts of well-lithified sediments. Likewise, a number of possibilities exist for the character of the boundary between the backstop and the overlying weaker material. It may be a sharp lithologic change, for example, from arc rock to sediment or from lithified sediment to newly accreted sediment; alternatively, it may be either a transitional boundary across which sediments become metamorphosed or further lithified (a lithification front as proposed by Byrne and Hibbard [1987]), or the surface of a previous convergent margin or truncated continental block now buried by sediments. The depth and dip of the top of the backstop are not known at most margins. We maintain, however, that because a stronger backstop at depth causes changes in morphology and in seismicity, its gross orientation and location might be inferred from observations of these phenomena.

Seismic imaging at many convergent margins is either too incomplete or too limited in depth to clearly show the

relationship between basement and shallow structures at the arcward end of forearcs. In some instances, however, such as the Lesser Antilles [Ladd et al., 1986], the Manila trench [Lewis and Hayes, 1985], the Peru margin [von Huene et al., 1987], and the Sulawesi trench [Silver et al., 1983], available multichannel seismic (MCS) lines show a reflector that dips trenchward and that appears to intersect the downgoing plate approximately beneath a major morphological or structural feature. A few examples of line drawings from MCS profiles that have such reflectors are shown in Figure 12. One interpretation of these reflectors is that they represent the upper surface of backstops within these forearcs [e.g., Silver et al., 1985].

Two commonly suggested alternative configurations for the backstop, those in which the backstop dips trenchward beneath the accretionary wedge and those in which the accretionary wedge dips arcward beneath the backstop (Figure 13), lead to quite different structures within the forearc [Silver et al., 1985, 1986]. This is also indicated in our simple laboratory models which are described below. The mechanics of a backstop geometry in which the bulk of the accretionary wedge dips arcward beneath the backstop (Figure 13b) fail to produce a forearc basin or an outer-arc high [Le Pichon et al., 1982; Silver et al., 1985]. Such a geometry has been proposed for the Franciscan Complex of California and Oregon based on surface geology [e.g., Ernst, 1970; Cloos, 1982]. Recent deep-penetration seismic studies in central California, however, show reflectors at depth that dip southwestward (trenchward) beneath both the Great Valley sequence and the Franciscan melange [Zoback and Wentworth, 1986]; these reflectors may mark the top of a trenchward-dipping backstop [Silver and Reed, 1988]. A backstop that dips trenchward beneath the accretionary wedge has sometimes been used in schematic cross sections [e.g., Westbrook, 1975; Le Pichon et al., 1982; Davis et al., 1983], and more recently, it has been discussed explicitly [e.g., Westbrook et al., 1984; Silver et al., 1985; Silver and Reed, 1988]. Here we will refer to this type of backstop as one that is trenchward-dipping. Such a backstop produces a topographic high above its intersection with the subducted plate, and a passive basin develops arcward of that point as discussed previously. When a massive thickness of young sediment is present, large amounts may be subducted beneath the backstop in addition to being accreted above it, resulting in a forearc that is intermediate in configuration between Figures 13a and b. A trenchward-dipping backstop seems applicable to many forearcs in which the abundance of young sediment is small to moderate [Silver and Reed, 1988].

### *Laboratory Modeling of Forearc Development*

We conducted a series of laboratory modeling experiments to investigate the effects of lateral variations in strength within the forearc. In particular, we studied how the presence and geometry of a backstop can influence forearc morphology. This modeling is similar to that used by Davis et al. [1983] to study the mechanics of accretionary wedges.

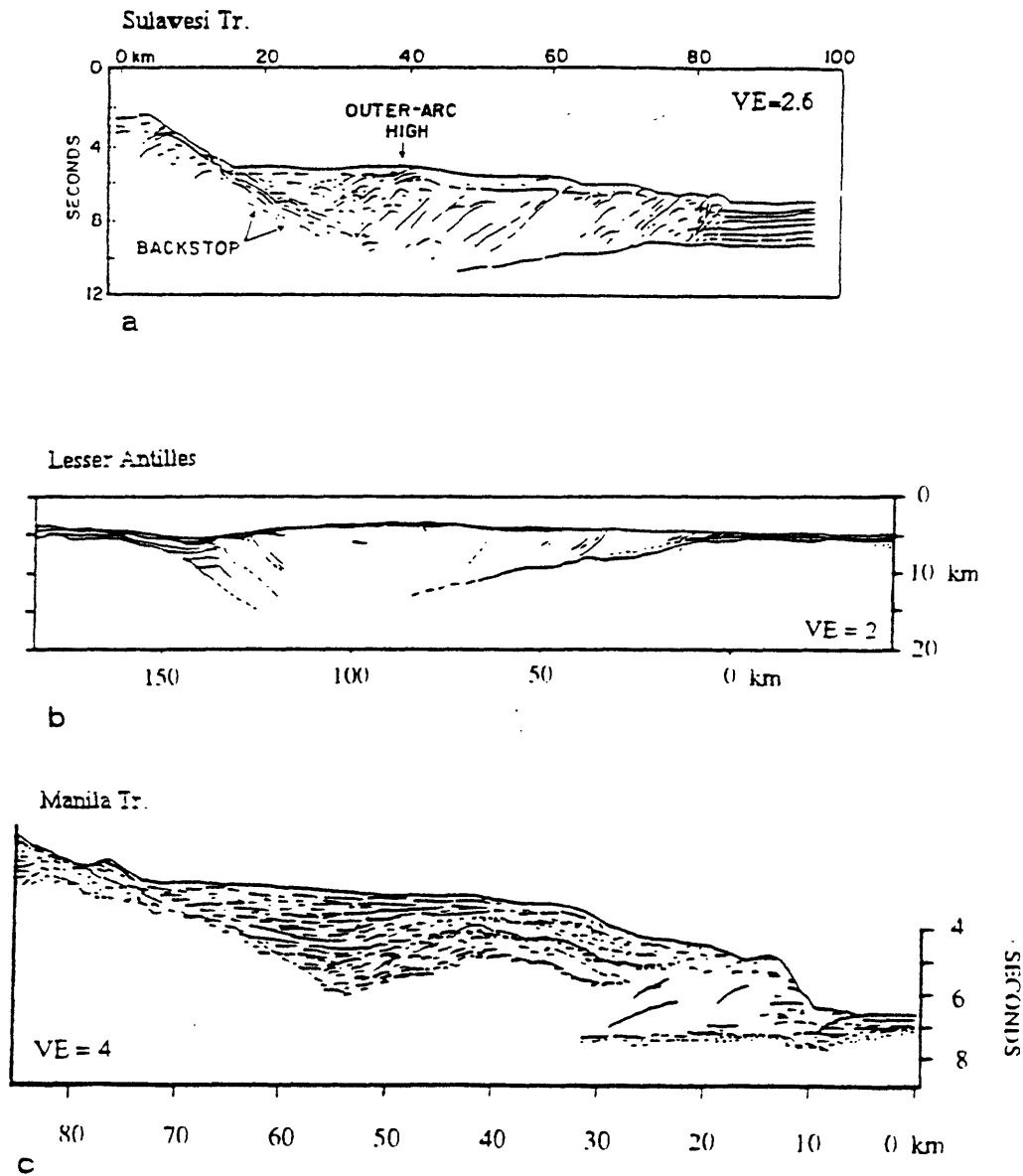


Fig. 12. Line drawings of multichannel seismic profiles across several forearcs. (a) Line 25 across the Sulawesi trench north of the north arm of Sulawesi, Indonesia, from Silver et al. [1983]. Trenchward-dipping reflectors beneath the southern part of the accretionary wedge are interpreted to be top of backstop. Note these reflectors and those from the top of the plate being subducted appear to intersect directly beneath the outer-arc high. Vertical scale is two-way travel time from the surface of the ocean in seconds. (b) Shell line C2114 across the Lesser Antilles island arc near 14°N. Travel time has been converted to depth. Note the trenchward dipping reflectors that, if extended, intersect the subducted plate beneath the outer-arc high. This forearc is approximately three times the size of that in 11a. More recent observations [Ladd et al., 1986] confirm the existence of the reflectors shown in this figure and trace them farther arcward. (c) Profile G across the Manila trench from Hayes and Lewis [1985]. Again, note that trenchward-dipping reflectors beneath the forearc basin, interpreted to be from the top of the Zambales ophiolite, would intersect the subducting plate approximately beneath the trench-slope break.

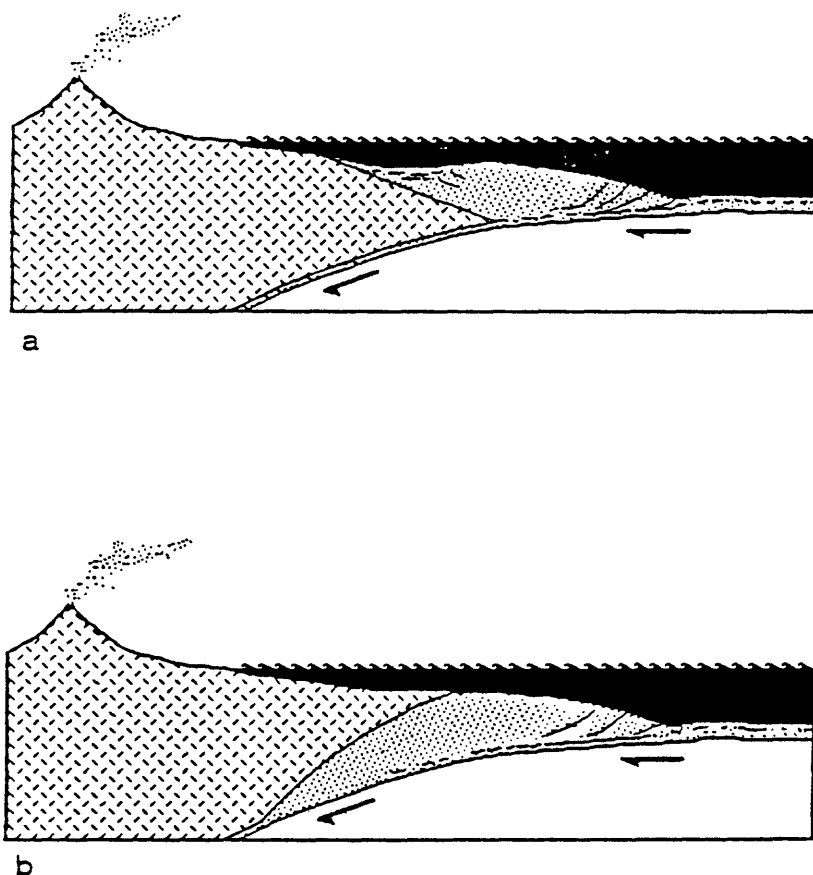


Fig. 13. Schematic illustration of two potential geometries for the **backstop** of forearc. Hatched region represents the stronger material of the overriding plate; dotted region, accreted and subducted sediments. Downgoing plate is in white. In top drawing the upper surface of the backstop dips trenchward beneath the accretionary wedge (stippled) while at bottom accretionary wedge dips arcward beneath backstop. In this paper we favor the upper, trenchward-dipping model for a number of the margins discussed in the text.

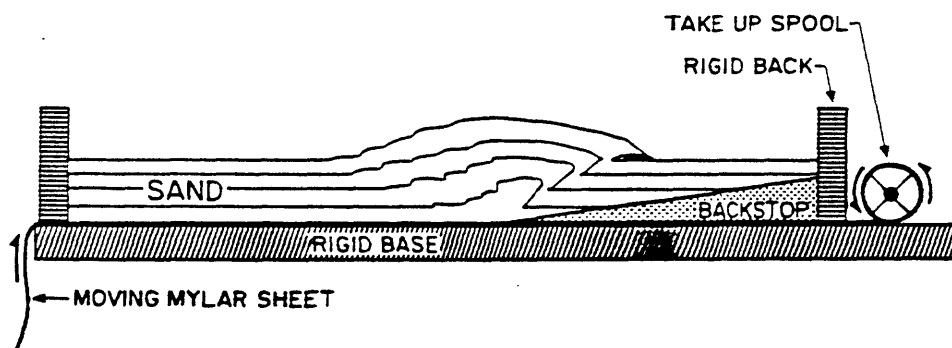


Fig. 14. Schematic diagram of laboratory sandbox model used to study the mechanical effects of a backstop within a forearc. Underlying Mylar sheet is pulled horizontally to right beneath originally flat-lying sand, backstop, and rigid ends of box (horizontal ruling) by the take-up spool, simulating motion along plate interface. Various geometries and materials were used for the backstop as described in the text.

A simple mechanical model with dry cohesionless sand was used to study the growth of forearcs with varying backstop configurations. The use of dry cohesionless sand as a modeling material has the advantage that, except for small dilatational effects, the behavior of the sand is independent of both time and length scales. The sandbox is an open-bottomed box with transparent side walls that is restrained against horizontal motion. A sheet of Mylar is placed between the box and the rigid base beneath it. A dipping backstop structure consisting of a material stronger than dry sand is placed on top of the Mylar and then the dry sand is added above it (Figure 14). Subduction is simulated by pulling the Mylar sheet horizontally under the box.

Experiments using a backstop with an upper surface dipping toward the incoming sand (trenchward) result in the development of a morphology highly reminiscent of many forearcs. A sequence of photographs of an experimental run using a wooden backstop (essentially infinite strength contrast) illustrates this development (Figure 15). The 'trenchward' tip of the backstop is a line of discontinuity both in the dip and in the velocity of the basement with respect to the sand. As convergence begins (Figure 15a), the sand above the tip of the backstop undergoes substantial uplift accommodated by both forward and backward dipping slip planes (Figure 15b). This results in the development of an outer-arc high centered over the intersection of the toe of the backstop and the moving Mylar sheet. At the same time a critically tapered wedge of sand develops in front of this high along trenchward verging slip planes or thrusts (Figure 15c). Further accretion of sand at the toe is accommodated by deformation along new slip planes that develop progressively farther trenchward. The topographic high grows with time and overthrusts the undeformed sand behind it along a narrow, arcward vergent shear zone (Figure 15c). Since the backstop material shields the sand above it from the movement of the Mylar sheet, that sand remains undeformed, resembling a forearc basin. The relative lack of slip along this backward vergent zone (compared to the total shortening in the accretionary wedge) causes it to act rather like a hinge as the greater slip on the trenchward side of the high, really a large pop-up feature, causes it to tilt away from the accretionary wedge (Figure 15d).

Modeling of cases in which the bulk of the accretionary wedge dips arcward beneath the backstop resulted in sand being underthrust beneath the backstop causing arcward rotation of the backstop. Such models do not produce a well-developed outer-arc high or forearc basin made up of sediment as is observed for most subduction zones.

Experiments such as those described above were conducted with a backstop made of wood, a material that has an essentially infinite-scaled strength compared to dry sand. The strength difference between actual materials of an accretionary wedge and backstop must be far less. To model the case of a smaller contrast in strength across a trenchward-dipping backstop, we used slightly dampened sand for the material of the backstop. Given the model length scale factor of

approximately  $10^5$ , the cohesive strength of the damp sand scales to nearly a kilobar, making it considerably stronger than the cohesionless dry sand above it.

In the experiments with wet sand (Figure 16a) the trenchward-dipping backstop itself is deformed and steepened during the early stages of convergence (Figure 16b). Because the backstop is not infinitely strong, a vertical column made up of just the toe of the backstop and dry sand does not have an integrated vertical strength sufficient to overcome the basal frictional resistance of the wedge trenchward of it. Thus the outer-arc high forms arcward of the toe of the backstop rather than directly above it (Figure 16c), and both dry and wet sand contribute to its formation through uplift along trenchward-dipping thrust faults. After the backstop is steep enough to be sufficiently strong, accretion steps out farther trenchward (Figure 16d). The passive region arcward of the high is similar to that observed in the wooden backstop experiments except that the backstop is involved in the thrusting at the arcward end of the high. The major differences between the infinite and finite strength contrast models are the arcward displacement of the high and the deformation within the backstop in the finite strength contrast model.

These simple laboratory models illustrate that a trenchward-dipping backstop that is stronger than the material above and trenchward of it is sufficient to account mechanically for the prominent forearc features commonly observed. Such a backstop also explains the distribution of forearc and plate boundary seismicity. Seismic activity would be expected to occur within the consolidated, lithified material of the backstop and along the plate boundary beneath it but not within the newer accreted sediments of the accretionary wedge and forearc basin or along the shallowest, sediment-lined part of the plate interface.

#### *Effect of Subduction of Massive Amounts of Sediment on the Seismogenic Zone*

In the southern Lesser Antilles, the Hikurangi subduction zone of New Zealand, the Makran margin of southern Iran and Pakistan, and the Cascadia subduction zone of North America few or no interplate thrust events are observed. These margins also all have large accretionary wedges with an abundance of young sediments. We think that the conditions favoring aseismic subduction beneath the accretionary wedge along the shallowest part of many subduction zones may persist to greater depths when sufficient amounts of young sediment are subducted, thereby decreasing the downdip width of the seismogenic zone. Given enough high-porosity sediment, it may be possible to reduce the width of the seismogenic zone to essentially zero, resulting in completely aseismic subduction [Byrne et al., 1987; Sykes et al., 1987].

#### CONCLUSIONS

An aseismic zone is observed at subduction zones along the shallowest part of the plate interface and in the overlying

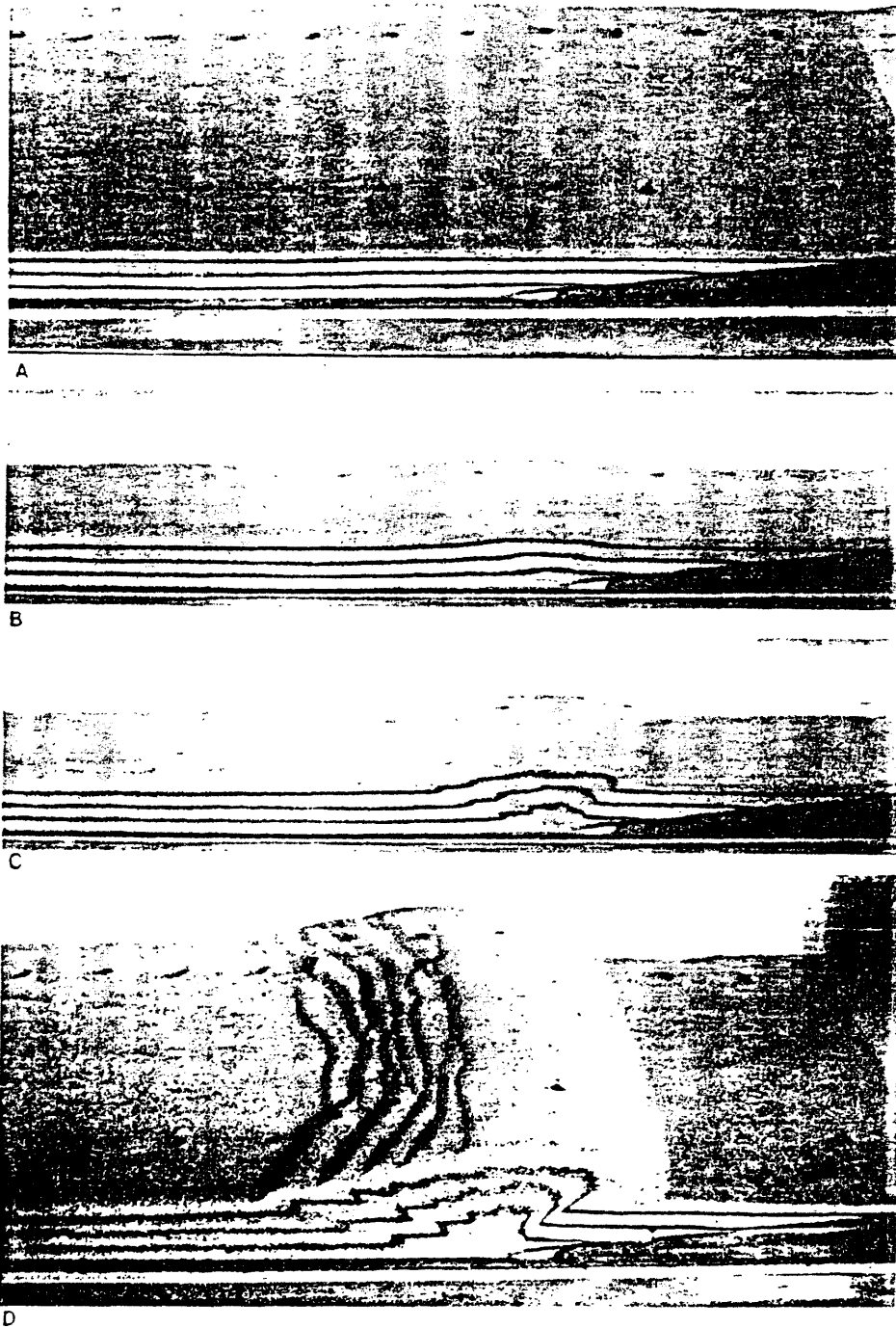
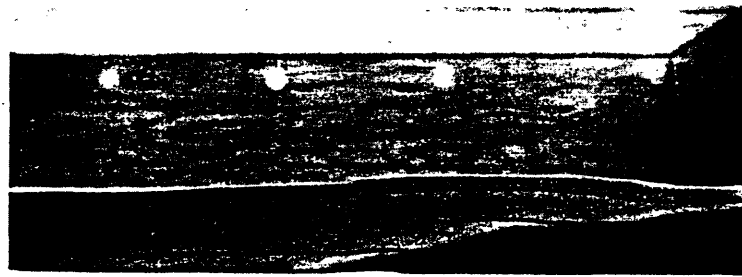


Fig. 15. Photographs of stages in deformation of sand during a run of the sandbox experiment. Configuration of experiments is the same as in Figure 14. Sand, undeformed and flat in the upper photograph, is increasingly compressed and deformed (subsequent pictures) until a crucial taper is attained in the accretionary wedge. Dark wedge in the lower right corner of each picture is composed of wood and simulates a backstop whose upper slope dips trenchward (to the left). Note that a topographic high develops over the toe of the backstop, and behind this high an undeformed region of sand remains, reminiscent of an outer-arc high/forearc basin pair. Black layers are passive marker beds.



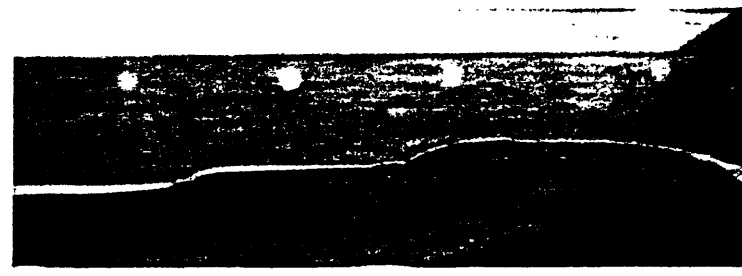
A



B



C



D

Fig. 16. Photographs of deformation in sand during an experiment run with a backstop of wet sand with a trenchward-dipping upper surface. Wet sand is intermediate in strength between dry sand and wood. Note that outer-arc high is located arcward (right of) the trenchward tip of the backstop and that deformation has occurred within the backstop itself. Otherwise, morphology is similar to that of Figure 15.

accretionary wedge. The shallowest part of the overriding plate at subduction zones is commonly composed of young, newly accreted and underplated sediments. Experimental work indicates that the slip properties of such unconsolidated material favor stable, aseismic slip. The aseismic zone is most likely caused by the presence of this unconsolidated sediment. In addition to the inherent slip properties of such material, the presence of elevated pore fluid pressure and, in some cases, an abundance of saturated marine clays, may also contribute to aseismic slip. The width of the aseismic zone is related to the abundance and state of sediments at any given margin, and may be quite large, exceeding several hundred kilometers in extreme cases. At the arcward end of the aseismic zone an onset of seismicity occurs, which we call the seismic front. The seismic front marks the transition between the shallow aseismic zone and the seismogenic zone that typically extends to greater depths along the plate interface.

The size of an earthquake is proportional to the area that it ruptures, and in subduction zones the size is very sensitive to the downdip width of the seismogenic zone,  $W$ . In fact, we argue that seismic moment is proportional to  $W$  to at least the third power. Because earthquake size is so sensitive to the width of the seismogenic zone, it is important to make accurate estimates of  $W$  when  $W$  is used to assess the seismic potential of regions. To that end, any estimate of the width of the seismogenic zone must not include the aseismic zone because that region does not contribute significantly to the seismic moment of large earthquakes. Previous studies that have made estimates of the seismic potential of various subduction zones based on parameters such as  $W$  have included the aseismic zone and have thus overestimated width and hence the maximum size of potential earthquakes and underestimated the average displacement, stress drop, and ratio of seismic to total slip,  $\alpha$ .

The distribution of seismicity within forearcs and along the plate interface is indicative of the distribution of material with unstable slip properties, and through inference, of the distribution of unconsolidated and semiconsolidated sediments. Information about the gross distribution of weaker sediments within forearcs is useful in modeling the mechanics of forearcs. We have used the critical taper wedge model of Davis et al. [1983] along with morphologic information and inferences about the distribution of relative material strength to develop a simple model for the growth and mechanics of forearcs. We are able to account for the development of major forearc features such as outer-arc highs and forearc basins through the presence of a body of stronger material within the forearc called the backstop. Laboratory modeling is also used to investigate the effects of backstop geometry and strength contrasts within the forearc on surface morphology. The model that is most consistent with the observed morphology of most forearcs uses a simple backstop whose upper surface dips trenchward, with its trenchward toe coming into contact with the subducting plate beneath the outer-arc high. Arcward of that point the stronger backstop supports the bulk of the

shear stress related to the convergence of the two plates, thus allowing weak sediments on top of the backstop, i.e., those of a forearc basin, to remain relatively undeformed (Figure 1). This model is oversimplified in that it does not consider the specific tectonic complexities of individual margins, but it is useful in illustrating how a backstop can produce an outer-arc high.

Basic observations about the distribution of seismicity in a number of subduction zones are therefore useful in understanding forearc mechanics and in the assessment of the seismic potential of subduction zones based on physical parameters such as the size of the rupture area of potential large earthquakes.

*Acknowledgments.* The authors thank R. Engdahl and C. Kisslinger for providing data on Aleutian earthquakes prior to publication, and J. Taber for furnishing data from the Shumagin Island network and for help with its analysis. We thank S. Kiorpes for assistance in the laboratory modeling, C. Marone for useful discussions of his experimental results, and J. Pacheco and C. Kisslinger for helpful discussions of this work. We also thank J. Beavan, N. Breen, M. Fisher, M. Marlow, C. Scholz and J. Taber for constructive reviews that greatly improved this manuscript. This work was supported by the National Science Foundation grants EAR 84-16635 (Lamont-Doherty Geological Observatory) and OCE 86-16894 (State University of New York at Stony Brook). Lamont-Doherty Geological Observatory contribution 4302.

## REFERENCES

- Abe, K., Reliable estimation of the seismic moment of large earthquakes, *J. Phys. Earth*, 23, 381-390, 1975.
- Aki, K., Earthquake mechanism, *Tectonophysics*, 13, 423-446, 1972.
- Aoki, Y., T. Tamano, and S. Kato, Detailed structure of the Nankai Trough from migrated seismic sections, *Am. Assoc. Pet. Geol.*, 34, 309-322, 1983.
- Astiz, L., and H. Kanamori, An earthquake doublet in Ometepec, Guerrero, Mexico, *Rhys. Earth Planet. Inter.*, 34, 24-45, 1984.
- Boyd, T. M., The Andreanof earthquake: Previous rupture history (abstract), *Eos Trans. AGU*, 67, 1082, 1986.
- Brandon, M. T., Comment on "Comments on the growth of accretionary wedges," *Geology*, 4, 184-185, 1986.
- Burk, C. A., Geology of the Alaska Peninsula - Island arc and continental margin, part 1, *Mem. Geol. Soc. Am.*, 99, 150 pp., 1965.
- Byerlee, J. D., and R. Summers, A note on the effect of fault gouge thickness on fault stability, *Int. J. Rock. Mech. Min. Sci.*, 13, 35-36, 1976.
- Byrne, D. E., L. R. Sykes, and D. M. Davis, Seismic and aseismic subduction, part 1, The role of young sediments in controlling the mode of slip along the plate boundary (abstract), *Eos Trans. AGU*, 44, 1468, 1987.

- Byrne, T., and J. Hibbard, Landward vergence in accretionary prisms: The role of the backstop and thermal history, *Geology*, *15*, 1163–1167, 1987.
- Chapple, W. M., Mechanics of thin-skinned fold-and-thrust belts, *Geol. Soc. Am. Bull.*, *89*, 1189–1198, 1978.
- Chen, A. T., The seismicity of forearc marginal wedges (accretionary prisms) and seismotectonics of convergent margins, Ph.D. dissertation, 151 pp., Univ. Texas at Dallas, 1981.
- Chen, A., C. Frolich, and G. Latham, Seismicity of the forearc marginal wedge (accretionary prism), *J. Geophys. Res.*, *87*, 3679–3690, 1982.
- Chinn, D. S., and B. L. Isacks, Accurate source depths and focal mechanisms of shallow earthquakes in western South America and in the New Hebrides island arc, *Tectonics*, *2*, 529–563, 1983.
- Chinnery, M. A., Theoretical fault models, *Publ. Dom. Obs. Ottawa*, *37*, 211–223, 1969.
- Cloos, M., Flow melanges: Numerical modeling and geologic constraints on their origin in the Franciscan subduction complex, California, *Geol. Soc. Am. Bull.*, *93*, 330–345, 1982.
- Dahlen, F. A., Noncohesive critical Coulomb wedges: an exact solution, *J. Geophys. Res.*, *89*, 10,125–10,133, 1984.
- Dahlen, F. A., J. Suppe, and D. Davis, Mechanics of fold-and-thrust belts and accretionary wedges: cohesive Coulomb theory, *J. Geophys. Res.*, *89*, 10,087–10,101, 1984.
- Davies, J. N., and L. House, Aleutian subduction zone seismicity, volcano-trench separation, and their relation to great thrust-type earthquakes, *J. Geophys. Res.*, *84*, 4583–4591, 1979.
- Davies, J., L. Sykes, L. House, and K. Jacob, Shumagin seismic gap, Alaska Peninsula: History of great earthquakes, tectonic setting, and evidence for high seismic potential, *J. Geophys. Res.*, *86*, 3821–3855, 1981.
- Davis, D., F. A. Dahlen, and J. Suppe, Mechanics of fold-and-thrust belts and accretionary wedges, *J. Geophys. Res.*, *88*, 1153–1172, 1983.
- Dieterich, J. H., Time dependent friction and the mechanics of stick-slip, *Pure Appl. Geophys.*, *116*, 790–806, 1978.
- Dieterich, J. D., Modeling of rock friction: 1. Experimental results and constitutive equations, *J. Geophys. Res.*, *84*, 2161–2168, 1979.
- Dieterich, J. H., Constitutive properties of faults with simulated gouge, in *Mechanical Behavior of Crustal Rocks*, *Geophys. Monogr. Ser.*, vol. 24, edited by N. L. Carter, M. Friedman, J. M. Logan, and D. W. Sterns, pp. 103–120, AGU, Washington D. C., 1981.
- Doser, D. L., and H. Kanamori, Depth of seismicity in the Imperial Valley region 1977–1983 and its relationship to heat flow, crustal structure, and the October 15, 1979 earthquake, *J. Geophys. Res.*, *91*, 675–688, 1986.
- Ekström, G., and E. R. Engdahl, Earthquake source parameters and stress distribution in the Adak Island region of the central Aleutian Islands (abstract), *Eos Trans. AGU*, *68*, 1352, 1987.
- Emerman, S., and D. Turcotte, A fluid model for the shape of accretionary wedges, *Earth Planet. Sci. Lett.*, *63*, 379–384, 1983.
- Engdahl, E. R., Seismicity and plate subduction in the central Aleutians, in *Island Arcs, Deep Sea Trenches, and Back-Arc Basins*, *Geophys. Monogr. Ser.*, vol. 1, edited by M. Talwani and W. C. Pitman, III, pp. 259–272, AGU, Washington, D. C., 1977.
- Engdahl, E. R., and D. Gubbins, Simultaneous travel-time inversion for earthquake location and subduction zone structure in the Central Aleutian Islands, *J. Geophys. Res.*, *92*, 13,855–13,862, 1987.
- Ernst, W. G., Tectonic contact between the Franciscan melange and the Great Valley sequence-crustal expression of a Late Mesozoic Benioff zone, *J. Geophys. Res.*, *75*, 886–901, 1970.
- Fisher, D., and T. Byrne, Structural evolution of underthrust sediments, Kodiak Islands, Alaska, *Tectonics*, *6*, 775–793, 1987.
- Frolich, C., S. Billington, E. R. Engdahl, and A. Malahoff, Detection and Location of Earthquakes in the Central Aleutian subduction zone using island and ocean bottom seismograph stations, *J. Geophys. Res.*, *87*, 6853–6864, 1982.
- Fuis, G. S., W. D. Mooney, J. H. Healy, G. A. Mehan, and W. J. Lutter, Crustal structure of the Imperial Valley region, The Imperial Valley, California, earthquake of October 15, 1979, *U.S. Geol. Surv. Prof. Pap.*, *1254*, 25–49, 1982.
- Hartzell, S., and D. Helmberger, Strong motion modeling of the Imperial Valley earthquake of 1979, *Bull. Seismol. Soc. Am.*, *72*, 571–596, 1982.
- Hasegawa, A., N. Umino, and A. Takagi, Fine structure of the deep-focus seismic planes in northeastern Japan (abstract) (in Japanese), *Annu. Meet. Seismol. Soc. Jpn.*, *1*, 17–18, 1976.
- Hayes, D. E., and S. D. Lewis, Structure and tectonics of the Manila trench system, western Luzon, Philippines, *Energy*, *10*, 263–279, 1985.
- Hirata, N., T. Yamada, H. Shimamura, H. Inatani, and K. Suyehiro, Spatial distribution of microearthquakes beneath the Japan Trench from ocean bottom seismographic observations, *Geophys. J. R. Astron. Soc.*, *73*, 653–669, 1983.
- Hirata, N., T. Kanazawa, K. Suyehiro, H. Shimamura, A seismicity gap beneath the inner wall of the Japan trench as derived by ocean bottom seismograph measurement, *Tectonophysics*, *112*, 193–209, 1985.
- House, L. S., and K. H. Jacob, Earthquakes, plate subduction, and stress reversals in the eastern Aleutian Arc, *J. Geophys. Res.*, *88*, 9347–9373, 1983.
- Kanamori, H., Great earthquakes at island arcs and the lithosphere, *Tectonophysics*, *12*, 187–198, 1971.
- Kanamori, H., The energy release in great earthquakes, *J. Geophys. Res.*, *82*, 2981–2987, 1977.
- Kanamori, H., and D. L. Anderson, Theoretical basis of some empirical relations in seismology, *Bull. Seismol. Soc. Am.*, *65*, 1073–1095, 1975.

- Karig, D. E., Evolution of arc systems in the western Pacific, *Annu. Rev. Earth Planet. Sci.*, 2, 51-75, 1974.
- Karig, D. E., Growth patterns on the upper trench slope, in *Island Arcs, Deep Sea Trenches, and Back-Arc Basins*, *Geophys. Monogr. Ser.*, vol. 1, edited by M. Talwani and W. C. Pitman, III, pp. 175-185, AGU, Washington, D. C., 1977.
- Karig, D. E., R. K. Cardwell, G. F. Moore, and D. G. Moore, Late Cenozoic subduction and continental margin truncation along the northern Middle America trench, *Geol. Soc. Am. Bull.*, 89, 265-276, 1978.
- Karig, D. E., M. B. Lawrence, G. F. Moore, and J. R. Curray, Structural framework of the forearc basin, N. W. Sumatra, *J. Geol. Soc. London*, 137, 77-91, 1980.
- Kawakatsu, H., and T. Seno, Triple seismic zone and the regional variation of seismicity along the northern Honshu arc, *J. Geophys. Res.*, 88, 4215-4230, 1983.
- Ladd, J. W., P. Buhl, and G. K. Westbrook, A seismic reflection section of an entire accretionary wedge: Barbados Ridge complex (abstract), *Eos Trans. AGU*, 67, 1217, 1986.
- LaForge, R., and E. R. Engdahl, Tectonic implications of seismicity in the Adak Canyon region, Central Aleutians, *Bull. Seismol. Soc. Am.*, 69, 1515-1532, 1979.
- Le Pichon, X., N. Lyberis, J. Angelier, and V. Renard, Strain distribution over the Eastern Mediterranean Ridge: A synthesis of new sea-beam data, *Tectonophysics*, 86, 243-274, 1982.
- Lewis, S. D., and D. E. Hayes, Forearc basin development along western Luzon, Philippines, *Energy*, 10, 281-296, 1985.
- Logan, J. M., N. Higgs, and M. Friedman, Laboratory studies on natural gouge from the U.S.G.S. Dry Lake No. 1 well, San Andreas fault zone, in *Mechanical Behavior of Crustal Rocks*, *Geophys. Monogr. Ser.*, vol. 24, edited by N. Carter, M. Friedman, J. Logan, and D. Sterns, pp. 121-134, AGU, Washington, D. C., 1981.
- Marone, C., and C. H. Scholz, The depth of seismic faulting and the upper transition from stable to unstable slip regimes, *Geophys. Res. Lett.*, in press, 1988.
- Marone, C., C. H. Scholz, and C. B. Raleigh, Constitutive modeling and frictional behavior of thick gouge layers, *Eos Trans. AGU*, 68, 1242, 1987.
- McCann, W. R., and R. Ryan, Seismic epicenters from local networks 1977-1981, in *Lesser Antilles Arc and Adjacent Terranes*, Atlas 10, Reg. Atlas Ser., Sheet 13, edited by R. C. Speed, G. K. Westbrook, and others, Ocean Margin Drilling Program, Marine Science International, Woods Hole, Mass., 1984.
- Mogi, K., Seismicity before and after large shallow earthquakes and their focal processes (abstract), *Gen. Assem. Int. Union Geol. Geophys. Abstr.*, 1, 343, 1987.
- Moore, J. C., and T. Byrne, Thickening of fault zones: A mechanism of melange formation in accreting sediments, *Geology*, 15, 1040-1043, 1987.
- Moore, J. C., B. Biju-Duval et al., Offscraping and underthrusting of sediment at the deformation front of the Barbados Ridge: Deep sea drilling project Leg 78A, *Geol. Soc. Am. Bull.*, 93, 1065-1077, 1982a.
- Moore, J. C., J. S. Watkins, T. H. Shipley, K. J. McMillen, S. B. Bachman, and N. Lundberg, Geology and tectonic evolution of a juvenile accretionary terrane along a truncated convergent margin: Synthesis of results from leg 66 of the Deep Sea Drilling Program, Southern Mexico, *Geol. Soc. Am. Bull.*, 93, 847-861, 1982b.
- Murauchi, S. and W. J. Ludwig, Crustal structure of the Japan Trench: The effect of subduction of ocean crust, Legs 56, 57, part 1, *Initial Rep. Deep Sea Drill. Proj.*, pp. 473-488, U. S. Govt. Print. Off., Washington, D. C., 1980.
- Nasu, N., et al., Multi-channel seismic reflection data across the Japan trench, *Int. Program Ocean Drill. Jpn. Basic Data ser.* 3, Ocean Res. Instit., Univ. of Tokyo, Japan, 1979.
- Peterson, E. T., and T. Seno, Factors affecting seismic moment release in subduction zones, *J. Geophys. Res.*, 89, 10,233-10,248, 1984.
- Quin, H., and J. Boatwright, Quasi dynamic faulting model for the October 15, 1979 Imperial Valley California earthquake (abstract), *Gen. Assem. Int. Union Geol. Geophys. Abstr.*, 1, 338, 1987.
- Reyners, M., and K. S. Coles, Fine structure of the dipping seismic zone and subduction mechanics in the Shumagin Islands, Alaska, *J. Geophys. Res.*, 87, 356-366, 1982.
- Robinson, R., Seismicity within a zone of plate convergence-The Wellington region, New Zealand, *Geophys. J. R. Astron. Soc.*, 55, 693-702, 1978.
- Robinson, R., Seismicity, structure and tectonics of the Wellington region, New Zealand, *Geophys. J. R. astr. Soc.*, 87, 379-409, 1986.
- Ruff, L., and H. Kanamori, Seismicity and the subduction process, *Phys. Earth Planet. Inter.*, 23, 240-252, 1980.
- Ruff, L., and H. Kanamori, Seismic coupling and uncoupling at subduction zones, *Tectonophysics*, 99, 99-117, 1983.
- Ruina, A., Slip instability and state variable friction laws, *J. Geophys. Res.*, 88, 10,359-10,370, 1983.
- Scherbaum, F., and C. Kisslinger, Variations of apparent stresses and stress drops prior to the earthquake of 6 May 1984 ( $m_b = 5.8$ ) in the Adak seismic zone, *Bull. Seismol. Soc. Am.*, 74, 2577-2592, 1984.
- Scholl, D. W., and H. F. Ryan, Crustal structure and evolution of the Aleutian forearc in the vicinity of the Andreanof earthquake (abstract), *Eos Trans. AGU*, 67, 1081, 1986.
- Scholz, C. H., The brittle-ductile transition and the depth of seismic faulting, *Geologische Rundschau*, in press, 1988.
- Silver, E. A., and D. L. Reed, Backthrusting in accretionary wedges, *J. Geophys. Res.*, 93, 3116-3126, 1988.
- Silver, E. A., R. McCaffrey, and R. B. Smith, Collision, rotation, and the initiation of subduction in the evolution of Sulawesi, Indonesia, *J. Geophys. Res.*, 88, 9407-9418, 1983.
- Silver, E. A., M. J. Ellis, N. A. Breen, and T. H. Shipley, Comments on the growth of accretionary wedges, *Geology*, 13, 6-9, 1985.
- Silver, E. A., N. A. Breen, M. J. Ellis, and T. H. Shipley,

- Reply on "Comments on the growth of accretionary wedges," *Geology*, *14*, 185–186, 1986.
- Singh, S. K., J. Havskov, K. McNally, L. Ponce, T. Hearn, and M. Vassiliou, The Oaxaca, Mexico, earthquake of 29 November 1978: A preliminary report on aftershocks, *Science*, *14*, 1211–1213, 1980.
- Stauder, W., Tensional character of earthquake foci beneath the Aleutian Trench with relation to seafloor spreading, *J. Geophys. Res.*, *73*, 7693–7701, 1968.
- Stein, S., J. F. Engeln, D. A. Wiens, K. Fujita, and R. C. Speed, Subduction seismicity and tectonics in the Lesser Antilles Arc, *J. Geophys. Res.*, *87*, 8642–8664, 1982.
- Stesky, R. M., Rock friction-effect of confining pressure, temperature, and pore pressure, *Pure Appl. Geophys.*, *116*, 690–704, 1978.
- Stewart, G. S., E. P. Chael, and K. C. McNally, The November 29, 1978, Oaxaca, Mexico, earthquake: A large simple event, *J. Geophys. Res.*, *86*, 5053–5060, 1981.
- Summers, R., and J. D. Byerlee, A note on the effect of fault gouge composition on the stability of frictional sliding, *Int. J. Rock Mech. Min. Sci.*, *14*, 155–160, 1977.
- Sykes, L. R., Aftershock zones of great earthquakes, seismicity gaps, and earthquake prediction for Alaska and the Aleutians, *J. Geophys. Res.*, *76*, 8021–8041, 1971.
- Sykes, L. R., and R. C. Quittmeyer, Repeat times of great earthquakes along simple plate boundaries, in *Earthquake Prediction: An International Review*, *Geophys. Monogr.*, Ser., vol. 4, edited by D. W. Simpson and P. G. Richards, pp. 217–247, AGU, Washington, D. C., 1981.
- Sykes, L. R., D. E. Byrne, and D. M. Davis, Seismic and aseismic subduction, part 2, Aseismic slip at zones of massive sediment supply and nature of great asperities at convergent margins (abstract), *Eos Trans. AGU*, *68*, 1468, 1987.
- Tse, S. T., and J. R. Rice, Crustal earthquake instability in relation to the depth variation of frictional slip properties, *J. Geophys. Res.*, *91*, 9452–9472, 1986.
- Tullis, T. E., and J. D. Weeks, Constitutive behavior and stability of frictional sliding of granite, *Pure Appl. Geophys.*, *124*, 383–414, 1986.
- Uyeda, S., and H. Kanamori, Back-arc opening and the mode of subduction, *J. Geophys. Res.*, *84*, 1049–1061, 1979.
- von Huene, R., Seismic images of modern convergent margin tectonic structure, *AAPG Studies In Geology*, vol. 26, Am. Assoc. Pet. Geol., 60 pp., 1986.
- von Huene, R. M., and H. Lee, The possible significance of pore fluid pressures in subduction zones, *Mem. Am. Assoc. Pet. Geol.*, *34*, 781–791, 1983.
- von Huene, R., M. Langseth, N. Nasu, and H. Okada, A summary of Cenozoic tectonic history along IPOD Japan Trench transect, *Geol. Soc. Am. Bull.*, *93*, 829–846, 1982.
- von Huene, R., E. Suess, and K. Emeis, Convergent tectonics and coastal upwelling: a history of the Peru continental margin, *Episodes*, *10*, 87–93, 1987.
- Ward, S. N., Body wave inversion: Moment tensors and depths of oceanic intraplate boundary earthquakes, *J. Geophys. Res.*, *88*, 9315–9330, 1983.
- Watanabe, T., M. G. Langseth, and R. N. Anderson, Heat flow in back-arc basins of the western Pacific, in *Island Arcs Deep Sea Trenches and Back-Arc Basins*, *Geophys. Monogr. Ser.*, vol. 1, edited by M. Talwani and W. C. Pitman, III, pp. 137–161, AGU, Washington, D. C., 1977.
- Watkins, J. S., K. J. McMillen, S. B. Bachman, T. H. Shipley, J. C. Moore, and C. Angevine, Tectonic synthesis, Leg 66: Transect and vicinity, *Initial Rep. Deep Sea Drill. Proj.*, *66*, pp. 837–849, U.S. Govt. Print. Off., Washington, D. C., 1982.
- Westbrook, G. K., The structure of the crust and upper mantle in the region of Barbados and the Lesser Antilles, *Geophys. J. R. Astron. Soc.*, *43*, 201–242, 1975.
- Westbrook, G. K., and M. J. Smith, Long decollements and mud volcanoes: Evidence from the Barbados Ridge complex for the role of high pore-fluid pressures in the development of an accretionary complex, *Geology*, *11*, 279–283, 1983.
- Westbrook, G. K., A. Mascle, and B. Biju-Duval, Geophysics and structure of the Lesser Antilles forearc, Leg 78A, *Initial Rep. Deep Sea Drill. Proj.*, pp. 23–48, U.S. Govt. Print. Off., Washington, D. C., 1984.
- Yoshii, T., A detailed cross-section of the deep seismic zone beneath northeastern Honshu, Japan, *Tectonophysics*, *55*, 349–360, 1979.
- Zhang, J., T.-F. Wong, and D. M. Davis, Failure modes as a function of porosity and effective pressure in porous sandstone (abstract), *Geol. Soc. Am. Abstr. Programs*, *19*, 901, 1987.
- Zhao, W.-L., D. Davis, F. A. Dahlen, and J. Suppe, The origin of convex accretionary wedges: Evidence from Barbados, *J. Geophys. Res.*, *91*, 10,246–10,258, 1986.
- Zoback, M. D., and C. M. Wentworth, Crustal studies in central California using an 800-channel seismic reflection recording system, in *Reflection Seismology: A Global Perspective*, *Geodyn. Ser.*, vol. 13, edited by M. Barazangi and L. Brown, pp. 183–196, AGU, Washington, D. C., 1986.

D. E. Byrne and L. R. Sykes, Lamont-Doherty Geological Observatory, Palisades, NY 10964.

D. M. Davis, Department of Earth and Space Sciences, State University of New York at Stony Brook, Stony Brook, NY 11794

(Received September 28, 1987;  
revised March 17, 1988;  
accepted March 28, 1988.)

## Seismic Activity in the Tokai Area, Central Japan

H.Aoki, F.Yamazaki, and T.Ooida (School of Science, Nagoya University, Nagoya, Japan, 464-01)

The seismic activity in the southern area is related with the subducting Philippine Sea (PHS) plate, whereas the activity in the northwest seems to occur within the upper crust. A relatively high activity in the lower crust is also recognized in some areas. In order to see these activities in more detail, epicenters of best determined events are classified according to the depth and shown in Figs. 1-3.

### 1. Sub-crustal activity

The majority of the events deeper than 30km seem to occur on a curved plane with a bend along a seismic belt extending NNW-SSE (Aoki, 1980). Yamazaki and Ooida (1984), adding new data, proposed a more complicated model for the plate, in which the subducted plate is divided into three slabs, (Tonankai (TN), Tokai (TK) and Suruga (SR) slabs) as shown by two chain lines in Fig.1. The boundary between SR and TK is a sharp bend, whereas the boundary between TK and TN is a big tear in the PHS plate. The bend or tear bears high potential to stop the rupture of great earthquake along the Nankai trough, along which seismic zoning was proposed by Utsu (1985). A more convincing evidence for the boundary is the east margin of the 1944 Tonankai earthquake constrained by revised data (Iwata and Hamada, 1986).

Subcrustal earthquakes do not spread northward but confined within an area shown by a dotted line in Fig.1. A sharp contrast of seismicity across the boundary may suggest the northern margin of the PHS plate, but it does not necessarily imply the lack of a sinking slab beyond the northern margin of the activity, as suggested by an extended H-V zone to the north of Izu peninsula (Ishida and Hasemi, 1988).

Another outstanding feature is the concentration of events within a narrow belt trending north and downward in the TK slab. The deepest point reaches 70km at the northern end. Focal mechanism solutions between normal and strike-slip faultings with tension axes nearly perpendicular to the belt are predominant. An offset of depth contour such as the one between TK and TN is not found at the seismic belt.

### 2. Seismic activity in the lower crust

Fig.2 shows a foci distribution at depths between 15 and 30km. Events in the lower crust are occurring in two areas: one is a triangle bounded by two tectonic lines (MTL and ISTL) and the Pacific coastline, and the other, a small area locating above the TK-TN boundary. Foci in the east area are shallow in the northwest, deepest near Shizuoka (S), where activity is high, and become shallow toward the Izu penin-

sula. Similar tendency is also recognized in the west area.

A cross section of foci distribution suggests that the eastern part beyond S is the shallow part of SR slab but the western side between S and MTL is an inclined seismic zone dipping toward the Suruga trough. A similar feature of focal depth variation is recognized not only in the west area but also in the Kii peninsula (ERI, 1987) and in Shikoku (Kochi Univ., 1988).

The focal mechanisms near MTL are characterized by an E-W compression, whereas an E-W extension predominates in the subducting plate. Various focal mechanisms are observed in S, where seismic activity has been steadily high. S might be a point of collision between two plates. There are two other seismic spots Y and H. Y is a seismic spot where events of  $M > 6$  occurred eight times in the last 100yr, though not uniform in time. The latest was an event of  $M = 6.0$  in 1983. Most of events shown at Y in Fig.2 are its aftershocks. The activity at H seems lower but more stable than at Y.

### 3. Seismic activity in the upper crust

Events at depths between 0-15km are shown in Fig.3. Shallow earthquakes are limited to the northwest of the Tokai area and in the Izu peninsula (some of the active spots in the central part are quarry blasts). Although many events have been registered, the activity seems not stable in terms of a historical time span, since most of them are aftershocks of remarkable earthquakes. It is important to eliminate or predict aftershock activity in order to find abnormal seismic activity prior to a great earthquake.

Recent shallow earthquakes of  $M > 6.5$  in the northwestern area of MTL are the 1891 Nobi ( $M = 8.0$ ), 1945 Mikawa ( $M = 6.8$ ), 1961 Kitamino ( $M = 7.0$ ), 1969 Gifu-ken-chubu ( $M = 6.6$ ), and the 1984 Nagao-ken-seibu ( $M = 6.8$ ) earthquakes. The biggest cluster of events in the figure is the aftershock activity of the 1984 event. Other aftershocks are shown by N, M, K, and G.

The 1891 Nobi earthquake: The aftershock sequence during 30yr was given by the rate of felt earthquake at Gifu (Utsu, 1961). Considering the relative location of Gifu, we estimated the average lower limit of magnitude as 3 for felt earthquakes.

The present activity is estimated as 0.03/day for  $M > 2$ . Assuming  $b = 0.9$ , the rate for  $M > 3$  is estimated as 0.004/day, which indicates a slightly lower level than expected from the data during first 30 yr.

The 1945 Mikawa earthquake: The rate of recorded aftershocks during 200 days were reported by Utsu (1961). The average lower limit of magnitude is estimated as 2.8 from the number of events whose magnitudes are known. Present activity for  $M > 2$  is 0.02/day, which implies a normal decay.

The 1969 Gifu-ken-chubu earthquake: Aftershocks recorded by a sensitive seismograph at Inuyama (Aoki, 1970) are available. Assuming that any event of similar size can be located by the

## MADE FROM BEST AVAILABLE COPY

present seismic network, yearly numbers of events are directly compared with the past data. The present activity is normal.

Thus shallow activity in the northwest area seems mainly consists of aftershocks of past remarkable earthquakes, except for the area shown on the left margin of Fig.3, where a number of events, though small in magnitude, were located along a remarkable active fault system (Isshi F.S.) striking NS and also on a belt trending towards the Mikawa aftershock area. No historic great-earthquake has been reported in this area. It reaches the subducting plate in a similar manner as mentioned above. Both activities are likely constrained by tectonic lines or large-scale faults.

#### 4. Foreshock activities prior to induced earthquakes

The 1945 Mikawa earthquake occurred 35 days after the 1944 Tonankai earthquake (M=7.9) near the northwest corner of the 1944 rupture. According to Iwata and Hamada (1986), spreading of aftershocks or induced earthquakes were recognized not only in the middle of Shizuoka prefecture but also in the area around the southern Izu peninsula and inland area of central Honshu. The 1945 event, the greatest among the induced earthquakes, is known as a typical case of foreshock activity. The roar of ground began to occur from two days before the mainshock. Several shocks could be recognized as foreshocks, because most of aftershocks concentrated in an area west of Mikawa but few in the Mikawa area. The 1984 Nagano-ken-seibu earthquake induced two events outside of the mainshock area. An event of M=6.2 occurred 24 hr after the mainshock to the west and preceded by foreshocks from 2 hr before the event. Another event of M=5.3 occurred 18 days after the mainshock to the east. Foreshocks began to occur within 13 hr and increased in number 3 hr before the event.

The common features between these induced earthquakes are 1) lack of foreshock activity prior to mainshock, and 2) the occurrence of event near the tip of main fault. These features are consistent with the results from rock failure experiments in laboratory. According to Mizutani et al.(1985), acoustic emission (AE) rate is very high for a high strain-rate experiment, compared with those for a low strain-rate experiment. If the data from laboratory experiment are extrapolated to a natural strain rate, the difference between the failure strength and AE threshold stress is so small that the main failure might occur without appreciable AE. Very low strain-rate in the nature may be one of the reasons why foreshocks are hardly observed in nature.

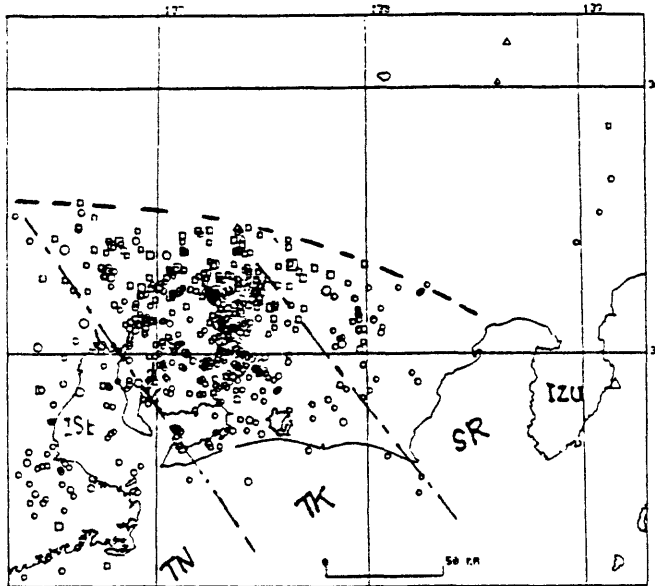
If this is the case for a main shock, we can expect a high probability of foreshock activity for the induced earthquake which is the most likely result of the rapid strain increase due to the main shock.

References

- Aoki, H., 1980, Proc. Earthq. Predic. Res. Symp. (1980), 97-102.  
 Aoki, H. et al., 1970, Bull. Earthq. Res. Inst. 48, 1181-1195  
 E.R.I., 1987, Rep. Cord. Com. Earthq. Predic. 37, 311-319  
 Ishida, M. and A.H. Hasemi, 1988, JGR, 93, 2076-2094  
 Iwata, T. and N. Hamada, 1986, Zisin, 39, 621-634  
 Kochi Univ., 1988, Rep. Cord. Com. Earthq. Predic.  
 Mizutani, H. et al., 1985; Earthq. Predic. Res. 3, 595-605  
 Yamazaki, F and T. Ooida, 1985, Zisin, 38, 183-192  
 Utsu, T., 1961, Geophys. Mag., 30, 521-605  
 Utsu, T., 1985, Chikyu, 7, 156-158

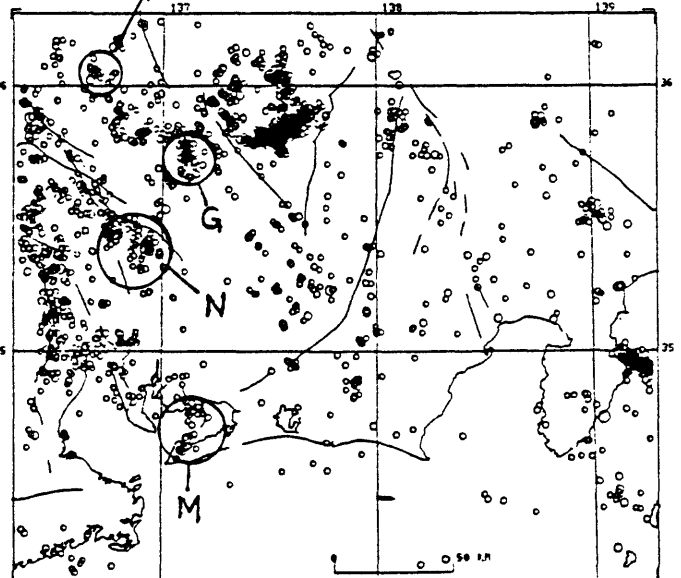
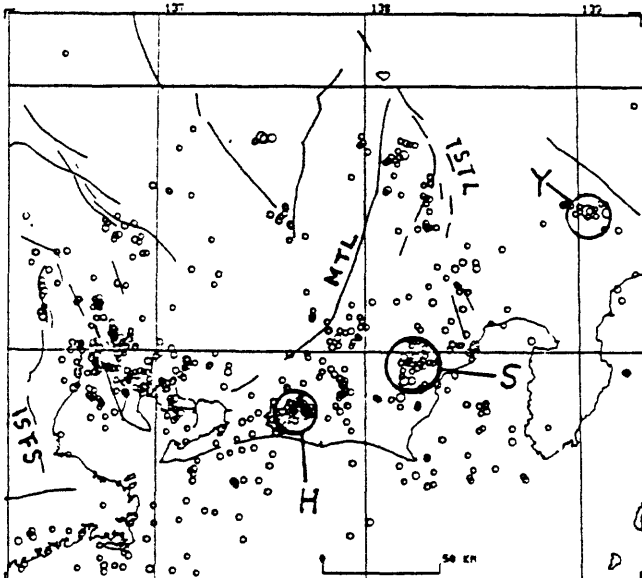
78 5 1 - 88 5 1

STDU < .10



Earthquake epicenters  
 May 1978 - Apr 1988  
 Magnitude > 2  
 Weighted mean residual of  
 travel time (P & S) < 0.1s.  
 ISTL; Itoigawa-Shizuoka Tec-  
 tonic Line, MTL; Median Tec-  
 tonic Line, ISFS; Isshi  
 Fault System.

- ← Fig.1 (depth; 30-80km)  
 ↙ Fig.2 (depth; 15-30km)  
 ↓ Fig.3 (depth; 0-15km)



## Recent Progress of Electromagnetic Studies for the Earthquake Prediction in Japan

Takesi Yukutake (Earthquake Research Institute, University of Tokyo, Tokyo)

In Japan the electromagnetic study for the earthquake prediction has been pushed forward mainly along two lines. One is geoelectric, and the other is geomagnetic. Geoelectric study includes studies of resistivity and electrical potential of the earth, and the geomagnetic those of magnetic structure and its time variation. There are some others which are not classified into these categories, such as electromagnetic wave emission. In this paper studies of the geoelectrical aspects will be described.

In association with an earthquake that took place in the central part of the Yamasaki fault on May 30, 1984, several kinds of electromagnetic phenomena were observed, changes in the resistivity, the electric potential differences and the magnetic field. Some are believed to be caused by movement of groundwater through the fault.

However, it is not known how the groundwater flows through the fault at the time of an earthquake. Since the electrical resistivity highly depends on the distribution of water, recent efforts have been concentrated on the study of the resistivity structure of the crust. Many faults are characterized by low resistivity. Some parts of the lower crust are confirmed to be low resistive, coincident with regions of aseismicity in the lower crust. The subducting oceanic plate has been found to have a thin low resistivity layer at its top surface, which is supposed to be caused by high water content.

Role of fluid in the deep crust is not well known. Clarification of detailed structures near the interface between high and low resistivity layers in the crust will be a task for the coming several years.

### 1. Electromagnetic phenomena observed before and after the earthquake in the central part of the Yamasaki fault on May 30, 1984

Located in the western part of Japan, the Yamasaki fault is a fault that has been most extensively investigated as a test site for the earthquake prediction. Several types of geomagnetic and geoelectric instruments are deployed in this area. On May 30, 1984, an earthquake of M 5.6 took place at a depth of about 17 km below the fault near its center.

Across the fault the electrical potential differences are being measured in a vault [Miyakoshi, 1986]. A notable change was observed for the electrode pairs of 34.4m separation. As shown in Fig. 1 by E-1, the change started about 55 hours preceding the earthquake, and recovered to the normal level 13 hours after the earthquake. Miyakoshi (1986) considers that this precursory change is likely due to an electrokinetic origin called streaming potential that was induced by movement of groundwater through the fractured zone along the fault.

It is widely known that the electrical potential at the earth's surface is often influenced by rainfall. Actually significant changes were observed in the potential difference across the fault at the time of rainfall as shown in Fig. 2, but there was no rainfall to be related to the precursory change [Miyakoshi,1986]. One thing to be noted is, however, that such close relationship to rainfall is observed only during the period of about two months before the earthquake occurrence. No clear changes were recognized before in association with rainfall.

Change in the electrical resistivity was remarkable. The resistivity is being measured by a direct current method with Schlumberger electrode arrangements in two directions, one in parallel with the fault and the other orthogonal to it [Sumitomo and Noritomi, 1986]. Measurement along the fault showed a conspicuous variation as in Fig. 3. The apparent resistivity increased from about 300 ohm.m to 1500 ohm.m after the earthquake. Although not so large, there was a significant change before the earthquake. Figure 4 shows that the apparent resistivity began to decrease about 70 days before the earthquake and reached a minimum around 30 days before. The decrement was about 30 percent of the original resistivity. Sumitomo and Noritomi (1986) attempt to explain this change by resistivity change of the outer part of the fault fractured zone.

It is noted that some of the anomalous changes mentioned above started about two months before the earthquake, resistivity change, change of relationship between the electric potential and rainfall. They are likely to be related to movement of groundwater. This seems to suggest that groundwater began to flow at some depths in the fault area two months preceding the earthquake.

## 2. Resistivity structure of the crust

It is not known, however, how the groundwater flows through the fault at the time of an earthquake. Many faults are known to have low resistivity zones along the faults, which are supposed to be caused by high water content of fractured rocks in the fault area [Research Group for Active Fault, 1982]. This implies that the fault can act as a water conduit. However it is not yet clarified to what depth the low resistivity nature of the fault extends. Considerable efforts are now concentrated on investigation of the resistivity structure of the crust.

Studies of the resistivity structure of the Japan island have been conducted under cooperative projects between universities and government institutions. The results so far obtained strongly suggest existence of low resistivity region in the lower crust [Research Group for Resistivity Structure, Japan, 1983; Yukutake, 1985; Ogawa et al., 1986; Utada et al., 1986]. Figure 5 shows a profile of the resistivity structure across the Japanese island arc in the Northeast Japan [Utada, 1987]. Low resistivity region extends in the lower crust from the aseismic front toward inland. The low resistivity is likely to be caused by fluids in the deep crust, and related to aseismicity of the lower crust.

Existence of a thin low resistivity layer has been also found at the

top of the subducting oceanic plate (Fig. 5). This is again considered to be caused by high water content. Consequently it is not unreasonable to suppose that at the time of an inter-plate earthquake considerable amount of water is squeezed out through this layer. Then electromagnetic changes like electric potential and resistivity would be expected if the measurements are conducted on the ocean floor.

### 3. Future programs

Although some of the low resistivity nature of the lower crust has been revealed, there are many things to be solved, such as what is the shape of the boundary between the resistive and the conductive crust, whether the low resistivity region along the fault reaches this layer or not. Since most of the large earthquakes occurs in the upper crust close to the upper and lower crust boundary, it seems highly important to clarify the resistivity structure near the boundary, and for the earthquake prediction particularly important to examine its time variation. Investigation of near-boundary structure is attempted by use of artificial as well as natural sources.

For prediction of the inter-plate earthquakes below the Japan island, it seems urgent to begin the ocean floor observation of the electric potential and the magnetic field. It is also important to develop techniques to measure the resistivity continuously of a shallower part of the oceanic crust.

### References

- Electromagnetic Research Group for the Active Fault, Low electrical resistivity along an active fault, the Yamasaki fault, J. Geomag. Geoelectr., 34, 103-127, 1982.
- Miyakoshi, J., Anomalous time variation of the self-potential in the fractured zone of an active fault preceding the earthquake occurrence, J. Geomag. Geoelectr., 38, 1015-1030, 1986.
- Ogawa, Y., T. Yukutake and H. Utada, Two dimensional modelling of resistivity structure beneath the Tohoku District, Northern Honshu of Japan, by a finite element method, J. Geomag. Geoelectr., 38, 45-79, 1986.
- Research Group for Crustal Resistivity Structure, Japan, Preliminary report on a study of resistivity structure beneath the Northern Honsyu of Japan, J. Geomag. Geoelectr., 35, 589-608, 1983.
- Sumitomo, N. and K. Noritomi, Synchronous precursors in the electrical earth resistivity and the geomagnetic field in relation to an earthquake near the Yamasaki fault, Southwest Japan, J. Geomag. Geoelectr., 38, 971-989, 1986.
- Yukutake, T., A review of studies on the electrical resistivity structure of the crust in Japan, Earthq. Pred. Res., 3, 345-356, 1985.
- Utada, H., Y. Hamano and T. Yukutake, A two-dimensional conductivity model across Central Japan, J. Geomag. Geoelectr., 38, 447-473, 1986.
- Utada, H., A direct inversion method for two-dimensional modeling in the geomagnetic induction problem, Dr. Sc. Thesis, Univ. Tokyo, 1987.

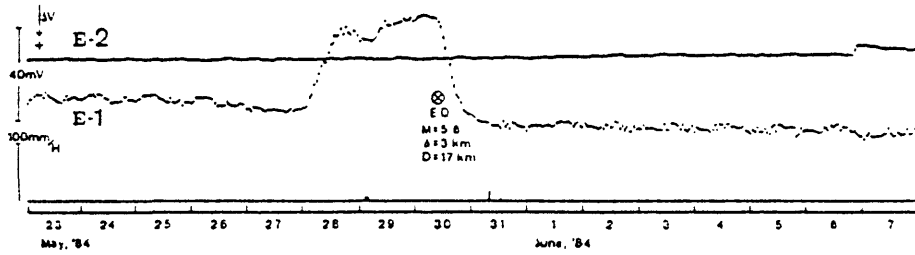


Fig. 1 Changes in the electric potential difference across the Yamasaki fault. E-1: Potential difference for the longer electrode separation, 34.4m. E-2: Potential difference for the shorter electrode separation, 23.0m. A precursory change started about 55 hours before the earthquake for E-1, whereas no remarkable change was recognized for E-2. Precipitation is plotted at the bottom. [Miyakoshi, 1986]

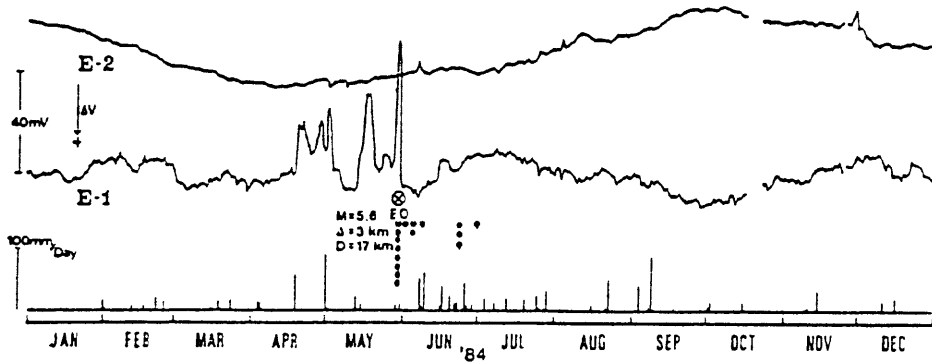


Fig. 2 Changes in the electric potential difference across the Yamasaki fault. Large changes have become to be observed since two months before the earthquake. Precipitation is plotted at the bottom. [Miyakoshi, 1986]

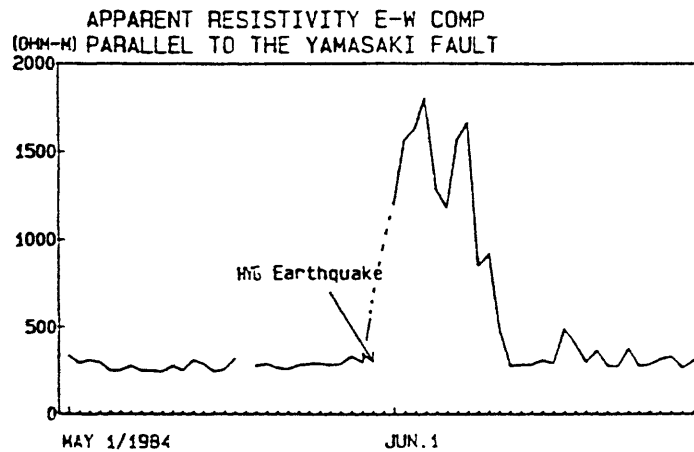


Fig. 3 Change in apparent resistivity obtained by a direct current method with electrodes aligned along the Yamasaki fault by Schlumberger arrangements. [Sumitomo and Noritomi, 1986]

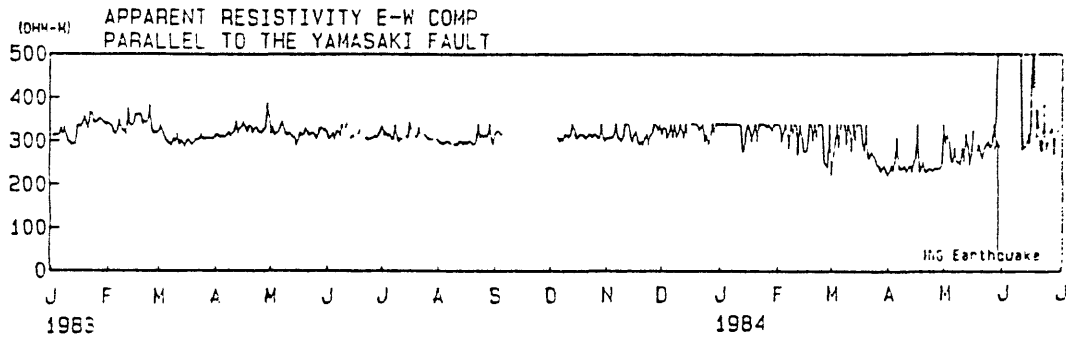


Fig. 4 Change in apparent resistivity before the earthquake. The resistivity started to decrease about 70 days preceding the earthquake. [Sumitomo and Noritomi, 1986]

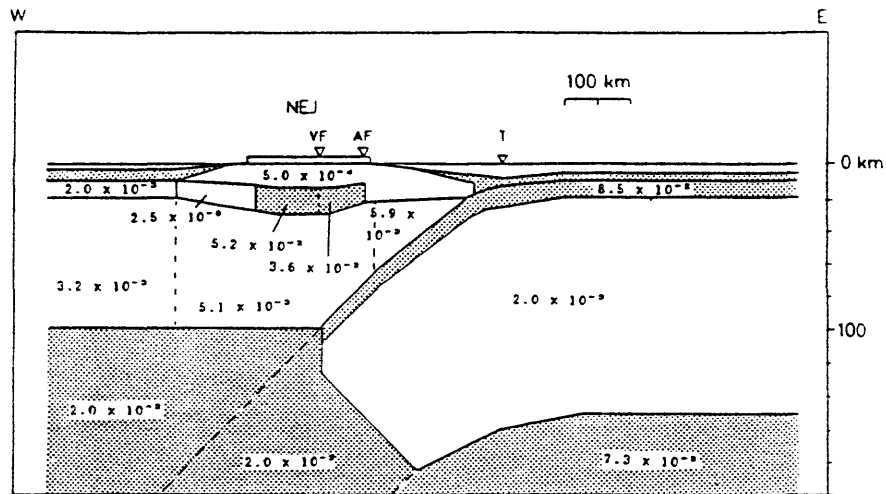


Fig. 5 Conductivity structure across the Japanese island arc in the Northeast Japan. Conductivity is given in the unit of S/m, which is inverse of resistivity (ohm.m). [Utada, 1987] The lower crust to the west of the aseismic front (AF) is conducting (low resistivity). VF denotes volcanic front, and T trench.

A thin conducting layer exists at the top of the subducting oceanic plate.

## PARKFIELD, CALIFORNIA EARTHQUAKE PREDICTION EXPERIMENT - A STATUS REPORT

BAKUN, W. H., U.S. Geological Survey - 345 Middlefield Rd.,  
MS 977, Menlo Park, CA. 94025

In 1985 the U.S. Geological Survey (USGS) issued a long-term prediction for an earthquake of about magnitude 6 to occur before 1993 on the Parkfield section of the San Andreas fault in central California. The rationale for the long-term prediction is outlined in Bakun and McEvelly (1984) and Bakun and Lindh (1985).

The prototype earthquake prediction experiment now in operation near Parkfield is designed to document the details of the final stages of the earthquake generation process. The design of the prototype prediction experiment is largely based on observations and accounts of historic Parkfield earthquakes, particularly the most recent shock on June 28, 1966. Foreshocks in 1966 and in the June 1934 sequence, as well as the main shocks in 1934 and 1966, were located beneath Middle Mtn. in the earthquake preparation zone at the northwest end of the rupture zone; monitoring of seismicity within the preparation zone is an important element of the prediction experiment. An irrigation pipeline that crosses the rupture zone broke and separated 9 hours before the 1966 main shock, and fresh en echelon cracks were observed near the center of the rupture zone 12 days before the 1966 main shock by Japanese seismologists visiting the Parkfield area as part of the Second US-Japan Earthquake Prediction Research Seminar. The broken irrigation pipeline and the observations of fresh cracks along the fault trace suggest significant precursory fault creep in 1966, and are a basis for detailed monitoring of crustal deformation along the Parkfield section of the San Andreas fault.

The prediction experiment includes active and passive borehole and surface seismic monitoring networks, creepmeters, a two-color laser geodimeter network, borehole volumetric and tensor strainmeters, borehole water level, geochemistry, and precision temperature measurements, tiltmeters, magnetic and electrical resistivity sensors, a radio frequency monitor, and leveling, alignment and geodimeter surveys (see Figure 1). The instrumentation is described in detail by Bakun et al. (1987).

The USGS, the Governor of California's Office of Emergency Services, the affected counties in central California and local officials have developed coordinated earthquake prediction response plans that will be implemented if the USGS issues a short-term prediction (see Bakun et al., 1987). Any short-term predictions will be based on a set of predetermined thresholds of unusual tectonic conditions detected by the geophysical networks listed above. Information material has been prepared and distributed to residents in areas near Parkfield likely to be affected by the predicted earthquake (see Figure 2).

### References

Bakun, W. H., and T. V. McEvelly, 1984, Recurrence models and Parkfield, California, earthquakes, *Journal of Geophysical Research*, vol. 89, pp. 3051-3058.

Bakun, W. H., and A. G. Lindh, 1985, The Parkfield, California, earthquake prediction experiment, *Science*, vol. 229, pp. 619-624.

Bakun, W. H., K. S. Breckenridge, J. Bredehoeft, R. O. Burford, W. L. Ellsworth, M. J. S. Johnston, L. Jones, A. G. Lindh, C. Mortensen, R. J. Mueller, C. M. Poley, E. Roeloffs, S. Schulz, P. Segall, and W. Thatcher, 1987, Parkfield, California earthquake prediction scenarios and response plans, U.S. Geological Survey Open-File Report 87-192, 45 pp.

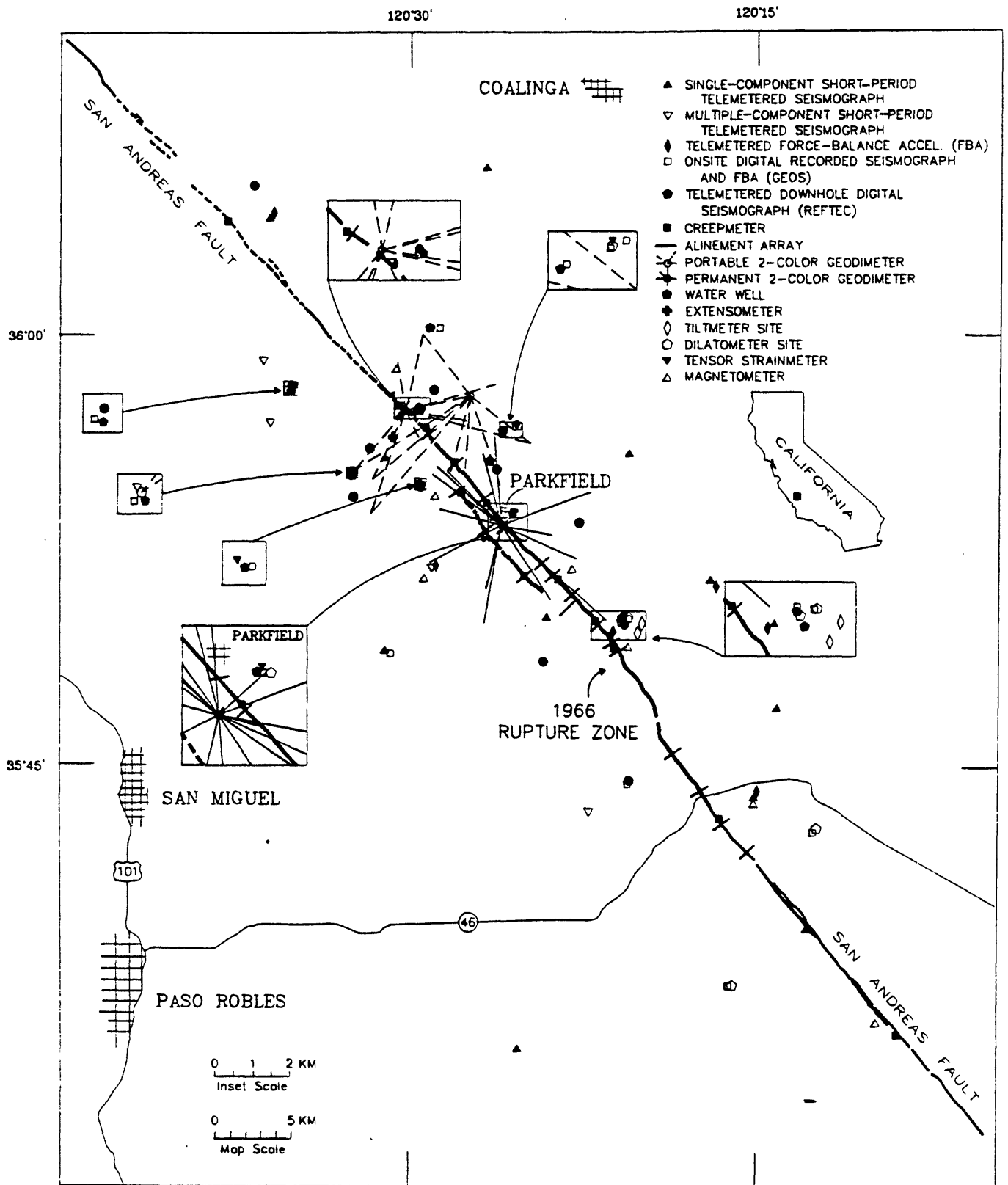
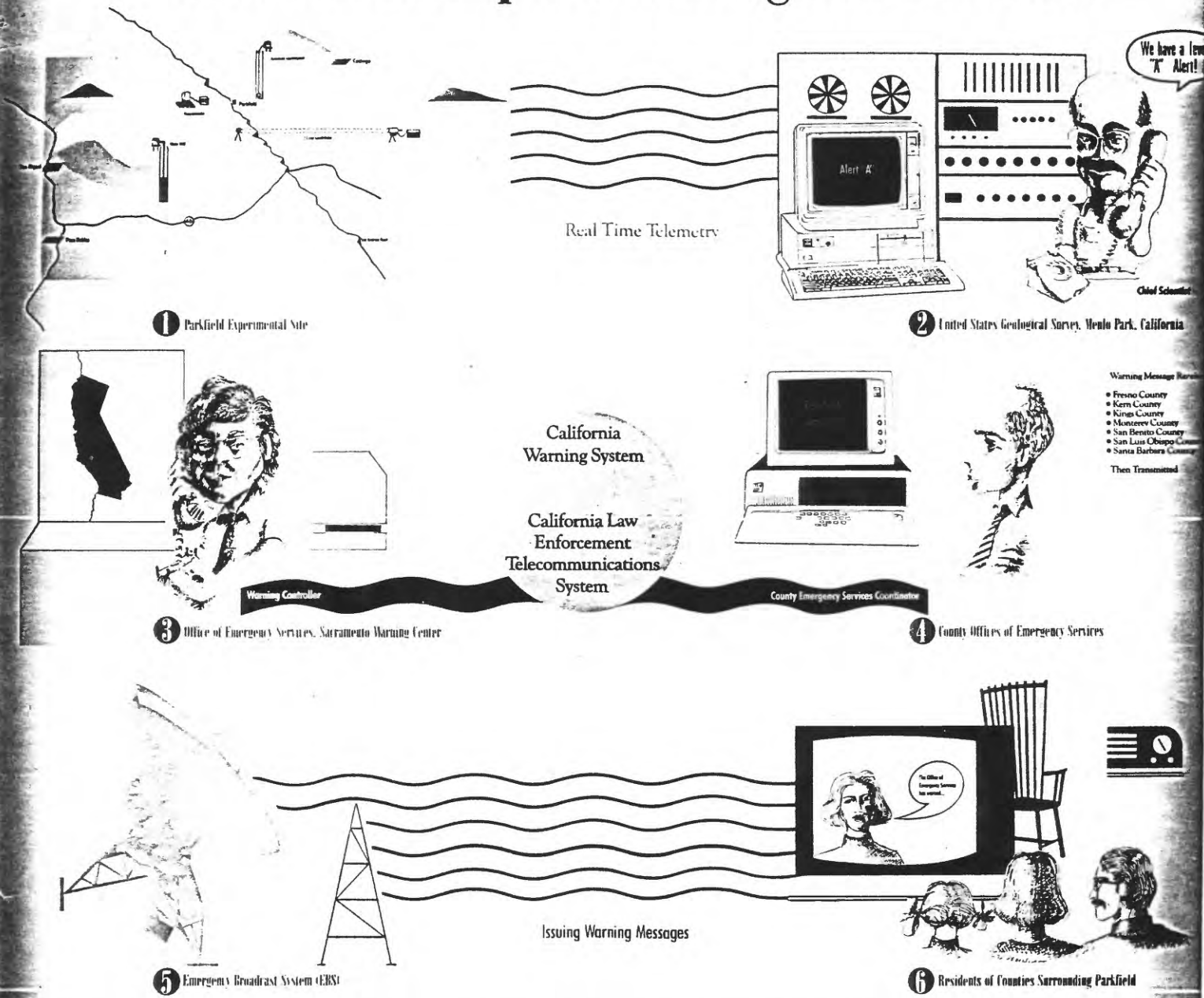


Figure 1. Locations of sensors in the prototype earthquake prediction experiment near Parkfield, CA.

# How The Earthquake Warning Will Be Issued



## How The Region Could Be Affected Intensity



- MODIFIED MERCALLI INTENSITY SCALE
- 0 III Damage slight in specially designed structures; considerable in ordinary substantial buildings with partial collapse; great in poorly built structures. Panel walls thrown out of frame structures. Fall of chimneys, factory stacks, columns, monuments, walls. Heavy furniture overturned. Sand and mud ejected in small amounts. Changes in the condition of well water.
  - I Felt by nearly everyone; many awakened. Some dishes, windows, etc., broken; a few instances of cracked plaster; unstable objects overturned. Disturbance of trees, poles, and other tall objects sometimes noticed. Pendulum clocks may stop.
  - II During the day felt indoors by many, outdoors by few. At night some awakened. Dishes, windows, doors, etc., cracked; cracking heard from walls. Parked cars rattle noticeably.
  - III Felt quite noticeably indoors, especially on the upper floors of buildings, but many people do not recognize it as an earthquake. Parked cars may rock slightly.
  - IV Not felt except by a few under especially favorable circumstances. Delicately suspended objects may swing.
  - V Felt by all. Some heavy furniture moved; a few instances of fallen plaster or damaged chimneys. Damage slight.
  - VI Damage slight to moderate in well-built ordinary structures; considerable in poorly built or badly designed structures; some chimneys broken. Noticed by persons driving motor cars.
  - VII Damage negligible in buildings of good design and construction; slight to moderate in well-built ordinary structures; considerable in poorly built or badly designed structures; some chimneys broken.
  - VIII Damage slight in specially designed structures; considerable in ordinary substantial buildings with partial collapse; great in poorly built structures. Panel walls thrown out of frame structures. Fall of chimneys, factory stacks, columns, monuments, walls. Heavy furniture overturned. Sand and mud ejected in small amounts. Changes in the condition of well water.
  - IX Damage considerable in specially designed structures; great in ordinary substantial buildings with partial collapse; very great in poorly built structures. Fall of chimneys, factory stacks, columns, monuments, walls. Heavy furniture overturned. Sand and mud ejected in small amounts. Changes in the condition of well water.
  - X Damage great in specially designed structures; complete in ordinary substantial buildings with partial collapse; very great in poorly built structures. Fall of chimneys, factory stacks, columns, monuments, walls. Heavy furniture overturned. Sand and mud ejected in small amounts. Changes in the condition of well water.
  - XI Damage very great in specially designed structures; complete in ordinary substantial buildings with partial collapse; very great in poorly built structures. Fall of chimneys, factory stacks, columns, monuments, walls. Heavy furniture overturned. Sand and mud ejected in small amounts. Changes in the condition of well water.
  - XII Damage complete in specially designed structures; complete in ordinary substantial buildings with partial collapse; very great in poorly built structures. Fall of chimneys, factory stacks, columns, monuments, walls. Heavy furniture overturned. Sand and mud ejected in small amounts. Changes in the condition of well water.



Figure 2. A 4:1 reduction of part of "The California Earthquake Prediction", a multicolor foldout information brochure mailed in May 1988 by the Governor of California's office of Emergency Services to 122,000 residences in Monterey Co., San Benito Co., Fresno Co., San Luis Obispo Co., and Kings Co., and Kern Co., California.

FN:classify

## CLASSIFICATION OF EARTHQUAKE PRECURSORS AND REGULARITY OF PRECURSOR APPEARANCE

Kazuo Hamada

National Research Center for Disaster Prevention  
Tsukuba Science City, 305 Japan

Abstract. A total of 750 precursory phenomena to earthquakes occurring in and around Japan were collected from literature. These phenomena are grouped into 40 items from many disciplines, such as geodesy, seismology, geo-electromagnetism, geo-chemistry and others. These items were classified into two categories according to their precursor times( $T_p$ ), which were defined as the time length from the commencement of the precursory phenomenon to the main shock, and the categories were labeled short-term precursors and long-term precursors. The short-term precursors included foreshocks, all kinds of anomalies detected by instruments for continuous measurements of crustal movement, most anomalies of geo-electromagnetism such as earth current, resistivity, and radio wave emission. They were clearly separated from the long-term precursors in terms of the frequency-distribution pattern with respect to  $T_p$ .

From the analysis of the frequencies of all the short-term precursors with  $T_p$ , the following probability density function( $P_d$ ) of  $T_p$  was derived:

$$\log P_d(T_p) = a - b \cdot \log T_p$$

$$a: \text{const.}, b = 0.926, 0.1 \leq T_p \leq 40 \text{ days.}$$

Approximately 50 % of  $T_p$  for short-term precursors are less than 3 days and 90 % of them are less than 30 days.

Comparing and discussing this formula with the empirical formula of probability( $\mu$ ) of fracture occurrence in rock with respect to applied stress( $\sigma$ ) by Mogi, the following relationship was derived, when  $P_d$  was assumed to be  $\mu$ :

$$\log P_d = A' + B' \sigma$$

$$\sigma = A'' - B'' \log T_p$$

$$A', A'', B', B'': \text{const.}$$

Such a relationship probably holds in the source region during a short period of time, approximately 40 days prior to the main shock.

### Introduction

A number of precursory phenomena to earthquakes which occurred in and around Japan were collected from literature. The collected precursors, which are probably the real precursors in the strictest sense, are complicated in terms of the way they appear. There seems to be no deterministic precursors so far. Therefore, a probabilistic approach based on observational facts seems to be the most practical way to predict earthquakes for the time being.

The collected precursors were classified into either short-term or long-term ones by each item, according to the precursor time( $T_p$ ) which is defined as the time interval from the commencement of the precursor to the mainshock. Then the frequency distribution of the short-term precursors with respect to the precursor time( $T_p$ ) was investigated from a macroscopic view point, where a variety of precursors in different items to different

earthquakes were treated together. Consequently, experimental probability density function(Pd) and distribution function(Pc) with respect to the Tp were derived for all the short-term precursors. And the Pd and Pc were found to be weak functions of the mainshock magnitude(M).

This is the first study which attempts to find a regularity in the appearance probability of short-term earthquake precursors in this way. It is hoped that this study will not only help to understand the source process at the preparation stage of an earthquake, but will also assist in predicting earthquakes in a practical way.

### Data

All the data used in this paper were of precursory phenomena to earthquakes occurring in and around Japan in the past 100 years or more, which were collected and selected by the author from literature, reports and other documents in many geo-science fields, as given in Table 1. Recently, an increasingly large number of precursory phenomena including even unusual behavior or the responses of animals or plants before earthquakes have been reported. In almost all these cases, the phenomena were recognized and reported by the observer after the main shock (Hamada, 1987). Since there is no established method of selecting real precursors from other anomalies which come from different sources, reported precursors possibly include noises. All the data sources could not be cited here because of space limitations, however, the main sources were the Earthquake Countermeasures Section of the Shizuoka Prefectural Office(1985), Suzuki(1985), and many of the Reports of the Coordinating Committee for Earthquake Prediction. Particularly, the last "Report" was a treasure house of information regarding precursory phenomena to earthquakes in Japan.

### Classification of earthquake precursors

The selected precursors for which precursor times(Tp) are known are given in Table 1. In the case of foreshock sequences, the number of precursors is not that of foreshocks but that of the sequences, and the commencement of the precursor is the first foreshock recognized. Out of the total 750 precursors, the majority(504) were seismological. Among the seismological precursors, more than half(287) were foreshocks.

At first, the earthquake precursors were classified by disciplines and items by instruments or apparent patterns of the precursors themselves. Then each item was classified into either short-term(S) precursors or long-term(L) ones. Where the majority of Tp was not greater than 30 days, the precursor was classified as short-term; where the majority of Tp was greater than 30 days, the precursor was classified as long-term. Immediate short-term(SS) precursors were considered as part of the short-term(S) ones. In those cases, a majority of Tp was not greater than 3 days. The short-term precursors included foreshocks, all kinds of anomalies detected by instruments for continuous measurements of crustal movement, most anomalies of geo-electromagnetism such as earth current, resistivity, and radio wave emission. All geodetic precursors were long-term. Precursors in seismology, geo-electromagnetism, and geo-chemistry were included in both the short-term and long-term categories. This classification however might be revised in the future according to the accumulation of observed data and knowledge or instrumental development.

The item of Utsu's criterion for foreshocks in seismology in Table 1 is not independent from the item of foreshock sequences. Therefore, this criterion of Utsu's was not counted as independent precursors in the

statistical investigation.

There is a very obvious difference in the probability distribution function( $P_c$ ) with  $T_p$  between the short-term and long-term precursors, as illustrated in Fig. 1. Where  $P_c(T_p)$  means a rate of the number of the short(or long)-term precursors whose precursor times are equal to or less than  $T_p$  per the total number of the short(or long)-term precursors in Table 1, respectively. For 85 % of the short-term precursors, the  $T_p$  is not greater than 30 days, while for only 14 % of the long-term precursors, the  $T_p$  is not greater than 30 days.

Figure 2 illustrates the frequency distribution of the short-term and long-term precursors in Table 1 with respect to the mainshock magnitude. This figure also shows a significant difference in the distribution pattern. That is, the long-term precursor has a tendency to appear for larger events than those for which the short-term precursor appears. Such differences between the short-term and long-term precursors seen in Figs. 1 and 2 may suggest different physical bases for them.

Figure 3 illustrates the  $P_c$  for the short-term precursors, where precursors are grouped according to the magnitude( $M$ ) of the main shock. The mean  $M$  of the  $M < 6$  group is approximately 5, that of the  $M \geq 6$  group, 7, and that of all the data, 6, as is seen in Fig. 2. Therefore, the  $P_c$  indicated by  $\blacktriangle$ ,  $\bullet$ , and  $\circ$  represent approximately those for  $M=5, 6,$  and  $7$ . The difference in  $P_c$  between mean magnitudes 5 and 7 events is at most 20 %, and variation in  $T_p$  is about a factor of 4 over the central half of the data, as seen in Fig. 3.

#### Regularity of precursors-appearance probability

Figure 4 illustrates the probability density for all the short-term precursors which was derived from the probability distribution in Fig. 1, where  $T_p$  is divided at 0.1, 0.3, 1, 3, 10, 30, and 100 days. The averaged probability density in the partitioned  $T_p$  is plotted at the middle of these  $T_p$  ranges. The figure shows an obvious linear relationship between  $\log P_d$  and  $\log T_p$  in the range roughly  $0.1 \leq T_p \leq 30$  days. For  $T_p >$  roughly 30 days, the  $\log P_d$  decreases more rapidly as the  $\log T_p$  increases.

The best fit straight line for the five plots for all the short-term precursors was derived by the least squares method as shown in Fig. 4. The empirical formula in Fig. 4 represents a drastic increase in the precursor-appearance probability with respect to time, approaching the main shock.

Here we consider, as a general problem, the probability distribution function( $P_c$ ) when the probability density function( $P_d$ ) is given by the formula in Fig. 4. The  $P_c$  is derived by integrating the  $P_d$  as follows:

$$\log_{10} P_d(T_p) = a - b \log_{10} T_p \quad (1)$$

$$a, b: \text{const.}, \infty \leq T_p \leq \infty$$

$$P_c(T_p) = 10^a (1/(1-b)) T_p^{1-b} + A \quad (b \neq 1) \quad (2)$$

$$P_c(T_p) = 10^a \ln_{10} \log_{10} T_p + B \quad (b = 1) \quad (3)$$

$$A, B: \text{const.}, \infty \leq T_p \leq \infty;$$

where, according to the definition,  $P_c(T_p) = \int_0^{T_p} P_d(T_p) dT_p$  and  $T_p$  is the precursor time. The  $P_d$  given by formula (1) is expressed with a straight line on the  $\log P_d$ - $\log T_p$  planes. And the corresponding  $P_c$  is expressed with an upward convex curve (if  $b > 1$ ), or a downward convex curve (if  $b < 1$ ), or a straight line (if  $b = 1$ ) on the  $P_c$ - $\log T_p$  planes.

The  $P_c$  value of formula (2) was calculated and compared with the observed data as illustrated in Fig. 5, where the  $b$  value was the same as that shown in Fig. 4, and "A" and "a" were determined by eye measurements

on the  $P_c$ - $\log T_p$  plane. There is an excellent agreement between the calculated  $P_c$  and the observed ones for  $0.1 \leq T_p \leq 40$  days, where the average discrepancy is only 1.2 %.

Such remarkable agreements as those in Figs. 4 and 5 suggest the existence of a simple regularity expressed by formula (1) for about 40 days prior to the main shock, in which approximately 90 % of all the short-term precursors are included.

#### Reliability and meaning of short-term precursors

One of the most important and most basic problems is the reliability of reported precursors. Unfortunately, since there is no established method to reject noises which come from different sources, noise contamination within the reported precursors is unavoidable, particularly just prior to earthquakes. Therefore, as the second best method, foreshocks, which most seismologists probably think are reliable precursors, and other short-term precursors were compared with each other in terms of  $P_c$  with respect to  $T_p$ .

Figure 6 shows the result of this comparison, where data from 287 foreshock sequences and 241 other short-term precursors were plotted together. As we can see in the figure, there is a surprisingly good agreement between the two, with no particular difference in the range  $0.1 \leq T_p \leq 10$  days. Most seismologists probably do not believe in the reliability of the anomalous precursor-like phenomena described in geochemistry geo-electromagnetism, continuous measurement of crustal deformation, and other fields to the same degree that they believe in foreshocks. However, Fig. 6 does not show a significant difference between foreshocks and the other phenomena mentioned. This suggests that noise contamination does not seriously affect  $P_c$ .

Thus far, the characteristic features of short-term precursors have been clarified; that is they have been clearly separated from long-term precursors in terms of  $P_c$ , their precursor-appearance regularity has been shown to be remarkable, and it has been shown that there is no significant difference between foreshocks and other short-term precursors in terms of  $P_c$ . These facts lead to the suggestion that a variety of short-term precursors in different disciplines are reflections of the common process in the preparation stage of the earthquake, namely, what has been called the "stress accumulation  $\rightarrow$  progress of strain  $\rightarrow$  commencement of pre-fracture and/or dislocation  $\rightarrow$  main rupture that is the main shock," and most of the short-term precursors appear corresponding to the phase of "pre-fracture and/or dislocation" which implies foreshocks and/or crustal deformation just prior to the mainshock.

#### A discussion related to the probability factor

The probability density function ( $P_d$ ) was compared with the following formula of fracture-occurrence probability by Mogi (1962).

$$\mu(\sigma) = A \exp(B\sigma) \quad (4)$$

$\sigma$ : stress

A, B: const.

This Formula (4) was rewritten as:

$$\log_{10} \mu = A' + B'\sigma \quad (5)$$

A', B': const.

A beautiful linear relationship between  $\log \mu$  and  $\sigma$  has been obtained for a granitic sample (Mogi, 1962). As discussed in the previous section if the short-term precursor is a reflection of a pre-fracture and/or dislocation in the source region, there is a possibility that the  $P_d$  is to be  $\mu$  in

formula (5). If the assumption  $Pd=\mu$  is permitted, the following can be derived from formulae (1) and (5):

$$\log_{10} Pd = A' + B' \sigma \quad (6)$$

$$\sigma = A'' - B'' \log_{10} T_p \quad (7)$$

$$A', A'', B', B'': \text{const.}$$

That is, approaching the main shock, increasing  $\log Pd$  corresponds to a linear increase of  $\sigma$ , which corresponds to linearly decreasing  $\log T_p$ .

### Conclusion

1. A total of 750 precursory phenomena to earthquakes have been collected, which consisted of 40 items from many disciplines. These items were classified into either short-term or long-term precursors, as seen in Table 1, depending upon whether the majority of the precursor times ( $T_p$ ) were 30 days or less, or greater than that, respectively. These short-term precursors, having been defined in this way, were clearly separated from the long-term ones in terms of the probability distribution function ( $P_c$ ) and the frequency distribution with the mainshock magnitude as shown in Figs. 1 and 2.

2. For the short-term precursors, the difference in  $P_c$  between mean magnitudes of 5 and 7 events is at most 20 % and the variation in  $T_p$  is about a factor of 4 over the central half of the data, as seen in Fig. 3.

3. It was shown that the probability density function ( $P_d$ ) and the probability distribution function ( $P_c$ ) for short-term precursors could be excellently expressed by formulae (1) and (2), as illustrated in Figs. 4 and 5, respectively, for the range  $0.1 \leq T_p \leq 40$  days.

4. It was also shown that no significant difference exists between the foreshocks which were considered to be representative short-term precursors and other short-term ones in terms of  $P_c$ , as is shown in Fig. 6. This leads to the suggestion that varieties of short-term precursors in different disciplines are a reflection of the common preparation process of the shock and correspond to a phase of "pre-fracture and/or dislocation" leading to the main shock.

5. If  $P_d$  is assumed to be  $\mu$  which is the fracture-occurrence probability under stress ( $\sigma$ ) derived by Mogi (1962), linear relationship related to  $\log Pd$ ,  $\log T_p$ , and  $\sigma$  can be derived as formulae (6) and (7).

### References

- Earthquake Countermeasures Section of Shizuoka Prefectural Office, The present state of analysis of precursors to an earthquake, 146pp., 1985, in Japanese.
- Hamada, K., Statistics of Precursory phenomena to Earthquakes Occurring in and around Japan, Proceedings of Earthquake Prediction Research Symposium (1987), 243-249, 1987.
- Mogi, K., Study of Elastic Shocks Caused by the Fracture of Heterogeneous Materials and its Relations to Earthquake Phenomena, Bull. Earthq. Res. Inst., 40, 125-173, 1962.
- Report of the Coordinating Committee for Earthquake Prediction, edited by Geographical Survey Institute, Japan, semi-annual.
- Suzuki, U., Records of Foreshocks, 164pp., published by the author, 1985, in Japanese.

Table 1. Precursors to Earthquakes Occurring in and around Japan

| Classification of Earthquake Precursors     |      |                                       |          | Number of Precursors |                   |                  |
|---|------|---------------------------------------|----------|----------------------|-------------------|------------------|
| Disciplines                                 | Coda | Classification items                  | Coda CRT | Total                | Tp <sub>≤30</sub> | Tp <sub>≤3</sub> |
| Gravity                                     | GR   |                                       | S        | 1                    | 1                 | 0                |
| Geodesy                                     | GD   |                                       |          | (20)                 | (2)               | (0)              |
|   |      | Levelling, uplift                     | u L      | 16                   | 2                 | 0                |
|   |      | Triangulation, trilateration          | t L      | 1                    | 0                 | 0                |
|   |      | Others                                | L        | 3                    | 0                 | 0                |
| Tide Gauge                                  | TD   |                                       |          | (11)                 | (2)               | (2)              |
|   |      | Uplift                                | u L      | 9                    | 1                 | 1                |
|   |      | Others                                | L        | 2                    | 1                 | 1                |
| Continuous Measurements of Crustal Movement | CN   |                                       |          | (108)                | (77)              | (39)             |
|   |      | Strainmeter                           | s S      | 21                   | 16                | 5                |
|   |      | Pendulum tiltmeter                    | t S      | 51                   | 32                | 9                |
|   |      | Water-tube tiltmeter                  | tw SS    | 11                   | 6                 | 6                |
|   |      | Volume strainmeter                    | v SS     | 25                   | 23                | 19               |
| Seismology                                  | SS   |                                       |          | (504)                | (331)             | (181)            |
|   |      | Anomalous seismic activity            | a L      | 71                   | 4                 | 0                |
|   |      | Microtremore                          | A SS     | 1                    | 1                 | 1                |
|   |      | b value change                        | b S      | 25                   | 13                | 8                |
|   |      | Foreshock sequences                   | f SS     | 287                  | 265               | 151              |
|   |      | Seismic wave from                     | F S      | 7                    | 4                 | 2                |
|   |      | Microearthquake swarms                | m L      | 16                   | 8                 | 1                |
|   |      | nu value change                       | nu SS    | 14                   | 14                | 12               |
|   |      | Pattern of seismic activity           | p L      | 31                   | 0                 | 0                |
|   |      | Seismic gap and quiescence            | q L      | 20                   | 5                 | 3                |
|   |      | Attenuation of seismic waves          | Q L      | 2                    | 0                 | 0                |
|   |      | Ground rumbling                       | r S      | 5                    | 5                 | 2                |
|   |      | Focal mechanism change                | s SS     | 1                    | 1                 | 1                |
|   |      | Utsu's criterion for foreshocks       | U SS     | 11                   | 11                | ?                |
|   |      | Change of seismic wave velocity       | v L      | 13                   | 0                 | 0                |
| Geo-electromagnetism                        | EL   |                                       |          | (63)                 | (50)              | (47)             |
|   |      | Geomagnetism                          | g L      | 4                    | 0                 | 0                |
|   |      | Earth current                         | e SS     | 11                   | 9                 | 8                |
|   |      | Potential at the sea bed              | ps SS    | 1                    | 1                 | 1                |
|   |      | Resistivity, Variometer               | r SS     | 30                   | 30                | 30               |
|   |      | Resistivity, Long-distance electrodes | R L      | 10                   | 3                 | 1                |
|   |      | Radio wave emission                   | w SS     | 7                    | 7                 | 7                |
| Geo-chemistry                               | CH   |                                       |          | (44)                 | (21)              | (10)             |
|   |      | Radon                                 | Rn S     | 15                   | 11                | 3                |
|   |      | Chlorine ion                          | cl L     | 5                    | 0                 | 0                |
|   |      | Groundwater temperature               | t L      | 11                   | 3                 | 2                |
|   |      | Groundwater level                     | l L      | 7                    | 3                 | 2                |
|   |      | Others                                | S        | 6                    | 4                 | 3                |
| Volcanic Activity                           | VL   |                                       | L        | 1                    | 0                 | 0                |
| Unusual Animal Behavior                     | AN   |                                       | SS       | 2                    | 2                 | 2                |
| Anomalous Potential of the Plant            | BT   | Albizzia plants                       | S        | 2                    | 2                 | 1                |
| Observation by the eye                      | NK   |                                       |          | (5)                  | (5)               | (4)              |
|   |      | Uplift                                | u SS     | 4                    | 4                 | 4                |
|   |      | Others                                | S        | 1                    | 1                 | 0                |

CPT: Classification by Tp, L(Long-term), S(Short-term), SS(Immediate short-term);  
 Tp: Precursor times in day from the commencement of the precursor to the main shock;  
 Numbers in parentheses are subtotal in that discipline.

FN:TPRC

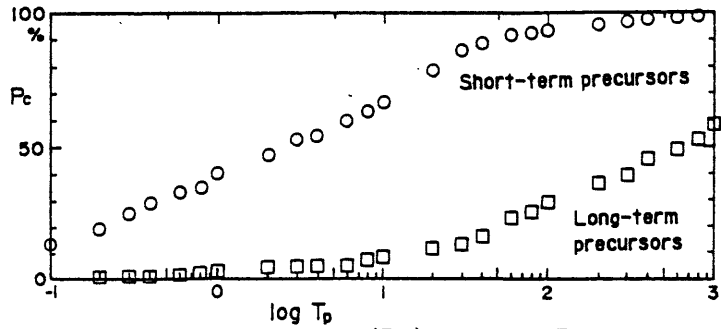


Fig. 1. Probability distribution( $P_c$ ) vs.  $\log T_p$  plot for the short-term and long-term precursors.  $T_p$  is the precursor time in days.

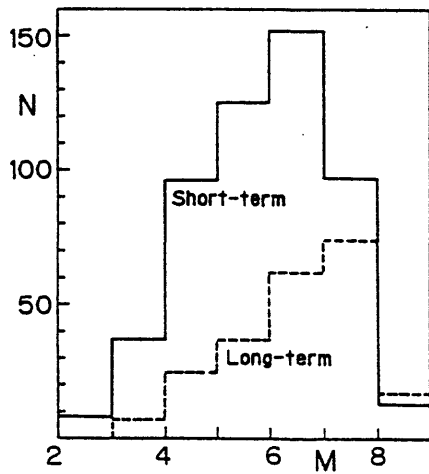


Fig. 2. Frequency( $N$ ) distributions of all the short-term and long-term precursors with respect to the mainshock magnitude( $M$ ).

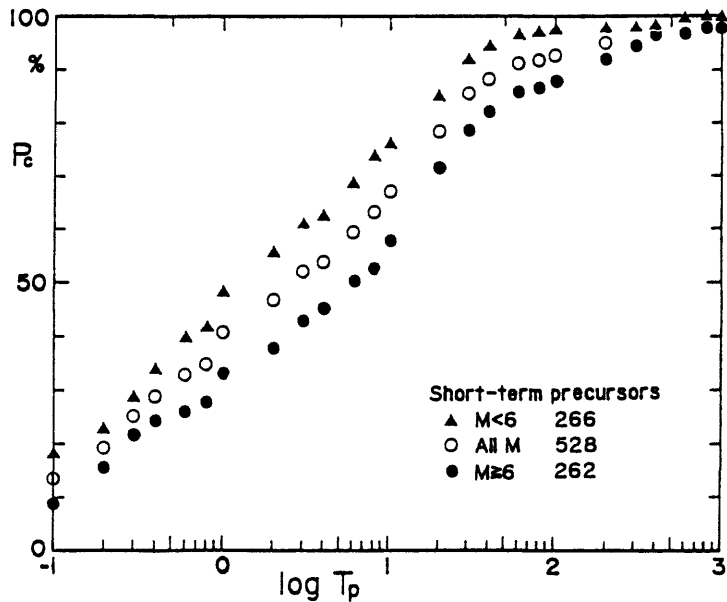


Fig. 3. Probability distribution( $P_c$ ) vs.  $\log T_p$  plot of the short-term precursors for different magnitudes( $M$ ) range of the main shock. Numerals show the number of data in each  $M$  range.

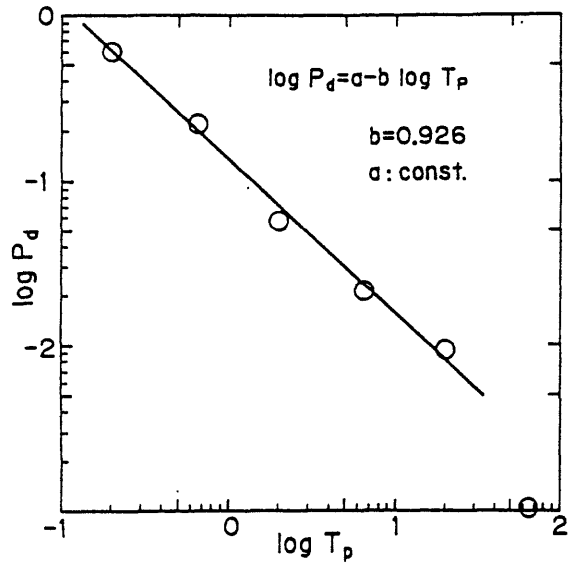


Fig. 4. Probability density( $P_d$ ) vs.  $\log T_p$  plot for all the short-term precursors and the estimated formula.

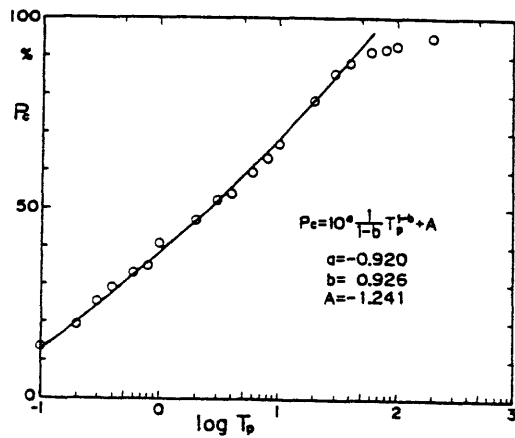


Fig. 5. Probability distribution( $P_c$ ) vs.  $\log T_p$  plot for all the short-term precursors and the estimated formula, which theoretically corresponds to that in Fig. 4.

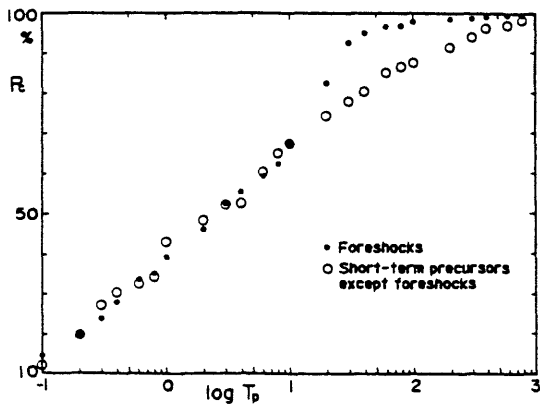


Fig. 6. Comparison of the  $P_c$  plot for foreshocks with that for all other short-term precursors.

CONCLUSIONS FROM SOCIAL SCIENCE RESEARCH ON EARTHQUAKE  
PREDICTION RESEARCH IN THE UNITED STATES  
FOR THE PERIOD OF 1974 THROUGH 1988

Dennis S. Mileti  
Director, Hazards Assessment Laboratory  
Professor, Department of Sociology  
Colorado State University  
Fort Collins, Colorado 80523, USA

The Prediction Research Record

The earliest efforts to estimate the social aspects of predicted earthquakes in the United States was by the Panel on Public Policy Implications of Earthquake Prediction in the National Research Council. This panel was established in 1974. The panel drew "... widely on experience with warning of other types of disaster ..." and made research recommendations including "... the need to study response to actual instances of earthquake prediction and warning as they occurred" (Turner et al. 1986:5). At about the same time a study of behavioral intentions in response to predicted earthquakes was performed (Mileti et al. 1981). This study was on key decision makers in commercial and noncommercial sectors and gathered data on anticipated measures that organizations thought would be adopted in response to a scientifically credible earthquake prediction. This study also estimated public prediction response. The major conclusion was that scientifically credible predictions for great earthquakes (with time, place and magnitude specified) would cause pre-event economic losses of major proportions. In 1978, the National Research Council issued a second report on the topic which was the result of the Committee on Socioeconomic Effects of Earthquake Prediction (1978). The Committee called for study of response to near predictions as well as to predictions. A third non-empirical report was also issued at about this same time; it was a technology assessment on earthquake prediction (Weisbecker et al. 1977).

In early February 1976, the U.S. Geological Survey reported that a land uplift about 25 centimeters in height was detected along a portion of the San Andreas fault just north of Los Angeles. The uplift was centered near the town of Palmdale in the Mojave desert. The Survey stated that the uplift was not fully understood; that is, it may or may not be a precursor of an earthquake. The USGS, however, did express concern because the uplift had occurred along a section of the San Andreas fault that has been inactive since the great 1857 earthquake in that area. This news led to a major social research effort by Ralph Turner and others (Turner, Nigg and Paz 1986). These researchers classified the announcement of the Palmdale Bulge as an approximate prediction since neither the place, time, nor magnitude was precisely stated. It was, in effect, earthquake hazard information that constituted a near prediction (1986:5). The investigation was intended, according to the authors, "... as a first step toward understanding how communities respond to the announcement of near predictions, and by inference, how they may respond to earthquake predictions in the future (1986:6). The major conclusion of

this work was that there was little evidence of serious individual or household preparedness for the earthquake despite the fact that nearly everyone believed that the quake was coming soon.

In 1980, Brady and Spence predicted an earthquake for Lima, Peru to occur in the summer of 1981. The former scientist's affiliation with the U.S. Bureau of Mines and the latter's with the U.S. Geological Survey gave the prediction scientific credibility. Assessment of the socioeconomic consequences of the prediction were performed by several researchers. Publications issued to date (cf. Echevarria, Norton and Norton 1986) suggest that "... over half of the population in Lima took some precautionary measures, that the total economic damage from the prediction was very roughly \$50 million, and that the poorer groups in society bore a disproportionate share of the prediction costs (1986:175).

The brief record in the U.S. regarding the social aspects of earthquake prediction suggests that on the one hand predictions may resemble disaster warnings with large-scale public response, while on the other hand predictions may resemble hazards or risk education with some potential for increased public awareness and, possibly, even preparedness and mitigation behavior. In fact, the conclusion which can be drawn from this research record is straightforward. It is likely that scientifically credible earthquake predictions vary from a social viewpoint in terms of specified time until the quake. First, long-term predictions (many years) are likely similar to general hazards education, increase public awareness, but do not elicit much public preparedness. Second, intermediate-term predictions (a couple of years) could have negative economic impacts as well as positive effects. Third, short-term predictions (a few days or hours) are likely similar to warnings of other disasters, for example, hurricanes.

#### Public Risk Communication Research

Earthquake predictions of any sort are efforts to communicate risk to the public. Much research has been performed on this topic. Findings suggest that people who receive risk information go through a sequential process that shapes their risk perceptions and subsequent behavior. A model of this process is the sequence hear-perceive (understand, believe and personalize)-respond (decide about alternative preparedness and/or mitigation actions and perform them). The sequence may not be the same for every person. The first stage is hearing the risk information. Second, the risk information must be understood. Understanding is not simply interpretation, but also the attachment of meaning to the information. Those meanings can vary among people and may or may not conform to the understandings intended. A 50 percent probability may be interpreted as certain by some or unlikely by others. In this sense, understanding includes the perception of risk. The third stage is belief in the risk information and in the accuracy of what is being communicated; in this way, belief also includes risk perception. The fourth stage is the personalization of risk; that is, the perceived implications of the risk being communicated on the receivers themselves; thus, personalization includes risk perception. The fifth stage is that people must decide what to do about the risk, and then, sixth, perform that behavior. Throughout

risk information communication a person typically goes through the stages of the model each time that new information is received. Thus, response to risk information follows from a series of decisions. The formation of perceived risk is not a single consequence of a singular communication but is instead the result of an emerging process. Additionally, people do not passively await the arrival of more information; most people actively seek out more. This results in what has typically been referred to as the confirmation process (Drabek 1969; Mileti et al. 1975).

Research on how risk information affects risk perceptions and response clearly catalogues that variation in public perceptions and response are the result of risk information factors (Sorensen and Mileti 1987). Empirical findings suggest that message attributes important to consider vary in reference to both message content and style. Message content is relevant to consider along three lines: information about risk location, the character of that risk (for example, effects of impact and time to impact), and guidance about what people should do before impact. Message style is also important. Important style attributes are:

- specificity (the degree to which the message is specific about risk, guidance, and location);
- consistency (the degree to which a message is internally consistent, as well as consistent across separate messages regarding risk, guidance, and location);
- accuracy (the extent to which message content about risk, location, and guidance is and is not perceived to be accurate);
- certainty (the degree to which those giving the warning message seem certain about what they are saying about risk, location, and guidance); and
- clarity (the degree to which risk, location and guidance information in the message is stated in words that people can understand).

Sender characteristics are as important as message attributes to consider in cataloging determinants of human response to warning response process factors. These include:

- channel attributes (the type of channel used--for example, personal versus impersonal--and the number of different channels used);
- frequency attributes (the number of times a particular message is conveyed, the number of different messages, and the pattern between difference conveyances--for example, every 15 minutes, randomly and so on); and
- source attributes (the level of familiarity of those giving the message to those receiving it, the degree to which the message giver is an official, and the credibility level of the message giver to those who receive the message).

## Conclusions

Each prediction type (long-term, intermediate-term, and short-term) is an attempt at public risk communication. Each prediction type raises different public response goals and problems. For example, long-term prediction raises awareness but little desired mitigation and preparedness, and short-term prediction requires quick public response.

The effect of risk communication factors on public response (preparedness and mitigation or protective action) has been documented in numerous studies. Although much more elaborate summaries are available elsewhere (Sorensen and Mileti 1987; Drabek 1986; Perry, Lindell and Greene 1981), the following conclusions illustrate this knowledge base regarding risk communication with the public. Public understanding of communicated emergency risk information and earthquake predictions would be enhanced if it is:

- specific regarding the risk, the hazard, what the public should do and how much time is available;
- consistent;
- certain;
- delivered personally;
- communicated over multiple channels;
- frequently disseminated
- from official sources; and
- confirmed.

## REFERENCES

- Committee on Socioeconomic Effects of Earthquake Prediction. 1978. A Program of Studies on the Socioeconomic Effects of Earthquake Prediction. Washington, D.C.: National Academy of Sciences, National Research Council.
- Drabek, Thomas E. 1969. "Social Processes in Disaster: Family Evacuation" Social Problems 16(Winter):336-349.
- Drabek, Thomas E. 1986. Human Systems in Disaster. New York: Springer-Verlag.
- Echevarria, Julio A., Kathryn A. Norton and Roger D. Norton. 1986. "The Socioeconomic Consequences of Earthquake Prediction." Earthquake Prediction Research 4:175-193.
- Mileti, Dennis S. 1975. Natural Hazard Warning Systems in the United States: A Research Assessment. Boulder: Institute of Behavioral Science, University of Colorado.

- Mileti, Dennis S., Janice Hutton and John Sorensen. 1981. Earthquake Prediction Response and Options for Public Policy. Boulder, Colorado: University of Colorado.
- Perry, Ronald W., Michael K. Lindell, and Marjorie R. Greene. 1981. Evacuation Planning in Emergency Management. Lexington, MA and Toronto: Lexington Books.
- Sorenson, John H., and Dennis S. Mileti. 1987. "Public Response to Emergency Warnings." Reston, Virginia: U.S. Geological Survey Conference Proceedings.
- Turner, Ralph H., Joanne M. Nigg, and Denise Heller Paz. 1986. Waiting for Disaster: Earthquake Watch in California. Los Angeles: University of California Press.
- Weisbecker, Leo w., Ward C. Stoneman and the Staff of the Stanford Research Institute. 1977. Earthquake Prediction, Uncertainty and Policies for the Future: A Technology Assessment of Earthquake Prediction. Menlo Park: Stanford Research Institute.

Temporal Variations in Seismic Activity and Some Precursors  
before Recent Intraplate Earthquakes in Southwest Japan

Takeshi Mikumo

Disaster Prevention Research Institute, Kyoto University, Uji, Kyoto, Japan

Temporal variations in seismic activity during the recent 7 years up to 1987 and some precursory phenomena observed before three moderate-size earthquakes in Southwest Japan are discussed here on the basis of regional and local seismic and geophysical observations.

1. Space-Time Distribution of Major Earthquakes

It has been pointed out ( Mogi, 1985 ) that major intraplate earthquakes with magnitudes greater than 6.0 that occurred along and near the Japan Sea coastal regions show alternate temporal variations of high activity and quiescence over Northeast and Southwest Japan. A more detailed space-time plot of seismicity including major to moderate-size events shows that these earthquakes in Northeast Japan are temporarily clustered around five periods, 1890-1900, 1910-1918, 1939-1950, 1960-1966 and after 1983, at about every 20 years ( Oike & Huzita, 1988 ). It also appears that the activity migrates from Northeast Japan to the northern Fossa Magna and even to Southwest Japan. It has also been suggested (e.g. Shimazaki, 1976 ; Mogi, 1981) that the space-time patterns of intraplate seismicity in Southwest Japan are closely related with large interplate earthquakes along the Nankai trough. The alternate temporal variations and apparent migration of the intraplate seismicity might be an indication of some enhancement and transfer of tectonic stress, which is possibly due to minor fluctuations of relative movements between the Pacific, Philippine Sea and Eurasian plates. These possibilities would be elucidated in a future from numerical modelling based on realistic crust and upper mantle structures composed of visco-elastic and visco-plastic materials.

The latest high seismic activity over the Japan Islands appears to have started some time in 1983, and one of the largest event was the May 26, 1983 earthquake (  $M=7.7$  ) that occurred off the west coast of Northeast Japan.

2. Temporal Variations of Recent Intraplate Seismicity in Southwest Japan

Since 1983, three major to moderate-size intraplate events took place in Southwest Japan ; the Tottori earthquake ( $M=6.2$ ) in late 1983, the Yamasaki fault earthquake ( $M=5.6$ ) in mid-1984, and the Western Nagano earthquake ( $M=6.8$ ) in late 1984 (See Fig.1), all of which have similar type of strike-slip mechanism. During the period between 1981 and 1987, more than 2000 local shocks with magnitudes greater than 3.0 occurred over the inland regions during the period between 1981 and 1987.

We investigate here detailed temporal variations of seismicity for earthquakes with magnitudes greater than 3.0 mainly on the basis of JMA data ( Ishikawa et al., 1985 ). The purpose here is to see if there is any correlation in the seismicity and hence in the stress state between several regions of Southwest Japan, and also to see if any seismicity quiescence can be identified before the three larger events. One of the reasons for

the choice of a magnitude threshold 3.0 is based on the detection capability of minor shocks by the JMA seismograph network, which provides homogeneous data set above this magnitude. Another reason comes from a recent work of Cao & Aki(1987), which correlates seismicity with a slip-weakening friction law.

We divide Southwest Japan into several sub-regions as shown in Fig. 2, taking into account the spatial distribution of seismicity and also the tectonic features. Region 1 is the zone close to the northern Fossa Magna and Region 2 includes its southern part and the eastern section of the Median Tectonic Line (MTL). Regions 3 and 4 cover the northern and southern parts of Quaternary active region, and Regions 5 and 6 are the central and western parts of the Inner Zone in Southwest Honshu. Regions 7 and 8 include the central and western sections of MTL.

Figure 3 shows the cumulative number of events included in each of the subdivided regions, plotted against time from 1981 to 1987, which indicates long-term seismicity. No techniques have been applied to remove dependent events such as swarms and aftershocks. It can be seen that Region 7 shows an extremely high seismicity and its rate of increase changed quite sharply in early 1983. Regions 1, 2 and 3 indicate a similar pattern of seismicity up to late 1986 with slight changes of its rate around mid-1983 or in early 1984. Likewise, a nearly parallel seismicity can be recognized in three adjacent regions, 4, 5 and 6, with a remarkable change of rate in early 1984. Region 8 also shows a similar trend to that in Region 6. Thus, the long-term seismicity in Southwest Japan consistently shows an appreciable increase over several regions around early to mid-1983 or early 1984.

The temporal behaviors of seismicity patterns observed before large earthquakes have been elaborately reviewed by Kanamori (1981). We classified these patterns into several categories, which may be expressed schematically in the form of cumulative seismicity diagram as shown in Fig. 4. Our numerical simulations ( Mikumo & Miyatake, 1983 ) on a three-dimensional fault subjected to a constant shear stress suggest that there could be several different types of seismicity patterns (See Table 1), which sometimes include precursory swarms, preseismic quiescence and foreshocks as in Case I, depending on the degree of fault zone heterogeneities. If the fault zone is extremely nonuniform including a number of small-scale heterogeneities, gradually increasing seismicity would be expected as in Case IV.

However, since the change in the long-term rate of seismicity in Fig. 3 can be recognized throughout all the regions in early to mid-1983 or in early 1984, this might be regarded as an indication of slight increase of regional tectonic stress. If this is actually the case, Region 7, which started to be active in early 1983 about 5 months before the largest event in N.E. Japan (J), appears to be most sensitive to the change of tectonic stress. Then, Regions 1 and 2 located close to the tectonic boundary between N.E. and S.W. Japan became activated in mid-1983. Although no precursory increase of seismicity has been observed before the 1983 Tottori earthquake (T) in the surrounding regions, the change of seismicity rate or the slight increase of tectonic stress prevailing over Regions 3 - 6 might have had some effects on the two moderate-size earthquakes in 1984 (Y & N).

The next two diagrams given in Fig. 5 show more detailed, cumulative

seismicity in two regions which are the sites of the above three earthquakes. Since these earthquakes were followed by a number of aftershocks, the two regions are treated separately. The lower one indicates the seismicity in Regions 6 and T which cover the site of the 1983 Tottori and the 1984 Yamasaki fault earthquakes. From this diagram, seismicity quiescence lasting for about 8 months may be identified before the 1983 event, but not before the 1984 event. The lower diagram shows the seismicity in Region N which is the site of the 1984 Western Nagano earthquakes. The rapid increase of seismicity in late 1978 is due to swarm earthquakes, but cannot be regarded as precursory activity to the 1984 event. The activity may be more or less related with the volcanic eruption of Mt. Ontake in October, 1979 located within this region. The seismicity rate in this region also increases in mid-1983 as in Regions 1 and 2, suggesting again a slight enhancement of tectonic stress over these regions. A clear seismicity quiescence can be identified for about 6 months before the 1984 event.

Besides the regional seismicity observations made by JMA, our local microearthquake observation network ( of the Disaster Prevention Research Institute, Kyoto University ) provided some additional evidence for the seismicity quiescence prior to the three events described here.

1) In the Tottori region, a large number of aftershocks, including micro-earthquakes, of the previous 1943 Tottori earthquake (  $M=7.4$  ) have been taking place for 40 years in the western section of the aftershock zone. Our recent observations indicate that microearthquake activity around there became inactive during 1978-1980 and completely quiet from mid-1982 to the October 31, 1983 event ( Oike, 1987 ).

2) Microearthquake activity around the Yamasaki fault show alternate temporal variations of high and low seismicity at every 12-13 years, and the latest high activity was in 1979-1980. A minor swarm took place in 1982 near the southeastern section of the fault, and after this time a complete seismic gap was formed there during 1983 up to the event on May 30 1984 ( Tsukuda, 1985 ).

3) In the Hida region, central Honshu, high seismicity has been observed just beneath the Hida mountain range extending in the N-S direction, and its southern end was the site of swarm earthquakes lasting since 1978. The space-time diagram of the seismicity plotted along the N-S profile clearly shows seismicity quiescence for larger shocks with magnitudes greater than 3.0 for about 5 months prior to the event on September 14, 1984, while this cannot be identified if all shocks down to a magnitude 0.5 are included ( Mikumo et al., 1985 ). This is consistent with the seismicity pattern derived from JMA data.

#### 4. Other Short-Term Precursors

Besides the temporal variations of seismicity, several short-term precursors have been recorded by different types of observations before the three events in Southwest Japan.

(1) Geochemical observations for chloride ion contents involved in underground water, which have been continuously made at several sites close to

the epicentral area of the 1983 Tottori earthquake, appear to indicate some variations after mid-1982 ( Yoshioka et al., 1984 ).

(2) 1) Geodetic distance-measurements, which have been repeated along several short-baselines across a part of the Yamasaki fault ( about 3 km from the epicenter ), indicate small contraction in areal strains around late 1983 about 6 months before the 1984 event ( Fujimori & Tanaka, 1985 ).

2) Apparent resistivity of rock materials observed close to the fault zone indicates a gradual decrease around mid-March to early April, 1984 and a rapid increase 10 days before the May 30 event ( Sumitomo, 1985 ). Also, the horizontal gradient of total magnetic force show a slight increase from mid-March up to the time of the earthquake ( Sumitomo, 1985 ).

3) A more pronounced precursory change has been identified in electric self-potential difference between two sites across the fault zone after mid-April to the time of the earthquake ( Miyakoshi, 1985 ).

(3) 1) Temporal variations of hydrogen gas contents observed at a hot spring 50 km apart from the epicenter indicate a rapid increase in early August, 1984 about one month before the September 14 event, and died out in mid-November. Also, a remarkable change in gas compositions such as He/Ar and H<sub>2</sub>/Ar has been observed at fumaroles on Ontake Volcano a week before the earthquake ( Sugisaka & Sugimura, 1986 ). Observations of radon concentration involved in soils, which have been made at 5 sites 60 km away from the epicenter, shows a consistent increase about 2 months before this event and decreases about three months later ( Ui, 1986 ).

## 5. Summary

Major intraplate earthquakes in the Japan Islands appear to indicate alternate temporal variations of high activity and quiescence, and the latest high activity appears to have started in 1983. The long-term rate of seismicity in Southwest Japan shows an appreciable increase around early to mid-1983 or in early 1984, suggesting slightly enhanced tectonic stress. A few regions close to tectonic boundaries appear more sensitive to the change of the tectonic stress. After this time three moderate-size events with magnitudes up to 6.8 occurred between late 1983 and late 1984. Seismicity quiescence has been identified from regional seismicity observations for magnitudes greater than 3 for several months before the two larger events, and also from local seismicity observations before all the three events. Several different types of precursors have been detected from geodetic, geochemical or geoelectro-magnetic observations before the three events.

## References

- Gao, T. and K. Aki, Physical basis for the magnitude cut-off dependence of seismicity quiescence, submitted to PAGEOPH, 1987.  
Fujimori, K. and Y. Tanaka, Geodetic baseline measurements across the Yamasaki fault, The Earth Monthly 7, 20-26, 1985 ( in Japanese ).  
Ishikawa, Y., K. Matsumura, H. Yokoyama and H. Matsumoto, SEIS-PC - its outline, Geol. Data Processing 10, 19-34, 1985 ( in Japanese ).  
Kanamori, H., The nature of seismicity patterns before large earthquakes,

Maurice Ewing Series 4, 1-19, Am. Geophys. Union, 1981.

- Mikumo, T. and T. Miyatake, Numerical modelling of space and time variations of seismic activity before major earthquakes, Geophys. J. R. Astr. Soc. 74, 559-583, 1983.
- Mikumo, T., H. Wada, S. Kaneshima, K. Imagawa and M. Koizumi, Seismic activity in the northern Hida region before and after the 1984 Western Nagano earthquake, and the faulting mechanism of the main shock event, Rep. Natural Disast. Sci. ( ed. K. Iida ), 21-33, 1985 ( in Japanese ).
- Miyakoshi, J., Temporal variations of self-electric potentials near the fault zone of the Yamasaki fault, The Earth Monthly 7, 38-42, 1985 ( in Japanese ).
- Mogi, K., Seismicity in western Japan and long-term earthquake forecasting, Earthquake Prediction, Maurice Ewing Series 4, 43-51, 1981.
- Mogi, K., Precursors of the 1983 Japan Sea earthquake, Earthq. Pred. Res., 3, 493-517, 1985.
- Oike, K., M 6.2 earthquake on October 31, 1983 in central part of Tottori Prefecture, Symp. Earthq. Pred. Res., 87-99, 1987.
- Oike, K. and K. Huzita, Relation between characteristics of seismic activity and neotectonics in Honshu, Japan, Tectonophysics, 148, 115-130.
- Shimazaki, K., Intra-plate seismicity and inter-plate earthquakes; Historical activity in Southwest Japan, Tectonophysics, 33, 33-42, 1976.
- Sugisaki, R. and T. Sugiura, Precursory change in gas compositions at mineral springs and fumarole before the Western Nagano Prefecture earthquake, ZISIN II, 39, 99-110, 1986 ( in Japanese ).
- Sumitomo, N., Geoelectric and geomagnetic observations around the Yamasaki fault, The Earth Monthly 7, 32-37, 1985 ( in Japanese ).
- Tsukuda, T., Seismic activity around the Yamasaki fault, The Earth Monthly 7, 9-14, 1985 ( in Japanese ).
- Ui, H., Fault zone as a strainmeter, Bull. Lab. Earthq. Chem. 4, 85-96, 1984 ( in Japanese ).
- Yoshioka, R., R. Nishida, T. Tsukuda, K. Mino, N. Koizumi, K. Kitaoka, S. Yabe and Y. Kishimoto, Anomalous features of self-spouting hot springs accompanied with the earthquake (M=6.2) on Oct. 31, 1983 at the central part of Tottori Pref., Annuals, DPRI, Kyoto Univ. 27B-1, 455-464, 1984 ( in Japanese ).

#### Figure Captions

- Fig. 1. Major to moderate-size earthquakes with magnitudes larger than 5.5 that occurred during the 7 years between 1981 and 1987, and the focal mechanism of four larger earthquakes.
- Fig. 2. Seismicity (  $M = 3$  ) in Southwest Japan during the period between Jan. 1, 1981 - Dec. 31, 1987 (upper), and tentatively sub-divided regions based on the seismicity and tectonic features (lower).
- Fig. 3. Cumulative number of events included in each of the sub-divided regions. Regions 1-8 refer to Fig. 1.
- Fig. 4. Schematic diagram of cumulative seismicity for several different precursory patterns expected from numerical modelling.
- Fig. 5. Cumulative seismicity in Region N and Regions 6+T. Note the seismicity quiescence prior to the two larger events.

MADE FROM BEST AVAILABLE COPY

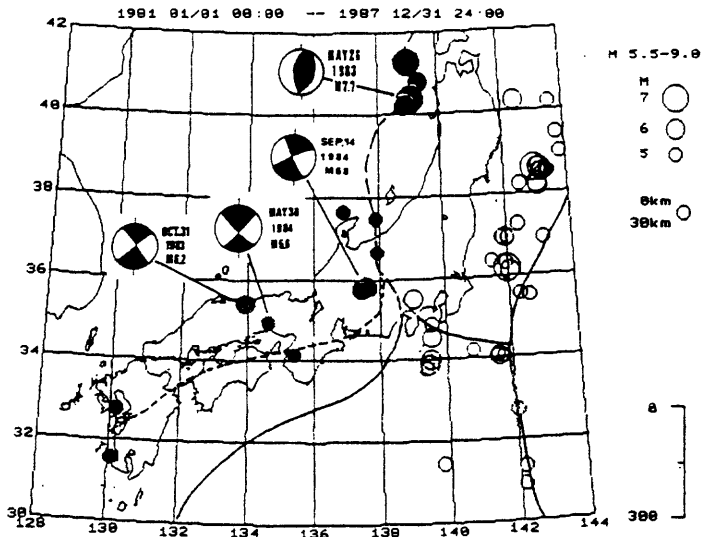


Fig. 1

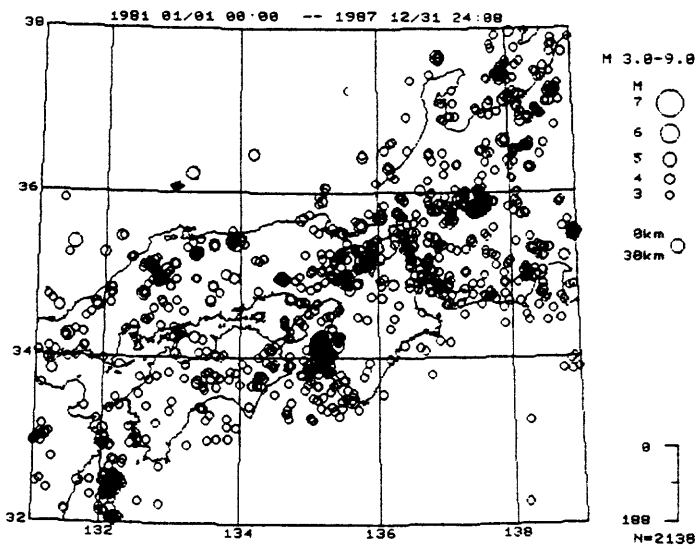
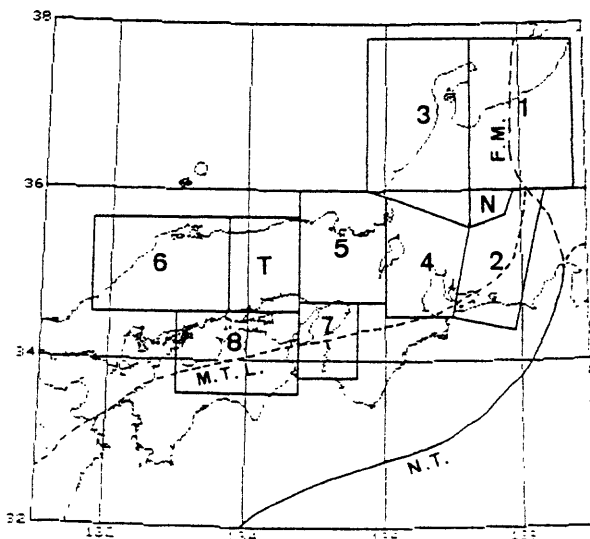


Fig. 2



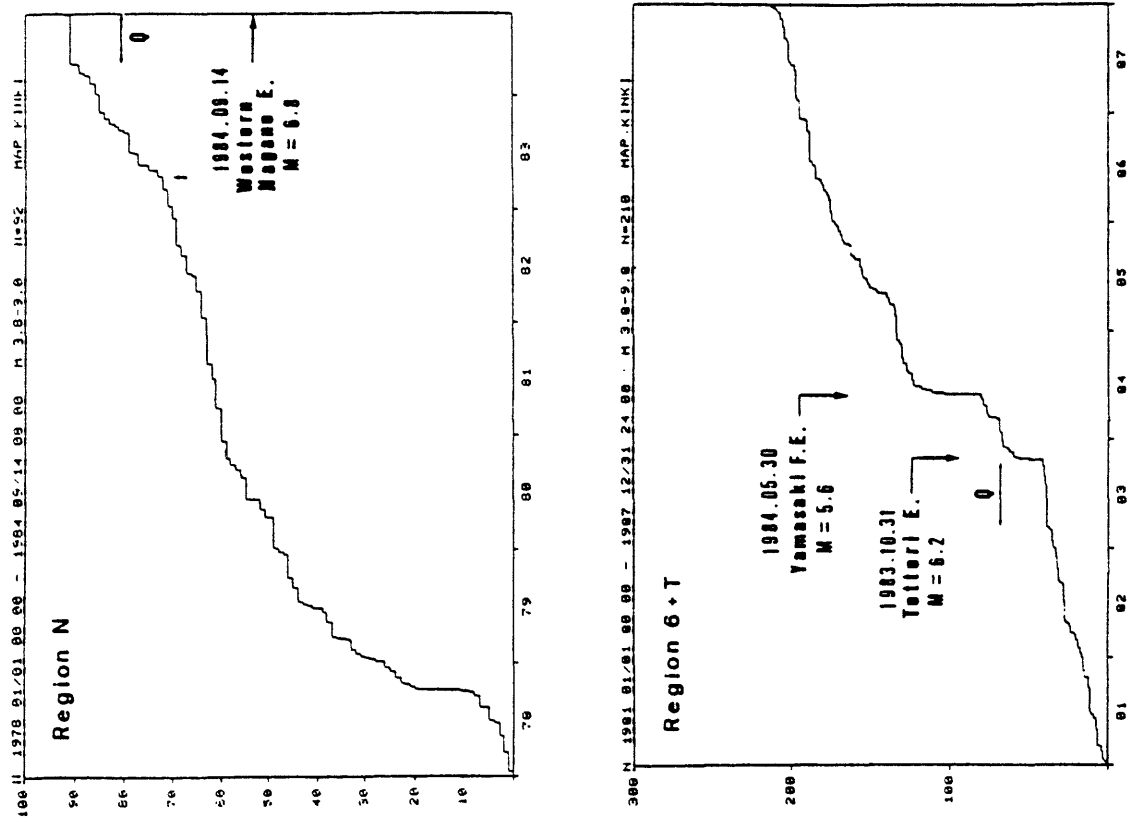


Fig. 5

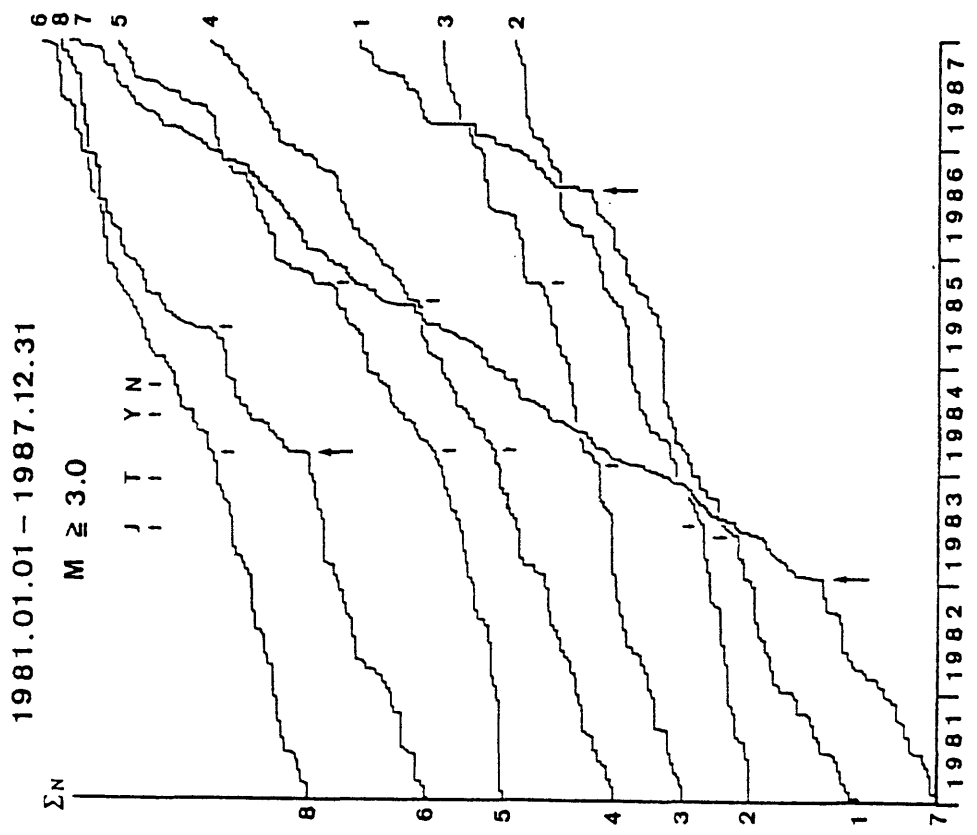


Fig. 3

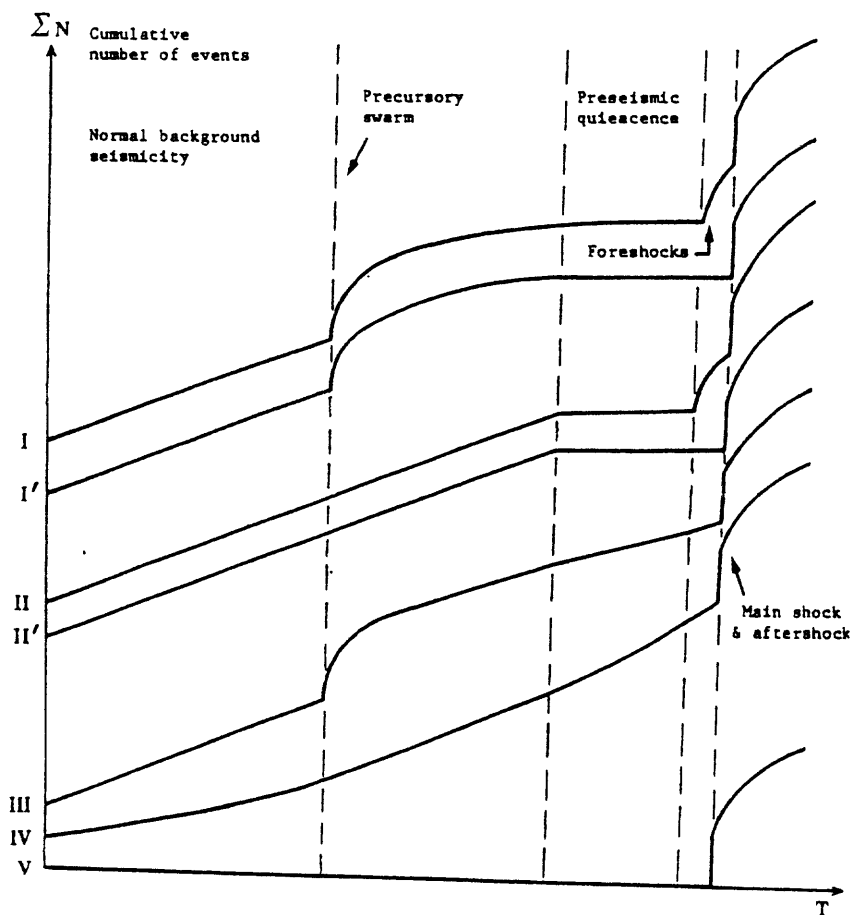


Fig. 4

Table 1. Different types of precursory changes of observed seismicity. ( after Mikumo & Miyatake, 1983 )

| Case | Normal stage                 | Precursory stage                                 | Main event                      | fault properties         |            |  |
|------|------------------------------|--|---------------------------------|--------------------------|------------|--|
| I    | Normal background seismicity | Precursory swarms or clustering                  | Pre-seismic quiescence          | Foreshocks or clustering | Main shock | heterogeneous, including small to moderate-size asperities with medium to high strengths |
| I'   | Normal background seismicity | Precursory swarms or clustering                  | Pre-seismic quiescence          | - - -                    | Main shock |  |
| II   | Normal background seismicity | - - -  | Pre-seismic quiescence          | Foreshocks or clustering | Main shock | heterogeneous, including moderate-size asperities with high strengths                    |
| II'  | Normal background seismicity | - - -  | Pre-seismic quiescence          | - - -                    | Main shock |  |
| III  | Normal background seismicity | Precursory swarms or clustering                  | Normal seismicity               | - - -                    | Main shock | extremely heterogeneous on small scales  |
| IV   | Normal background seismicity | - - -  | Gradually increasing seismicity | - - -                    | Main shock |  |
| V    | - - -                        | No background seismicity or precursory phenomena | - - -                           | - - -                    | Main shock | relatively homogeneous   |

# Prediction of Large Aftershocks on the Basis of Quiescence

R.E. Habermann

NOAA / National Geophysical Data Center, Boulder, Colorado

Frederic H. Creamer

CIRES, NOAA / University of Colorado, Boulder, Colorado

Seismic quiescence has been clearly demonstrated prior to some large mainshocks and has been used to successfully predict several others. Matsu'ura (1986) proposed that quiescence may also occur prior to large aftershocks that follow many major earthquakes. It is clearly important to test this proposal carefully, for predicting the occurrence of large aftershocks would obviously be significant. We have expanded and improved on the foundation laid by Matsu'ura in several important ways. First, we have substantially expanded the data base used in the study, including primarily modern data from both teleseismic and local networks. Second, we have conducted a study which is aimed at testing the real-time application of the concepts which Matsu'ura developed. Finally, we have systematically determined success rates, false alarm rates, and missed event rates.

## METHOD

The general approach to identification of quiescence in aftershock sequences is similar to that used in studies of precursors to mainshocks. The principal task is the definition of an expected rate of occurrence and the recognition of deviations in observed activity from that expectation. In aftershock studies the expected rate is determined using Omori's law of aftershock decay. The steps taken in this study were:

- 1) Aftershocks were isolated from normal seismicity.
- 2) The Gutenberg-Richter cumulative frequency versus magnitude relation was used to determine the minimum magnitude of completeness and a magnitude cutoff was made at that level.
- 3) The modified Omori formula parameters ( $K$ ,  $c$ , and  $p$ ) were estimated by the maximum likelihood technique developed by Ogata (1983).
- 4) An expected cumulative number (ECN) was computed and compared to the observed cumulative number (OCN) of aftershocks.
- 5) Thirty aftershock sequences were used to test various alarm criteria for identifying quiet periods in a simulated real-time experiment. When the alarm criteria were satisfied the quiet period was classified as a successful prediction or as a false alarm.

## DIFFERENCES BETWEEN OUR TECHNIQUE AND MATSU'URA'S

There are two principal differences between Matsu'ura's study and ours. First, the emphasis in our study was on the real-time identification of quiescence. Second, the details of the aftershock sequence models were different. Matsu'ura modeled an aftershock sequence using only data prior to the onset of a particular quiet period. During the quiet period, the sequence was modeled by setting the rate of decay ( $p$ ) = 0. This allowed any quiescence to be identified by a large negative residual. In our study, all data available up to a given time were used to model the aftershock sequences, including the quiet period. This degraded the fit prior to the quiet period, but improved it over the entire

time period. This also alleviated the problem of explicitly modeling every quiet period between aftershocks. Warnings were issued on the basis of a decrease in residuals rather than on large negative residuals.

### ALARM CRITERION

It is clearly important to determine the success rate (number of successes / number of alarms), the false alarm rate (1 - success rate), and the missed aftershock rate (number of successes / number of targets) associated with any proposed precursor. In order to do this, one must construct a quantitative description of an alarm, an alarm criterion, and then systematically search many data sets for occurrences of alarms. In this research the principal parameter examined for variations was the residual between the observed and expected numbers of events. When the derivative of this residual reached a minimum (-1), a potential alarm was started and the amount of decrease in subsequent time steps was computed in units of standard deviations of the residuals. If the amount of decrease was larger than the threshold being tested, an alarm was declared.

Figure 1A shows residuals versus ECN for the first 48 hours of the Livermore, California aftershock sequence of January, 1980. The upper and lower lines are drawn at two standard deviations above and below the mean to provide a scale. Figure 1B shows the derivative of the residuals. This derivative reaches -1 at 41 hours, indicating the onset of quiescence. The residuals at 40 and 48 hours are 6.9 and 0.10, so a drop of 1.42 standard deviations occurred during the last 8 hours of this sequence (see Figure 1B). These numbers, a drop of 1.42 and a duration of 8 hours, describe this quiet period. One other number which was used to describe the quiescence was the position of the start of the quiescence in the sequence. In this case, the quiescence starts 83% of the way through the sequence.

It is worth noting that the largest aftershock of the Livermore sequence (ML=5.3) occurred 55.5 hours after the mainshock. This quiet period, therefore, might be considered as a precursor. In this study, however, the secondary aftershock is not large enough, and the decrease in residuals is not large enough to predict the aftershock with a reasonable false alarm and missed event rate.

### SUCCESS, FALSE ALARM AND MISSED AFTERSHOCK RATES

In order to simulate a real-time environment in the search, only events which occurred prior to some time in a sequence were considered. That time was moved through the sequence in 12 hour increments to create a series of data sets. Each data set was fitted using the maximum likelihood scheme and the last half of each data set was searched for quiet periods. The alarm criterion was varied from a decrease in residuals of more than 1.4 standard deviations to a decrease of more than 3.6 standard deviations. When quiet periods which satisfied a warning criteria were identified, their occurrence time was noted and they were classified as successes or false alarms. Successes were followed within 21 hours by an aftershock with a magnitude within 0.5 units of the mainshock magnitude. False alarms were not followed by such events. A major aftershock that did not have quiescence that was recognizable at the time increments described above, was counted as a missed event.

The search for quiet periods was carried out on thirty aftershock sequences from teleseismic and local catalogs and the success, false alarm, and missed aftershock rates were determined for any combination of amount of residual decrease and start time of the quiet periods. Figure 2 shows the success rates for the western Pacific region. We will discuss the results for a drop of at least 2.2 standard deviations beginning no earlier than at 78% of the observed time period. This warning criteria was successful in four of eleven

occurrences and twelve of 16 large aftershocks were missed.

A clear regional variation in occurrence of large aftershocks and performance of this alarm criteria was observed. In the West Pacific region, many events are followed by large aftershocks. This warning criteria was successful in four of six occurrences and eleven of fifteen large aftershocks were missed. In the East Pacific and California, only one event was followed by a large aftershock (Michoacan, 1985). This aftershock was preceded by quiescence which lasted six hours and was recognized 5 hours before the large aftershock. This quiescence was missed in our systematic study because of the time of occurrence (from 24 to 30 hours). These numbers show that if an anomaly is observed, there is a fairly good chance that it will be followed by a large aftershock, particularly in the western Pacific. On the other hand, many large aftershocks are not preceded by anomalies of this magnitude.

The following major aftershocks were preceded by a decrease of 2.2 standard deviations during the last 22% of the time period between the mainshock and the aftershock which was recognized successfully in our search:

| Region             | Mainshock                   | Aftershock                            |
|--------------------|-----------------------------|---------------------------------------|
| New Ireland        | July 14, 1971 (7.9 $M_s$ )  | July 19 (7.1 $M_s$ ), 26 (7.9 $M_s$ ) |
| Kuriles            | June 10, 1975 (7.0 $M_s$ )  | June 13 (6.4 $M_s$ )                  |
| Kuriles (Figure 3) | March 23, 1978 (7.5 $M_s$ ) | March 24 (7.6 $M_s$ )                 |

The following large aftershocks had precursory quiescences which satisfied the criteria but were not recognized in the systematic search.

|                |                            |                                 |
|----------------|----------------------------|---------------------------------|
| Santa Cruz     | July 8, 1980 (7.5 $M_s$ )  | July 17 (7.9 $M_s$ )            |
| Nihonkai-Chubu | May 26, 1983 (7.7 $M_s$ )  | June 9 (5.6 $M_s$ , 6.3 $m_b$ ) |
| Michoacan      | Sep. 19, 1985 (8.1 $M_s$ ) | Sep. 21 (7.6 $M_s$ )            |

The following large aftershocks had precursory quiescence which was identified, but did not satisfy the criterion. The drops (D) and start times (S) are given.

|                   |                            |                            |
|-------------------|----------------------------|----------------------------|
| Nemuro-oki Japan  | June 17, 1973 (7.7 $M_s$ ) | June 24 (7.1 $M_s$ ) S=39% |
| Livermore, Calif. | Jan. 24, 1980 (5.9 $M_L$ ) | Jan. 28 (5.3 $M_L$ ) D=1.8 |
| T'ang-shan China  | July 27, 1976 (8.1 $M_s$ ) | July 28 (7.4 $M_s$ ) D=2.0 |
| Kuriles           | June 13, 1975 (6.4 $M_s$ ) | June 15 (6.2 $M_s$ ) D=2.0 |
| New Hebrides      | Dec. 28, 1973 (7.5 $M_s$ ) | Jan. 10 (7.2 $M_s$ ) Late  |

The following major aftershocks were not preceded by quiescence:

| Region           | Mainshock                   | Aftershock                            |
|------------------|-----------------------------|---------------------------------------|
| Nemuro-oki Japan | June 17, 1973 (7.7 $M_s$ )  | June 17 (7.1 $M_s$ )                  |
| Kuriles          | March 23, 1978 (7.5 $M_s$ ) | Mar. 23 (6.8 $M_s$ )                  |
| Kuriles          | June 13, 1975 (6.4 $M_s$ )  | June 15 (6.2 $M_s$ ), 22 (6.1 $M_s$ ) |
| Mindanao         | Aug. 16, 1976 (7.9 $M_s$ )  | Aug. 17 (6.8 $M_s$ ), 29 (5.4 $M_s$ ) |
| Santa Cruz       | July 8, 1980 (7.5 $M_s$ )   | July 9 (6.7 $M_s$ )                   |
| New Hebrides     | Dec. 28, 1973 (7.5 $M_s$ )  | Dec. 30 (6.6 $M_s$ )                  |

Matsu'ura, R.S., Precursory quiescence and recovery of aftershock activities before some large aftershocks, Bull. Earthquake Res. Inst. University of Tokyo, 61, 1-65, 1986.

Ogata, Y., Estimation of the parameters in the modified Omori formula for aftershock frequencies by the maximum likelihood procedure, J. Phys. Earth, 31, 115-124, 1983.

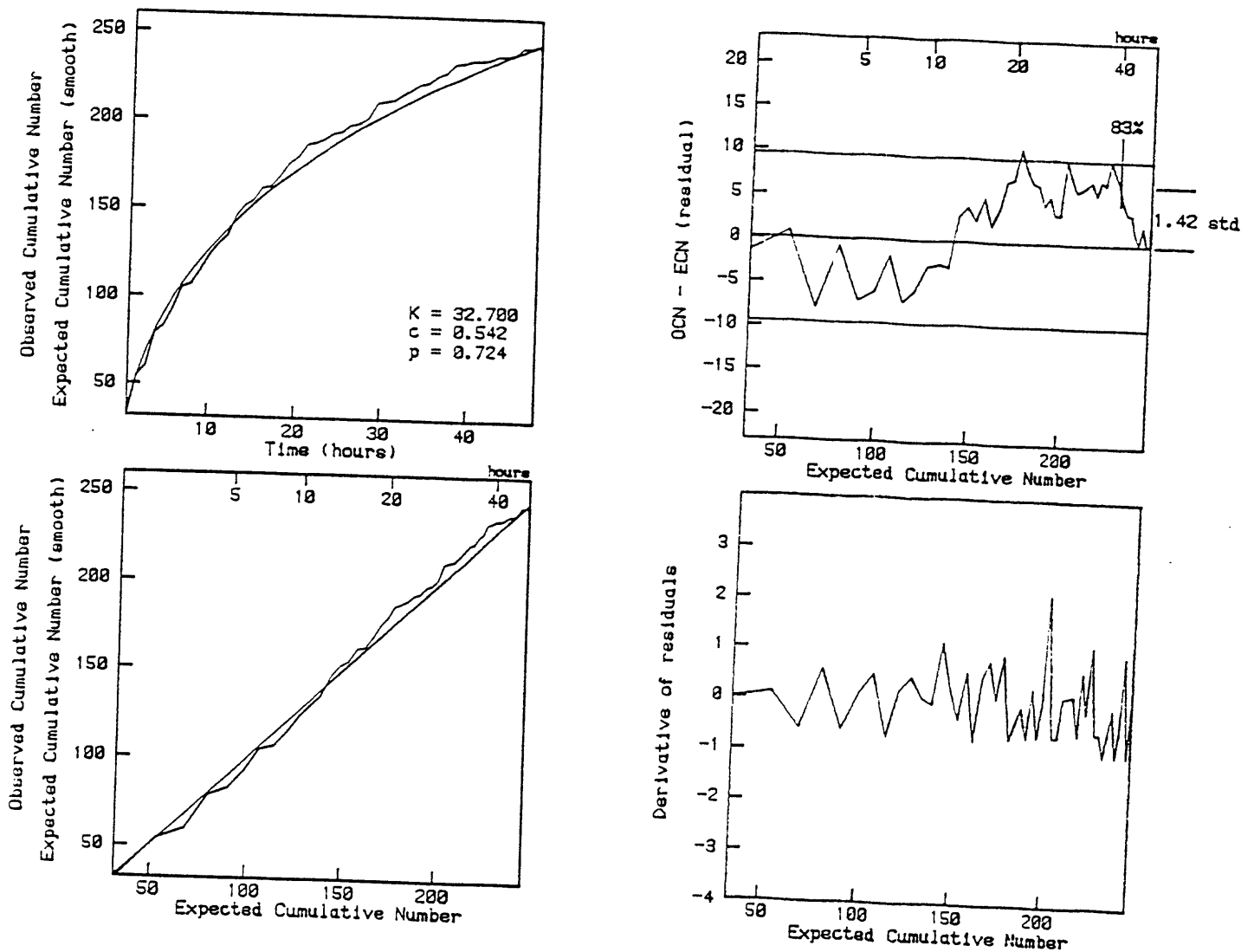


Figure 1. (A) Cumulative number of aftershocks as a function of time for the first 48 hours of the Livermore, California aftershock sequence. The observed number is the jagged line and the model with the parameters shown is smooth. (B) Observed and expected number of events as a function of expected number of events (frequency linearized time of Ogata and Matsu'ura). The expected number of events is a straight line with a slope of one in this presentation. (C) Residuals for the first 48 hours of the sequence with time of the alarm and amount of decrease marked. (D) Derivatives of the residuals. The minimum possible value of the derivative is -1 which occurs when no events have occurred in a time interval. The occurrence of a derivative of -1 is used as an to trigger the alarm algorithm.



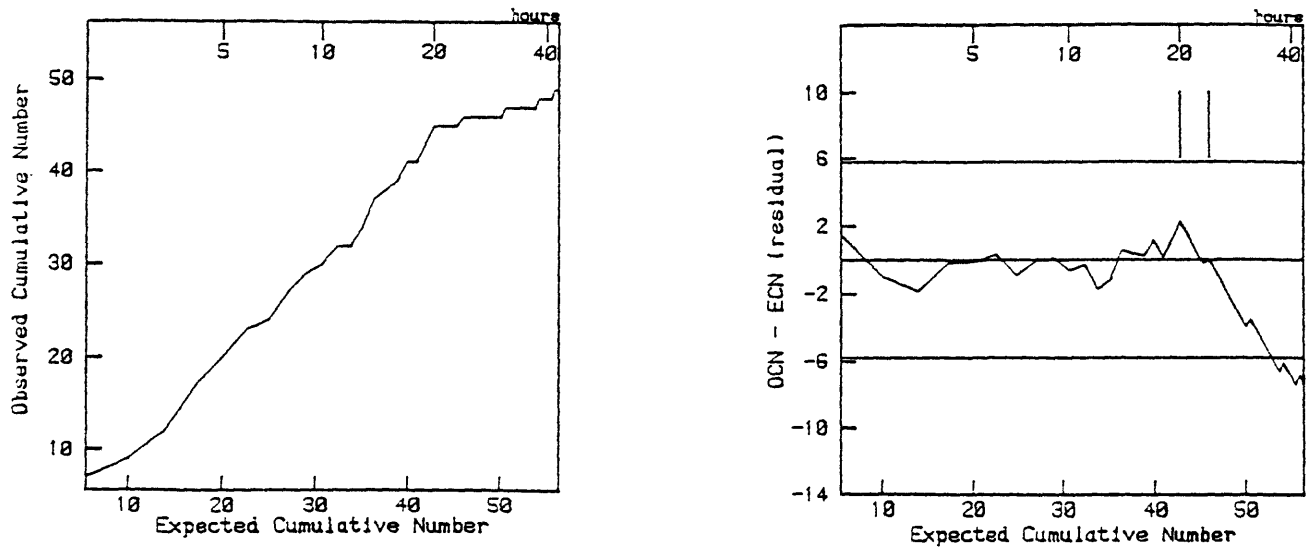


Figure 3. Precursory quiescence prior to the March 24, 1978 aftershock 43.28 hours after the March 23, 1978 Kuriles mainshock. (A) Observed versus expected cumulative number of events for the first 43 hours of this sequence. If the observed cumulative number fit the expected exactly this curve would be a straight line with a slope of one. (B) Residuals for the first 43 hours of this sequence. The vertical lines show the initial alarm recognized 24 hours into the sequence. The quiescence continues after it is initially identified, providing over 19 hours of warning prior to this aftershock.

## Coseismic Changes in Groundwater Radon

H. Wakita, G. Igarashi, Y. Nakamura, Y. Sano and K. Notsu

Laboratory for Earthquake Chemistry, Faculty of Science,  
University of Tokyo, Bunkyo-ku, Tokyo, Japan

Coseismic changes in the radon concentration of groundwater were consistently observed at a sensitive observation station for nearby earthquakes with magnitudes of 6.0 and over and were observed for most earthquakes of a similar size occurring up to about 400 km away. A total of 14 coseismic changes were observed for 16 earthquakes which occurred during the observation period, between January 1984 and July 1988. A similar change was also found for an M7.9 earthquake with a hypocentral distance of about 1000 km. The decreases in radon concentration lasting a few days which were observed for most changes can be interpreted to be caused by changes in the stress field.

It is well known that precursory changes are only observed at extremely small numbers of observation sites. Even coseismic changes are observed at only a few of many stations. This suggests the presence of a site sensitive to earthquake occurrence. The detection of a sensitive site by coseismic changes is important to earthquake prediction study.

Continuous measurements of the radon concentration of groundwater have been carried out by the University of Tokyo for over ten years at nine stations in Japan. Precise description of the measuring method (NOGUCHI and WAKITA, 1976), type of groundwater and characteristics of background fluctuations in the observed data (WAKITA et al., 1985; 1986) have already been reported. During the observation period precursory changes of the 1978 Izu-Oshima-kinkai earthquake with a magnitude of 7.0 were also observed at one of the stations (WAKITA et al., 1980).

Long-term variations in the radon data from the KSM observation site were examined in terms of occurrence of nearby earthquakes. The site, with a 200-meter-deep drilled hole, is positioned on the fracture zone of the Futaba fault (Fig. 1), one of the major active faults in Northeast Japan, with a length of about 60 km trending in a north-south direction parallel to the Japan trench. The upper layer is composed of sandstone and shale; mylonite granodiorite is found in the layers deeper than 130 m.

An iron casing pipe with a diameter of 10 cm is installed in the hole. The extremely small amounts of groundwater with a flow rate of about 30 ml/min that issue from the strainer positioned between 124 and 129 m is used for the radon measurement. Because such a small amount of water is used, several changes were made in the usual measuring system. In order to quicken response time to the possible changes in radon concentration, flowing water at the strainer position is siphoned, through a small pipe with a

diameter of 13 mm, to the measuring chamber, which was also modified for the small quantity of water. As a result of these modifications, the measuring system was too easily affected by change in external conditions. The observed radon data fluctuate, most notably affected by temperature changes in the measuring system, since emanation of radon depends on temperature changes. In spite of this fluctuation, however, several significant decreases in the radon concentration are observed. These are likely to correlate with large earthquakes that occurred in the adjacent region.

In order to remove the temperature effects, a Bayesian approach developed by ISHIGURO et al. (1983) was applied. The computer program "BAYTAP (Baysian Tidal Analysis Program)", was successfully used to analyze earth tide data (ISHIGURO et al., 1984). Since the tidal component in the radon data at KSM site is not significant, the original radon data were decomposed into the trend, the temperature response, and the irregular (residual) components by "BAYTAP". In contrast with the conventional filtering method, the procedure is based on a time domain model which includes the response of radon variation to the observed temperature input. The basic assumption of this approach is smoothness of the trend component, and this requirement is represented in the form of prior probability of the Bayesian model. The method allows an objective decision on the choice of the maximum lag of the response functions as a problem of selecting a statistical model. A precise description of the application of this procedure, including the selection of various parameters, will be reported elsewhere.

Radon data collected between January 1984 and July 1988 were processed by "BAYTAP". Downward spike-like changes were clearly observed in the temporal variations of the trend component (Fig. 2). Some of them were matched to those previously recognized in the original data. These radon changes were compared with occurrences of earthquakes in the region close to the KSM site.

Northeast Japan is situated in a typical island arc system. This region is characterized by the double-planed structure of its deep seismic zone. Many large earthquakes occur as a result of the coupling of the descending Pacific plate and the Eurasian plate. Owing to slab pull force, the stress distribution of the upper seismic plane is dominantly down-dip compression; that of the lower plane is down-dip extension (HASEGAWA et al, 1985). Figure 1 shows the epicentral distribution of  $M \geq 6.0$  earthquakes in the region during January 1984 and July 1988. A total of 16 earthquakes, including 7 nearby earthquakes with magnitudes of 6.0 to 6.7, are plotted. Their focal mechanisms are much more complicated in the southern region where three plates converge: the Pacific plate, the Eurasian plate and the Philippine Sea plate. In addition, volcanic activities are significant in the area along the Izu-Mariana arc. Coseismic changes are observed for 14 earthquakes: 13 caused substantially by movements of the Pacific plate and one related to the 1986 eruption of Izu-Oshima Volcano. For two earthquakes related to the movements of the

Philippine Sea plate, radon changes are not significant. A similar change was found for the largest earthquake with a magnitude of 7.9 and hypocentral distance of about 1000 km.

Some other changes in the trend also coincide with smaller earthquakes, for example, a change caused by an M5.8 nearby earthquake on November 29, 1986. Other observed changes not associated with earthquakes may be attributed to crustal movements reflecting changes in the stress field but not resulting in an earthquake.

No relationships between the amplitude of the radon change and hypocentral distance and earthquake magnitude are observed. No simple correlation is found to the direction of P wave first motion. The magnitudes of nearby earthquakes are not large enough to allow analysis of the relation to estimated principal strain and dilatation using a computer program based on SATO and MATSU'URA (1975). A peculiarity of the KSM site -- the presence of the fault, which may act to either amplify or distort small strain changes -- has to be considered. In fact no meaningful radon changes were observed at the NRH site positioned at the southern part of the Futaba fault.

Figure 3 shows the result of statistical treatment by "BAYTAP". The occurrences and patterns of the radon decreases in the trend component differ with earthquakes. The observed lag in response time which exceeds the 9 hours required in the present system owing to the low flow rate of the water, and the presence of a kind of relaxation process suggests that the mechanism causing radon changes is not related to direct propagation of seismic waves but is likely to reflect viscoelastic movements with a certain time constant. A decrease in radon emission eliminates the possibility that the change is due to ground vibration originating from the shock events, when the radon emission is enhanced.

This is the first paper reporting systematic observation of coseismic radon changes. Complete understanding of the mechanism causing decrease in radon emission remains in the future. In order to clarify the mechanism, field experiments changing hydraulic pressure and precise study of crustal deformations are needed. The detection of precursory changes will be facilitated by improving measuring conditions.

Acknowledgments-The authors appreciate the use of the computer program of "SEIS-PC" from Dr. Y. ISHIKAWA, and "BAYTAP" from Drs. M. ISHIGURO and Y. TAMURA, and valuable discussion with Drs. T. ASADA, M. ISHIDA, M. MATSU'URA, S NIHEI and A. TAKAGI.

#### REFERENCES

- HASEGAWA, A. N. UMINO, and A. TAKAGI, Seismicity in the Northeastern Japan Arc and seismicity patterns before large earthquakes, *Earthq. Predict. Res.*, 3, 607-626 (1985).  
ISHIKAWA, Y., K. MATSUMURA, H. YOKOYAMA, and H. MATSUMOTO, SEIS-PC -Its outline-, *Geol. Data Process.*, 10, 19-34 (1985).  
ISHIGURO, M., H. AKAIKE, H. OOE, and S. NAKAI, A Bayesian approach

to the analysis of earth tides, Proc. 9th Intern. Symposium on earth tides, Ed. J.T. KUO, 283-292, E Schweizerbart'sche Verlagsbuchhandlung, 1983, Stuttgart.

ISHIGURO, M., T. SATO, Y. TAMURA, and M. OOE, Tidal data analysis -An introduction to BAYTAP-, Proc. Inst. Stat. Math., 32, 71-85 (1984).

NOGUCHI, M., and H. WAKITA, A method for continuous measurement of radon in groundwater for earthquake prediction, J. Geophys. Res., 82, 1353-1357 (1977).

SATO, R., and M. MATSU'URA, Strains and tilts on the surface of a semi-infinite medium. J. Phys. Earth, 22, 213-221 (1974).

WAKITA, H., Y. NAKAMURA, K. NOTSU, M. NOGUCHI, and T. ASADA, Radon anomaly: A possible precursor of the 1978 Izu-Oshima-kinkai earthquake, Science, 207, 882-883 (1980).

WAKITA, H., Y. NAKAMURA, and Y. SANO, Groundwater radon variations reflecting changes in regional stress fields, Earthq. Predict. Res., 3, 545-557 (1985).

WAKITA, H., Y. NAKAMURA, and Y. SANO, Background fluctuations in groundwater radon observation, J. Phys. Earth, 34, S81-S89 (1986).

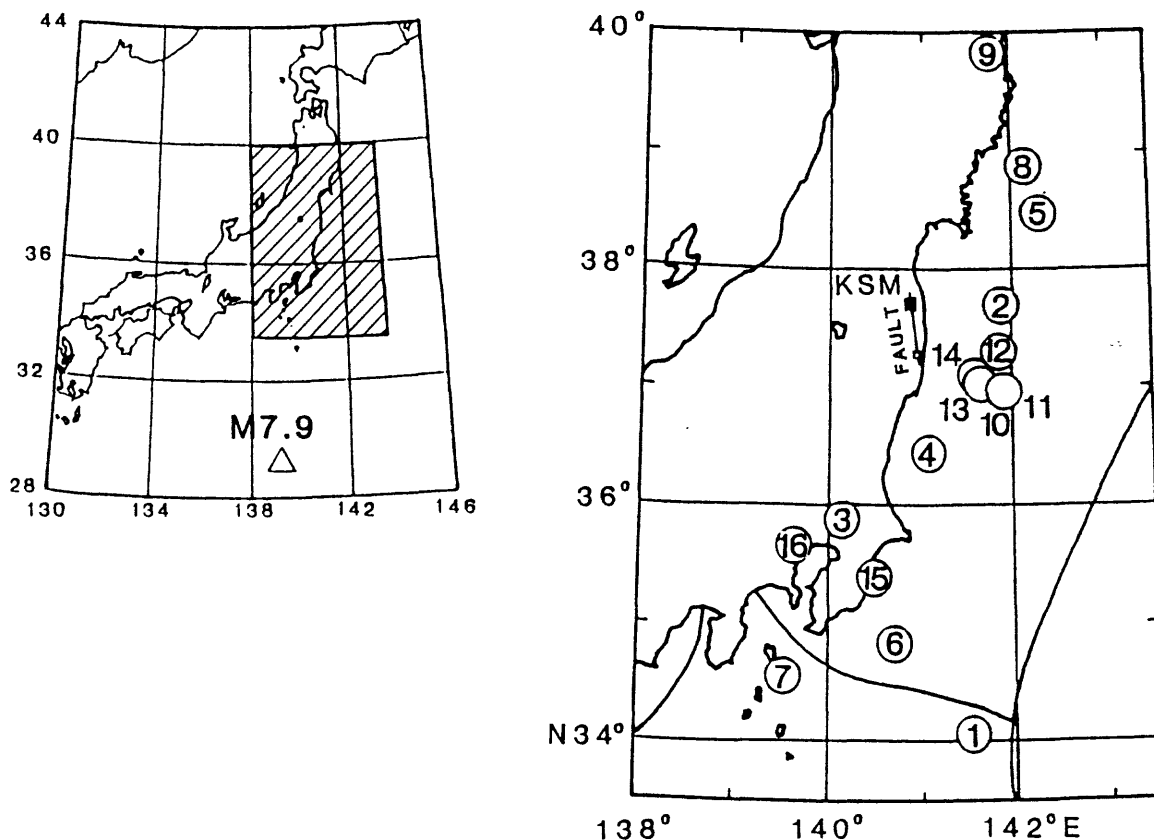


Fig. 1. Epicentral distribution of  $M \geq 6.0$  earthquakes (January 1984 and July 1988), including a M7.9 earthquake (JMA). Drawing made by the computer program "SEIS-PC" (ISHIKAWA et al., 1985).

KSM

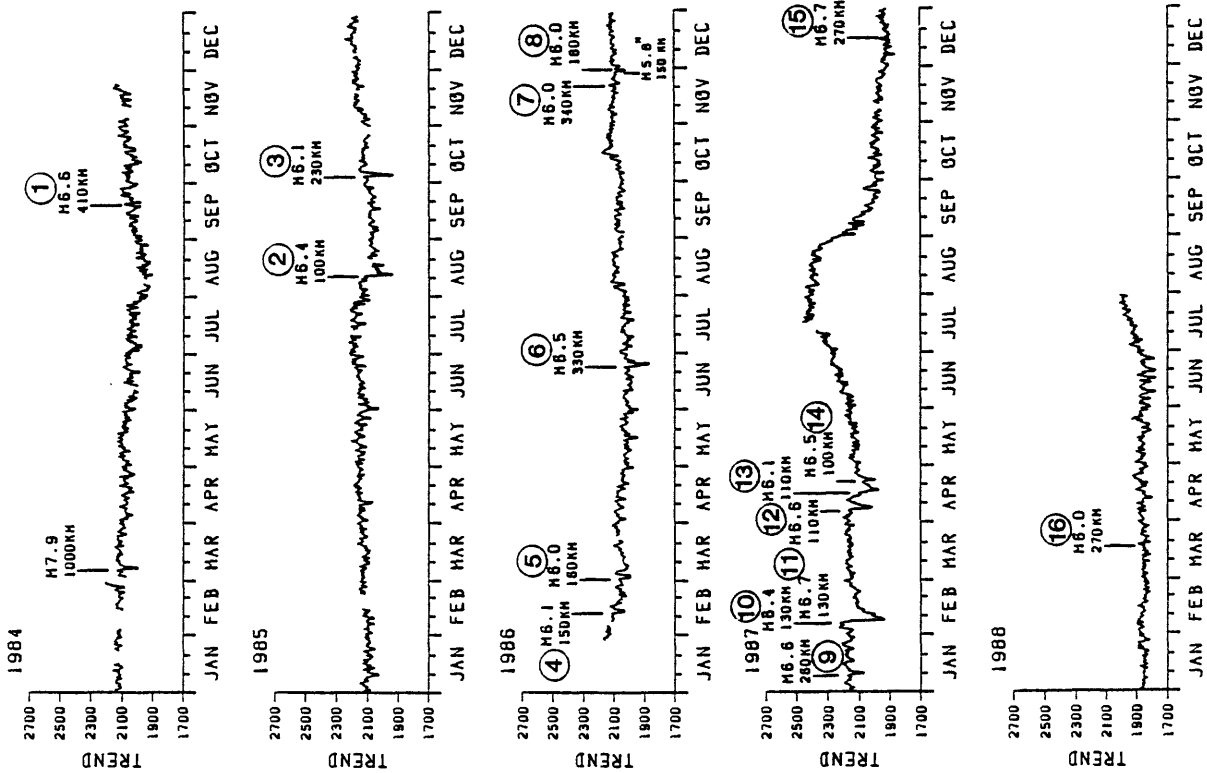
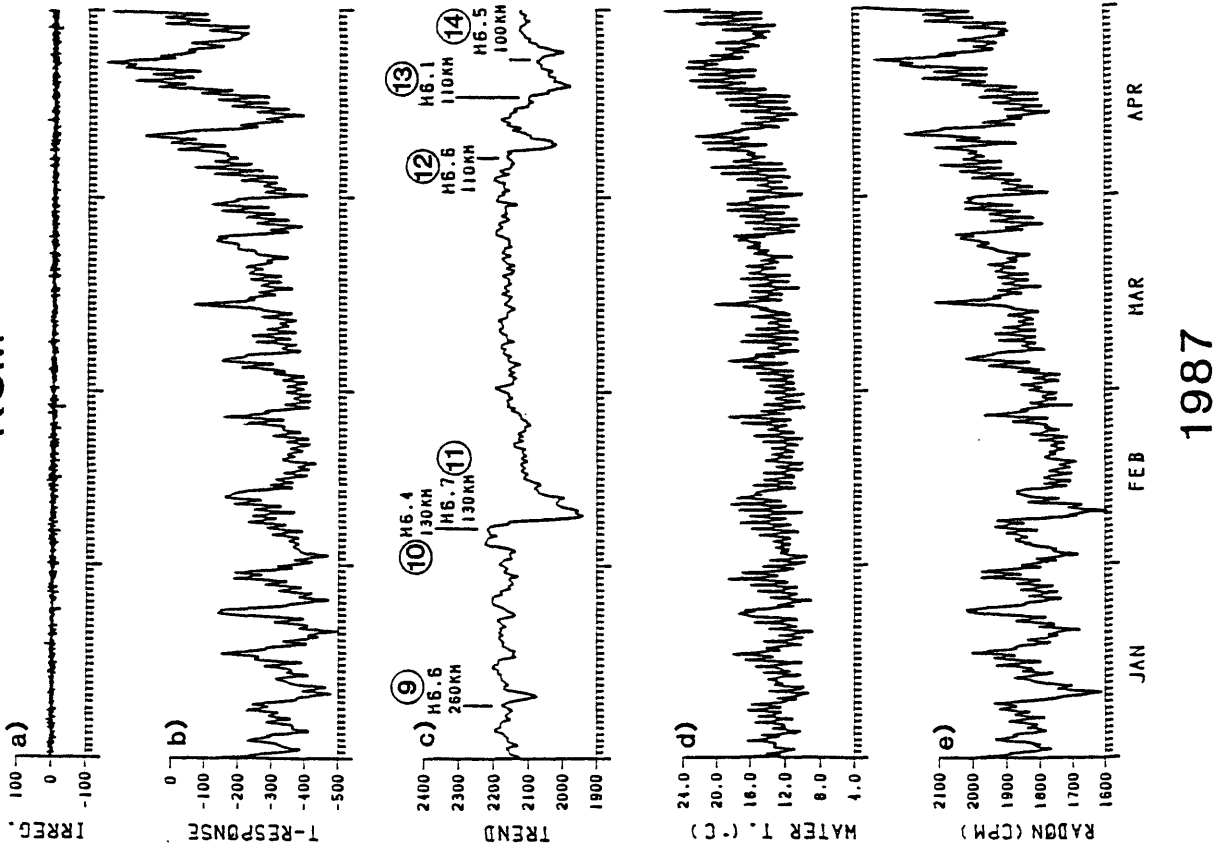


Fig. 3. Result of a Bayesian approach (ISHIGURO et al., 1984) to radon data: a) estimated irregular component, b) estimated temperature-response component, c) estimated trend component, d) observed data of temperature in the measuring chamber, and e) observed radon data.

KSM



1987

Fig. 2. Temporal variation in the estimated radon trend with occurrence of the 17 earthquakes (JMA) shown in Fig. 1 and a M5.8 earthquake.

**A MORE PRECISE CHRONOLOGY OF EARTHQUAKES  
PRODUCED BY THE SAN ANDREAS FAULT IN SOUTHERN CALIFORNIA**

Kerry Sieh,<sup>1</sup> Minze Stuiver<sup>2</sup> and David Brillinger<sup>3</sup>

**ABSTRACT**

Improved methods of radiocarbon analysis have enabled us to date more precisely the earthquake ruptures of the San Andreas fault that are recorded in the sediments at Pallett Creek. Previous dates of these events had 95%-confidence errors of 50 to 100 calendar years. New error limits are less than 23 calendar years for all but two of the dated events. This greater precision is due to larger sample size, longer counting time, lower background noise levels, more precise conversion of radiocarbon ages to calendric dates and better stratigraphic constraints and statistical techniques. The new date ranges, with one exception, fall within the broader ranges estimated previously, but the average interval between the latest 10 episodes of faulting is now about 132 years, which is about a decade less than previous estimates. Coincidentally, the new mean interval equals the present period of dormancy. This reduction of the mean interval does not result in a higher probability of a large earthquake during the next few decades, however, because variability about the new mean is much greater than was suspected previously. Five of the nine intervals are shorter than a century; three of the remaining four intervals are about two to three centuries long. Despite the wide range of these intervals, a pattern in the occurrence of large earthquakes at Pallett Creek is apparent in the new data. The past 10 earthquakes occur in four clusters, each of which consists of two or three events. Earthquakes within the clusters are separated by periods of several decades, but the clusters are separated by dormant periods of two to three centuries. This pattern may reflect important mechanical aspects of the fault's behavior. If this pattern continues into the future, the current period of dormancy will probably be greater than two centuries. This would mean that the section of the fault represented by the Pallett Creek site is currently in the middle of one of its longer periods of repose between clusters, and sections of the fault farther to the southwest are much more likely to produce the next great earthquake in California. The greater precision of dates now available for large earthquakes recorded at the Pallett Creek site enables speculative correlation of events between paleoseismic sites along the southern half of the San Andreas fault. A history of great earthquakes with overlapping rupture zones along the Mojave section of the fault remains one of the more attractive possibilities.

---

<sup>1</sup> Division of Geological and Planetary Sciences, 170-25, California Institute of Technology, Pasadena, California 91125

<sup>2</sup> Dept. of Geological Sciences and Quaternary Research Center, AK-60, University of Washington, Seattle, WA 98195

<sup>3</sup> Department of Statistics, University of California, Berkeley, CA 94720

## New Directions in the U.S. Earthquake Prediction Program

by

Robert L. Wesson  
U.S. Geological Survey  
Reston, Virginia 22092

This paper briefly highlights areas of research that seem to be likely candidates for increased emphasis in the earthquake prediction program in the United States in the years ahead. Over the last decade progress has been more rapid than originally anticipated in some areas and less rapid than anticipated in others. Perhaps most rapid progress has been made in the areas of geologic studies for long-term prediction, seismologic studies of the earthquake source, and geodetic studies of strain accumulation and release. Significant progress has been made in continuous instrumental measurements of strain, although this has proved to be a more difficult problem than perhaps originally anticipated. The reliable detection of short term precursors has also proven to be more difficult than was anticipated a decade ago, although the Parkfield Earthquake Prediction Experiment is designed to make progress in that area. Wesson and Filson (1981) outlined the basic strategy of the U.S. earthquake prediction program as it was formulated in the late 1970's. Hanks (1985) and Wesson and Wallace (1985) presented reviews of progress through about 1984. Maintaining a sound strategy for earthquake prediction research requires a continuing analysis of scientific results and a posing of new questions, and of the opportunities for new measurements, analysis and understanding presented by technological advances. This paper attempts to highlight several areas where scientific and technological advances present exciting opportunities in U.S. earthquake prediction studies.

### Geologic and seismologic studies for long-term prediction

The original ideas about seismic gaps proposed by Mogi and Fedotov and first applied in the United States by Sykes and Kelleher provided a starting point for a rich collection of geological and seismological studies leading to estimates of the long-term probabilities for large earthquakes in several parts of the western United States and Alaska. Recent estimates for the probabilities of large earthquakes in the next few decades in California (Working Group on California Earthquake Probabilities, 1988) and Alaska (Nishenko and Jacob, 1988, submitted) incorporate geologic and seismologic estimates of recurrence intervals and identify candidate areas for increased emphasis in intermediate and short-term earthquake prediction studies. In California increasing emphasis will be placed on extending these studies to other faults, to attempting to refine the long-term estimates by obtaining more recurrence data, and to develop studies for intermediate and short-term prediction studies in some of the most critical areas, particularly in southern California and the eastern portion of the San Francisco Bay region.

## New opportunities for geodetic measurements

At present most geodetic measurements for regional strain and earthquake prediction studies in the United States are carried out by the relatively tedious and expensive techniques of leveling for vertical deformation, and geodolite surveys with airplane or helicopter temperature measurements along the line of sight for horizontal deformation. The new Global Positioning System (GPS) utilizing a system of satellites flying in known orbits broadcasting signals and sophisticated ground receivers offers the possibility for increasing the speed and efficiency of these measurements, without compromising accuracy. Initial experiments comparing GPS and classical geodolite surveys in the San Francisco Bay region area and elsewhere in California are very promising (Prescott and others, in press). While considerable work remains to be done, GPS technology clearly will be playing a larger and larger role in geodetic measurements for earthquake prediction studies.

## Measurements of stress and other borehole measurements

The Cajon Pass scientific borehole (DOSECC, 1987) was originally intended to reach a depth of about 5 km adjacent to the San Andreas fault in southern California and was designed to sample and measure the physical and geological environment in an active seismic zone at seismogenic depths (4-10 km). Although funding limitations did not allow completion of the hole, the efforts surrounding the project have already added considerable vigor to the discussion of the state of stress in a seismically active region of the Earth's crust and the physical and mechanical processes operating there. Preliminary results of the investigations will appear soon in a Special Issue of Geophysical Research Letters. Despite the expense, future efforts to obtain direct measurement at seismogenic depths are critical in order to constrain the largely speculative models of the processes and conditions at these depths.

## Characterizing the rheology of fault zones

Geodetic studies of regional deformation, geologic and seismologic studies of fault displacement during and following earthquakes, and fault creep studies all suggest the importance of understanding the aseismic processes of fault deformation and their interrelationships with the generation of earthquakes. The 1987 Superstition Hills earthquake provides a striking example of these aseismic processes in that at least 80% of the surface fault displacement (approaching a maximum of nearly 1 m) occurred as afterslip. Previously minor "sympathetic" fault displacement occurred along the Superstition Hills fault associated with the 1968 Borrego Mountain and 1979 Imperial Valley earthquakes. A collection of studies of the 1987 earthquake will appear in a Special Issue of the Bulletin of the Seismological Society of America early in 1989. Fault creep may provide important clues

in intermediate-term earthquake prediction (Wesson and Nicholson, 1988). Detailed field studies and computer modeling of aseismic deformation will provide opportunities to deduce models of fault zone rheology and to test models based on laboratory measurements. Obviously characterizing the aseismic processes that lead to the redistribution and concentration of stress is important to a mechanistic approach to earthquake prediction.

#### Opportunities for combined use of short-period and broad-band seismic networks

During the 1970's and 1980's significant advances were made in developing and deploying telemetered, short-period seismic networks, and in analyzing their data output. These networks have proven invaluable as tools to study the details of the space-time patterns of seismicity and their relationship to geologic structure. Now technology is becoming available to compliment these networks with digital, broadband, high-dynamic range seismic systems. Such systems, which are becoming available as parts of the National Science Foundation/Incorporated Research Institutions for Seismology Global Seismographic Network and the U.S. Nuclear Regulatory Commission/U.S. Geological Survey National Seismographic Network, will provide capability for studies of seismic source processes and seismic wave propagation.

#### Computer modeling of earthquake processes

Fortunately, just as the measurement and observation systems are beginning to provide measurements to constrain models of the strain accumulation and earthquake generation processes, computers are becoming widely available that can make realistic predictions of measurable quantities from physically-based models of these processes. The increasing availability of such computers will provide the opportunity to greatly increase intuition and understanding of these processes through computer modeling.

#### The Parkfield Earthquake Prediction Experiment

The Parkfield Earthquake Prediction Experiment will be described in more detail at this meeting in the paper to be presented by Bakun and has been described previously by Bakun and Lindh (1985 a and b). The Parkfield experiment is particularly important to the U.S. earthquake prediction program for several reasons. First, it provides a unique opportunity to test the emerging ideas about the mechanics and interrelation of seismic and aseismic deformation processes along the San Andreas fault. Second, the Parkfield experiment provides a critical opportunity to deploy, test and compare various techniques for instrumental measurement of crustal strain in a very active tectonic environment. Instruments deployed at Parkfield for strain measurement include borehole dilatometers and tensor strainmeters, water level recorders, creepmeters and a two-color laser strainmeter. Evidence is beginning to accumulate for episodes of crustal deformation that can be detected on several kinds of instruments. Third, because of the commitment to a short-

term prediction of the next Parkfield earthquake, the experiment provides an opportunity to explore the communication and public utilization of a short-term earthquake prediction.

#### Selected References

Bakun, W.H., and A.G. Lindh, The Parkfield, California, earthquake prediction experiment, *Earthq. Predict. Res.*, 3, 285-304, 1985a.

Bakun, W.H., and A.G. Lindh, The Parkfield, California, earthquake prediction experiment, *Science*, 229, 619-624, 1985b.

Hanks, T.C., The National Earthquake Hazards Reduction Program--Scientific Status, *U.S. Geol. Survey Bull. 1659*, 40 p., 1985.

Nishenko, S.P., and K. Jacob, Seismic potential of the Queen Charlotte-Alaska-Aleutian seismic zone, *submitted to Jour. Geophys. Res.*, 1988.

Prescott, W.H., G. Svarc, and K. Wendt, Comparison of GPS baseline measurements with geodolite observations in the San Francisco Bay region, California, *Jour. Geophys. Res.*, *in press*.

Wesson, R.L., and J.R. Filson, Development and strategy of the earthquake prediction program in the United States, in Simpson, D.W., and P.G. Richards, eds., *Earthquake Prediction: An International Review*, *Am. Geophys. Union Monograph, Maurice Ewing Series 4*, 671-680, 1981.

Wesson, R.L., and C. Nicholson, Intermediate-term, pre-earthquake phenomena in California, 1975--1986, and preliminary forecast of seismicity for the next decade, *Pure and Applied Geophysics*, 126, 407-446, 1988.

Wesson, R.L., and R.E. Wallace, Predicting the next great earthquake in California, *Scientific American*, 252, 35-43, 1985.

Working Group on California Earthquake Probabilities, Probabilities of large earthquakes occurring in California on the San Andreas fault, *U.S. Geol. Survey, Open-File Report 88-398*, 62 p., 1988.

THE OUTLINE OF  
THE SIXTH EARTHQUAKE PREDICTION PLAN OF JAPAN

Kazuhiko Otake  
Geographical Survey Institute

Introduction

The Geodesy Council of the Ministry of Education, Science and Culture has proposed the 1st - 5th Earthquake Prediction plans to the Cabinet Ministers concerned, since July 1964. The 5th Plan expiring in this fiscal year, the Council made an evaluation of progress under this plan, base on which studies on a new plan (fiscal 1989 -1993) were conducted. The plan was approved at the plenary meeting held on July 28, 1988, and was subsequently proposed by the Chairman of the Council to the Prime Minister, the Minister of Education, Science and Culture, the Minister of International Trade and Industry, the Minister of Transport, the Minister of Posts and Telecommunications, and the Minister of Construction.

The Sixth Plan is summarized in the following.

Policies underlying the Plan

Under the former earthquake prediction plans, periodic surveys and observations have been conducted on a nationwide scale for long-term predictions, followed by concentrated observations looking for short-term precursory phenomena. At the same time, basic research on explanations of various phenomena preceding the occurrence of earthquakes had been promoted.

The Sixth Plan proceeds in accordance with the same fundamental concept. Focus on observations and researches in the Area of Intensified Observation and such areas (Fig. 1) will be further emphasized. For a more precise understanding of short-term precursory phenomena, the development of comprehensive analyzing method should be encouraged. Also on the basis of wide fundamental research on earthquake prediction, the research on inland earthquake prediction, active application of space techniques and other new techniques, and comprehensive utilization of various observation data should be especially encouraged.

Contents of the Plan

1. Intensification of Observation and Research Effective for Long-term Prediction

In order to improve accuracy in the prediction of the location and magnitude of earthquakes by the quantitative evaluation of long-term crustal

activities, efforts in nation wide observation and mobile observations aimed at identifying the regional characteristics should be made in parallel.

For that purpose, promoting application of new techniques, such as the space techniques, further repletion should be made in geodetic survey and seismological observation, conducted on a nationwide scale. At the same time, comprehensive mobile observation and research should be undertaken in the Areas of Intensified Observation, the Areas of Specified Observation, and other areas by mobile parties, especially observations on the sea bottom are emphasized.

Furthermore, surveys of active crustal techtonics and historiographical researches, which play important roles in the quantitative evaluation of characteristics of crustal activities, should be further promoted.

- 1) Periodic surveys and observations
  - A. Geodetic surveys
    - a) Precise geodetic survey (GSI)
    - b) High density and short-term periodic geodetic survey (GSI, HD)
    - c) Gravity and magnetic surveys (GSI, HD)
  - B. Observation by space techniques, such as VLBI, SLR, GPS (CRL, GSI, HD)
- 2) Continuous observations
  - A. Seismological observations
    - a) Large, moderate and small scale earthquake observations (JMA)
    - b) Microearthquake observation (Univ., NRCDP)
  - B. Tide gauge observation (GSI, JMA, HD)
  - C. Geomagnetic observation (JMA, HD, GSI, Univ.)
- 3) Mobile observation
  - A. Comprehensive overland observation (Univ., NRCDP, JMA, GSI, HD)
  - B. Various observations at ocean bottom (Univ., NRCDP, HD)
- 4) Fundamental investigations
  - A. Survey of active techtonics (Univ., GSI, NRCDP, JMA, GSJ, HD)
  - B. Histriographical investigation (Univ., NRCDP)

## 2. Intensification of Observation and Research Effective for Short-term Prediction

In order to detect the precursory phenomena and to grasp their characteristics, high density long-term observations of various items should be made in different areas. Improvement of observation and data analysis methods against the decrease of S/N ratio due to environmental changes, and renewal of observation facilities should be promoted.

In order to reinforce the monitoring system for the Tokai region, precise observations of various items which may be effective for short-term prediction should be made, and also data collection and processing ability should be improved.

With respect to the Metropolitan area, various observations with new techniques should be done on the basis of preceding results, such as the

development of observation methods and research and development aimed at improvement of detecting ability of short-term precursory phenomena and data accumulation should be also priorities.

- 1) Continuous observations of crustal movements
    - A. Observation by bore-hole volume strainmeter (JMA)
    - B. Composite observations by bore-hole type meters (NRCDP)
    - C. Observation by tiltmeter and extensometer (Univ., JMA, GSI)
    - E. Comprehensive survey of crustal activity along observation arrays (Univ.)
    - F. Tide difference observations (GSI, JMA, HD)
  - 2) Gravity change measurements (GSI, JMA, Univ.)
  - 3) Seismological observations (JMA, NRCDP, Univ.)
  - 4) Geoelectromagnetic observation (JMA, Univ., HD, GSI, NRCDP, CRL)
  - 5) Earth chemistry, ground water observation (GSJ, Univ.)
  - 6) Observation and Research for earthquake prediction in the Metropolitan area
    - A. Deep well observation in the central area, composite observation surrounding area and GPS observation at fixed points (NRCDP)
    - B. Precise strain, precise levelling and gravity surveys in the Metropolitan area. Application of GPS (GSI)
    - C. Strain survey by GPS and active fault study by magnetic survey and geological survey (Univ.)
    - D. Research and development of various observation methods in high noise areas (JMA)
    - E. Intensification of ground water observation on the basis of geological structure survey (GSJ)
    - F. Survey of submarine topography and geological structure (HD)
3. Promotion of Fundamental Research in Earthquake Prediction and Development of New Techniques

In order to understand the phenomena preceding earthquakes, further rock-breaking tests should be promoted.

In order to map the concentration of stress, further measurement of crustal stress, and detailed surveys of the crust and upper mantle as well as crustal activities should be made.

Especially for inland earthquake prediction, in order to carry out efficient study, surveys for selecting the study areas should be done. And also comprehensive observation and research should be tried in the area where seismological activities reflect the field of the complex plate motions.

Furthermore, to improve the study on earthquake prediction, development of techniques including space technique, and improvement and development in ocean bottom observation technique should be highly promoted.

- 1) Rock-breaking test (Univ., GSJ, NRCDP, JMA)
- 2) Measurement of crustal stress (Univ., NRCDP, GSJ)

- 3) Survey and research on crustal structure and physical property (Univ., GSJ, GSI, JMA, HD, NRCDP)
- 4) Fundamental research on inland earthquake
  - a) Precise survey for crustal, physical properties and regional characteristics of crustal activities (Univ.)
  - b) Geological structure survey, related to inland earthquake (GSJ, JMA, GSI)
  - c) Various observations and researches in high density and high accuracy in the Sagami Bay region (NRCDP, GSJ, HD, GSI, Univ.)
- 5) Development of new techniques
  - a) Development of small VLBI equipment, improvement of GPS observation accuracy (CRL, NRCDP, GSI)
  - b) Development and improvement of submarine observation technique (NRCDP, HD, Univ, JMA)

#### 4. Reinforcement of Earthquake Prediction System

- 1) Reinforcement of data collection and processing system in earthquake, crustal deformation and ground water (JMA, NRCDP, HD, GSJ, Univ.)
- 2) Preservation and application of various materials concerning earthquake prediction
- 3) Strengthening the routine monitoring system
 

For short-term prediction of the Tokai area, observation data thought to be effective are successively concentrated to JMA..

Concerning the South Kanto area, necessary data should be concentrated to JMA successively and reinforce the monitoring under intimate cooperation with the Coordinating Committee of Earthquake Prediction, and prompt and adequate application for the observation research should be reinforced.
- 4) Reinforcement of the organizations involved in earthquake prediction
- 5) Promotion of training and acquisition of staffs
- 6) Promotion of International Cooperation
 

International exchange of information about seismic observation data, symposiums, cooperative research and international cooperation at various aspects

NRCDP: National Research Center for Disaster Prevention  
 GSJ: Geological Survey of Japan  
 CRL: Communications Research Laboratory  
 JMA: Japan Meteorological Agency  
 HD: Hydrographic Department, Maritime Safety Agency  
 GSI: Geographical Survey Institute

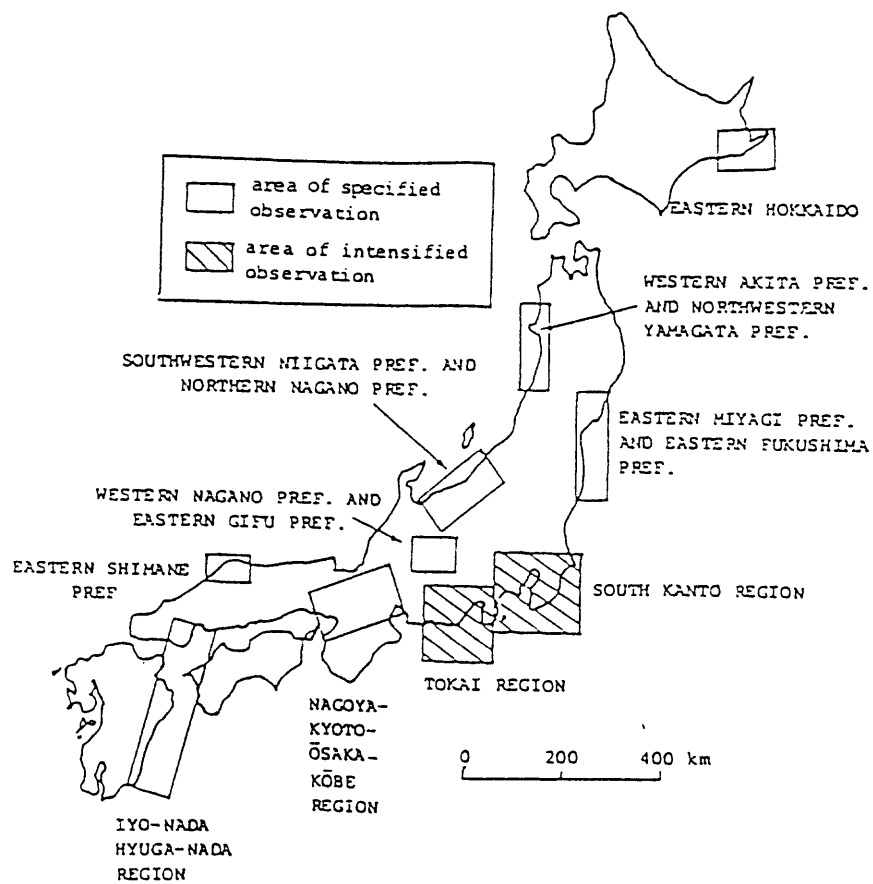


Fig. 1. Areas of Specified Observation and Intensified Observation

## Rapid Determination of Source Parameters

Adam M. Dziewonski, Harvard University, Cambridge, Ma. 02138

Rapid determination of earthquake parameters, including the source mechanism and an initial estimate of the source time function are of practical significance. The technological developments of the last few years provide new opportunities to shorten the interval between the occurrence of an event and the time that its tectonic significance can be assessed. For large events,  $M_S > 6.5$ , inclusion of data from globally distributed stations is important, because the local arrays are likely to be saturated and the finite spatio-temporal dimensions of the source complicate interpretation of local or regional data.

A new generation of seismographic stations is now being deployed. In addition to the dynamic range in excess of 200 db and the pass band from some tens of Hertz to the tidal frequencies, these stations are equipped with micro-computers having the capabilities of the mainframes of one decade ago. These micro-computers can perform varied, multiple tasks including 'housekeeping' duties, event detection, real-time filtration, internal and external communications and intensive 'number crunching'. With the availability of the automated, public access, international communication systems allowing for data transmission (telex, telephone, packet switching networks), there is an opportunity to consider the new global seismographic network as a distributed computer system. However, the transmission is can be slow, introduce errors and is expensive. It is desirable, therefore, to minimize the number of transmitted bits.

The example given here deals with determination of the seismic moment tensor, but the extension of the outlined approach to other tasks is straightforward. The inverse problem for seismic moment tensor consists of finding the linear combination its six independent components,  $f_i$ , that minimizes the expression:

$$\sum_k \int_{t_{k1}}^{t_{k2}} [u_k(t) - \sum_{i=1}^6 f_i \cdot \psi_{ik}(t)]^2 dt = \min; \quad (1)$$

where  $u_k(t)$  is the  $k$ -th observed seismogram and  $\psi_{ik}$  is the excitation function for the  $i$ -th component of the moment tensor appropriate for the  $k$ -th record. The excitation functions depend on the (known) Earth structure, locations of the source ( $\mathbf{x}_s$ ) and the receiver ( $\mathbf{x}_r$ ). The time is measured with respect to the origin time,  $t_0$ ;  $t_{k1}$  and  $t_{k2}$  are the time intervals for which the  $k$ -th waveform is considered. The least squares approach leads to:

$$\sum_{j=1}^6 f_j \cdot \left( \sum_k A_{ijk} \right) = \sum_k b_{ik}; \quad (2)$$

where:

$$A_{ijk} = \int_{t_{k1}}^{t_{k2}} \psi_{ik} \cdot \psi_{jk} dt \quad (3)$$

$$b_{ik} = \int_{t_{k1}}^{t_{k2}} u_k \cdot \psi_{ik} dt \quad (4)$$

It is only computation of the elements of the  $b$ -vector that requires the observed waveforms. If the hypocentral location ( $\mathbf{x}_s, t_0$ ) is transmitted to the station, then the excitation kernels  $\psi$  and the integral (4) can be computed there, and instead of transmitting several hundred, or even thousand, data points per component, only six or five numbers need to be transmitted from the station to the central location.

# EARTHQUAKE PHENOMENA OBSERVATION SYSTEM (EPOS)

## --- NEW JMA SYSTEM FOR EARTHQUAKE PREDICTION AND TSUNAMI WARNING SERVICES ---

Kenshiro Tsumura  
Japan Meteorological Agency  
Tokyo, Japan

### 1. Introduction

The Japan Meteorological Agency (JMA) is responsible for tsunami warning services in Japan. The JMA operates nationwide seismological observation network and six local tsunami warning (forecasting) centers to which seismic and tidal data in each area are telemetered. These local centers issue tsunami warnings and/or advisories as quickly as possible, whenever a large earthquake occurs, using telemetered data and telegrams sent from meteorological offices. ( Figure A )

The JMA is also responsible for the short-term prediction of the coming Tokai earthquake. The JMA continuously monitors various data telemetered from observation stations in the Tokai and surrounding areas, including those maintained by related institutions and universities. ( Figure B ) When anomalous changes are found in the data, the Earthquake Assessment Committee (EAC) will be summoned promptly and evaluate the possibility of occurrence of the Tokai earthquake. On basis of the EAC's assessment, the Earthquake Warnings Statement will be announced by the Prime-Minister.

The JMA has developed and installed a new comprehensive data processing system, Earthquake Phenomena Observation System (EPOS) in the Headquarters, Tokyo, in March 1987. Main purposes of EPOS are; (1) to shorten the time for issuance of tsunami warnings/ advisories and earthquake/tsunami information, and (2) to enhance the capability to monitor large amount of telemetered data for the Tokai earthquake prediction and to provide materials necessary for the assessment by the EAC more quickly and comprehensively. EPOS aims at a system for practical uses to issue warnings for the prevention and mitigation of seismic and tsunami disasters, especially loss of lives. Therefore, EPOS has been designed as a reliable and easy operational system that functions well in case of emergency.

EPOS can process maximum 512 CH seismic data and 512 CH other (crustal) data such as sea-level, strain, tilt, groundwater etc. on an on-line realtime basis. The results of processing can be shown on many color graphic displays.

### 2. Configuration of EPOS

The configuration of EPOS is schematically given in Figure 1. The main processing unit is composed of three sets of super-mini-computers (MELCOM 350/60-300, 16MB); the first for seismic data processing, the second for crustal data processing and the third for data editing/storing respectively. The interface unit is composed of several sets of telemetering units and two communication control units linked with high speed optical bus. The interface unit receives large amount of seismic and crustal data telemetered from various observation networks, converts them into unified format data in EPOS, and inputs them into the main processing unit. The interface unit is also linked to the ADESS (Automated Data

Editing and Switching System for meteorological data communication services) to receive and transmit telegrams concerning seismological services.

The peripheral devices of EPOS are installed in groups for each major specified purposes. Each group is mostly composed of several sets of color graphic displays with semi-functional keyboard, a color hardcopy device and a laser-beam printer. A large panel installed at the center of surveillance room is linked to the main unit and displays such essential information as state of tsunami forecasting, seismic intensity distribution, abnormality in monitored seismic activity and/or crustal activity in the Tokai region, and various alerts for duty personnel.

A special console is provided for preparing and sending tsunami warning/advisory telegrams instantaneously by the simplest operation.

In the meeting room for the EAC, a large screen is installed, on which almost all the information processed in EPOS can be directly displayed easily.

Magnetic disk units and optical disk unit with large capacity are used as the temporal and final storage of original and processed data.

### 3. Processing of seismic data

Main flow of the seismic data processing in EPOS is shown in Figure 2.

#### (1) Processing for seismic event detection

Signals telemetered from seismic stations are continuously checked in order to monitor the function of telemetering devices and to detect arrival of seismic waves examining STA/LTA ratio, then approximate onset times are estimated examining the variations in amplitude and frequency of input signals. The occurrence of a major earthquake is monitored by checking the number of stations at which seismic waves are detected and the maximum amplitudes at selected stations. When some conditions on these elements are satisfied, the "major earthquake mode processing" for emergent determination of hypocenter and magnitude is initiated automatically.

#### (2) Processing of seismic wave signals (First Processing)

The portion of telemetered signals which has been judged to includes seismic waves in the previous processing, are analyzed by the method using the AR-model (Yokota et al., 1981) to determine accurate onset times of P and S waves, the maximum amplitude and period, sense of initial motion and duration. Then the hypocenter and magnitude are determined using these data and the results are displayed on the graphic displays and the panel. If the magnitude thus determined exceeds 4.0, the "major earthquake mode processing" is also activated immediately. These processes are executed immediately after the detection of seismic waves within 2-3 minutes, while the secondary processing for revisional determination is executed after the end of the event with more delay.

#### (3) Major earthquake mode processing (Emergent processing for tsunami warning and earthquake information services)

To issue tsunami warnings/advisories and earthquake information promptly, the "major earthquake mode processing" is started as soon as the recognition of major earthquake is obtained in the previous processes and executed with highest priority. Telemetered data from selected 30 stations and seismic telegrams are used to reduce the calculation time. To get better result, the calculation is repeated when the time elapsed a constant interval or new data from additional 5 stations are available. The results of the calculation with seismograms used are displayed on the

graphic displays on an on-line realtime basis. Besides, operators can modify the results with interactive procedure confirming the results on the display to get final estimates. When the hypocenter and magnitude are determined with sufficient accuracy, tsunami grade on each coastal area is estimated automatically on the same principle as used in the conventional procedure using tsunami forecasting chart and the result is indicated by lighting the lamps of corresponding keys on tsunami forecasting console. The operator may modify the result on his experience by setting other key(s) indicating different grade. Confirming final decision the operator push down the release key to send out warnings/advisories which have been automatically composed as telegrams. Then they are disseminated immediately to meteorological offices, disaster prevention organs and the mass media through ADESS. Simultaneously, EPOS compiles and disseminates related information in the form of facsimile and international telegrams to PTWC etc. with minimum operation.

#### **4. Processing of crustal data**

Non-seismic data such as volume strain, linear strain, tilt, sea-level, groundwater-level etc. are called as "crustal data" in EPOS, and treated in unified procedure. The original crustal data with different sampling rates are averaged into minutely, hourly and daily values, and these values are used for monitoring and analysis with different time spans. EPOS automatically corrects barometric and tidal effects on crustal data on an on-line realtime basis and displays the results as colorful graphics, of which parameters can be easily changed. These corrections are very effective for detection of minute strain changes especially at stations near the coast as shown in Figure 3. The rate of variation of corrected values are checked regularly to alert the operator when it exceeds predetermined threshold. Since the technique to correct the effect of rainfall has not yet been established well, hourly amounts of precipitation, of which data are supplied to EPOS from AMeDAS (Automated Meteorological Data Acquisition System) are displayed with strain data to check the possibility of rainy effect visually.

#### **5. Conclusion**

By the introduction of EPOS, the time for issuing tsunami warnings/advisories is expected to be shorten by about 5 minutes compared to the conventional system. Actually, average time for the recent six cases issuing tsunami advisories with EPOS was 7 minutes as shown in Table 1. EPOS has made it possible to offer high quality data to the EAC very quickly. The committee members can examine almost any data in EPOS including realtime ones on the large screen in the meeting room, although, in case of emergency, how to select most effective data for the evaluation from huge amount of data in limited time is to be studied further.

#### **Reference**

Yokota, T., S. Zhout, M. Mizoue, and I. Nakamura, An automatic measurement of arrival times of seismic waves and its application to an on-line processing system, Bull. Earthq. Res. Inst., 56, 449-484, 1981.

Table 1. Tsunami forecast with EPOS at the JMA Headquarters, Tokyo  
 ( E:Elapsed Time in minutes, F: Tsunami Forecast, T: Tsunami Observed,  
 A:Tsunami Attention, N:No tsunami ) ( August 1987 -September 1988 )

| Date      | Time (JST) | E | F | T | Hypocenter & Magnitude |       |       |     |        |        |       |     |
|-----------|------------|---|---|---|------------------------|-------|-------|-----|--------|--------|-------|-----|
|           |            |   |   |   | Emergent               |       |       |     | Final  |        |       |     |
|           |            |   |   |   | Lat                    | Long  | Depth | M   | Lat    | Long   | Depth | M   |
| 1987/9/24 | 1355       | 8 | N | N | 36.6                   | 141.3 | 30    | 5.6 | 36.71  | 141.31 | 43    | 5.8 |
| /12/17    | 1108       | 6 | A | N | 35.3                   | 140.5 | 70    | 6.6 | 35.37  | 140.50 | 58    | 6.7 |
| 1988/3/18 | 0534       | 8 | N | N | 35.7                   | 139.7 | 90    | 6.1 | 35.66  | 139.65 | 96    | 6.0 |
| 7/31      | 0840       | 9 | N | N | 34.9                   | 139.3 | 10    | 5.4 | *34.93 | 139.22 | 19    | 5.2 |
| 8/12      | 1415       | 6 | N | N | 35.1                   | 139.9 | 70    | 5.3 | *35.10 | 139.54 | 66    | 5.3 |
| 9/ 5      | 0049       | 7 | N | N | 35.5                   | 139.0 | 40    | 5.4 | *35.48 | 139.03 | 31    | 5.6 |

\*semi-final

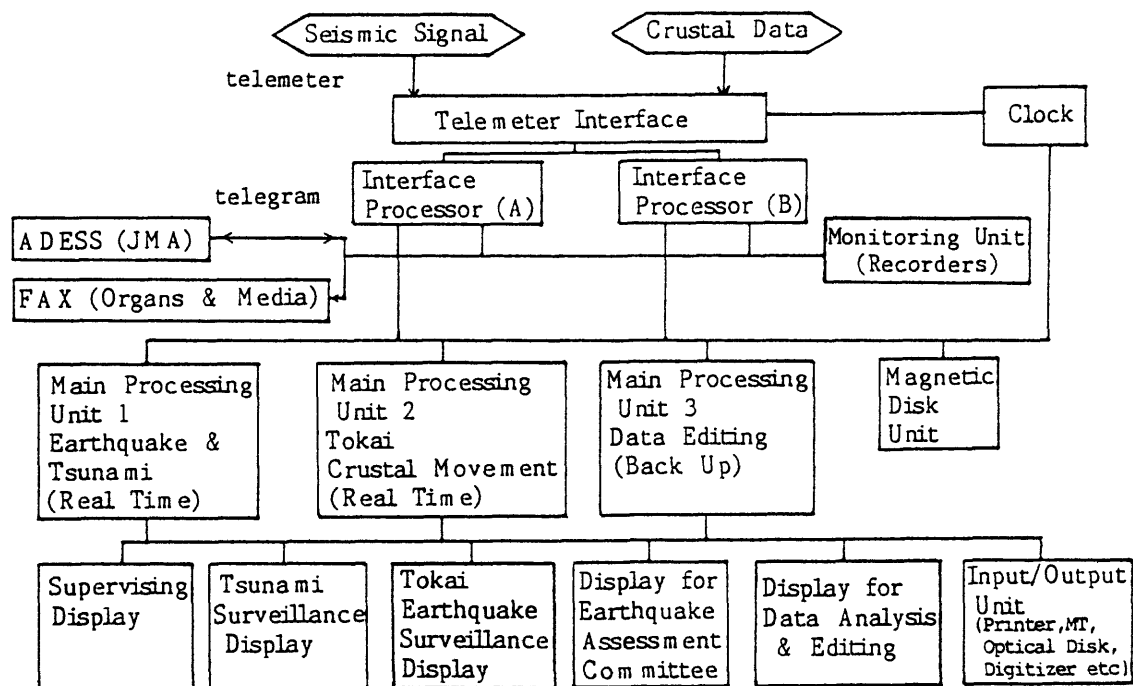
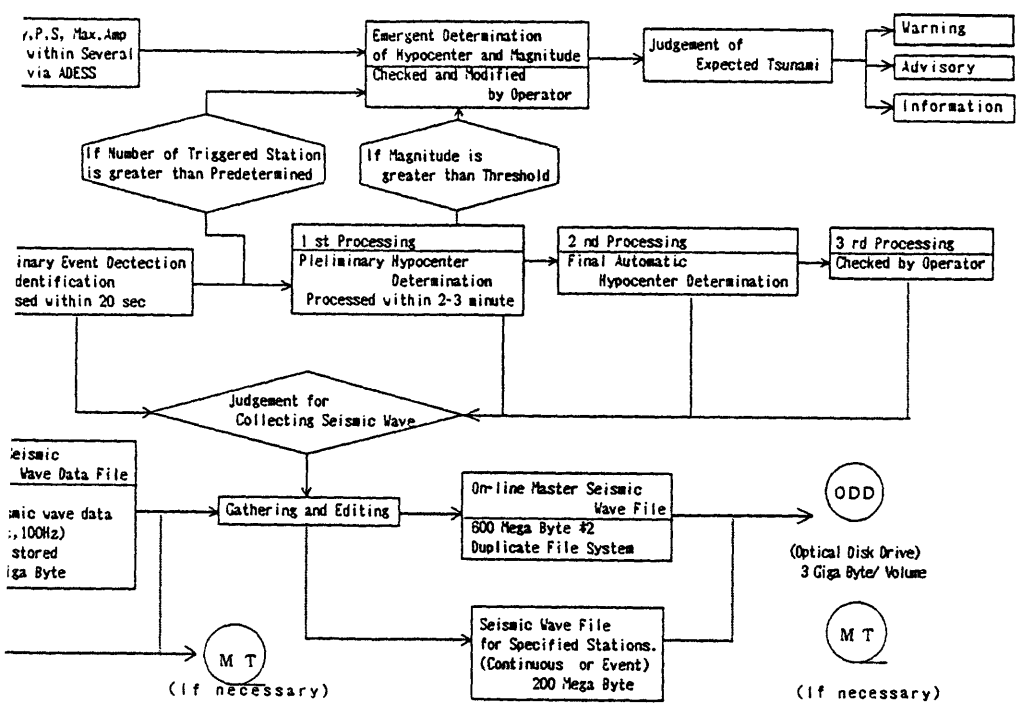
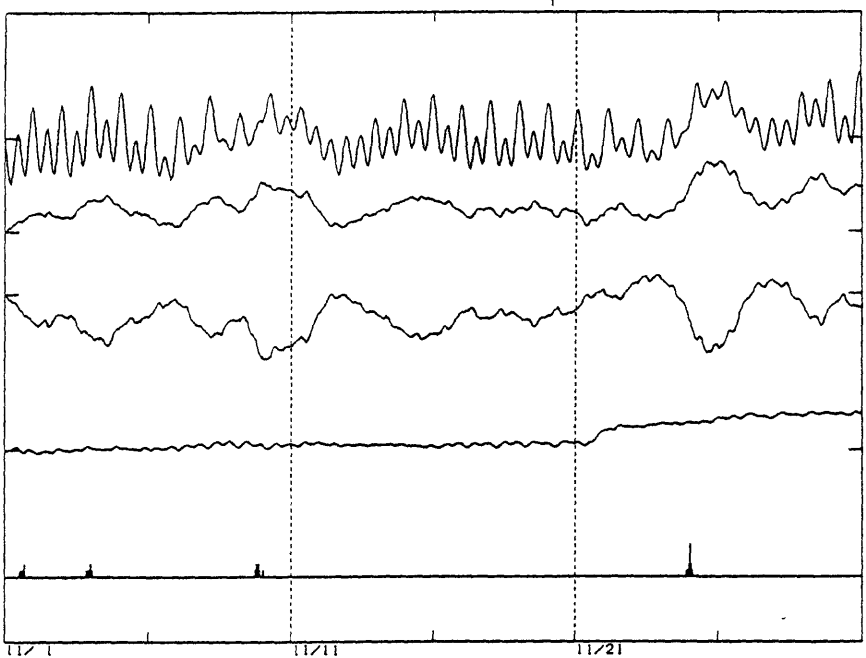


Figure 1. Schematic configuration of Earthquake Phenomena Observation System (EPOS).



Flowchart and processing flow of EPOS for tsunami warning, surveillance and information services.

時間値  
 0: 0 -- 1986/12/ 1 0: 0 >



Effectiveness of the tidal and barometric corrections for... A minute volume strain change at Toi station due to... eruption, November 21, 1986, impossible to be... original data, is easily detected on the corrected

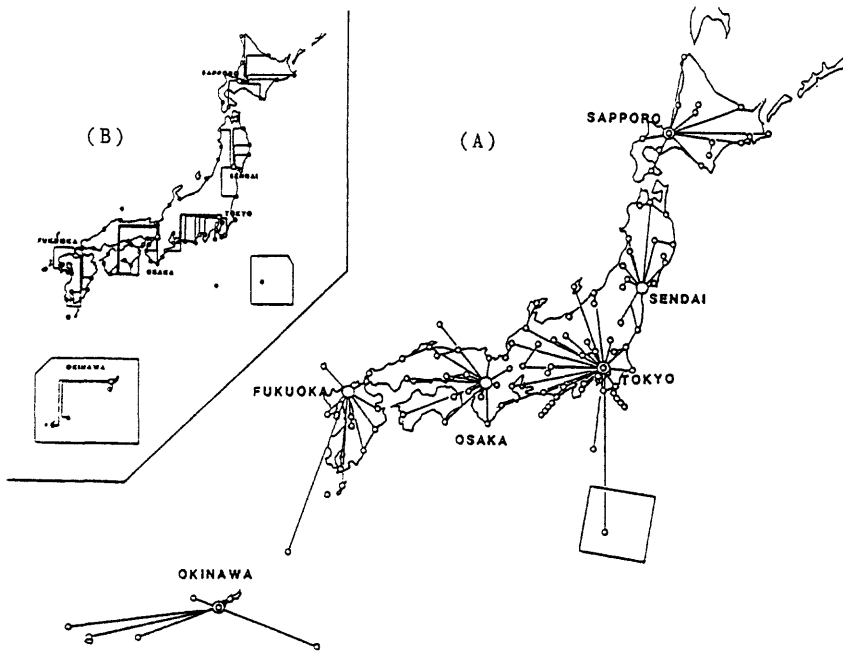


Figure A. The JMA seismic(A) and tidal(B) observation networks for tsunami warning services, telemetered to six local tsunami warning centers.

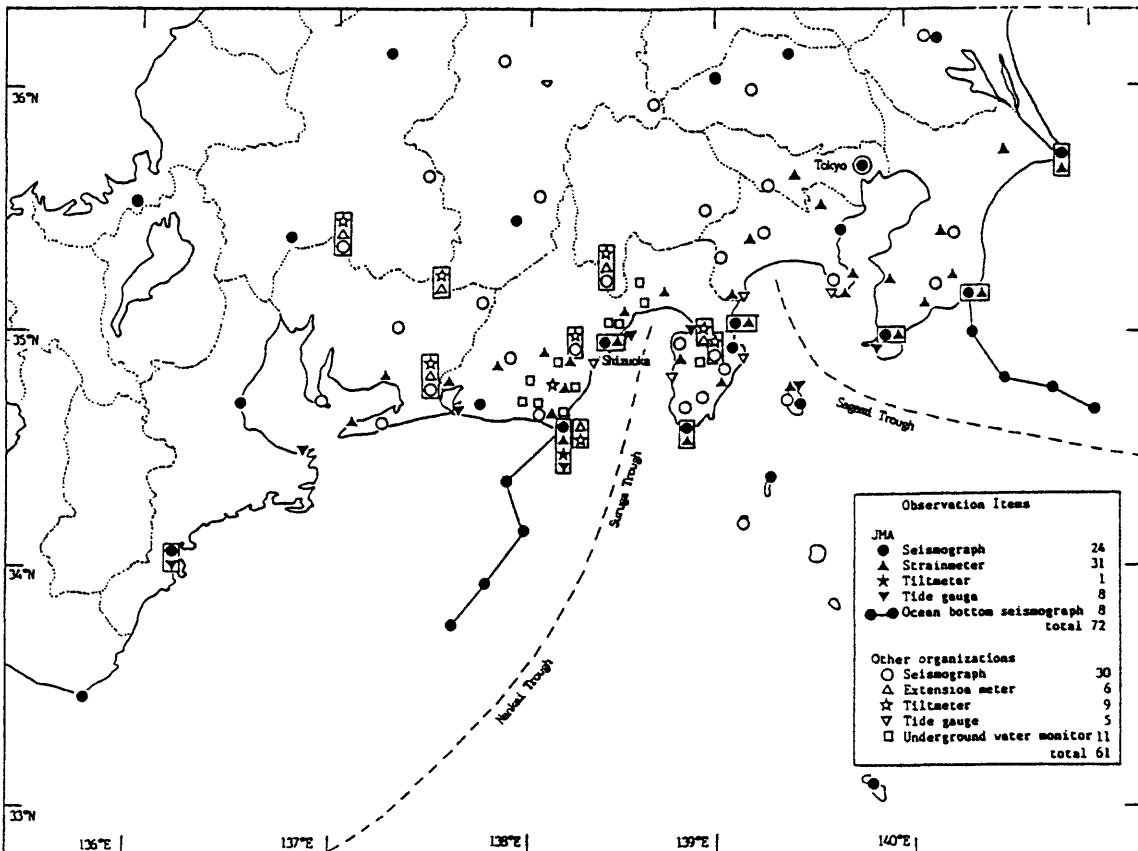


Figure B. Continuous earthquake observation network in the Tokai area and its vicinity.(Other organizations:Earthquake Research Institute of Tokyo Univ., Nagoya Univ., National Research Center for Disaster Prevention, Geographical Survey Institute, and Geological Survey of Japan).

## Appendix

### Recent results of the volume strainmeter observation

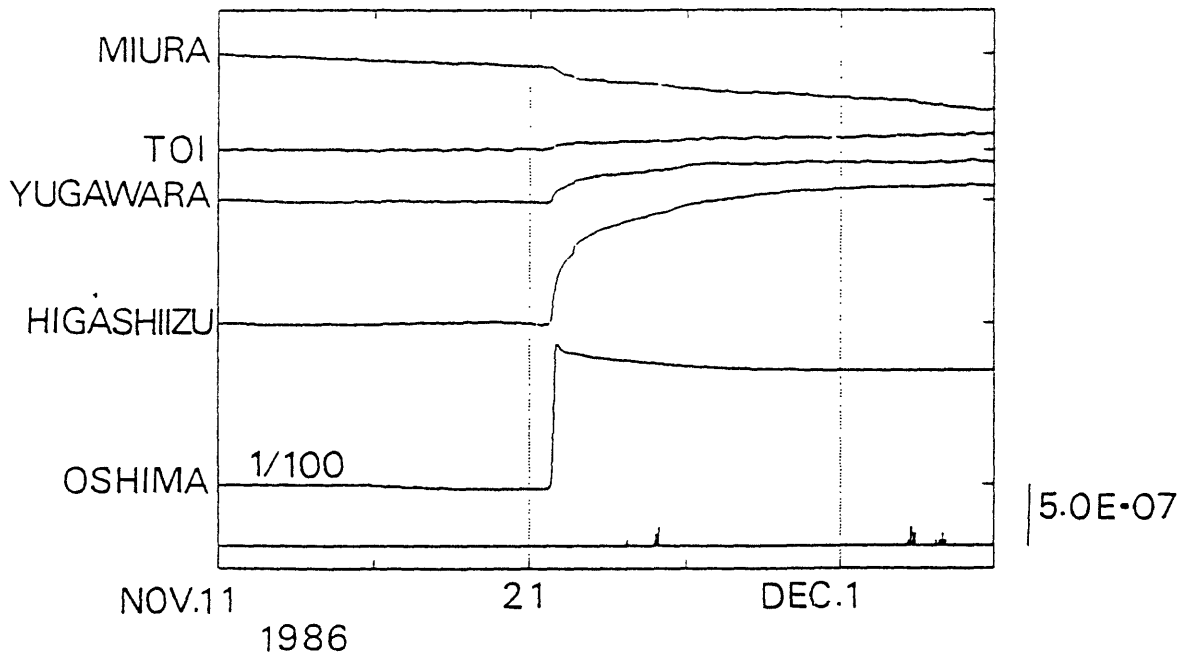
The following two results obtained by the JMA volume strainmeter network in the Tokai and South Kanto areas proved reliability of the instrument and suggested possibility of detecting minute precursors of the coming Tokai earthquake with much more reality than ever imagined.

(1) Before and after the large eruption of Izuoshima island on November 21, 1986, strain changes not coseismic but gradual, were recorded at several stations, not only at Oshima station located very close to the volcano but also at other stations located as far as 60 km from the volcano. (Figure A-1,A-2)

(2) Since 1978, active earthquake swarm activities have repeatedly occurred in the area east off the Izu Peninsula, central Honshu. The volume strainmeter at Higashiizu station, located about 20 km from the epicentral area of these swarms, recorded strain changes clearly related to the seismic activities three times; in October 1986, October 1987 and July-August 1988. The largest earthquakes in these activities were M 3.8, 4.6 and 5.2, respectively. (Figure A-3) But there were other earthquake swarm activities in the same region without any strain changes at the station. The reason of such difference is not clear at present.

The corrections for tidal and barometric effects on the strain data are indispensable for the detection of very minute strain changes as in these cases.

# STRAIN CHANGES AT OSHIMA AND IT'S SURROUNDING STATIONS



## VALUES AND SENSES

THE SHADES SHOW THE CONTRACTIVE  
ZONE CALCULATED BY THE OPEN CRACK  
MODEL

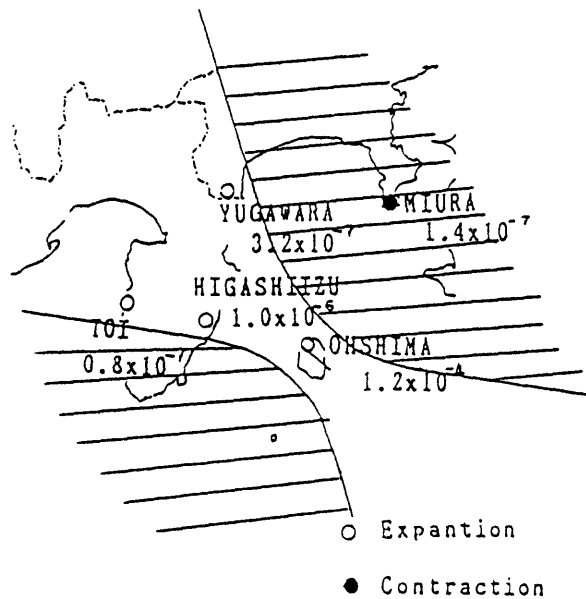
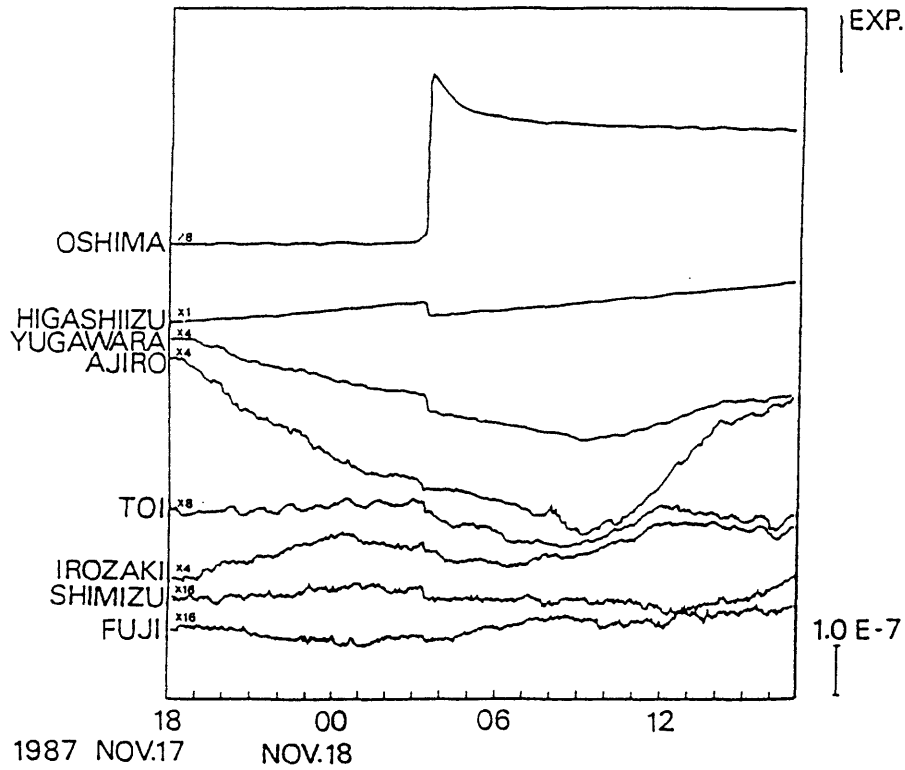


Figure A-1. Strain changes before and after the large eruption of Izuoshima on November 21, 1986.

# STRAIN CHANGES AT OSHIMA AND IT'S SURROUNDING STATIONS



## VALUES AND SENSES

THE SHADE SHOW THE CONTRACTIVE ZONE

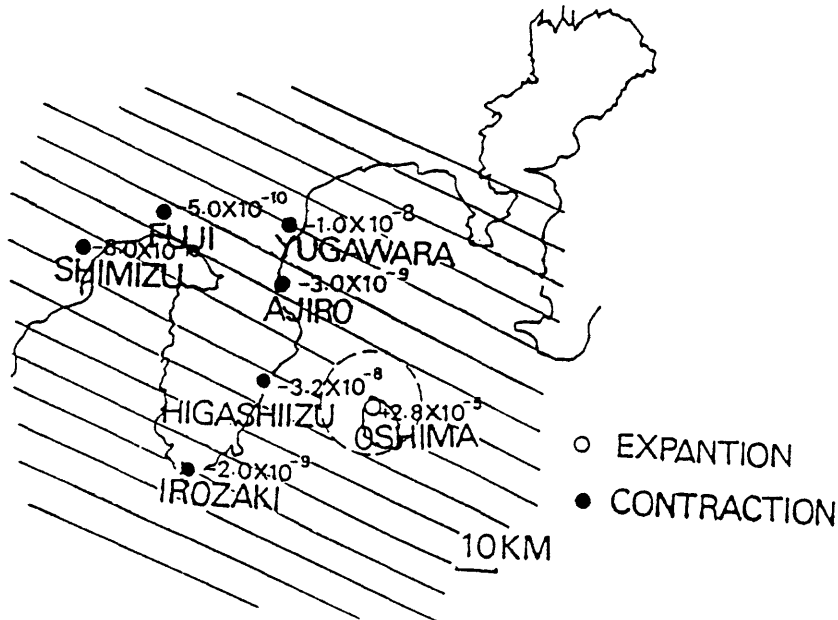
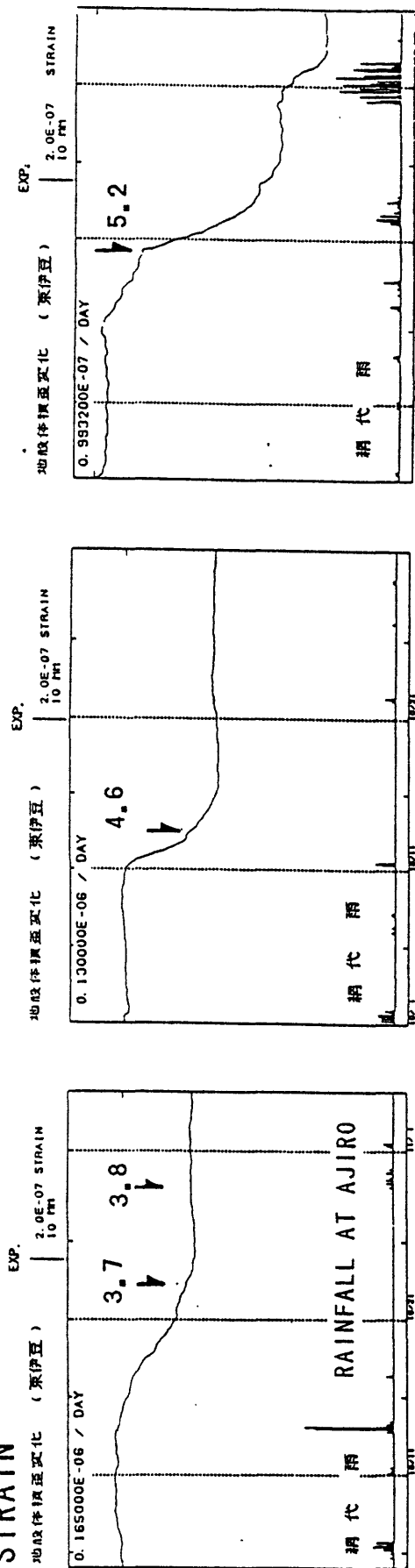


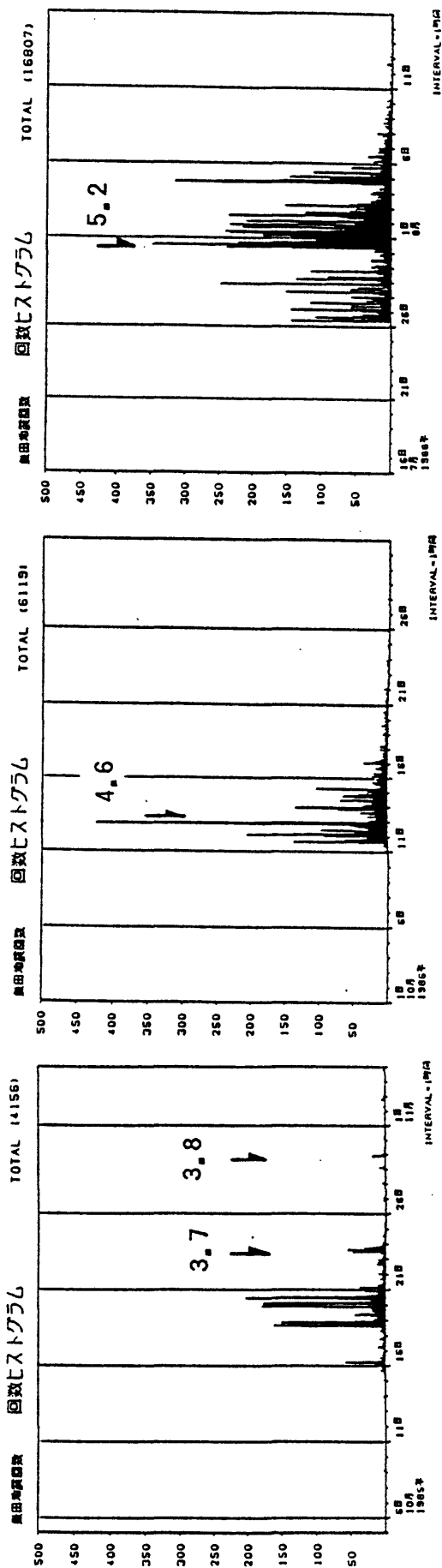
Figure A-2. Strain changes before and after the small eruption of Izuoshima volcano on November 18, 1987.

Strain Change at Higashi-Izu (epicentral distance about 20km) and Seismic Activity in the region of East off Izu Peninsula

STRAIN



HOURLY NUMBER OF EARTHQUAKES



1985/10/5 ---1985/11/4 1986/10/1 ---1986/10/31 1988/7/16 ---1988/8/15

Figure A-3. Strain changes related to the earthquake swarms recorded at Higashiizu station.

# On Mitigating Rapid Onset Natural Disasters: Project THRUST

## (Tsunami Hazards Reduction Utilizing Systems Technology)

*E. N. Bernard,<sup>1</sup> R. R. Behn,<sup>1</sup> G. T. Hebenstreit,<sup>2</sup> F. I. Gonzalez,<sup>1</sup> P. Krumpe,<sup>3</sup> J. F. Lander,<sup>4</sup> E. Lorca,<sup>5</sup> P. M. McManamon,<sup>6</sup> and H. B. Milburn<sup>1</sup>*

Rapid onset natural hazards have claimed more than 2.8 million lives worldwide in the past 20 years. This category includes such events as earthquakes, landslides, hurricanes, tornados, floods, volcanic eruptions, wildfires, and tsunamis. Effective hazard mitigation is particularly difficult in such cases, since the time available to issue warnings can be very short or even nonexistent. This paper presents the concept of a local warning system that exploits and integrates the existing technologies of risk evaluation, environmental measurement, and telecommunications. We describe Project THRUST, a successful implementation of this general, systematic approach to tsunamis. The general approach includes pre-event emergency planning, real-time hazard assessment, and rapid warning via satellite communication links.

### Introduction

Throughout history, natural disasters have killed, injured, and displaced people of every nation on the globe. Rapid onset natural hazards, such as earthquakes, landslides, tsunamis, hurricanes, tornados, floods, volcanic eruptions, and wildfires, have claimed more than 2.8 million lives worldwide in the past 20 years and have adversely affected 820 million people. The world's vulnerability and the social and economic cost of these hazards will only increase in the future because of population growth and urban concentration, increased capital investment coupled with new technologies, the existence of vulnerable critical facilities and fragile lifelines, and increasing interdependence of local, national, and international communities (Housner, 1987).

The tsunami is one example of these rapid onset hazards. Lander and Lockridge [1986] have found that 99% of all tsunami-related fatalities occur within 400 km of the earthquake epicenter. Since tsunamis are generated over the area of uplift (which could extend up to 600 km in length), most of the fatalities occurred on the coasts directly opposite the source. Travel times to these areas are much shorter than 30 minutes.

Existing tsunami warning systems are effective on a Pacific-wide time scale of 1 hour and a regional time scale of 10 minutes. They are not effective, however, on a local time scale, that is, within 2 minutes of a local, potentially tsunamigenic earthquake. Project THRUST (Tsunami Hazards Reduction Utilizing Systems Technology) has successfully designed and developed a warning system to meet this need and has established a pilot system in Valparaiso, Chile. The three major components that make up the THRUST sys-

tems approach to tsunami hazard mitigation on the local level are

- Pretsunami preparedness, consisting of
  - historical data base studies,
  - numerical model simulations, and
  - development of a detailed emergency operations plan;
- Real-time local hazard assessment, achieved by utilizing seismic triggers with predetermined threshold levels; and
- Rapid dissemination of information to local officials, achieved by exploiting satellite communications technology.

After the pilot system was installed, the Project THRUST researchers began a lengthy evaluation program. Over a period of 9 months, the average response time of the system was found to be 2 minutes — a significant improvement over the original target response time of 10 minutes. Transmission performance tests conducted during this period also demonstrated that the GOES (Geostationary Operational Environmental Satellite) communication system could be used in a warning mode. The THRUST team found that after 1 year of operation, hardware reliability was acceptable for first-generation pilot instrumentation. Furthermore, it seems apparent that the level of reliability required in a true operational setting will be achievable in the second generation of THRUST equipment.

The major objective of project THRUST has thus been achieved — the development of a low-cost system to deliver tsunami warnings rapidly enough to be useful on a local level. Hardware costs for the most basic THRUST system configuration, consisting of a seismic station and tsunami warning station, are about \$15,000. Furthermore, this fundamental system delivers the primary THRUST product — life-saving tsunami hazard information — in an average elapsed time of 2 minutes.

### Tsunami Hazard and Warning

Tsunamis are long ocean waves that are usually generated by the sudden displacement of the seafloor by large, shallow-focus submarine earthquakes. The initial damage to coastal structures is caused directly by the enormous forces that characterize an incident wave. Destruction continues, however, through a number of indirect mechanisms that can wreak havoc in a coastal community, ultimately causing much greater damage than that inflicted directly by the tsunami. Flotation and drag forces move houses and overturn railroad cars; inundation turns floating debris such as autos, logs, and pieces of destroyed buildings into dangerous projectiles; strong tsunami-induced currents lead to the erosion of foundations and the collapse of bridges and seawalls; fires result from the combustion of oil spilled by damaged ships or

<sup>1</sup>NOAA Pacific Marine Environmental Laboratory, Seattle, Wash.

<sup>2</sup>Science Applications International Corporation, McLean, Va.

<sup>3</sup>Agency for International Development, Office of U.S. Foreign Disaster Assistance, Washington, D.C.

<sup>4</sup>NOAA National Geophysical Data Center, Boulder, Colo.

<sup>5</sup>Instituto Hidrografico de la Armada de Chile, Valparaiso, Chile.

<sup>6</sup>CyberLink Corporation, Boulder, Colo.

storage facilities [Bernard and Goulet, 1981]. The ultimate loss, however, is that of human life.

Over 51,000 coastal residents have been killed by 94 destructive tsunamis in the last century. To protect coastal inhabitants, some local authorities have initiated mitigation measures such as the identification of tsunami inundation areas, the construction of protective barriers, and the establishment of tsunami warning systems. Currently available tsunami warning systems provide two levels of coverage for coastal inhabitants around the Pacific Ocean. The first level of coverage is Pacific-wide (represented in Figure 1 by the letter A) and provides warning to all Pacific nations of large, basin-wide destructive tsunamis. The second level of coverage is regional (represented by the letters B-F in Figure 1) and provides quick warnings for tsunamis generated within that region.

The Pacific-wide system is operated by the U.S. National Oceanic and Atmospheric Administration (NOAA) Pacific Tsunami Warning Center (PTWC) near Honolulu, Hawaii. This international monitoring network consists of some 30 seismic stations and 78 tide stations throughout the Pacific basin. Two criteria are used to identify earthquakes with tsunamigenic potential: the estimated  $M_s$  magnitude must be greater than 7.0, and the estimated epicenter must be located in a known tsunamigenic region. If an earthquake that meets these two criteria occurs, then nearby tide stations are monitored for evi-

dence of a tsunami. If a tsunami is detected, and if it is large enough to be dangerous, then a Pacific-wide warning is issued, with estimates of arrival times at selected coastal locations. This system is presently capable of determining epicenter locations to within  $\pm 50$  km, computing initial magnitude estimates to within  $\pm 0.2$  on the Richter scale, reporting wave height observations with an accuracy of  $\pm 10$  cm, and estimating tsunami arrival times with an accuracy of  $\pm 10$  minutes (PTWC, personal communication, 1987). The minimum time presently required to complete these procedures and issue a warning is 1 hour; since a typical deep ocean tsunami speed is  $\sim 750$  km/h, the Pacific-wide warning system provides effective warning only for those coastal areas that are more than 750 km distant from the earthquake.

Regional warning systems, the second level of protection, are effective in providing warnings for coastal areas within 100–750 km of the tsunami source. These regional systems have been established in a number of areas that are known to be prone to earthquake, such as French Polynesia, Japan, the Soviet Union, Hawaii, and Alaska (Figure 1). An important procedural difference distinguishes these regional systems from the Pacific-wide system: If the criteria for earthquake magnitude ( $M_s > 7.0$ ) and location are met, then a regional warning is issued immediately. Subsequent observations at sea level stations are used to make decisions regarding cancellation of the regional warning or extension of the warning to other areas of the Pacific. Regional systems estimate earthquake magnitude and location by processing local seismic data, which is available in real time via telephone lines or dedicated transmission circuits. Typically, a regional system can process these data and issue a warning within 12 minutes of earthquake occurrence [Sokolowski et al., 1983]. The special processing involves various algorithms dependent on amplitude and duration measurements from low-gain seismometers. Such techniques gain speed at the expense of some accuracy. The magnitude of large earthquakes is particularly difficult to estimate with near-source data, because the effects of the local crust and differential radiation from the fault are poorly known. Nonetheless, it appears that magnitudes can be estimated with an accuracy of  $\pm 0.3 M_s$ , and epicenters can be located to within  $\pm 20$  km. Regional centers also provide wave heights observations to within  $\pm 5$  cm and estimate arrival times to within  $\pm 5$  minutes [Sokolowski et al., 1983].

The effectiveness of such systems is demonstrable and impressive. Before establishment of the Japanese regional system, more than 6000 people were killed by 14 tsunamis; in contrast, 20 local tsunamis have killed 215 Japanese since the regional system became operational. Similar savings of life are credited to the other regional systems. Unfortunately, it is clear from Figure 1 that many coastal areas remain unprotected by such systems, primarily because of a high initial cost of about \$1,000,000 (U.S.) and typical operating costs of \$500,000/yr. As a result, 5646 people have been killed by six tsunamis in the last 11 years at coastal sites unprotected by such regional systems.

The U.S. Agency for International Development's Office of Foreign Disaster Assistance (AID/OFDA) saw the need for a much

less expensive system, and in 1982 the office commissioned NOAA's Pacific Marine Environmental Laboratory (PMEL) to develop and evaluate a low-cost pilot. The resulting activity became known as the Project for Tsunami Hazard Reduction Utilizing Systems Technology (Project THRUST). Three general requirements were ultimately adopted by the project as design criteria for the final end-to-end system:

- maximum compatibility with local needs and resources,
- minimum cost, and
- proven reliability.

The project team assured local compatibility by working closely with local authorities at the specific site chosen. Low cost was achieved primarily through the use of existing technology. Reliability was proven through the 1-year evaluation program with routine monitoring and periodic testing of the system (mentioned above). The resulting pilot system can provide critically needed tsunami warnings on a local level at low cost and functions effectively as a valuable complement to Pacific-wide and regional tsunami warning networks. Furthermore, the basic THRUST unit can be viewed as a fundamental building block that could be duplicated and linked to form additional regional networks.

This report describes the design and development of the three THRUST components mentioned above, as well as the results of the yearlong evaluation study performed on the pilot local tsunami warning system established in Valparaiso, Chile.

## Pre-tsunami Preparedness

Of the three THRUST components, the first — pretsunami preparedness — bears most directly on the issue of THRUST system compatibility with a particular location. Bernard et al. [1982] identified three separate but related tasks that are needed to assess the local tsunami threat systematically and ensure that the final system was indeed compatible with the needs and resources of a specific site:

- historical data base studies,
- numerical model simulations, and
- development of a detailed emergency operations plan.

The site chosen for the location of the pilot system had to have a clear need for a warning system and the local resources to analyze, maintain, and evaluate the new THRUST technology. The Valparaiso area has a clear need: It has long been recognized as a region that is seismically active. It lies in a subduction zone formed by the Nazca tectonic plate thrusting under the South American continent. Great earthquakes ( $M_s > 7.8$ ) occurred in 1575, 1647, 1730, 1822, and 1906, with rupture lengths of  $\sim 300$  km [Comte et al., 1986]. Nishenko [1985] placed Valparaiso in the middle of a seismic gap with an estimated recurrence interval of  $83 \pm 9$ . A significant probability therefore exists that the next great earthquake in this region will occur during  $1989 \pm 9$  years. Furthermore, Chile has experienced 123 tsunamis since 1562, 24 of which have caused extensive loss of life and property. Figure 2 shows that Valparaiso lies in the middle of a region characterized by

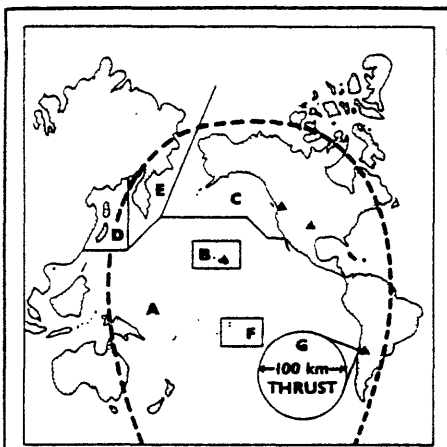


Fig. 1. Two types of tsunami warning systems exist for the Pacific basin. The Pacific-wide system warns populations in about 1 hour or  $> 750$  km from the source, while regional systems warn in about 10 minutes or between 100 and 750 km from the source. THRUST was designed as a low-cost system to warn local populations within 100 km of the source area. Areal coverage for GOES West satellite communications and locations of THRUST receivers during project, are also depicted. Pacific-wide warning system (over 750 km): A—the Pacific Tsunami Warning System. Regional warning systems (100–750 km): B—Hawaii, C—Alaska, D—Japan, E—Soviet Union, and F—French Polynesia. Local warning system (less than 100 km): G—THRUST system. Dashed line encloses area of communications coverage by the GOES West satellite; solid triangles are the locations of THRUST receivers.

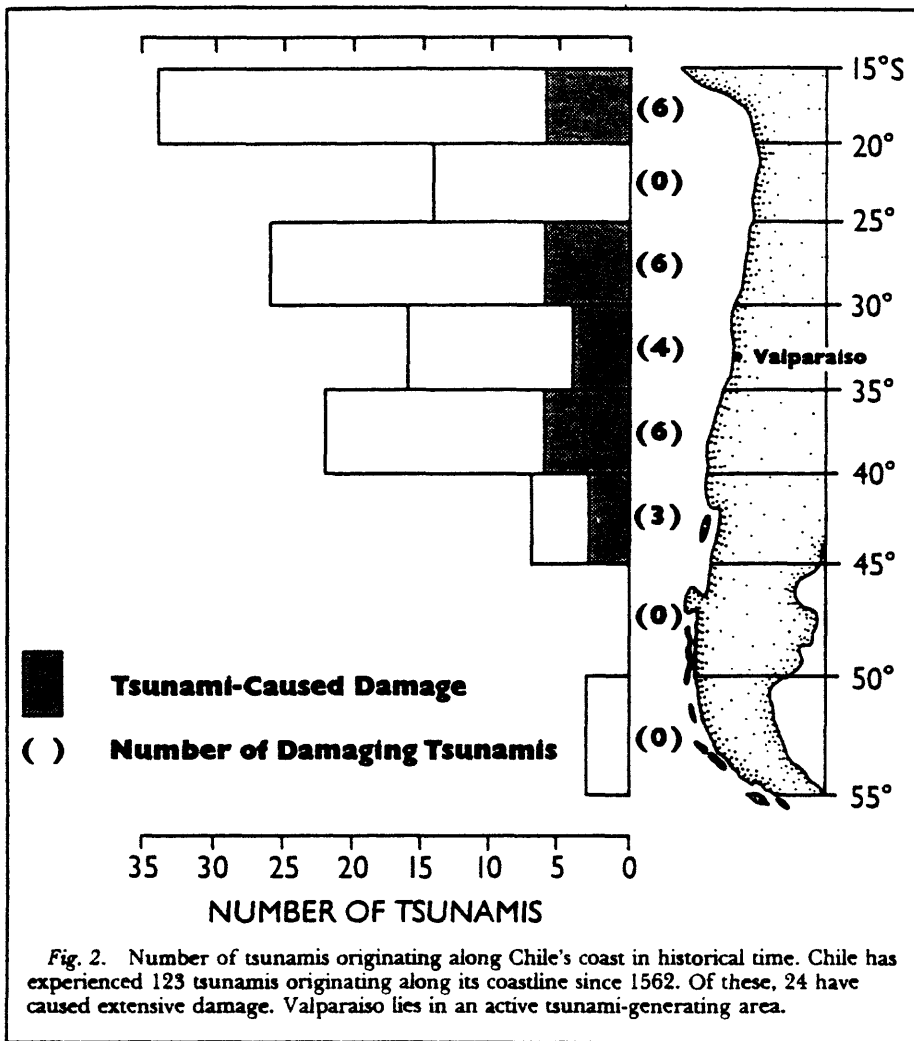


Fig. 2. Number of tsunamis originating along Chile's coast in historical time. Chile has experienced 123 tsunamis originating along its coastline since 1562. Of these, 24 have caused extensive damage. Valparaiso lies in an active tsunami-generating area.

destructive tsunamis that have killed over 1500 residents since 1900 [Lockridge, 1985].

The requisite local disaster warning expertise was also available. The National Tsunami Warning Center for Chile, located in Valparaiso, is under the operational control of the Instituto Hidrografico de la Armada (IHA). IHA maintains 10 tide stations along the Chilean coast as part of its tsunami hazard mitigation effort, and a communication link with the PTWC ensures warning of distantly generated tsunamis. For these reasons, after careful examination of several other sites, the city of Valparaiso was selected as the ideal site.

#### Historical Data Base Studies

To develop the relevant historical data base, the National Geophysical Data Center (NGDC) of NOAA's National Environmental Satellite, Data, and Information Center (NESDIS) searched published data and technical reports, journal articles, and tsunami warning logs and communicated personally with data management personnel worldwide. These data were then incorporated into the NGDC tsunami data base, which now includes information on 1,989 tsunamis. Subsequent analysis of these data provided several important products: a statistical summary of tsunami characteristics for the Peru-Chile region [Lockridge, 1985], an evaluation of the nature of tsunami risks specific to Chile [Lander,

1986], and a wall-sized multicolored map summarizing the historical tsunami record in the Pacific basin [Lockridge and Smith, 1984]. The map has found extensive use as a valuable tool in the tsunami educational program of Chile and elsewhere.

These statistical studies showed that the tsunami hazard mitigation problem is primarily near-field in nature. Of all tsunami fatalities that have occurred in the Pacific, 99% were found to occur within 400 km of the earthquake epicenter. This general result was also true for the specific site of Valparaiso. Six of the 23 Chilean tsunamis experienced at Valparaiso were damaging, but the most damaging tsunamis were generated within 100 km of the city. This implies a response time of less than 10 minutes for an effective local warning system.

#### Numerical Model Simulations

Modeling techniques can provide insight into local tsunami hazards and have been used extensively in estimating inundation areas [Houston et al., 1975; Brandsma et al., 1979]. A weakly nonlinear model that allows flooding [Reid et al., 1977] was selected for the THRUST Valparaiso study because of previous success in using this model to evaluate tsunami threats in South America [Hebenstreit and Whitaker, 1983]. The model was first

validated by simulating the 1960 tsunami in Corral, Chile, where run-up data were available.

The final results of the historical data base analysis suggested that two specific cases should be numerically simulated. These simulations were intended to provide worst-case scenarios, and the results are thus believed to be very conservative indicators of tsunami hazard, that is, they ensure a substantial margin of safety if used as a basis for the development of emergency response procedures. Critical results from these numerical simulations were the findings that such a worst-case tsunami could be expected to cause extensive flooding of Valparaiso (Figure 3) and to arrive within 3 minutes of the generating earthquake.

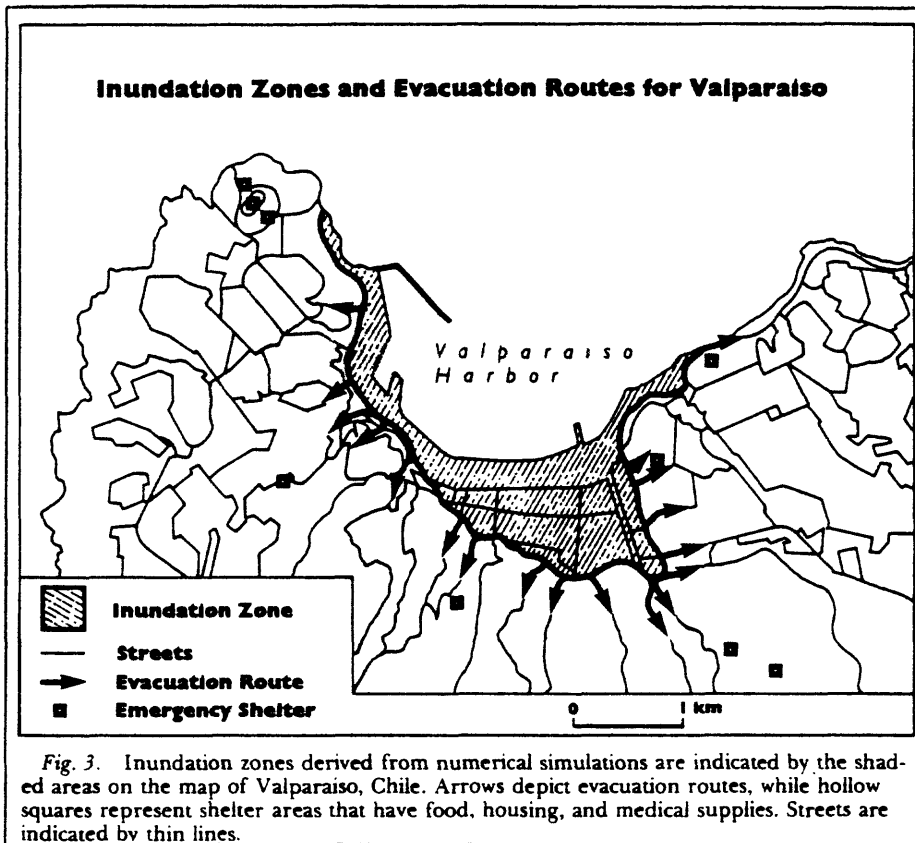
#### Development of a Detailed Emergency Operations Plan

The results of the numerical simulations were used as an aid in disaster planning, both for short-term measures to be taken on issuance of a tsunami warning and for longer-term relief efforts once the tsunami had receded. The simulated inundation maps were combined with baseline topography and street maps to identify emergency resources and tools that must be available on short notice during such a disaster, including hospitals, staging areas, and evacuation routes. They also indicated those resources that might not be available because of their location within the flood zone.

With this information in hand, the Office of National Emergency for the Ministry of Interior (ONEMI) in Valparaiso organized a series of meetings with all local officials involved in emergency operations. The result was the "THRUST Project Tsunami Emergency Operations Plan for Chile" [Lorca, 1987], which includes maps depicting probable inundation areas, evacuation routes, security areas, hospitals, and other important disaster resources. In addition to detailing emergency procedures, this plan facilitates documentation of the disaster by providing standardized forms for reporting field situations and damage assessments. Useful reference material is also provided in four appendices that describe the Chilean emergency relief structure, local tsunami hazard analysis, public education, and ham radio emergency network regulations. Finally, to ensure continued coordination among the various agencies, the document outlines simulation exercises to be conducted and evaluated at regular intervals.

#### Real-Time Hazard Assessment

The worst case scenario would be one in which a large earthquake just offshore of Valparaiso generated a tsunami that arrived within 3 minutes. The first warning of possible tsunami generation would be local ground motion, and residents should be educated to act accordingly (a public education program is a critical component of the comprehensive emergency plan). In the first few minutes following any local earthquake, authorities will be in urgent need of information to assess the earthquake danger and make critical decisions regarding a tsunami threat. Therefore, if real-time environmental monitoring is to be



effective in reducing tsunami fatalities and property loss, then the information must, first, bear directly on evaluating the tsunami threat, and second, be available within 3 minutes.

Meeting the second requirement via satellite communication is discussed in the next section; here we address the first requirement. We also discuss the use of seismic stations to assess potential hazard and automatically trigger a predetermined response and the use of water level stations for continuing rapid evaluation of tsunami risk.

### Local Seismic Acceleration Sensors: The Trigger

Seismic information is the first signal of an earthquake and must be interpreted in terms of the probability of tsunami generation. Almost instantaneous emergency response to a local earthquake can be provided by accelerometers. These devices are now routinely used to monitor local earthquake activity and immediately trigger hazard mitigation procedures, such as stopping an elevator or closing a bridge to traffic, when a predetermined acceleration threshold is exceeded [MacDonald and Viskne, 1986]. We reasoned that this same principle could be applied to reduce the response time (and cost) of a local tsunami warning system significantly if the acceleration signal could be related to the local tsunami threat, that is, to the earthquake magnitude and location. Kanamori and Jennings [1978] have demonstrated that accelerometers could be used to accurately determine earthquake magnitude, and Saragomi *et al.* [1985] have recently developed an empirical relationship for major earthquakes in central Chile that models the observed accelerations

as a function of both the magnitude and epicentral distance.

The THRUST seismic instrumentation consisted of two Kinemetrics Vertical Seismic Triggers, characterized by a sensitivity to acceleration of 0.001 g and a range of 0.025–0.25 g. The first trigger is located at IHA in Valparaiso, while the second is 110 km southeast at the University of Chile in Santiago. This placement provided directional information for rough estimates of whether the earthquake is inland or offshore. The acceleration threshold is set to 0.126 g at Valparaiso and 0.143 g in Santiago. Since the acceleration is a continuous function of two variables, these specific threshold settings do not correspond to a unique solution pair ( $M$ , magnitude, epicentral distance from Valparaiso). Rather, the thresholds represent a continuum of possible solutions that, in this particular case, include those from 7.0  $M_s$ , 80 km to 6.2  $M_s$ , 33 km. As a rough index of potential tsunami danger, this ambiguity is acceptable, since the hazard would be expected to increase not only with earthquake magnitude but also with proximity to the epicenter.

### Local Water Level Sensors

In the existing regional tsunami warning systems, water level information is not required to initiate the evacuation of people. It is imperative, however, that water level information be available quickly and continuously to assist in subsequent decisions (such as the end of the hazard). For the THRUST project, water level stations were designed and built so that the data were accessible through satellite communications after the initial warning. The design included consideration of accuracy, location, survivability, reliability,

and timeliness. These criteria were established to test a new type of water level station designed specifically for tsunami warning operations.

Existing water level sensors in the regional warning centers and the Pacific-wide systems are not well suited to tsunami measurements because these instruments were designed to measure tides. Because tide gages mechanically damp waves of shorter periods than the 12-hour tidal cycle, reported measurements with tide gages are less than tsunami wave amplitudes. Ohada [1985] reported that during the 1983 Sea of Japan tsunami, one tide gage measured only one half of the actual wave amplitude. We selected bottom-mounted pressure sensors to provide 1-cm accuracy for tsunami waves in the 4–90-minute period range and avoided these problems.

To avoid exposure of the water level sensor during the worst case tsunami, two instruments were placed in 10 m water depth. To provide earliest shoreline detection, these sensors were located on the seaward side of the Valparaiso breakwater. Two water level sensors provided redundancy for improved system reliability and survivability. Satellite communications insured timely transmission of data.

Data is collected continuously in one of two formats, tidal mode or Tsunami Detection Mode (TDM). The normal mode of operation is tidal, in which each data point consists of a 15-minute average. Tripping of a seismic trigger automatically activates the tsunami detection mode, in which the data rate is increased and each sample represents a 1-minute average. Twenty samples are transmitted every 10 minutes to provide data from 10 minutes before receipt of the alarm (available from a data buffer) to 50 minutes after the alarm is received. One hour after TDM is invoked, the water level sensors return to the tidal mode. Clearly, activation of the TDM requires a communication link between the water level sensor and each of the distant seismic stations. This particular link and the additional communication links required for the rapid delivery of both seismic and water level information to local authorities are described in the next section.

### Rapid Dissemination of Information

The final component of THRUST is a satellite-based communication system that will allow information delivery within minutes after the earthquake. NOAA's GOES system offers both rapid data collection and information dissemination capabilities, with broad geographic coverage that extends from western Europe and Africa, through the Americas, to eastern Australia [Bernard *et al.*, 1982; MacCallum *et al.*, 1983]. Figure 1 illustrates GOES coverage and the locations of THRUST stations linked via the GOES communication system. Figure 4 summarizes how THRUST stations (seismic, tsunami warning, and water level) interact with GOES satellites and the Command and Data Acquisition (CDA) facility at Wallops Island, Va., to achieve rapid dissemination of the required information.

On receipt of the emergency message via satellite, THRUST receivers simultaneously activate visual and audio alarms and then print a tsunami alert message. This message,

the primary end product of the THRUST system, consists of important guidance information for warning center personnel. Delivery of this message formally establishes the tsunami warning status, thereby activating a series of automatic emergency procedures established in the Tsunami Emergency Operations Plan. It also provides travel time estimates of the potential tsunami to various coastal regions and provides names and phone numbers of key personnel to be notified.

Two THRUST receivers are located at the water level sensor sites in Valparaiso. When the emergency message is received, these receivers change the data sampling scheme of each sensor from the normal tidal mode to the Tsunami Detection Mode. These data are then immediately available to local officials from the CDA via dial-in communication link.

## System Evaluation

A 9-month test program was conducted from September 1, 1986, to May 31, 1987. Three specific procedures were utilized to assess the reliability of the hardware, evaluate the response time of the system, and test the success rate of transmissions.

**12-Hourly Maintenance Tests (Seismic Station).** At a random time within each successive 12-hour period, each of the two seismic stations would activate itself and initiate the sequence culminating in the printing of a test message at Valparaiso, Boulder (Colorado), Seattle (Washington), and Honolulu (Hawaii). As illustrated in Figure 4, this tested the seismic sensor, GOES satellite, CDA relay procedures, THRUST receivers, and printers.

**24-Hourly Maintenance Tests (Water Level Station).** At a random time within each successive 24-hour period, the water level station would initiate TDM and transmit 1-min-

ute data, which were then retrieved from the Central Data Distribution Facility (CDDF) by PMEL via telephone link. This procedure tested the water level sensors, water level transmitters, GOES satellites, and CDA archiving procedures (Figure 4).

**Random End-to-End Test by Earthquake Simulation.** The accelerometers were physically shaken to simulate an earthquake 30 times during the 9-month test to exercise the entire THRUST system, using the GOES satellite.

## THRUST Hardware Reliability

Separate maintenance records were kept for the seismic and water level stations, a method that helped to identify problems in each system. The seismic station had hardware reliability of 96%, while the water level station had 88% reliability. These numbers are reasonable for a pilot project. Such routine monitoring of subsystems is an integral part of any truly operational system and serves to increase the reliability of the end-to-end system. Details of the performance of the system can be found in the work of *Milburn and Behn* [1987].

## System Response Time

The average response time during the 28 successful end-to-end tests by earthquake simulation was 2.5 minutes. For the 1088 seismic test messages (2 seismometers  $\times$  2 tests/day  $\times$  272 days), the average response time was 1.16 minutes, with a standard deviation of 2.24 minutes. Similar response times were recorded at all THRUST receivers (Figure 1), verifying simultaneous receipt of information.

## Communication System Reliability

As expected for a pilot project, the reliability of communications varied greatly from month to month because of problems with THRUST hardware, inexperienced person-

nel, and the GOES satellite system. However, after excluding THRUST hardware outage time to obtain an accurate assessment of the performance of the GOES communication system alone, we find that an overall average of approximately 70% of the 1088 test messages were correctly received. However, one station (Boulder) was characterized by a 9-month average of nearly 80%; Each of the four stations experienced at least 1 month in which receipt of twice-daily test messages was approximately 90%. Furthermore, of the 30 alert messages generated by earthquake simulations to test the entire end-to-end system, 28 were received at the primary site in Valparaiso, for a 93% success rate. Finally, the receipt of twice-daily test messages at IHA were also monitored during the more recent 8-month period from August 28, 1987, to April 25, 1988; 240 of these 242 tests were executed properly, corresponding to a success rate of approximately 99%. These are exceptional communication reliability rates for a pilot project, and they are an indication of the evident robustness of the GOES satellite operations and the validity and feasibility of the overall THRUST concept.

## THRUST Hardware Costs

To survive a major earthquake, all equipment must be durable and self-powered by independent, uninterruptible sources. Low hardware cost was achieved by using existing technology whenever possible, and all THRUST hardware was available commercially, except for a data collection interface between the sensor and the THRUST receiver. However, some computer software development was necessary. The software for the data collection was provided by Synergetics and that in the Commodore 64 by Cyber-Link. Detailed descriptions of the equipment are provided by *Milburn and Behn* [1987] and *McManamon and Cateora* [1988].

The THRUST system can be conveniently thought of in modular terms. In general, three THRUST stations perform distinctly different functions at physically separate sites:

- a tsunami warning center station, requiring a THRUST unit, printer, and an uninterruptible power supply (UPS);
- a seismic trigger station, requiring an accelerometer, transmitter, and UPS, and
- an optional water level monitoring station, requiring a water level sensor, transmitter, THRUST unit, and UPS.

Approximate 1986 hardware (U.S.) costs for each of these THRUST stations are

|                                |          |
|--------------------------------|----------|
| tsunami warning station        | \$9,000  |
| seismic trigger station        | \$6,000  |
| water level station (optional) | \$15,700 |

Note that these are basic hardware costs only; the one-time engineering development costs incurred by project THRUST for expenses related to engineering design, assembly, travel to the site, and installation are not included. Future THRUST stations will be free of much of this overhead, although there will inevitably be additional expenses. If installation and maintenance are performed by local personnel, however, these expenses will be minimized. Specific installation and maintenance costs will naturally vary with particular

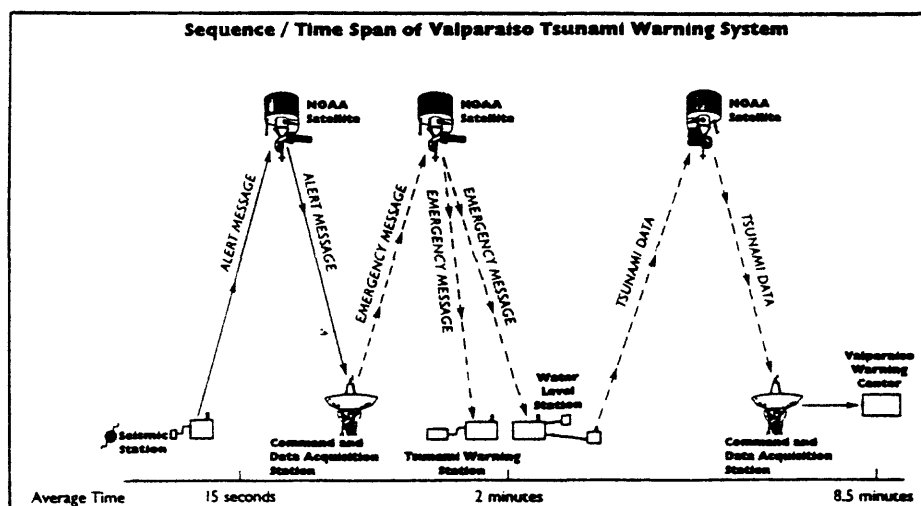


Fig. 4. Sequence/time span of the Valparaiso tsunami warning system. NOAA GOES weather satellites 22,300 miles (~35,700 km) above Earth serve as the THRUST communication system. A major earthquake activates the entire system by triggering an accelerometer/transmitter that sends, via the satellites, an alert message to the Valparaiso Tsunami Warning Center, to the water level stations in Valparaiso harbor, and to the Pacific Tsunami Warning Center near Honolulu. At the same time, the water level sensors begin to transmit wave information through the GOES system. Less than 3 minutes after an earthquake has triggered the system, the dimensions of the threat have been defined for those responsible for executing the local emergency action plan.

site characteristics, such as logistical convenience and available shelter for equipment.

## Conclusions

Project THRUST has demonstrated the feasibility of using satellite communications for a low-cost local tsunami warning system. On the basis of 1 year of testing and evaluating the pilot system, the level of reliability required in a true operational setting appears to be achievable in the second generation of THRUST equipment.

We conclude that

- the three basic components of the THRUST system's approach to local hazard mitigation are easily generalized to other natural hazards — that is, pre-event preparedness, real-time local hazard assessment through environmental monitoring, and rapid alert through satellite communications; and
- the modular nature of a THRUST-type system easily lends itself to interlinking of multiple units to form larger regional systems.

Thus, in addition to establishing an effective, low-cost local tsunami warning network, we also consider this project to be a successful demonstration of the viability of the THRUST system's approach in local mitigation of rapid onset natural disasters.

## Acknowledgments

This project was supported by the U.S. Agency for International Development's Office of Foreign Disaster Assistance, the National Oceanic and Atmospheric Administration (NOAA), and the Government of Chile. We are grateful for the enormous assistance provided by NOAA/NESDIS in allowing the use of the GOES satellite system for this pilot project. In particular, we thank Gordon Vaeth and Mike Nestlebusch of NESDIS, who made this project possible. This report is contribution 997 from NOAA's Pacific Marine Environmental Laboratory.

## References

- Bernard, E. N., and R. Goulet, Tsunami research opportunities, report, 50 pp., National Science Foundation, Washington, D.C., 1981.
- Bernard, E. N., J. F. Lander, and G. T. Hebenstreit, Feasibility study on mitigating tsunami hazards in the Pacific, *NOAA Tech. Memo. ERL PMEL-37*, 1982.
- Brandtsma, M., D. Divoky, and L. Hwang, Tsunami atlas for the coasts of the United States, *Rep. NUREG/CR-1106*, Tetra Tech Inc., Pasadena, Calif., 1979.
- Comte, D., A. Eisenberg, E. Lorca, M. Pardo, L. Ponce, R. Saragoni, S. K. Singh, and G. Suarez, The 1985 central Chile earthquake: A repeat of previous great earthquakes in the region?, *Science*, 233, 449, 1986.
- Hebenstreit, G. T., and R. E. Whitaker, Tsunami hazard modeling and mitigation: Runup and inundation studies, *SAI Rep. SAI-83/1236*, Sci. Appl. International Corp., McLean, Va., 1983.
- Housner, G. W., *Confronting Natural Disasters: An International Decade for Natural Hazard Reduction*, National Academy Press, Washington, D.C., 1987.
- Houston, J. R., R. W. Whalin, A. W. Garcia, and H. L. Butler, Effect of source orientation and location in the Aleutian Trench on tsunami amplitude along the Pacific coast of the continental United States, *Waterways Exp. Stn. Rep. H-75-4*, U.S. Army Corps of Eng., Vicksburg, Miss., 1975.
- Kanamori, H., and P. J. Jennings, Determination of local magnitude,  $M$ , from strong-motion accelerograms, *Bull. Seismol. Soc. Am.*, 68, 471, 1978.
- Lander, J. F., THRUST: Final report, report, Natl. Geophys. Data Ctr., Boulder, Colo., 1986.
- Lander, J. F., and P. A. Lockridge, Uses of a tsunami data base for research and operations (abstract), *Eos Trans. AGU*, 67, 1003, 1986.
- Lockridge, P. A., Tsunamis in Peru-Chile, *Rep. SE-39*, World Data Center A, Boulder, Colo., 1985.
- Lockridge, P. A., and R. H. Smith, Tsunami in the Pacific basin 1900–1983, report, Natl. Geophys. Data Ctr., Boulder, Colo., 1984.
- Lorca, E., THRUST Project tsunami emergency operations plan for Chile, Inst. Hidrograf. de la Armada, Valparaiso, Chile, 1987.
- MacDonald, R. B., and A. Viksne, Strong motion instrumentation in Bureau of Reclamation program, *Rep. NBS IR 86-3364*, pp. 85–97, National Bureau of Standards, Gaithersburg, Md., 1986.
- MacCallum, D. H., and M. J. Nestlebusch, The Geostationary Operational Environmental Satellite data collection system, *NOAA Tech. Memo. NESDIS 2*, 1983.
- McManamon, P. M., and J. Cateora, THRUST final report, CyberLink Corp., Boulder, Colo., 1988.
- Milburn, H. B., and R. R. Behn, Instrumentation for the THRUST Project, report, Pac. Mar. Environ. Lab., Seattle, Wash., 1987.
- Nishenko, S. P., Seismic potential for large and great interplate earthquakes along the Chilean and southern Peruvian margins of South America: A quantitative appraisal, *J. Geophys. Res.*, 90, 3589, 1985.
- Okada, M., Response of some tide wells in Japan to tsunamis, in *Proceedings of the International Tsunami Symposium*, pp. 209–213, Institute of Ocean Sciences, Sidney, Canada, 1985.
- Reid, R. O., A. C. Vastano, and T. J. Reid, Development of SURGE II Program with application to the Sabine-Calcasieu for Hurricane Carla and design hurricanes, *Rep. TP77-13*, Coastal Studies Inc., College Station, Tex., 1977.
- Saragoni, R. H., P. S. Gonzalez, and M. B. Fresaro, Analisis de los acelerogramas del terremoto del 3 Marzo de 1985, *Rep. SES199*, Univ. of Chile, Santiago, Chile, 1985.
- Sokolowski, T. H., G. W. Fuller, M. E. Blackford, and W. J. Jorgensen, The Alaska Tsunami Warning Center's automatic earthquake processing system, *Proceedings of the 1983 Tsunami Symposium, Rep. NTIS PB84-183482*, U.S. Dept. of Commer./Pac. Mar. Environ. Lab., Seattle, Wash., 1983.

## Deep Ocean Tsunami and Seismic Wave Observations: Three Recent Gulf of Alaska Events

F.I. Gonzalez and E.N. Bernard

Pacific Marine Environmental Laboratory  
National Oceanic and Atmospheric Administration  
7600 Sand Point Way, N.E.  
Seattle, WA 98115

The Pacific Tsunami Observation Program (PacTOP) was established in August, 1986 by the Pacific Marine Environmental Laboratory (PMEL) of the National Oceanic and Atmospheric Administration (NOAA) [1]. The PacTOP network employs bottom pressure recorders (BPRs) to monitor portions of the seismically active Aleutian trench which possess high potential for tsunamigenic earthquakes that might threaten Alaska, the U.S. west coast and Hawaii; two regions of particular concern are known as the Shumagin and Yakataga Seismic Gaps (Figure 1), named for their proximity to the Shumagin Islands and Cape Yakataga [2].

Recently, three large earthquakes occurred a few hundred kilometers south of Cape Yakataga. The dominant fault mechanism for each was horizontal strike-slip rather than vertical dip-slip motion [3], so that the transfer of seismic energy to the overlying water column was relatively inefficient. Nonetheless, each earthquake generated a small tsunami which was recorded at a number of coastal tide stations in Alaska and Hawaii; Table 1 summarizes the observations for the two tide stations closest to the earthquake epicenters, Yakutat Bay and Sitka, Alaska. Two of these tsunamis were also observed at three of the deep ocean BPR stations; furthermore, apparent seismic wave signals are also evident in a number of the BPR records (Table 1 and Figure 2).

From Table 1, we see that the largest maximum wave was observed at both Yakutat and Sitka on 30 November, intermediate amplitudes were recorded on 6 March, and the smallest tsunami apparently occurred on 17 November during the smallest magnitude earthquake. All observed deep water tsunami amplitudes were one to two orders of magnitude smaller than coastal amplitudes (Table 1); as might be expected, no tsunami energy was recorded on 17 November at any of the BPRs. However, in contrast to the Yakataga and Sitka observations, the largest deep water tsunami amplitudes were recorded on 6 March, rather than 30 November. This may be due partly to the fact that the 6 March event was somewhat closer to the deep water gauges, but 30% farther away from Yakutat than the 30 November epicenter (Figure 1). However, both epicenter distances to Sitka were comparable, suggesting more complicated mechanisms were important, such as differences in source geometry and size, source orientation, and bathymetric effects.

Significantly, we note that the largest deep water amplitudes were recorded at station WC9 on both 30 November and 6 March, even though WC9 was 50 to 60 percent farther from the epicenters than any of the other gauges. Again, this suggests either substantially directional source mechanisms or bathymetric effects which selectively focus the energy toward the west coast.

Rough estimates of arrival times were provided by the Pacific Tsunami Warning Center for each of the deep water stations, using  $C_g=(gh)^{1/2}$  on a 1-degree depth-averaged grid. Epicenter and station locations used were approximate, and they are plotted as plus signs in Figure 1; the arrival times are indicated by a vertical dashed line in Figure 2. Agreement with the observations is reasonable, considering the approximations made and the ambiguity in defining the observed arrival time.

Finally, seismic disturbances can induce ocean bottom pressure variations through vertical accelerations of the oceanic water column; although not presented here, estimates of the magnitude of the vertical motion of the sea floor can be obtained with a simple model [4]. We have computed seismic wave speeds, using the source distance and estimates of arrival time at each station ( $\pm 30$  sec); these are presented in Table 1. However, the values obtained for the weakest event on 17

November may be subject to substantial error because of the inherently lower signal-to-noise ratio; similarly, the record for station WC9 is sufficiently noisy (the station is in the Axial Caldera on the Juan de Fuca ridge) that the signal-to-noise ratio is unfavorable even for the larger events. The apparently low seismic speeds observed at AK10 are also not simply interpreted, since this station is situated on the landward slope of the Aleutian Trench, and interactions of the seismic waves with the trench must be taken into account. However, the clearest and least ambiguous signals, i.e. those received at AK7 and AK8 for the two largest earthquakes, yield values which range from 3.0 to 4.5 km/sec; these correspond to speeds which might be expected for Rayleigh (R1) waves and/or vertical shear (SV1) waves in oceanic crust [4].

**Table 1.** Summary of seismic and tsunami parameters.  $r$  is the epicentral distance from each station;  $V_S$  is the observed seismic wave speed;  $a_{max}$  and  $p_{max}$  are the amplitudes of the largest observed wave (i.e. half of the largest peak-to-trough excursion). (1 mb is approximately equal to a sea water head of 1 cm.)

| Date   | 17 Nov 1987      | 30 Nov 1987      | 6 Mar 1988       |
|--|------------------|------------------|------------------|
| <b>Earthquakes:</b>                                  |                  |                  |                  |
| Time (GMT)   | 08:46:53.32      | 19:23:19.59      | 22:35:35.80      |
| Latitude (deg N)                                     | 58.586           | 58.679           | 57.270           |
| Longitude (deg W)                                    | 143.270          | 142.786          | 142.790          |
| Magnitude ( $M_{sz}$ )                               | 6.9              | 7.6              | 7.6              |
| Magnitude (mb)                                       | 6.6              | 6.7              | 6.8              |
| Depth (km)   | 10               | 10               | 10               |
| $r(\text{km})/p_{max}(\text{mb})/V_S(\text{km/s})$ : |                  |                  |                  |
| Yakutat  | 230/-/-          | 200/-/-          | 310/-/-          |
| Sitka  | 500/-/-          | 475/-/-          | 450/-/-          |
| AK7  | 980/0.8/1.6-1.8  | 1010/2.5/3.4-4.2 | 925/2.4/3.1-3.9  |
| AK8  | 1050/0.6/2.5-2.9 | 1080/2.8/3.6-4.5 | 1005/2.7/3.0-3.7 |
| WC9  | 1660/Noisy/Noisy | 1650/Noisy/Noisy | 1530/Noisy/Noisy |
| AK10   | 1050/0.0/None    | 1080/1.2/2.0-2.3 | 1035/1.1/1.8-2.0 |
| <b>Tsunamis:</b>                                     |                  |                  |                  |
| $a_{max}$ (cm)                                       |                  |                  |                  |
| Yakutat  | 5.               | 42.              | 19.              |
| Sitka  | 0.               | 13.              | 5.               |
| $p_{max}$ (mb):                                      |                  |                  |                  |
| AK7  | 0.0              | 1.0              | 2.4              |
| AK8  | 0.0              | 0.5              | 1.6              |
| WC9  | 0.0              | 1.7              | 2.8              |
| AK10   | 0.0              | 0.0 ?            | 0.0 ?            |

### References

- [1] Gonzalez, F.I., E.N. Bernard, H.B. Milburn, D. Castel, J. Thomas, J.M. Hemsley, 1988: The Pacific Tsunami Observation Program (PacTOP), in *Proceedings of the International Tsunami Symposium*, IUGG XIX General Assembly, 18-19 August 1987, Vancouver, British Columbia, 3-19.
- [2] Jacob, K.H., 1984: Estimates of Long-Term Probabilities for Future Great Earthquakes in the Aleutians. *Geophys. Res. Letters*, **11**, 295-298.
- [3] J.C. Lahr, C.D. Stephens, R.A. Page, K.A. Fogleman, 1988: Alaska Seismic Studies, in *National Earthquake Hazard Reduction Program Summaries of Technical Reports*, 26, U.S. Geological Survey Open-File Report (in press).
- [4] Filloux, J.H., 1983: Pressure Fluctuations on the Open-Ocean Floor off the Gulf of California: Tides, Earthquakes, Tsunamis, *J. Phys. Oceanogr.*, **13**, 783-796.

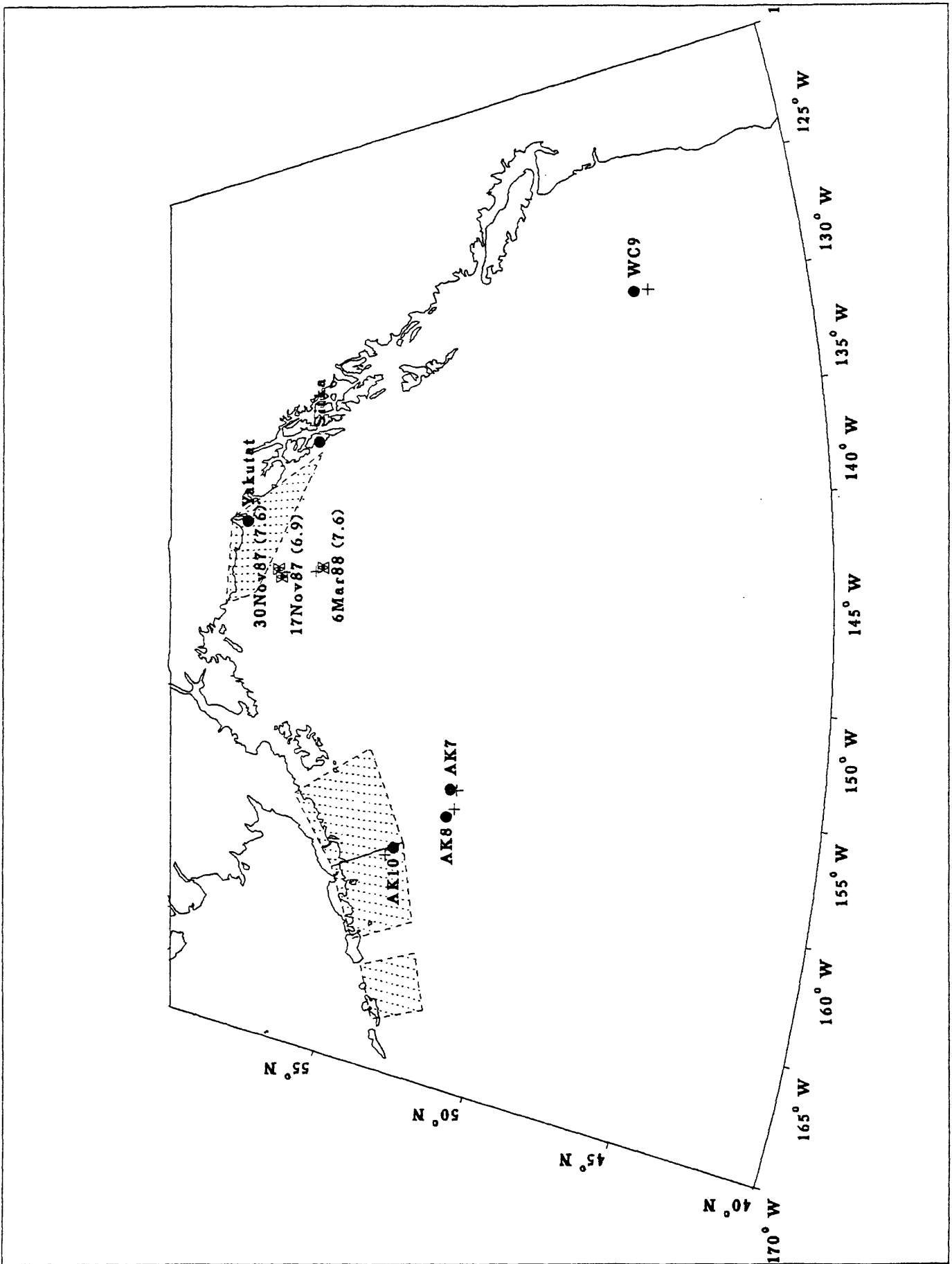
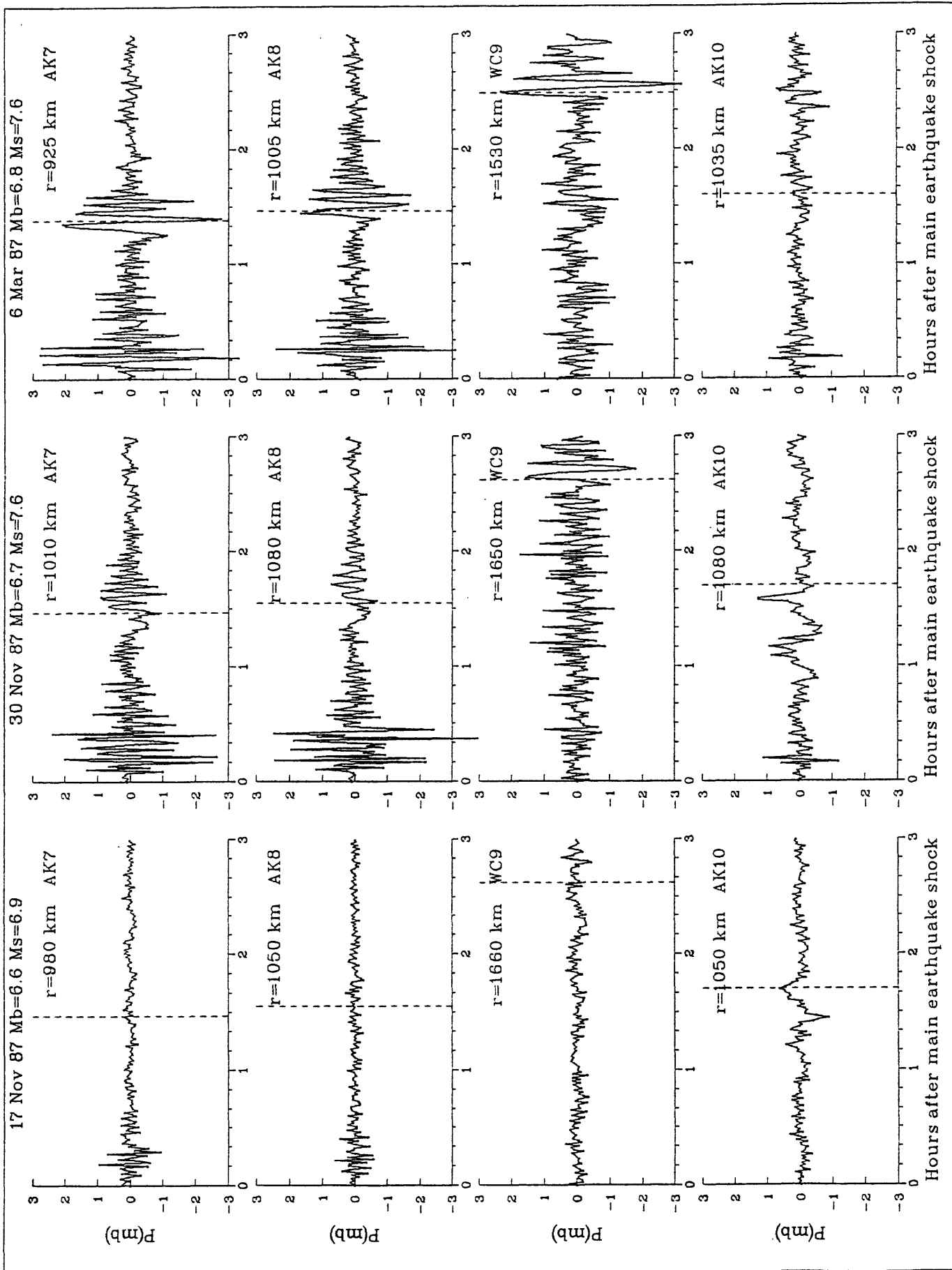


Figure 1. Station locations and earthquake epicenters, with magnitude  $M_s$  indicated in parentheses. Hatched regions delineate the Shumagin Seismic Gap (encompassing AK10) and the Yakutat Seismic Gap (encompassing Yakutat). A plus sign indicates an approximate location used in the computation of tsunامي travel times (that for the 17 Nov 87 and 30 Nov 87 earthquake location is obscured by the epicenter symbols). Map projection is gnomonic, so that great circles are straight lines.



**Figure 2.** PacTOP bottom pressure recorder (BPR) observations. Each observation is a 56.25 sec average, recorded every 56.25 sec (64 samples per hour). One millibar (mb) corresponds to approximately one cm of sea water.  $r$  is the epicenter distance from each station. The vertical dashed line represents arrival time estimates computed by the Pacific Tsunami Warning Center. Station locations are shown in Figure 1.

## Extended Abstract

### Pasadena Very-Broad-Band System and Its Use for Real-time Seismology

Hiroo Kanamori

Seismological Laboratory, California Institute of Technology  
Pasadena, California 91125

As a joint project between California Institute of Technology, The University of Southern California, The United States Geological Survey, and The Incorporated Research Institutions for Seismology, a very broadband seismograph system was installed in November 1987 at the Kresge Laboratory of California Institute of Technology (Figure 1). The system consists of a 3-component Wielandt-Streckeisen seismometer, Kinematics FBA-3 accelerometer and a Quanterra 24-bit data logger with telephone dial-up capability. The system is essentially similar to the one developed by Stein(1985) and installed at the Harvard Observatory, Massachusetts. One significant difference is a 3-component strong-motion data channel which is added to obtain on-scale recordings of large regional earthquakes. The overall dynamic range is about 200 db. The response of the system is approximately flat in velocity over a period range from 0.2 to 370 sec. The sampling interval is 20 samples per second.

The dual (Streckeisen + 24-bit digitizer and FBA3 + 16-bit digitizer) system with telephone dial-up capability allows semi-real-time determination of local magnitude of large regional events.

Figure 2 shows the recordings of an  $M_L=5$  earthquake in the Whittier Narrows area. The acceleration at Pasadena was about  $1 \text{ cm/sec}^2$ , which was large enough to clip the N-S component of the very-broadband channel. The low-gain (strong motion) channel recorded this motion without clipping, and produced undistorted displacement records as shown in the figure. The peak-to-peak amplitude of the ground motion is approximately 1 mm. The saturation level of the low-gain channel is 1 g ( $980 \text{ cm/sec}^2$ ) so that this system can provide on-scale recordings of practically all large regional events.

Figure 3 compares four earthquakes in the Whittier Narrows area with the local magnitudes of approximately 5, 4, 3, and 1.5.

A significant difference in the wave form between different events suggests a difference in the mechanism of these events. For example the P-wave polarity of 1/19 event is opposite to that of the other events. The amplitude ratio of NS to EW components of 2/11 event is larger than that of the others.

These wave-form data combined with the results from the existing Southern California Seismic Network can be used to determine source mechanisms quickly. For the three earthquakes in the Whittier Narrows area ( $M_L=3, 4, \text{ and } 5$ ), integration of the broadband records yielded simple displacement records from which the source time functions could be easily inferred. Figure 4 shows the displacement records rotated into the transverse(T) and the radial(R) components. The wave form of the SH wave recorded on the T component represents the moment rate function of the source (e.g. far-field source time function). A good estimate of the mechanism and the seismic moment of these events could then be obtained through inversion of the wave-form data. Here we used a very simple scheme. The basic data used are the amplitudes of the vertical component of the P wave, and the transverse and the radial components of the S wave. Since the number of unknown parameters is 4 (dip, rake, strike, seismic moment), it is not possible to determine the source parameters uniquely. We look for the solution that satisfies the observed amplitude data in the closest neighborhood of the first approximation obtained from the local P-wave first-motion data. Figure 5 shows the comparison between the observed and synthetic wave forms computed for the first approximation and the final solution. The first-motion mechanisms were provided by Lucy Jones (personal communication, 1988). If we have two or more stations, the non-uniqueness can be removed, and the method allows rapid determinations of the source parameters of regional events.

Since the broadband data provide undistorted source time functions, they allow quick and intuitive source mechanism determinations.

### Figure Captions

Fig. 1

A simplified block diagram of the Kresge VBB system.

Fig. 2

Wave forms of an  $M_L=5$  earthquake in the Whittier Narrows area, southern California. Upper left: Wood-Anderson records

simulated from the broadband (Streckeisen) records. Note the clipping on the NS component. Lower left: Wood-Anderson records obtained from the low-gain (strong motion) channel. The ground motion is recorded without clipping. Lower right: Ground motion displacement obtained from the low-gain (strong motion) record.

Fig. 3

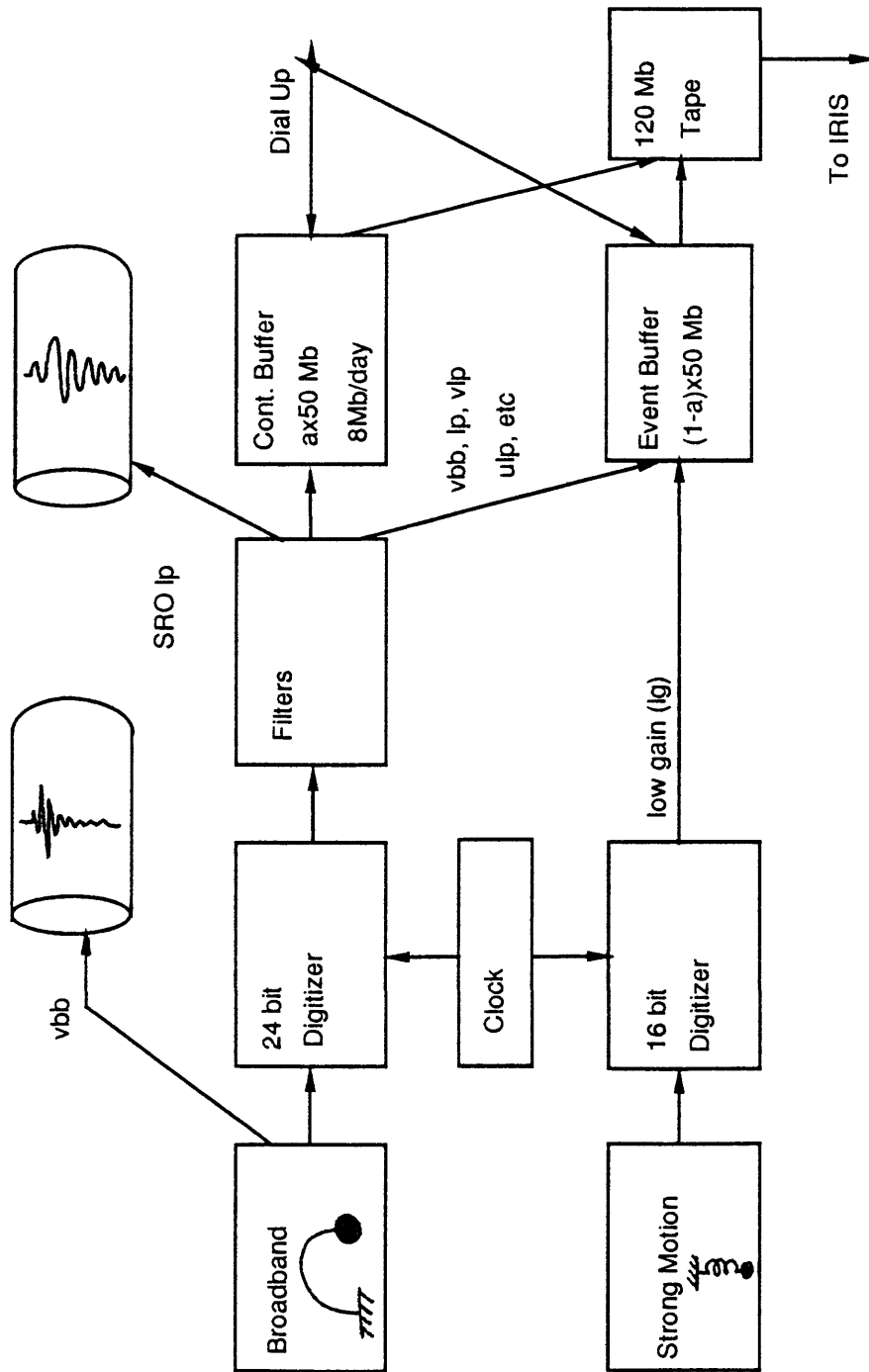
Wood-Anderson records of four earthquakes in the Whittier Narrows area with local magnitudes ranging from 1.5 to 5. Note the difference in the amplitude scale for different events.

Fig. 4

Rotated seismograms of ground-motion displacement of the three earthquakes in the Whittier Narrows area. Note the difference in the pulse width and amplitude. The S waves on the vertical and radial components exhibit the effects of interaction between the free surface and the incoming SV waves.

Fig. 5

Comparison between the observed (top) and synthetic records (middle and lower) for the three earthquakes in the Whittier Narrows area. The synthetics shown in the middle are computed for the mechanism determined from P-wave first-motion data (Lucy Jones, personal communication, 1988). The synthetics at the bottom are obtained by inversion of P and S wave amplitudes.  $M_w$  is calculated from the seismic moment.



Kresge Very-Broadband System

Fig. 1



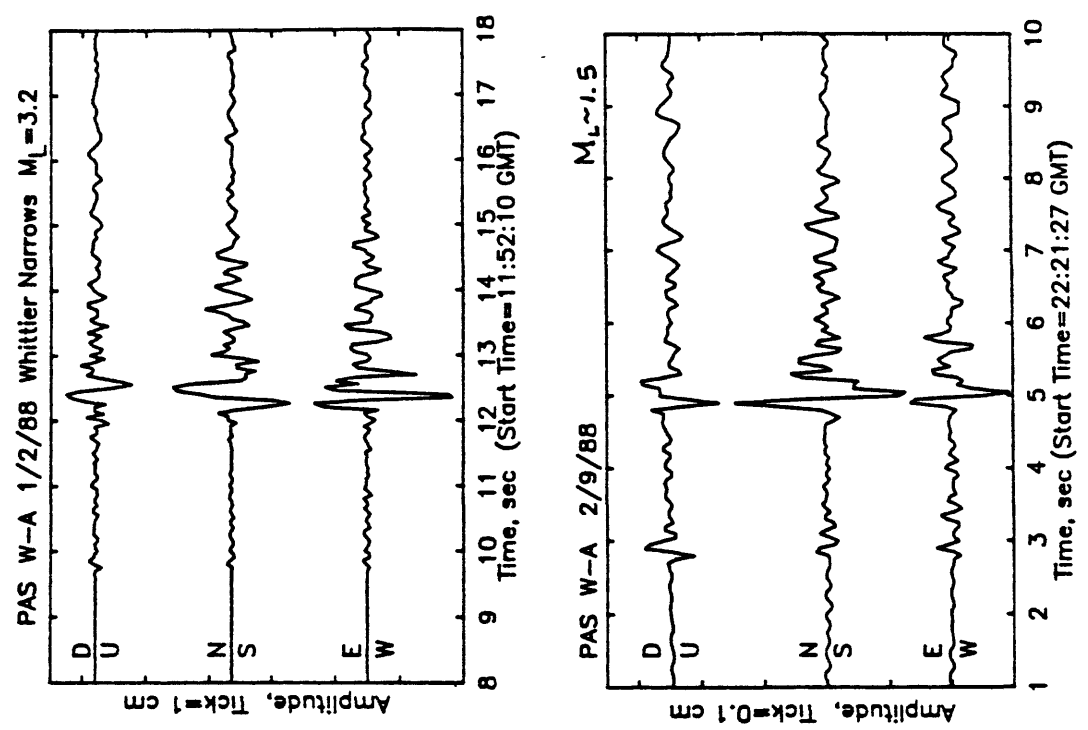
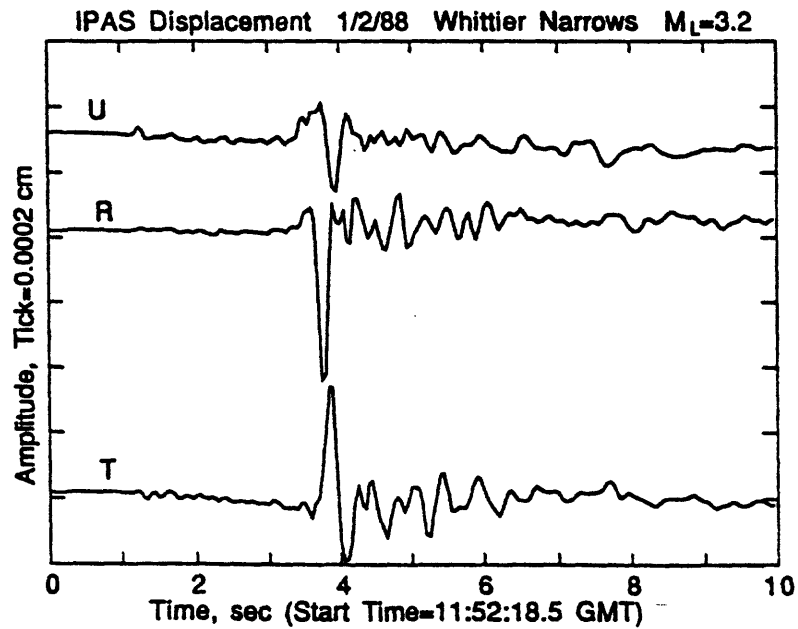
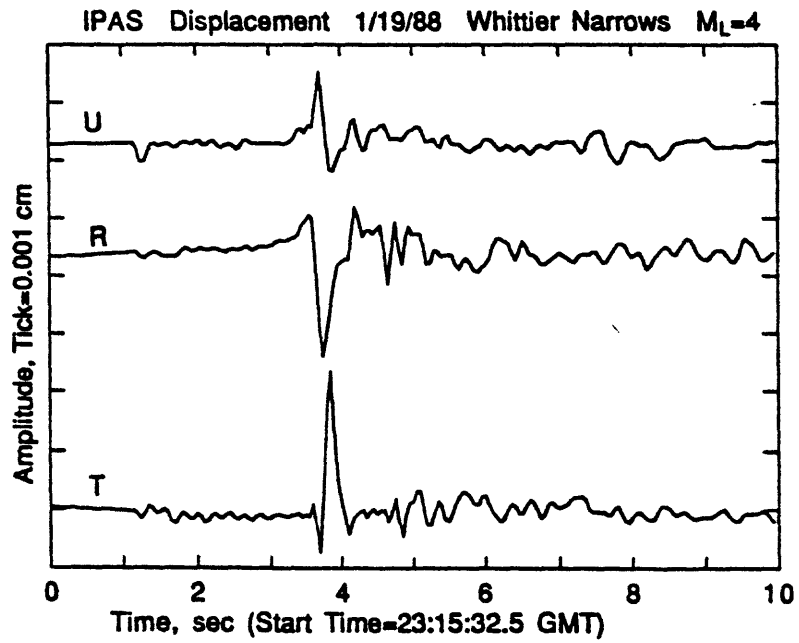
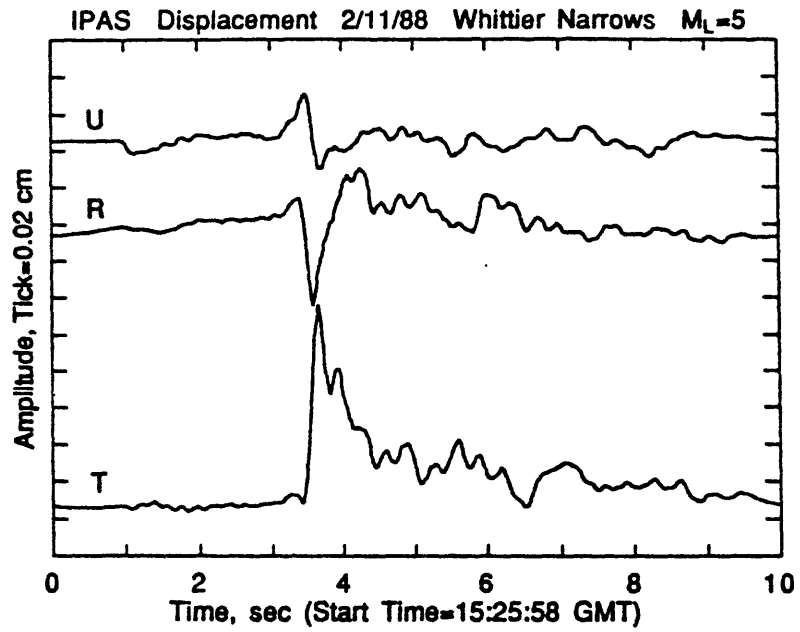
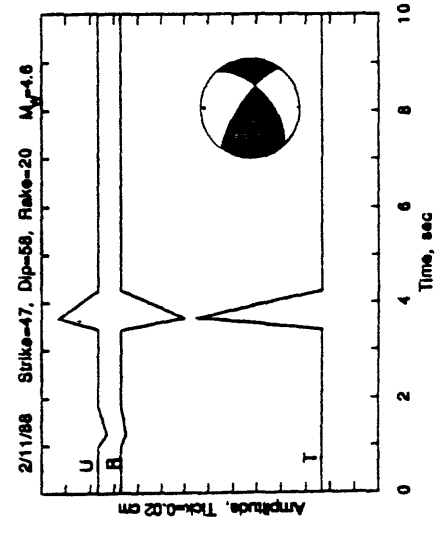
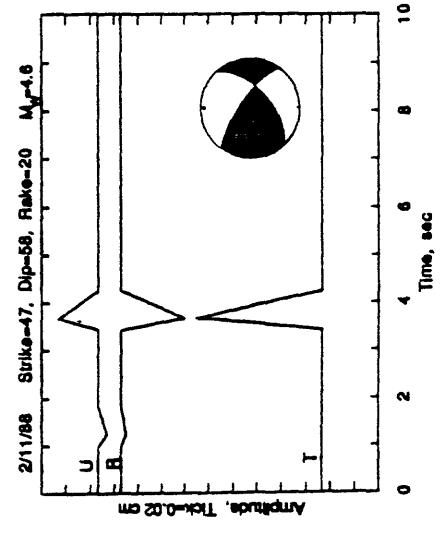
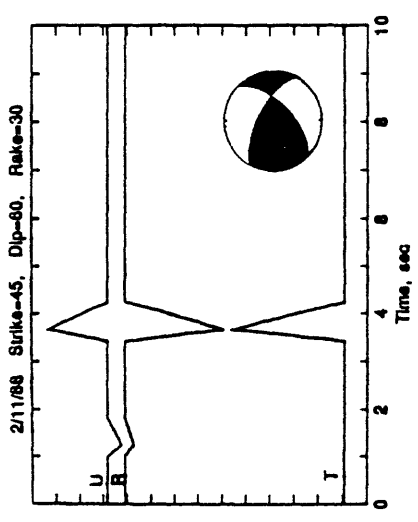
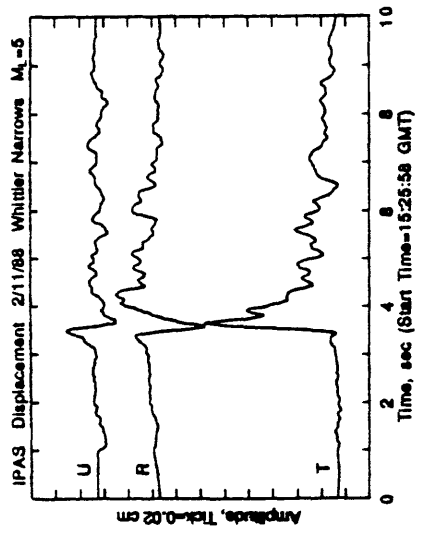


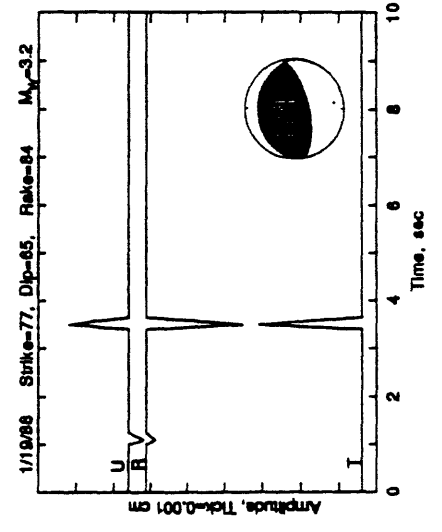
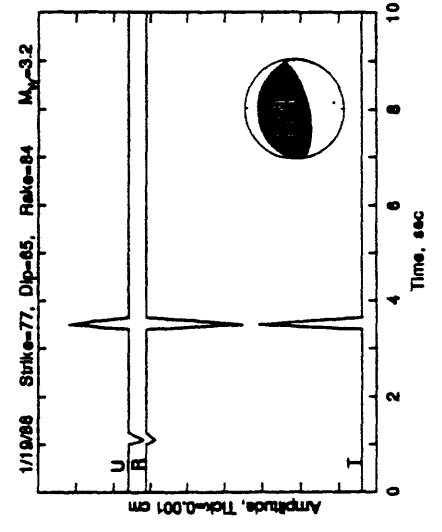
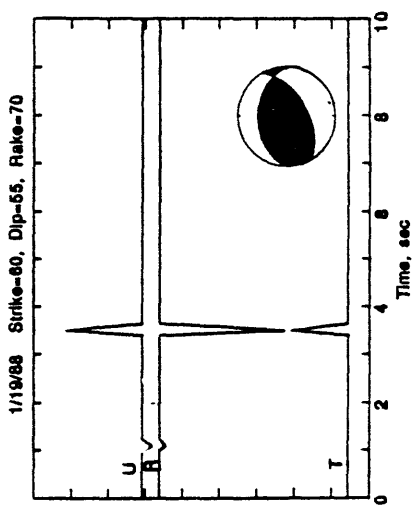
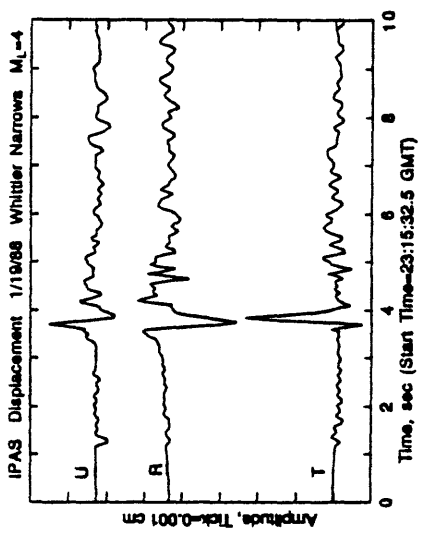
Fig. 3



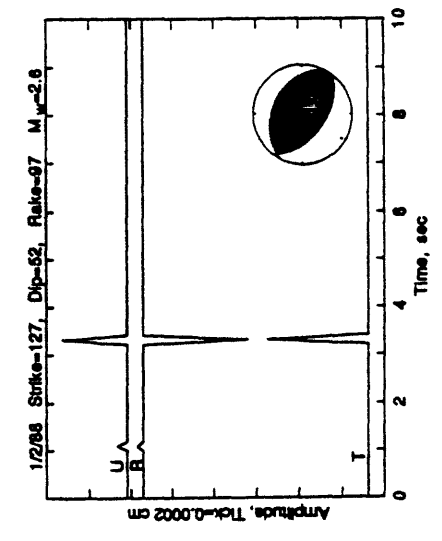
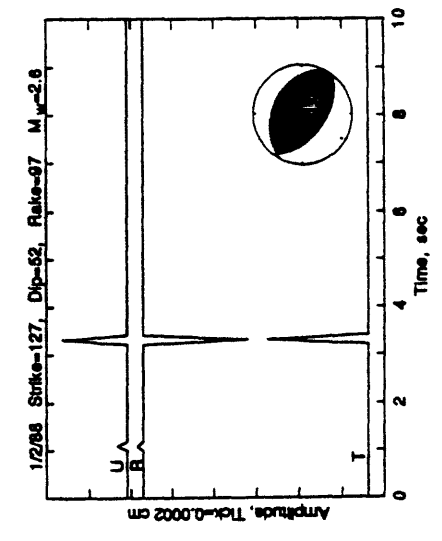
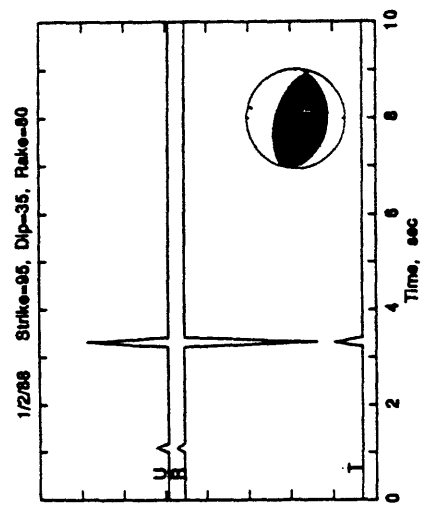
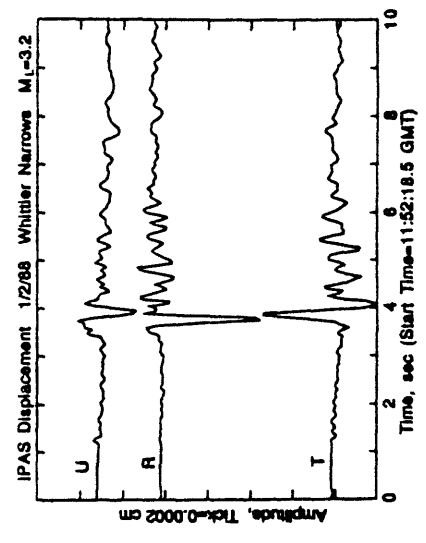
a



b



c



# A REAL-TIME PROCESSING SYSTEM OF TOHOKU UNIVERSITY SEISMIC NETWORK AND RECENT MICROEARTHQUAKE ACTIVITY

Akira HASEGAWA, Norihito UMINO and Akio TAKAGI  
(Observation Center for Prediction of Earthquakes and Volcanic Eruptions, Faculty of Science, Tohoku University)

An automatic event detection and location system has been developed to process microearthquake data collected by the telemetered seismic network of Tohoku University, which covers the northeastern part of Honshu, Japan (Fig.1). The system is composed of three subsystems. The first one is a pre-processing system whose main function is event detection. Detection of seismic signal at each station is made by using the ratio of short-term amplitude to long-term average in the seismogram of high-gain vertical component. Triggered time at each station is used for preliminary determination of hypocenter in this pre-processing system.

Automatic picking of P- and S-wave first arrivals and hypocenter location for events detected by the pre-processing system are performed by the second subsystem. Akaike's information criterion (AIC) is applied for picking of arrival times of P- and S-waves [e.g., Yokota et al., (1981)]. The other phase data, such as maximum amplitude, P- and S-wave periods, P-wave first motion, etc., are also read automatically in this second subsystem. Earthquake hypocenters are located by an iterative method. First, P arrivals are picked with reference to the triggered times formerly obtained by the pre-processing system, and are used to locate the hypocenter for the event. Then the system picks S arrivals by using the expected arrival times from the hypocenter already determined from P arrivals. Hypocenter location is made again by using both P and S arrivals. Subsequently, arrival time data which do not agree with this location or data which are missed in the first step of picking are re-picked, and the event is relocated. This process is repeated until a reasonable result is obtained. In the location procedure included is an algorithm which can remove wrong data or can discriminate two or more events occurred almost at the same time. After the hypocenter is finally located, the system determines the magnitude for the event from maximum amplitude data [Watanabe, (1971)] already read. The third subsystem is a batch processing system to check and revise, if necessary, the results obtained by the second subsystem.

In June 1984, the system was linked with the telemetered network system, and since then it has been working in real time. About 9,000 events per one year are located in and around the network by this automatic system. When hypocenter parameters determined by the automatic system are compared to those determined by the manual processing, it is found that more than

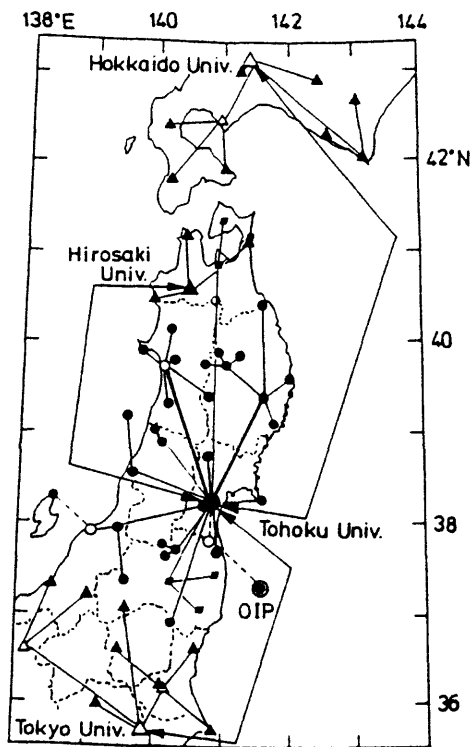


Fig.1 Map showing locations of stations of the microearthquake observation network of Tohoku University.

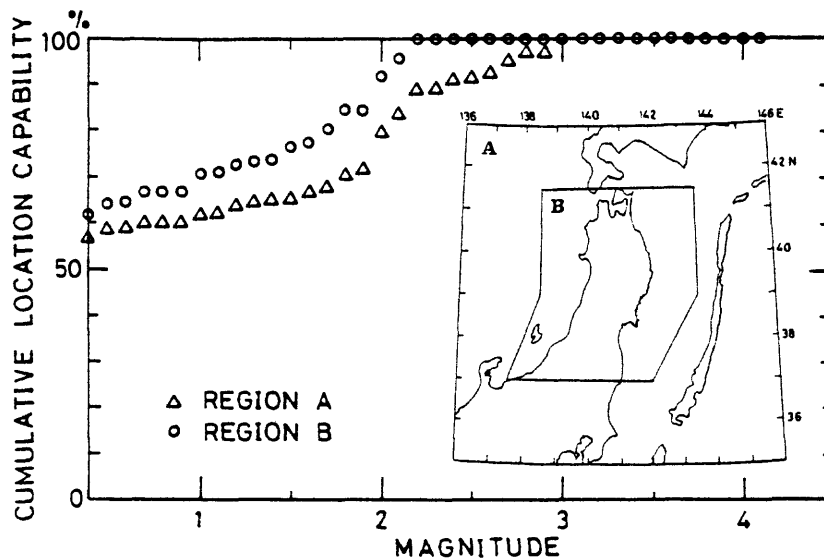


Fig.2 Cumulative location capability of the automatic processing system plotted against magnitude [after Hasegawa et al. (1986)].

90% of the events with magnitude larger than 2.0 located in and around the network by the manual processing are well located by the automatic system (Fig.2). Differences between hypocenter locations determined by the automatic and manual processing systems are mostly within a standard deviation of determined

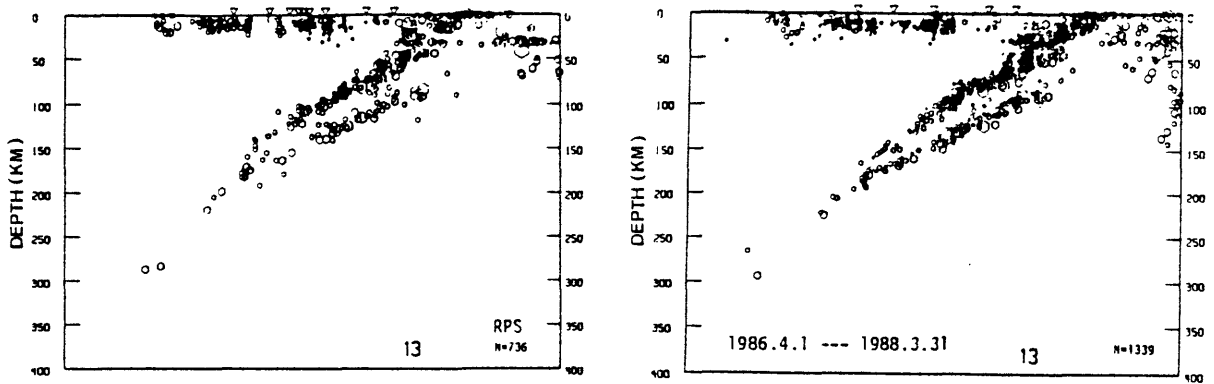


Fig.3 Vertical sections of earthquakes located in the central part of the Tohoku District by the automatic (left) and manual (right) processing system.

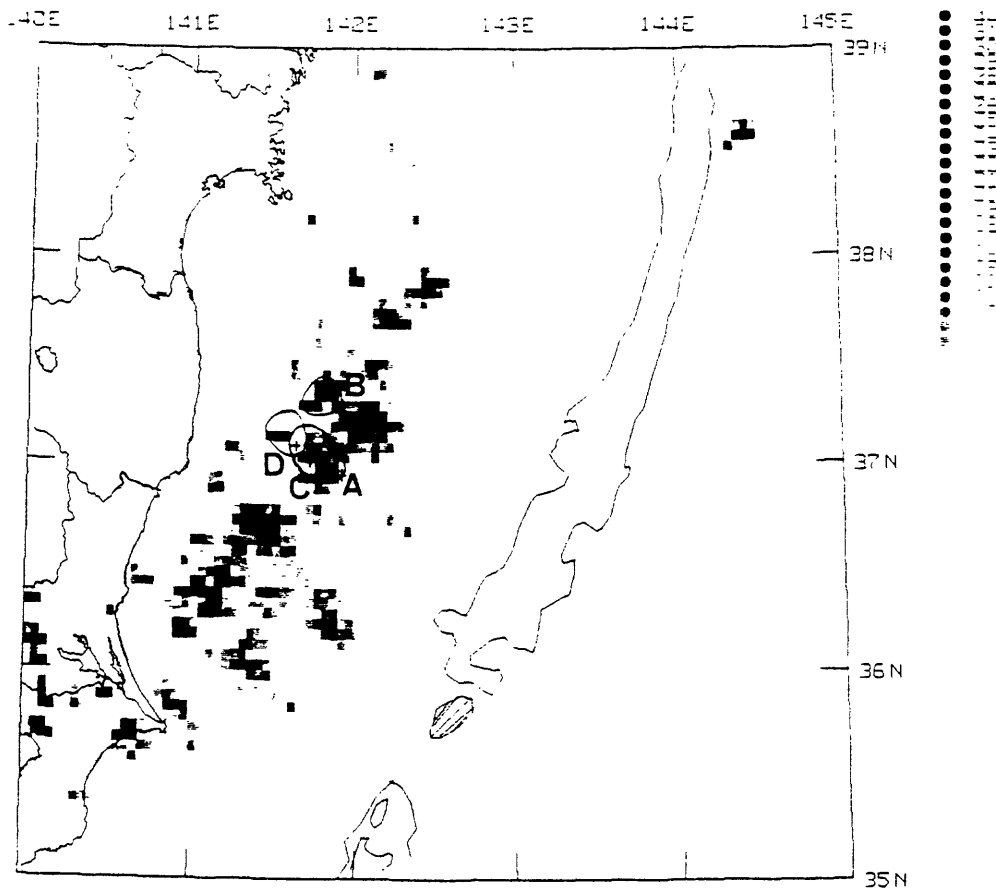


Fig.4 Spatial distribution of microearthquake activity shown with light and shade for 4 years before the occurrence of the 1987 events. Shades represent the regions of high seismic activity. Areas A through D, enclosed by solid lines, denote the rupture areas of February 6 (M6.7, M6.4), April 7 (M6.6), April 17 (M6.0) and April 23 (M6.6), 1987, events, respectively.

hypocenters. Hypocenter distribution obtained from the automatic system clearly shows double-planned deep seismic zone beneath the network (Fig.3), which demonstrates hypocenter locations by the automatic system are quite reliable.

In February to April, 1987, there occurred several earthquakes with magnitude larger than 6 off Fukushima Prefecture, the southern part of the Tohoku District. These are the largest earthquakes occurred in and around the network since the starting of the operation of the automatic system. The system detected and well located these earthquakes and their aftershocks.

A hydrophone station, which was set up about a half year before the occurrence of the present activity near its focal area, detected these events and played an important role to improve the accuracy of focal depths [Hasegawa et al., (1987)]. Rupture areas of these events, along the boundary between the descending Pacific plate and the overriding continental plate, correspond to the hypocenters (i.e., the point of rupture initiation) of the large Fukushima-Oki Earthquakes of 1938 with magnitude 7.5 and 7.3, though the rupture areas of the 1938 events are much larger than those of the present events. It is found that microearthquake activity for 4 year period before the occurrence of the present events is concentrated on their rupture areas (Fig.4). Concentrations of microearthquake activity are also seen in some other areas along the plate boundary off Fukushima and Ibaraki Prefectures (Fig.4). Many of the hypocenters of large earthquakes occurred for the last 60 years are located in these areas of concentrations of the recent microearthquake activity, which, it seems, shows the spatial distribution of the asperity along the plate boundary off Fukushima and Ibaraki Prefectures.

#### REFERENCES

- Hasegawa, A., N. Umino, A. Yamamoto, and A. Takagi, Automatic event detection and location system of microearthquake observation network, J. Seism. Soc. Japan, Ser. 2, 39, 381-395, 1986.
- Hasegawa, A., A. Yamamoto, N. Umino, A. Takagi, and T. Sato, Continuous seismic observation by hydrophones at a point 40km off Iwaki, Fukushima Prefecture, J. Seism. Soc. Japan, Ser. 2, 40, 535-540, 1987.
- Watanabe, H., Determination of earthquake magnitude at regional distance in and near Japan, J. Seism. Soc. Japan, Ser. 2, 24, 189-200, 1971.
- Yokota, T., S. Zhou, M. Mizoue, and I. Nakamura, Automatic measurement of arrival time of seismic waves and its application to an on-line processing system, Bull. Earthq. Res. Inst., Tokyo Univ., 55, 449-484, 1981.

## Seismic Monitoring in Southern California; Plans for the Future and Present Realities

Thomas H. Heaton, Scientist in Charge  
Pasadena Office, U.S. Geological Survey  
525 S. Wilson Ave, Pasadena CA 91106  
818-405-7814

What are the long-term goals of seismic monitoring in southern California; what resources are required to fulfill those goals; and where do we currently stand? The U.S. Geological Survey and the Seismological Laboratory at Caltech jointly operate a 250-station telemetered seismic network in southern California. The following is an outline of a plan for seismic monitoring in southern California. The plan can be separated into two categories: 1) the development of systems that utilize relatively well-understood seismological principles to decrease risk during earthquake crises, and 2) the development of a system for obtaining new seismological data that is likely to spawn breakthroughs in our understanding of earthquake physics.

### Goals for Reducing Earthquake Risk

#### Near real-time estimation of damage patterns after significant earthquakes.

The goal here is to provide a rapid assessment of the overall distribution of shaking following a significant earthquake. Such information is vital for rapid allocation of emergency management resources following a large earthquake. Such information is necessary in order to provide appropriate instructions to the general populace (through the Emergency Broadcast System) regarding important issues such as advice on transportation. Furthermore this information is essential for rapid damage control of all lifelines. Other areas of concern are national defense, financial markets, etc.

#### Real-time probabilistic assessments of current risk.

Long-term estimates of seismic risk can be developed from studies of fault slip rates and historic seismicity. Seismic risk estimates can also change significantly over short time scales because of temporal changes in seismicity (or perhaps strain rate, as well). The most obvious example is the problem of estimating the chance that any given earthquake is a fore-shock. Probabilistic models can be developed which include information regarding the specific site being considered. An obvious example of this is the warning system developed for the Parkfield experiment. Similar risk estimation techniques should be applied to specific regions in southern California.

#### Short-term warning of imminent ground shaking.

In very large earthquakes, substantial damage often occurs at great distances from the earthquake's epicenter. Because of the relatively slow speed of seismic waves, it is possible to elec-

tronically warn a region of imminent strong shaking as much as several tens of seconds before the onset of strong shaking. Automated defensive responses could be triggered by users after receiving estimates of the arrival time and strength of shaking expected at an individual site. The seismological community should have the goal of providing such real-time alerting information, whereas the responsibility of how to utilize such information should rest on individual users.

#### Prediction of site effects in strong ground motions

The variation in strength of ground shaking from earthquakes of a given magnitude and at a given distance is usually about a factor of ten. Much of the variation can be shown to be caused by wave propagation effects that can consistently be seen in many records from the same site. We therefore should record ground motions of numerous small earthquakes at sites of engineering importance. Portable event recorders that collect data for several months should provide valuable site response information.

#### **Monitoring Goals to further Basic Research**

The fundamental goal here is to provide as complete a description of the deformations (static and dynamic) as is possible. In the long run, we endeavor to understand the basic physics of deformation in southern California. Where is deformation occurring; how much of it occurs during earthquakes, how much of it occurs as steady creep, and how much of it occurs as episodic creep? In order to really understand these problems, we need to record three components of ground motion over a very broad range of frequencies (20 Hz to static deformations) at several hundred sites in southern California. Furthermore data should be relatively accessible to the research community.

#### **Data Systems Required to meet Goals**

In order to meet the stated long-term seismic monitoring goals in southern California, we need to deploy systems that have the following characteristics.

Large dynamic range. Ground motions should be recorded on scale from ambient earth noise to very strong ground shaking. This requires a total dynamic range of about 180 dB (9 orders of magnitude). Sensitive seismic sensors together with engineering strong motion sensors are capable of spanning this dynamic range. 24-bit digitizers are highly desirable if this goal is to be met.

#### 3-component data.

Large frequency bandwidth. 10 to 0.1 Hz is the main frequency band of earthquake engineering interest. The study of microearthquake sources requires yet higher frequencies (up to 30 Hz may be practical). Episodic creep motions may occur on time scales of minutes to days. Although this frequency band cannot be achieved by any single system, high quality seismometers can detect ground motions at periods in excess of 10 minutes as well tilt from solid earth body tides. Furthermore, the rapid development of Global Positioning Satellite (GPS) systems should allow

millimeter-level monitoring of static deformations on time scales of minutes and longer.

High spatial density. Several hundred high-quality recorders are necessary to fully realize the stated goals. Some significant fraction of those stations should be placed in densely populated regions.

Portable instrumentation. Several dozen 6-channel portable event recorders should be available to supplement a fixed array to study aftershocks, to study site response, etc.

#### Information Management Systems required to meet Goals

The installation of numerous high-quality seismic sites is only one piece of the problem. Systems must be developed to manage the data and to manipulate the data to produce useful warning information.

Data management system. Data must be analysed, documented, archived, and made accessible on random-access media using standard formats.

Warning systems. Automated systems must be developed to locate earthquakes, recognize episodic strain events, and to produce real-time risk maps. Systems must also be developed to automatically produce maps of shaking intensity following significant earthquakes. Finally, systems must be developed to broadcast early warning information during an ongoing sequence.

Site response microzonation. Practical methodologies for prepared and distributing site response information would have to be developed.

#### Currently Operating Systems (USGS/Caltech/Pasadena)

A 250-station telemetered seismic network is currently operated jointly by the USGS (Pasadena Office) and Caltech. Signals are continuously telemetered via FM telemetry through a combination of commercial telephone, radio, and microwave links to Pasadena where they are digitized at a rate of 100 samples per second. Most of the stations are high-gain, vertical, short-period seismometers having an approximate dynamic range of 40 dB. In general, close in stations are off scale by M 2.5. There are also about six sites having one additional low-gain horizontal component and there are two sites having 3-component strong-motion accelerometers.

Digital seismograms are saved only when events are detected and data analysis is generally within several days of real time (except during a significant sequence). Approximately 15,000 earthquakes are located each year with the system. Data is analysed and stored using the Caltech/USGS Seismic Processing System (CUSP) which runs only on VAX/VMS computing systems. Catalog and phase information are saved on one set of magnetic tapes (FREEZE) and digital seismograms are stored on a separate set of tapes (ARKIVE). Currently, FREEZE tapes can only be read on a machine supporting CUSP (VAX/VMS). 64 stations in the network are also automatically scanned for seismic phases (RTP) and earthquakes are located automatically within approximately 10 minutes. Summaries of seismicity and descriptions of the network

attributes and data management systems are published in semi-annual network bulletins.

In December 1987 a new seismic recording system (Quanterra/Streckeisen/Kinematics) was installed at the station PAS as a cooperative project between Caltech, the University of Southern California, USGS (Pasadena), and IRIS. This system records over a frequency band which ranges from 8 Hz to 0.001 Hz and has a dynamic range in excess of 180 dB (24-bit digitizers). Data is accessed through dial-up modem telemetry that is open to all interested scientists.

Portable instrumentation is limited to four analog strong-motion recorders without absolute time (SMA1's). Despite their lack of sophistication, important records have been obtained from deploying these instruments during aftershock sequences.

There are currently several operational alarm systems. One alarm system triggers whenever a set of seismic signals exceeds a maximum threshold. This alarm alerts the Caltech security office which then activates commercial radio pagers that are carried by key personnel. In addition, automated alarms have been installed that are triggered by the RTP automated location hardware. These alarms can be adjusted to notify key personnel when seismic activity occurs in specific locations. Communications with the USGS headquarters (Reston, VA) and the National Earthquake Information Center (USGS, Golden, CO) are coordinated by telephone and by the EASY system. The EASY system is a closed computer mail system that provides printed messages to key personnel. Communications with the State of California are done via telephone in consultation with USGS officials in Reston. No formal policies have yet been developed to define when and what types of information should be relayed to the State of California. The California Office of Emergency Services has assigned a person with a portable telephone to the Seismological Laboratory at Caltech during recent significant earthquake sequences.

### Discussion

We currently operate a real-time 250-station seismic network that does a good job of providing locations of earthquakes as small as M2.0. Furthermore recently installed systems (and systems under development) should allow location of earthquakes in near real time. Unfortunately, the limitations of one-component data, small dynamic range, and limited frequency bandwidth prevent our current system from supplying the data necessary to meet the long-range goals that are defined here. A new generation of seismic stations similar to that installed at PAS will allow these goals to be met. Currently, we are planning to install a system with similar performance characteristics near San Bernardino, CA, as a joint project with the U.S. Army Corps of Engineers. Unfortunately, funding has not yet been obtained to deploy the large number of such stations if our goals are to be met. Furthermore, much work remains on developing warning algorithms and systems to convey information to emergency management officials. Although we believe that our strategy is fundamentally sound, we are currently a long way from accomplishing these goals.

The Application of Foreshocks to Real-Time  
Earthquake Hazard Assessment in Southern California

Lucile M. Jones  
U. S. Geological Survey  
Seismological Laboratory 252-21  
California Institute of Technology  
Pasadena, CA 91125

and

Paul A. Reasenber  
U.S. Geological Survey MS/977  
345 Middlefield Road  
Menlo Park, CA 94025

presented at  
U. S. - Japan Conference on Earthquake Prediction  
Morro Bay, California  
September 12-15, 1988

## Introduction

Foreshocks have been proposed as a basis for short-term earthquake prediction. Indeed, since 1985, the U. S. Geological Survey has issued three earthquake warnings concerning the possibility that an earthquake or earthquake sequence may be followed by a larger event. However, to better use the observation of foreshocks in real-time earthquake hazard assessment, we need to understand the characteristics of foreshock sequences. We need to describe the temporal, spatial and magnitude distributions of foreshocks with respect to their mainshocks so as to determine the probability of a mainshock of some magnitude occurring at some time after a possible foreshock. The variations in these distributions with location need to be understood. We also need to search for discriminating characteristics of foreshock sequences that may allow them to be recognized as such before the mainshock occurs.

We present an analysis of four aspects of foreshocks in southern California. First, foreshocks are defined through a clustering procedure. Second, the rate of foreshock activity is determined both to estimate earthquake hazard but also to provide a random probability against which to measure the success of any possible discriminant. Third, the magnitude and temporal distributions of the foreshocks and mainshocks are determined to parameterize the increased earthquake hazard arising from the occurrence of a possible foreshock. Fourth, the data are searched for possible distinguishing characteristics of foreshock sequences.

## Data Analysis

Earthquake sequences in the southern California catalog since 1932 have been identified using an algorithm by Reasenber (1985). This algorithm groups earthquakes into clusters on the basis of individual earthquake's interaction zones in time and space. This algorithm has been shown to produce a "declustered" catalog (where clusters are replaced by individual earthquakes with a moment equal to the sum of the moments of the original cluster) that is Poissonian. Foreshocks are then defined as any earthquakes preceding the largest member of the cluster. Thus an arbitrary definition for foreshocks has not been used; rather, as much as possible, the data are allowed to control the extent of both foreshock and aftershock sequences. Aftershocks are also defined from the clustering algorithm.

The southern California catalog since 1932 is complete above  $M_L = 3.0$ . Excluding aftershocks, it includes 6480  $M \geq 3.0$ , 863  $M \geq 4.0$ , 113  $M \geq 5.0$ , 23  $M \geq 6.0$  earthquakes. The area included is shown in Figure 1. To examine regional variations in foreshock behavior, this area has been divided into the compressional regime west of the San Andreas fault, called southwestern California and the extensional regime east of the San Andreas fault, called eastern California. Subdivisions of these regions are also considered—the primarily reverse-faulting Transverse Ranges and the primarily normal faulting (and volcanic) Mammoth region.

**Rate of Foreshock Activity.** 28% of  $M \geq 5.0$  mainshocks in southern California (1932-1988) were preceded by foreshocks of  $M \geq 3.0$ . The percentage of  $M \geq 3.0$  earthquakes followed by a larger earthquake within 1 week is 6.6%. These numbers were

determined counting each foreshock sequence as one earthquake with the magnitude of the largest foreshock. These are comparable to the results of Jones (1985) where foreshocks in southern California were arbitrarily defined as earthquakes within 5 days and 10 km of the mainshock and a rate of 6% was found. Unlike the previous study, however, these results suggest a possible dependence of the rate on the magnitude of the possible foreshock. Larger earthquakes ( $M \geq 5$ ) could be twice as likely to be foreshocks as  $M=3.0$  earthquakes. The difference in probability is greater than one but less than two standard deviations apart (Figure 2).

The rate of foreshock activity varies strongly by region, with foreshocks most common in extensional regimes, less common in strike-slip environments and least common in compressional regimes (Table 1). If applicable outside of California, this dependence of foreshock rate on tectonic environment could explain the apparently lower rate of foreshock activity in Japan compared to California.

TABLE 1. Rate of Foreshock Activity in Southern California

| Region                  | % of $M \geq 5.0$ Mainshocks<br>Preceded By Foreshocks | % of $M \geq 3.0$ Earthquakes<br>Followed By Mainshocks |
|-------------------------|--|---|
| All Southern California | 28%  | 6.6%  |
| Southwestern California | 20%  | 4.1%  |
| Eastern California      | 40%  | 9.9%  |
| Transverse Ranges       | 15%  | 2.3%  |
| Mammoth                 | 40%  | 15.4%   |

**Characteristics of Foreshock Sequences.** The frequency of foreshocks with magnitude  $M_f$  prior to mainshocks of magnitude  $M_m$  can be fit by an exponential distribution. For mainshocks of  $M_m \geq 3.0$ ,

$$N(M_f) = 780 * 10^{-0.85(M_m - M_f)}.$$

For mainshocks of  $M_m \geq 4.0$ .

$$N(M_f) = 160 * 10^{-0.58(M_m - M_f)}.$$

The difference in b-value between the  $M_m \geq 3.0$  and  $M_m \geq 4.0$  mainshocks suggests that the magnitude dependence of the foreshock probabilities seen above is real. There is a slight variation in the b-value between eastern and southwestern California (Figure 3). Eastern California also showed a greater difference in probabilities of being a foreshock for  $M \geq 5.0$  and  $M < 5.0$  earthquakes which could be related.

The decay with time of the occurrence of mainshocks after foreshocks is best fit by a power-law decay like the modified Omori's law. The occurrence of mainshocks after the largest foreshock of a sequence decays with a p-value of 1.30 (Figure 4). This value does not vary between regions. The spatial distance between foreshocks and mainshocks is also small, with almost all foreshocks within 8 km of their mainshocks (Figure 5). This

varies slightly with region, with southwestern California foreshocks located closer to their mainshocks than eastern California foreshocks.

**Comparison of Foreshocks and Aftershocks.** The occurrence of mainshocks after foreshocks follows both the modified Omori's Law and the Gutenberg-Richter b-value relationship determined for the occurrence of aftershocks after mainshocks. This finding suggests that there might not be a physical difference between foreshocks, mainshocks and aftershocks, but rather that the relative magnitudes of earthquakes within a sequence are the expression of underlying stochastic laws.

One way to examine this possibility is through the magnitude frequency relation. The number of aftershocks per unit magnitude can be plotted with respect to the difference in magnitude between aftershock and mainshock as shown in Figure 6a. By using the magnitude difference, many aftershock sequences can be summed together as shown in Figure 6b. In this figure the total number of aftershocks is normalized by the number of sequences. We can thus see that 50% of the aftershock sequences had aftershocks 1.5 units smaller and 4% had aftershocks .1 units of mainshock smaller than the mainshock. If the magnitude frequency line in Figure 6b were extended beyond  $M_{after} - M_{main} = 0$ , the number of "mainshocks" per unit magnitude with "aftershocks" larger than themselves would be similar to the rate of mainshocks after foreshocks determined above. One would expect that if foreshocks, mainshocks and aftershocks result from the same failure process, this line would extend smoothly above zero when foreshock-mainshock pairs are included; if foreshocks result from a different process, an inflection of the line at zero might be expected.

The results are ambiguous. Figure 6c shows the number of earthquakes per unit magnitude versus the magnitude difference of that earthquake and the largest earthquake to have preceded the event in the sequence. Thus for a true aftershock this quantity is  $M_{after} - M_{main}$  as shown above and for a mainshock with a foreshock, it is  $M_{main} - M_{fore}$ . Depending on one's outlook, the data could support either a straight line or inflected interpretation. Perhaps some foreshock-mainshock sequences are a statistical extension of aftershock sequences while others result from a different failure process.

### Parameterization of Foreshock and Aftershock Sequences

Several of the parameters describing the rate of occurrence of earthquakes in sequences have been suggested as possible foreshock discriminants. The rate of occurrence of earthquakes in sequences ( $\lambda(t, M)$ ) can be modeled, assuming the modified Omori's Law and the Gutenberg-Richter relationship, as

$$\lambda(t, M) = 10^{A+b(M_m - M)} \cdot (t + c)^{-p}$$

where A, b, c, and p are constants (Reasenberg and Jones, 1988). Previous investigators have suggested that foreshock sequences may have lower than normal b-value (e.g., Mogi, 1963), p-value (Liu, 1986) or A-value (general rumor).

We have used the southern California sequences to systematically search for evidence of any of these relationships. The constants, (A, b, and p) have been estimated for 69 aftershock sequences and 14 foreshock sequences related to mainshocks ( $M \geq 4.5$ ) in California

since 1933. For the foreshock sequences, the largest foreshock is treated as a mainshock and the foreshocks occurring after the largest foreshock and before the mainshock are considered aftershocks. This corresponds to the real-time situation in which an earthquake occurs and is followed by some smaller events, and we want to know if these earthquakes will be followed by an even larger earthquake.

These parameters are approximately normally distributed for the 69 aftershock sequences (Figure 7). The mean values for Californian aftershocks are  $b=0.89$ ,  $p=1.05$  and  $A=-1.71$ . The  $b$ - and  $p$ -values do not vary significantly with location but the  $A$ -value may be higher in eastern California. The mean values for the 14 foreshock sequences are different from the aftershocks for all of the parameters, lower for  $b$ - and  $p$ -values but higher for the  $A$ -value. T-tests (a test of the probability that 2 data sets could be drawn from the same parent distribution) were run on these distributions. The probability that the  $b$ -value distributions of the aftershocks and foreshocks are different is 92%; for the  $p$ -values, it is 98% and for the  $A$ -values it is  $> 99.9\%$ .

An examination of the data set shows a subgroup of 4 of the 14 foreshock sequences analysed have lower  $p$ -values and higher  $A$ -values than were estimated for any of the aftershock sequences (Table 2). One other foreshock sequence has a lower  $p$ - and higher  $A$ -values than all but 3 aftershock sequences. All of these distinctive low- $p$ , high- $A$  foreshock sequences have occurred since 1975 and all have occurred in the extensional regions east of the San Andreas fault. Three of these low- $p$ , high- $A$  sequences also had very low  $b$ -values. The nine other foreshock sequences had  $p$ -values similar to aftershock sequences. In fact, the  $p$ -value for 2 foreshock sequences was 1.50, higher than all but 1 of the 69 aftershock sequences. For all foreshock sequences, the  $A$ -value was high though not necessarily as extremely high as for the 5 sequences that also had a high  $p$ -value.

TABLE 2. Sequence Parameters of Foreshocks in Southern California

| Year | Mon | Day | Location         | Mag | Nfor | Naft | $b \pm 1\sigma$ | $p$  | $A$   |
|------|-----|-----|------------------|-----|------|------|-----------------|------|-------|
| 1934 | 6   | 5   | Parkfield        | 5.0 | 2    | 4    | $0.42 \pm 0.21$ | 1.03 | -1.19 |
| 1939 | 12  | 5   | Borrego          | 4.0 | 0    | 6    | $0.67 \pm 0.27$ | 0.83 | -1.22 |
| 1950 | 7   | 28  | Niland           | 5.4 | 24   | 12   | $1.00 \pm 0.29$ | 0.92 | -0.91 |
| 1968 | 6   | 29  | Santa Barbara    | 4.4 | 13   | 12   | $1.02 \pm 0.29$ | 1.03 | -0.80 |
| 1969 | 10  | 22  | Point Conception | 5.4 | 1    | 24   | $0.77 \pm 0.16$ | 1.18 | -1.23 |
| 1975 | 1   | 23  | Brawley          | 4.4 | 11   | 23   | $0.46 \pm 0.10$ | 0.50 | 0.58  |
| 1975 | 11  | 15  | Goat Mountain    | 4.6 | 0    | 32   | $0.84 \pm 0.15$ | 0.91 | -1.66 |
| 1978 | 3   | 11  | Baja             | 4.8 | 269  | 293  | $1.00 \pm 0.06$ | 0.82 | -1.20 |
| 1979 | 3   | 15  | Homestead        | 4.9 | 6    | 22   | $1.14 \pm 0.26$ | 0.50 | -1.19 |
| 1980 | 5   | 25  | Mammoth          | 6.4 | 215  | 95   | $0.80 \pm 0.12$ | 1.50 | -1.29 |
| 1981 | 4   | 25  | Westmoreland     | 4.1 | 15   | 101  | $0.76 \pm 0.08$ | 0.50 | 0.08  |
| 1983 | 10  | 19  | Durrwood         | 4.0 | 1    | 19   | $0.68 \pm 0.16$ | 0.59 | -0.67 |
| 1986 | 7   | 20  | Chalfant Valley  | 5.9 | 7    | 72   | $0.89 \pm 0.12$ | 0.72 | -1.27 |
| 1987 | 11  | 24  | Superstition     | 6.2 | 4    | 164  | $0.67 \pm 0.06$ | 1.50 | -1.25 |

Nfor = Number of foreshocks before largest foreshock

Naft = Number of foreshocks after largest foreshock

From these results, guidelines can be drawn for real-time assessment of the foreshock potential of ongoing sequences. First a sequence with a high A-value ( $> -1.3$ ) is more likely to be a foreshock sequence; over 40% of the sequences with  $A > -1.3$  are foreshock sequences. A low A-value may make it less likely to be a foreshock (the smallest recorded foreshock A-value is larger than the mean aftershock A-value) but because A-values were not determined for foreshock sequences with small numbers of events because of lack of data, this inference is not confirmable. If, in addition to a high A-value, the sequence has a low p-value, it is even more likely to be a foreshock; 70% of sequences with  $p < .75$  and  $A > -1.3$  were foreshocks. However, many foreshock sequences have also had high p-values including the 1980 Mammoth and 1987 Superstition Hills foreshock sequences. A low b-value also makes a sequence more likely to be a foreshock; 32% of sequences with  $b \leq .8$  have been foreshocks.

## Discussion

This results suggests that determination of model parameters (A, b and p) in real-time could contribute useful information for the purpose of earthquake prediction. It is worthwhile considering the requirements for a real-time data acquisition and processing system to allow these results to be used. Most obviously, earthquakes must be quickly detected and located. It is likely during a foreshock sequence to have a substantial number of events so the system must handle periods of high seismicity without generating large backlogs. Earthquakes within a minimum of three (preferably four) units of magnitude of the mainshock are needed to get reasonable estimates of the parameters, especially the b-value, and the potential foreshocks to M6 mainshocks are usually in the M4-M5 range so recording down to M1.5-2.0 level is important. To use these results, processing of even smaller earthquakes is not needed.

The *automatic and accurate* determination of magnitudes for larger ( $M \geq 4$ ) earthquakes is a crucial requirement for a real-time system. The determination of A-value is very sensitive to the magnitude of the "mainshock" (i.e., potential largest foreshock) and the b-value is also strongly affected by the magnitudes of the largest events in the sequence. Thus onscale recording of larger earthquakes (requiring ultra low-gain or wide dynamic range stations) must be part of the routine processing stream. Magnitudes determined from paper records or digital systems not in real-time communication with the processing computers are not sufficient. The information should be accessible to the automatic real-time processor.

## References

- Jones, L. M., 1985, Foreshocks and time-dependent earthquake hazard assessment in southern California, *Bull. Seismol. Soc. Amer.*, **75**, 1669-1680.
- Liu, Z. R., Earthquake frequency and prediction, *Bull. Seismol. Soc. Amer.*, **84**, 255-265.
- Mogi, K., 1963, Some discussions on aftershocks, foreshocks and earthquake swarms. The fracture of a semi-infinite body caused by an inner stress origin and its relation to earthquake phenomena (third paper), *Bull. Earthq. Res. Inst.*, **41**, 615-658.

Reasenber, P., 1985, Second-Order Moment of Central California Seismicity, 1969–1982, *J. Geophys. Res.* 90 5479–5496.

Reasenber, P., and L. M. Jones, 1988, Earthquake hazard immediately after a mainshock in California, *Trans. Amer. Geophys. U.*, in press.

### Figure Captions

Figure 1. A map of the areas used in this study.

Figure 2. (a) The percentage of earthquakes in southern California that were foreshocks to a larger earthquake within 1 week as a function of the magnitude of the earthquake (see text). (b) The percentage of  $M \geq 5$  and  $M \geq 6$  earthquakes in southern California that were preceded by foreshocks within 1 week as a function of the magnitude of the foreshock.

Figure 3. The cumulative number of foreshock-mainshock pairs versus difference in magnitude between foreshock and mainshock for mainshocks (a)  $M \geq 3.0$  and (b)  $M \geq 4.0$ .

Figure 4. The rate per day of the occurrence of mainshocks as a function of time after the largest foreshock for (a) southwestern California and (b) eastern California.

Figure 5. The number of foreshock-mainshock pairs as a function of distance between foreshock and mainshock for (a) aftershocks and (b) foreshocks.

Figure 6. (a) The number of aftershocks per unit magnitude as a function of difference in magnitude between aftershock and mainshock for the 1983 Coalinga earthquake. (b) The number of aftershocks per unit magnitude normalized by number of sequences as a function of difference in magnitude between aftershock and mainshock for all  $M \geq 5.0$  mainshocks in this study. (c) The number of earthquakes per unit magnitude as a function of difference in magnitude between that earthquake and the largest earthquake preceding it in its cluster for all sequences with a mainshock of  $M \geq 5.0$  in this study.

Figure 7. Distribution of  $b$ ,  $p$  and  $A$  parameters determined for (a) 14 foreshock sequences and (b) 69 aftershock sequences to  $M \geq 4.5$  mainshocks in California, from 1933 to 1987. Solid bar indicates mean  $\pm 1$  standard deviation.

Regions in Southern California

**MADE FROM BEST AVAILABLE COPY**

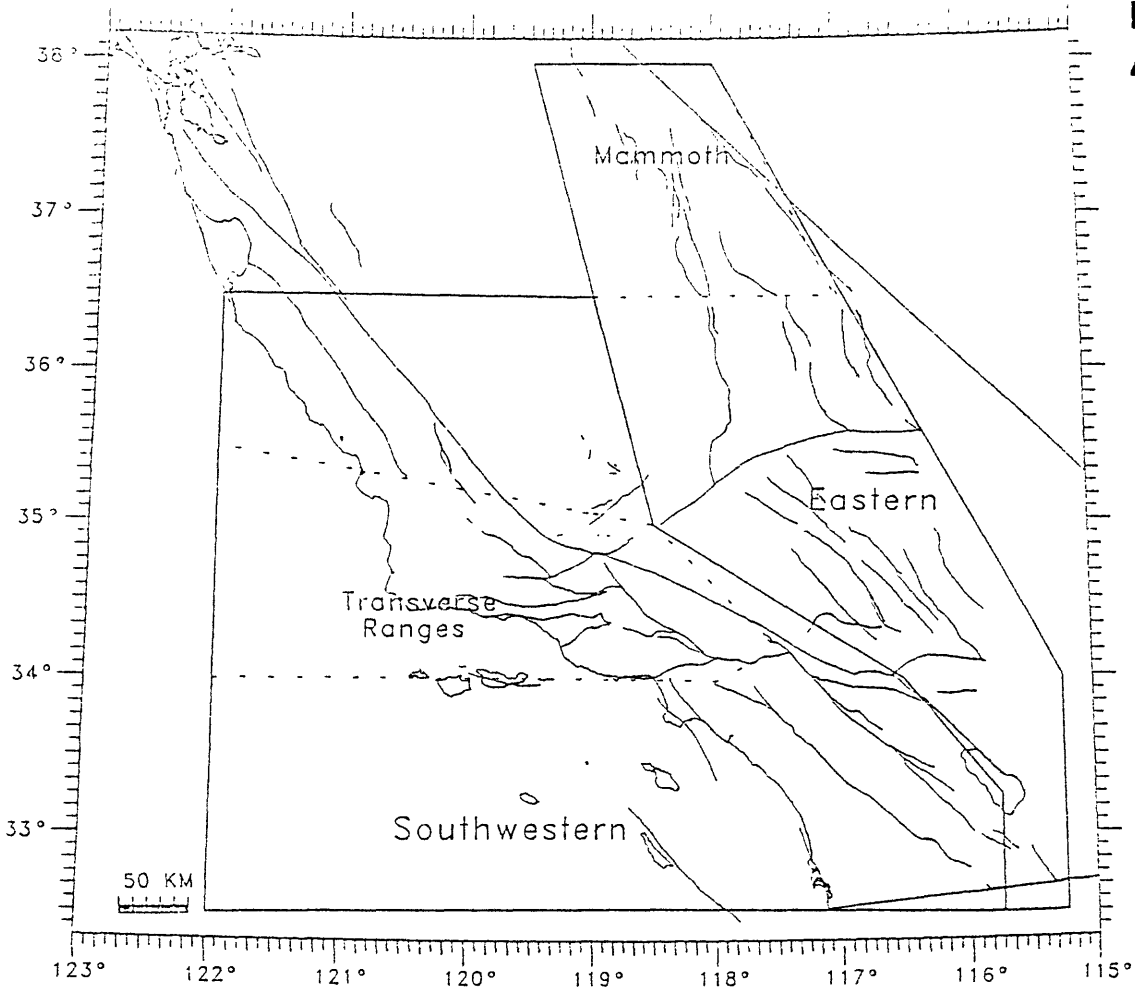


Figure 1

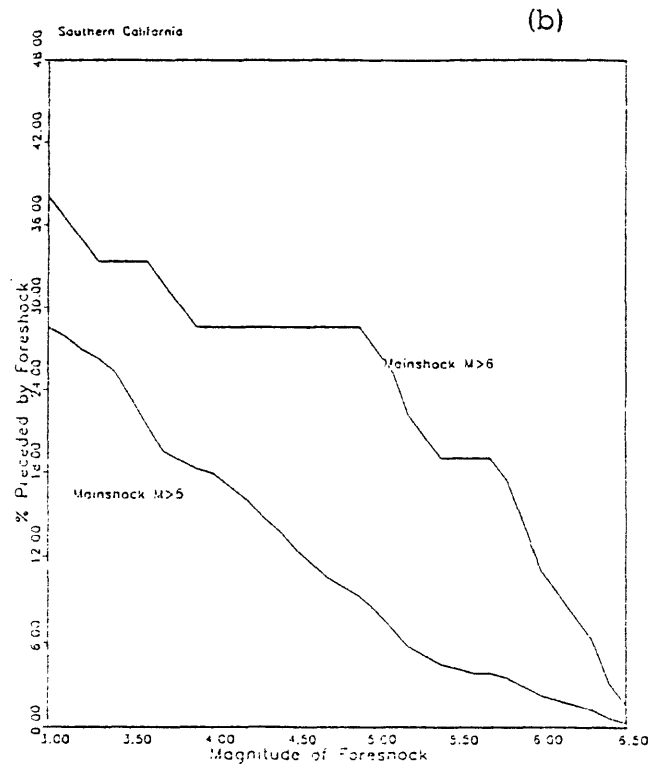
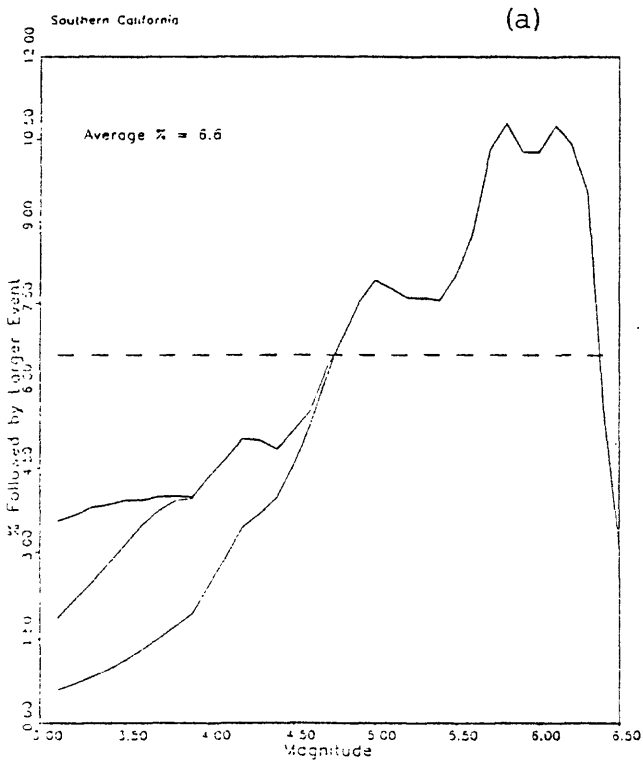
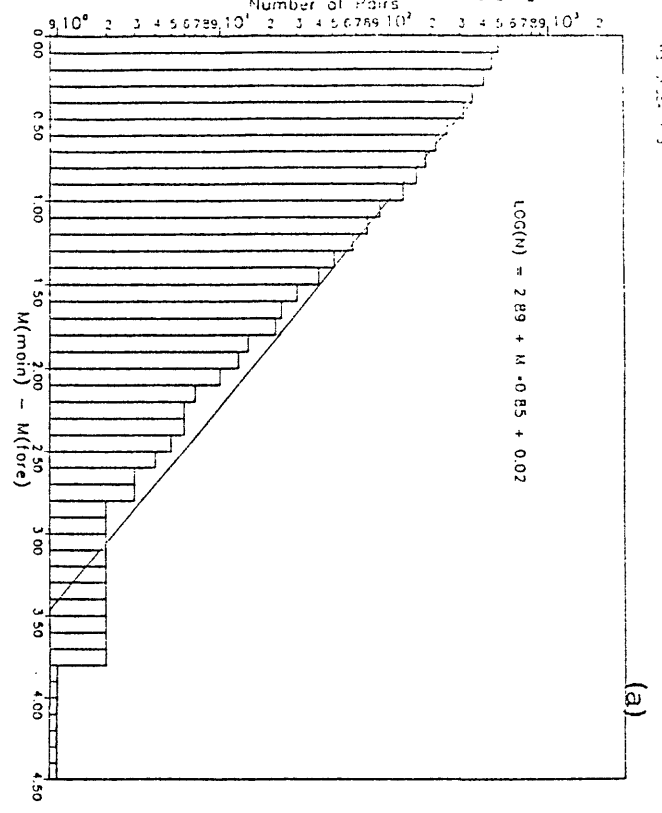
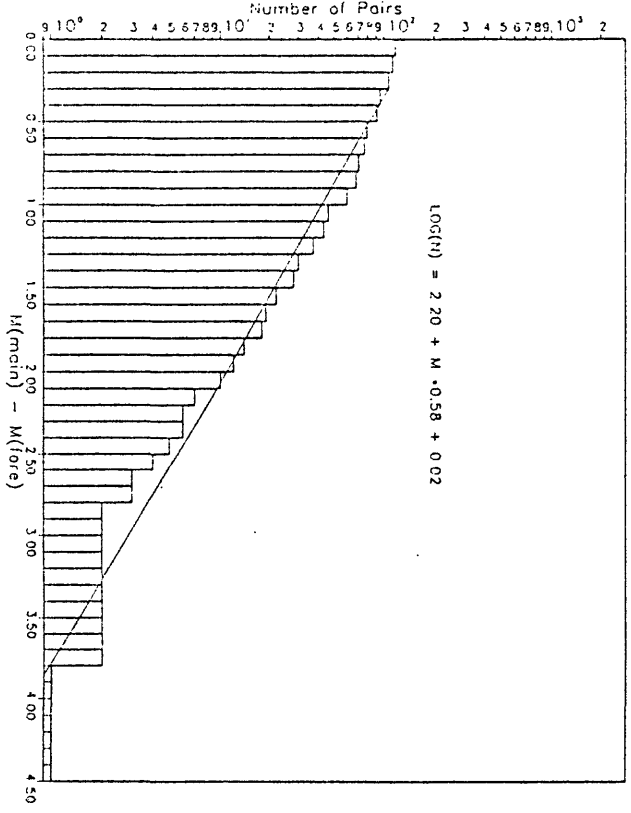


Figure 2



(a)



(b)

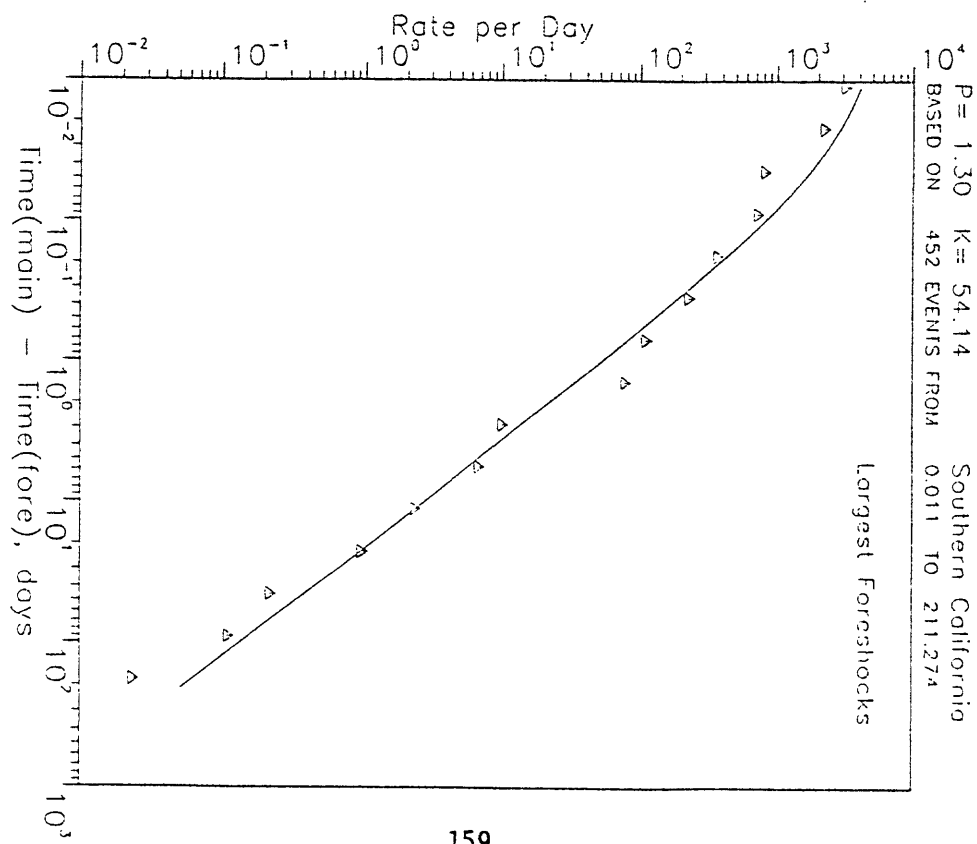


Figure 4

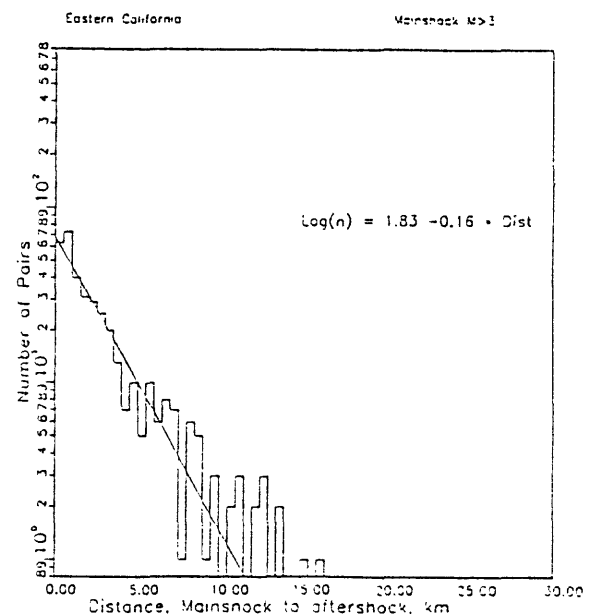
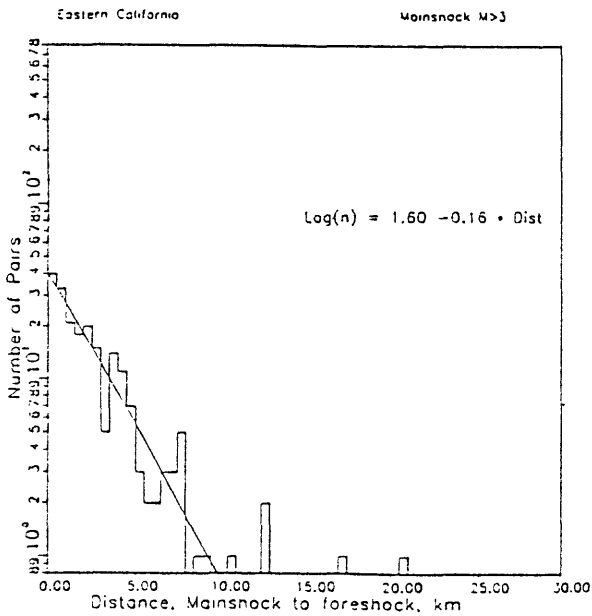
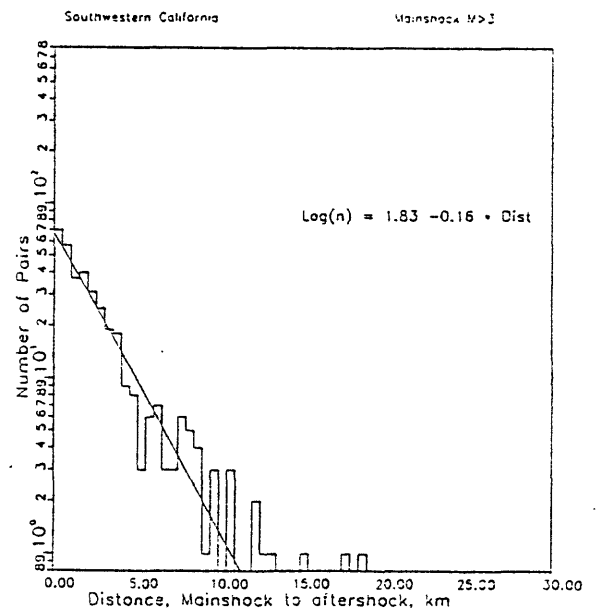
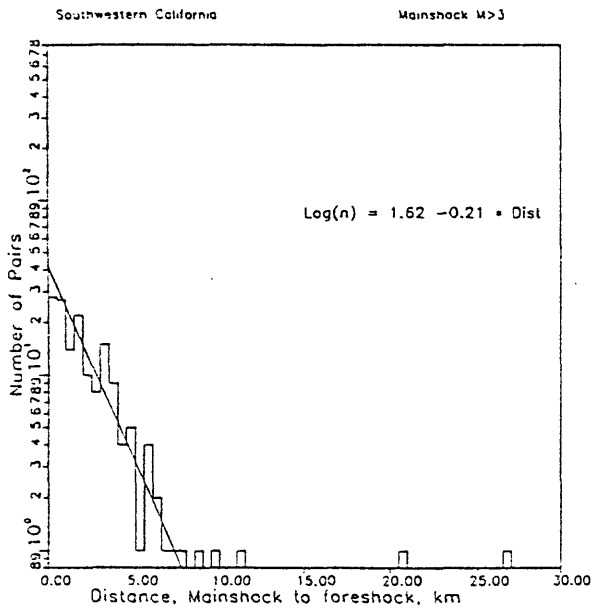
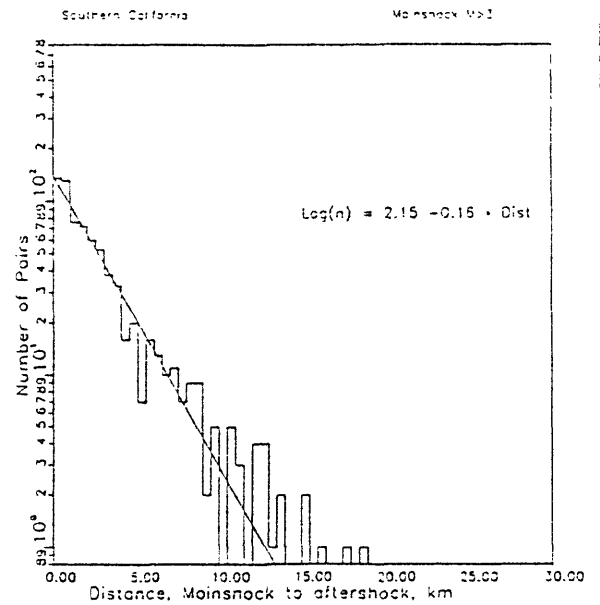
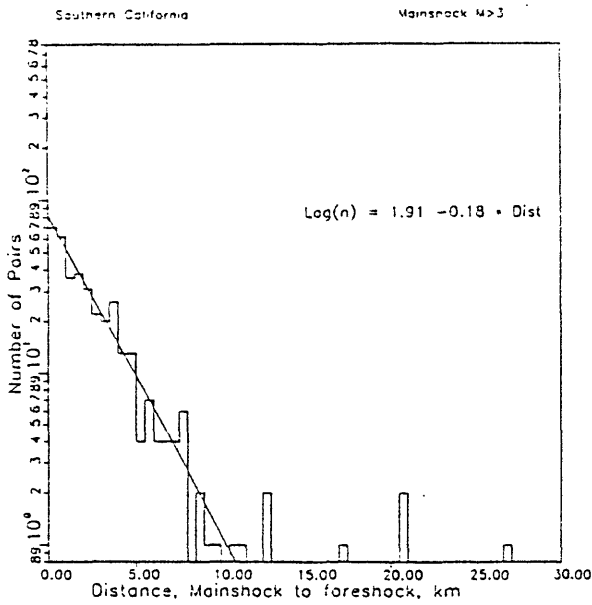


Figure 5

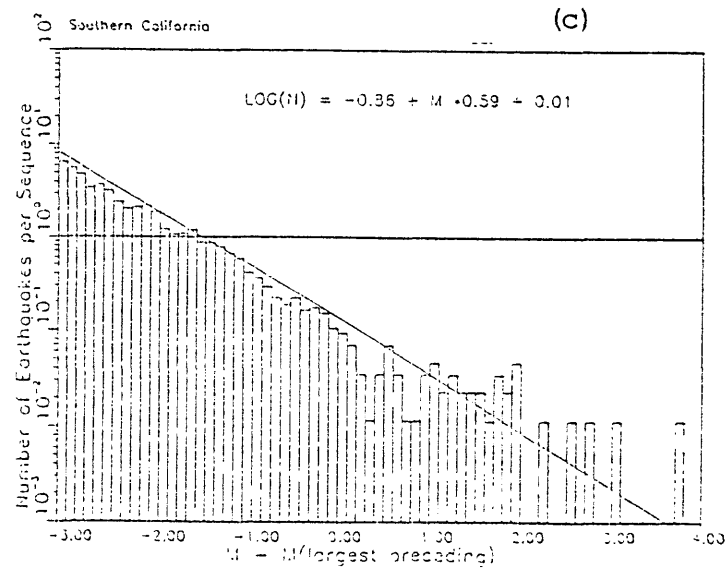
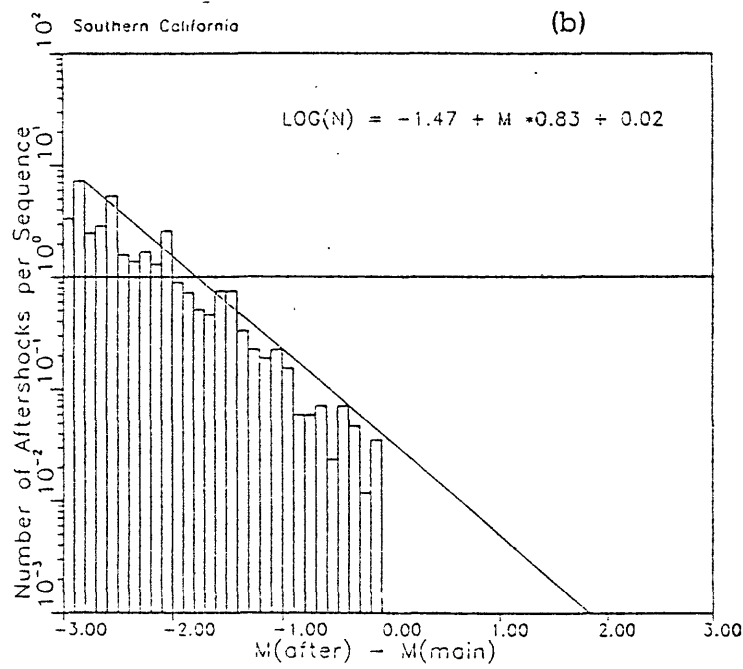
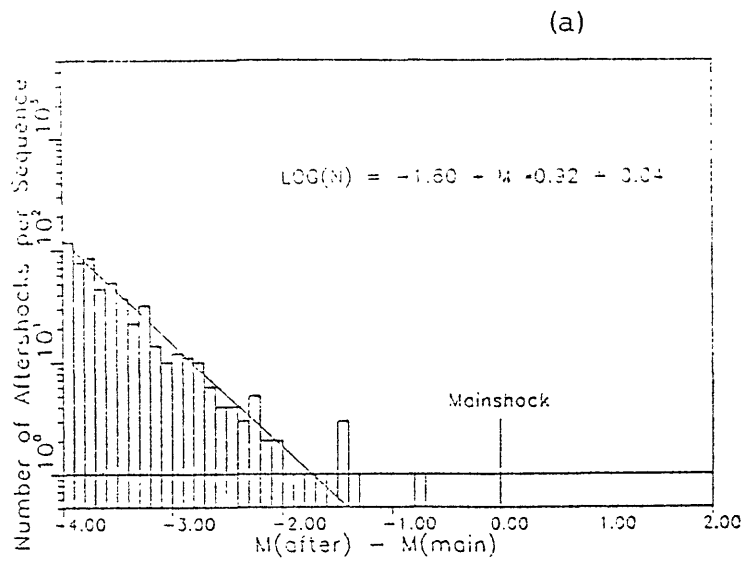
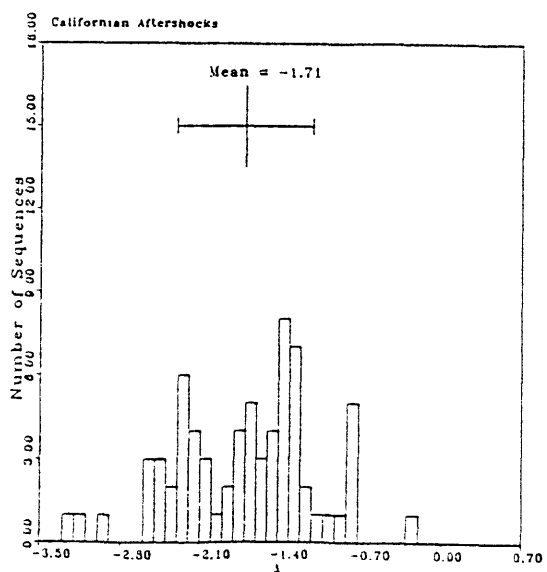
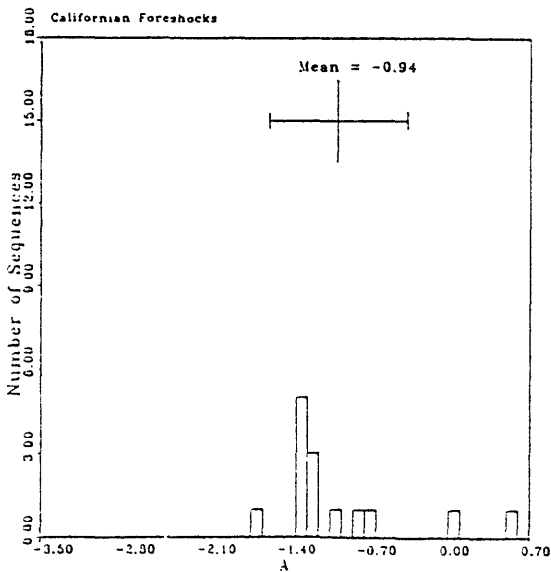
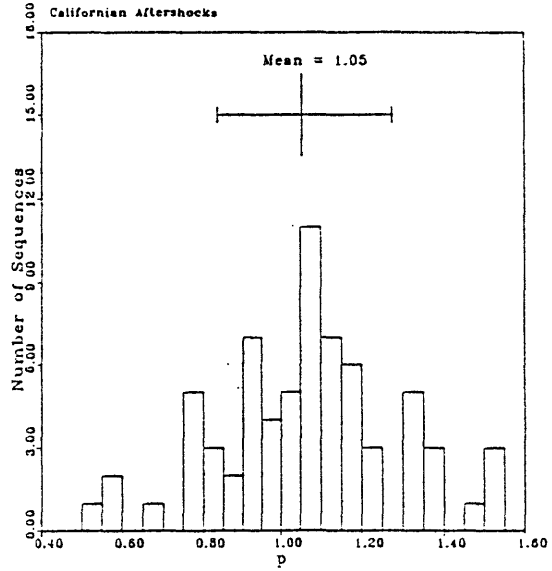
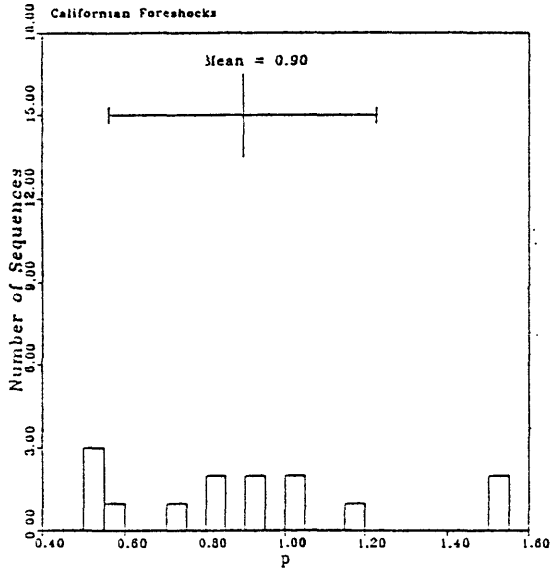
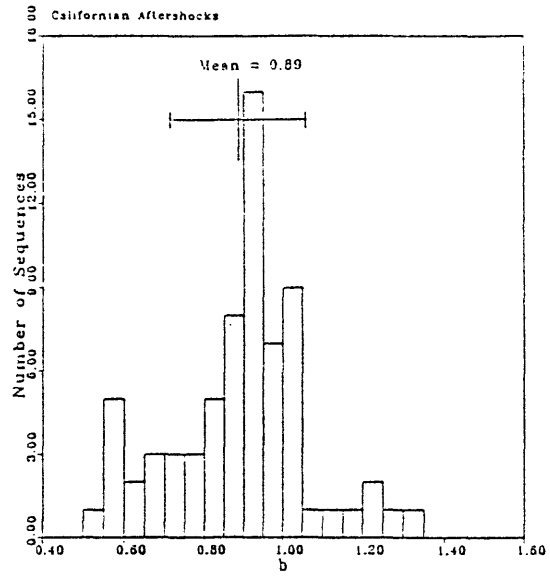
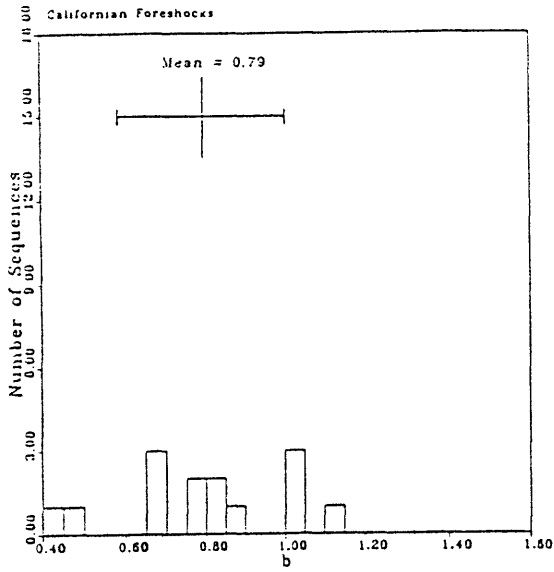


Figure 6



## REAL-TIME EARTHQUAKE WARNING

M. Nafi Toksöz, Anton M. Dainty, John T. Bullitt and Robert Cicerone  
Department of Earth, Atmospheric, and Planetary Sciences  
Massachusetts Institute of Technology  
Cambridge MA 02139

To be effective, a real-time earthquake warning system should provide estimates of the epicenter, origin time and size of an earthquake within tens of seconds, and then use these to calculate the area at risk. The problem of estimating the size of the earthquake has been the primary focus of our effort. There is a large body of work on efficient and robust methods of determining epicenter and origin time, and Heaton (1985) has discussed the calculation of the area at risk and its limitations. Conventional methods of estimating earthquake size (e.g., coda duration), however, do not seem adequate for real time applications. Furthermore, the problem is important: to be credible, the system must discriminate between magnitude 4, magnitude 6 and magnitude 8 events.

We present a prototype warning system designed for use on the strike slip faults of the San Andreas system. Our philosophy of system design has been to design the system for deployment on a known fault (the San Andreas) and to use knowledge about this fault in an expert system. By doing this we seek to reduce the computational load on the expert system by reducing the generality of the rules it must consider. The strike-slip San Andreas system was chosen because of the characteristics of near fault strong motion discussed below. An alternative approach would be to design a more general and more widely distributed system that, for example, monitored all the faults in a region. While ultimately this would be desirable, designing a simpler system allows us to look at the problem of real-time estimation of the size of the event in a situation where a lot of prior information is available. Once this crucial problem is understood, the principles can be applied to the more general problem.

The approach to the problem is conceived as follows. A network of strong motion accelerometers will be laid out around a potential causative fault and will continuously telemeter instantaneous ground acceleration and/or velocity to a central station (Figure 1). The real time analysis of these signals shall be: a) detection of potential signals of interest; b) use of an expert system to locate events and estimate size and to distinguish potentially damaging events from smaller earthquakes; c) similarly, calculation of the area of strong shaking; d) the taking of appropriate measures to mitigate damage and casualties. In this presentation we address part (a) and especially part (b).

In the "standard" model of earthquakes (e.g., Aki, 1968), an event begins through the initiation of slip at a point on a fault plane. The slip then propagates as a rupture front across the fault plane at close to the shear wave speed in the faulted material. The moment  $M_o$  of the earthquake is given by

$$M_o = \mu A d \quad (1)$$

where  $A$  is the faulted area,  $d$  is the average slip and  $\mu$  is the shear modulus of the faulted rock. We have chosen the moment as the appropriate measure of earthquake size; from (1) determination of moment requires measurements of both  $A$  and  $d$ . To assess the possibility of doing this in real time for strike-slip earthquakes, we have reviewed results reported in the literature from the analysis of near fault strong motion records for the 1966 Parkfield earthquake (Aki, 1968), the 1979 Imperial Valley earthquake (Hartzell and Heaton, 1983), and the 1984 Morgan Hill earthquake (Hartzell and Heaton, 1986), as well as simulations of the 1857 Fort Tejon earthquake (Bouchon and Aki, 1980). Successful attempts to synthesize the ground motion records using the standard faulting model have demonstrated that the total ground motion is the sum of the radiation from different parts of the fault with the appropriate travel time delay and radiation pattern. On the horizontal components, especially at low frequencies, S waves dominate, while on the vertical components high frequency P waves are seen. An interesting special case, however, occurs for instruments close (within about a kilometer) to a near surface strike slip fault trace. The horizontal ground displacement and ground velocity components are dominated by a large pulse due to radiation from the rupture front as it passes the instrument (Aki, 1968; Bouchon, 1980). The detection of this pulse would indicate passage of the rupture near a given station. If an epicenter estimate is available, the distance between the epicenter and the station gives an estimate of the "current length"  $L$  of the ruptured fault; if a width  $W$  can be assigned to the fault then a "current area"  $A = L \times W$  can be calculated.

Two methods have been used to estimate the local slip  $d$ . The amplitude of the pulse on the horizontal velocity component perpendicular to the fault trace is directly proportional to the local slip  $d$  (Aki, 1968) for stations very close to the fault and provides a means for making a spot measurement of  $d$  immediately after the rupture front has passed. Furthermore, this component does not change sign upon crossing the fault and thus is tolerant of lack of knowledge of the exact position of the fault trace. This method has been used for analysis of observed ground motion records from the 1979 Imperial Valley and 1984 Morgan Hill earthquakes. The local slip in cm has been taken as equal to the peak ground velocity in cm/sec on the perpendicular component. This empirical rule was derived by comparing the observed peak velocity on the Cholame station for the 1966 Parkfield earthquake with the corresponding local slip (Aki, 1968). The second method is to compute the ground displacement parallel to the fault for a station very close to the fault. This should give half the local slip directly, and has been used for the 1857 Fort Tejon simulation. There is, however, one major difficulty in both methods: studies of fault rupture using strong motion records indicate that the distribution of slip is highly variable across the fault plane (Hartzell and Heaton, 1983; Kanamori and Stewart, 1978; Toksöz *et al.*, 1987). Thus the "current slip" should be estimated as the average of all stations for which local measurements can be estimated.

The requirements for the proposed earthquake warning system outlined above can be most effectively fulfilled by an expert system, i.e., a computer program that uses artificial intelligence techniques to draw reliable conclusions from the data provided to it. The relevant aspects of the theory of seismic wave propagation near a vertical strike-slip fault can be distilled into a set of rules, by which inferences regarding earthquake location and size may be drawn from the seismic data. Examples of such rules are shown in Table 1.

In our simplified model of a prototype system, we consider a one-dimensional array of seismic sensors deployed along the trace of a vertical strike-slip fault. Signals from these sensors, after some preprocessing, are made available to the expert system in real time. The sensors have been assumed to be three component accelerometers from which ground velocity and displacement may also be obtained by appropriate filtering or integration. The expert system is activated when a station in the array is first triggered by large ground accelerations. The location of the first triggered sensor is assumed to be at the earthquake epicenter, and the trigger time at that sensor is assumed to be the origin time.

The estimate of the seismic moment is updated whenever the estimates of either the average slip on the fault or the rupture length change. The rupture length is taken to be the distance between the first triggered sensor and the sensor that most recently reported the passage of the rupture. The average slip on the fault is taken to be the average of the local slip at all sensors that detected the passage of the rupture. In calculating the moment, we assume a fault width of 10 km, a value typical for moderate to large earthquakes on the San Andreas system, and a shear modulus,  $\mu$ , of  $2.5 \times 10^{11}$  dynes/cm<sup>2</sup>, which is appropriate for crustal rocks in the fault zone.

To test the prototype we have used recorded strong motion digital data from the 1979 Imperial Valley and 1984 Morgan Hill earthquakes. In each earthquake, four sensors located close to the fault trace are used in the simulations. The strong motion stations and the velocity data are shown in Figure 2. The raw data consist of the vertical component of the corrected acceleration (for establishing trigger times) and the horizontal component of ground velocity perpendicular to the fault (for estimating the slip). The data are processed by calculating the peak absolute amplitude of the trace in evenly-spaced time intervals. Peak acceleration is computed every 0.1 seconds; peak velocity every 0.5 seconds. These rectified peak amplitude traces (Figure 2) constitute the input data for the expert system and are given to the system in the proper time order, i.e., as if they were being received in real time.

Time histories showing the results of the simulations are shown in Figure 3. Figure 3A summarises the calculations for the Imperial Valley earthquake by showing the current values of the rupture length, average slip and seismic moment computed by the expert system as a function of time after triggering of the Bonds Corner sensor, the first sensor to trigger. The rupture length is zero until the expert system decides that the rupture has passed the Meloland station (Figure 2), then jumps to 14 km, the distance between Bonds Corner and Meloland. It remains constant for a time, then increases again when the rupture passes El Centro 6. After the rupture has passed El Centro 6 the rupture length remains constant because the horizontal velocity at Brawley never exceeds the peak velocity at Bonds Corner, indicating to the expert system that the rupture does not extend to Brawley. The resulting estimate of the fault length is 22 km, shorter than the true length. The slip increases steadily from time zero as the horizontal velocity at Bonds Corner increases and then increases more rapidly as an estimate from Meloland is added to the average; as more information is added the average slip continues to increase, although the program does not require this. This effect is presumably due to downfault focussing of energy due to radiation

pattern (Bouchon, 1980), the distribution of asperities (Hartzell and Heaton, 1983; Toksöz *et al.*, 1987) and the focussing effect of the low velocity fault zone (Cormier and Spudich, 1984). The first estimate of the current moment is taken when the first estimate of the current rupture length is available, and then increases steadily until it reaches its stable, final value. This steady increase is expected on physical grounds.

The final estimate of seismic moment for the Imperial Valley earthquake computed using (1) (Figure 3A) is  $4.9 \times 10^{25}$  dyne-cm, obtained within 9.5 sec of the time of the triggering of the first sensor (Bonds Corner). This value agrees well with that of  $5.0 \times 10^{25}$  dyne-cm obtained from seismic measurements (Hartzell and Heaton, 1983). Since the estimated rupture length is known to be too short, the average slip must be too large: this will be discussed in more detail in connection with the Morgan Hill earthquake, where a similar effect occurs. The epicenter is placed at the Bonds Corner station, about 4 km North of the true epicenter, and the origin time is taken as the trigger time at Bonds Corner, about 3 sec after true origin.

For the Morgan Hill earthquake (Figure 3B) a similar sequence of calculations is shown. The rupture is determined to propagate from Halls Valley to Gilroy 6, leading to an estimate of rupture length (52 km) that is somewhat too long. Because of the large amplitude pulse at the Coyote Lake Dam, the expert system jumps directly to a first non-zero estimate of the rupture length from Halls Valley to Coyote Lake Dam, bypassing Anderson Dam. Again, the average slip increases with time, although there is no theoretical reason why it should. A final moment estimate of  $5.4 \times 10^{25}$  dyne-cm was obtained 13 sec after the time of triggering of the earliest sensor, Halls Valley. This value is about 2.5 times greater than that given by Hartzell and Heaton (1986), equivalent to a difference of 0.25 magnitude units. Again the discrepancy seems to be due to a high estimate of the average slip—the error in the rupture length is not sufficient. This high estimate of slip may be due to use of the Cholame record at Parkfield for calibration or the focussing effects alluded to above, but we suspect that the influence of asperities is the most likely explanation. There appears to be a large asperity near Anderson Dam which causes large velocity amplitudes at the downfault stations (Hartzell and Heaton, 1986), and since averaging only occurs over a few stations the final estimate is too high. A similar explanation can be advanced for Imperial Valley, where a large asperity near Meloland has been proposed (Hartzell and Heaton, 1983). We note, however, that for the purposes of earthquake warning moment estimates within about a factor of two of the true value would be quite acceptable. The epicenter for the Morgan Hill earthquake is placed at the Halls Valley station, 5 km NW of the true epicenter, and the origin time is estimated as the trigger time at Halls Valley, 3 sec after true origin.

As a final example, we present calculations of the local slip and moment by our method for a simulation of the 1857 Fort Tejon earthquake. This simulation was provided to us by M. Bouchon and is similar to that given in Bouchon and Aki (1980), except that frequencies up to 5 Hz are considered and the simulation covers only the first 200 km of the fault. We have used the parallel component of ground motion for stations spaced every 10 km down the fault starting at the epicenter; the stations are 100 m from the fault trace. In Figure 4 at top we show the estimated local slip

at each station compared to the input local slip. There is general agreement on the size, but after about 100 km downfault there are also spurious features in the estimated slip: we are presently investigating these discrepancies. The bottom panel shows the estimated current moment in time; the final value of  $4.4 \times 10^{27}$  dyne-cm is in reasonable agreement with the result  $5.3 - 8.7 \times 10^{27}$  dyne-cm given by Sieh (1978), whose models were used as input to the simulation.

The ongoing Parkfield Earthquake Monitoring Experiment offers an ideal setting for field testing a warning system. Because of the problems due to unpredictable wave amplification effects within the fault zone and small-scale heterogeneity of the rupture noted in the cases above, a denser network of sensors (accelerometers) laid out along the fault trace may be required in order to obtain a more accurate estimate of the moment. Off fault sensors would be desirable to discriminate between events on and off the fault. The output from the sensors would be telemetered to a central point, where they would be received by a data processing computer. This computer would digitise the data, if necessary, compute the velocity from the acceleration inputs and find the appropriate envelopes. The processed data would be the input to the expert system, which would implement rules of the type described in this note. The final part of the system would be some means of evaluation of system performance in terms of success or failure to detect significant events and estimate their size, and false alarms.

## ACKNOWLEDGEMENTS

We thank Michel Bouchon for many illuminating discussions on the nature of ground motion produced by faulting and supplying us with the simulation of the 1857 Fort Tejon earthquakes. Anthony Shakal of the Office of Strong Motion Studies, Division of Mines and Geology, California Department of Conservation supplied the data for the Meloland station; other strong motion data was supplied by the U. S. Geological Survey.

## REFERENCES

- Aki, K. (1968). Seismic displacements near a fault, *J. Geophys. Res.* **73**, 5359-5376.
- Bouchon, M. (1980). The motion of the ground during an earthquake, I: the case of a strike slip fault, *J. Geophys. Res.* **85**, 356-366.
- Bouchon, M. and K. Aki (1980). Simulation of long-period, near-field motion for the great California earthquake of 1857, *Bull. Seis. Soc. Am.* **70**, 1669-1682.
- Cormier, V. F. and P. Spudich (1984). Amplification of ground motion and waveform complexity in fault zones: examples from the San Andreas and Calaveras faults, *Geophys. J. Roy. Astron. Soc.* **79**, 135-152.

- Hartzell, S. H. and T. H. Heaton (1983). Inversion of strong ground motion and teleseismic waveform data for the fault rupture history of the 1979 Imperial Valley, California, earthquake, *Bull. Seism. Soc. Am.* **73**, 1553-1583.
- Hartzell, S. H. and T. H. Heaton (1986). Rupture history of the 1984 Morgan Hill, California, earthquake from the inversion of strong motion records, *Bull. Seism. Soc. Am.* **76**, 649-674.
- Heaton, T. H. (1985). A model for a seismic computerized alert network, *Science* **228**, 987-990.
- Kanamori, H. and G. S. Stewart (1978). Seismological aspects of the Guatemala earthquake of February 4, 1976, *J. Geophys. Res.* **83**, 3427-3434.
- Sieh, K. E. (1978). Slip along the San Andreas fault associated with the great 1857 earthquake, *Bull. Seis. Soc. Am.* **68**, 1421-1448.
- Toksöz, M. N., A. M. Dainty and J. Nabelek (1987). Earthquake source mechanisms: case studies, in *Strong Ground Motion Seismology*, Mustafa Özder Erdik and M. Nafi Toksöz, Editors, NATO ASI Series C: Mathematical and Physical Sciences, vol. **204**, D. Reidel Publishing Co., Dordrecht, Holland, 41-84.

## TABLE 1

Example of two rules used in the expert system for rapid earthquake warning. The rules are activated whenever new data from a sensor becomes available to the expert system. Rule 1 is used to detect the passage of the rupture past a given sensor. If it tests **TRUE**, then a new fact is added to the system ("rupture has reached sensor **X**"). The addition of this fact to the system causes Rule 2 (among others) to be activated. When Rule 2 tests **TRUE**, it invokes a computational procedure to compute the earthquake's "rupture length" (the distance between the most widely-separated sensors that have detected rupture passage).

### Rule 1:

**IF** the peak velocity at sensor **X** is greater than that at the epicentral sensor  
**THEN** the rupture has reached sensor **X**.

### Rule 2:

**IF** the rupture has just passed sensor **X**  
**THEN** compute rupture length.

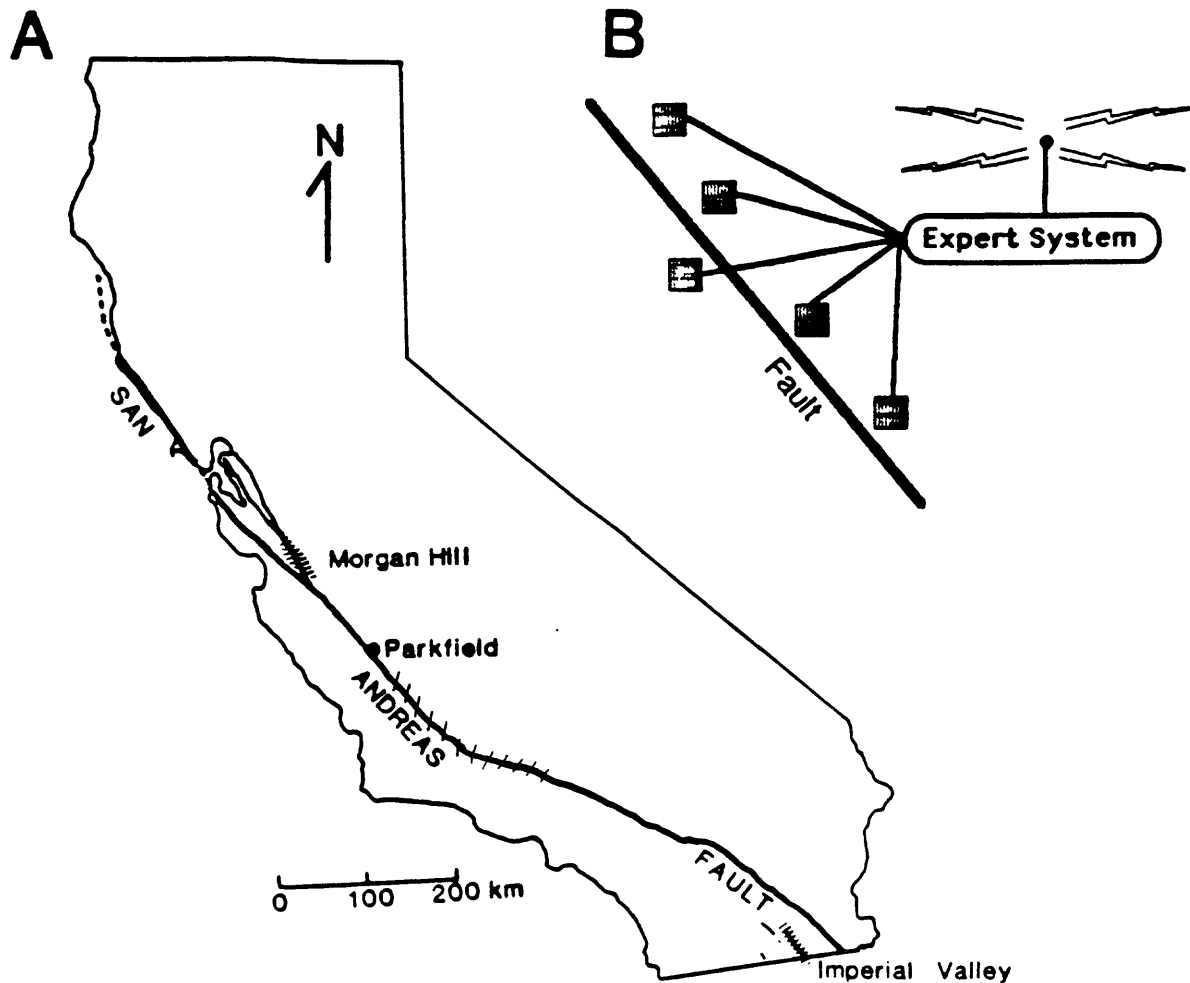


Figure 1: (A) Sketch of the San Andreas Fault system. The hatched regions denote zones of earthquake rupture associated with the 1979 Imperial Valley and 1984 Morgan Hill earthquakes and the 1857 Fort Tejon earthquake simulation.

(B) Schematic of proposed implementation of an automated earthquake warning system. A network of accelerometers (boxes) is deployed along a suspected seismogenic fault. Data from the sensors are telemetered in real time to a central station, where the signals are preprocessed and passed to the expert system. If the expert system determines that a potentially damaging earthquake is in progress, advance warning may be sent via radio link to critical facilities before the onset of strong shaking.

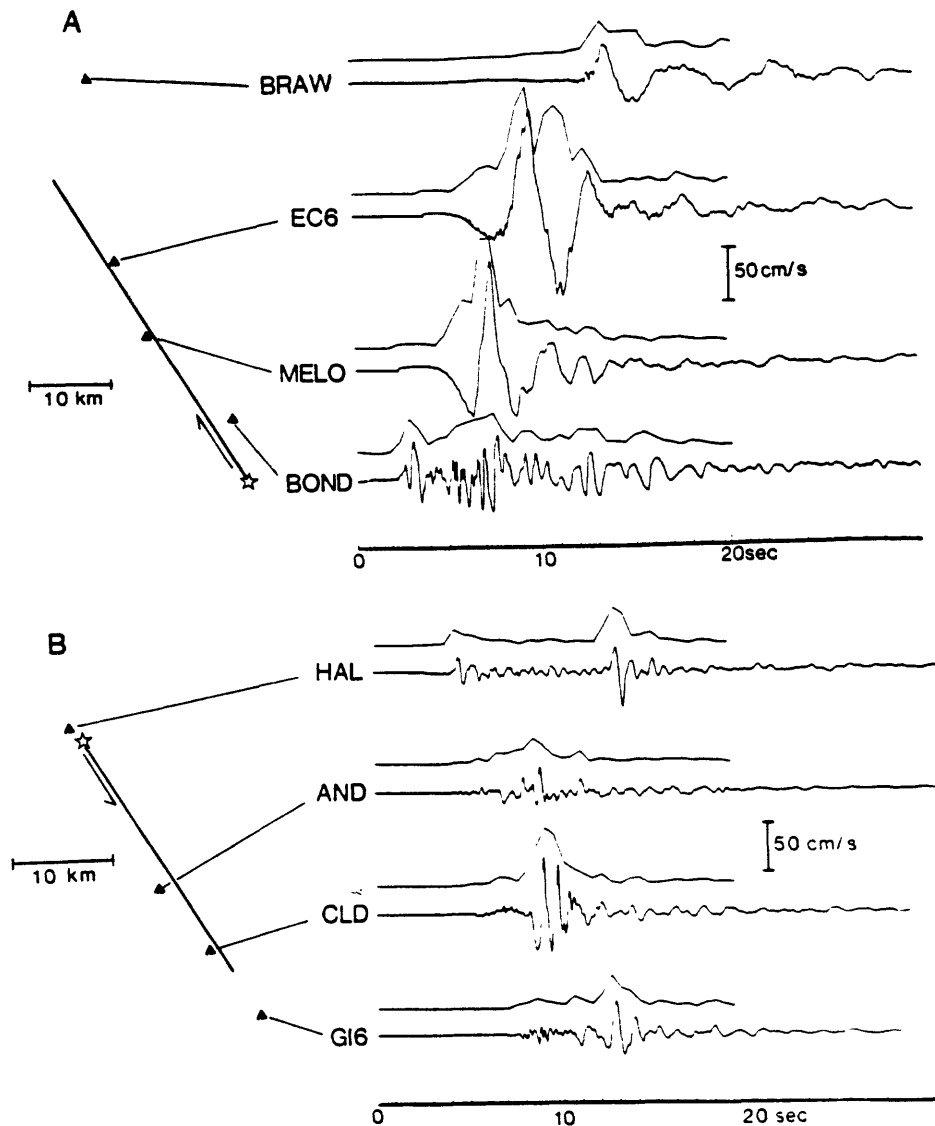
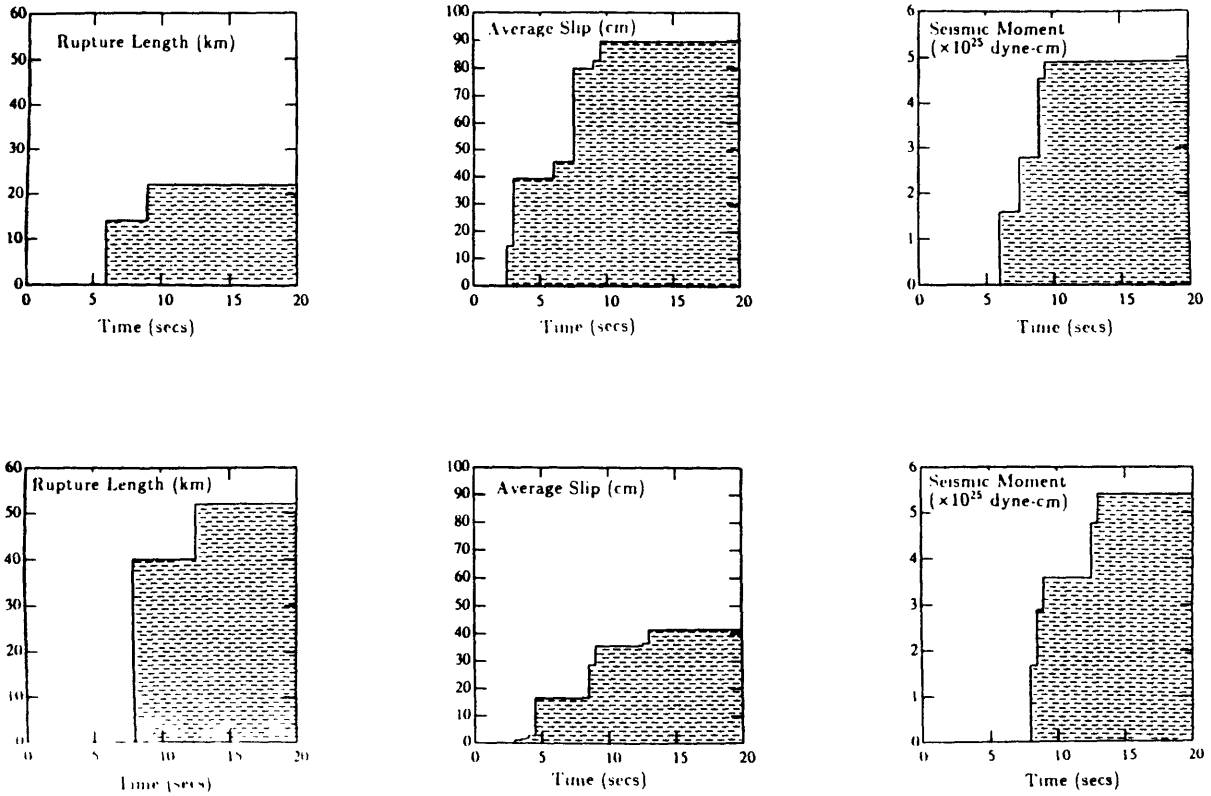


Figure 2: Signals used by the expert system in estimating the magnitude of slip on the fault and the length of rupture. Peak absolute amplitudes of horizontal ground velocity in the direction perpendicular to the fault are computed in 0.5 sec time windows; these signals are plotted immediately above the corresponding raw velocity waveforms. Data from each of the four sensors used in the simulations are shown for the 1979 Imperial Valley (A) and 1984 Morgan Hill (B) earthquakes. The maps to the left of the waveforms indicate the relative location of the sensors (triangles) along the fault trace (heavy line). The epicenter is indicated by the crossed star; the direction of rupture propagation is indicated by the arrow. The station designations are as follows: BRAW, Brawley; EC6, El Centro Differential Array No. 6; MELO, Meloland Overcrossing; BOND, Bonds Corner; HAL, Halls Valley; AND, Anderson Dam; CLD, Coyote Lake Dam; GI6, Gilroy Array 6.

**MADE FROM BEST  
AVAILABLE COPY**



**Figure 3: Time histories of the estimates of rupture length, average fault slip, and seismic moment for the 1979 Imperial Valley, California earthquake (A), and the 1984 Morgan Hill, California earthquake (B). The times are measured from the time of triggering of the first sensor. In each case, the alarm threshold of seismic moment ( $5 \times 10^{25}$  dyne-cm) is reached in about ten seconds or less after the start of the fault rupture. The computation time is negligibly short (less than 1 sec) relative to seismic wave propagation time so that an alarm can be issued while fault rupture is still in progress.**

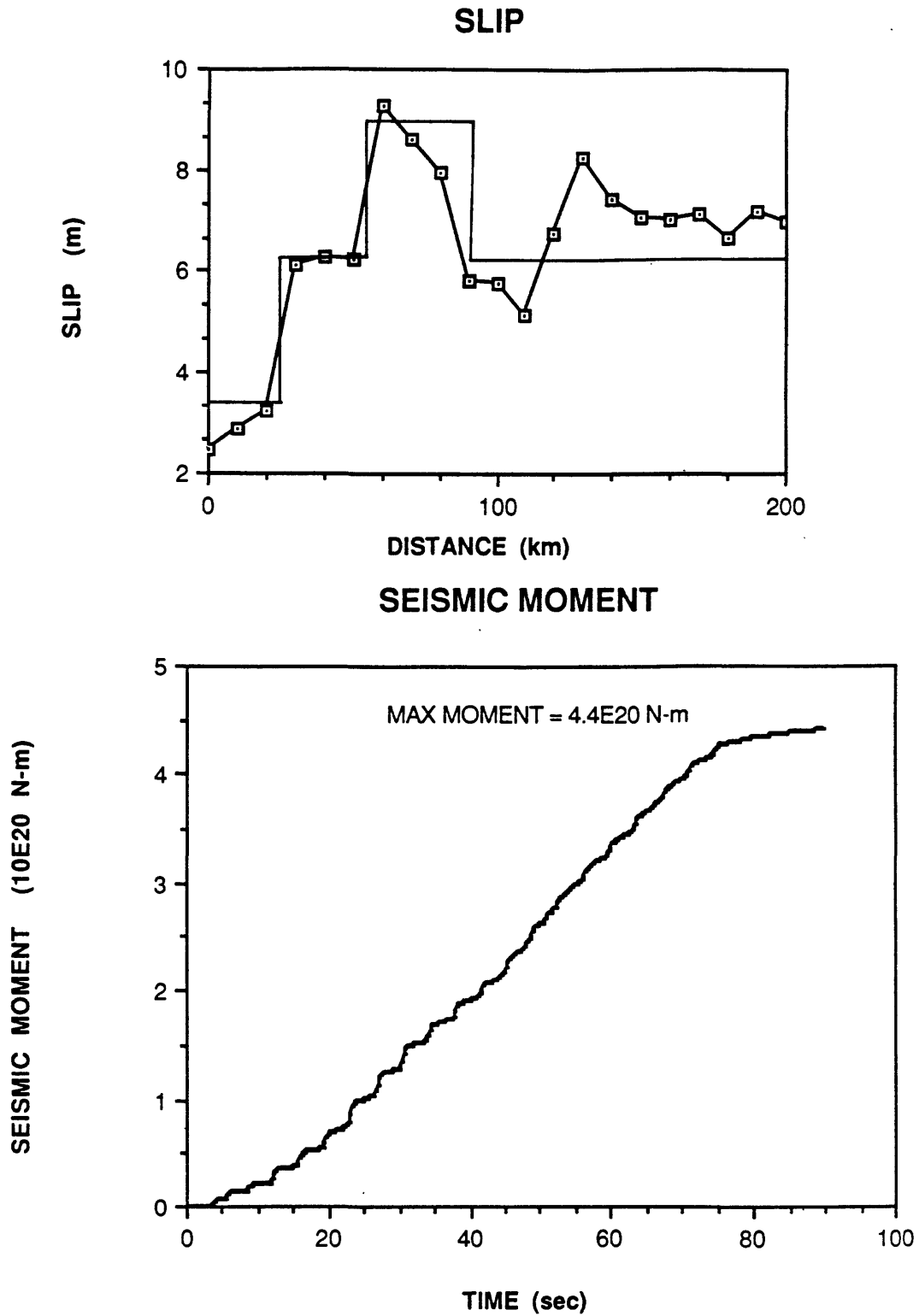


Figure 4: (Top) Local slip along the fault for a simulation of the 1857 Fort Tejon earthquake. Curve with points is estimated from the computed ground displacement parallel to the fault trace, while the curve without points is the input slip. (Bottom) Current seismic moment as a function of time for the simulation.

A Model for Real Time Advisories of Large Earthquakes ( $M \geq 7$ )

Dr. Karen C. McNally

C.F. Richter Seismological Laboratory  
University of California, Santa Cruz, CA 95064

## Introduction

In 1984 a committee of California scientists and representatives from the state of California [California Earthquake Prediction Evaluation Council (CEPEC) Southern California Earthquake Preparedness Program (SCEPP) and the Seismic Safety Commission, local jurisdictions, and the private sector] and federal agencies concluded investigations to establish a standardized earthquake prediction terminology for California. It was designed to be systematic, conform to the present state of scientific knowledge, respond to public earthquake preparedness, warning and response needs, and also flexible to allow for further refinements in the future (Wallace et al., 1984). Earthquake predictions were subdivided into three time scales: "long-term" (a few years up to a few decades), "intermediate-term" (a few weeks to a few years), and "short-term" (a few hours to a few weeks). "Short-term" predictions are subdivided into "alert" (3 days to a few weeks) and "imminent alert" (hours to 3 days). Wallace, et al. concluded that probabilities should be divided into a three-fold division of percentage values regardless of time period: 0-10% - 'slight'; 11-49% - 'moderate'; 50-100% - 'high', regardless of time period. Following discussions with members of the news media it was suggested that some members of the lay public understand percentage better if stated as, e.g. "one chance in ten", as chances of rain are commonly stated. This work further urged that scientists distinguish between their statements regarding earthquake 'predictions' and those pertaining to earthquake 'potential', for conformance with public planning efforts statewide.

Subsequent public applications of this terminology framework revealed that short term 'imminent alert' prediction time scales ( $\leq$  few hrs) did not allow for both scientific deliberations and also timely public warnings for the maximum public safety. This problem was brought to the attention of CEPEC, which advises The California Governor's Office of Emergency Services (OES) on earthquake and volcano predictions and related State science policy decisions. CEPEC was questioned: is it possible to develop a model for preplanned rapid responses on short time scales (for either potential foreshocks or aftershocks)? Such a plan could allow warning and readiness procedures to begin while CEPEC scientists conferred. In addition, it could provide a regular framework for advance planning, preparedness activities and warning procedures by the State of California.

Of primary concern are possible large ( $M \geq 7$ ) earthquakes and their aftershocks. At the present time, state preparedness and response planning is relatively well developed for moderate earthquakes, which mainly affect a single county-wide jurisdiction. Emergency officials, fire, police, school officials, etc. are reasonably well networked for a coordinated response. However, a large ( $M \geq 7$ ) earthquake is likely to affect multiple jurisdictions on a regional, rather than local, scale. The extensive planning and

agreements needed for a coordinated response to earthquake damage on a regional scale are the most crucial, and can benefit from the preplanning activities by OES based on CEPEC advice. Advance warning is most needed, therefore, for such large earthquakes ( $M \geq 7$ ), which present the greatest danger. For this reason our attention is concentrated on large events,  $M \geq 7$ . A further complicating factor is that there are a number of locations statewide which scientists agree could produce such large earthquakes at any time, not just a single location on which state and local governments should be concentrating their attention.

Because large California earthquakes are relatively infrequent compared with smaller ones, scientists have the least up-to-date information and modern instrumental data about them. Knowledge can be accelerated by gathering data from the sites of large earthquakes elsewhere in the world, but at present these efforts are still in progress. The most similar fault structures are found in New Zealand, Northern Chile, and Turkey. In fact, little is known about large shallow strike-slip interplate earthquakes such as those expected in California. Studies of small and moderate earthquakes are more developed because they occur more frequently. However, it is not known to what degree their characteristics can be extrapolated to the case of large earthquakes. In fact, recent research argues that the physics of moderate earthquakes might differ from that of large earthquake because the brittle upper crust can contain the complete source rupture area of the former, but not the latter, (which are bounded by the free surface and the lower depth of ~15 km, below which there is not seismicity or brittle failure in the California seismotectonic environment; see, eg., Shimazaki, 1986; Lackenbruch and Sass, 1973).

Against this background one can reasonably ask: What information do scientists now have which could be brought to bear in the interests of public safety, while scientists continue research? (A related point is: Which research problems are the most important for scientists to prioritize, because large earthquakes might be imminent?) A "catch-22" situation exists because scientists cannot wait for the occurrences of large California earthquakes in order to measure them, after the fact. This report suggests an interim approach utilizing the information that scientists now have, with systematic 'advisories' following the occurrence of potential foreshocks to large earthquakes. A public policy benefit of concentrating on larger earthquakes for preplanned advisories is that they and their potential foreshocks occur less frequently than smaller ones, and the 'false alarm' rate is significantly lower (by a factor of ~6). This fact will allow OES to take a statewide perspective, with a total 'false alarm' rate of about 1 per 3 years, on average (see below).

Additional work, when confirmed, can be used to refine public advisories for greater reliability and safety with an evolution toward increased probability levels and more specific short term predictions of large earthquakes. The possibility for damaging

aftershocks following large earthquakes is also a concern, particularly those which might occur on relatively short time scales (up to a few days). Suggestions concerning preplanned responses for potential aftershocks are also included.

### A Model for Preplanned Real-time Advisories of Large Earthquakes

In 1986 the California Earthquake Prediction Evaluation Council (CEPEC) and the California Governor's Office of Emergency Services (OES) began developing a procedure for preplanned, real-time advisories of large earthquakes ( $M \geq 7$ ) in 8 seismic gaps statewide. Figure 1 shows a summary of the seismic gaps in California which are known to have a potential for large earthquakes (as reported in various publications, see general references). In terms of public hazard, the seismic gaps numbered #3-9 are likely to be the most significant in the southern and northern California regions. (Two seismic gaps in the Sierra Nevada - State of Nevada region are also being evaluated for possible inclusion in these procedures.) Experience indicates that California benefits from having short term earthquake advisories. These notifications are designated as 'advisories' in public announcements.

Statewide preplanned advisories are based on seismic data. The concept of a 'practical approach' to preplanned short term advisories of future large ( $M \geq 7.0$ ) earthquakes in California is suggested. Below we outline the suggested approach.

Every  $M \geq 6$  earthquake within 50 km of 4 seismic gaps in Southern California is assumed to be a foreshock to a  $M \geq 7$  mainshock, to occur within 5 days. Figure 2 shows the seismic gaps, the proposed advisory zones and the historic earthquakes ( $M \geq 6$ , 1/1/1932-6/30/1988) within them. After 5 days the warning would expire. Every  $5 \leq M \leq 6.9$  earthquake within 20 km of 4 seismic gaps in Northern California would be treated the same. Figure 3 shows the seismic gaps, the proposed advisory zones, and the historic earthquakes ( $M \geq 5$ , 1910-1987) (see, eg, Bolt and Miller, 1975) within them. The average rate of 'false alarms' statewide should not exceed approximately one per year. In fact, if no mainshock occurs, the 'false alarms' will average about one per 3 years if the suggested procedure is followed. Perhaps as many as 30-45% of the mainshocks ( $M \geq 7$ ) in western North America (i.e., California, Nevada, and Baja, see Figure 4) are preceded by foreshocks, but data are not sufficient for detailed statistics. Nor are such details necessarily useful for public warnings and response purposes at the present time. In fact, broad probability ranges of slight (0-10%), moderate (11-49%), and high (>50%) are probably the most useful for public response planning purposes (Wallace et al., 1984). Short-term advisories, despite the 'false alarms' (which are viewed as useful exercises), are beneficial and in the interests of public safety. The probability level of these advisories is 'slight', in the absence of further information.

It is not the issuance of 'false alarms' that is the major problem, nor the total number of them. The rate of false alarms can be a problem, however, when the average exceeds ~1 per year over several years. The duration of the advisory period is constrained by state budgets: advisory conditions are not practical for more than a few days because of the costs. The temporal characteristics of foreshock behavior which need to be known are that most mainshocks will follow within 5 days, together with the common knowledge that the probability of subsequent earthquakes generally decreases with increasing time longer than a few weeks.

To examine the implications of prior ('foreshock') activity and preplanned response, we (1) rely on existing reports and (2) adopt a 'practical' perspective because very little data exist regarding the largest earthquakes in California, and a purely statistical approach to 'foreshock' analysis is not meaningful. We thus adopt a conservative, prudent approach in the interests of public safety. Ideally, one would take a large ensemble of  $M \geq 7$  earthquakes within a specific seismic gap and calculate the number of cases in which the mainshock was preceded by events of a certain magnitude and distance and time, and also the number of times that such prior events were followed or not followed by a mainshock in order to determine the probability distribution, and, hence, the probability values. However, it is clear that such data are too sparse for purely statistical criteria to be meaningful. We therefore examine available data from this 'practical' perspective in order to estimate the rates of 'false alarms' and 'successes' for preplanned short term advisories of the largest mainshocks expected in California. It is clear that there are many uncertainties in the existing database, eg., locations, magnitudes, etc. Special studies could upgrade these data but they can not compensate for the paucity of data pertaining to large California earthquakes, which is the inevitable limit on the reliability of existing statistics. Reliability could be improved, however, with further constraints derived from physical models and additional observations of precursors.

All large earthquakes ( $M \geq 7.0$ ) in the western North America tectonic region from 1857-1987 are shown in Figures 4 and 5 and listed in Table 1. Tables 2 and 3 summarize the prior activity reported for 8 of the 16 largest earthquakes (Richter, 1958; Hileman et al., 1973; Bolt and Miller, 1975; Sieh, 1978; Topozada et al., 1978, 1979). [Note that here we treat the 1954 earthquakes, a 'doublet' occurring 1 minute apart, as one earthquake. Also, see aftershock discussion, below. The 1903, 1915 and 1980 earthquakes were not reviewed.] In 7 of these 8 cases, the 'prior events' were probably magnitude  $5 \leq M \leq 6.8$ . Based on this review it thus appears that perhaps as many as 7 out of 16, or approximately 44%, of the large ( $M \geq 7$ ) earthquakes might be preceded by  $M \geq 5$  earthquakes in the near vicinity. Five out of 16, or 31%, were  $M \geq 6$ .

Below we review the available data to find a "composite" definition of "prior time" and "near vicinity" using a 'quasi-physical' approach, because, again, the data are not sufficient to support a purely statistical interpretation, nor to determine the statistical distributions relative to the largest earthquakes. Table 4 reviews 5 and 10 cases in which  $M \geq 6$  and  $M \geq 5$  events preceded  $M \geq 7+0.5$  earthquakes, respectively. We find that the distributions are similar at either magnitude threshold for the prior activity: i.e., ~30% and 80-89% of the prior activity occurs within  $\leq 25$  km and  $\leq 50$  km of the mainshock epicenter, respectively, and 40-50% and 60% within  $\leq 1$  day and  $\leq 5$  days, respectively.

In Figures 2 and 3 we outline the boundaries of 50 and 20 km distance from the seismic gaps in the southern and northern California regions, respectively. Because the mainshock epicenter is most likely to be near either end or near the midpoint of each seismic gap, we suppose that the prior activity could be anywhere along the edge of each gap, if such activity is within  $\sim \pm 25$  to 50 km of the mainshock epicenter. Using southern California and the Sierra Nevada regions as an example (gaps #1-5, Figure 1), we find that there were 7 magnitude  $6 \leq M < 7$  earthquakes in the 40 year period 1932-1972, or  $\sim$  one per 6 years, within 50 km of each seismic gap; there were  $\sim 4$  within 25 km, or one per 10 years. In contrast there was roughly one event per year with magnitude  $5 \leq M < 7$  within the same regions, which would result in too many 'false alarms' statewide if northern California is also considered.

The above example suggests that if no large ( $M \geq 7$ ) earthquake occurred along the seismic gaps #1 through 5 during the next 40 years the number of 'false alarms' for preplanned warnings could be one per 6 years versus one per year at a  $M \geq 6$ , or  $M \geq 5$  threshold. Conversely, if all gaps #1-5 should break in the next forty years, about 31% of the 6 mainshocks [i.e. two] might be preceded by  $M \geq 6$  'foreshocks', and perhaps two of the 7 expected earthquakes with  $6 \leq M < 7$  might be followed by mainshocks. If warnings were issued for each 'foreshock', then perhaps only 5 of them would be 'false alarms'. This ratio of 2 successful warnings per 6 false alarms per 40 years would seem to be quite reasonable in view of the potential benefits of the successful warnings. The time window can be selected at  $\leq 1$  day or  $\leq 5$  days, corresponding to  $\sim 40\%$  and  $60\%$  of the cases, respectively, for 'foreshocks' with  $M \geq 6$  (see Table 4), and according to budgetary and/or other constraints on public warnings, stages of alert, and readiness activities.

#### A Model for Preplanned, Real-Time Advisories for Damaging ( $M \geq 6$ ) Aftershocks Following Large ( $M \geq 7$ ) Earthquakes

The term 'aftershock' here means a secondary earthquake(s) that occur after a first [large] earthquake according to the most basic definition.

Large mainshocks [ $M \geq 7$ ] and damaging aftershocks [ $M \geq 6.0$ ] are

emphasized because a large mainshock can weaken structures which subsequently collapse in a damaging aftershock, causing as much damage as the mainshock itself. [In urban areas a moderate aftershock ( $5 < M < 6$ ) following a  $6 < M < 7$  mainshock can also be very dangerous, and are also discussed, further below.] We review data from existing catalogs to evaluate whether preplanned real-time warnings might be appropriate.

The time scale [ $\leq 1$  year] and distance criteria [ $\leq 125$  km in a structural association with the mainshock] to identify aftershocks were selected following a review of the actual case histories for large earthquakes in western north America (1857-1980) viewed in the context of public safety and planning needs.

Terms that describe subcategories of aftershocks, eg. doublets, multiplets, sympathetic rupture, triggered slip, conjugate faulting, complex rupture, etc., are often used by scientists, but are not necessary for the present purposes. However, when all of these subcategories are considered, the distance criterion of 125 km is not unreasonable, particularly in view of the fact that many of these phenomena are not well understood, nor even precisely defined. Aftershocks can continue for decades, but usually at smaller magnitudes than those considered here. In any case, such large late aftershocks require long-term planning, beyond the present scope of short term planning in this report.

We also note that the physical nature of aftershock processes, described statistically by Omori in 1894, still remains a complex problem of lively research; no simple physical model has yet been confirmed on a universal basis. Accordingly, we here attempt to compile information which is now known for Western North America and which is also relevant for public planning purposes.

Of the 20 large mainshocks ( $M \geq 7$ ) listed in Table 1, only 5 (25%) are reported as being followed by significant 'aftershocks' ( $M \geq 6$ ) within one year and 125 km distance of the epicenter (see Table 5). Of these, one 'aftershock' was within one minute [a 'doublet'] and two were 55 and 202 days following the mainshock. The two remaining cases are worthy of note. The 1952 Kern County mainshock was followed by 3 significant aftershocks: at 13 minutes, 1.5 days, and 8 days after the main event. The latter two aftershocks were ~50 and ~46 km from the mainshock and caused serious damage. In the final case, the 1872 mainshock produced significant aftershocks in 3 1/2 hours and also in 8 days at distances of ~25 km from the epicenter, and then again after 16 days, at a distance of ~98 km.

It appears that significant aftershocks are not very frequent, but the data for large mainshocks are few and some aftershocks in the pre-instrumental or early instrumental periods last century and around the turn of the century may not have been identified, and, again, it would not be prudent to follow a purely statistical approach. Viewed from a 'practical' perspective the data suggest the following. Time periods of 1 minute and 13 minutes are too short for public advisories; 55 and 202 days are

too long for a sustained advisory period. However, a public advisory that there is at least a 'slight' chance of a damaging aftershock at any time within the next 8 days [and within ~100 km of the epicenter] is recommended for safety, following a large ( $M \geq 7$ ) mainshock anywhere statewide. Situation monitoring by OES should continue for another 8 days. [These recommendations are based on the time and distance scales for the Kern County (1952) and Owens Valley (1872) mainshock-aftershock case histories.]

In the strictest sense, 2 of 20 large ( $M \geq 7$ ) mainshocks (10%) (see Tables 1 and 5) had aftershocks ( $M \geq 6$ ) in the time period 3 1/2 hours to 16 days, which corresponds to a probability range of 'slight'. For northern California, 5 out of 6 events were in the Mendocino to California/Oregon border region, and none had aftershocks  $M \geq 6$ . However, aftershocks could have occurred in the offshore region in 1873 and 1898 and gone unnoticed. Also, the remainder of the northern California region is represented by only one event, the 1906 earthquake, and statistics are not possible. It would seem prudent, therefore, to provide an advisory at the probability level of 'slight' for northern California.

In the southern California/Baja region, 3 of 9 (33%) of the large ( $M \geq 7$ ) mainshocks had aftershocks ( $M \geq 6$ ); [one was in the time period 3 1/2 hours to 16 days, but, again, the numbers are too small for meaningful statistics]. The Sierra/Nevada region is similar, i.e., 2 of 5 (40%), for the same magnitudes. These case histories suggest a probability level of 'moderate' for both regions. Two of the 5 mainshocks (40%) with magnitudes greater than 7.4 statewide had  $M \geq 6$  aftershocks. These two were in the southern California/Baja and Sierra/Nevada regions, and both were within the suggested time period. [In the southern California/Baja region one of the 2 (50%) mainshocks  $M > 7.4$  had  $M \geq 6$  aftershocks, and the same was true for the Sierra/Nevada region.]

We therefore, conclude that an advisory with the probability level of at least 'slight' is justified for the southern California/Baja and Sierra/Nevada regions following all mainshocks  $M \geq 7.0$ , and especially those  $M > 7.4$ .

It is worth mentioning that this review does not reveal significant differences in aftershock likelihood for mainshocks with dip-slip versus those with strike-slip fault mechanisms. In fact, within the same seismotectonic environment, 2 of 5 (40%) had significant aftershocks in the Imperial Valley/Baja region, and the same for the Nevada/Owens Valley region, with no correlation to the size of the mainshock. It thus appears that a greater understanding of the physical processes of large ( $M \geq 7$ ) mainshock-aftershock sequences is needed before further refinements are justified for public policy purposes. We also reiterate that some aftershock information could well be missing from existing catalogs and recommend that OES encourage further data investigations to be undertaken.

Urban Areas. (To be provided for review at CEPEC.)

Summary. We follow the above approach to recommend a preplanned real-time short term advisory scenario for southern and northern California (Figures 2 and 3). All earthquakes  $6 \leq M \leq 6.9$  in the 'advisory zones' for southern California (Figure 2) trigger an advisory pertaining to the seismic gaps indicated. All earthquakes  $5 \leq M \leq 6.9$  in the 'advisory zones' for northern California trigger an advisory for the seismic gaps indicated in Figure 3. Based on the historic seismicity ( $6 < M < 6.9$ ) from 1932-6/30/1988 in the southern California advisory zones, the average 'false alarm' rate will be one per 6.4 years if no mainshock occurs. The historic seismicity ( $5 \leq M \leq 6.9$ ) from 1910-1987 in the northern California advisory zones suggests an average 'false alarm' rate of one per 6.0 years, if there is no mainshock. The combined statewide rate thus averages one per 3 years. However, if [for example] three large mainshocks occur in the next 20 years, and as many as ~30-45% are preceded by foreshocks, there might be one successful advisory per 5.5 false alarms. The advisories should trigger a preplanned (short-term) "response" lasting 1-5 days. Note that, in the absence of any further information, ~ 69% of the 5 mainshocks [i.e. 3.5] are expected with no prior activity  $M \geq 6.0$ .

Important research at hand is to discriminate which seismic gap is more likely to break when a [possible] foreshock occurs. Studies of stress distributions and real-time, accurate fault mechanisms are needed. A serious scientific problem to be solved is that of inconsistent reportings of magnitudes for felt earthquakes. Recently an earthquake was reported simultaneously as being  $M=5$  and  $M=5.7$  by two eminent institutions. Subsequently a complaint was filed with state offices and at a statewide meeting. This problem may be solved by 'legislating' that one (and only one) magnitude will be issued by designated institutions unless scientists can resolve their differences. If this occurs, seismologists will have lost an important opportunity to obtain public encouragement for research to discover the nature of wave propagation through heterogeneous media, utilizing a new generation of high quality seismic data.

The suggested new CEPEC/OES procedures, if adopted, should be explained to the scientific community [e.g., via scientific publication] to avoid a confusing situation. A serious policy problem can arise if scientific experts state to the media that they are "pessimistic about whether earthquakes can ever be predicted" because they are confused. Furthermore, procedures for handling the response to public inquiries following the issuance of an advisory should be preplanned and coordinated with scientists in the state, as well as with local jurisdictions. Many scientists and different institutions are certain to be contacted for information, despite published 'instructions' to the contrary, at least initially. [For example, OES brochures which direct the public to a centralized real-time information line might be distributed to scientists].

Finally, and of utmost importance, OES should encourage the development of a complete, systematic, and reliable database of earthquake information for the state of California. This database should utilize present technology for rapid accessibility as earthquakes occur. OES and CEPEC should maintain an up-to-date list of knowledgeable scientists whose input might be a resource to CEPEC. (Final decisions and discussions should continue to be among CEPEC members, however, in order to avoid inconsistent judgements and advice to OES.)

The present approach of preplanned advisories should not replace scientific deliberations by CEPEC, but rather, should complement CEPEC by allowing OES to begin activities immediately. CEPEC could conclude, for example, that the advisory probability level should be 'moderate' or 'high', rather than 'slight', if further information is available. The present 'advisory' approach can be refined as further information or research developments are confirmed in the future.

Recommendations for other topics to be considered by CEPEC. Research results suggest that real-time monitoring and analysis of seismic data on sustained, intermediate term time scales (few weeks to few years) can significantly increase the reliability for short term advisories. We find evidence that at least 6 seismic phenomena may exhibit changes within approximately 2-4 years before large mainshocks (Figure 6). These are: (1) seismicity below locked zones; (2) swarms at edges of locked zones; (3) seismic quiescence within locked zones; (4) stress induced changes in earthquake fault mechanisms around edges of locked zones; (5) attenuation change within locked zones; (6) resumption of seismicity within quiescent zones. Several of these phenomena begin changing prior to the 2-4 year time window before mainshocks; the combination, however, increases the 'signal-to-noise' ratio, for greater reliability of the final predictions. A real-time seismograph monitoring system for California predictions should thus have a wide dynamic range (for monitoring earthquakes from M=2.5 to 8.0) as well as a broad band frequency response.

The success of this joint government and scientific effort will depend critically on the quality of seismographic instruments and a real-time analysis capability statewide. Consistent magnitudes and accurate earthquake locations in real time are crucial. A recent test of this system occurred on June 27, 1988, with a M=5 earthquake in Northern California.

## General References

- Bolt, B. and R. Miller, 1975. Catalog of Earthquakes in Northern California and Adjoining Areas, 1 January 1910 - 31 December 1972, Seismographic Stations, University of California, Berkeley.
- Hileman, J.A., Allen, C.R., and J.M. Nordquist, 1973. Seismicity of the Southern California Region 1 January 1932 to 31 December 1972, Seismological Laboratory, California Institute of Technology, Pasadena, CA.
- Lachenbruch A., and J. Sass, 1973, Thermo-mechanical aspects of the San Andreas fault system, in Proc. of Conf. on Tectonic Problems of the San Andreas Fault System, Stanford Univ., Stanford, CA, pp. 192-205.
- Lind, A., Open File Report 83-0063.
- NEPEC, 1987, Internal Report
- Richter, C.F., 1958, Elementary Seismology, W.H. Freeman, San Francisco, CA.
- Shimazaki, K., 1986, Small and large earthquakes: The effects of the thickness of seismogenic layer and the free surface, in Maurice Ewing v. 6, AGU, Wash. D.C., pp. 209-216.
- Sieh, K., 1978, Central California foreshocks of the great 1857 earthquake, Bull. Seism. Soc. Am., V68, pp. 1731-1749.
- Topozada, T., Parke, D., and C. Higgins, 1978. Seismicity of California 1900-1931, Special report 135, Calif. Div. of Mines & Geol., Sacramento, CA., 39 pp.
- Topozada, T., Real, C., Bezore, S. and D. Parke, 1979. Compilation of pre-1900 California Earthquake History, Open-File Report OFR 79-6SAC, Calif. Div. Mines & Geol., Sacramento, CA, 271 pp.
- U.S. Geological Survey, Denver, CO
- The Working Group on California Earthquake Probabilities, 1988, Probabilities of large earthquakes occurring in California on the San Andreas Fault, Open File Rpt., 88-398, USGS, Menlo Park, CA, 62 pp.
- Wallace, R.E., 1978, Patterns of Faulting and Seismic Gaps in the Great Basin Province, USGS Conf. VI, Methodology for Identifying Seismic Gaps and Soon-to-Break Gaps, Open File Report 78-943, Menlo Park, CA, pp. 857-868.

Wallace, R.E., J.F. Davis and K.C. McNally, 1984, Terms for expressing earthquake potential, prediction and probability, Seismol. Soc. Am. Bull., v. 74, n. 5, p. 1819-1827.

Wesnousky, 1986, Earthquakes, Quaternary Faults, and Seismic Hazard in California, Journal of Geophysical Research, v. 91, N.B12, pp. 12,587-12,632.

Wesson, R. and Wallace, R.E., 1985, Predicting the Next Great Earthquake in California., Sci. Amer. v 252 N.Z., pp. 35-43.

**MADE FROM BEST  
AVAILABLE COPY**

**SEISMIC GAPS WITH SIGNIFICANT POTENTIAL  
FOR  $M > 7$  EOS AND POPULATION HAZARD**

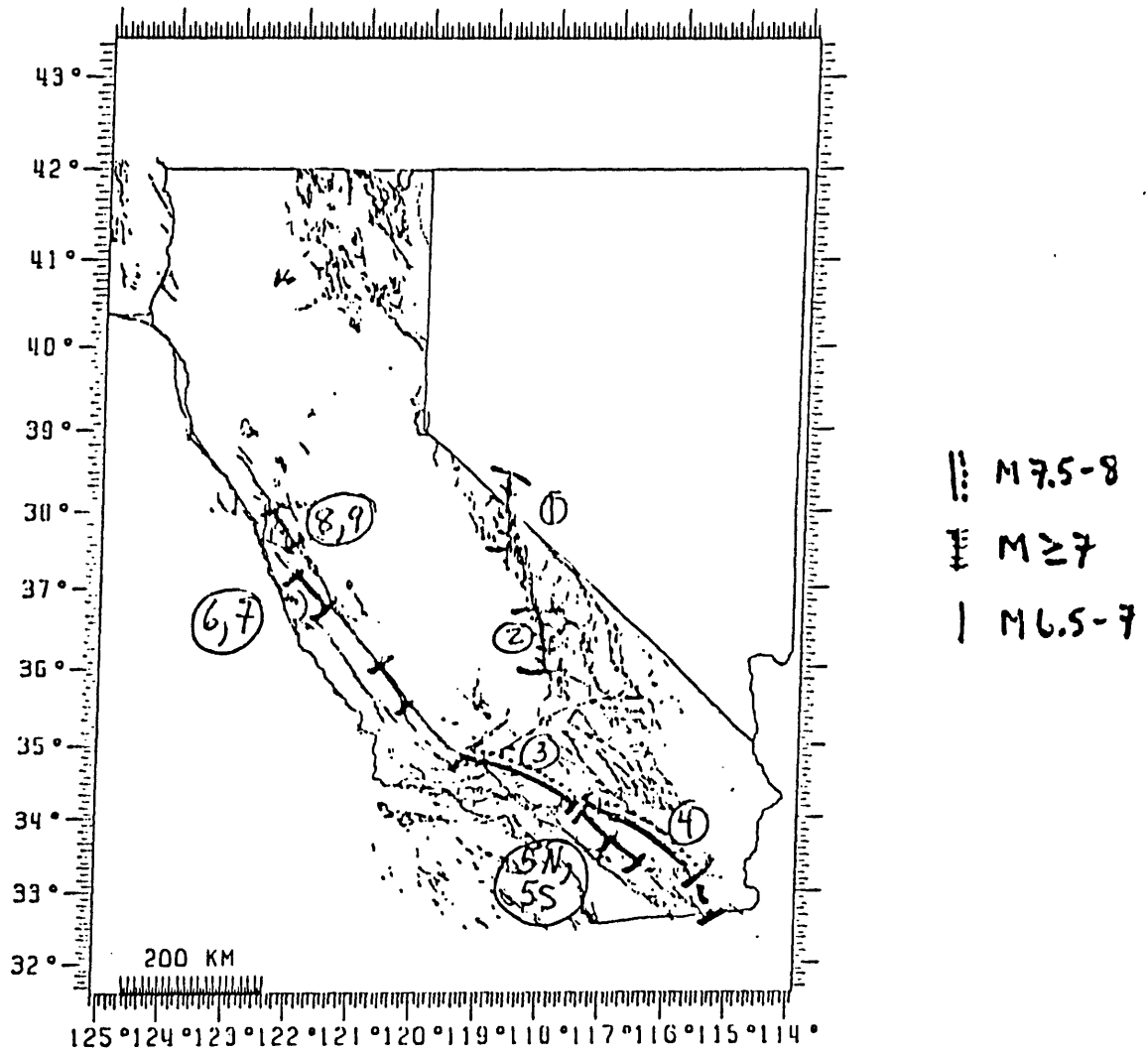


Figure 1

**MADE FROM BEST  
AVAILABLE COPY**

**SEISMIC GAPS WITH SIGNIFICANT POTENTIAL  
FOR  $M > 7$  EOS AND POPULATION HAZARD**

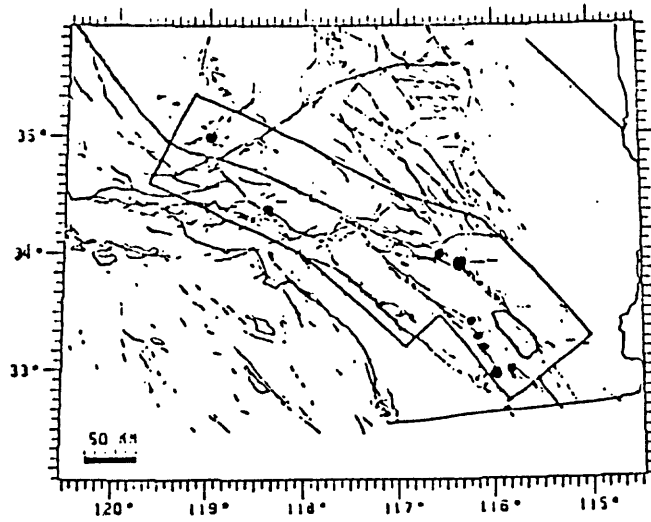
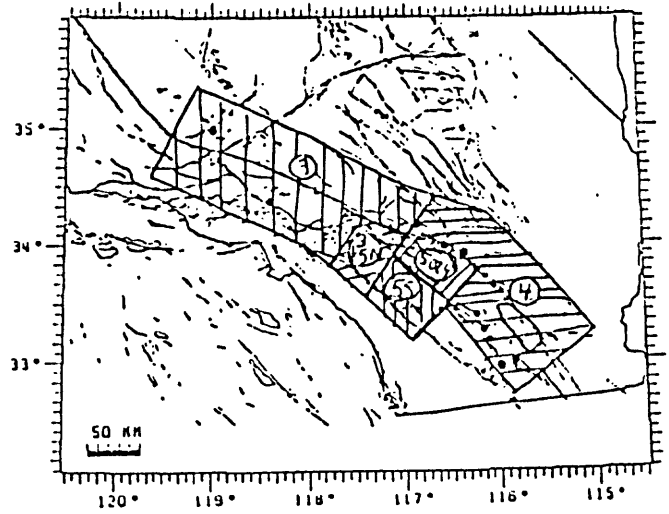
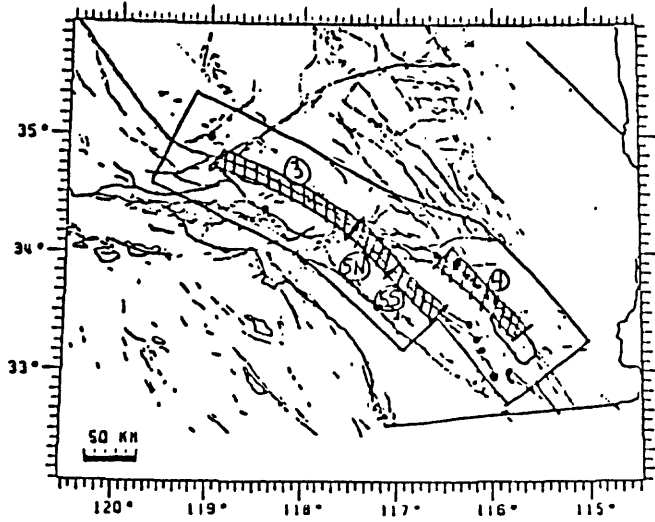


Figure 2

**MADE FROM BEST  
AVAILABLE COPY**

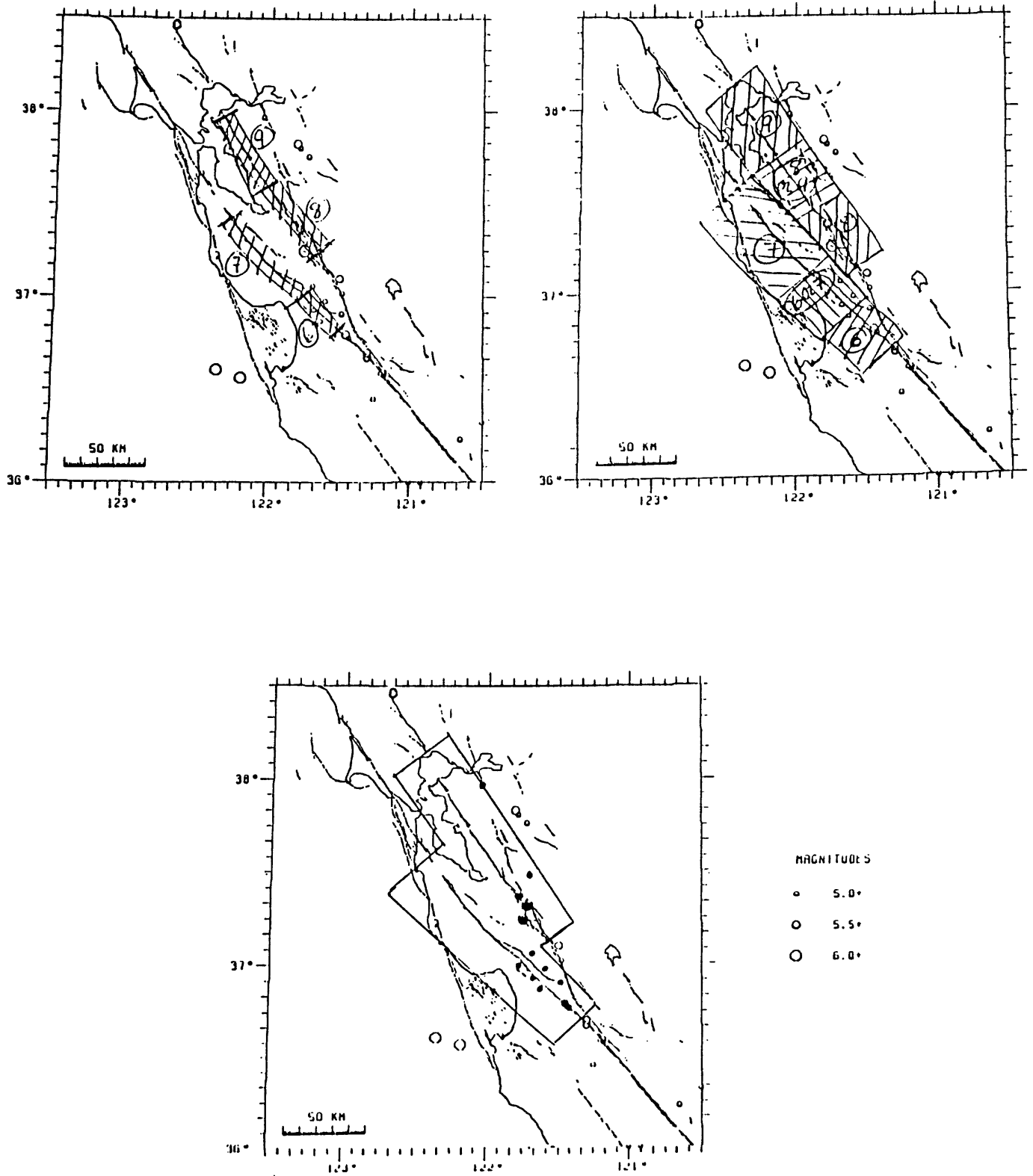


Figure 3

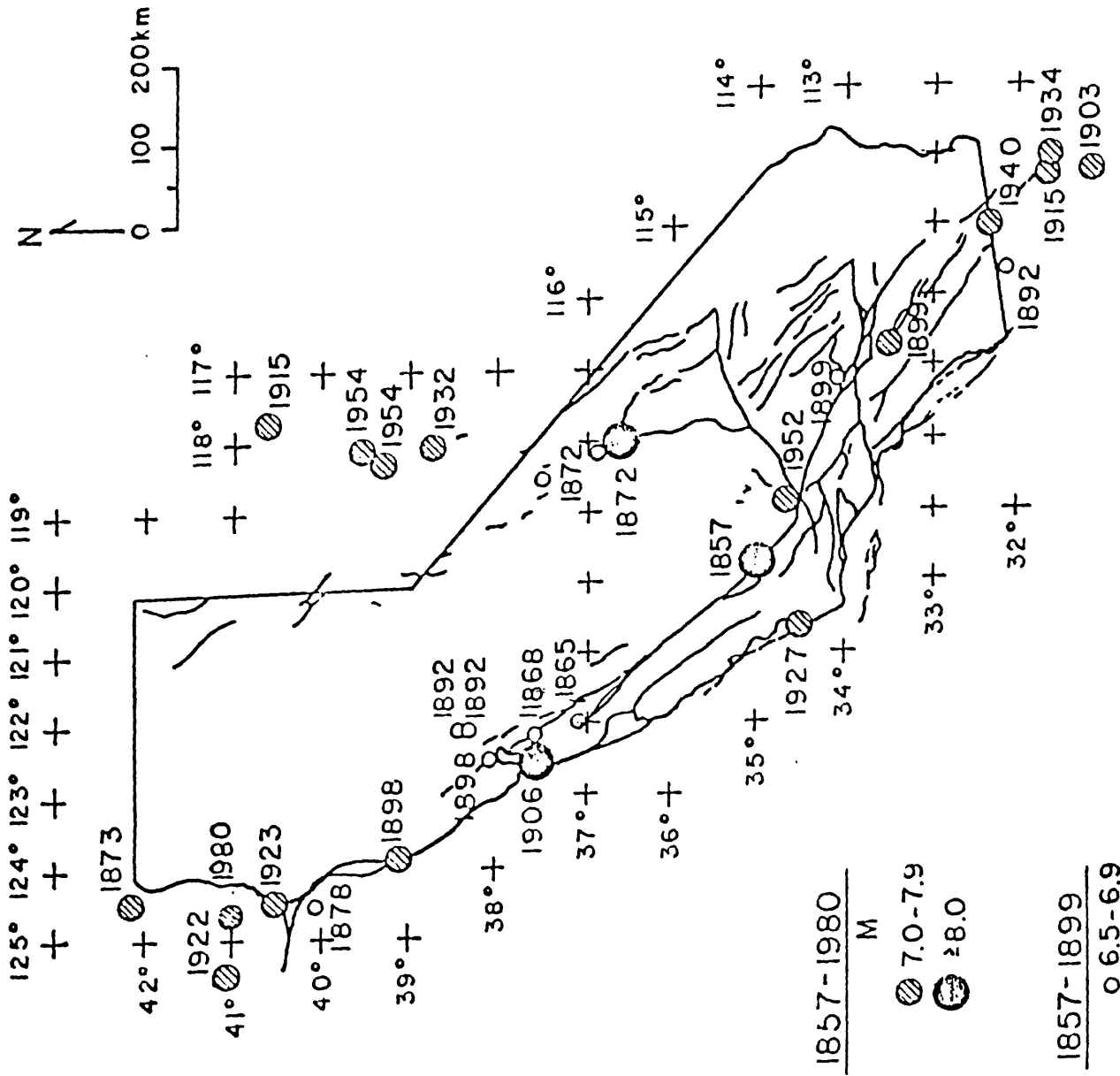


Figure 4

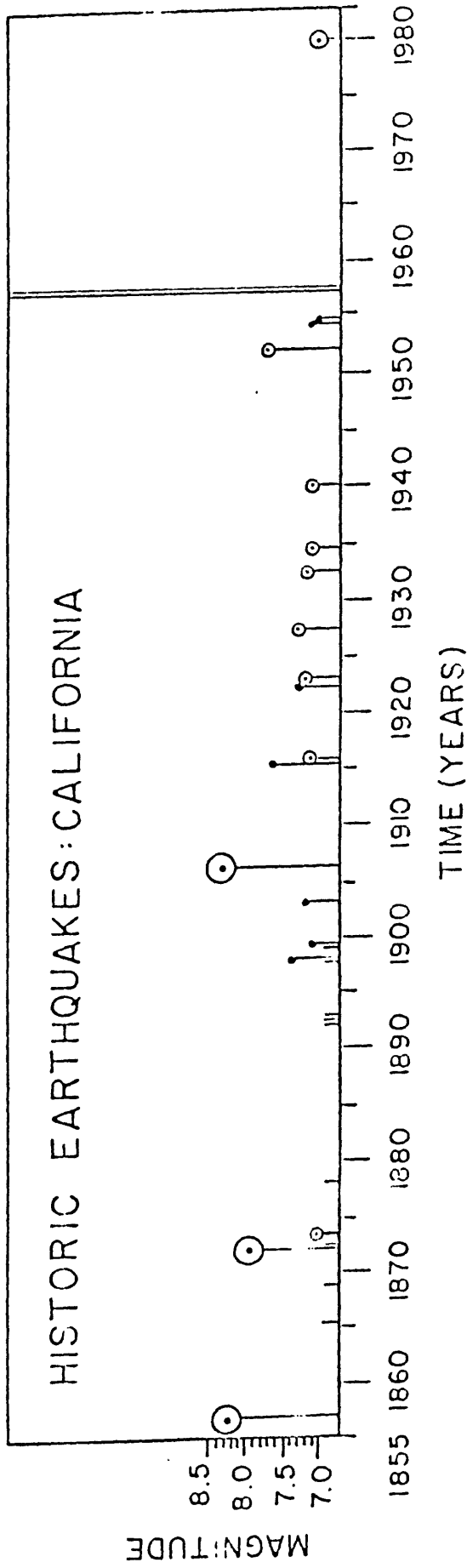


Figure 5

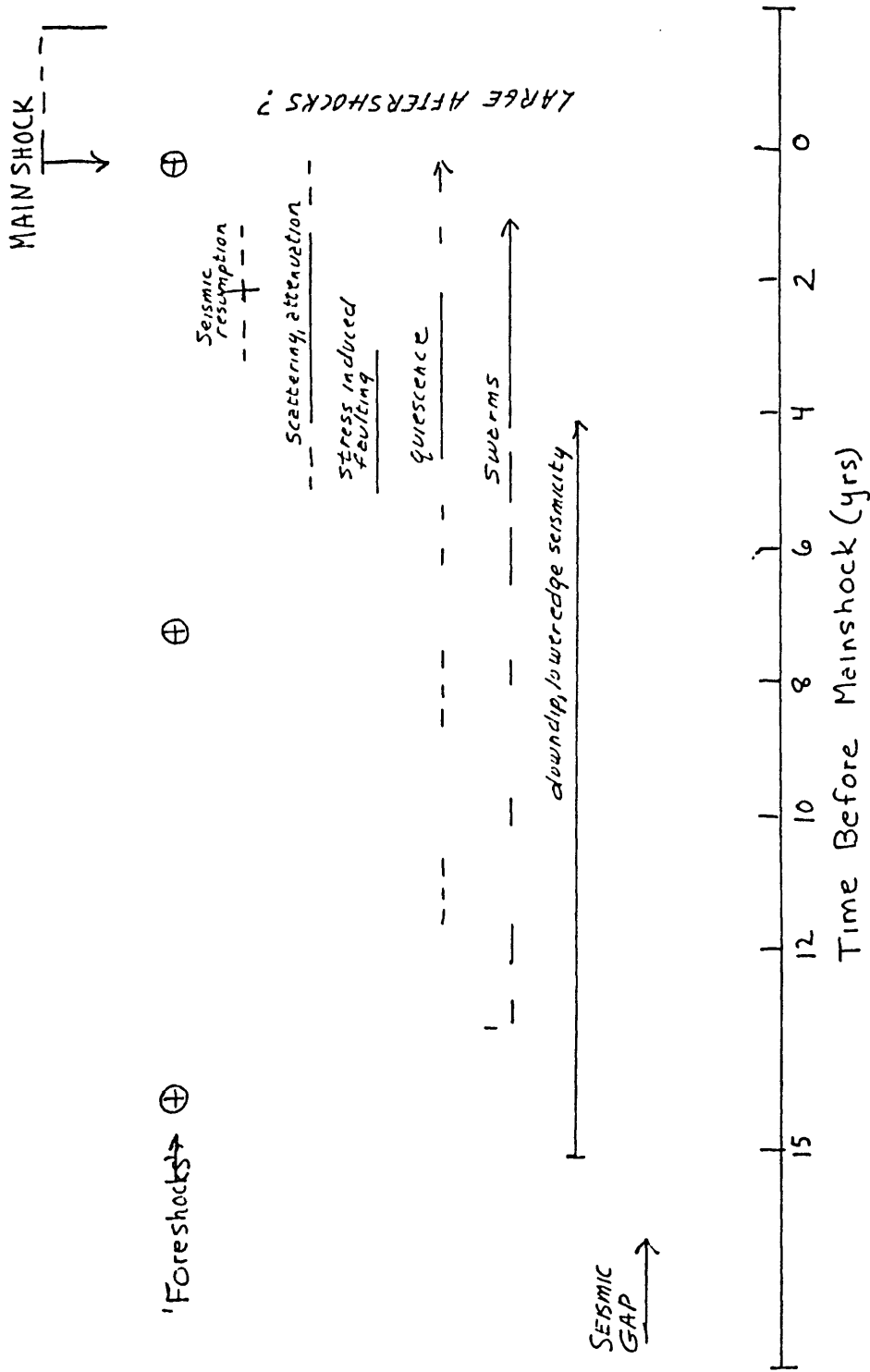


Figure 6

TABLE 1. EARTHQUAKES IN (AND AROUND) CALIFORNIA WITH MAGNITUDE LARGER THAN 7.0, 1/1857 - 7/1980

| REF  | DATE        | TIME<br>GMT | LOCATION |           | Mag. Ref.          | COMMENTS                      |
|--|-------------|-------------|----------|-----------|--------------------|-------------------------------|
|  |             |             | lat ( N) | long ( W) |                    |                               |
| 1  | 09 Jan 1857 | 16:00       | 35.3     | 119.8     | 8 1/4 <sup>2</sup> | Ft. Tejon, CA                 |
| 1  | 26 Mar 1872 | 10:30       | 36.7     | 118.1     | 8.0+               | Owens Valley, CA              |
| 1  | 23 Nov 1873 | 05:00       | 42.0     | 124.2     | 7.0+               | Offshore, CA-OR border        |
| 1  | 24 Feb 1892 | 07:20       | 32.6     | 116.3     | 6.9+               | Baja, CA                      |
| 1  | 15 Apr 1898 | 07:07       | 39.2     | 123.8     | 7.4 *3(6.7+)       | Offshore Mendocino County, CA |
| 1  | 25 Dec 1899 | 12:25       | 33.8     | 117.0     | 7.1 *3(6.7+)       | San Jacinto, CA               |
| 3  | 24 Jan 1903 | 05:5        | 31.5     | 115.0     | 7.2 *3             | Lower California              |
| 4,5,6  | 18 Apr 1906 | 13:12:21    | 37.7     | 122.5     | 8.3 *7             | San Francisco, CA             |
| 8  | 03 Oct 1915 | 06:52.8     | 40.5     | 117.5     | 7.7 *7             | Pleasant Valley, NV           |
| 4,5,9  | 21 Nov 1915 | 00:13:42    | 32.0     | 115.0     | 7.1 *9             | Baja, CA                      |
| 10   | 31 Jan 1922 | 13:17:22    | 41.0     | 125.5     | 7.3 *9             | West of Eureka, CA            |
| 4,5  | 22 Jan 1923 | 09:04:18    | 40.5     | 124.5     | 7.2 *9             | Off Cape Mendocino, CA        |
| 4,5  | 04 Nov 1927 | 13:50:53    | 34.9     | 120.7     | 7.3 *9             | Off Point Arguello, CA        |
| 4,8  | 21 Dec 1932 | 06:10:05    | 38.8     | 118.0     | 7.2 *9             | Cedar Mtn., NV                |
| 4,9,10   | 31 Dec 1934 | 18:45:45    | 32.0     | 114.75    | 7.1 *9             | Baja, CA                      |
| 10   | 19 May 1940 | 04:36:40.9  | 32.73    | 115.5     | 7.1 *11(6.7 4,10)  | Imperial Valley               |
| 4,9,10   | 21 Jul 1952 | 11:52:14    | 35.0     | 119.02    | 7.7 *9             | Kern County, CA               |
| 12   | 16 Dec 1954 | 11:07:13    | 39.32    | 118.20    | 7.2 <sup>12</sup>  | Fairview Peak, NV             |
| 12   | 16 Dec 1954 | 11:11:29    | 39.50    | 118.00    | 7.1 <sup>12</sup>  | Dixie, NV                     |
| 13   | 08 Nov 1980 | 10:27:33    | 41.01    | 124.64    | 7.0 <sup>14</sup>  | Offshore Eureka               |
| EARTHQUAKES WITH MAGNITUDE POSSIBLY AS LARGE AS 7, 1857-1899 |             |             |          |           |                    |                               |
| 1  | 08 Oct 1865 | 20:46       | 37.2     | 121.9     | 6.5+               | Santa Cruz, CA                |
| 1  | 21 Oct 1868 | 15:53       | 37.7     | 122.1     | 6.8+               | Hayward, CA                   |
| 1  | 26 Mar 1872 | 14:06       | 36.9     | 118.2     | 6.7+               | Owens Valley, CA aftershock   |
| 1  | 03 Apr 1872 | 12:15       | 36.9     | 118.2     | 6.6+               | Owens Valley, CA aftershock   |
| 1  | 11 Apr 1872 | 19:00       | 37.5     | 118.5     | 6.9+               | Owens Valley, CA aftershock   |
| 1  | 09 May 1878 | 04:25       | 40.0     | 124.5     | 6.5+               | Cape Mendocino, CA            |
| 1  | 19 Apr 1892 | 10:50       | 38.5     | 122.0     | 6.8+               | Vacaville, CA                 |
| 1  | 21 Apr 1892 | 17:43       | 38.6     | 121.9     | 6.5+               | Winters, CA                   |
| 1  | 31 Mar 1898 | 07:43       | 38.2     | 122.4     | 6.5+               | Mare Island, CA               |
| 1  | 22 Jul 1899 | 20:32       | 34.3     | 117.4     | 6.5+               | Lytle Creek, CA               |
| 5  | 21 Jul 1918 | 22:32       | 33.8     | 117.0     | 6.8+               | San Jacinto and Hemet         |

Magnitude based on geologic data + Magnitude based on intensity

\* M<sub>s</sub>

## Table 1 - References

1. Topozada, T., Real, C., Bezore, S. and D. Parke, 1979. Compilation of pre-1900 California Earthquake History, Open-File Report OFR 79-6SAC, Calif. Div. Mines & Geol., Sacramento, Ca., 271 pp.
2. Sieh, K., 1978. Slip along the San Andreas fault associated with the great 1857 earthquake, Bull. Seism. Soc. Am., v. 68, n. 5, pp. 1421-1448.
3. Kanamori, H. and Abe, K., 1979. Reevaluation of the turn-of-the-century seismicity peak, J. Geophys. Res., 84, pp. 6131-6139.
4. Real, C. and Topozada, T., 1978. Earthquake Catalog of California, January 1, 1900-December 31, 1974, Special Publication 52, Calif. Div. Mines and Geol., Sacramento, CA, 15 pp.
5. Topozada, T., Parke, D., and C. Higgins, 1978. Seismicity of California 1900-1931, Special Report 135, Calif. Div. of Mines & Geol., Sacramento, Ca., 39 pp.
6. Bolt, B.A., 1968. The focus of the 1906 California earthquake Bull. Seism. Soc. Am., v. 58, pp. 457-472.
7. Geller, R., and H. Kanamori, 1977. Magnitudes of great shallow earthquakes from 1904 to 1952, Bull. Seism. Soc. Am., v. 67, n. 3 pp. 587-598.
8. Slemmons, D., Gimlett, J., Jones, A., Greensfelder, R. and J. Koenig, 1965. Earthquake Epicenter Map of Nevada, Map 29, Nevada Bureau of Mines, Nevada.
9. Gutenberg, B. and C.F. Richter, 1954. Seismicity of the Earth and Associated Phenomena, 2nd ed., Princeton Univ. Press, Princeton, 310 pp.
10. Hileman, J.A., Allen, C.R., and J.M. Nordquist 1973. Seismicity of the Southern California Region 1 January 1932 to 31 December 1972, Seismological Laboratory, California Institute of Technology, Pasadena, CA.
11. Kanamori, H., and P. Jennings, 1978. Determination of local magnitude, M, from strong-motion accelerograms, Bull. Seism. Soc. Am., v. 68, n. 2, pp. 471-485.
12. Bolt, B. and R. Miller, 1975. Catalog of Earthquakes in Northern California and Adjoining Areas, 1 January 1910-31 December 1972, Seismographic Stations, University of California, Berkeley.

13. McKenzie, M.R., Miller, R.D. and R.A. Uhrhammer, 1982. Earthquakes and the Registration of Earthquakes from July 1, 1980 to December 31, 1980, V. 50, N. 2, pp. 88-156, Seismographic Station, University of California, Berkeley.
14. Earthquake Data Report, U.S. Dept. Interior, Geological Survey.

## Table 2

### MAINSHOCKS, YEAR AND PRIOR ACTIVITY

#### M-8

1857 as shown, Table 3  
1872 as shown, Table 3  
1906 no significant prior activity reported

#### M > 7 ( $\pm 0.5$ )

1873 no significant prior activity reported  
1892 no significant prior activity reported  
1898 no significant prior activity reported  
1899 as shown, Table 3  
1915 as shown (Nevada), Table 3  
1922 as shown, Table 3  
1923 no significant prior activity reported  
1927 no significant prior activity reported  
1932 no significant prior activity reported  
1934 as shown, Table 3  
1940 no significant prior activity reported  
1952 as shown, Table 3  
1954 'doublet'; M = 7.2 and 7.1; 4 min. apart; distance ( $\Delta$ ) -20 km  
1954 as shown, Table 3:

(Not reviewed: 1903, 1915 Baja, 1980)



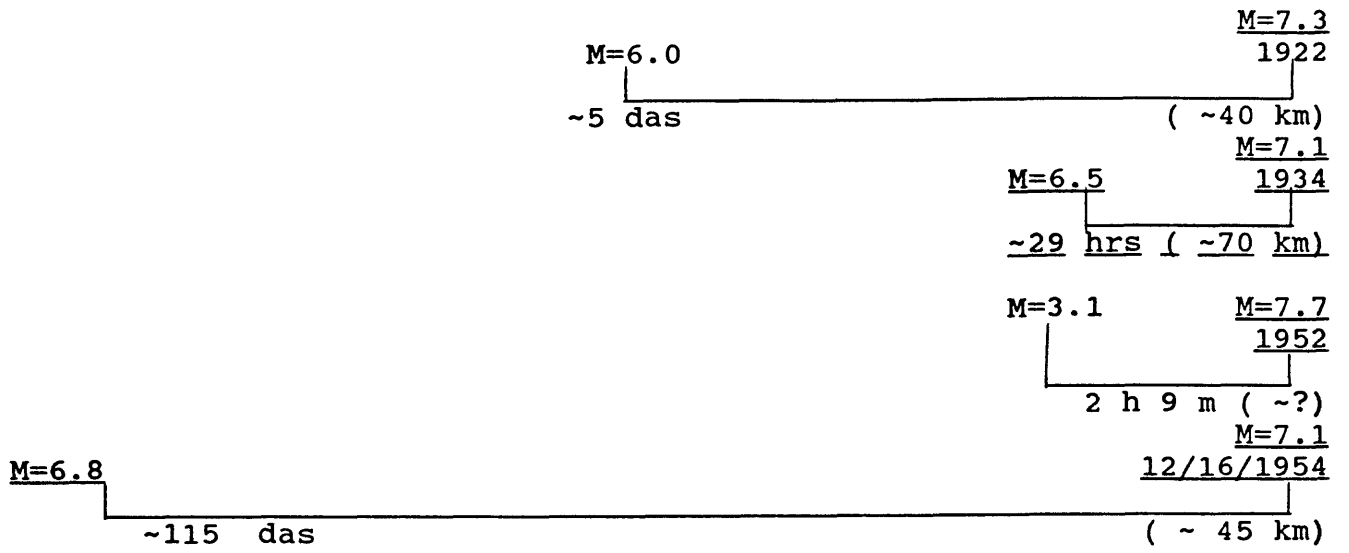


**Table 4**

| PRIOR<br>EVENT                                | LARGER<br>EARTHQUAKES | DISTANCE<br>$\Delta$ | TIME<br>$\Delta t$      | YEAR                                      |
|---|-----------------------|----------------------|-------------------------|---|
| M 6-7   | M > 7+.5              | (20-70 km)           | (~1 da -<br>9 mos)      |   |
| 5-6   | 8                     | ~30 km (?)           | 7 hrs                   | 1857                                      |
| 6.5   | 7.1                   | ~70                  | 1 da                    | 1934 Baja                                 |
| 6.0   | 7.3                   | ~40                  | 5 da                    | 1922                                      |
| 6.6, 6.4                                      | 6.8                   | ~20                  | 48 da                   | 1954                                      |
| 6.8   | 7.1                   | ~45                  | 115 da                  | 1954                                      |
| -----   |                       |                      |                         |   |
| M 5-6   | M > 7+.5              |                      |                         |   |
| 5.5   | 6.5                   | < 20 (?)             | 52 min                  | 1934 Nevada,<br>UCB loc.,<br>Richter Mag. |
| 5-6   | 8                     | ~40-50               | < 7 hrs<br>(2-3 events) | 1857                                      |
| 'large'                                       | 7.6                   | ?                    | 7 hrs 14 m(2)           | 1915                                      |
| 5.8   | 7.1                   | ~50                  | 5 mos 3 da              | 1899                                      |
| 5.2   | 8                     | 22                   | 9 mos (9 da?)           | 1872                                      |
| -----   |                       |                      |                         |   |
| SUMMARY                                       | KM:N                  |                      | t:N                     |   |
| (N=number<br>of cases,<br>prior event<br>≥ 6) | ≤ 25: 30%             |                      | ≤ 1 da: 40%             |   |
|   | ≤ 50: 80%             |                      | ≤ 5 da: 60%             |   |
|   | ≤ 70: 100%            |                      | ≤ 9 mos: 100%           |   |
| -----   |                       |                      |                         |   |
| (N=number<br>of cases,<br>prior event<br>≥ 5) | ≤ 25: 30%             |                      | ≤ 1 da: 50%             |   |
|   | ≤ 50: 89%             |                      | ≤ 5 da: 60%             |   |
|   | ≤ 70: 100%            |                      | ≤ 9 mos: 100%           |   |

Table 5

'Aftershocks' ( $M \geq 6$ )Mainshocks ( $M \geq 7$ )

| Date        | Location<br>lat<br>(N) | Location<br>long<br>(W) | Mag | Date                     | Location<br>lat<br>(N) | Location<br>long<br>(W) | Mag | $\Delta t$<br>( $\leq 1$ yr<br>from main) | $\Delta$<br>( $< 125$ km) |
|-------------|------------------------|-------------------------|-----|--------------------------|------------------------|-------------------------|-----|---|---------------------------|
| 26 Mar 1872 | 36.7                   | 118.1                   | 8.0 | 26 Mar 1872              | 36.9                   | 118.2                   | 6.7 | <u>-3 1/2 hrs</u>                         | <u>-25</u>                |
|             |                        |                         |     | 03 Apr 1872              | 36.9                   | 118.2                   | 6.9 | <u>-8 das</u>                             | <u>-25</u>                |
|             |                        |                         |     | 11 Apr 1872              | 37.5                   | 118.5                   | 6.6 | <u>-16 das</u>                            | <u>-98</u>                |
| 31 Dec 1934 | 32.0                   | 114.75                  | 7.1 | 24 Feb 1935              | 31.98                  | 115.2                   | 6.0 | (55 das)                                  | -50                       |
| 19 May 1940 | 32.73                  | 115.5                   | 7.1 | 07 Dec 1940              | 31.67                  | 115.08                  | 6.0 | (202 das)                                 | -125                      |
| 21 Jul 1952 | 35.0                   | 119.02                  | 7.7 | 21 Jul 1952              | 35.0                   | 119.02                  | 6.4 | (13 min)                                  | 0                         |
|             |                        |                         |     | 23 Jul 1952              | 35.37                  | 118.58                  | 6.1 | <u>-1.5 das</u>                           | <u>-50</u>                |
|             |                        |                         |     | 29 Jul 1952              | 35.38                  | 118.85                  | 6.1 | <u>8 das</u>                              | <u>-46</u>                |
| 16 Dec 1954 | 39.32                  | 118.20                  | 7.2 | 16 Dec 1954<br>(doublet) | 39.50                  | 118.00                  | 7.1 | (1 min)                                   | -70                       |

# **EARTHQUAKE FAULT SLIP ESTIMATION FROM GEOLOGIC, GEODETIC AND SEISMOLOGIC OBSERVATIONS: IMPLICATIONS FOR EARTHQUAKE MECHANICS AND PREDICTION RESEARCH**

by

Wayne Thatcher and Manuel G. Bonilla

U.S. Geological Survey, Menlo Park, CA 94025

The spatial distribution of coseismic fault slip provides clues to the mechanics of earthquake strain release and sheds light on the nature and importance of fault segmentation in controlling the strain release process. Although the true slip distribution is not accessible to direct observation, several methods can be applied to recover informative features of its spatial pattern. Figure 1 illustrates this schematically, showing how geologic, geodetic, and seismologic observations sample different aspects of the coseismic slip distribution. Each approach produces a pattern of slip that is in varying degrees a filtered and biased version of the true slip, and the advantages and limitations of each method thus deserve careful attention in examining the results that follow.

When sufficiently numerous, fault slip (geologic) data can provide a very detailed picture of surface slip distribution along the fault rupture (figure 1, top). However, this pattern is seldom wholly representative of the slippage on the fault at seismogenic depths and even surface values will be biased where the fault zone is complex or coseismic deformation is distributed over a zone wider than that spanned by an offset feature.

Geodetic slip estimates are usually free of these shortcomings but are at best a rather coarse spatial averaging of fault slip in the zone of principal strain release (figure 1, middle). Furthermore, geodetic estimates are subject to the usual vagaries of network distribution relative to the coseismic rupture and this factor, along with measurement uncertainty, limits the precision and spatial resolution of derived slip estimates.

Seismic measurements of sufficient number and quality can in principle supply details of two dimensional slip distribution not provided by either geologic or geodetic methods. However, even for earthquakes with both near-source and distant seismic recordings from a range of source-receiver azimuths there is as yet a significant degree of nonuniqueness in the derived slip estimates. In the more common condition of less-than-complete observations, only large-scale features of the pattern of seismic moment release on the rupture plane are reliably obtained (figure 1, bottom).

The purpose of this paper is to examine case histories of earthquakes for which seismic slip has been estimated by one or more of the methods illustrated in figure 1 and to extract any significant generalizations that are indicated by these results.

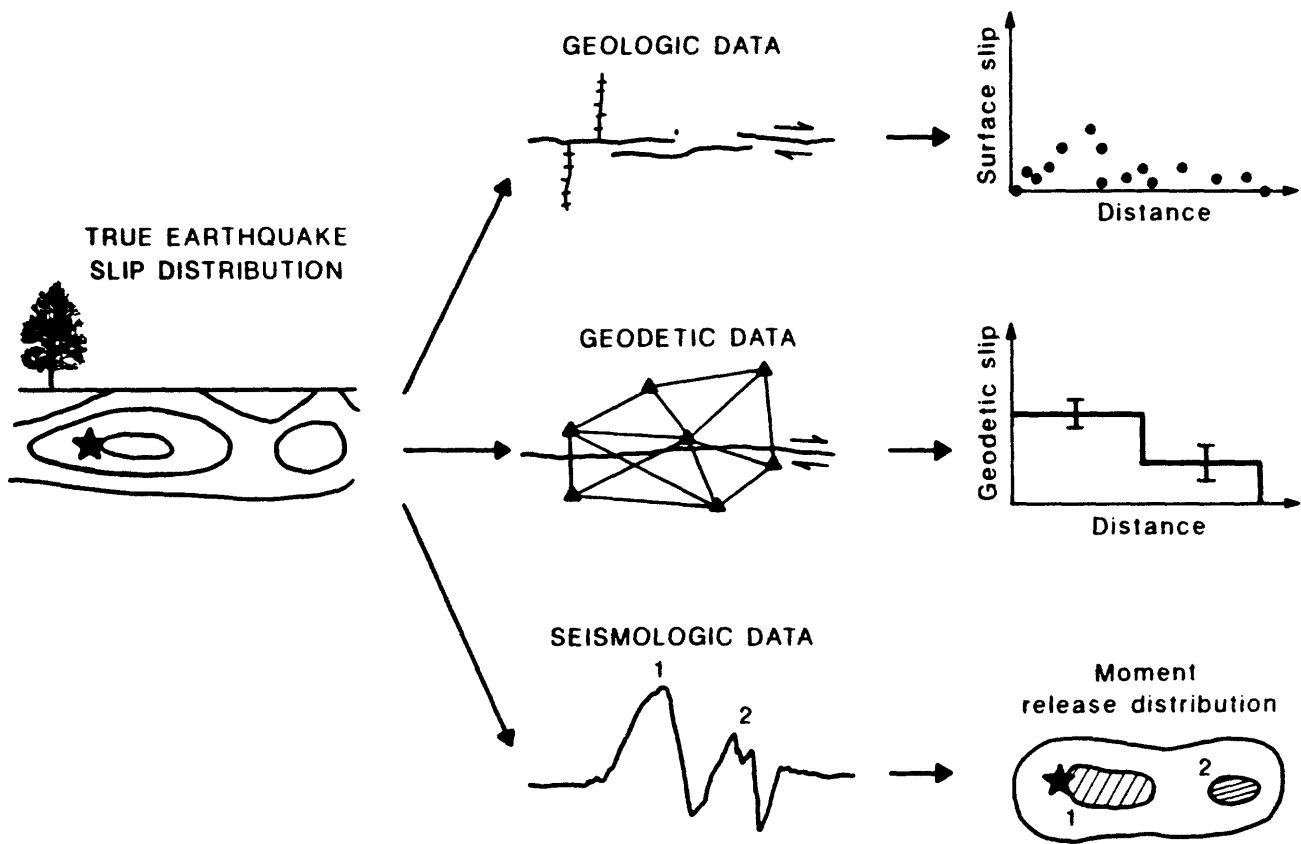


**FIGURE 1.** Three methods of earthquake slip estimation. True slip distribution is shown on cross-section at left. Geologic observations of offset features at the fault trace (center frame, top) provide information for plotting surface slip versus distance along fault (top right). Repeat geodetic measurements of angles, baseline lengths, or elevation changes for networks located near surface rupture (center frame, middle) provide data from which average fault slip at seismogenic depths can be estimated for various segments of fault and plotted versus distance along the fault (middle right, straight lines with error bars on each determination). Seismograms (center frame, bottom) can be analyzed to locate regions of concentrated seismic moment release; frame at bottom right schematically shows aftershock zone, with two regions of high moment release determined from seismograms and indicated by diagonal ruling within aftershock zone.

## GEOLOGIC DATA

To date we have examined surface slip and faulting patterns for 22 earthquakes from active regions around the world. The events range from  $M_w$  6.0 to 8.1 and have fault lengths from 15 km to 460 km. Fifteen of the shocks show predominantly strike-slip faulting and the remaining events have either normal or reverse slip. Representative features are summarized in figures 2, 3, and 4. Each figure has the same format, showing surface slip plotted against distance along the fault. A map view of the surface rupture is plotted at the same scale as the graph, a star locates the mainshock epicenter, and the geodetic slip estimates (when available) are indicated by straight lines with one standard deviation error bars.

Whenever surface slip determinations are sufficiently closely spaced we have observed considerable irregularity in slip magnitude over distances of a few kilometers or less. Occasionally these variations are systematic, pointing to a single cause such as local fault geometry. More commonly the origin of these local variations is unknown. Where observations are numerous such short wavelength fluctuations in surface slip can, for this study, be identified as noise and discarded. However, where data distribution is sparse, unrepresentative sampling of this local noise can introduce significant bias into the long wavelength variations in surface slip that are the main focus of this study.

For those cases in which such aliasing is not a problem and where fault zone complexity introduces no additional biases, the surface slip data for many earthquakes we have examined show notable variations over length scales of  $\sim 10$  km and greater. Figures 2, 3, and 4 illustrate this, showing that surface slip profiles are typically highly irregular and bear little resemblance to the smooth elliptical slip distributions predicted by models of uniform stress release across planar cracks that are occasionally still used to represent seismic faulting. Often, as for the 1940 El Centro and 1968 Dasht-e Bayaz earthquakes (see figures 3 and 4), this irregularity is characterized by regions of locally high slip on a rupture that otherwise shows considerably smaller slip amplitudes. We have found no simple relation between the locations of these high slip regions and fault geometry. For example, note the linearity and relative simplicity of the Imperial fault in the region where 1940 surface slip increases to more than 6 meters (figure 3). Similar features are documented for the 1976 Guatemala earthquake [Bucknam *et al.*, 1978] and for the great California earthquakes of 1857 and 1906 [Sieh, 1978; Lawson, 1908].

Surface slip profiles often reveal the effects of fault segmentation, with the magnitude of slip being a maximum near the center of each segment and dying off towards both ends. This feature is illustrated well by the 1968 Borrego Mountain earthquake (figure 2) and is also seen in the offset profiles for the 1915 Pleasant Valley (Nevada) and 1891 Mino-Owari (Japan) earthquakes [Wallace, 1984; Matsuda, 1974]. For those earthquakes that involve failure of only one or a few identifiable segments the surface slip patterns are sometimes simpler than those shown for the majority of the larger events. For example, the 1968 Meckering and 1987 Superstition Hills earthquakes [Gordon and Lewis, 1980; P. Williams and H. Magistrale, unpublished manuscript 1988] have surface slip profiles that are roughly



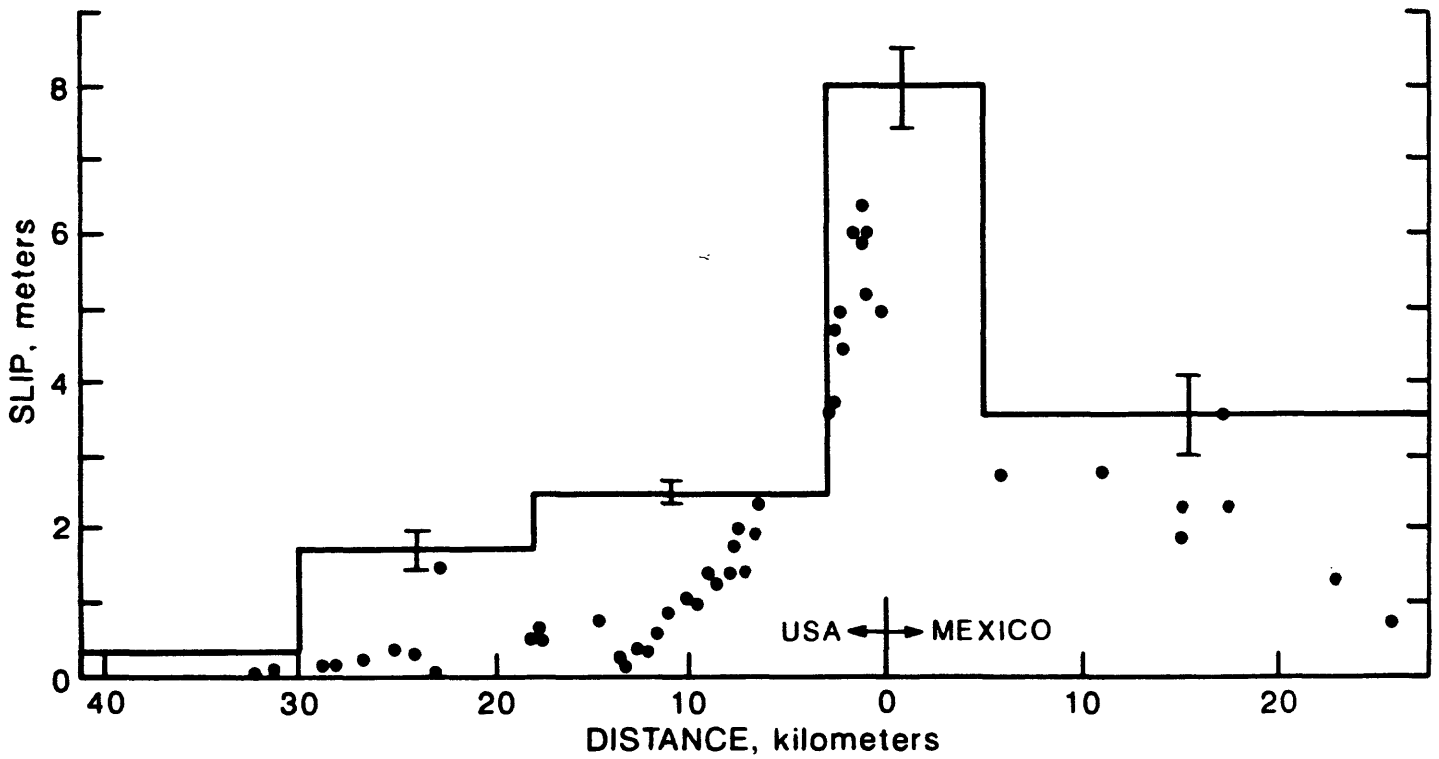


**FIGURE 3.** 1940 El Centro earthquake. Surface slip distribution versus distance along fault strike. Map view of surface faulting is shown at top of figure at the same scale, with north arrow indicating map orientation. Geologic data from *Sharp* [1982]. Star locates mainshock epicenter, initiation point of seismic rupture [*Richter*, 1958]. Geodetic estimates of fault slip are indicated by straight lines with one standard deviation error bars [*Zhang and Thatcher*, 1988, unpublished manuscript].

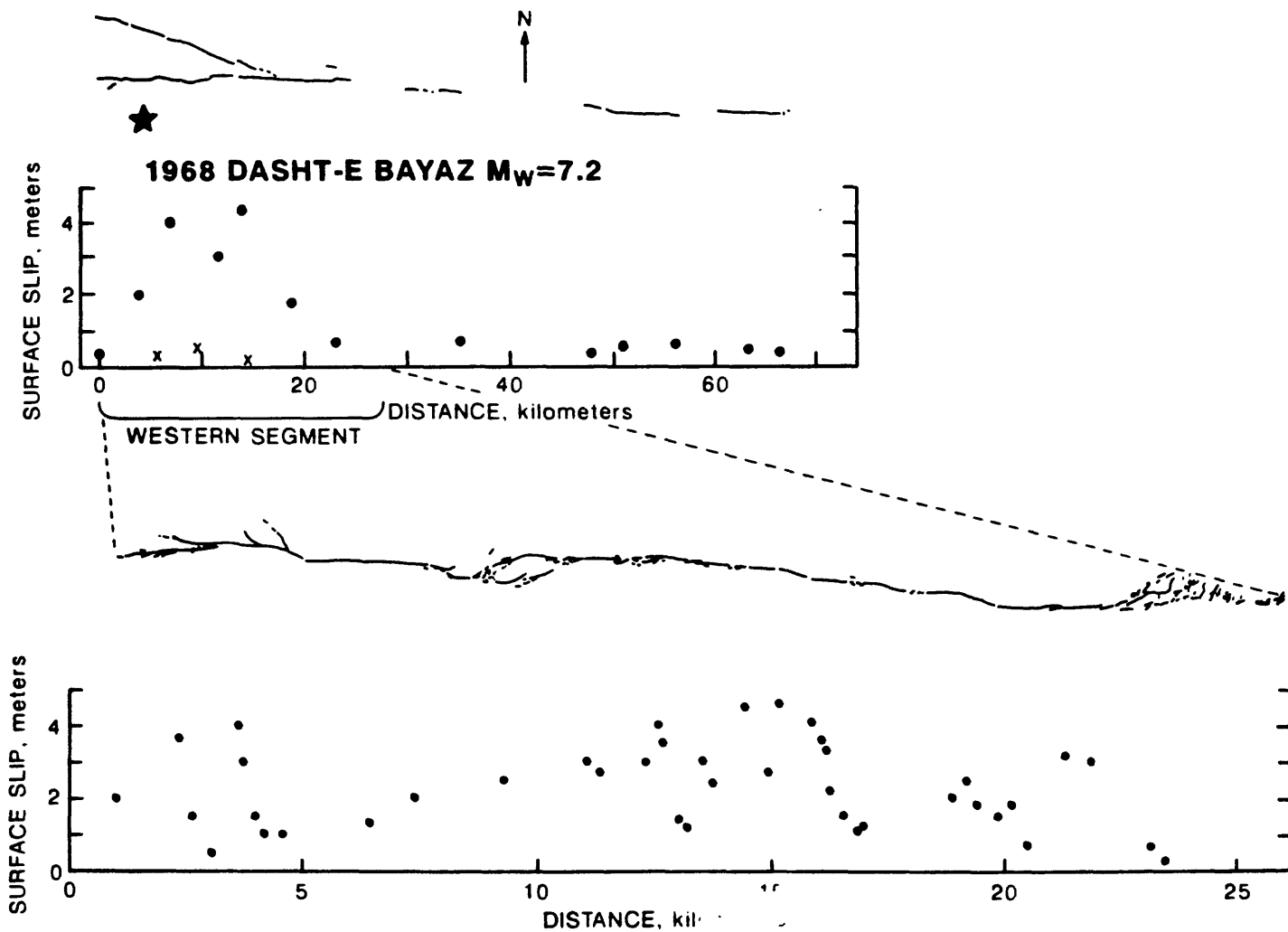


**FIGURE 4.** 1968 Dasht-e Bayaz (Iran) earthquake. Top frame of figure shows surface faulting map, north arrow indicating map orientation, and slip distribution along fault for entire 80-km-long rupture (crosses show surface slip on northwestern segment). Star locates mainshock epicenter, initiation point of seismic rupture. Bottom frame shows detailed map of surface faulting and slip along westernmost 25 km of the 1968 rupture. All data from *Ambraseys and Tchalenko* [1969].

symmetric, with maxima near the center of the rupture and relatively uniform decreases in slip amplitude towards the ends of the zone of surface faulting.

We have also noted some systematic features in the location of the mainshock epicenter along the zone of surface faulting. First, as many other studies have shown, we find that the mainshock epicenter, the initiation point of seismic rupture, is preferentially located towards the ends of the zone of surface faulting – in only four of the earthquakes studied here did the mainshock nucleate within the central 50 percent of the surface rupture. Furthermore, there is a tendency for the mainshock to locate in or near the region of maximum surface slip, although this is by no means a universal feature. For example, while the 1968 Borrego Mountain and 1968 Dasht-e Bayaz epicenters are, within location uncertainties, inside the maximum slip zone, the 1940 epicenter is not. Other events fall into one or the other of these classes, although significant epicentral uncertainty degrades the strength of the test of this hypothesis for many of the events examined here. We shall return to this issue when discussing seismologic observations, where the evidence is more conclusive.

## GEODETIC DATA

Ten of the earthquakes with surface faulting and slip distributions also have geodetic estimates of fault slip reliable enough to afford a comparison between the two methods. Figures 2 and 3 show specific examples, and a summary of all the comparisons is presented in figure 5. Each independent estimate of geodetic slip is shown by a vertical block. Error bars are small, generally less than 10% of each slip estimate, and are omitted in the figure. Surface slip (solid dots give maximum slip, crosses are average values) is compared with each independent geodetic estimate. Histogram shows ratio of maximum surface slip to geodetic slip (in percent) plotted against number of examples that occur in 20 percent increments for 0% to 100% and for ratios greater than 100%.

The comparisons illustrate that in cases where the geologic data are sufficiently numerous (*e.g.*, 1906 San Francisco, 1940 El Centro), the surface slip distributions are qualitatively similar to those indicated by the geodetic estimates. However, even the maximum slip is usually less than the geodetically estimated slip at seismogenic depths. The ratio shows considerable dispersion but its average is about 80%. Both the large scatter among surface slip observations and their biases relative to the geodetic determinations of slip underline a truth of which Quaternary fault geologists are acutely aware, that it is a rare fault locality where either total event slip or long-term slip rate can be reliably obtained.

## SEISMOLOGICAL DATA

During the past five years broad-band seismic recordings from large earthquakes have found increasing use in delineating those regions of the earthquake rupture surface where seismic moment or energy release are concentrated [*e.g.*, *Ruff and Kanamori*, 1983; *Kikuchi and Kanamori*, 1982; *Kikuchi and Fukao*, 1987]. Although the dimensions of these zones are seldom constrained well enough to reliably convert moment release into fault slip, the

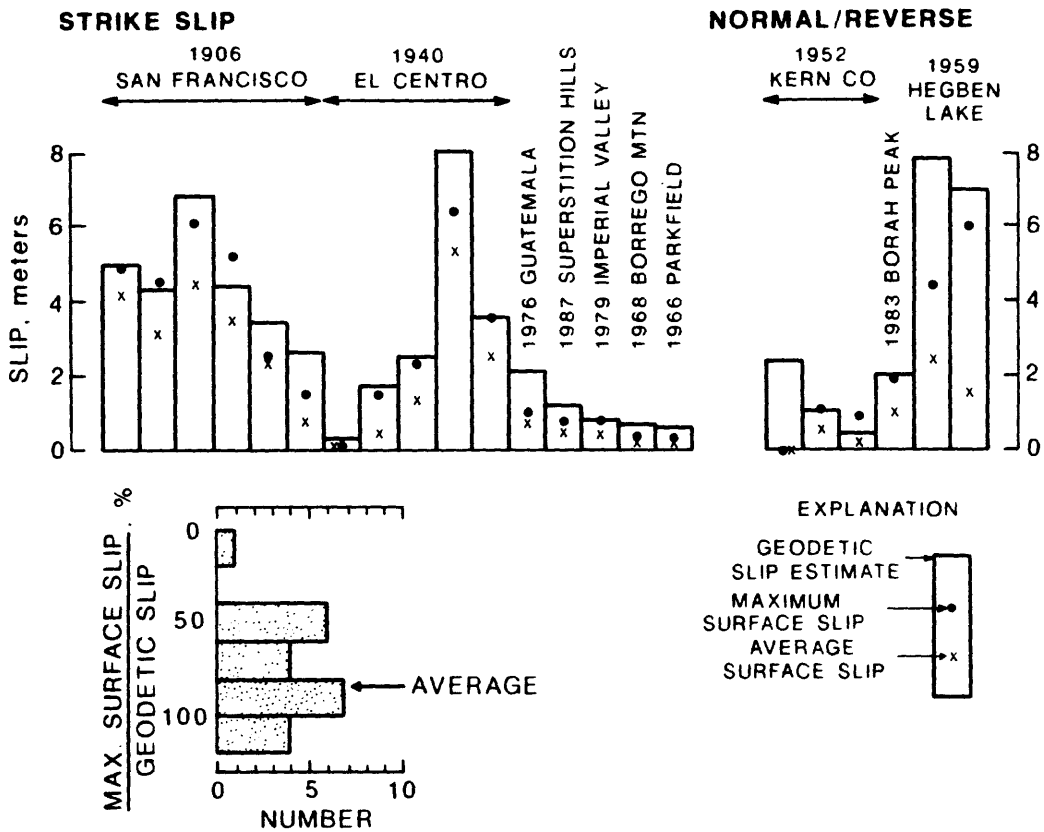


**FIGURE 5.** Geodetically-estimated slip (bars) compared with maximum surface slip (solid dots) and arithmetic average of reported surface slip (crosses) for strike slip (left) and normal or reverse faulting earthquakes (right). Note slip estimates on more than one fault section for 1906 San Francisco, 1940 El Centro, 1952 Kern County, and 1959 Hebgen Lake earthquakes. Bottom of figure shows histogram of ratio of maximum surface slip and geodetically-estimated slip, plotted as a percent, in twenty percent increments from 0 to 100% and for ratios greater than 100%.

results provide at least qualitative indications of two-dimensional slip distribution. All practitioners in this field have commented on the high degree of spatial heterogeneity in moment release revealed by their results, and the patterns shown are reminiscent of the long wavelength irregularity in slip distribution seen in the geologic and geodetic results discussed here.

Thus far in our review of the seismologic data we have examined analyses done for 16 earthquakes, all but one with  $M_w \geq 7.5$ , the great majority of these being great shallow focus underthrust events. The results of over a dozen separate studies by L. Ruff, M. Kikuchi, H. Kanamori and their coworkers of 14 of these events are summarized in greatly simplified cartoon fashion in figure 6. For each earthquake the aftershock zone is outlined in map view (north is towards the top of the figure), with the regions of high moment release shown by diagonal ruling and the mainshock epicenter indicated by a star. For the underthrust events the trench axis is shown as a line with teeth on the overthrust lithospheric plate. In this study we have followed convention and assumed that aftershock zones delimit the regions of coseismic fault slip. Although this may in some instances lead to overestimates of the true extent of the earthquake rupture plane, we do not think this bias is very great.

The most striking feature of figure 6 is the generally small area of the zone or zones of high moment release relative to the entire rupture plane. Equally notable is the usual location of mainshock epicenter either inside or immediately adjacent to one of these zones. The 1979 Colombia and 1977 Sumba Sea earthquakes are exceptions to this general rule, and for several other events (1968 Tokachi-oki, 1976 Mindinao, 1976 Guatemala) the regions of high moment release comprise such a large proportion of the aftershock zone that the rule is only weakly confirmed. Nonetheless, the coincidence of mainshock epicenter with zones of high moment release is striking. Figure 7 summarizes the evidence favoring systematic mainshock location relative to both maximum surface slip region (geologic data) and zones of concentrated moment release (seismologic results). Clearly the geologic observations only suggestively support such a systematic localization of mainshock epicenter, while the seismologic evidence is much stronger. Although our study has focussed on shallow crustal earthquakes it may be noteworthy that for 14 of 18 intermediate- and deep-focus events analyzed by *Fukao and Kikuchi* [1987] the mainshock also lay within the zone of high moment release.

## IMPLICATIONS

Earthquake slip distributions obtained by all three methods examined here are typically highly irregular, with maximum slippage often localized in one or a few restricted regions that together comprise only a small proportion of the entire rupture plane. This complexity does, however, contain some systematic elements, since rupture has a tendency to initiate towards the ends of the zones of seismic faulting and near or within regions of high coseismic slippage. Although this latter feature is an assumption or consequence of several simple models of uniformly propagating earthquake rupture, it is a perhaps somewhat surprising property of complex ruptures of the type illustrated here. For

## ZONES OF CONCENTRATED MOMENT RELEASE FOR MAJOR EARTHQUAKES

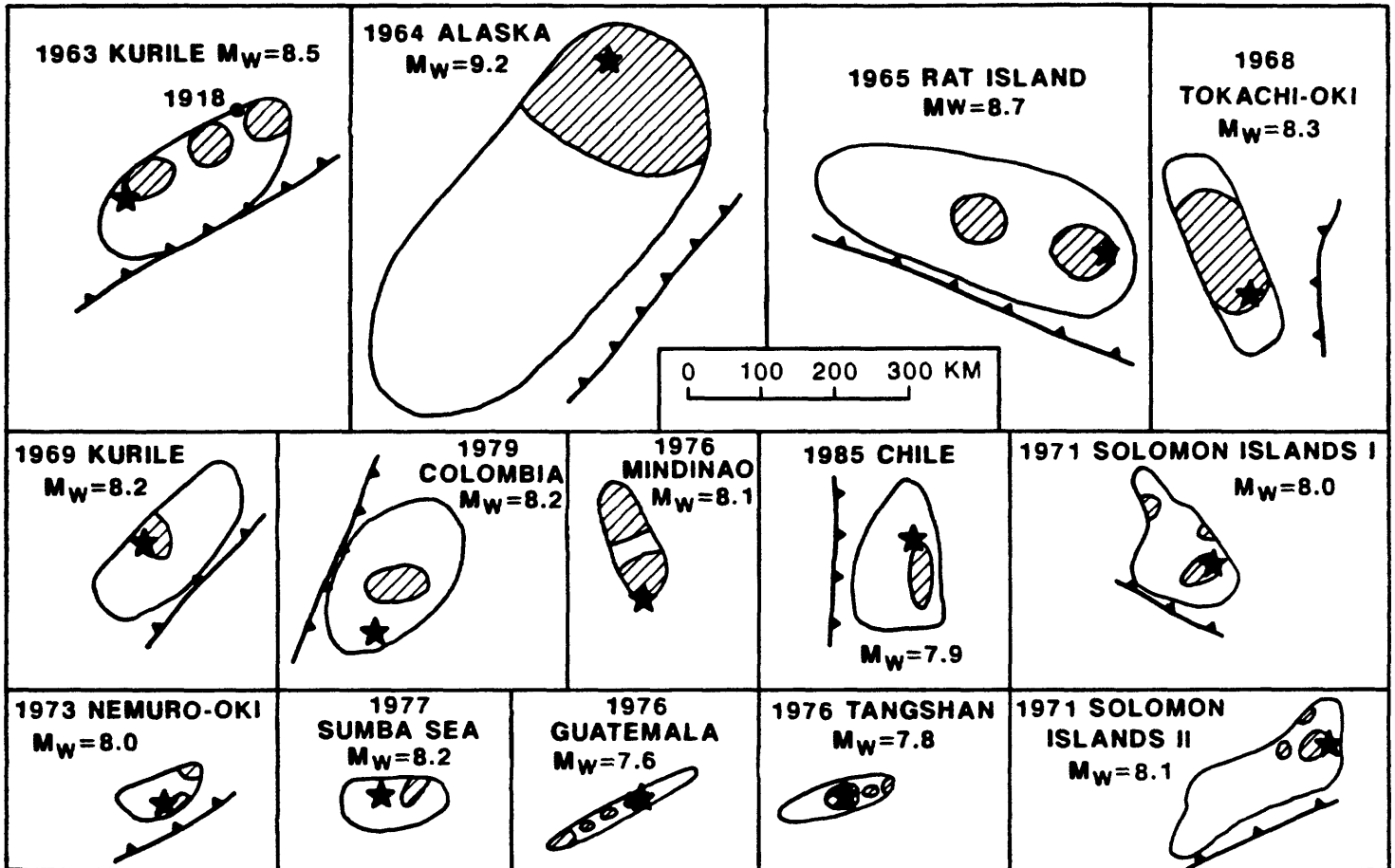


**FIGURE 6.** Schematic map-view summaries of aftershock zones (solid line) and regions of high seismic moment release (diagonal ruling) for 14 major earthquakes. Star locates mainshock epicenter, initiation point of seismic rupture. For interplate underthrust earthquakes, trench axis is shown, with teeth on overthrust lithospheric plate. North is towards top of figure for each map. In the 1963 Kurile earthquake zone (top left) the epicentral location of the most recent preceding great earthquake, which occurred in 1918, is shown for reference.

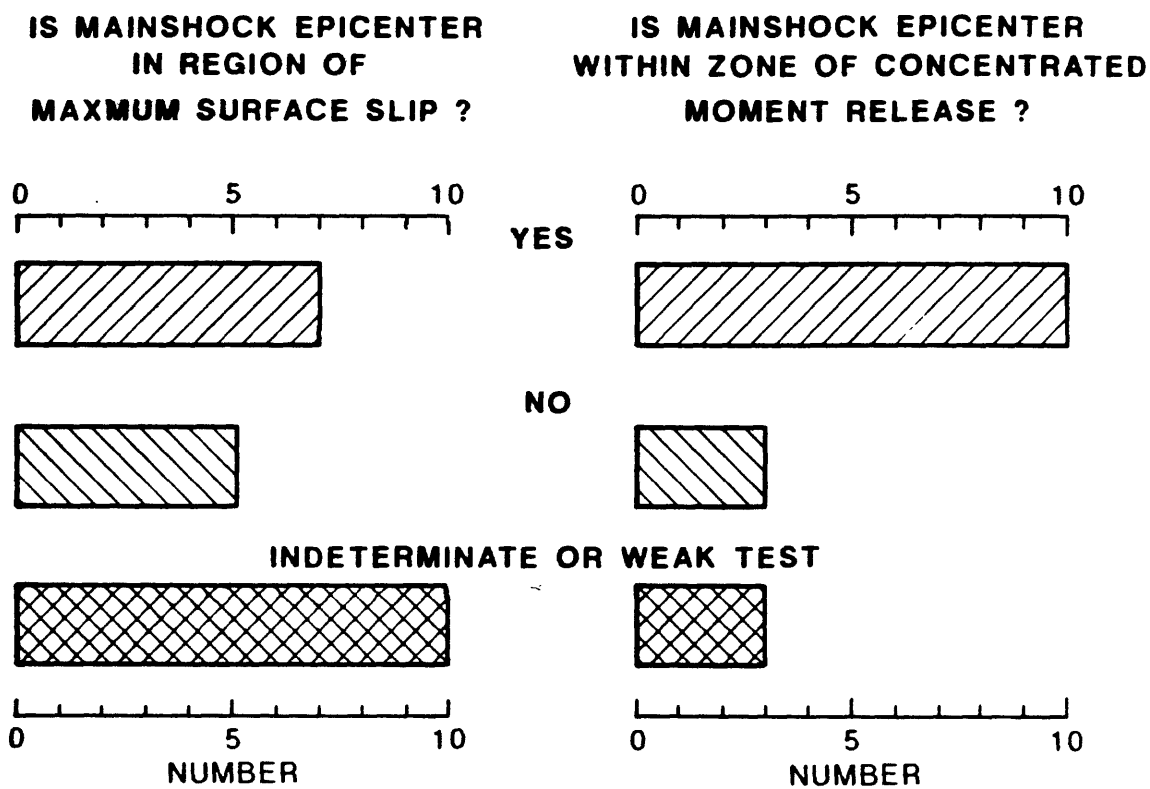


**FIGURE 7.** Summary of geologic and seismic observations that constrain the location of mainshock epicenter relative to (a) maximum surface slip region and (b) regions of high seismic moment release.

example, at one extreme, it has suggested that large-scale seismic failure might be triggered by a small shock randomly located on the rupture plane [Brune, 1979]. On the other hand, the generalizations we argue for here hint at some considerable order in the earthquake preparation process that has perhaps not hitherto been sufficiently appreciated, and our results provide observational evidence that seismic faulting may indeed be controlled by the physical properties of very localized regions of the rupture zone where slip nucleates ('asperities').

The ultimate significance of these observations depends to a considerable extent on an issue not addressed in this study, the degree to which large earthquakes repeatedly rupturing the same fault segment have similar slip distributions. Some historical and paleoseismic data suggest strong repeatability from event to event, as for example in the rupture zone of the 1966 Parkfield earthquake, along parts of the 1857 San Andreas rupture, and for several prehistoric Wasatch fault (Utah) events [Bakun and McEvilly, 1984; Sieh, 1978; Schwartz and Coppersmith, 1984]. In contrast, observations from a number of subduction zones indicate notable variability from one event to the next, both in the inferred slip and in the along strike extent of the source region. Examples include the 1906 and 1979 Colombia earthquakes [Kanamori and McNally, 1982], the 1985 and earlier Valparaiso (Chile) events [Christensen and Ruff, 1986], the 1894 and 1973 Nemuro-oki (Japan) shocks [Abe, 1977] and the 1957 Aleutian and 1986 Andreanof Islands earthquakes [Huang and Kanamori, 1986]. The currently available evidence bearing on this matter is thus equivocal and may suggest a range of behavior.

However, if recurrent earthquakes on the same segment of fault retain even grossly similar characteristics from event to event then the observations reported here have obvious implications for earthquake prediction research and for the issues that are the principal focus of this workshop. The tendency for rupture to initiate near regions of maximum slip suggests that it is this maximum value that controls the recurrence characteristics for the segment. Provided the regions of high slip and/or concentrated moment release can be identified from historical data or paleoseismic investigation, geologic studies and intensified monitoring might then be especially concentrated in areas that comprise only a small portion of the entire earthquake source region and yet may well lie near the eventual location of rupture initiation.

## REFERENCES

- Abe, K., 1977, Some problems in the prediction of the Nemuro-oki earthquake, *J. Phys. Earth*, Suppl. Issue, **25**, p. 261-271.
- Allen, C.R., and Nordquist, J.M., 1972, Foreshock, mainshock, and larger aftershocks of the Borrego Mountain earthquake, *U.S. Geol. Survey Prof. Paper 787*, p. 16-23.
- Ambraseys, N.N., and Tchalenko, J., 1969, The Dasht-e Bayaz earthquake of August 31, 1968 in Iran, *Bull. Seismol. Soc. Amer.*, **59**, p. 1751-1792.
- Bakun, W.H., and McEvelly, T.V., 1984, Recurrence models and the Parkfield, California, earthquakes, *J. Geophys. Res.*, **89**, p. 3051-3058.
- Brune, J.N., 1979, Implications of earthquake triggering and rupture propagation for earthquake prediction based on premonitory phenomena, *J. Geophys. Res.* **84**, p. 2195-2198.
- Bucknam, R.C., Plafker, G., and Sharp, R.V., 1978, Fault movement (afterslip) following Guatemala earthquake of February 4, 1976, *Geology*, **6**, p. 170-173.
- Christensen, D.H. and Ruff, L.J., 1986, Rupture process of the March 3, 1985 Chilean earthquake, *Geophys. Res. Lett.*, **13**, p. 721-724.
- Clark, M.M., 1972, Surface rupture along the Coyote Creek fault, *U.S. Geol. Survey Prof. Paper 787*, p. 55-86.
- Fukao, Y., and Kikuchi, M., 1987, Source retrieval for mantle earthquakes by iterative deconvolution of long-period P-waves, *Tectonophys.*, **144**, p. 249-269.
- Gordon, F.R., Lewis, J.D., 1980, The Meckering and Calingiri earthquakes, October 1968 and March 1970, *Geol. Survey W. Australia, Bull. 126*, 229 pp.
- Huang, L., and Kanamori, H., 1986, On the May 7, 1986 Andreanof Islands earthquake source parameters, *Geophys. Res. Lett.*, **13**, p. 1426-1429.
- Kanamori, H., and McNally, K., 1982, Variable rupture mode of the subduction zone along the Ecuador-Colombia coast, *Bull. Seismol. Soc. Amer.*, **72**, p. 1241-1254.
- Kikuchi, M. and Fukao, Y., 1987, Inversion of long-period P-waves from great earthquakes along subduction zones, *Tectonophys.*, **144**, p. 231-247.
- Kikuchi, M., and Kanamori, H., 1982, Inversion of complex body waves, *Bull. Seismol. Soc. Amer.*, **72**, p. 491-506.

- Lawson, A.C. (Chairman), 1908, The California Earthquake of April 18, 1906, Report of the State Earthquake Investigation Commission, 2 vol., 641 pp., Carnegie Institution of Washington, Washington, D.C.
- Matsuda, T., 1974 (in Japanese), Surface faults associated with Nobi (Mino-Owari) earthquake of 1891, Japan, *Spec. Rep. Earthq. Res. Inst.*, **13**, p. 85-126.
- Richter, C.F., 1958, Elementary Seismology, Freeman, San Francisco, 768 pp.
- Ruff, L. and Kanamori, H., 1983, The rupture process and asperity distribution of three great earthquakes from long-period diffracted P-waves, *Phys. Earth Planet. Int.*, **31**, p. 203-230.
- Schwartz, D.P., and Coppersmith, K.J., 1984, Fault behavior and characteristic earthquakes, examples from the Wasatch and San Andreas fault zones, *J. Geophys. Res.*, **89**, p. 5681-5698.
- Sharp, R.V., 1982, Comparison of 1979 surface faulting with earlier displacements in the Imperial Valley, in *The Imperial Valley, California, Earthquake of October 15, 1979*, U.S. Geol. Surv. Prof. Paper 1254, p. 213-221.
- Sieh, K., 1978, Slip along the San Andreas fault associated with the great 1857 earthquake, *Bull. Seismol. Soc. Amer.*, **68**, p. 1421-1448.
- Snay, R.A., Cline, M.W., and Timmerman, E.L., 1983, Regional deformation of the earth model for the San Diego region, California, *J. Geophys. Res.*, **88**, p. 5009-5024.
- Wallace, R.E., 1984, Faulting related to the 1915 earthquakes in Pleasant Valley, Nevada, *U.S. Geol. Surv. Prof. Paper 1274-A*, p. A1-A33.
- Zhang, Y., Thatcher, W., 1988. Coseismic deformation accompanying the May 8, 1940 Imperial Valley, California earthquake, to be submitted to *J. Geophys. Res.*

Data Collection Network System of University Group and Some Recent Results of Crustal Movements

Hiroshi Ishii  
Earthquake Research Institute, University of Tokyo

Data Collection Network System

In Japan about a hundred of continuous crustal movement observatories are operated for earthquake prediction research by a university group. Most of the observatories are equipped with some among vault- and borehole-type instruments such as extensometers, watertube tiltmeters, borehole tiltmeters, borehole strainmeters and others. A series of Monitoring Chains on Crustal Activities (MOCCA) shown in Fig. 1 is established during the fourth phase of the National Earthquake Prediction project (1979-1983).

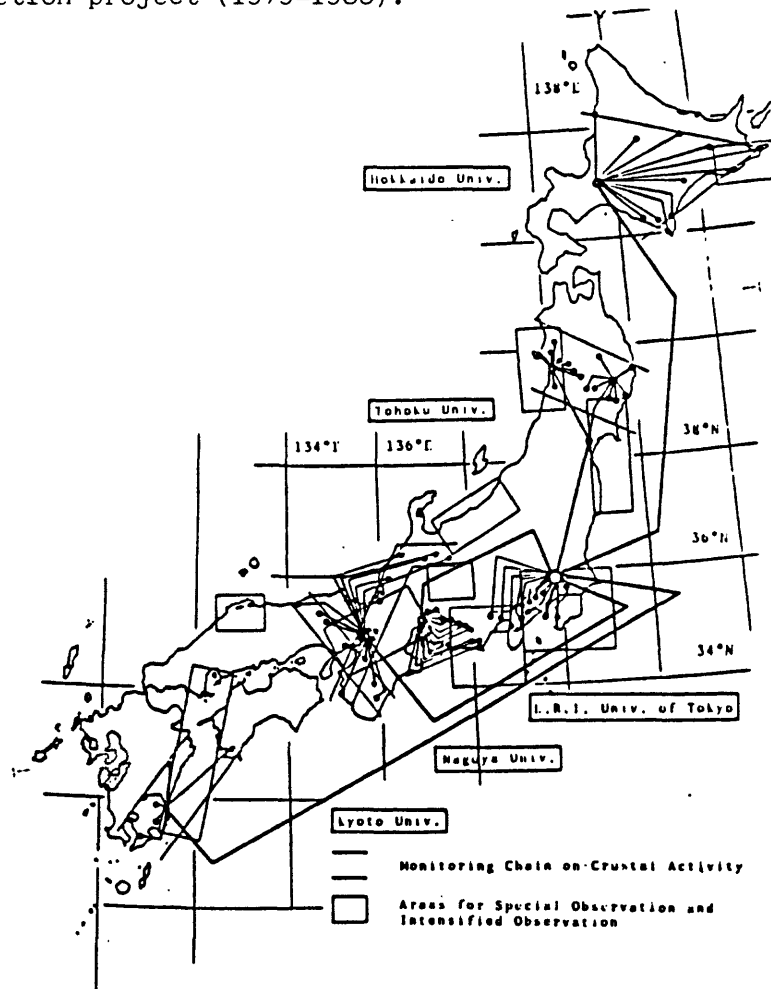


Fig. 1 Location of Monitoring Chain of Crustal Activity and flow of data collection

The Chains are station system deployed for observing multi-dimensional data and are arranged across zones of seismotectonic importance. Development of data processing system for multi-disciplinary multi-channel data has been performed by each university

In the fifth phase of the project (1984-1988) data collection network system is under construction. Flow of data obtained from the Monitoring Chains is also illustrated in Fig. 1. Data observed at local stations belonging to each Monitoring Chain are assembled at a regional center utilizing public telephone line or exclusive line. Then the collected data are sent to Earthquake Prediction Data Center (EPDC) of Earthquake Research Institute of the University of Tokyo by utilizing DDX (Digital Data Exchange) telephone lines. Outline of the crustal movement data collection network system is presented in Fig. 2.

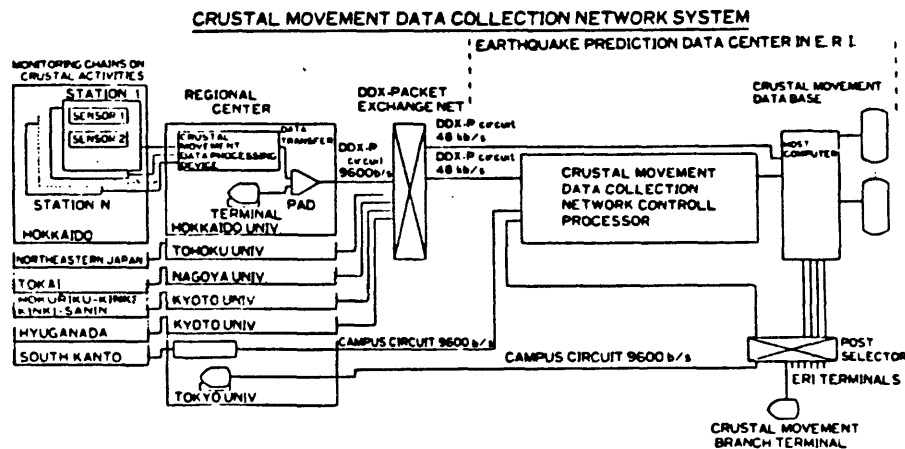


Fig. 2 Crustal movement data collection network system

There are 7 Monitoring Chains. Data observed at stations are firstly sent to regional centers. Then data assembled at regional centers are processed by crustal movement data processing device and transferred to EPDC through DDX-PACKET EXCHANGE NET of DDX-P circuit of NTT company. Data stored in DATA BASE in EPDC can be searched and processed from a terminal in a regional center. The data base terminal can run programs stored in the host computer and perform various works. Development of processing and analysis programs is now progressing.

### Vertical Movements in the Tokai region and the Izu Peninsula

The Izu Peninsula is located at the northern end of the Philippine sea plate sinking under the continental plate, and crustal activities are very high. The Philippine sea plate is sinking beneath the Tokai region from the Suruga trough where an occurrence of a great earthquake is expected with enormous damage. Therefore, research of both the Tokai region and the Izu Peninsula are of very interest and important from a view point of earthquake prediction. We discuss in detail about recent vertical deformation of the two regions as shown in Fig. 3.

#### 1. Tokai Region

A fault model of an earthquake expected in the Tokai region (Mogi, 1985) is drawn in Fig. 4. The Omaezaki is placed just above the fault and is expected to reflect a precursory phenomena of a

MADE FROM BEST  
AVAILABLE COPY

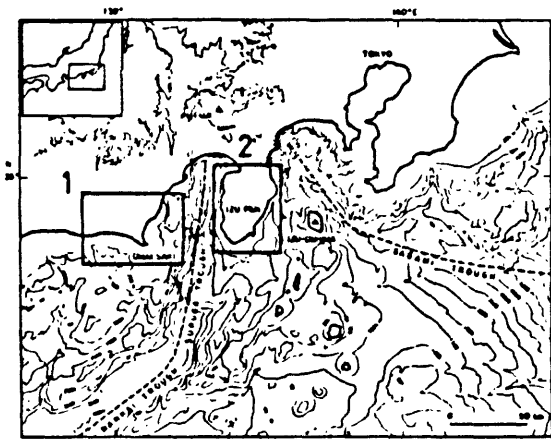


Fig. 3 Two regions where temporal and spatial vertical movements are investigated

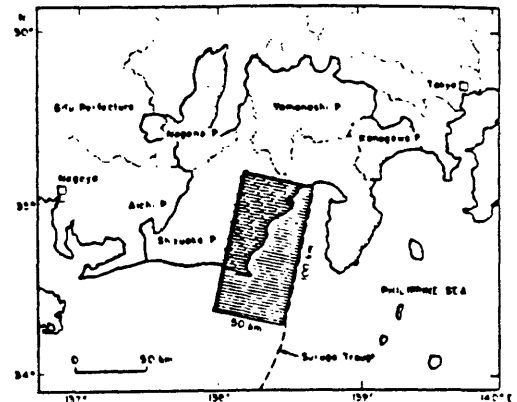


Fig. 4 A fault model of an earthquake expected in the Tokai region (after Mogi, 1985)

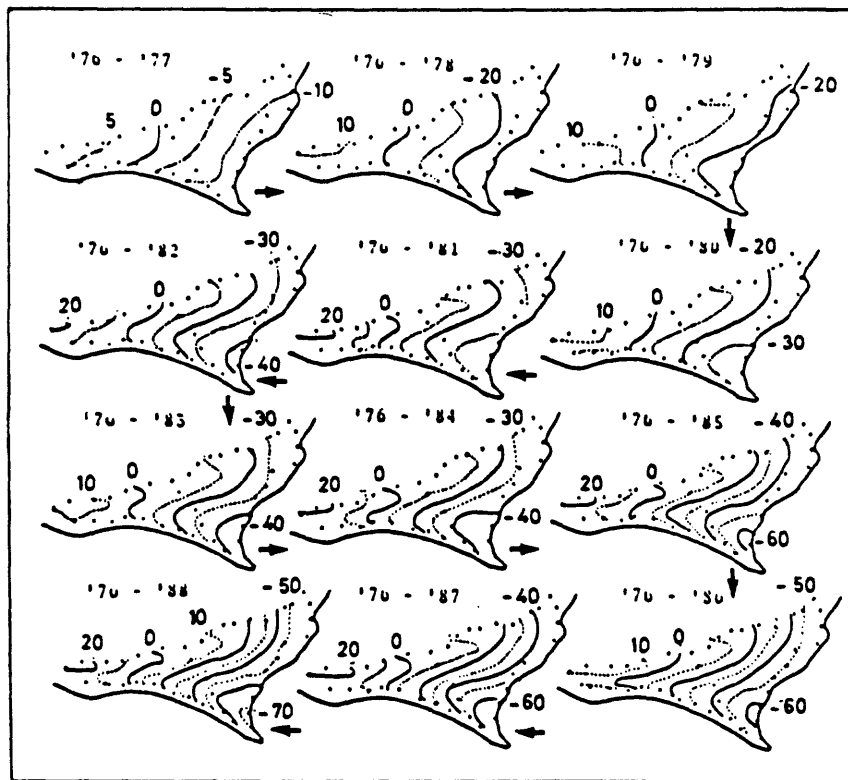


Fig. 5 Accumulated vertical deformations from 1976 to 1988 in the Tokai region

MADE FROM BEST  
AVAILABLE COPY

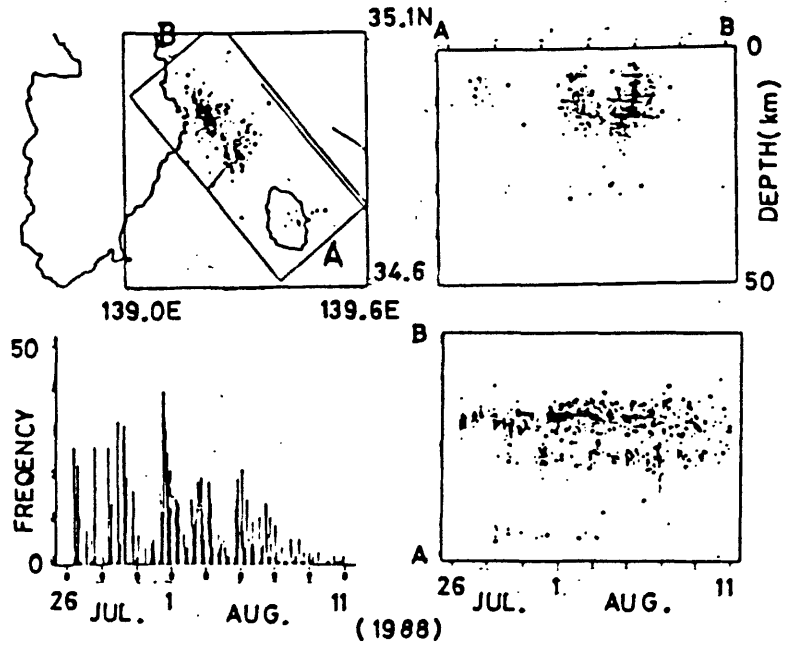


Fig. 6 Distribution of hypocenters and frequency of earthquake swarms occurring in August of 1988 (after E.R.I.)

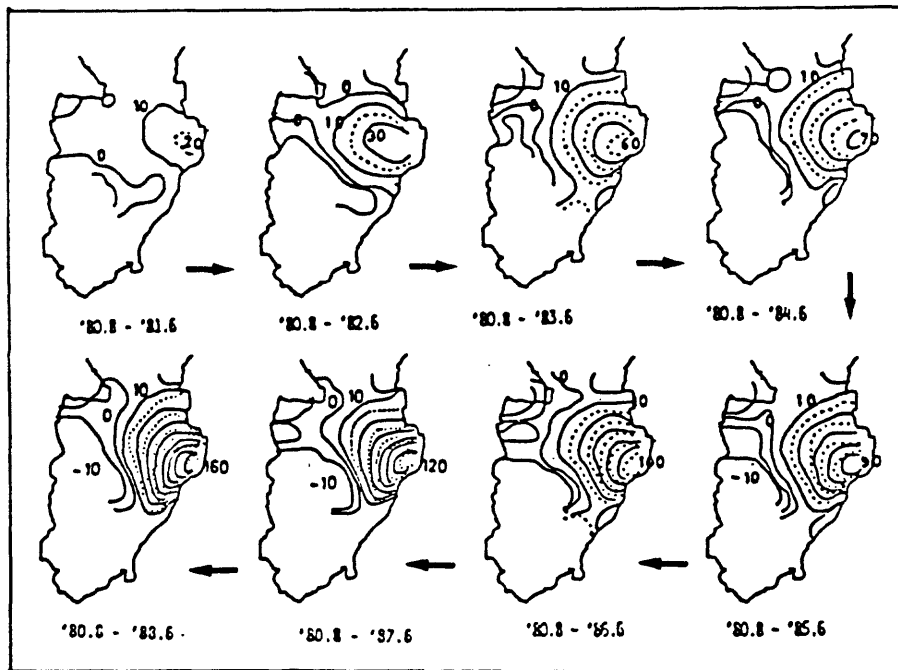


Fig. 7 Accumulated vertical deformations from 1980 to 1988 in the Izu Peninsula

great Tokai earthquake. In the Tokai region, a precise leveling survey is repeated every year since 1976. By applying the method devised by us (Miura et al., 1988), we investigated temporal and spatial variations of vertical movements. Accumulated vertical displacements from 1976 to 1988 are shown in Fig. 5 by contours for every year. Bench marks on leveling routes employed for drawing contours are also plotted by circles.

The east coast is continuously subsiding. A maximum subsidence appears at the north of the cape Omaezaki with a rate of about 0.6 cm/year. A subsidence at the south coast indicates less subsidence with a distance from the cape. Though the variations of the accumulated deformations are rather simple, differences between two years are complex. Accumulated contours are almost perpendicular to the direction of the plate subduction. The temporal variation of the maximum subsidence plate indicates well coincidence with temporal variation of the vertical movement obtained from the sea level data at Omaezaki.

## 2. Izu Peninsula

Earthquake swarms happened this summer off the northeast of the peninsula. Distribution of the epicenters and frequency are presented in Fig. 6 (E.R.I., 1988). In this area earthquake with magnitude 6.7 occurred in 1980. Therefore, temporal and spatial variations of vertical deformation are of very interest.

The analyzed period is from 1980 to 1988 and the survey was performed by use of the same method as before. Accumulated vertical displacements from August of 1980 to June of 1988 are shown in Fig. 7 by contours for every year. The uplifting range becomes clear with the lapse of time. The center of the uplifting area with a radius of about 14 km is located at the northeast of the peninsula.

Slow migration of the uplift peak with a velocity of about 10 km/year was found from the time history of yearly vertical movements. Discussions are presented by taking into account other geophysical facts.

## References

- Earthquake Research Institute, Materials at the 84th meeting of the coordinating committee for the earthquake prediction, 4-5, 1988  
Miura, S., H. Ishii and A. Takagi, Migration of vertical deformations and coupling of island arc plate and subducting plate, A.G.U. Geophysical Monograph (accepted) 1988.  
Mogi, K., Earthquake prediction, 355 pp., Academic Press, 1985.

# SPATIAL AND TEMPORAL CORRELATION BETWEEN CODA $Q^{-1}$ AND SEISMICITY

by

Keiiti Aki  
Department of Geological Sciences  
University of Southern California

## ABSTRACT

From the observed strong correlation between coda  $Q^{-1}$  and seismicity in space, we conclude that coda  $Q^{-1}$  represents the degree of fracture in the lithosphere. As compared to coda  $Q^{-1}$ , the crustal seismic velocities are insensitive to the current seismicity, while seismic velocities and attenuations at the top of the mantle may be related to the tectonic activity originating in the asthenosphere. Temporal variations in coda  $Q^{-1}$  are also related to seismicity, but the relation is more complex than for spatial variations.

From the analysis of local earthquake coda waves recorded by the Benioff short-period vertical seismograph at Riverside, California, we found a surprisingly large and systematic temporal variation in coda  $Q^{-1}$  in southern California during the 55 year period from 1933 to 1987. Comparison of the coda  $Q^{-1}$  variation with the b-value obtained for earthquakes with  $M_{\geq 3}$  occurred in the area within 180 km from Riverside (corresponding to the area for which  $Q^{-1}$  is estimated by the coda method), led to an extraordinary discovery that coda  $Q^{-1}$  correlates positively with b-value with the correlation coefficient of 0.79. The significance of correlation cannot be rejected at the confidence level of 0.974. Since the data used for measuring  $Q^{-1}$  namely seismograms, and the data used for measuring b, namely catalog,

are totally independent, the observed correlation supports strongly the physical reality of temporal change in both coda  $Q^{-1}$  and b-value.

The correlation between coda  $Q^{-1}$  and b-value has been observed for several cases, but the correlation was positive in some cases, and negative in others. Our current preferred model for explaining the observed correlation is the following. A seismic creep is going on from time to time over various sizes of cracks in a seismic region. Creep activities tend to increase the crack density and coda  $Q^{-1}$  in the region. If the creep occurs with a certain predominant crack size, spatial stress concentration may enhance seismicity for earthquakes with the comparable size. If this characteristic size is in the lower part of the magnitude range for which b-value is estimated, the enhanced seismicity will increase b. On the other hand, if it is in the upper part of the magnitude range, it will decrease b. Thus, we can explain the observed strong correlation between coda  $Q^{-1}$  and b-value for both positive and negative cases.

Comparative strain measurement of the NRLM tunnel  
by an interferometer and a distance meter

Tadanao OH'ISHI and Katuo SETA

National Research Laboratory of Metrology  
Umezono 1-1-4, Tsukuba, Ibaraki 305 Japan

The main tasks of National Research Laboratory of Metrology are to establish and maintain state level metrology standards, develop techniques for precision measurements.

Among physical quantities length is one of the most important ones. In the region of geodetic measurement, a laser extensometer, a CO<sub>2</sub> laser synthetic interferometric distance-measuring system, a distance measuring equipment using inter-mode beat of He-Ne laser has been developed. And a three color distance meter is now being developed.

A 310 m long tunnel has been constructed in the site of the NRLM eight years ago. Performance tests of those instruments mentioned above have been done in the tunnel. Strain changes of the tunnel also has been observed<sup>1)</sup>. And several unusual distortion changes which begun before earthquakes around Tsukuba area have been noticed. Observation by using a laser extensometer has been carried out from 1980. In order to get much information about strain changes of the tunnel, an observation of 300 m span by using a distancemeter has been carried out for two years from 1986 to 1988.

### NRLM tunnel

The NRLM tunnel is made of reinforced concrete. No joint was introduced. It is because easy deformation of it is inconvenient to set base lines in the tunnel. Many piles were driven into the soil to make the base of the tunnel. The direction of the NRLM tunnel is 28 degree counter clockwise from east-west direction. The tunnel is not for geodetic observation but for experimental room developing distance measuring techniques using optical method. About six hundred meter depth of soil is under the tunnel and the under ground water level is few meter beneath the ground surface.

The cross section and the plan of the tunnel is shown in Fig.1 (a) and (b), respectively. The floor of it is 5 m beneath the ground surface. 3.5 m thick soil is piled over it. The tunnel consists of coaxial dual tunnels. The outer one has many cracks in its body and rain water comes inside through those cracks. The inner one prevents water to sink into the inside of it. Two small

dehumidifiers are installed in the tunnel and they keep the humidity between 50 % and 60%. The condition is favorable to maintain the instruments.

### Laser Extensometer<sup>2)</sup>

The laser extensometer, as shown in Fig. 2, is michelson type interferometer with cube corner reflectors. Span of it is 25 m and most of optical path is covered with sealed tube which has glass windows on both ends. Optical paths of both arm in the air are adjusted to be equal length in order to prevent being affected by changes of the refractive index of air. The light source is a frequency stabilized He-Ne laser. Interference fringes are periodically swept with an optical pathlength modulator. The interference fringes are detected by two photodiodes and converted into electric signals, which fed to a bidirectional counter. The count number is converted into voltage signal. A deformation of the tunnel is shown by the averaged voltage signal. Its resolving power reaches to  $0.01 \mu\text{m}$ , namely  $4 \times 10^{-10}$  of the span.

### Distance meter using beat signal of longitudinal modes of laser<sup>3)4)</sup>

The light source is 633 nm He-Ne laser operating with two longitudinal oscillation modes. The frequency of beat note of two modes is about 550 MHz. The beat signal is used to measure distance and this signal can be treated as the signal obtained from amplitude modulated laser beam. A modulation ratio of 100 % can be obtained easily without a modulator. The 100 % modulation ratio provides high signal to noise ratio and it gives high resolution in distance measurement.

Schematic diagram of this distance measuring equipment is shown in Fig. 3. The laser beam transmits through a polarizer in order to two oscillation modes have equal amplitude of light signal in the same polarization state. The beam is divided into two part in amplitude by the beamsplitter. Therefore those two part have each two mode components. The transmitted one reaches at far target reflector and return to the beamsplitter. Then the beam is reflected and illuminates a avalanche photo diode. A high frequency electric signal is generated in the avalanche photo diode. The reflected one is detected by the other avalanche photodiode and it is changed into high frequency electric signal, too. Both of electric signals has the 550 MHz frequency and the phase difference of them are measured by a vector voltmeter HP8405. A distance is read from the phase difference. The Integral number of wavelength of 550 MHz signal is measured with somewhat different beat frequencies around 550 MHz.

### Result of comparative measurement

The result of comparative measurement is shown in Fig. 4. Rough trends of both curves have same tendency. But some differences are noticed. Firstly, phases of one year period components in both curves are different by about two months; 48 days. The reason of it is not explained yet, but temperature may be a main factor. In near future the temperature distribution along the tunnel will be measured. From the result we may have some informations about the phase difference. The amplitudes of the one year period components show small difference, namely  $4.0 \times 10^{-6}$  and  $4.5 \times 10^{-6}$ . Secondary, the trends for more than few years which can be consider to be linear are also different. The value of the extensometer was  $6.7 \times 10^{-6}$  and that of distance meter was  $2.6 \times 10^{-6}$ .

The fact mentioned above means that the deformation of the tunnel is not unique along the tunnel. Therefore the laser extensometer measures local deformations. A simple model may be inadequate to explain the local deformation.

### References

- 1) T. Oh'ishi and I. Fujima: Strain Changes of NRLM Tunnel before Earthquakes, Proceedings of 5th Joint Meeting of the UJNR Panel on earthquake Prediction Technology (1986) pp.87-101.
- 2) T. Ohishi, S. Seino and Y. Sakurai: Laser Extensometer for Earth Strain Measurement, J. Geod. Soc. of Japan Vol.22, No.4 (1976) pp.287-289.
- 3) K. Seta and T. Oh'ishi: Optical Distance Measurement Using Inter-Mode Beat of Laser, Jpn. J. Appl. Phys. Vol. 24, No. 10 (1985) pp.1374-1375.
- 4) K. Seta, T. Oh'ishi and I. Fujima: A Distance Meter using Inter-Mode Beat of He-Ne Laser, Proceedings of 5th Joint Meeting of the UJNR panel on earthquake Prediction Technology (1986) pp.350-365.

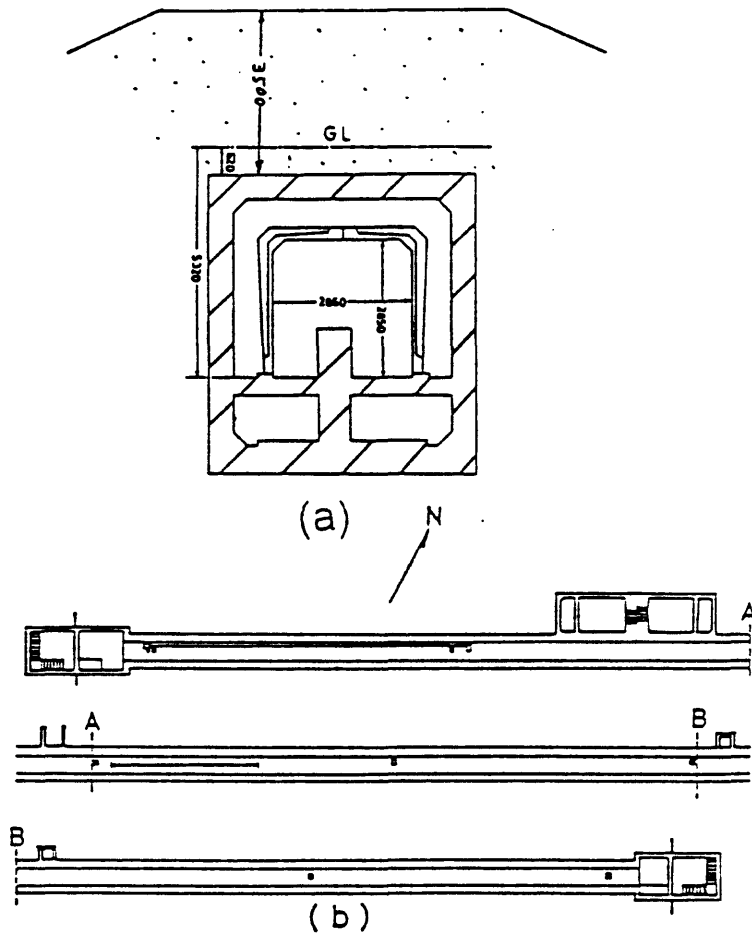


Fig. 1 Cross section (a) and plan (b) of NRLM tunnel

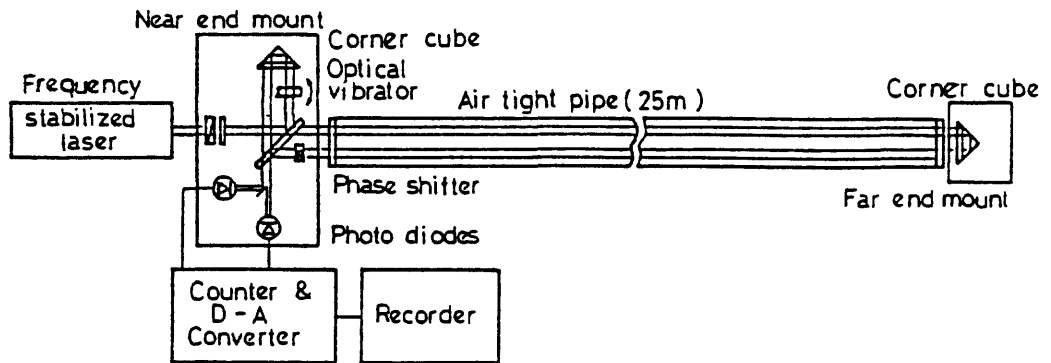


Fig. 2 Laser extensometer

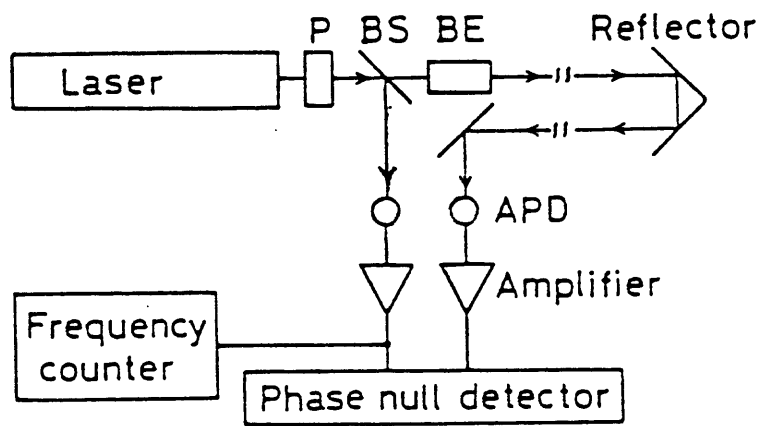


Fig.3. Schematic diagram of optical distance meter.

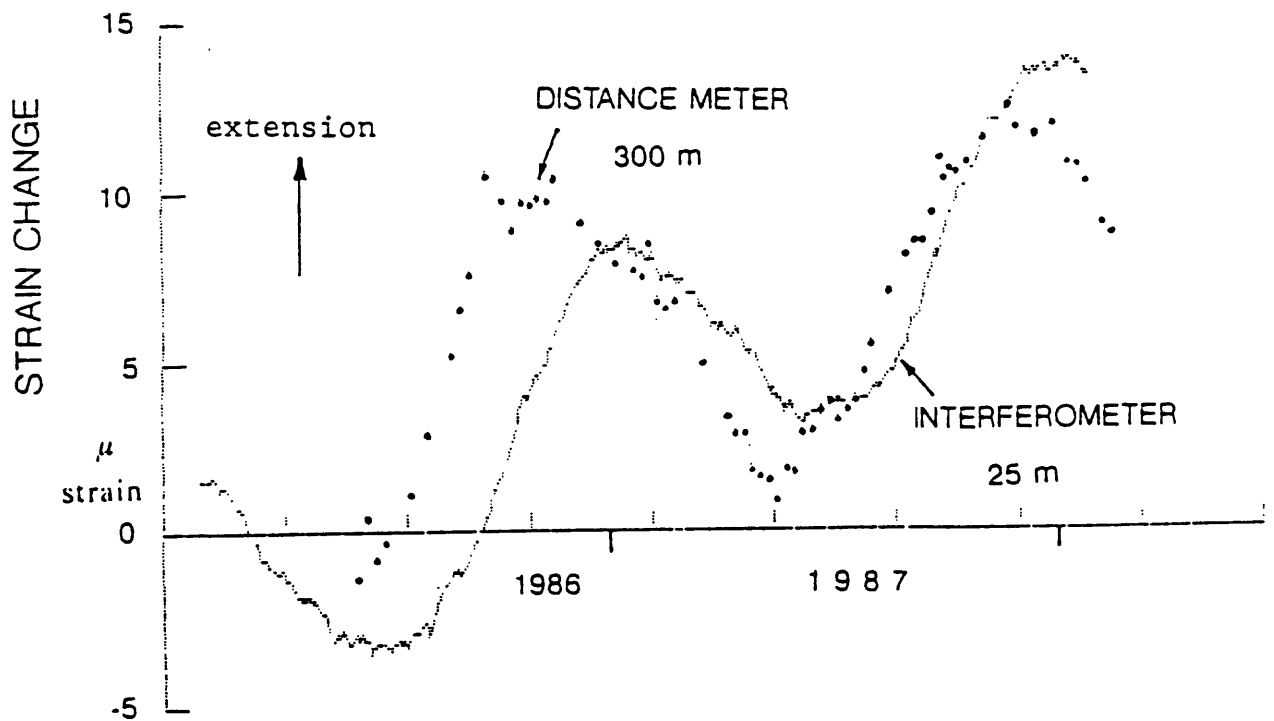


Fig. 4 Result of comparative measurement

## Repeating Earthquakes: Characteristics and Implications

*William L. Ellsworth and Lynn D. Dietz*

U. S. Geological Survey  
345 Middlefield Road  
Menlo Park, CA 94025

In this study we examine the nature of earthquake recurrence through the analysis of multiple cycles of faulting -- repetitive movement of the same part of the fault plane -- in a variety of tectonic settings and over a wide magnitude range. Our purposes in this work are twofold: to develop a better understanding of properties of recurrence intervals and their application to the problem of long-term earthquake forecasting; and to bring new observational data to bear on the problem of earthquake nucleation.

The principal approach we use is the intercomparison of seismograms for pairs events at one or more common stations. Through both simple visual comparison and cross spectral analysis of seismogram pairs we can establish (or rule out) the kinship of potentially paired events. Where adequate network data exist, we can also determine the relative position of the event centroids (Poupinet, and others, 1984). Auxiliary data, such as aftershock distributions, also contribute important constraints on the spatial relation of associated events.

The paradigm of the repetitive recurrence of a "characteristic" earthquake, as exemplified by the series of M 6 Parkfield earthquakes (Bakun and McEvelly, 1984), receives strong support in our observations. The central property is the occurrence of nearly identical earthquakes rupturing the same part of the fault through many cycles of strain accumulation and release. In the cases where the distribution of pre- and post-mainshock seismicity can be related to the slip distribution in the mainshock it is clear that little if any seismicity occurs on the part of the fault plane that produces the mainshock. Further, we find that the amount of coseismic slip determined from records of the mainshock equals the amount predicted by the product of the long-term slip rate and the interevent interval, at least in those cases where this comparison can be made.

The existence of discrete regions on the fault plane that move only in events with a characteristic displacement defines the fundamental properties of the asperity model (e.g. Wesson and Ellsworth, 1973). Simple measures of the parameters of the earthquake cycle for each repeating source place constraints on the strength of these locked patches on the fault plane. The results suggest that the peak shear stress acting on the asperity at the time of failure approaches laboratory values for static friction.

## References cited

- Bakun, W. H. and T. V. McEvilly, 1984, Recurrence models and Parkfield, California, earthquakes: *Journal of Geophysical Research*, v. 89, p. 3051-3058.
- Cockerham, R. S. and J. P. Eaton, 1987, The earthquake and its aftershocks, April 24 through September 30, 1984: *U. S. Geological Survey Bulletin 1639*, p. 15-28.
- Ellsworth, W. L., 1975, Bear Valley, California, earthquake sequence of February-March 1972: *Bulletin of the Seismological Society of America*, v. 65, p. 483-506.
- Frémont, M. and S. D. Malone, 1987, High precision relative locations of earthquakes at Mount St. Helens, Washington: *Journal of Geophysical Research*, v. 92, p. 10223-10236.
- Hartzell, S. H. and T. H. Heaton, 1983, Inversion of strong ground motion and teleseismic waveform data for the fault rupture history of the 1979 Imperial Valley, California, earthquake: *Bulletin of the Seismological Society of America*, v. 73, p. 1553-1583.
- Hartzell, S. H. and T. H. Heaton, 1986, Rupture history of the 1984 Morgan Hill, California earthquake from the inversion of strong motion records: *Bulletin of the Seismological Society of America*, v. 76, p. 649-674.
- Keilis-Borok, V. I., 1959, On the estimation of the displacement in an earthquake source and of source dimensions: *Ann. Geofis.*, v. 12, p. 205-214.
- Liu, H. and D. V. Helmberger, 1983, The near-source ground motion of the 6 August 1979 Coyote Lake, California, earthquake: *Bulletin of the Seismological Society of America*, v. 73, p. 201-218.
- Mendoza, C. and S. H. Hartzell, 1988, Aftershock patterns and main shock faulting: *Bulletin of the Seismological Society of America*, v. 78, p. 1438-1449.
- Porcella, R. L., R. B. Matthiesen, and R. P. Maley, 1982, Strong-motion data recorded in the United States: *U. S. Geological Survey Professional Paper 1254*, p. 289-318.
- Poupinet, G., W. L. Ellsworth, and J. Fréchet, 1984, Monitoring velocity variations in the crust using earthquake doublets: an application to the Calaveras fault, California: *Journal of Geophysical Research*, v. 89, p. 5719-5731.
- Reasenber, P. and W. L. Ellsworth, 1982, Aftershocks of the Coyote Lake, California earthquake of August 6, 1979: a detailed study: *Journal of Geophysical Research*, v. 87, p. 10637-10655.
- Sharp, R. V., 1982, Comparison of 1979 surface faulting with earlier displacements in the Imperial Valley: *U. S. Geological Survey Professional Paper 1254*, p. 213-221.
- Shimizaki, K. and T. Nakata, 1980, Time-predictable recurrence model for large earthquakes: *Geophysical Research Letters*, v. 7, p. 279-282.
- Wesson, R. L. and W. L. Ellsworth, 1973, Seismicity preceding moderate earthquakes in California: *Journal of Geophysical Research*, v. 78, p. 8527-8546.

## Figure Captions

### Figure 1.

This old figure (Wesson and Ellsworth, 1973) illustrates the simple model for the seismic source that we believe best satisfies our observations. The shaded area on the fault plane represents a region that only slips during an earthquake: an "asperity". Outside this region the fault is free to creep, and the contours schematically illustrate the build-up of strain (or a slip deficit) on the stuck patch. A major question about this model that remains to be answered is whether or not the shaded area participates in the afterslip process. If it does not, then the tractions acting on the asperity are a significant fraction of the static frictional strength.

### Figure 2.

Seismicity of the Calaveras fault before and after the M 5.8 1979 Coyote Lake earthquake from Reasenber and Ellsworth (1982). Coseismic slip contours from Liu and Helmberger (1983) are tied to the common hypocenter of the Coyote Lake earthquake. Note the striking absence of seismic activity within the coseismic source zone. Reasenber and Ellsworth proposed that this earthquake was preceded by a similar event in 1897 and noted that if the coseismic source zone was locked during the intervening 82 years, 1.2 m of slip deficit should have accumulated on the fault. Thus, within the high-slip zone, the magnitude of the fault displacement is approximately slip-predictable.

### Figure 3.

Strong support for the asperity model comes from the M 6.2 1984 Morgan Hill earthquake on the Calaveras fault. These figures, courtesy of David Oppenheimer, show the seismicity on the fault plane before and after the earthquake. The contours represent the coseismic displacements determined by Hartzell and Heaton (1986). Several authors (Cockerham and Eaton, 1984; Mendoza and Hartzell, 1988) have noted the strong anti-correlation of the coseismic slip and the aftershocks. Note also that little, if any, seismicity occurs within the coseismic source before the event. Also note that the aftershocks essentially replicate the pre-earthquake pattern. This appears to be a general feature of San Andreas system earthquakes (see also Ellsworth, 1975).

### Figure 4.

Six earthquakes of highly regular character, as revealed by their seismograms, have occurred on the San Andreas fault near Bear Valley since 1934. Reported local magnitude values range from M 4.0 to M 4.2. We believe that all six earthquakes ruptured the same spot on the fault plane, on the basis of the high coherency between the seismograms of all six events recorded on Wood-Anderson seismographs. The last three have also been compared using digitized copies of high-quality FM recordings. The cross correlation timing method of Poupinet and others (1984) has been applied to the seismograms of the 1977 and 1987 members of Set 10 for the stations shown. Joint location of the

hypocentroids of the two events places them within 32 m of each other. These two events must have ruptured the same asperity.

Figure 5.

Seismicity of the San Andreas fault in the Bear Valley - Stone Canyon region from 1971 to 1986, M 1.5. Cross section runs from northwest (left) to southeast and includes only events on the fault plane. Set 10 is located near the base of the seismic zone and underlies the source area of set 2.

Figure 6.

Cumulative moment versus time for Set 10. The recurrence intervals are neither strictly slip- nor time-predictable. For example, the 1942 earthquake occurs early, while the 1956 event occurs late. The intervals do not appear to be a Poisson random variable either, as there is a marked absence of short intervals.

Figure 7.

Spectral ratios of the horizontal components of motion recorded by the broad-band Press-Ewing at Berkeley for the 1966 and 1977 members of Set 10. The data were digitized at 20 samples/sec with a 4-pole high-cut filter applied at 5 Hz. The spectral ratios are virtually flat between d.c. and 7-8 Hz. The coherency is near unity over this band as well.

Figure 8.

Seismograms of the 1977 and 1987 members of Set 10 recorded by Calnet station CAO at a distance of 90 km. Also shown is the immediate foreshock of the 1987 earthquake. The seismograms are highly correlated at frequencies below 5 Hz. At higher frequencies there are clear differences between the higher frequency 1977 event and the lower frequency 1987 event. Note that the high frequency character of the foreshock virtually eliminates all but a source effect to explain the difference.

Figure 9.

Spectral ratio of mainshock seismograms at station CAO for the 1977 and 1987 members of Set 10. The data were digitized at 100 samples/sec. Differences between the two records are greatest near 8 Hz. Contrast this spectral ratio with the one obtained for the 1966 - 1977 pair, as shown in figure 7.

Figure 10.

The circular crack model of Keilis-Borok (1959) can be used to place a bound on the minimum stress change produced by an earthquake within the region of coseismic displacement. For this model, the stress drop is constant within the rupture surface. All other models must have a larger stress change at some point within the slip surface. Application of this bound to Set 10 indicates that the stress drop must locally be a large fraction of the static frictional stress. The critical assumption here is the association of the potential slip (i.e. length of the interseismic period times the long-term slip rate) with the peak slip. If the asperity

continues to slip after the earthquake is over, the stress drop will be overestimated by this method.

Figure 11.

Map and cross section showing the mainshock location for ten sets of earthquakes in the Stone Canyon region exhibiting repeating behavior. Set 10 is the same as described above. The 38 events belonging to these ten sets represent all of the events  $M \geq 4.0$  known to locate on the San Andreas fault in this region. All unpaired  $M \geq 4.0$  events that have occurred since the establishment of the local seismographic network in 1970 locate to the northeast of the fault and have been omitted from this figure.

Figure 12.

Wood-Anderson seismograms recorded at Mt. Hamilton form the primary basis for associating the members of each event set. These seismograms for two members of Set 9 display the high coherence required for association throughout the legible portion of the records. The differences between different families are so large that there is virtually no chance of erroneously associating two events.

Figure 13.

Aftershocks of three Bear Valley earthquakes classified as members of Set 2. These events exhibit the least characteristic behavior of all events examined. Also included in Set 2 is the 1951 earthquake, which appears to be essentially the same as the 1972 event, on the evidence of their seismograms. The third cycle of slip on this part of the fault deviated from the prior pattern when the northwestern half of the 1972 zone failed in 1982. Four years later, the other half of the zone ruptured in an event that initiated at or near the 1972 hypocenter. It is of some note that the sum of the moments of the 1982 and 1986 events total only 40% of the moment of the 1972 event. Approximately half, but not more, of the moment discrepancy can be explained by slip-predictable behavior, given the relatively short intervals following the 1972 event.

Figure 14.

Table of Stone Canyon region repeating earthquake sets.

Figure 15.

Relative seismic moment distribution for Stone Canyon earthquake sets. All moments have been normalized for each set. Note that the small magnitude tail is due to Set 2.

Figure 16.

Relative interevent time distribution for Stone Canyon earthquake sets with 3 or more members. Histograms are shown for the observed distribution (top), and for the intervals computed using the time-predictable model and the slip-predictable model of Shimizaki and Nakata (1980). The model calculations have been made in two ways: first assuming that the coseismic slip is proportional to the seismic moment (constant

source area); alternatively assuming that the stress drop is constant. S.D. is the standard deviation of the mean. The results display a slight preference for slip-predictable behavior. Note also that the observed interevent time distribution does as well or better at forecasting the time of the next event as the time-predictable model. This is not to imply that time-predictability is disproven. Rather, knowledge of more than the gross properties of past earthquakes will be needed if it is to be of practical value.

Figure 17.

Repeating earthquake behavior is not restricted to the central San Andreas fault. Multiple repetitions of the same source also occur on volcanoes. This example from Frémont and Malone (1987) illustrates seismograms for some of the 73 members of multiplet M0. Relative locations for the centroids of these events (right) imply that the same source is repeating itself time and time again as the volcano strains immediately prior to a dome-building eruption.

Figure 18.

The 1940 and 1979 Imperial Valley earthquakes were both recorded by the same strong motion instrument located 6.5 km southwest of the Imperial fault. Contours on the fault plane show the coseismic dislocation determined by Hartzell and Heaton (1983) for the 1979 event from an extensive array of strong motion instruments in the region. Surface slip along the Imperial fault generalized from Sharp (1982) compares and contrasts the slip north of the U.S.-Mexican border. While the 1940 event was substantially larger, extending well to the south of the international border, the similarity in the surface slip in 1979 with the overlapping part of the 1940 rupture raises the question of their similarity at depth.

Figure 19.

Accelerograms recorded by station El Centro #9 in 1940 (NS 40 and EW 40) and 1979 (NS 79 and EW 79). Note the overall similarity in amplitude, frequency content and duration for the first 8 seconds of both records (Porcella and others, 1982).

Figure 20.

Preliminary comparison of a portion of the north-south accelerograms for the 1940 and 1979 Imperial Valley earthquakes. The 2.56 s window of data used is highlighted. The spectral ratio (upper plot) and coherency (lower plot) display a high degree of correlation in the 3.5 - 6 hz band. The preceding window (not illustrated) also shows a similar degree of correlation, but has slightly different timing, arriving  $\frac{1}{4}$  sec. earlier in 1979 than in 1940. If each subevent is produced by the rupture of the same collection of asperities, then minor variations in the phasing of rupture within the common collection of asperities comprising each event could account for the differences between the seismograms.

Figure 1.

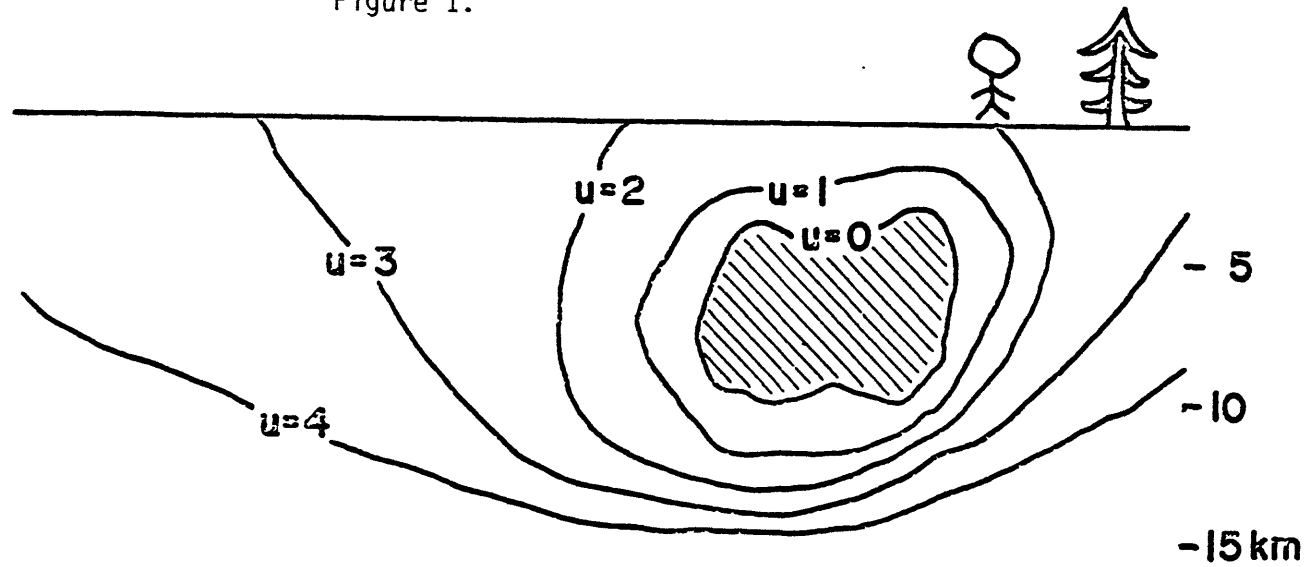


Figure 2.

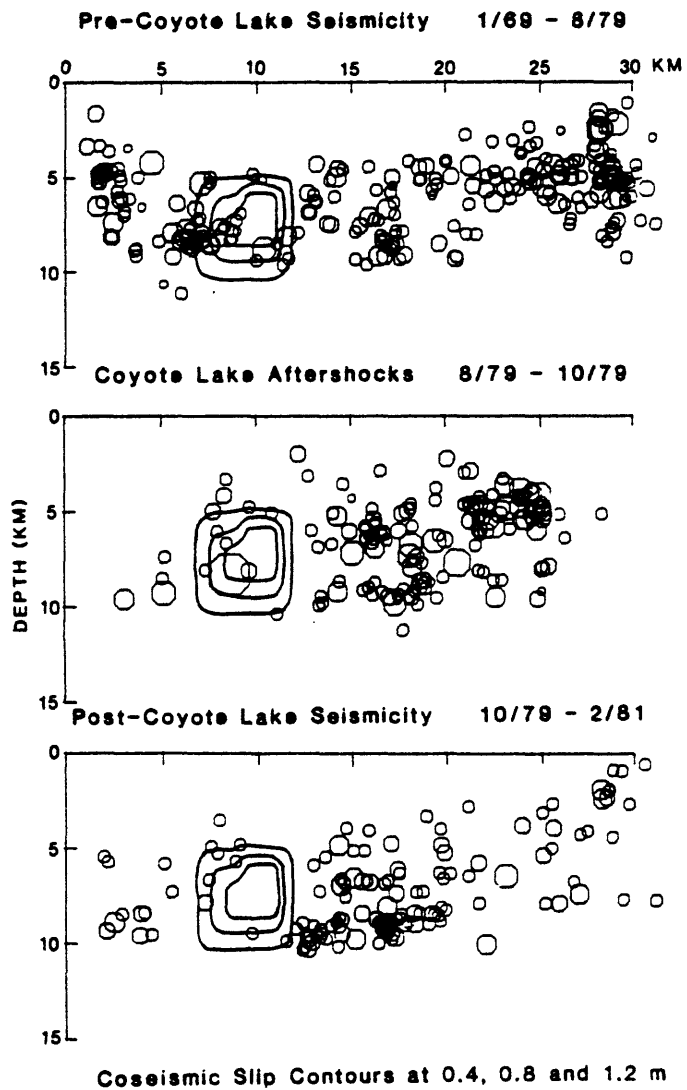


Figure 3.

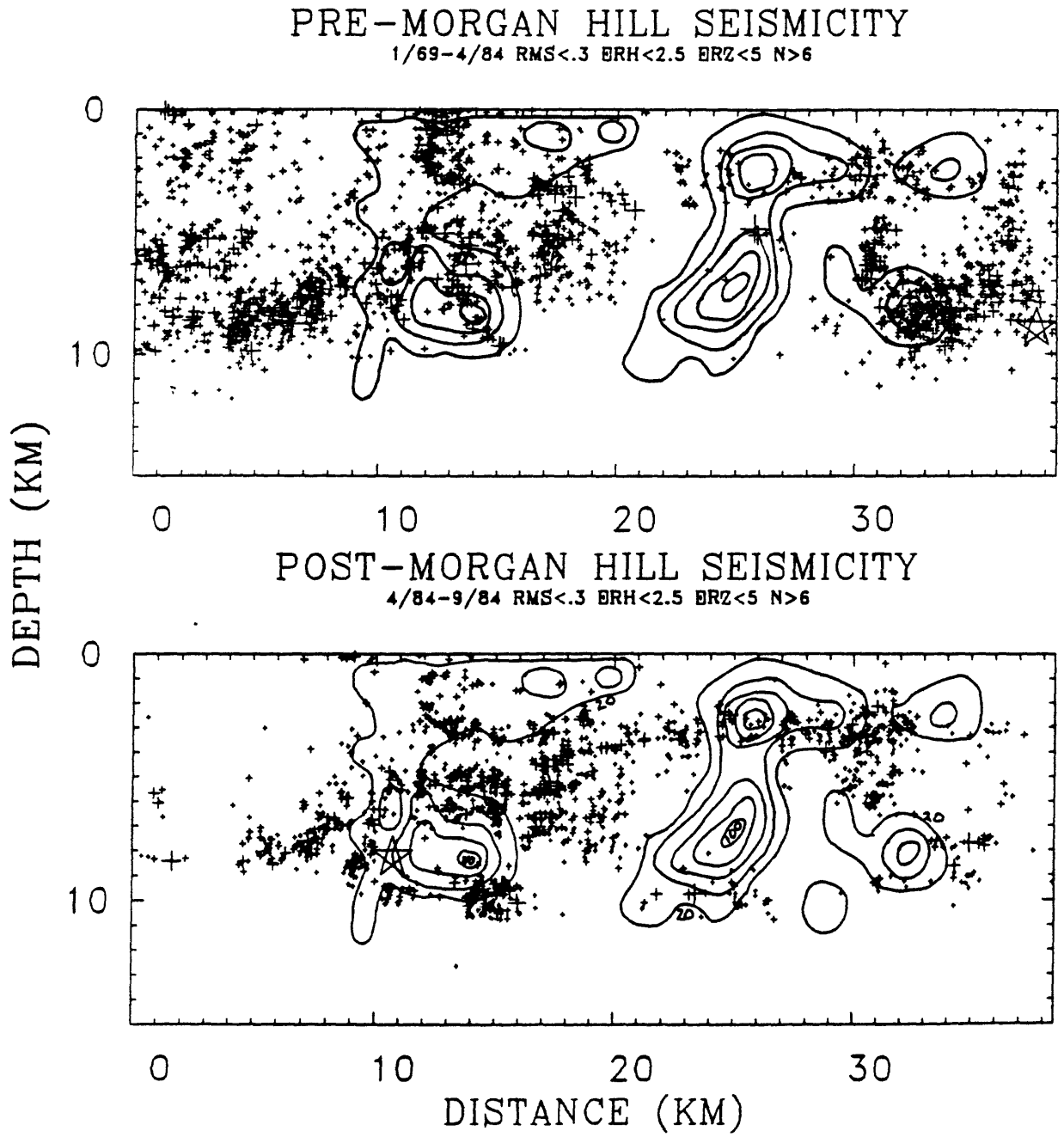


Figure 4.

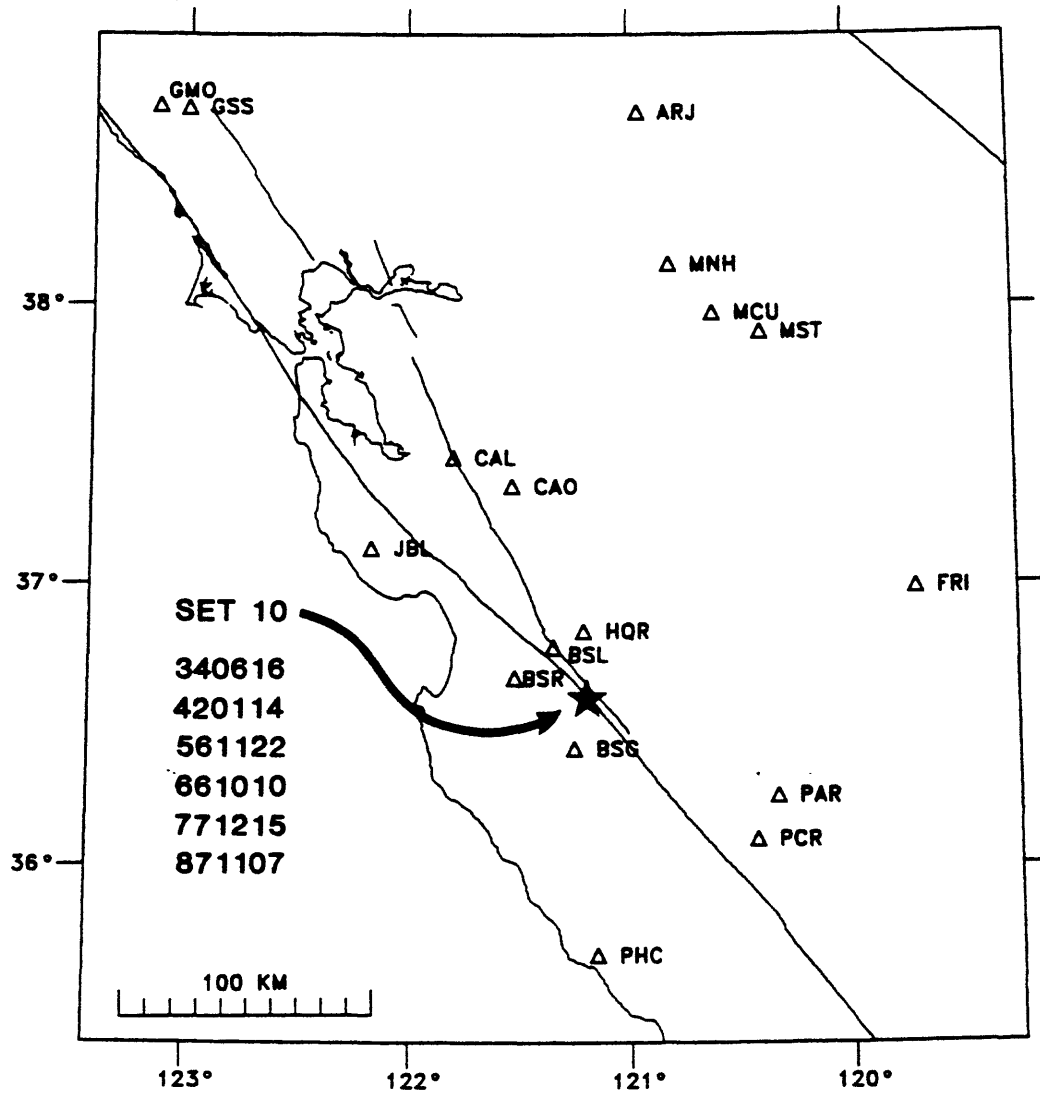


Figure 5.

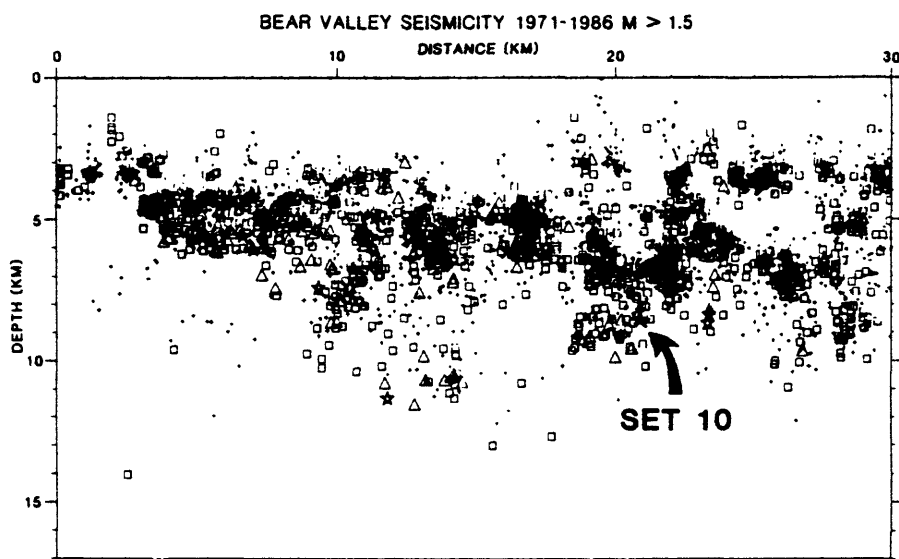


Figure 6.

# SET 10

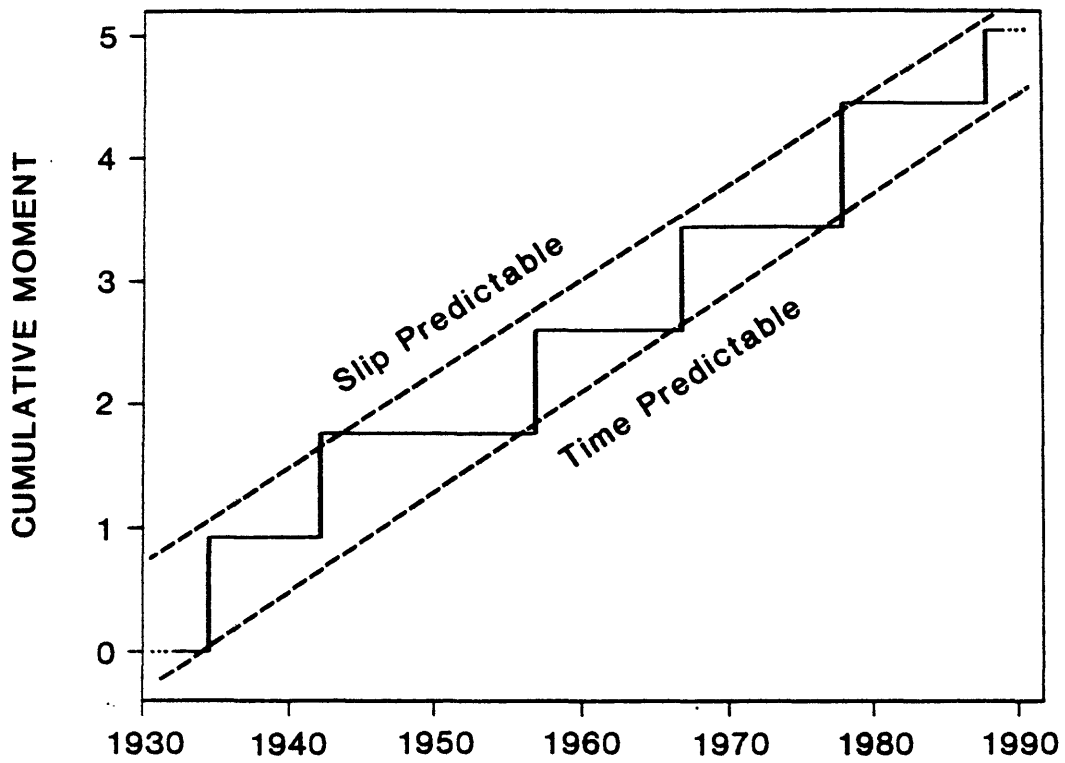


Figure 7.

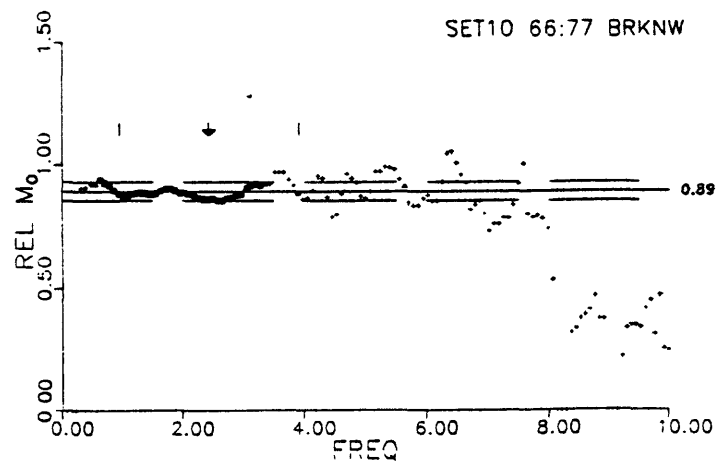
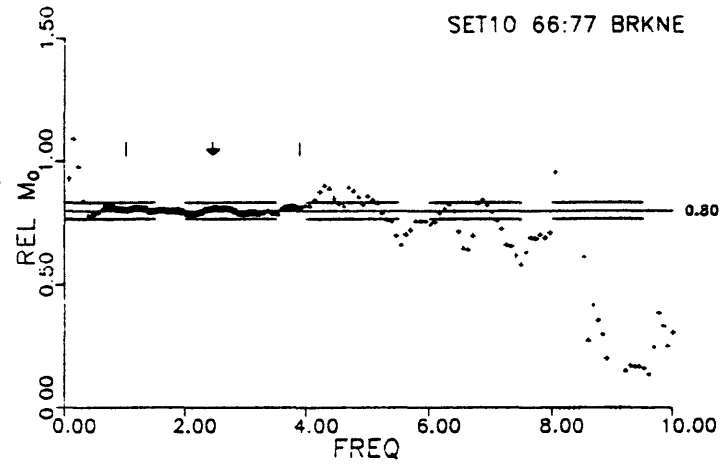


Figure 8.

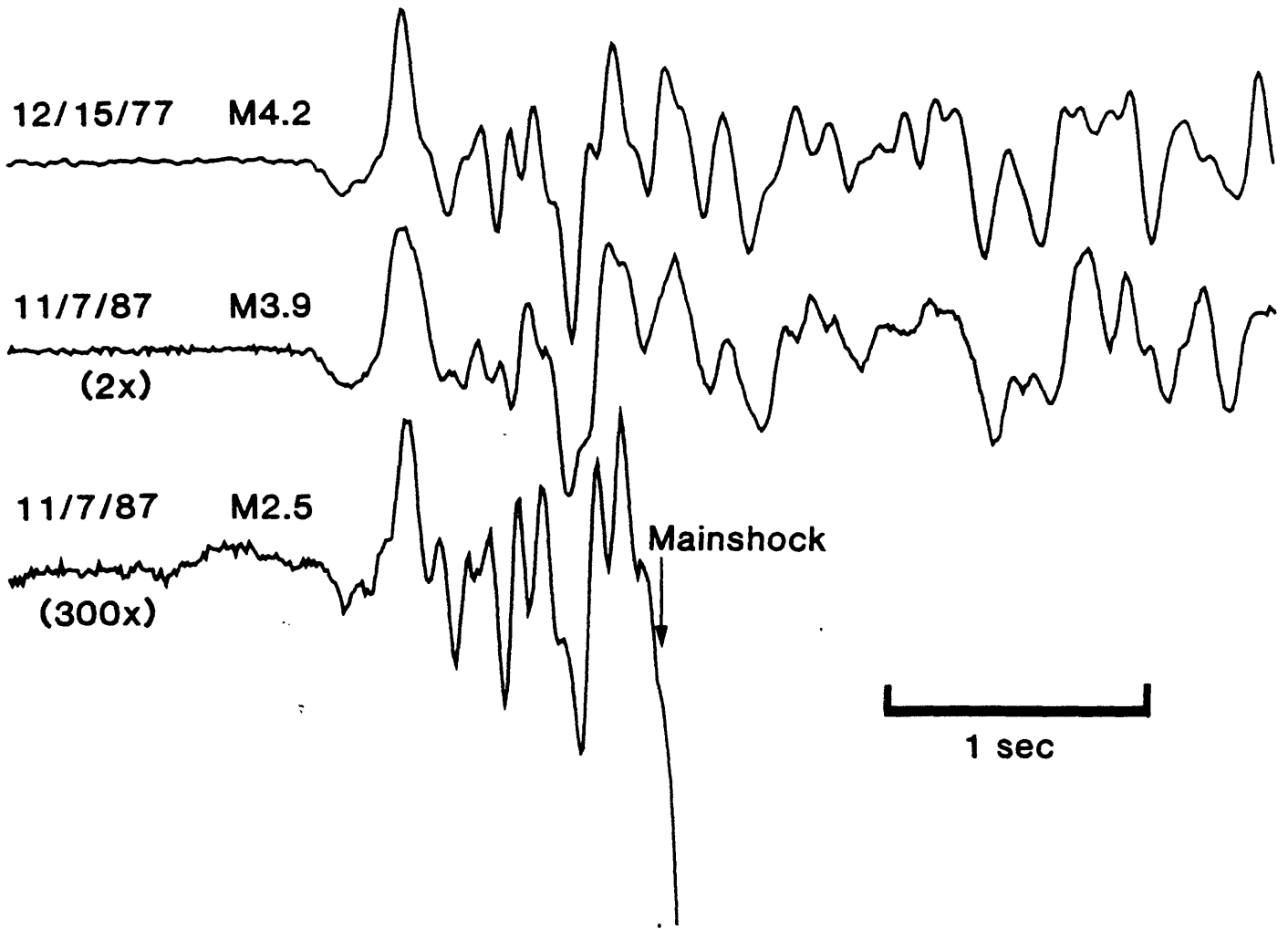


Figure 9.

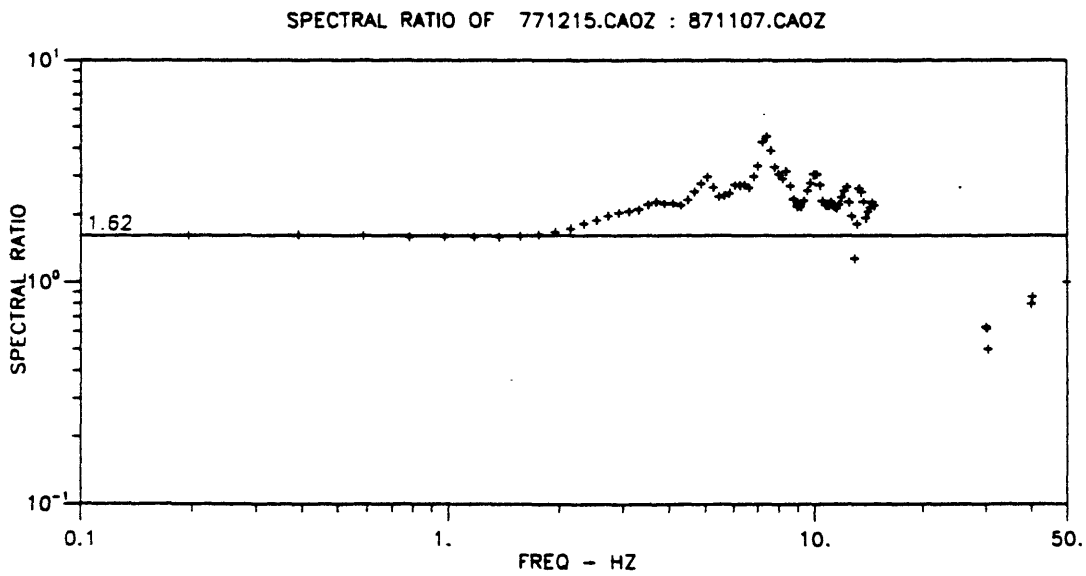


Figure 10.

## Bounds on Stress Drop

### Assumptions:

1. Some point on the fault remains locked during the interevent period.
2. Coseismic slip at this point = slip rate ( $\dot{u}$ )  $\times$  time interval ( $\Delta t$ ).

If we know  $M_0$ , the stress drop for a circular crack model (Keilis-Borok, 1959) can be written as a function of  $M_0$ ,  $\dot{u}$  and  $\Delta t$ .

$$\Delta\sigma = \frac{7}{16} \left( \frac{2}{3} \pi \mu \dot{u} \Delta t \right)^{\frac{3}{2}} M_0^{-\frac{1}{2}}$$

### 1977 Earthquake:

$$M_0 = 7 \times 10^{21} \text{ dyne-cm}$$

$$\Delta t = 11 \text{ years}$$

$$\dot{u} = 2.5 \text{ cm/a}$$

$$\Delta\sigma = 375 \text{ bars}$$

### 1987 Earthquake:

$$M_0 = 4 \times 10^{21} \text{ dyne-cm}$$

$$\Delta t = 10 \text{ years}$$

$$\dot{u} = 2.5 \text{ cm/a}$$

$$\Delta\sigma = 430 \text{ bars}$$

Figure 11.

# REPEATING EARTHQUAKES NEAR STONE CANYON, CALIF.

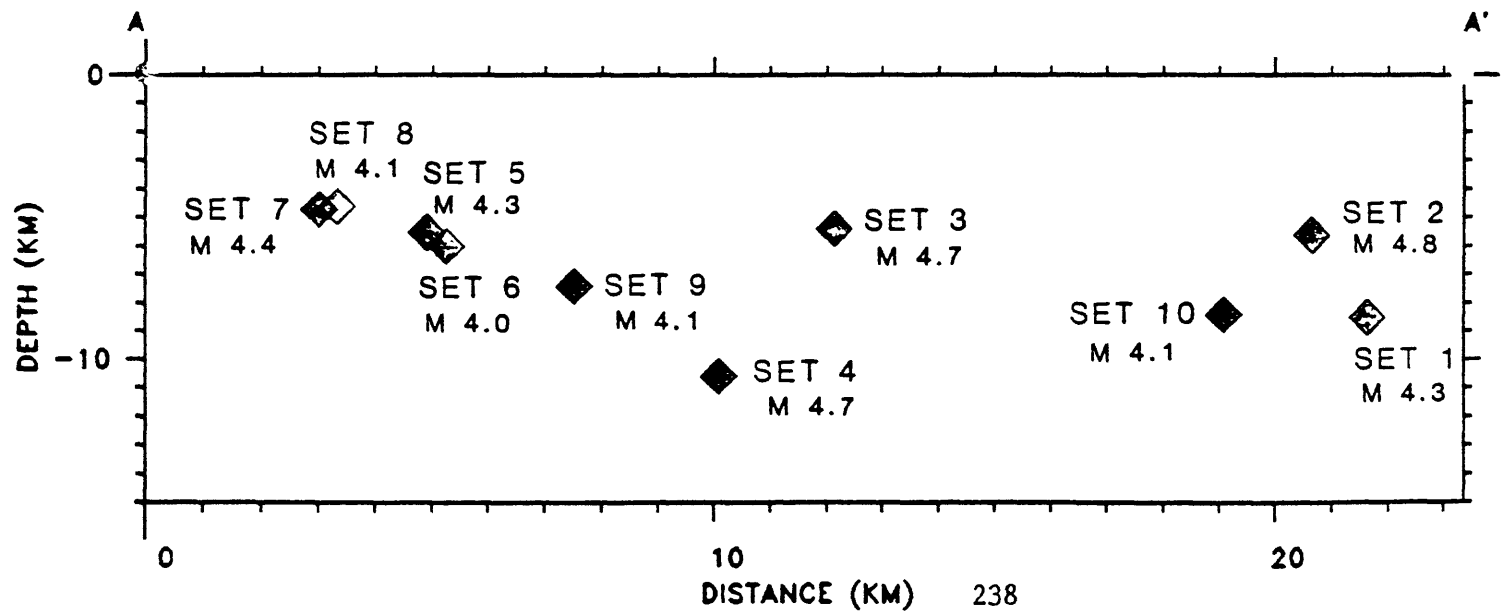
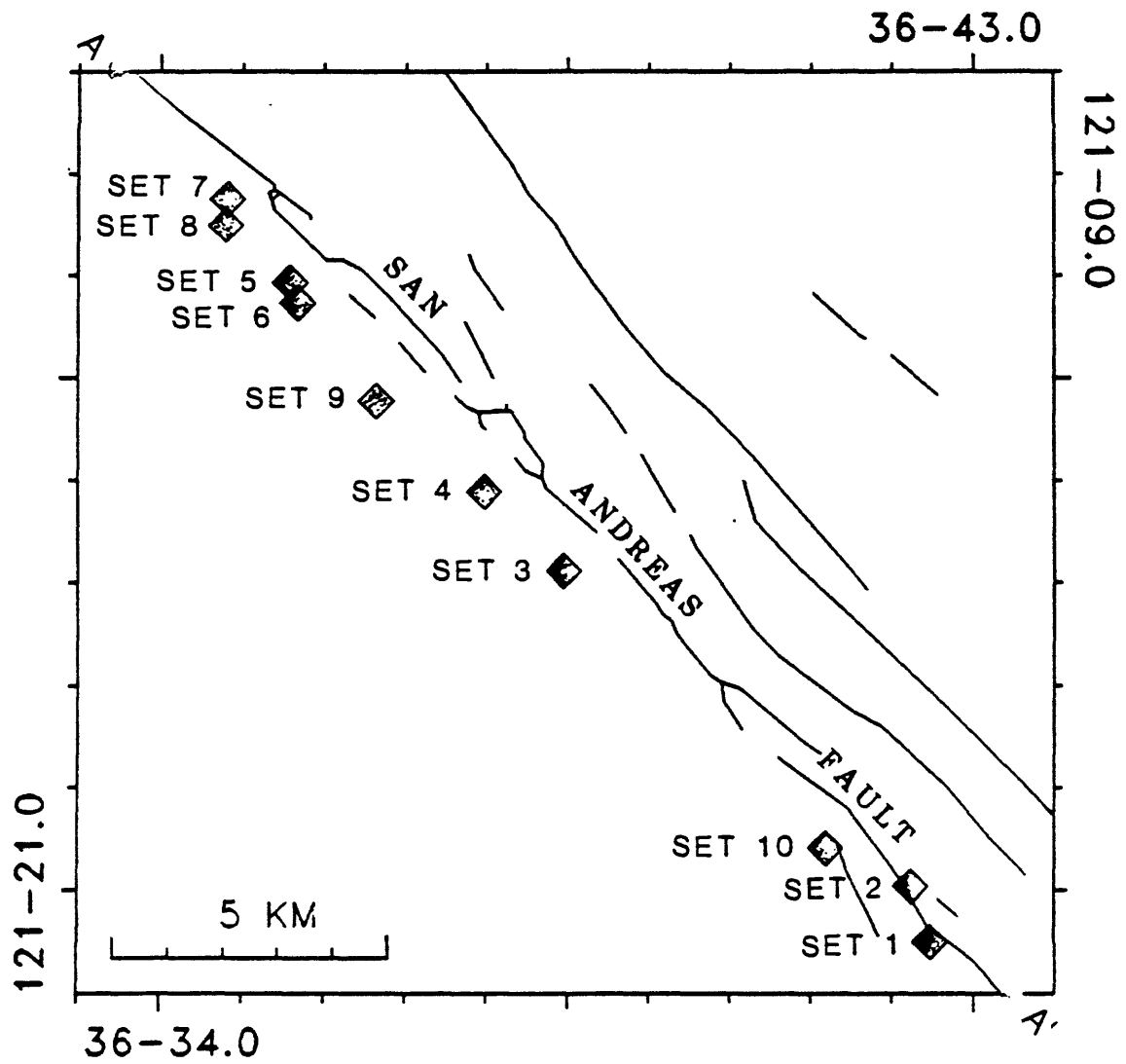
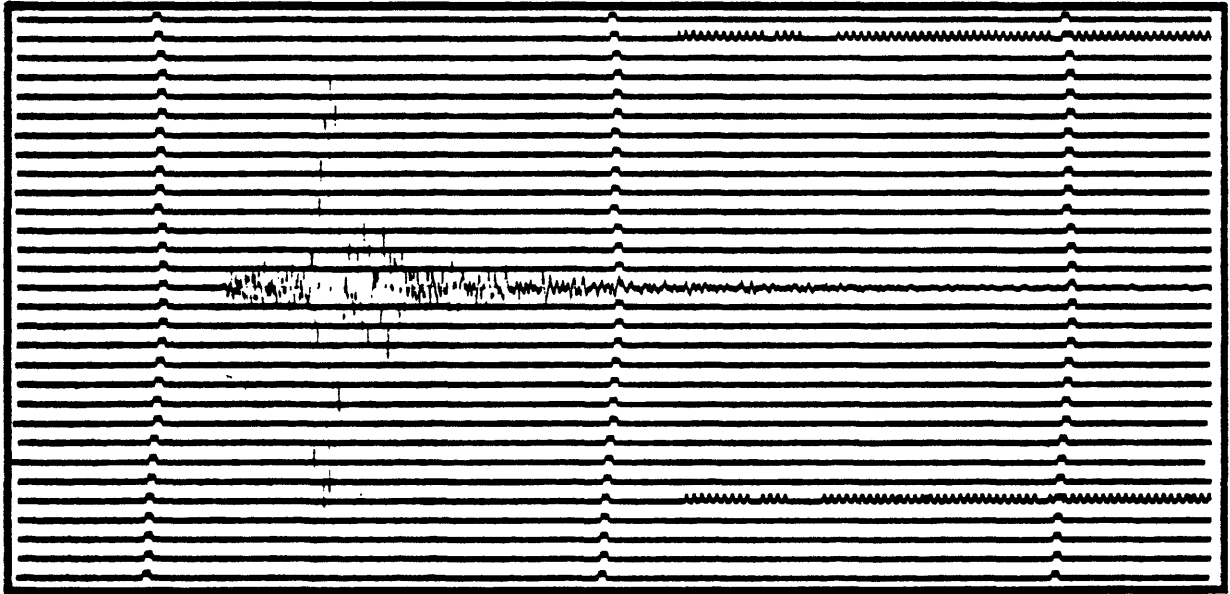


Figure 12.

MHC Wood-Anderson EW

650914 0909



820831 0311

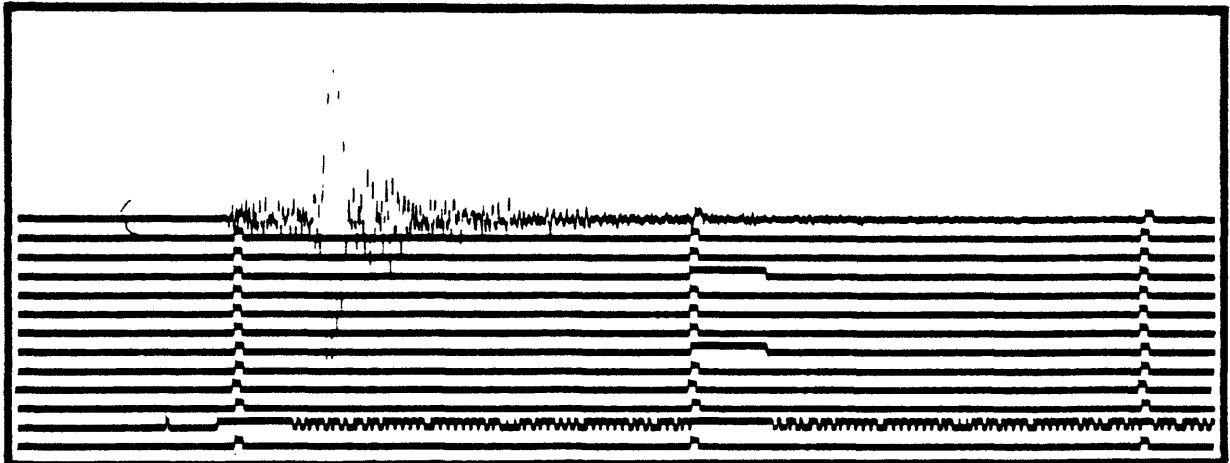


Figure 13.

# SET 2 3 DAYS OF AFTERSHOCKS (M>1.2)

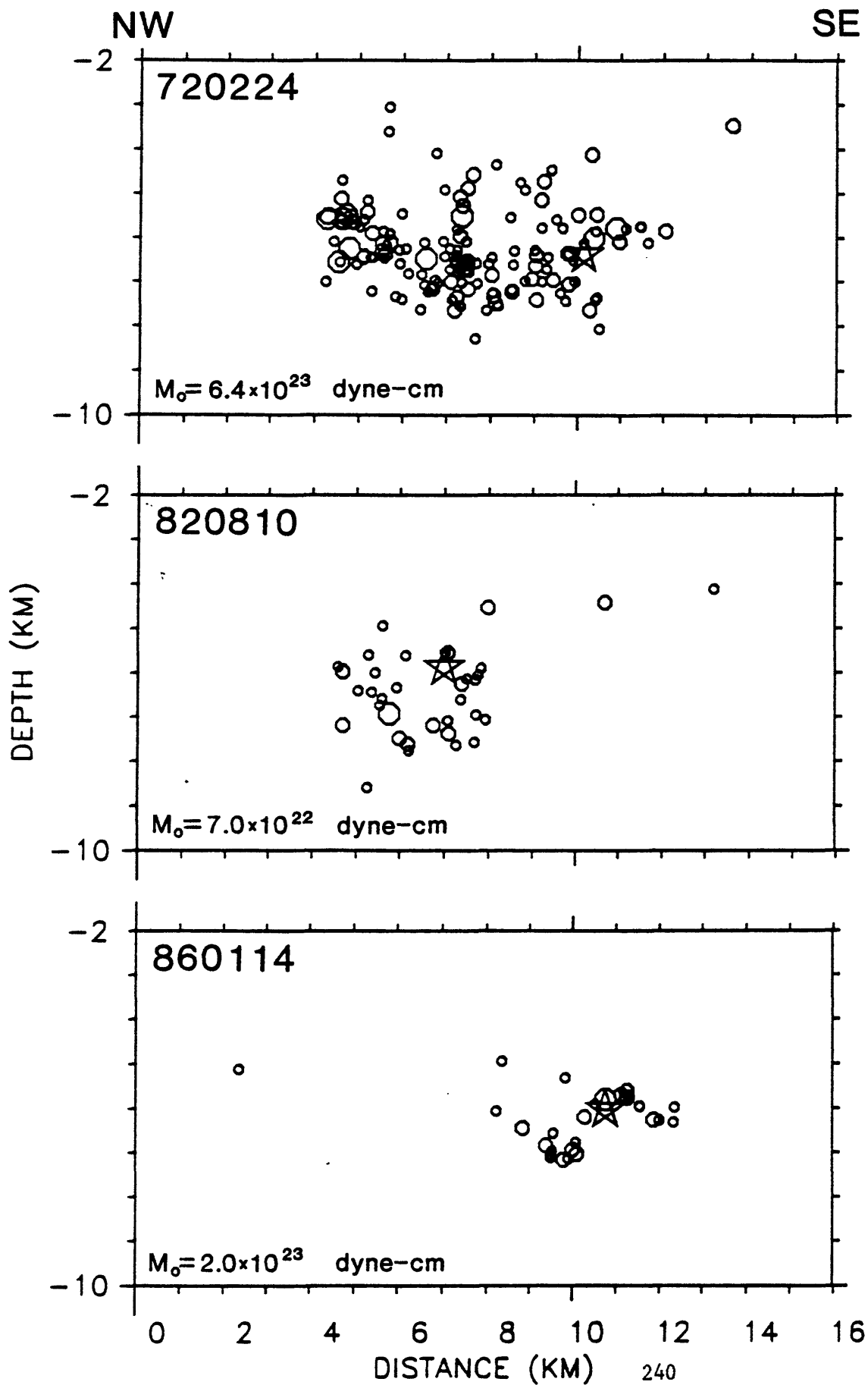


Figure 14.

## STONE CANYON CHARACTERISTIC EARTHQUAKE SETS

| SET | LATITUDE<br>N | LONGITUDE<br>W | DEPTH<br>km | DATE<br>yrmo da hrmm | M <sub>L</sub> |
|-----|---------------|----------------|-------------|----------------------|----------------|
| 1   | 36-34.50      | 121-10.53      | 8.5         | 370217 0333          | 4.3            |
|     |               |                |             | 540327 1543          | 4.4            |
|     |               |                |             | 730622 0129          | 4.2            |
|     |               |                |             | 841005 1616          | 4.1            |
| 2   | 36-35.04      | 121-10.77      | 5.6         | 510729 1053          | 5.1            |
|     |               |                |             | 720224 1556          | 5.1            |
|     |               |                |             | 820810 0211          | 4.3            |
|     |               |                |             | 860114 0309          | 4.5            |
| 3   | 36-38.12      | 121-14.98      | 4.9         | 510806 0905          | 4.7            |
|     |               |                |             | 720904 1804          | 4.7            |
|     |               |                |             | 860531 0847          | 4.5            |
| 4   | 36-38.89      | 121-16.03      | 11.3        | 380927 1223          | 4.9            |
|     |               |                |             | 820811 0746          | 4.5            |
| 5   | 36-40.93      | 121-18.42      | 5.5         | 371027 1553          | 4.3            |
|     |               |                |             | 480427 2022          | 4.6            |
|     |               |                |             | 560218 2358          | 4.1            |
|     |               |                |             | 730115 0943          | 4.1            |
| 6   | 36-40.73      | 121-18.32      | 6.0         | 371027 2025          | --             |
|     |               |                |             | 480427 2032          | --             |
|     |               |                |             | 560219 0006          | 3.8            |
|     |               |                |             | 730115 1023          | 3.7            |
|     |               |                |             | 820924 0805          | 4.3            |
| 7   | 36-41.75      | 121-19.19      | 4.7         | 400907 1302          | 4.3            |
|     |               |                |             | 540622 1250          | 4.4            |
| 8   | 36-41.49      | 121-19.21      | 4.6         | 400907 1038          | 4.1            |
|     |               |                |             | 540622 1149          | 4.4            |
|     |               |                |             | 711229 0025          | 3.9            |
|     |               |                |             | 800306 1105          | 4.0            |
| 9   | 36-39.78      | 121-17.36      | 7.4         | 381024 1339          | 4.1            |
|     |               |                |             | 480111 0537          | 4.1            |
|     |               |                |             | 650914 0909          | 4.0            |
|     |               |                |             | 820831 0311          | 4.1            |
| 10  | 36-35.41      | 121-11.82      | 8.4         | 340616 2303          | 4.0            |
|     |               |                |             | 420114 0944          | 4.0            |
|     |               |                |             | 561122 1643          | 4.2            |
|     |               |                |             | 661010 0653          | 4.1            |
|     |               |                |             | 771215 1115          | 4.2            |
|     |               |                |             | 871107 1506          | 4.0            |

Figure 16.

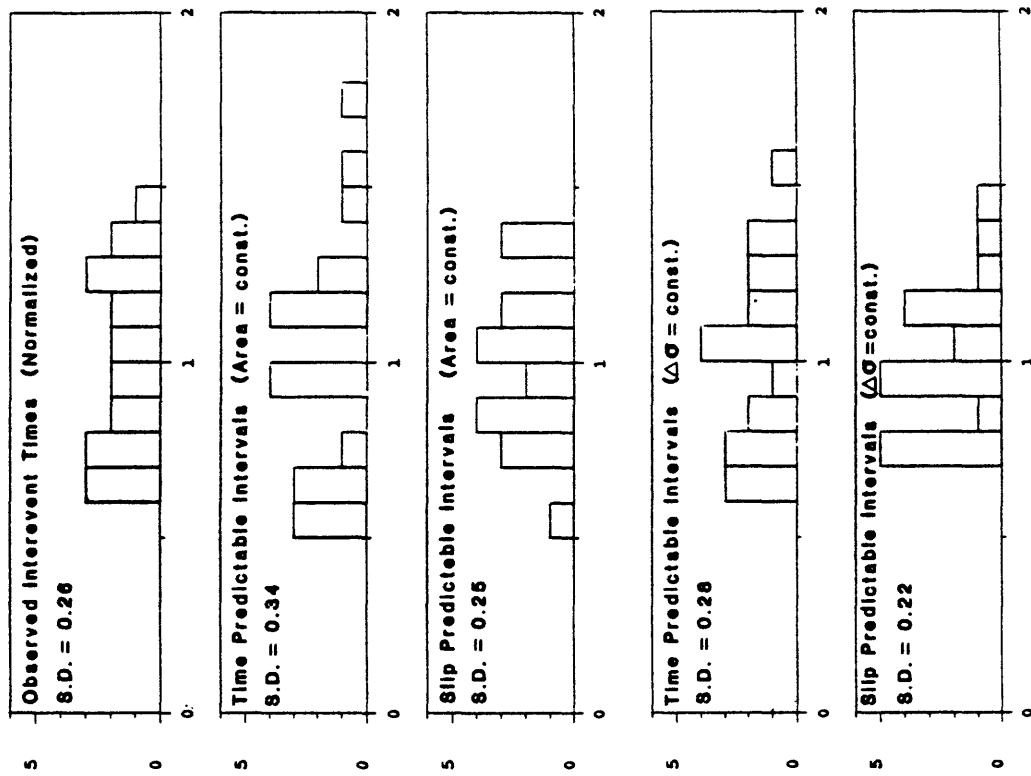
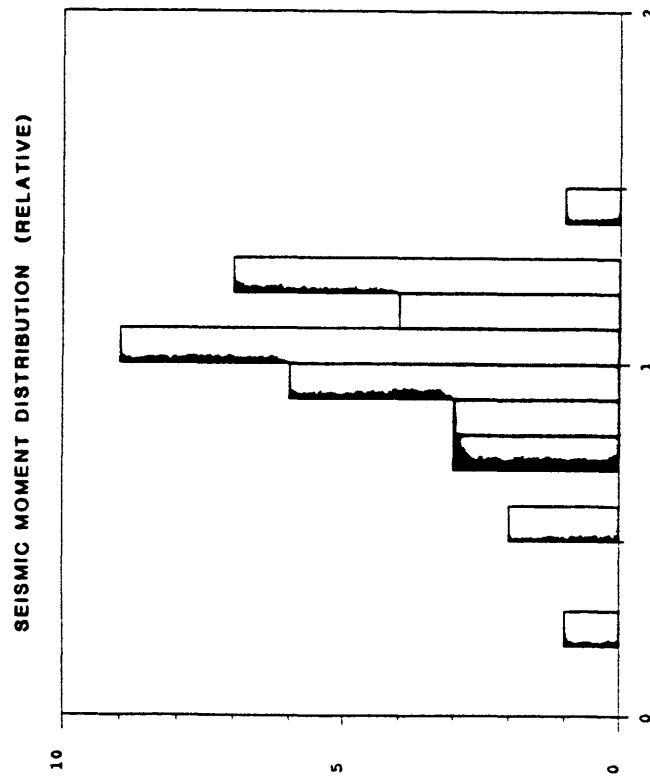


Figure 15.



Pre-Eruption Earthquake Multiplet Mt. St. Helens

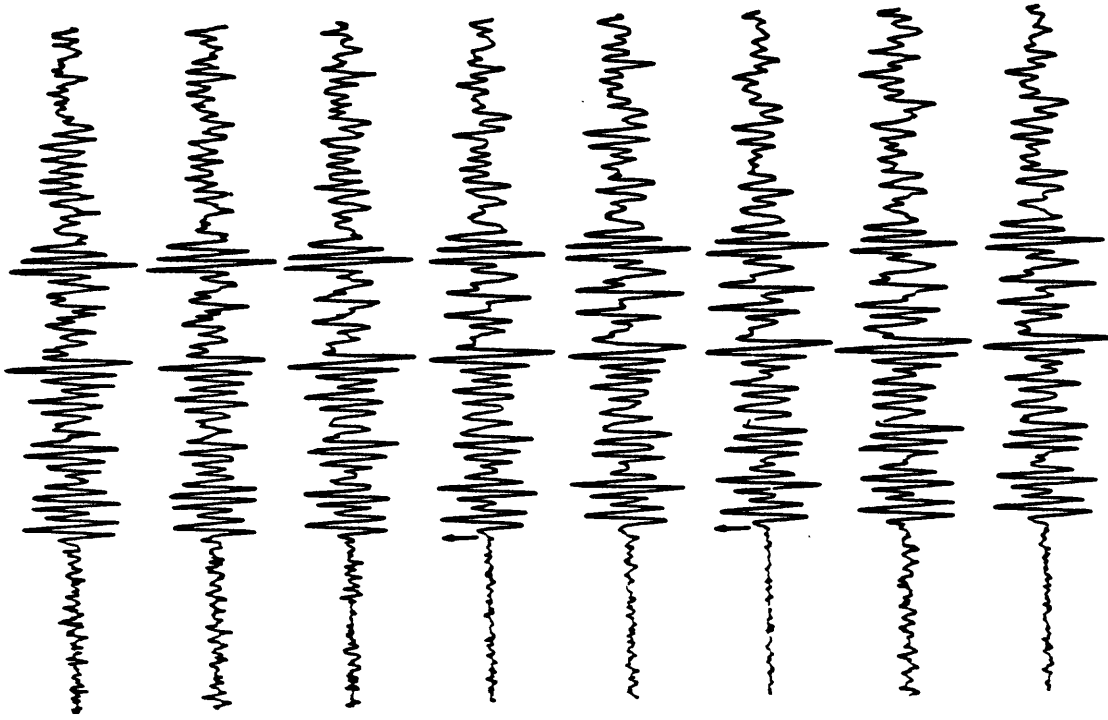
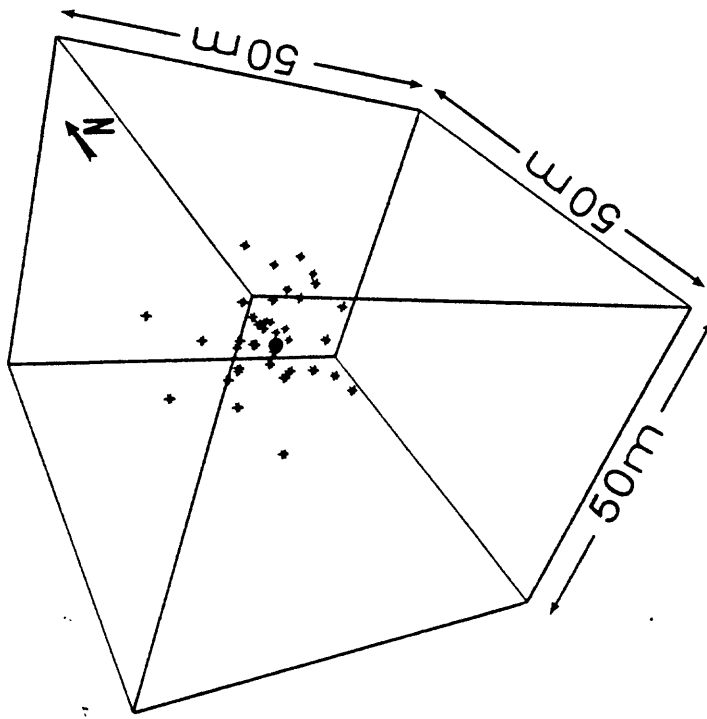


Figure 17.



Joint Centroid Determination

Figure 18.

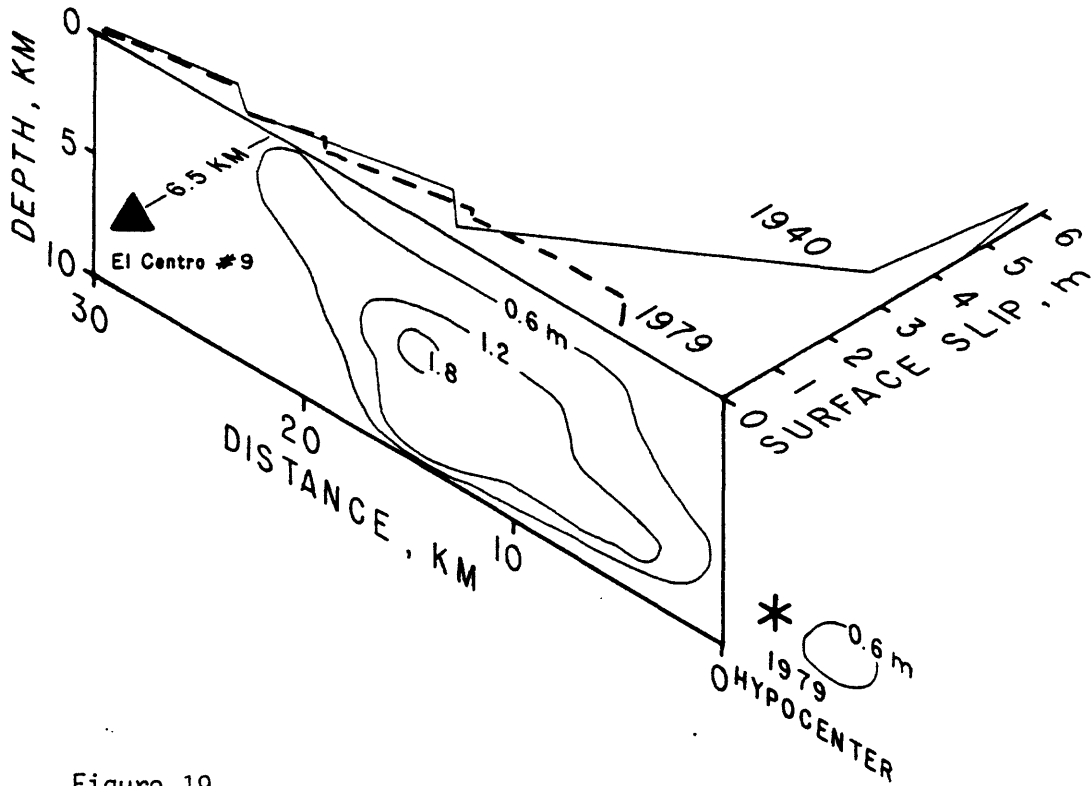


Figure 19.

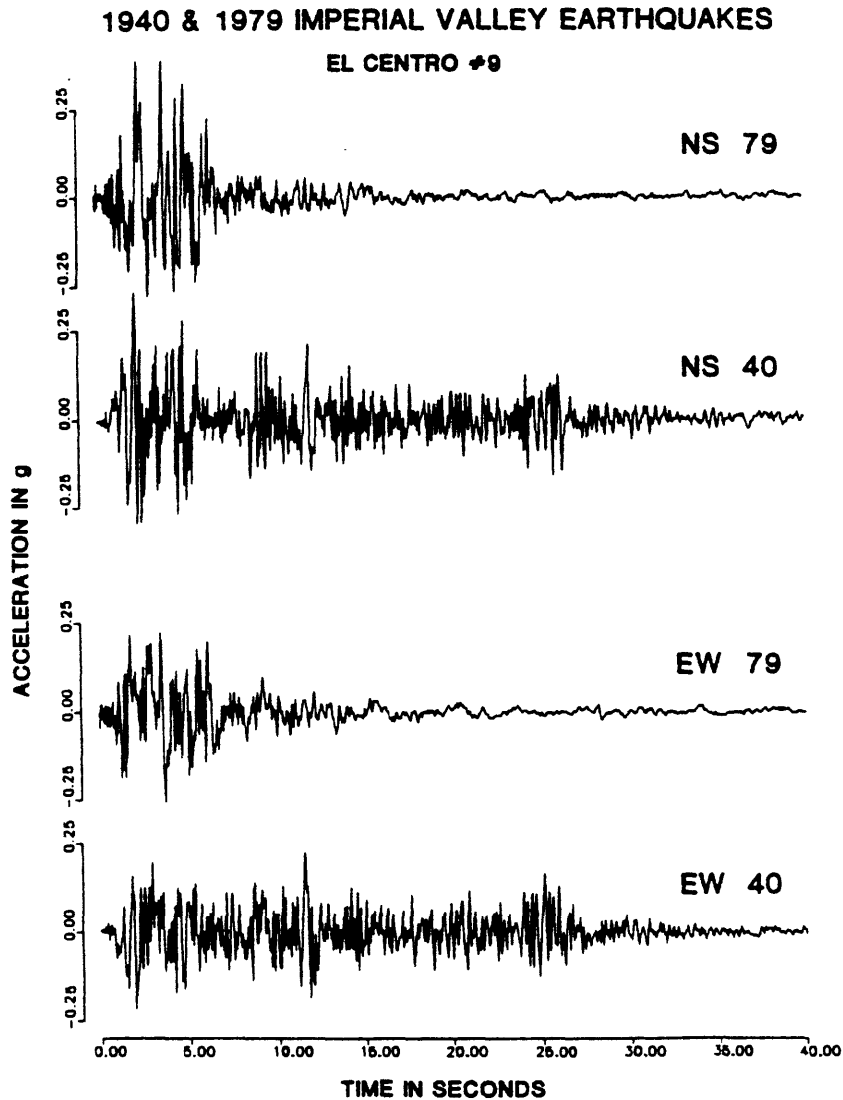
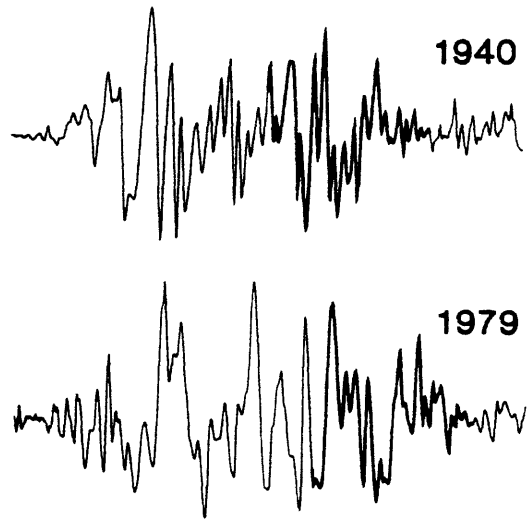
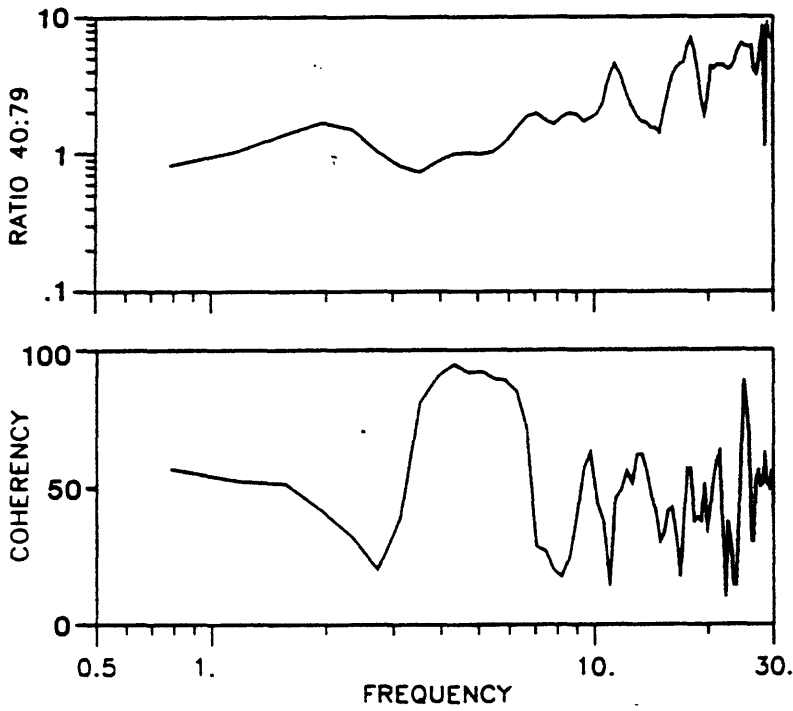


Figure 20.

### EL CENTRO #9 NS



## Gravity Studies of Active Faults in Japan

YUKIO HAGIWARA

Earthquake Research Institute, University of Tokyo

In the beginning of nineteen eights, the gravity studies of active faults was relatively quiescent in Japan. By contrast, the years since the 5th National Project for Earthquake Prediction (1984-1988) have been bursting with new applications of the gravity method and development of interpretation. The first outburst was a gravimetric discovery of the seismogenic fault of the 1984 Western Nagano Prefecture Earthquake by Nagoya University surveyors. Since then university mobile surveys have intensified gravity studies of active faults. We introduce here the highlights of the gravity work conducted by the Earthquake Research Institute for the past three years.

### Residual Gravity Anomaly

Separation of gravitational attraction of shallow subsurface structures from the Bouguer anomaly is mostly made by two-dimensional space-domain filtering techniques. The residual Bouguer anomaly obtained by subtracting the lowpass-filtered anomaly from the original Bouguer anomaly can reflect the shallow structures. We use a two-dimensional lowpass filter with the cut-off wavelength of 160 km to obtain the residual Bouguer anomaly. The reason why we adopt the wavelength of 160 km is that the topography of long wavelengths over 160 km is related to isostasy (Tsuboi and Yamaguchi, 1940). The shorter wavelength topography can be sustained by the crustal elasticity.

We made a nationwide color map of the residual Bouguer anomaly of Japan. In Fig. 1, shallow earthquake epicenters and active faults are plotted on the residual Bouguer anomaly map. We see in this map that active faults are mostly located on negative anomaly zones (green zones in the original color map), and that shallow earthquakes are much more active in those zones.

Fig. 2(a) shows shallow microearthquake epicenters on the residual Bouguer anomaly map of the northern part of the Tohoku district. The related seismic energy releases are also shown in Fig. 2(b). It is clear that both the shallow microearthquake epicenters and their energy releases coincide very well with the negative anomaly zones. The breaking point of upper-crustal materials against the tectonic stress may be relatively low in the negative anomaly zones. In the Tohoku district, the positive anomaly zones in most cases are found on outcropped or shallow-seated granitic or basic rocks, while the negative anomaly zones on volcanic or sedimentary layers.

Ishida and Hasemi (1988) have recently pointed out as a result of the three-dimensional velocity analysis that relatively high velocity zones coincide with positive residual Bouguer anomaly zones.

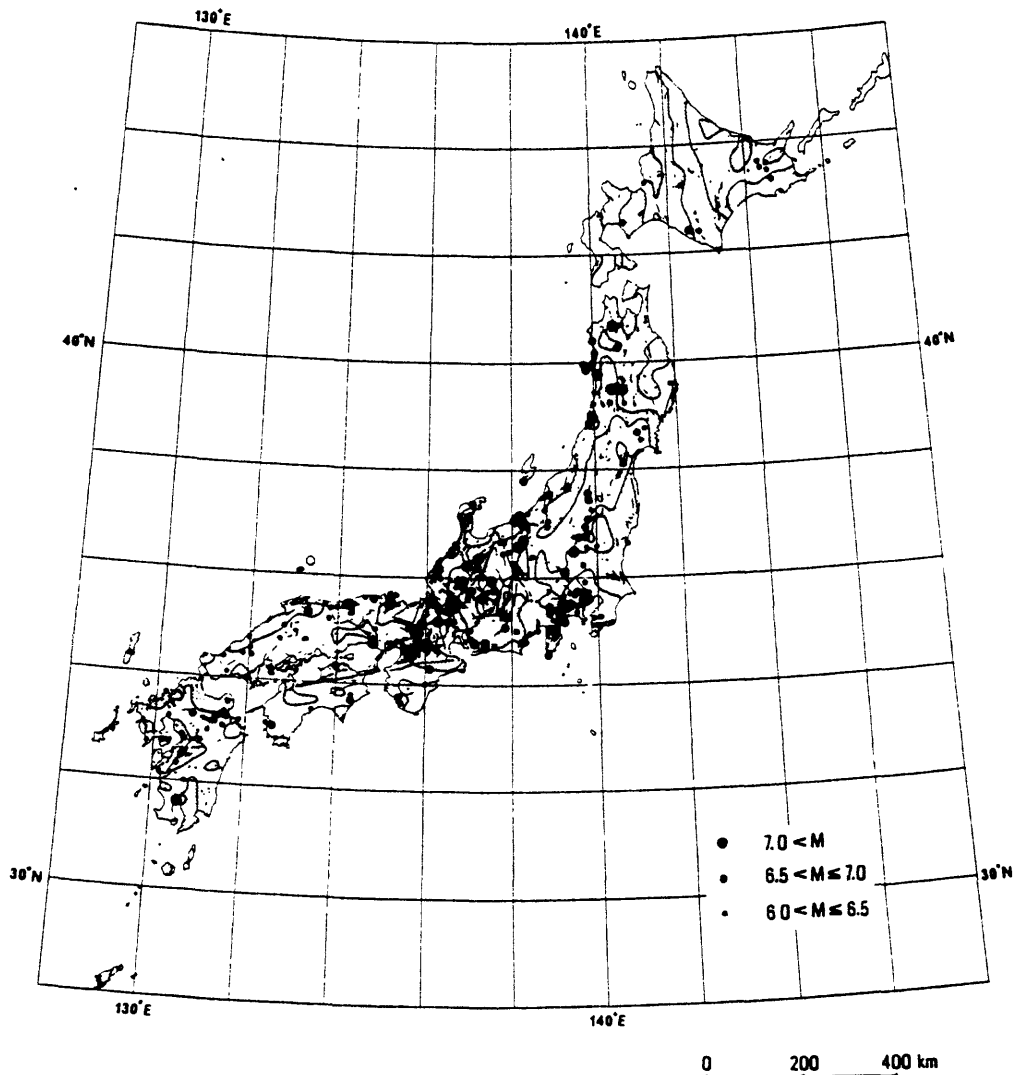


Fig. 1. Residual Bouguer anomaly of Japan (the shaded areas represent positive), active faults discovered by geological surveys, and epicenters of destructive earthquake ( $M \geq 6.5$ ) occurred before 1884 and shallow earthquakes (0-20 km) occurred for the period 1885-1986.

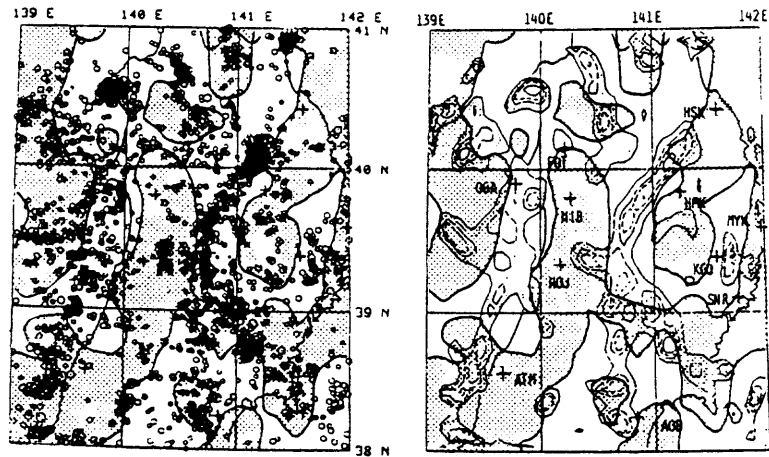


Fig. 2. (a) Epicenters of shallow microearthquakes (0-20 km) in the northern part of the Tohoku district for the period 1976-1982, and (b) the accumulated seismic energy (minimum contour indicates  $10^{10}$  erg and its increment is  $10^2$  erg; Ishii et al., 1983) plotted on the residual Bouguer anomaly map (the shaded areas represent positive).

#### Gravity Surveys for Active Faults

During the period of the 5th National Project for Earthquake Prediction (1984-1988), university mobile surveys have conducted gravimetries for tracing and detecting active faults. Most of the efforts were concentrated on Central Japan. Here we introduce the gravity survey result obtained around the Kushibiki fault in the western Kanto district.

Abe (1974) determined a 20 km-long seismogenic fault model for the 1931 West Saitama Earthquake of M7.0. Its epicenter is just located on the Kushibiki fault, but the length of 20 km is much longer than that estimated from geological surveys. For tracing the extension of the fault we made detailed gravity survey over there. We see in the Bouguer anomaly map (Fig.3) that the fault "KS" cuts the slope of the massive Paleozoic block at an acute angle and extends northwest- and southeastward for about 20 km in totality. The present gravity survey proves useful for discovering an active fault concealed by overburden.

The vertical displacement of the Kushibiki fault is about 1 m on the ground surface. According to Abe's model, the fault slip is left-lateral, but there is no geological evidence of any lateral slip. The Bouguer anomaly indicates that Ara River changes stream leftward at the site where the southeastern extension of the fault crosses it. That fact is considered to be one of the evidences of the left-lateral slip motion.

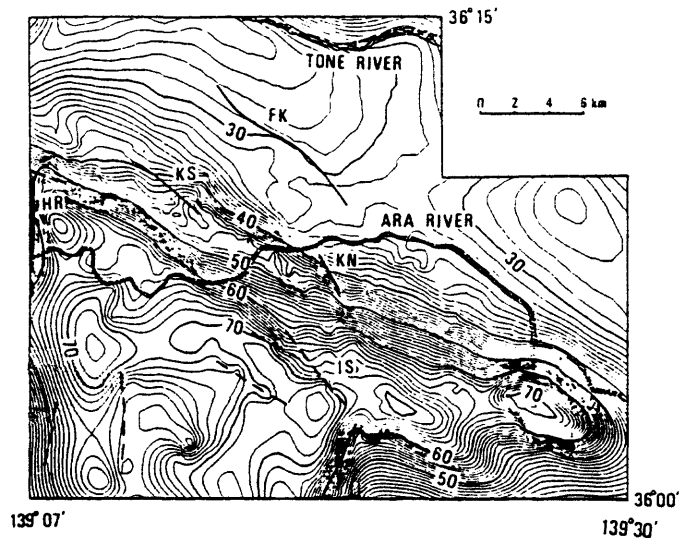


Fig. 3. Bouguer anomaly (unit:mgal) around the Kushibiki fault.  
 FK : Fukaya fault HR : Hirai fault KS : Kushibiki fault  
 KN : Konan fault IS : Imaichi-Sugaya fault

#### Gravity Field Change during Volcanic Eruption

Following the summit eruption, a fissure eruption took place on the Izu-Oshima volcano in November 1986. The Geographical Survey Institute and the Earthquake Research Institute conducted levelling surveys and detected coeruptive elevation change. As seen in Fig. 4(a), a subsidence zone runs in the NW-SE direction parallel to the fissure. Concurrently high-precision gravity surveys were repeated to detect the related gravity change (Fig. 5(a)).

Okubo and Watanabe (1988) presented a physical model explaining both the gravity and elevation changes. The model assumes (1) a spherical pressure source and (2) formation of a fracture zone where a large number of microcracks open. The density of the crack-filling material is estimated to be  $0.3$  to  $1.3 \text{ g/cm}^3$ , which is far smaller than the value expected from the dyke-intrusion model. We see the almost perfect coincidences between the observed elevation change (Fig. 4(a)) and the calculated one (Fig. 4(b)) based on the fracture model and between the observed gravity change (Fig. 5(a)) and the calculated one (Fig. 5(b)).

The northwestern extension of the volcanic fissure zone reaches the eastern coast of the Izu peninsula, where the seismic swarm activity has been continuously occurring since 1978. The marked crustal upheaval located beside the swarm area is still going on with an almost constant speed of about  $0.6 \text{ cm/year}$ . Assuming that the swarm results from the microcrack generation in the fissure zone, a similar fracture model can be applied to gravity field changes observed on this upheaval.

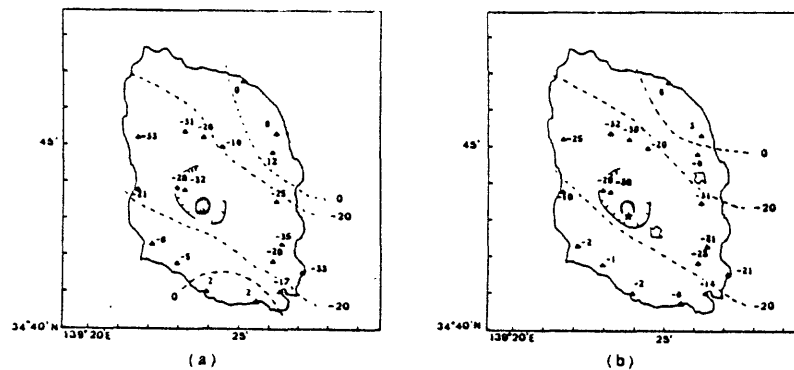


Fig. 4. (a) Elevation change (unit:cm) observed on Izu-Oshima island before and after the 1986 eruption, and (b) that calculated from the fracture model (Okubo and Watanabe,1988). The symbol ★ marks the position of the magma chamber.

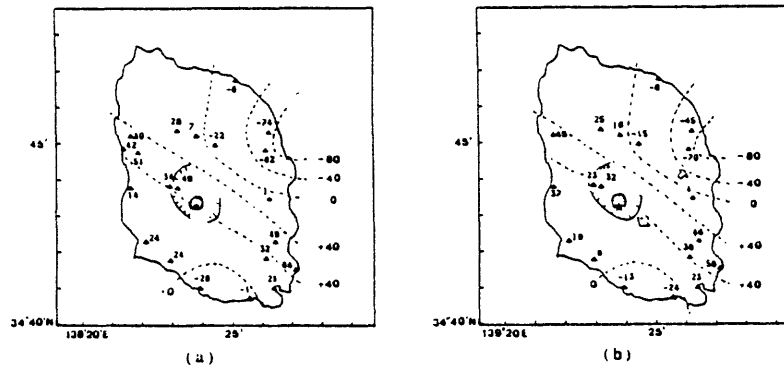


Fig. 5. (a) Gravity change (unit:  $\mu\text{gal}$ ) observed on Izu-Oshima island for the period 1983-1986, and (b) that calculated from the fracture model (Okubo and Watanabe,1988). ★ see Fig. 4.

#### REFERENCES

- Abe, K., Seismic displacement and ground motion near a fault: the Saitama earthquake of September 21, 1931, *J. Geophys. Res.*, 79, 4393-4399, 1974.
- Ishida, M., and A. H. Hasemi, Three-dimensional fine velocity structure and hypocentral distribution of earthquakes beneath the Kanto-Tokai district, Japan, *J. Geophys. Res.*, 93, 2076-2094, 1988.
- Ishii, H., Sato, T., Tachibana, K., Hashimoto, K., Murakami, E., Mishina, M., Miura, S., Sato, K., and A. Takagi, Crustal strain, crustal stress and microearthquake activity in the Northeastern Japan Arc, *Tectonophy.* 97, 217-230, 1983.
- Okubo, S., and H. Watanabe, Gravity changes caused by tensile faulting, submitted to *Geophys. Res. Lett.*, 1988.
- Tsuboi, C., and S. Yamaguchi, Relation between the gravity anomalies and the corresponding subterranean mass distribution (VI), *Bull. Earthquake Res. Inst., Univ. Tokyo*, 19, 26-38, 1940.

## FORESHOCKS, AFTERSHOCKS AND EARTHQUAKE RECURRENCE

James H. Dieterich  
U. S. Geological Survey  
345 Middlefield Road  
Menlo Park, California 94025

### SUMMARY

It is proposed that aftershocks represent a perturbation of background seismicity resulting from step-like increase of stress at the time of a main shock. Observations that aftershocks cluster in those areas near a mainshock that experience an increase of shear stress and aftershock-like bursts of seismicity near sites of rapid intrusions (Dvorak and Tanigawa, 1985) support the idea that sudden increase of stress underlies spatial and temporal aftershock patterns. Foreshocks have many of the characteristics of aftershocks, including decrease of foreshock-mainshock frequency with time that is similar to aftershock decay (Jones and Molnar, 1979; and Jones, 1985). These similarities suggests that foreshock may involve processes operating in the generation of aftershocks. This study examines and tests some specific predictions of a model for the occurrence of earthquakes in the presence of stressing variations using aftershock data.

The perturbation of earthquake rates by a stress step has been modeled using a theory of time-dependent nucleation of earthquake instability. The nucleation model is based on fault constitutive properties observed from laboratory experiments (Dieterich, 1979, 1981; Ruina, 1983; Tullis and Weeks, 1986). Previously (Dieterich, 1986, 1987, 1988), it has been shown that: a) dynamically unstable slip nucleates on fault patches having a characteristic size, b) above a critical threshold stress the nucleation process on a fault patch is self-driven and consists of accelerating creep on the fault patch, c) and the time required to nucleate an instability is highly dependent on stress level and stressing rates. This model considers only the nucleation process for onset of unstable slip and not the magnitude of the subsequent

earthquake which is controlled by rupture propagation processes.

Analytic solutions for earthquake rates originating from a population of nucleation patches following a stress perturbation have been obtained. The model assumes a constant rate of background seismicity,  $R$ , in the absence of a stressing perturbation and constant shear stressing rate,  $\dot{\tau}$ , before and after the stress step. Following a sudden stress step the earthquake rate at any location on a fault is found to be given by:

$$\frac{dn}{dt} = \frac{R}{1 + [ \exp(-\Delta\mu/A) - 1 ] [ \exp(-t/t_a) ]} \quad (1)$$

where  $\Delta\mu$  is the stress step (change in shear stress divided by the normal stress,  $\Delta\tau/\sigma$ ) and  $A$  is a constitutive parameter with values in the range 0.003-0.007 (Dieterich, 1988). The duration of the perturbing effect of the stress step,  $t_a$ , corresponds to the duration of aftershocks or possibly the limiting interval separating a mainshock from a foreshock.  $t_a$  is inversely proportional to stressing rate:

$$t_a = \frac{\sigma A}{\dot{\tau}} = \frac{\sigma A t_r}{\Delta\tau_e} \cong \frac{A t_r}{B \ln(t_r)} \quad (2)$$

In (2) the stressing rate is assumed to be the earthquake stress drop,  $\Delta\tau_e$  divided by recurrence time,  $t_r$ , of the earthquake stress drop (effects of fault creep or contributions from small events are not considered). The approximation giving  $t_a$  in terms of  $t_r$  is based on the constitutive relation. The units of  $t_a$  and  $t_r$  are seconds.  $B$  is a constitutive parameter with experimental values in the range 0.006-0.010 and from experiments and stability considerations the ratio of  $A/B$  is expected to have values in the range 0.5 - 1.0 (Dieterich, 1981; Rice and Ruina, 1983; Tse and Rice, 1986). In equation (1) the increase in stress,  $\Delta\mu$ , may be expressed as a multiplying factor,  $k$ , of the earthquake stress drop, which yields:

$$\frac{\Delta\mu}{A} = \frac{k \Delta\tau_e}{\sigma A} \cong \frac{k B}{A} \ln(t_r) \quad (3)$$

Some characteristics of the response of earthquake rates to a stress step as predicted by (1) are illustrated in Figure 1. Several features are of possible interest. First, the logarithm of the seismicity rate increases to an initial level that is proportional to the magnitude of

the local stress step. Second, for different locations having different amplitude stress steps and different initial rates of seismicity, the rates all asymptotically approach and follow the same  $1/t$  decay law. Third, the duration of the aftershocks is independent of the magnitude of the stress step, but depends upon stressing rate or recurrence time as given by (2).

The proposed relationship (1) yields a predicted response that is remarkably similar to Omori's law for aftershock decay:

$$\frac{dn}{dt} = \frac{a}{b + t} \quad (4)$$

This includes a decay of aftershock rates that is asymptotic to  $1/t$  over some interval of time. The principal quantitative difference is that Omori's relationship does not include the background rate. As shown by Figure 1,  $t_a$  as given in (2) is defined as the time at which the relation of Omori (4) intersects the background rate. In addition to this rough agreement of the model with overall aftershock decay observations, specific features of the model noted above suggest several detailed tests of the model.

One such test is the prediction of the model that aftershock duration as defined in Figure 1 is related to earthquake recurrence time (2) and independent the magnitude of the stress step. This relationship has not been proposed previously and if confirmed, it could suggest some new approaches for analysis and use of aftershock data. A study is underway to evaluate the validity of the predicted relationship. Figure 2 plots the predicted relationship between recurrence time and aftershock duration assuming  $A/B = 0.8$ . Some preliminary determinations with recurrence times from 10 years to 5000 or more years are plotted for comparison. The preliminary results appear to support the proposed relationship. This result suggests that aftershock duration could provide a rough, independent estimate of recurrence time. Such estimates could prove especially useful in areas where other recurrence data are absent.

Other potential applications of the model are suggested by the quantitative relationship of earthquake rates and magnitude of shear stress increases. For example, for the general case of a spatially nonuniform stress step, the spatial and temporal seismicity can be calculated from (1). The initial rate following the stress step is found at  $t=0$  from (1):

$$\frac{dn}{dt} = R \exp(\Delta\mu/A) \quad (5)$$

The time  $t_s$ , when the rate asymptotically merges with the  $1/t$  decay:

$$t_s = t_a \exp[-\Delta\mu/A] \quad (6)$$

See Figure 1 for graphical definition of  $t_s$ .

The relationships (5) and (6) provide explanations for the characteristic clustering of aftershocks at the edges of the mainshock rupture where the stress step is greatest and the spread of aftershocks with time. The spreading of aftershocks is an apparent effect in which earthquake rates at locations with a large stress step merge with regions with progressively lower stress steps at the time  $t_s$ . This effect is illustrated by combining (6) with elasticity solutions for changes of stress due to a shear crack. For example, combining Starr's solution for a shear crack in plane strain with (7) yields:

$$t_s = t_a \exp \left\{ - \left[ \frac{t_r}{t_a} \right] \left[ \frac{x}{(x^2 - c^2)^{1/2}} - 1 \right] \right\} \quad (6)$$

where,  $c$  is the half length of a constant stress drop slip patch and  $x$  is the position along the fault from the center of the slip patch. Hence, at the ends of the faulted patch (where  $x > c$ ) the apparent end of the aftershock zone will be at position  $x$  (where  $x > a$ ) at time  $t_s$ . Quantitative comparison with aftershock sequences will be presented.

The possible relevance of the model to aftershocks is somewhat problematical because foreshock sequences are not as well characterized as aftershock sequences. The decay of frequency of occurrence of foreshock-mainshock pairs with time and distance (Jones and Molnar, 1979; Jones, 1985) is similar to that of aftershocks, suggesting the possibility of similar mechanisms. If indeed this is the situation, then a mainshock following a foreshock simply represents a perturbation of background seismicity by the foreshock, where the rupture propagation subsequent to nucleation results in a larger event (*i.e.* the rupture propagation controls magnitude and is independent of nucleation processes). Alternatively, foreshocks may be a response of the background seismicity to accelerating deformation for the nucleation of the mainshock. In this case, the dimensions of mainshock nucleation patches must be significantly larger than the patches for the background seismicity and cause

significant stressing in adjacent regions as the accelerating slip progresses toward mainshock nucleation. The local background seismicity would accelerate and appear as foreshocks in those regions in response to the accelerating stressing rate.

#### REFERENCES

- Dieterich, J. H., "Modeling of rock friction: 1 Experimental results and constitutive equations, *J. Geophys. Res.*, 84, 2161-2168, 1979.
- Dieterich, J. H., "Constitutive properties of faults with simulated gouge", in: *Mechanical Behavior of Crustal Rocks*, Geophysical Monograph 24, American Geophysical Union, 103-120, 1981.
- Dieterich, J.H., "A model for the nucleation of earthquake slip", in: *Earthquake Source Mechanics*, Am. Geophys. Union Monograph 37, 37-47, 1986.
- Dieterich, J.H., "Nucleation and triggering of earthquake slip: Effect of periodic stresses", in press, *Tectonophysics*, 1987.
- Dieterich, J. H., "Probability of Earthquake recurrence with nonuniform stress rates and time-dependent failure", *PAGEOPH*, 126, 589-617, 1988.
- Dvorak, J. J. and W. R. Tanigawa, "Generation of earthquake swarms along the south Flank of Kilauea volcano, Hawaii", *Eos Trans. AGU*, 66, 851, 1985.
- Jones, L. M. and P. Molnar, "Some characteristics of foreshocks and their possible relation to earthquake prediction and premonitory slip", *J. Geophys. Res.*, 84, 3596-3608, 1979.
- Jones, L.M., "Foreshocks and time-dependent earthquake hazard assessment in southern California", *Bull. Seism. Soc. Am.*, 75, 1669-1680, 1985.
- Rice, J.R., and Gu, J.-C., "Earthquake aftereffects and triggered seismic phenomena", *PAGEOPH*, 121, N. 2, 187-219, 1983.
- Rice, J.R. and A.L. Ruina, "Stability of steady frictional slipping", *Trans. ASME, J. Appl. Mech.*, 50, 343-349, 1983.
- Ruina, A.L., "Slip instability and state variable friction laws", *J. Geophys. Res.* 88, 10359-10370, 1983.
- Tse, S. T. and J. R. Rice, "Crustal earthquake instability in relationship to the depth variation of frictional slip properties", *J. Geophys. Res.*, 91, 9452-9472, 1986.
- Tullis, T. E. and J. D. Weeks, "Constitutive behavior and stability of frictional sliding of granite, *PAGEOPH.*, , 1986.

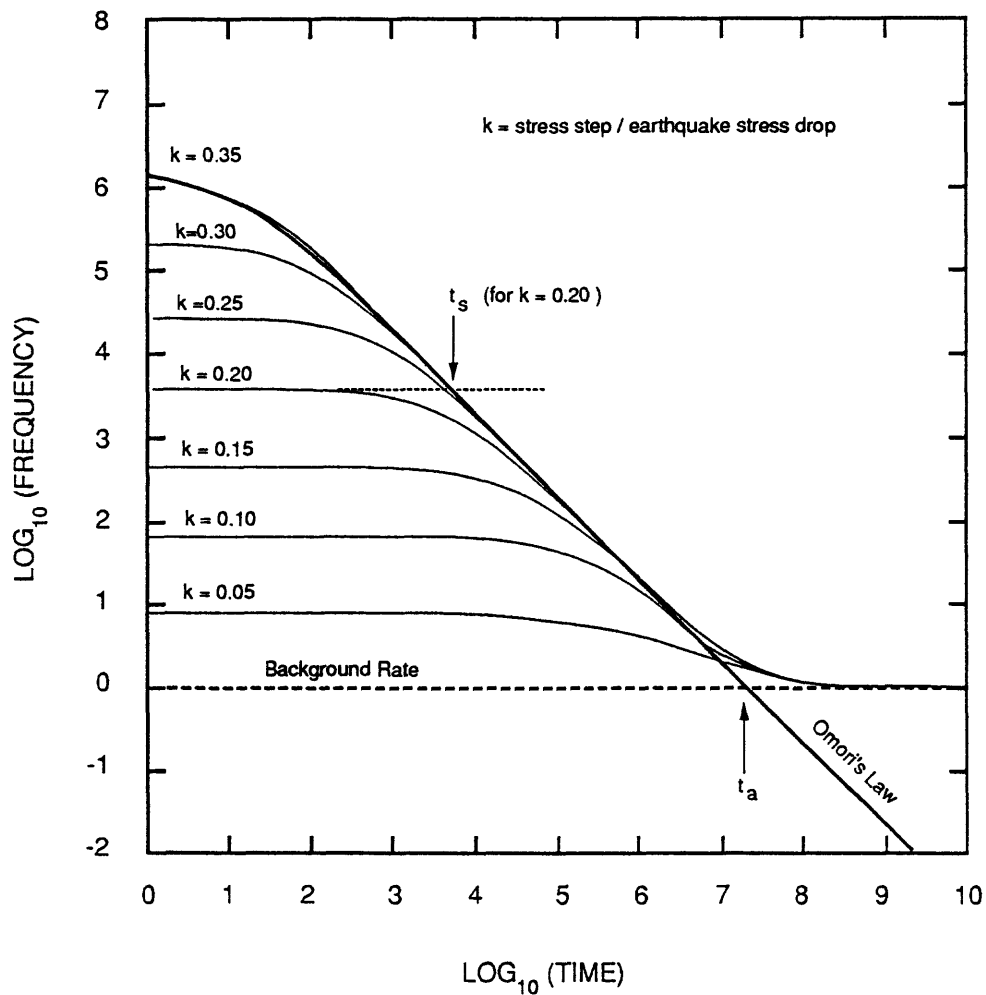


Figure 1. Earthquake frequency following a stress step. Heavy line is Omori's law fit to the  $k = 0.035$  theoretical curve. The ratio of constitutive parameters  $A/B$  is 0.5 and the recurrence time is 22 years.

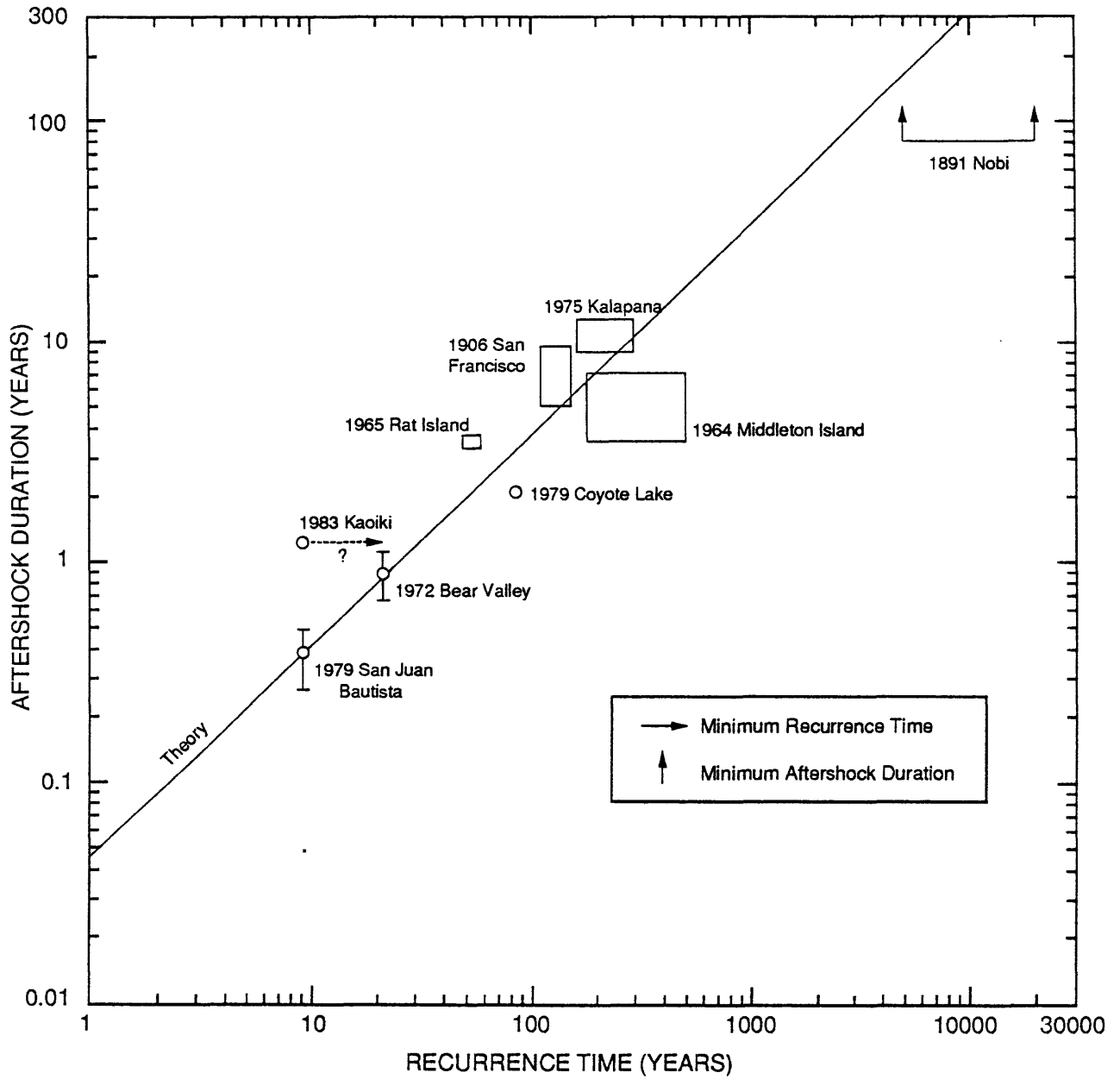


Figure 2. Preliminary determination of aftershock duration and earthquake recurrence time. Theory is given by equation (2) with  $A/B = 0.8$ .

# Implications of Fault Creep Studies for the Mechanics of Faulting

by

Robert L. Wesson  
U.S. Geological Survey  
Reston, Virginia 22092

Observations along the surface traces of active faults in California and elsewhere indicate that tectonic displacement can occur as seismic slip, or as aseismic fault creep. Fault creep occurs as secular fault displacement, as episodic displacement called "creep events", as periods of continuing surface fault displacement after the occurrence of an earthquake ("afterslip"), and as "sympathetic" slip triggered by an earthquake on another fault elsewhere in the same region. Observations of fault creep, afterslip, and triggered slip along active faults and analytic and numerical studies of the dynamics of fault creep suggest the following: 1) the long-term creep rate (or afterslip rate) at a point along an active fault is controlled by the long-term loading rate and by the geometric distribution of stuck and creeping areas on the fault zone, 2) creep events represent the failure of one or more discrete "creep asperities" that fail at a finite yield stress, then heal to reaccumulate stress, 3) afterslip and triggered slip are fundamentally the transient response of the weak, creeping, portions of the fault zone to changes in the static stress field resulting from the sudden, deep-seated, dislocation that caused the preceding earthquake. Thus, it appears that fault creep is a fundamental process that acts to redistribute and concentrate changes in stress, from either long-term loading or nearby earthquakes, onto the stuck portions of the fault that fail in earthquakes. Inasmuch as episodes of creep, afterslip, and triggered slip are periods of relatively rapid stress increase on the stuck portions, these intervals of time should be regarded as periods of higher earthquake probability in the affected areas.

Fault creep can be viewed as arising from the interplay of three factors: stress applied to the fault from external sources; stress caused by the geometry and distribution of displacement on the fault--arising from the elastic response of the surrounding medium to the displacements within the anelastic fault zone itself; and the constitutive relations characterizing the resistance to slip on the fault. Wesson (1988) presents analytic solutions for some cases of viscous and quasi-plastic (power law creep) fault zone rheology, and a matrix formulation for calculating dislocation stresses on a fault zone in a halfspace or plate as the basis for numerical simulation of one- and two-dimensional propagating creep.

## Long-term Creep Rates

Long-term creep rates are determined by the distribution of stuck and creeping portions of the fault zone and by the rate of change of the regional stress. Referring to Figure 1,

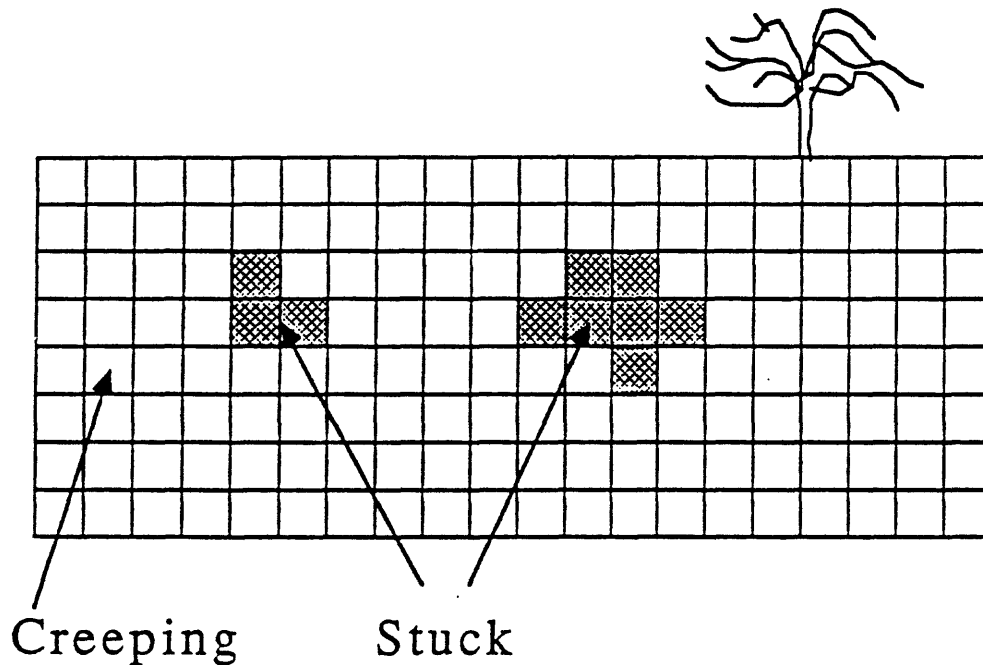


Figure 1.

consider the quasi-static equilibrium at each point (and in particular at the center of each element) then

$$\tau_{\text{res}} = \tau_{\text{ext}} + \tau_{\text{dis}} \quad (1)$$

where  $\tau_{\text{res}}$  is resistance to slip (dependent on the rheology of the fault zone),  $\tau_{\text{ext}}$  is external stress (derived from crustal loading and the static stress changes associated with nearby earthquakes), and  $\tau_{\text{dis}}$  is dislocation stress (derived from the geometry of the stuck and creeping portions of the fault zone and elastic constants). The dislocation stress on each element can be written as the product of a matrix of geometric factors and a vector of displacement on all elements:

$$\tau_{\text{dis}} = A u$$

Then (1) can be rewritten and partitioned into creeping and stuck parts

$$\tau_{\text{res}} = \begin{pmatrix} \tau_{\text{crp}} \\ \tau_{\text{stk}} \end{pmatrix} = (\tau_{\text{ext}}) + \begin{pmatrix} A_{\text{crp}} & | & B_{\text{stcr}} \\ \hline B_{\text{crst}} & | & A_{\text{stk}} \end{pmatrix} \begin{pmatrix} u_{\text{crp}} \\ u_{\text{stk}} \end{pmatrix}$$

Differentiating with respect to time and noting that for steady-state creep

$$\frac{d}{dt} \tau_{\text{crp}} = 0 \text{ and } u_{\text{stk}} = 0,$$

then

$$\frac{d}{dt} \tau_{\text{res}} = \begin{pmatrix} 0 \\ \frac{d}{dt} \tau_{\text{stk}} \end{pmatrix} = \left( \frac{d}{dt} \tau_{\text{ext}} \right) + \begin{pmatrix} A_{\text{crp}} & | & B_{\text{stcr}} \\ \hline B_{\text{crst}} & | & A_{\text{stk}} \end{pmatrix} \begin{pmatrix} \frac{d}{dt} u_{\text{crp}} \\ 0 \end{pmatrix}$$

and

$$\frac{d}{dt} u_{\text{crp}} = - A_{\text{crp}}^{-1} \frac{d}{dt} \tau_{\text{ext}}$$

Thus the long term-creep rates are shown to be equal to the product of a matrix of geometric factors times the rate of external loading.

### Creep Events

Fault creep events last a few hours to days and include from a millimeter or less to a few tens of millimeters of displacement. Instrumental measurements of displacement versus time during creep events show that many events have a characteristic, simple form including a steep beginning, followed by a gradual decay in the rate of displacement. Some creep events display small amounts of precursory slip, and many seem to be composed of several discrete "simple" events. Propagation of creep events along the San Andreas, Calaveras and Imperial faults in California has been inferred from the nearly simultaneous observation of creep events at nearby creepmeters, and from kinematic modeling of continuous measurements of strain during creep events. A simple, one-element, quasi-plastic model is in agreement with the form of creep events observed at Melendy Ranch, California. Wesson (1988) presents results of numerical modeling of a propagating creep event observed along the southern Calaveras fault, central California, during July, 1977,

suggesting that on the southern Calaveras fault, observations of propagating creep indicate a yield stress near zero at the surface and throughout much of the fault zone. However these observations also indicate the presence of a zone at a depth of about 0.5 km, and about 5 km long, with a yield stress of about 15 bars (1.5 MPa).

### Afterslip

Measurements of the continuing surface fault displacement (afterslip) following earthquakes are widely reported to follow a relation of the form  $u(t) = a + b \log t$ , where  $u(t)$  is the surface fault displacement,  $t$  is time and  $a$  and  $b$  are constants. Thus, the rate of fault displacement  $du/dt$  decays as  $1/t$ . Sets of measurements that extend to large times (years) typically show a gradual change to a more rapid rate of decay as  $u(t)$  asymptotically approaches an upper bound. The limited number of measurements available within a few hours following an earthquake (principally from the 1987 Superstition Hills, Calif., earthquake), as well as results from numerical modeling, indicates that the initial displacement rate is less than  $1/t$ . Assume that the displacement rate on the fault is a function of the applied shear stress and that the displacement on the fault asymptotically approaches an equilibrium configuration in which the dislocation stress from the afterslip balances the static stress change from the buried displacement at the instant of the earthquake. A bootstrap technique can then be used to estimate the dependence of displacement rate on shear stress. As the fault displacement approaches equilibrium, the shear stress can be shown to be proportional to the difference between the displacement at any time and its final equilibrium value. The constant of proportionality can be calculated from the geometry of the initial buried earthquake dislocation and the fault experiencing afterslip. Thus, a table of displacement rate and shear stress can be constructed. Observations of afterslip along the Superstition Hills earthquake provide an example. The commonly observed form  $u(t) = a + b \log t$  implies that the displacement rate is proportional to  $\exp(k \tau)$ , where  $k$  is a constant and  $\tau$  is shear stress.

### Reference

Wesson, R.L., Dynamics of fault creep, Jour. Geophys. Res., 93, 8929-8951, 1988.

Observation Status of the Japanese Geodetic Satellite  
"Ajisai" and Precise Baseline Determination by using  
the Transportable Laser Ranging Station (HTLRS)

YOSHIO KUBO and MINORU SASAKI  
Hydrographic Department, Maritime Safety Agency  
3-1, Tsukiji 5-chome, Chuo-ku, Tokyo 104 Japan

Abstract

The Japanese Geodetic Satellite was launched in August 1986 and named Ajisai. The launch orbit is circular with an inclination of 50 degrees and altitude of 1500 km.

The Satellite Laser Ranging (SLR) observation has been continued at more than 20 SLR stations in the world. The range precision given by some NASA laser ranging systems reached 1 cm.

A transportable laser ranging station has been developed by the Hydrographic Department of Japan (JHD) for observations of Ajisai and other geodetic satellites to construct a marine geodetic controls around Japan. After collocation observations with the fixed SLR system at the Simosato Hydrographic Observatory the transportable station was shipped to an isolated island, Titi-sima, and SLR observation was continued from mid-January to mid-March, 1988. The analysis for baseline length

determination between Titi-sima and Simosato by means of a short arc method for seven sets of simultaneously observed successive passes of Lageos gives a result as

baseline = 937,665.041 m  $\pm$  0.004 m (rms).

#### 1. Observation status of the Geodetic Satellite "Ajisai"

The Japanese Geodetic Satellite was launched in August, 1986 and named "Ajisai" which means "hydrangea" of flower in Japanese. The launch orbit is almost complete circular with an inclination of 50 degrees and altitude of 1500 km.

The functions of Ajisai are 1) to reflect input laser light back toward the ground for precise ranging and 2) to reflect solar light to determine the direction to the satellite from an observation site. The satellite is a hollow sphere, 2.15 m in diameter, and weighs 685 kg. The surface is covered with corner cube reflectors and separate solar light reflectors.

The laser tracking has been made by the Simosato Hydrographic Observatory (SHO) of the Maritime Safety Agency, the Goddard Laser Tracking Network (GLTN) of the National Aeronautics and Space Administration (NASA) of the United States and other international cooperative SLR stations.

Total amount of SLR observation for Ajisai made at the

SHO and other stations in the world is given in Table 1. As for the range precision, some high precision SLR systems of NASA reach 1 cm. Despite of the large sphere radius as 2.15 m, rather good range precision is realized as our simulation[1] gave before the launch.

## 2. Preliminary analysis of Ajisai SLR data

As a preliminary result of analysis of Ajisai SLR data by using an orbital processor developed in the Hydrographic Department of Japan[2], an estimate of baseline length between Quincy and Monument Peak in California crossing over the San Andreas Fault is given as following. The Ajisai SLR data for successive passes simultaneously obtained at the both sites from January to February 1987 were used for the analysis. A preliminary result for the baseline between reference points of each SLR systems at the both sites is

$$\text{baseline} = 883\,602.11 \text{ m} \pm 0.05 \text{ m (rms)}$$

An example of the residuals of raw range minus range derived from determined orbit for a set of data in Oct. 9, 1986 is given in Fig. 1.

### 3. Completion of a Transportable Laser Ranging Station (HTLRS)

The transportable SLR system named the Hydrographic Department Transportable Laser Ranging Station (HTLRS) had completed by the end of October 1987. The outline of HTLRS is presented in Figs. 2 and 3 and the principal specifications are shown in Table 2.

The output laser pulse is propagated through the Coude path along the azimuth axis and reflected by a small mirror to the central part of a large mirror measuring 50 cm x 35 cm of the transmitter/receiver on the elevation axis. The return signal from a satellite comes to the whole part of the transmitter/receiver mirror and goes to a receiver telescope 35 cm in diameter. The detector for the return signal is mounted on a bench on the azimuth axis behind the receiver telescope.

Tracking control is made mainly by a microcomputer. Some on site softwares for tracking and preliminary signal data selection from a number of noises give good operability on the screen using a joystick like some computer games. The HTLRS is capable for ranging not only to Ajisai but also Lageos.

Clock subsystem is composed of a Rubidium frequency standard and of a Loran-C receiver for time comparison. The station is housed by two separate shelters measuring 2.1 m x 2.3 m x 3.3 m and 2.1 m x 2.3 m x 4.0 m. The total weight is

around 5 tons. The system can be transported to isolated islands lacking port facilities by a transport plane.

The testing observation and collocation observation with Simosato fixed SLR system were made at the Simosato site. Range precision to Lageos and Ajisai were 3-4 cm level and no specific bias compared with the Simosato system was found.

#### 4. Start of field observation using the HTLRS

The HTLRS was shipped to Titi-sima (island), which consists a primary station of the Marine Geodetic Control of Japan[3] (Fig. 4), in Ogasawara (Bonin) islands as the first field observation in early January 1988. The SLR observations to Lageos, Ajisai and Starlette was started both at the island and the Simosato site. The total numbers of the range data obtained at both sites in the duration are presented in Table 3.

An analysis for baseline length determination between Titi-sima and Simosato site by means of a short arc method for 11,139 shots in seven sets of simultaneously observed successive passes of Ajisai using the software developed at the Hydrographic Department gives a result as

$$\text{baseline} = 937,665.041 \text{ m} \pm 0.004 \text{ m (rms)}.$$

The precise determination of the baseline lengths between the Simosato site and each station of the nine primary stations in Fig. 4 will be made in the following

five years in the Northwest Pacific Region.

The re-determination of these baselines after that will clarify the plate motion in this region.

#### references

- [1] Sasaki, M. and H. Hashimoto : "Launch and Observation Program of the Experimental Geodetic Satellite of Japan", IEEE transactions on Geoscience and Remote Sensing, Vol. GE-25, 526-533, 1987.
- [2] Sasaki, M. : "Algorithm for Determination of Satellite Orbit and Geodetic Parameters by using Laser Ranging Data and Preliminary Results of its Application", Rept. of Hydrogr. Res., No.19, 107-133, 1984.
- [3] Yamazaki, A. and T. Mori : "Marine Geodetic Controls around Japan", Marine Geodesy, Vol. 7, 331-344, 1983.

Table 1. Observation status of "AJISAI"

| year         | Simosato site<br>passes | site<br>shots | other world SLR sites<br>passes |
|--------------|-------------------------|---------------|---------------------------------|
| 1986         | 169                     | 139,000       | 1160                            |
| 1987         | 277                     | 171,000       | 2016                            |
| Jan-Jun 1988 | 174                     | 72,000        | 1116                            |

Table 2. Principal specifications of HTLRS

|                     |   |
|---------------------|---|
| receiver diameter   | 35 cm   |
| type                | elevation axis and receiving<br>electronics over azimuth axis |
| laser output energy | 50 mJ   |
| pulse width         | 100 - 200 psec  |
| repetition rate     | 5 pps   |
| range precision     | 3 - 4 cm  |
| clock               | Rubidium / Loran C  |
| shelter             | two housings (air transportable)                              |
| size                | 2.1 m x 2.3 m x 3.3 m and<br>2.1 m x 2.3 m x 4.0 m            |
| wight               | 5 tons  |

Table 3. Range data obtained in the field work duration  
(Jan. - Mar. 1988)

| satellites     | Titi-sima<br>(HTLRS) |        | Simosato<br>(fixed-SLR system) |        |
|----------------|----------------------|--------|--------------------------------|--------|
|                | passes               | shots  | passes                         | shots  |
| Ajisai         | 38                   | 19,700 | 94                             | 36,400 |
| Lageos         | 11                   | 5,500  | 22                             | 1,500  |
| Starlette      | 4                    | 600    | 22                             | 2,900  |
| mean precision | 9 cm                 |        | 3.6 cm                         |        |

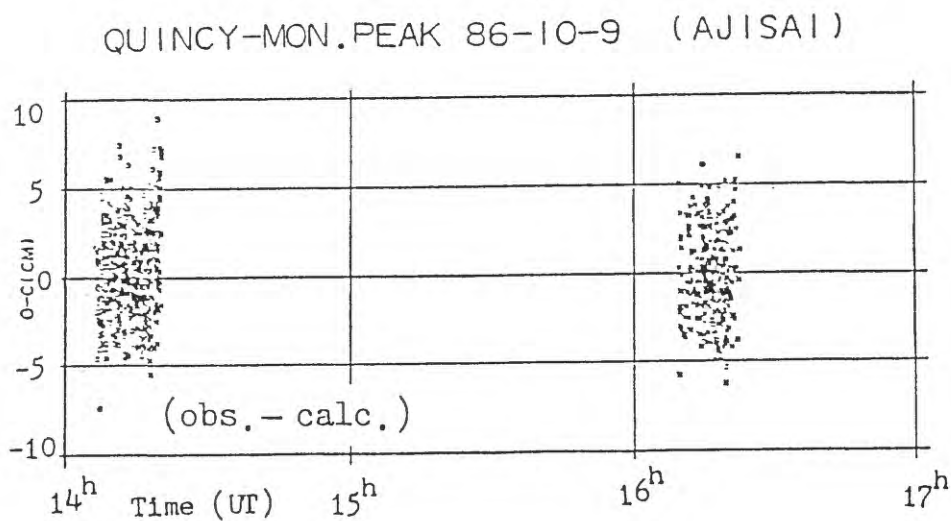


Fig. 1. RMS for (O-C) of Ajisai SLR data and best fit orbit of short arc.

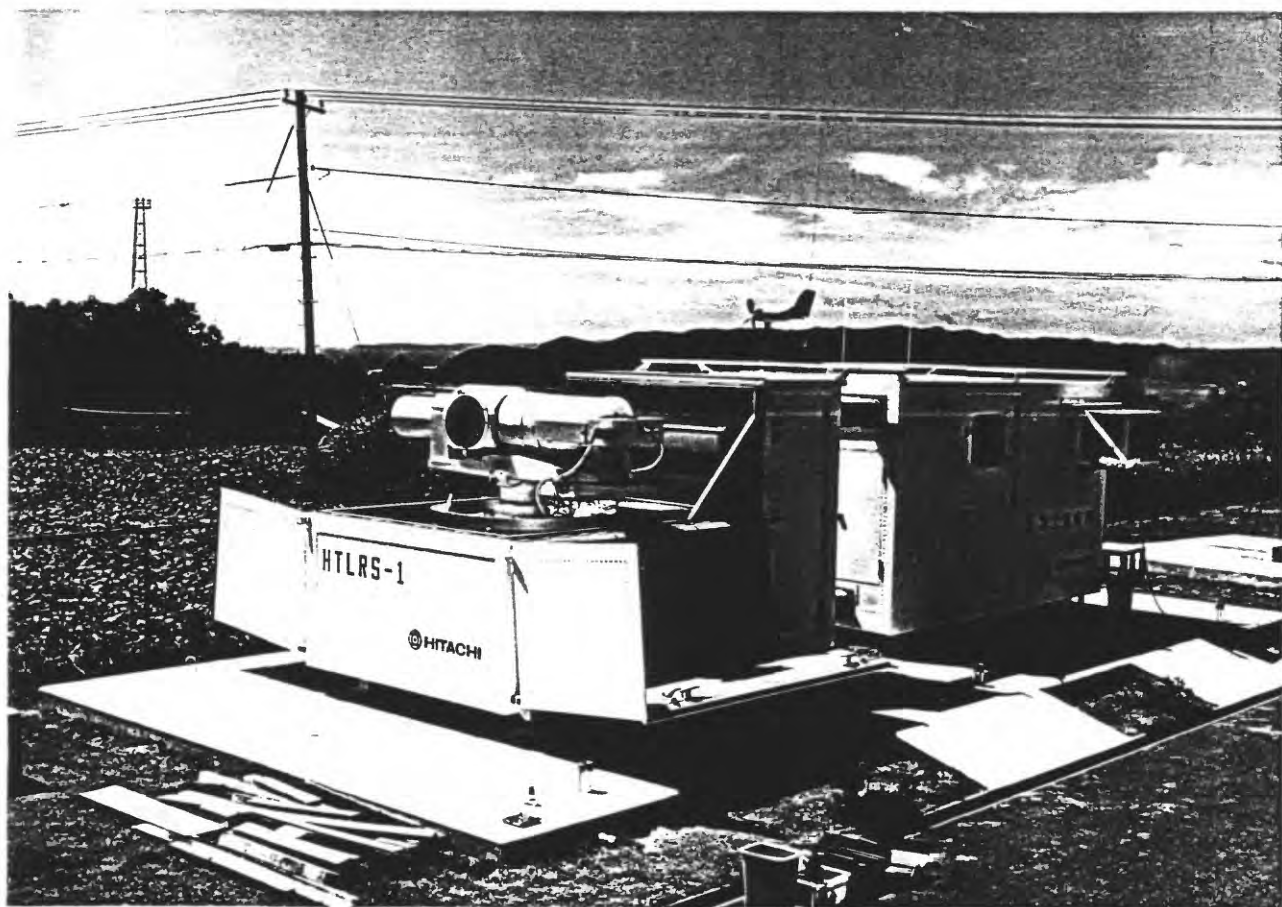


Fig. 2. Overview of the Hydrographic Department Transportable Laser Ranging Station (HTLRS).

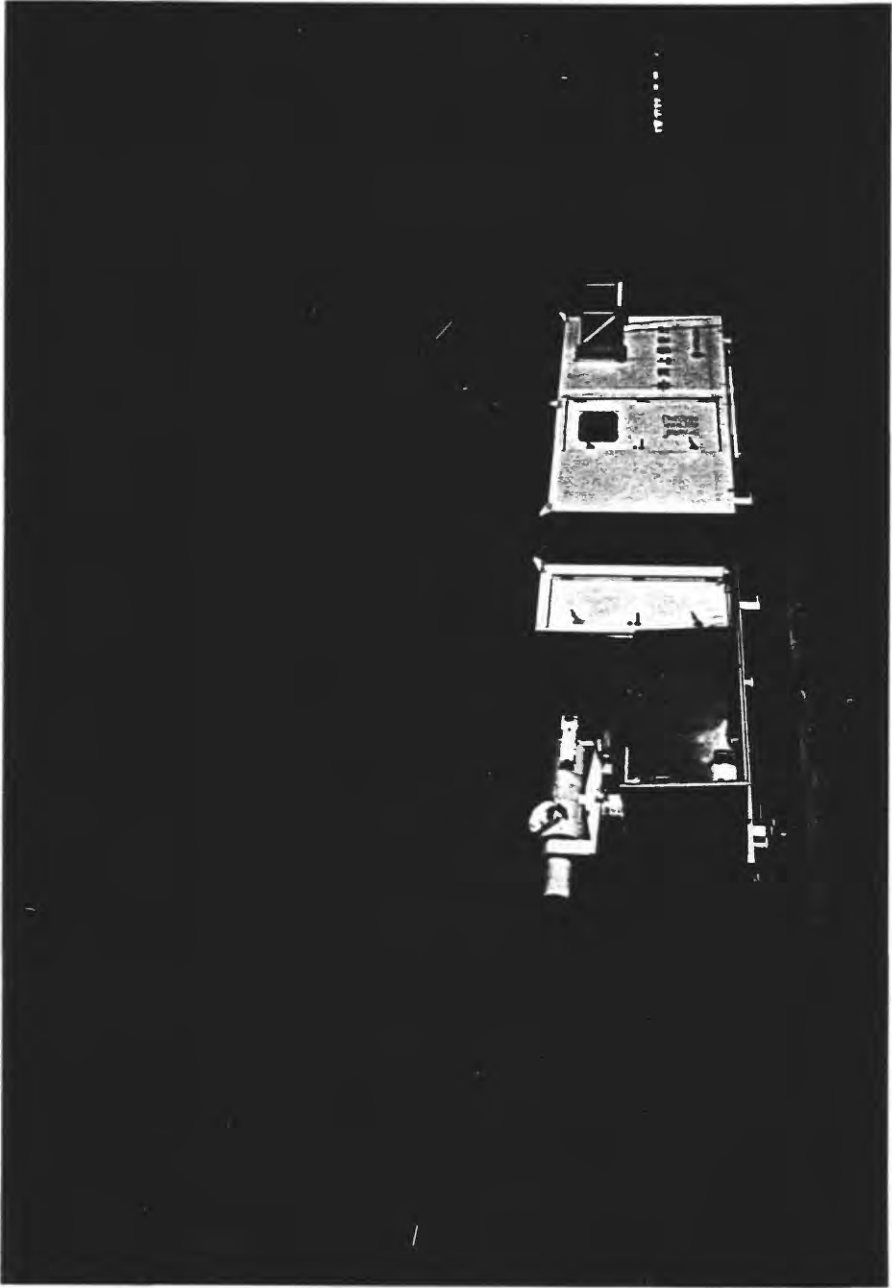


Fig. 3. A scene of SLR observation of the HTLRS in the evening.

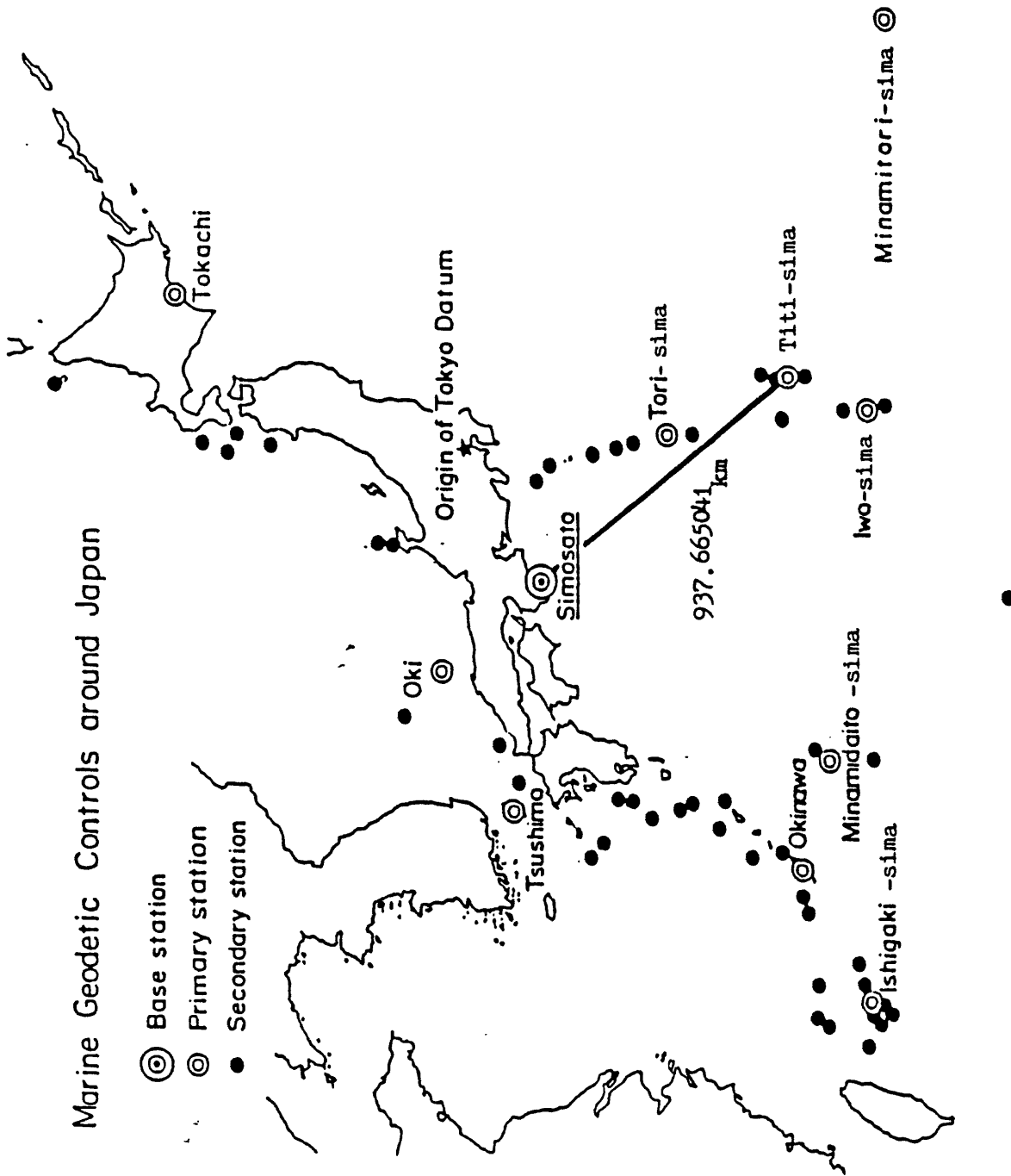


Fig. 4 Configuration of the Marine Geodetic Controls of JHD.

## CONFERENCES TO DATE

- Conference I Abnormal Animal Behavior Prior to Earthquakes, I  
Not Open-Filed
- Conference II Experimental Studies of Rock Friction with Application to Earthquake Prediction  
Not Open-Filed
- Conference III Fault Mechanics and Its Relation to Earthquake Prediction  
Open-File No. 78-380
- Conference IV Use of Volunteers in the Earthquake Hazards Reduction Program  
Open-File No. 78-336
- Conference V Communicating Earthquake Hazard Reduction Information  
Open-File No. 78-933
- Conference VI Methodology for Identifying Seismic Gaps and Soon-to-Break Gaps  
Open-File No. 78-943
- Conference VII Stress and Strain Measurements Related to Earthquake Prediction  
Open-File No. 79-370
- Conference VIII Analysis of Actual Fault Zones in Bedrock  
Open-File No. 79-1239
- Conference IX Magnitude of Deviatoric Stresses in the Earth's Crust and Upper Mantle  
Open-File No. 80-625
- Conference X Earthquake Hazards Along the Wasatch and Sierra-Nevada Frontal Fault Zones  
Open-File No. 80-801
- Conference XI Abnormal Animal Behavior Prior to Earthquakes, II  
Open-File No. 80-453
- Conference XII Earthquake Prediction Information  
Open-File No. 80-843
- Conference XIII Evaluation of Regional Seismic Hazards and Risk  
Open-File No. 81-437
- Conference XIV Earthquake Hazards of the Puget Sound Region, Washington  
Open-File No. 82-19
- Conference XV A Workshop on "Preparing for and Responding to a Damaging Earthquake in the Eastern United States"  
Open-File No. 82-220
- Conference XVI The Dynamic Characteristics of Faulting Inferred from Recording of Strong Ground Motion  
Open-File No. 82-591
- Conference XVII Hydraulic Fracturing Stress Measurements  
Open-File No. 82-1075
- Conference XVIII A Workshop on "Continuing Actions to Reduce Losses from Earthquakes in the Mississippi Valley Area"  
Open-File No. 83-157
- Conference XIX Active Tectonic and Magmatic Processes Beneath Long Valley  
Open-File No. 84-939

Conference XX A Workshop on "The 1886 Charleston, South Carolina, Earthquake and its Implications for Today"  
Open-File No. 83-843

Conference XXI A Workshop on "Continuing Actions to Reduce Potential Losses from Future Earthquakes in the Northeastern United States"  
Open-File No. 83-844

Conference XXII A Workshop on "Site-Specific Effects of Soil and Rock on Ground Motion and the Implications for Earthquake-Resistant Design"  
Open-File No. 83-845

Conference XXIII A Workshop on "Continuing Actions to Reduce Potential Losses from Future Earthquakes in Arkansas and Nearby States"  
Open-File No. 83-846

Conference XXIV A Workshop on "Geologic Hazards in Puerto Rico"  
Open-File No. 84-761

Conference XXV A Workshop on "Earthquake Hazards in the Virgin Islands Region"  
Open-File No. 84-762

Conference XXVI A Workshop on "Evaluation of the Regional and Urban Earthquake Hazards in Utah"  
Open-File No. 84-763

Conference XXVII Mechanics of the May 2, 1983 Coalinga Earthquake  
Open-File No. 85-44

Conference XXVIII A Workshop on "The Borah Peak, Idaho, Earthquake"  
Open-File No. 85-290

Conference XXIX A Workshop on "Continuing Actions to Reduce Potential Losses from Future Earthquakes in New York and Nearby States"  
Open-File No. 85-386

Conference XXX A Workshop on "Reducing Potential Losses from Earthquake Hazards in Puerto Rico"  
Open-File No. 85-731

Conference XXXI A Workshop on "Evaluation of Regional and Urban Earthquake Hazards and Risk in Alaska"  
Open-File No. 86-79

Conference XXXII A Workshop on "Future Directions in Evaluating Earthquake Hazards of Southern California"  
Open-File No. 86-401

Conference XXXIII A Workshop on "Earthquake Hazards in the Puget Sound, Washington Area"  
Open-File No. 86-253

Conference XXXIV A Workshop on "Probabilistic Earthquake-Hazards Assessments"  
Open-File No. 86-185

Conference XXXV A Workshop on "Earth Science Considerations for Earthquake Hazards Reduction in the Central United States"  
Open-File No. 86-425

- Conference XXXVI A Workshop on "Assessment of Geologic Hazards and Risk in Puerto Rico"  
Open-File No. 87-007
- Conference XXXVII A Workshop on "Earthquake Hazards Along the Wasatch, Utah"  
Open-File No. 87-154
- Conference XXXVIII A Workshop on "Physical & Observational Basis for Intermediate Term Earthquake Prediction"  
Open-File 87-154
- Conference XXXIX Directions in Paleoseismology  
Open-File No. 87-673
- Conference XL A Workshop on "The U.S. Geological Survey's Role in Hazards Warnings"  
Open File No. 87-269
- Conference XLI A Review of the Earthquake Research Applications in the National Earthquake Hazard Reduction Program: 1977-1987  
Open-File No. 88-13-A
- Conference XLII A Workshop on "Evaluation of Earthquake Hazards and Risk in the Puget Sound and Portland Areas"  
Open File No. 88-541
- Conference XLIII A Workshop on "Earthquake Risk: Information Needs of the Insurance Industry"  
Open-File No. 88-669
- Conference XLIV A Workshop on "Geological, Geophysical, and Tectonic Settings of the Cascade Range"  
Open-File No. 89-178
- Conference XLV A Workshop on "Fault Segmentation and Controls of Rupture Initiation and Termination"  
Open-File No. 89-315
- Conference XLVI The 7th U.S.- Japan Seminar on Earthquake Prediction  
Open-File No. 90-98
- Conference XLVII A Workshop on "USGS'S New Generation of Probabilistic Ground Motion Maps and their Applications to Building Codes"  
Open-File No. 89-364
- Conference XLVIII A Workshop on "Earthquake Hazards in the Puget Sound, Portland Area"  
Open-File No. 89-465

For information on ordering the above publications, please contact:

U.S. Geological Survey  
Books and Open-File Reports Service Section  
Building 41, Box 25425  
Federal Center  
Denver, Colorado 80225